

Monopulse Principles and Techniques

SECOND EDITION

Samuel M. Sherman • David K. Barton

Monopulse Principles and Techniques

Second Edition

For a listing of recent titles in the *Artech House Radar Series*,
turn to the back of this book.

Monopulse Principles and Techniques

Second Edition

Samuel M. Sherman
David K. Barton



**ARTECH
HOUSE**

BOSTON | LONDON
artechhouse.com

Library of Congress Cataloging-in-Publication Data

A catalog record for this book is available from the U.S. Library of Congress.

British Library Cataloguing in Publication Data

A catalogue record for this book is available from the British Library.

ISBN-13 978-1-60807-174-6

Cover design by Vicki Kane

© 2011 ARTECH HOUSE

685 Canton Street

Norwood, MA 02062

All rights reserved. Printed and bound in the United States of America. No part of this book may be reproduced or utilized in any form or by any means, electronic or mechanical, including photocopying, recording, or by any information storage and retrieval system, without permission in writing from the publisher. All terms mentioned in this book that are known to be trademarks or service marks have been appropriately capitalized. Artech House cannot attest to the accuracy of this information. Use of a term in this book should not be regarded as affecting the validity of any trademark or service mark.

10 9 8 7 6 5 4 3 2 1

Contents

Preface to the Second Edition xiii

Preface to the First Edition xv

Chapter 1 Introduction 1

 1.1 Review of Radar Principles 1

 1.2 Tracking Radars and the Evolution of Monopulse 2

 1.3 A “Baseline” Monopulse Radar 6

 1.4 Advantages and Disadvantages of Monopulse 13

 1.5 Nonradar Uses of Monopulse 15

 References 16

Chapter 2 Terminology, Definitions, and Notation 19

 2.1 The Meaning of Monopulse 20

 2.2 Apertures and Illumination Functions 22

 2.3 Patterns, Lobes, and Beams 22

 2.4 Sum and Difference Patterns 24

 2.5 Sum and Difference Notation 26

 2.6 Error Signals 27

 2.7 Complex Signal Representation and Complex
 Envelopes 27

 2.8 Elevation, Azimuth, and Traverse 31

 References 38

Chapter 3 The Monopulse Output as a Complex Ratio 39

 3.1 General Principles 39

 3.2 Relative Phase of Difference and Sum 41

 3.3 Some Useful Relationships and Formulas 41

 References 44

Chapter 4	Components Used in Monopulse	45
4.1	Antenna Mounts	45
4.2	Antennas	46
4.2.1	Lens Antennas	47
4.2.2	Single-Reflector Antennas	50
4.2.3	Cassegrain (Double Reflector) Antennas	51
4.2.4	Polarization-Twisting Reflector Systems	52
4.3	Feeds	54
4.4	Devices for Forming Sums and Differences	57
4.4.1	Hybrid Junctions	57
4.4.2	Directional Couplers	60
4.4.3	Comparators	63
4.4.4	Other Methods of Obtaining Monopulse Sum (or Reference) and Differences	65
4.4.5	Graphical Symbols	66
4.5	Receivers	68
	References	69
Chapter 5	Amplitude-Comparison and Phase-Comparison Classification	71
5.1	Definitions and Examples	72
5.1.1	Definitions	72
5.1.2	Interpretation	72
5.1.3	Optimum Monopulse	74
5.1.4	Amplitude-Comparison Monopulse Antenna Example	78
5.1.5	Phase-Comparison Monopulse Antenna Example	80
5.2	Phase Fronts, Phase Centers, and Related Concepts	82
5.2.1	Transmitting Antennas	82
5.2.2	Receiving Antennas	85
5.2.3	Targets	85
5.2.4	An Example: Phase Fronts of a Two-Element Source	86
5.2.5	Simplification at Large Distances	87
5.2.6	Phase Centers of Array Antennas	90
5.2.7	Phase Centers of Reflector Antennas	93
5.3	Distinguishing Between Phase- and Amplitude- Comparison Monopulse	93
5.3.1	Reflector Antenna Examples	93
5.4	Distinction Based on Relative Phase of Illumination Functions	98
5.5	Distinction Based on Sum and Difference Patterns	99
5.6	Apparent Conversion of One Class to the Other	100

5.7	Summary of Amplitude-Comparison and Phase-Comparison Classification	102
	References	103
Chapter 6	Optimum Feeds for Space-Fed Amplitude-Comparison Monopulse Antennas	105
6.1	Nature of Optimization	105
6.2	f/D Ratio	107
6.3	Effect of Squint Angle in a Four-Horn Feed	108
6.4	Optimization of Squint Angle	111
6.5	Comparison with Measured Patterns	113
6.6	Beacon Operation	116
6.7	Comparison of Beam Squint Angle and Feed Offset Angle	116
6.8	Effect of Squint Angle on Normalized Difference Pattern	117
6.9	Other Feed Configurations	118
6.10	Summary of Feed Optimization	122
	References	123
Chapter 7	Monopulse in Array Antennas	125
7.1	Principles of Operation	125
7.2	Array Coordinates	128
7.3	Arrays with Space Feeds	128
7.4	Arrays with Constrained Feeds	132
	7.4.1 Constrained-Fed Arrays Divided into Quadrants or Subarrays	132
	7.4.2 Constrained-Fed Arrays with Independent Illuminations	134
	7.4.3 Efficient Illumination Tapers for Phased Arrays	136
7.5	Classification as Amplitude or Phase Comparison	138
7.6	Special Types of Arrays	141
	References	141
Chapter 8	Monopulse Processors	143
8.1	Functions and Properties of Monopulse Processors	144
8.2	Range Gating	146
8.3	Angular Coordinates for Monopulse Calibration	147
8.4	Exact Monopulse Processor	148
8.5	Processor Using Phases and Linear Amplitudes of s and d	150
8.6	Processor Using I and Q	152

8.7	Processor Using Phases and Logarithmic Amplitudes of s and d	153
8.8	Processor Using Dot-Product Detector with AGC	155
8.9	An Approximate Dot-Product Detector	158
8.10	Noncoherent Processor Using Sum and Difference of $ v_1 $ and $ v_2 $	162
8.11	Processor Using $s + d$ and $s - d$	165
8.12	Processor Using $\log v_1 $ and $ v_2 $	166
8.13	Processor Using $s \pm jd$	170
8.14	Two-Channel Monopulse Using $s + d$ and $s - d$	174
8.15	Phase-Amplitude Monopulse	177
8.16	Multiplexed Monopulse Receivers	178
8.17	Conopulse	181
8.18	Summary of Monopulse Processors	182
	References	185
Chapter 9	Response to Unresolved Targets	187
9.1	Review of Monopulse Response to a Point Target	190
9.2	The Meaning of Unresolved Targets	191
9.3	Superposition as an Approximation	191
9.4	The Two-Target Problem	193
9.5	The Complex Indicated Angle	195
9.6	Physical Interpretation	200
9.7	Measurement of the Imaginary Part (Quadrature- Phase) Component	201
9.8	Effect of Local-Oscillator Frequency	203
9.9	Detection of Presence of Unresolved Targets	203
9.10	Mean and Variance of Indicated Angle	204
9.11	Weighted Mean of Indicated Angle	207
9.12	Possibility of Determining Angles of Unresolved Targets	209
9.13	Information Derivable from Real Part	214
9.14	Removal of Initial Assumptions	216
9.15	Extensions of Monopulse Techniques and Fundamental Limitations	217
9.16	Closed-Loop Tracking	218
9.17	More Than Two Targets	219
9.18	Nonindependent Targets	221
	References	222
Chapter 10	Monopulse Angle Errors	225
10.1	Error Due to Noise	226
10.1.1	Analytical Model	227

10.1.2	Noise Statistics	227
10.1.3	Conversion of Voltages to Powers	229
10.1.4	Conversion of d/s Error to Angular Error	229
10.1.5	Bias in Monopulse Ratio	231
10.1.6	Exact Solution for Probability Density Function of d/s	233
10.1.7	First-Order Approximation for $S/N \gg 1$	235
10.1.8	Higher-Order Approximation for $S/N > 1$	238
10.1.9	Multiple-Pulse Estimates	241
10.1.10	Fluctuating Targets	242
10.1.11	“Inexact” Monopulse Processors	247
10.1.12	Closed-Loop Versus Open-Loop Operation	247
10.2	Errors Due to Clutter	247
10.2.1	Random Error from Clutter Distributed Across the Beam	248
10.2.2	Number of Independent Clutter Samples	249
10.2.3	Random Error from Clutter at a Specific Angle in the Beam	250
10.2.4	Bias Error Due to Clutter	252
10.3	Dynamic Lag Error	252
10.3.1	Tracking-Loop Error Coefficients	252
10.3.2	Pass-Course Problem	254
10.4	Radar-Dependent Errors	256
10.4.1	Monopulse Network Effects on the Boresight Axis	256
10.4.2	Boresight Axis Shift with Radar Frequency	259
10.4.3	Polarization Effects	261
10.5	Target-Dependent Noise Errors	263
10.5.1	Glint Error	263
10.5.2	Scintillation Error	266
	References	269
Chapter 11	Multipath	271
11.1	Flat-Earth Specular Model	272
11.2	Effect on Detection	276
11.3	Effect on Closed-Loop Elevation Tracking	277
11.4	Types of Multipath Remedies	280
11.5	Beam Pattern Design	281
11.6	Range and Doppler Resolution	282
11.7	Smoothing and Averaging	285
11.8	“Low-E” Modes	286
11.9	Offset-Null Tracking	288

11.10	Elevation Patterns Having a Symmetrical Ratio . . .	288
11.11	Double-Null Tracker	293
11.12	Use of the Complex Indicated Angle	294
11.13	Independent-Target Methods	301
11.14	Diffuse Multipath Effects on Monopulse	302
11.14.1	Power of Specular and Diffuse Multipath Reflections	303
11.14.2	Distribution of Multipath in Elevation Angle	305
11.14.3	Multipath Error for Closed-Loop Tracking	305
11.14.4	Effect of Range or Doppler Resolution and Smoothing	307
11.14.5	Low-E Mode	308
11.14.6	Offset-Null Tracking	308
11.14.7	Diffuse Multipath in Patterns Having a Symmetrical Ratio	308
11.14.8	Complex Indicated Angle with Diffuse Multipath	309
11.14.9	Diffuse Multipath Effect on Independent-Target Methods	311
11.14.10	Summary of Multipath Mitigation Methods	312
	References	313
Chapter 12	Monopulse Countermeasures and Countercountermeasures . .	317
12.1	Range and Doppler Denial and Deception	318
12.1.1	Range and Doppler Denial	318
12.1.2	Range and Doppler Deception	319
12.1.3	Chaff Deception	320
12.2	Generic Monopulse ECM	321
12.2.1	Formation Jamming	321
12.2.2	ECCM Against Formation Jamming	323
12.2.3	Cross-Eye Jamming	323
12.2.4	Surface-Bounce Jamming	326
12.2.5	Bistatic Jamming	328
12.3	Exploitation of Radar Faults	329
12.3.1	Cross-Polarized Jamming	330
12.3.2	Exploiting Phase and Gain Imbalance	332
12.3.3	Exploiting AGC Response	333
12.3.4	Exploiting Image Response	334
12.3.5	Two-Frequency Jamming	335
12.3.6	Jamming at the Commutation Frequency	336
	References	336

Chapter 13	Tracking Radar Applications of Monopulse	337
13.1	Surface-Based Monopulse Tracking Radars	337
13.1.1	AN/FPS-49 and TRADEX Radars	337
13.1.2	Patriot AN/MPQ-53 Multifunction Radar	339
13.1.3	Russian Surface-to-Air Missile (SAM) Guidance Radars	340
13.1.4	Aegis AN/SPY-1 Radar	342
13.2	Airborne Monopulse Tracking Radars	344
13.2.1	Multimode Fighter Radars	344
13.2.2	Electronically Scanned Fighter Radars	344
13.3	Monopulse Homing Seekers	346
13.3.1	Semiactive Homing	346
13.3.2	Active Homing	347
	References	349
Chapter 14	Nontracking Radar Applications of Monopulse	351
14.1	Monopulse 3-D Surveillance Radars	351
14.1.1	Scanning-Beam 3-D Radars: AN/TPS-59 and AN/FPS-117 Examples	352
14.1.2	Stacked-Beam 3-D Radars: Martello S-723 Example	354
14.2	Monopulse Secondary Surveillance Radars	355
14.3	Other Radar Applications	357
14.3.1	Terrain-Avoidance Radar	357
14.3.2	Aircraft Low Approach Radar	358
14.3.3	Target Recognition	358
14.3.4	Displaced Phase Center Antenna Applications	359
	References	359
Chapter 15	Special Topics	361
15.1	Difference and Sum Patterns Having a Ratio Proportional to Angle	361
15.1.1	General Properties	361
15.1.2	Applications and Implementation	362
15.1.3	Derivation of Equations	363
15.1.4	Characteristics of the Patterns and Illumination Functions	364
15.1.5	Computation of Patterns at Indeterminate Points	366
15.1.6	Other Pattern Pairs Having a Constant Monopulse Slope	367

15.1.7	Extension to Electronically Steerable Arrays	370
15.2	The Diagonal Difference Signal	371
15.3	Units of Angle and Sine Space	374
15.4	Comparison with Rhodes' Terminology and Classification	376
	References	378
	List of Symbols	381
	About the Authors	389
	Index	391

Preface to the Second Edition

The favorable reception of the first edition of *Monopulse Principles and Techniques* in 1984 confirmed the need for a book of that type. However, much work has been done and much has been learned since 1984 and much of the accumulated knowledge has not been available in an organized and readily accessible form. When the publisher requested a new edition, the author agreed provided that he could be joined by his former colleague David K. Barton.

The two of us have now pooled our experience and our efforts in the preparation of this new edition. In short, our aim has been to produce a book that would have been very valuable to us when we were learning and working in this field. We hope that others will also find it helpful.

The theoretical treatment from the first edition remains, since the fundamentals of monopulse had been well developed at the time that edition was published. Material has been added in Chapter 5 to relate monopulse performance measures to the optimum monopulse described in George Kirkpatrick's pioneering work, and to apply those measures to both reflector and array antenna systems. The same measures are also invoked in Chapter 6, on optimum feeds for space-fed amplitude-comparison monopulse antennas. New material has been added to Chapter 7 on monopulse in array antennas.

The treatment of monopulse angle errors in Chapter 10 retains the analysis of first- and second-order effects of noise, and this is now applied further to clutter errors. Discussions of the many other sources of monopulse angle errors have been added. In Chapter 11, the effects of diffuse components of multipath are considered, along with the specular component. Chapter 12 on monopulse countermeasures and countercountermeasures is new, as are Chapters 13 and 14 on applications of monopulse to tracking and nontracking radars.

Preface to the First Edition

Monopulse, also known as simultaneous lobe comparison, is a method of determining the angular location of a source of radiation or of a “target” that radiates part of the energy incident upon it. Monopulse is used in certain types of radars, and the same or analogous techniques (not limited to pulsed operation or to electromagnetic radiation) are also applied in fields such as direction-finding, communications, missile guidance, and sonar. The principles presented in this book are valid for any use of monopulse but the examples, photographs, and descriptions of equipment are drawn from monopulse radar, which since its conception and early development in the 1940s and 1950s has become a highly successful type of instrument, widely used for precise angle measurement and tracking.

The proliferation of new applications and designs has led to a wide diversity of forms of monopulse, all based on the fundamental principle of comparison of signals received simultaneously by different antenna patterns (or patterns of other types of transducers). The basic concept is simple, but there are many theoretical and practical considerations that must be understood in order to achieve the full capability of monopulse, as well as to recognize the limits of that capability. The theory has a fascination of its own which has attracted the efforts of a number of investigators. The results of some of their studies have helped to guide the application of advanced technology to produce the high level of performance available today. Further improvements and new applications can be expected in the future.

In this book I have tried to present a balanced combination of theory and up-to-date practice and application. The style is tutorial. The book explains the principles of monopulse, categorizes and describes its various forms, and analyzes their capabilities and limitations. Although not intended to be a design manual, it devotes considerable space to monopulse circuits, components, and design features, especially those that distinguish monopulse from other techniques for angle measurement and tracking, or one form of monopulse from another. In the ana-

lytical portions the emphasis is on the relation of theory to physical concepts and applications rather than on theory alone. I have tried to avoid unnecessary complication in the mathematics without sacrificing rigor. The explanations, proofs, and derivations include all the essential steps; but those who wish to bypass the details can extract needed facts, formulas, descriptions, and diagrams.

I have devoted considerable space to definitions and to explanations of terminology and notation because some of the mystery of a specialized subject often lies in unfamiliar terms and symbols as well as in the subject matter itself. The discussions on these subjects will also aid in “translating”—and I hope standardizing—the nonuniform, loose, and even erroneous monopulse terminology sometimes encountered. A complete list of symbols I have used is provided.

My intent is to serve a broad spectrum of users, from senior or graduate students to experienced engineers, scientists, analysts, and managers, preferably with some basic knowledge of radar, communications, or a related field. Experienced designers who are already familiar with monopulse components and circuits can benefit from a better understanding of monopulse theory. On the other hand, system analysts can improve the relevance and validity of their theoretical models by learning about the physical processes and devices that the models are supposed to represent. Engineering managers can enlarge their knowledge of monopulse in order to communicate with the specialists in their organizations.

Because monopulse literature is scattered in numerous papers and reports, many of which deal only with narrow, specialized topics, and some of which are not readily available, I believe this book will fill the need for a unified treatment of monopulse. There are excellent books on radar in general, but they devote relatively little space to monopulse. Books devoted exclusively to monopulse are very few. *Introduction to Monopulse*, by Donald R. Rhodes, originally published by McGraw-Hill Book Co. in 1959 (reprinted by Artech House), was and still is an important contribution to the radar literature, but it covers only a restricted scope, mainly from a theoretical viewpoint, and of course it does not reflect developments since 1959. Another book, *Monopulse Radar*, compiled and edited by David K. Barton and published by Artech House in 1974, is a collection of reprints of selected papers by various authors, with supplementary comments by Barton on the significance and highlights of the different papers. Some of the papers are classics in the field of monopulse, including two that had not previously appeared in open literature because they were originally classified. The book is highly useful as a reference source but it is not intended as a unified treatment of the entire subject of monopulse. There is also a Russian book by A. I. Leonov and K. L. Fomichev which has been translated into English (by edited machine translation) under the title *Monopulse Radar*. It is available in photocopy form (identified by the number AD 742 696) from National Technical Information Service, Springfield, Virginia. It contains a large amount of useful information, drawn largely from U.S. sources (including descriptions of several U.S. monopulse radars). The figures and equations are reproduced “as is” from the Russian originals,

with English translations of figure labels added. Unfortunately, the translation is not always clear, and the poor quality of the reproduction makes many of the equations difficult to read and some of the figures unrecognizable. Furthermore, there is no index.

In gathering material I have drawn on many sources, but the organization and method of presentation are my own. I have added original material and many new or revised illustrations and plots. The largest amount of space is devoted to topics that I believe will be useful to most readers, or which are not adequately or clearly treated (or are not treated at all) elsewhere in the technical literature. For some of the specialized or peripheral topics that are covered well in other readily available sources, brief summaries are given and readers are referred to those sources for more detailed information.

My interest in monopulse was acquired and nurtured during my many years as a manager and staff scientist in the Missile and Surface Radar organization of the RCA Government Systems Division. There, I was fortunate in being associated with experts in the theory, design, operation, and testing of various types of radars, many of which included monopulse. Dr. Josh T. Nessmith, formerly Manager of Systems Engineering in that organization, suggested that some of my papers, reports, and internal memoranda might be expanded into a book. He provided encouragement and administrative support, and our technical discussions helped to clarify some difficult points. I am grateful to Bernard J. Matulis, Chief Engineer of Missile and Surface Radar, for the personal interest that he took in this project and for the support services and facilities that he made available. Many other colleagues at RCA have shared their knowledge and experience with me and have given constructive suggestions and criticisms on portions of the manuscript. I have also had helpful discussions with Dean D. Howard, of the U.S. Naval Research Laboratory, Warren D. White, formerly of AIL (a division of Cutler-Hammer), and David K. Barton, of the Raytheon Company.

Samuel M. Sherman
1984

Chapter 1

Introduction

Monopulse, also known as simultaneous lobe comparison, is a technique for measuring the direction of arrival of radiation. The radiation may emanate from an active source such as a distant transmitting antenna, a beacon, a jammer, an astronomical body, or from a passive source—that is, a target or scatterer that reradiates some of the power incident on it. Monopulse has many actual and potential applications not limited to electromagnetic radiation, but it has reached a particularly high state of development in certain types of radar. This book therefore deals specifically with monopulse as used in radar, but much of the material applies as well to other uses, some of which will be pointed out.

1.1 REVIEW OF RADAR PRINCIPLES

A very brief summary of radar principles will be given as a framework within which to introduce the elementary concepts of monopulse. The treatment of the advanced aspects of monopulse in later chapters will presuppose a more extensive general knowledge of radar than can be provided here. The reader is presumed to have such knowledge already, or to be pursuing it concurrently. It can be obtained from any one of a number of books, not to mention a wealth of technical literature in journals. Recent books covering radar from a broad viewpoint include those by Skolnik [1], Barton [2], Peebles [3], Eaves and Reedy [4], and Richards [5]. The handbook edited by Skolnik [6] contains a vast store of information on a wide range of radar topics, better suited for reference than for a tutorial exposition. These books devote only a small fraction of their total pages specifically to monopulse.

The basic functions of radar are to detect the presence of electromagnetic scatterers (radar *targets*) in the antenna beam and to determine their positions. In a

typical radar the transmitter generates pulses of electromagnetic radiation, usually at a regular rate called the *pulse repetition frequency*. The antenna radiates the transmitter output into space, typically in a directional pattern that concentrates most of the power into a major lobe or beam which is narrow in one angular dimension (*fan beam*) or in both angular dimensions (*pencil beam*). The same antenna, in most cases, is also used for reception, but not necessarily with the same pattern. The received signals are converted from radio frequency (RF) to intermediate frequency (IF), amplified and filtered by one or more receivers, and then processed for visual display or for automatic (usually digital) detection and extraction of information.

If there is a target in the beam, the radar receives an echo from it following each transmitted pulse. The target *range* or distance is readily determined by multiplying half the time delay between the transmitted and received pulses by the speed of light.

A crude way of determining angular position of a target is to move the antenna beam past the target direction and note the pointing direction that gives the maximum echo amplitude. This method, in effect, is used in many search radars where measurement precision on the order of tenths of the beamwidth is acceptable, but it is not adequate in applications requiring much finer precision. Furthermore, it is not suitable for closed-loop angle tracking because as the beam axis deviates from the target, the echo amplitude decreases regardless of the direction of deviation; thus, there is no directional or sense information to tell the servo which way to drive the antenna to bring it back to the target. Even if sense information is provided, the sensitivity is very poor, since the slope of the response curve is zero at the maximum.

The need for continuous, accurate angle and range measurements on a designated target led to the development of tracking radars, starting with the relatively crude tracking radars of World War II and culminating in the sophisticated precision instruments of today. The most important single improvement in angle tracking was the introduction of monopulse, which is now used also for nontracking angle measurements.

1.2 TRACKING RADARS AND THE EVOLUTION OF MONOPULSE

A *tracking radar* is a radar that automatically keeps the antenna beam axis aligned with a selected target. Such a radar usually has a highly directional antenna pattern (i.e., a narrow beam). The beamwidth is typically of the order of 1° in each angular coordinate, but it varies considerably from one radar to another, and in any one radar it need not be the same in both coordinates.

Any deviation of the target from the beam axis produces a *correction signal* (usually called an “error” signal) for each coordinate, approximately proportional to the angular deviation in that coordinate, with a sign or polarity that indicates the

sense of the deviation (up or down, left or right). The correction signal is used to drive the axis toward the target.

A tracking radar also tracks the target in range, by keeping a range (time) gate centered on the target. Only signals received during the gate are accepted for tracking. The time interval between centers of the transmitted pulse and range gate provides the range measurement. Deviation of the target echo pulse from the center of the range gate produces a correction signal, which tends to keep the range gate centered on the target. In some radars, the Doppler-shifted frequency of the target is also tracked by sensing the difference between that frequency and that of a tunable narrowband filter, and deriving a Doppler correction signal that tends to keep the filter band centered on the target frequency.

This book discusses angle tracking, or more generally, angle measurement, which can be accomplished with an accuracy of a small fraction of a beamwidth.

The earliest application of tracking radars was to provide range and pointing direction for artillery. This background is reflected in some of the terminology of tracking radars, such as *track*, *target*, *boresight*, and *range* (meaning distance to the target). Present-day tracking radars are used in many applications besides direct fire-control support. Examples will be given later in this section.

Early in the history of radar, an angle-tracking technique called *lobe switching* came into use. In this technique the radar beam or lobe, instead of pointing directly at the target, points slightly to one side and then to the other, alternating rapidly. Figure 1.1 illustrates lobe switching in elevation; in traverse¹ it would be

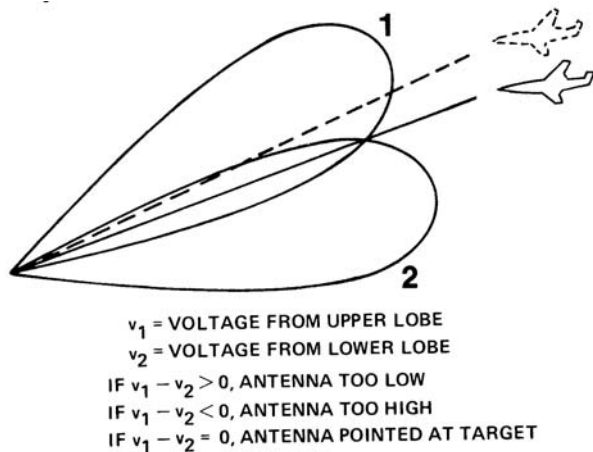


Figure 1.1 Sequential lobing in elevation.

¹ Traverse angle is measured in the slant plane containing the target. This is to be distinguished from azimuth, which is measured in a horizontal plane. See Section 2.8 for a fuller discussion.

similar. If the target is above or below the axis, the echoes are unequal. Suppose the target is above the crossover axis, as shown by the dotted line. Then the echo from lobe 1 is greater than from lobe 2. The voltage difference $v_1 - v_2$ in this case is positive, which means that to center the target on the crossover axis, the antenna must point higher. The two signals can be displayed visually, side by side, to enable an operator to make the necessary correction, or their difference can be used in a servo loop to position the antenna automatically.

The same operation can be interleaved in both angular coordinates. Sequential lobing in elevation and traverse can be combined, permitting complete angle tracking, requiring four successive beam positions, as shown in Figure 1.2(a). The beam can be moved electronically or by mechanically rotating or nutating the feed around the axis. If it is done mechanically, then instead of moving the beam in four discrete steps, it is preferable to move it continuously in a circular path centered around the crossover axis, resulting in *conical scan*. Lobe switching and conical scan are both included in one general term—*sequential lobing*. Although the beam motion is continuous in conical scan, the target is illuminated only when each transmitted pulse reaches it, as illustrated in Figure 1.2(b). If the scanning rate is 30 cycles per second (a typical value), and the pulse repetition rate has an illustrative value of 240 pulses per second, there are eight beam positions per scan. When the target is anywhere but on the crossover axis, the echo strength, modulated approximately sinusoidally at the scanning frequency, is greatest when the beam axis is closest to the target direction. Demodulation of the received signal yields the modulation envelope, which, when normalized and compared to a reference sinusoid at the scanning frequency in a pair of phase-sensitive detectors, yields correction signals indicating the two orthogonal components of axis deviation from the target. The conical-scan type of tracking radar gave successful service long after World War II for applications where the utmost precision was not needed.

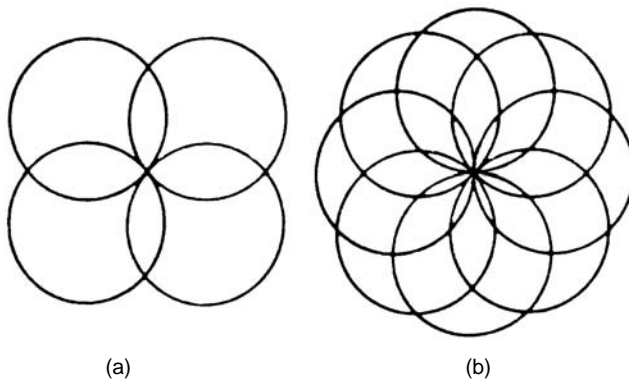


Figure 1.2 Two types of sequential lobing: (a) lobe switching in traverse and elevation; and (b) conical scan.

A principal source of error in sequential lobing is the fluctuation that occurs in the echo strength of most targets. This fluctuation often has considerable power spectral density in the vicinity of the lobing or scanning frequency, and therefore causes erroneous angle indications. In simple language, the radar cannot distinguish between pulse-to-pulse variations in echo amplitude due to target displacement from the antenna axis and those due to target fluctuations.

Another disadvantage of sequential lobing is the limitation on the data rate imposed by the necessity of obtaining at least four successive echo pulses for each pair of angle estimates. This can be a serious limitation in the tracking of targets that have large angular accelerations, whether actual or apparent (i.e., geometrically induced). In the case of conical scan there is the further disadvantage that the mechanical vibration makes it hard to maintain accurate boresight alignment.

The solution that overcomes or alleviates these problems is *monopulse*, also called *simultaneous lobing* or *simultaneous lobe comparison*.

One category of monopulse, called *amplitude-comparison* monopulse, is similar in concept to lobe switching, but instead of comparing the target echoes obtained in four sequential beam positions (up-down, left-right), it forms the four receiving beams simultaneously and makes the comparisons on each pulse. (If monopulse is used in only one angular coordinate, only two simultaneous receiving beams are needed.) A single transmitting beam suffices, being just wide enough to encompass the receiving beams. Another category is *phase-comparison* monopulse. This operates a little differently, but the common feature of all monopulse is the use of simultaneous receiving beams. Since angle information is available from every received pulse instead of requiring a cycle of successive beam positions, monopulse can provide a higher data rate than sequential lobing.

Ideally, monopulse radars are free of errors due to pulse-to-pulse fluctuations in target echo strength, because the fluctuations have no effect on the ratios of signals received simultaneously from different lobes on each pulse. In practice, because of design and cost constraints, these errors are not always entirely eliminated, but they are at least greatly reduced.

The advantages of monopulse over the other angle tracking techniques are obtained at the price of greater equipment complexity and cost. For example, monopulse requires multiple receivers, while the other techniques need only one. The receivers must be carefully designed and matched so that they track one another in gain and phase (see Section 1.3). For some applications the simpler systems are quite adequate.

The practical development and use of monopulse radar received great impetus after World War II, but the concept originated and the early development occurred well before that (although not under that name). Brief historical summaries are given by Rhodes [7] and Barton [8], and further details can be found in references that they cite. The earliest unclassified paper on monopulse appears to be a brief one (actually only an abstract) by Page [9], who was active in its early develop-

ment. That paper was based on a 1944 U.S. Naval Research Laboratory report by Page, classified at the time but later declassified and reprinted in [8].

Most tracking radars in use today are of the monopulse type. Throughout the world thousands of monopulse radars have been built and installed on land, at sea, on aircraft and guided missiles, and in space. They perform a large variety of functions, of which some major categories can be listed as:

1. Tactical control of gunfire and of missile launching and guidance.
2. Strategic military applications such as tracking of potentially hostile aircraft or missiles at long range.
3. Space applications, including tracking of space vehicles, satellites, and other space objects, both U.S. and foreign.
4. Intelligence applications, including analysis not only of trajectories but also of echo variations as the target moves, from which certain information about target size, shape, rotation, and other characteristics can be deduced. This would be difficult or impossible with sequential lobing because of the modulation that those techniques superimpose.
5. Support applications for both military and space purposes, including monitoring and evaluation of exercises at test ranges, and tracking space vehicles during launch to determine what orbit or trajectory corrections are needed, if any, or to give the signal for destruction if the path is faulty beyond correction. Tracking radars designed for such support applications are called *instrumentation radars*, and these are among the most precise radars in existence [10–12]. Accuracies in the order of $1/200$ of a beamwidth (a “beam-splitting” ratio of 200:1) are attainable.

Although the original and most common mode of operation of monopulse is tracking in the strict sense of keeping the beam axis pointed at the target, this is not the only mode. In some radars, off-axis measurements are used; the beam axis may be as much as a half-beamwidth removed from the target direction. Monopulse can also be used in one or both coordinates in a search radar or the search mode of a multifunction radar. In these cases the open-loop monopulse output signal indicates (by way of a calibration function) the target angle in one or both coordinates relative to the known direction of the beam axis at each instant, and thus the absolute target angles are determined.

1.3 A “BASELINE” MONOPULSE RADAR

Before entering into the more detailed aspects of monopulse, an example of monopulse radar configuration is presented. Although this example represents only one of the various forms of monopulse, and is idealized and simplified besides, it

illustrates the basic principles and serves as a “baseline” reference for some of the material in later chapters. This particular type of radar belongs to the general category known as *amplitude-comparison* monopulse, which was introduced in Section 1.2 and will be examined in more detail later. Another category, known as *phase-comparison* monopulse, will also be examined later.

The radar that will serve as the model has a paraboloidal-reflector antenna² fed by a cluster of four feed horns in the focal plane, symmetrically offset about the axis, as shown in Figure 1.3. The two feed horns that are visible in Figure 1.3(a) are displaced from the axis toward the viewer and the other two are displaced in the opposite direction. When viewed axially from the center of the reflector, the horns appear as in Figure 1.3(b). (Although drawn as squares, the horns are rectangular in many cases.) The four feed horns produce four squinted beams, as shown in Figure 1.4.³ Note that the upper horns produce the lower beams. The beams are such that if their outputs were connected to four separate, identical receivers, their responses to an incident plane wave (i.e., to the radiation

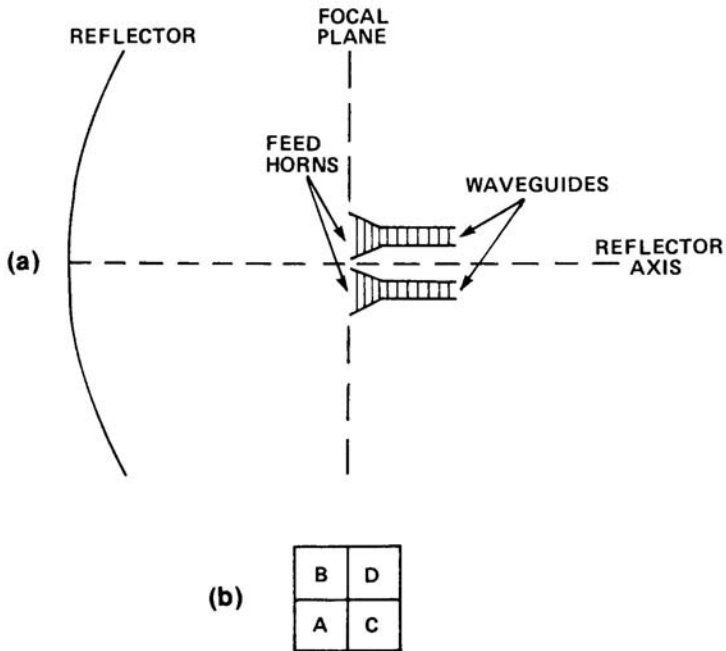


Figure 1.3 Reflector and feed horns: (a) side view; and (b) axial view of feed horns from reflector.

² Also called a parabolic-reflector antenna, since any section parallel to the axis is a parabola.

³ The sidelobes are omitted from the figure.

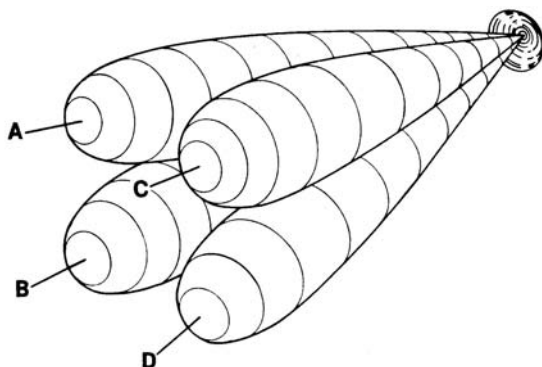


Figure 1.4 Four squinted beams in amplitude-comparison monopulse.

from a distant source or scatterer) would all be in the same phase but would generally differ in amplitude in accordance with the beam patterns and the direction of arrival of the wave. The common crossover point is on the paraboloid axis. Only a target on the axis of symmetry of the antenna assembly gives equal amplitudes in the four beams. From the ratios of the amplitudes, the two angular components of the source direction relative to the axis can be determined. Three beams, yielding two independent ratios, would suffice to determine the two angular components of a single target. Four beams are generally used because of the practical advantages of symmetrical design.

The four beams are shown in cross section in Figure 1.5. Let *A*, *B*, *C*, and *D* represent the corresponding received voltages. In theory, the outputs of the four horns could be connected to four identical receivers, the outputs of which could then be compared. In practice, the four receivers, even if adjusted initially for equal gain and phase, would vary unequally as a function of time, signal level, radio frequency, and environmental conditions. The result, as was learned in some

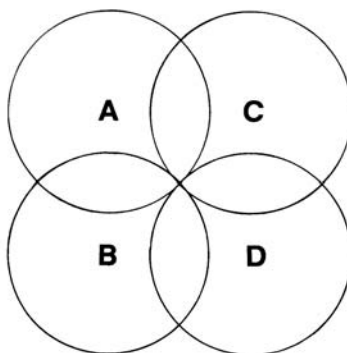


Figure 1.5 Cross section of amplitude-comparison monopulse beams.

of the early monopulse development, would be large drifts in the electrical axis (boresight direction) and in the measurement of off-axis target angles.

The usual method, therefore, is to form the sum, an elevation difference, and a traverse difference of the horn outputs at RF, prior to the receivers, by means of RF combining devices known as hybrid junctions (described in Chapter 4). Being electrically and mechanically compact and rigid, these devices have much less drift than the active circuits of receivers; therefore the null axis is more stable. The sum and the differences are:

$$\text{Sum} \quad s = \frac{1}{2}(A + B + C + D) \quad (1.1)$$

$$\text{Traverse difference} \quad d_{tr} = \frac{1}{2}[(C + D) - (A + B)] \quad (1.2)$$

$$\text{Elevation difference} \quad d_{el} = \frac{1}{2}[(A + C) - (B + D)] \quad (1.3)$$

The factor 1/2 in these equations is due to the equality of total input power and total output power, assuming lossless combiners (see Section 2.4).

The shapes of the sum and difference voltage patterns are shown in Figure 1.6 for either traverse or elevation. Also shown are the voltage patterns v_1 and v_2 of the pairs of squinted beams from which the sum and difference are formed:

$$\begin{aligned} \text{For traverse:} \quad v_1 &= (C + D)/\sqrt{2} \\ v_2 &= (A + B)/\sqrt{2} \end{aligned} \quad (1.4)$$

$$\begin{aligned} \text{For elevation:} \quad v_1 &= (A + C)/\sqrt{2} \\ v_2 &= (B + D)/\sqrt{2} \end{aligned} \quad (1.5)$$

The sum and difference (in each coordinate) are related to v_1 and v_2 by the equations

$$\begin{aligned} s &= (v_1 + v_2)/\sqrt{2} \\ d &= (v_1 - v_2)/\sqrt{2} \end{aligned} \quad (1.6)$$

yielding the result shown in (1.1) to (1.3). All the patterns are one-way. Also plotted in Figure 1.6 is the ratio of the difference to the sum, d/s .

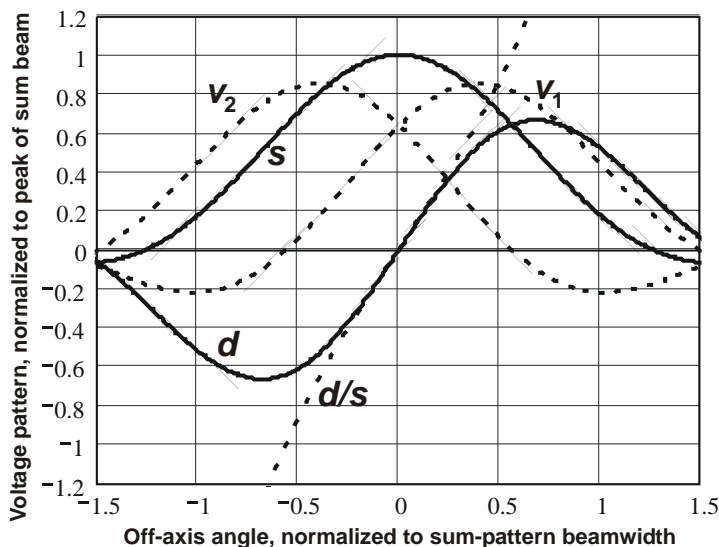


Figure 1.6 Amplitude-comparison monopulse patterns in either coordinate: sum (s), difference (d), squinted beams (v_1 and v_2), normalized difference (d/s).

The direction in space in which the traverse and elevation difference patterns both have their nulls is called the *monopulse axis*, the *boresight axis*, the *tracking axis*, or the *electrical axis*. Ideally it coincides with the geometric or mechanical axis of the reflector, but in practice there is usually some deviation. To determine the monopulse axis as the reference for angular readings, it is necessary to *bore-sight* or *collimate* the antenna. This process consists essentially of pointing the antenna so as to obtain a null on a test target at a known direction, then adjusting the angle readouts to the correct values in that direction. When the word “axis” is used alone in a monopulse context, it is understood to mean the electrical rather than the mechanical axis.

The sum pattern is a pencil beam with its peak on the monopulse axis. (In practice the directions of the sum peak and the difference null may differ slightly because of imperfect symmetry.) Unless otherwise specified, the beamwidth of a monopulse antenna is customarily defined as the one-way half-power beamwidth of the sum pattern—that is, the angular interval between the points where the sum voltage is $1/\sqrt{2}$ times its peak value. The horizontal scale of Figure 1.6 is normalized to that beamwidth. The half-power width of the sum beam is somewhat greater than that of each squinted beam.

Figure 1.7 is a functional diagram that includes, in simplified form, the processing steps described so far and those that follow.

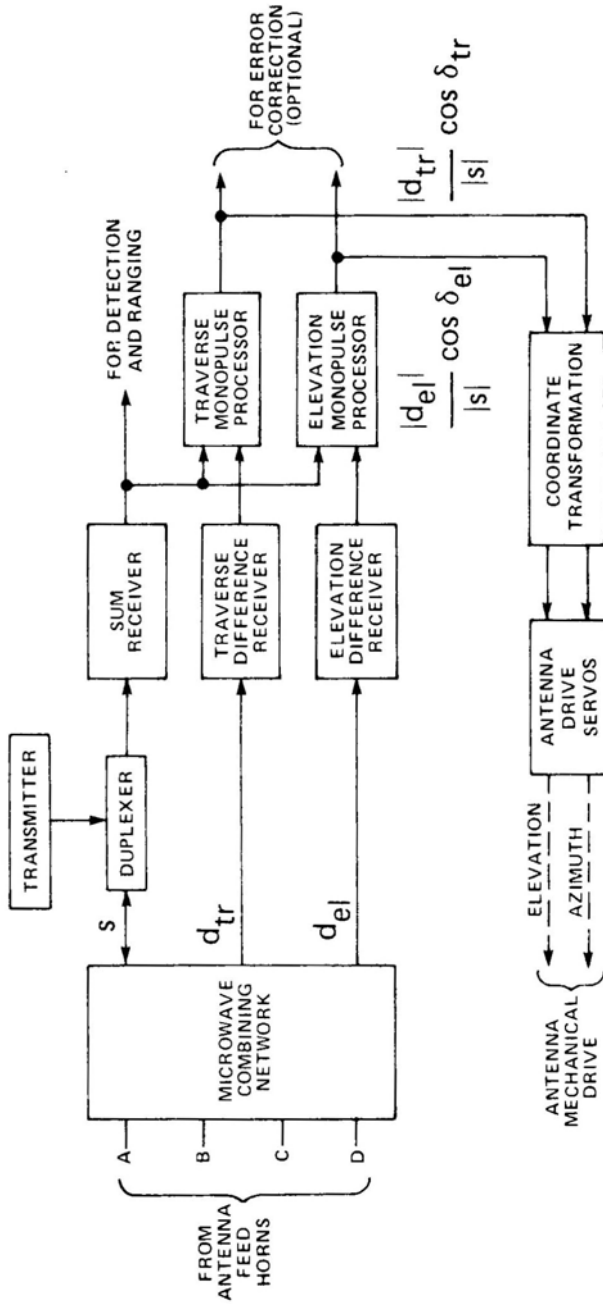


Figure 1.7 Functional diagram of one form of monopulse radar.

The same channel that forms the sum pattern for reception is also used in the reverse direction for transmission. (The duplexer permits two-way operation.) Thus, the transmitting pattern is the same as the sum pattern in Figure 1.6. In reception the sum signal is used for detection, ranging, and displays, in addition to the monopulse function.

In the receivers for the sum and difference channels the radio frequency (RF) voltages from the microwave combining network are converted to intermediate frequency (IF) by mixing with the output of a local oscillator, then amplified and filtered at IF. The filter bandwidth is approximately the reciprocal of the radar pulse width.

For each coordinate there is a monopulse processor. This processor can take any one of several forms, some of which will be described in Chapter 8. A common feature of all monopulse processors is that they respond to voltage *ratios* or phase *differences* or both, not to absolute voltages or phases.

In our baseline radar the two inputs to each processor are the sum signal and the difference signal for one coordinate. The output is the ratio of difference voltage amplitude to the sum voltage amplitude, multiplied by the cosine of the relative phase angle between the two voltages. The relative phase is denoted by δ_{tr} in traverse and δ_{el} in elevation. In our idealized baseline model, the sum signal and the difference signals from a single point target always have 0° or 180° relative phase, because they are derived from four individual beams whose outputs are assumed to have exactly the same phase. Therefore, the cosine is $+1$ if the target is on one side of the axis and -1 if it is on the other side. We will find in later chapters, however, that under practical conditions the cosine is not necessarily confined to ± 1 .

The amplitude ratio indicates how far the target is off the axis and the cosine factor provides the sense (left or right of the axis, above or below the axis). The cosine factor also serves to reject the quadrature-phase component of noise and thus it reduces errors caused by noise.

The output in each coordinate, consisting of the voltage amplitude ratio multiplied by the cosine of the relative phase is often called the “error” signal in that coordinate but we will avoid this name because, as explained in Section 2.5, an “error” signal is not necessarily associated with an error in determining target angle. A more descriptive name is the *normalized difference signal*, or more specifically, the in-phase component of the normalized difference signal, because it is also possible to measure the quadrature-phase component by replacing the cosine by the sine. In our baseline radar model, the quadrature component is zero (except for noise contributions) in response to a point target, and so nothing would be gained by measuring it. In other cases, however, it is nonzero and may contain useful information, as we will see in later chapters.

A more general term for the output is simply the *monopulse processor output*, which includes not only the type of output produced by the baseline radar but also the outputs of other types of monopulse processors, to be described later.

The antenna patterns are so designed that the normalized difference signal d/s in either coordinate, in response to a single point target, is: (1) nearly proportional to the target angle off axis in that coordinate out to about one-half beamwidth on either side, as can be seen in Figure 1.6, and (2) nearly independent of the target angle in the other coordinate. The normalization makes the output independent of echo strength and dependent only on target angle. The echo strength has the effect of a common multiplying factor on the sum and difference signals and therefore “cancels out.”

Our baseline model is a mechanically steered tracking radar. The monopulse processor outputs, after coordinate transformation, become inputs to the servo-amplifier channels, and the servos turn the antenna in the proper direction until a null in the monopulse processor output is reached. The reason for the coordinate transformation is that the mechanical rotation coordinates of the antenna mount are usually azimuth and elevation while the difference signals are functions of target traverse and elevation relative to the antenna axis. A simple approximate transformation usually suffices. This consists of multiplying the traverse monopulse output by the secant of the antenna elevation angle to drive the azimuth servo, and using the elevation monopulse output without transformation to drive the elevation servo.

Ideally the antenna axis would follow the target direction exactly. In practice there are deviations. While the servo does the best it can to keep the tracking axis on a moving target, it will lag by some amount. The lag may be caused by target angular rates or accelerations exceeding the maximum capabilities of the servo, or by higher-order derivatives of target angular motion. Wind forces may also cause the antenna axis to deviate from the target. In either case—lag or wind forces—there is a residual voltage at the monopulse processor output that the servo cannot null out. The resulting error can be largely removed by an optional feature called *error correction* or *electrical correction signal*. The residual monopulse output that the servo is unable to null out is measured and converted to the corresponding off-axis angle by a known calibration function. The off-axis angle, added to the pedestal shaft rotation angle either in real time or in postmission analysis, gives a corrected value of the target angle.

1.4 ADVANTAGES AND DISADVANTAGES OF MONOPULSE

Advantages of monopulse over sequential lobing, some of which have already been mentioned, are summarized here. More detailed comparisons, including analysis of sequential lobing in greater depth than can be given here, are available elsewhere [13–18].

1. Errors due to amplitude fluctuations of target echoes are eliminated or greatly reduced in monopulse.
2. In a monopulse radar, angle information is derivable from each pulse rather than requiring a complete cycle of pulses or a complete scan. The full capability of single-pulse measurement is not generally utilized in continuous tracking of a single target, since the signals are usually integrated (or measurements are smoothed) over several pulses. Nevertheless, that capability increases the available data rate and permits the use of a higher bandwidth when needed to reduce lag error or loss of track on an accelerating target. The single-pulse capability is highly important in some surveillance radars and in multifunction radars with electronically steered antennas, which perform interleaved tracks on several targets by switching the beam direction rapidly from one to another. Each dwell on each target may allow time for only a few pulses or even a single pulse, and a measurement on each pulse may be required.
3. Since the sum beam, both in transmission and reception, is pointed at the target rather than to one side or the other, the signal-to-noise ratio is higher in monopulse, assuming that the other radar parameters are the same. This results in better detection capability (required before track can be initiated) and less tracking error (by a factor of roughly two) due to thermal noise.
4. Monopulse radar is free of the mechanical vibration and wear and tear of the rotating feed or reflector needed to produce conical scan, and therefore has better stability of the boresight axis.
5. Transmission from a sequential-lobing radar reveals the presence and periodicity of the switching or scanning⁴ and makes the radar vulnerable to certain countermeasures that take advantage of that information. Monopulse transmission is unmodulated.
6. In certain applications, information about the nature and orientation of a target that is being tracked is derived from analysis of pulse-by-pulse amplitude fluctuations of the echo. This is difficult or impossible in sequential lobing because of the modulation imposed by the lobe switching or scanning. In a monopulse radar the received sum signal can be used for this purpose, since it is unmodulated.
7. The tracking range in conical scan is limited by the scan rate. This is because the beam direction must not be allowed to move too much between transmission and reception. Monopulse is free of this restriction; the maximum unambiguous range is limited only by the pulse repetition frequency.

⁴ There are, however, special techniques of using switching or scanning in reception only, leaving the transmission unmodulated.

The principal disadvantage of monopulse is that, in order to realize its inherent superior capability, it needs more equipment and more painstaking design and adjustment of components. It is therefore more expensive.

Conventional monopulse requires three receiver channels for two-coordinate angle tracking, compared with one receiver channel for sequential lobing; the three channels must “track” one another in gain and phase over a wide range of conditions. Special monopulse configurations have been devised which use fewer than three channels (see Sections 8.14–8.17) but either they cause some sacrifice in performance or they pose difficult design problems.

The RF circuitry is more complex in monopulse, since the sum signal and the two difference signals (or signals from the individual feed horns) must be brought down from the antenna. The RF channels must be kept balanced to prevent errors.

There are additional factors which, although not directly attributable to the use of monopulse techniques, increase the cost of a monopulse system. For example, a pedestal and drive system that is adequate for a conical scan radar (because its error contributions and dynamic limitations are masked by those of the conical-scan process itself) may have to be replaced by a higher-performance, more costly pedestal and drive in order not to limit the accuracy and dynamic performance achievable with a monopulse radar.

Ordinary monopulse (such as the baseline system described in the preceding section) has smaller advantages over other tracking techniques when the radar resolution cell contains multiple targets, multiple reflection points on one target, or a target and multipath, since these conditions distort the arriving wave front and affect all tracking systems. However, monopulse in a broader sense (meaning the use of simultaneous receiving patterns not confined to those in the baseline system) makes possible special techniques that can be used in some cases to reduce those errors.

1.5 NONRADAR USES OF MONOPULSE

Although the emphasis in this book is on monopulse as used in radar, the same or analogous techniques are used for other purposes as well. Other radio-frequency applications include passive direction-finding [19, 20], communications (for example, keeping an Earth-station antenna pointing at a communications satellite) [21], radio astronomy [22, 23], and missile guidance [24, 25]. The monopulse principle is also used in both active and passive sonar [26, 27] and in some optical trackers.

In applications not involving pulsed transmission the technique is often called simultaneous lobing or simultaneous lobe comparison rather than monopulse. In radio astronomy a technique known as interferometry derives information about the angular distribution of radiating sources by correlating the signals received by two or more widely spaced antennas; in a broad sense this can be considered a

form of phase-comparison monopulse, or it might more properly be called “time-delay-comparison monopulse.”

References

- [1] M. I. Skolnik, *Introduction to Radar Systems*, 3rd ed., New York: McGraw-Hill, 2001.
- [2] D. K. Barton, *Radar System Analysis and Modeling*, Norwood, MA: Artech House, 2005.
- [3] P. Z. Peebles, *Radar Principles*, New York: John Wiley & Sons, 1998.
- [4] J. L. Eaves and E. K. Reedy, *Principles of Modern Radar*, New York: Van Nostrand Co., 1987.
- [5] M. A. Richards, *Principles of Modern Radar*, Raleigh, NC: Scitech Publ., 2010.
- [6] M. I. Skolnik, *Radar Handbook*, 3rd ed., New York: McGraw-Hill, 2008.
- [7] D. R. Rhodes, *Introduction to Monopulse*, New York: McGraw-Hill. Reprint, Dedham, MA: Artech House, 1982.
- [8] D. K. Barton, (ed.), *Radars: Vol. 1, Monopulse Radar*, Dedham, MA: Artech House, 1974.
- [9] R. M. Page, “Monopulse Radar,” *IRE Convention Record*, 1955, Part 1, pp. 132–134.
- [10] D. K. Barton, “The Future of Pulse Radars for Missile and Space Range Instrumentation,” *IRE Trans. on Military Electronics*, Vol. MIL-5, No. 4, October 1961, pp. 330–351. Reprinted in *Monopulse Radar*, D. K. Barton, (ed.), Dedham, MA: Artech House, 1974.
- [11] D. K. Barton, “Recent Developments in Radar Instrumentation,” *Astronautics and Aerospace Engineering*, July 1963, pp. 54–59.
- [12] J. T. Nessmith, “Range Instrumentation Radars,” *IEEE Trans. on Aerospace and Electronic Systems*, Vol. AES-12, No. 6, November 1976, pp. 756–766.
- [13] S. F. George and A. S. Zamanakos, “Multiple-Target Resolution of Monopulse vs. Scanning Radars,” *Proc. National Electronics Conf.*, Vol. 15, 1959, pp. 814–823. Reprinted in *Monopulse Radar*, D. K. Barton, (ed.), Dedham, MA: Artech House, 1974.
- [14] J. H. Dunn and D. D. Howard, “Precision Tracking with Monopulse Radar,” *Electronics*, April 22, 1960, pp. 51–56. Reprinted in *Monopulse Radar*, D. K. Barton, (ed.), Dedham, MA: Artech House, 1974.
- [15] D. K. Barton, *Radar System Analysis*, Englewood Cliffs, NJ: Prentice-Hall, 1964.
- [16] D. K. Barton, “Tracking Radars,” Part VI, Ch. 7 of *Modern Radar*, R. S. Berkowitz, (ed.), New York: John Wiley & Sons, 1965.
- [17] D. K. Barton and H. R. Ward, *Handbook of Radar Measurement*, Englewood Cliffs, NJ: Prentice Hall, 1969. Reprint, Norwood, MA: Artech House, 1984 (see p. 35).
- [18] J. H. Dunn, D. D. Howard, and K. B. Pendleton, “Tracking Radar,” Chapter 21 of *Radar Handbook*, M. I. Skolnik, (ed.), New York: McGraw-Hill, 1970.
- [19] L. G. Bullock, G. R. Oeh, and J. J. Sparagna, “An Analysis of Wide-Band Microwave Direction-Finding Techniques,” *IEEE Trans. on Aerospace and Electronic Systems*, Vol. AES-7, No. 1, January 1971, pp. 188–203.

- [20] V. C. Sundberg and D. F. Yaw, "ECM and ESM Antennas," Chapter 40 of *Antenna Engineering Handbook*, R. C. Johnson, (ed.), New York: McGraw-Hill, 1984.
- [21] J. H. Cook, "Earth Station Antennas," Chapter 36 of *Antenna Engineering Handbook*, R. C. Johnson, (ed.), New York: McGraw-Hill, 1984.
- [22] J. D. Kraus, *Radio Astronomy*, New York: McGraw-Hill, 1966.
- [23] J. S. Hey, *The Radio Universe*, Oxford, U.K.: Pergamon Press, 1971.
- [24] J. F. Gulick, "Overview of Missile Guidance," *IEEE Eascon '78 Record*, Washington, D.C., September 25–27, 1978, pp. 194–198.
- [25] E. R. Feagler, "The Interferometer as a Sensor for Missile Guidance," *IEEE Eascon '78 Record*, Washington, D.C., September 25–27, 1978, pp. 203–210.
- [26] V. C. Albers, *Underwater Acoustics Handbook II*, University Park, PA: Pennsylvania State University Press, 1964.
- [27] C. A. Roberts and A. Favret, "Applications of Monopulse Tracking Techniques to Passive Linear Arrays," *Journal of the Acoustical Society of America*, Vol. 51, No. 1 (Part 1), January 1972, pp. 31–37.

Chapter 2

Terminology, Definitions, and Notation

In the early days of monopulse development and even to the present time, different terminology and symbols have been used by various companies, government organizations, and individuals, and have often been only loosely defined. The lack of standardization has sometimes been a source of confusion. The purpose of this chapter is to define the terms and symbols used in this book and to help the reader “translate” some of the terminology found elsewhere. Many of the terms have been defined in standards of the Institute of Electrical and Electronic Engineers (IEEE), compiled in [1], and reference will be made to those definitions as appropriate. Although the IEEE standards reflect the consensus of panels of experts and authors, they are not compulsory standards, and of course they cannot retroactively standardize terminology in older radar literature. Furthermore, they do not include *all* radar terms. As a result, there are differences in terms and definitions (not to mention symbols) used by various writers. They may require occasional “translation” but need not cause confusion if the reader pays careful attention to each writer’s definitions and notation.

In this book the terminology and definitions are consistent with those in the IEEE standards but are expanded for tutorial purposes. The reader is assumed to be already familiar with basic general radar terminology. Therefore, emphasis will be given to those terms that are peculiar to monopulse or that have special meanings when applied to monopulse. Attention is also given to some terms, which although not limited to monopulse or even radar, are subject to more than one interpretation and therefore require clarification. Important terms are defined or explained wherever they are introduced throughout the book, and a list of symbols is provided at the back of the book.

Some terms, however, are so fundamental to the subject of monopulse (including the word “monopulse” itself) that they deserve special attention at the outset. Such terms are discussed in this chapter.

Monopulse action takes place on reception. However, some of the terms, particularly those pertaining to antennas and associated components, are transmission terms, because some of the concepts are easier to explain in that form. By reciprocity, the receiving pattern of an antenna is the same as if the antenna (including the feed system, combiners, and beamformer) were used for transmission.

2.1 THE MEANING OF MONOPULSE

The word *monopulse* was first introduced by H. T. Budenbaum of the Bell Telephone Laboratories in 1946, according to his later paper [2]. The word is entrenched in the technical terminology not only of the English language but of several foreign languages as well, with minor variations. It was coined because it clearly expressed the ability to collect from each pulse the information needed for a pair of two-coordinate angle estimates, whereas the older angle-sensing techniques of sequential lobing required several (at least four) pulses to form a pair of angle estimates.

The term *simultaneous lobing*, synonymous with monopulse, is a more accurate description of the technique, although it is less commonly used. It is the *simultaneity* rather than the “one pulse” that is essential. As a matter of fact, many monopulse radars *do not* extract angle estimates from each pulse. The usual practice is to smooth or integrate the raw single-pulse estimates, in order to improve the estimates, provide Doppler resolution, or simplify the processing. Furthermore, as already mentioned, monopulse is not confined to pulsed radars. The simultaneity of reception prevents errors due to fluctuation in the signal strength. Because many monopulse systems use design compromises for economy, these errors may not be completely prevented, but they are at least smaller than in sequential lobing.

There are many monopulse radars that do provide complete angle estimates from each pulse. Examples include certain precision instrumentation radars whose outputs are used for fine-grain, pulse-by-pulse analysis of target trajectories and reflection characteristics, and phased array radars that maintain tracks on several targets, interleaved with one another and with search, so that the time available for a dwell on each target is very short.

A variety of definitions of monopulse can be found in the technical literature. The following definition, taken from an earlier version of the IEEE Standard [1], is adopted here with minor changes in order to include nonradar applications:

A technique in which information concerning the angular location of a source or target is obtained by comparison of signals received simultaneously in two or more antenna patterns, as distinguished from techniques such as lobe switching or conical scanning, in which angle information is derived from a series of sequential antenna patterns. In radars using monopulse the simultaneity of the patterns makes it possible to obtain a two-dimensional angle estimate from a single pulse (hence the

name monopulse), although multiple pulses are usually employed to improve the accuracy of the estimate, provide Doppler resolution, or simplify the processing. The monopulse principle can be used in continuous-wave as well as pulsed radar, and also in non-radar applications.

The wording of this definition expresses several important points:

1. The words “information concerning” are intended to emphasize that what is obtained from the monopulse is an *estimate* of angular location subject to various errors. The word “information” may be interpreted, as in information theory, to mean reduction of uncertainty.
2. “Angular location” means a single angular coordinate or a pair of angular coordinates, such as azimuth and elevation (see Section 2.8).
3. Since a “target” reradiates energy back to the radar, it might be considered to be included under the more general term “source” (meaning a source of radiation). However, a source is usually interpreted to mean an active radiator such as a transmitting antenna or transponder, as distinguished from a target that reradiates passively by reflection. Monopulse is used in reception, not transmission—therefore it works on active sources as well as targets. To avoid needless repetition, the word “target” will frequently be used in this book to include sources as well, except where a distinction is being made.
4. “Comparison of signals” can take many forms, depending on the monopulse classification. In most cases, the comparison is not made directly between signals from individual feed horns or antenna elements, but indirectly—for example, between the sum and the differences. A comparison must take the form of an amplitude ratio or a phase difference or both¹ so that the resulting angle indication will not depend on absolute signal strength or phase.
5. The definition mentions “two or more” patterns. For measurement of a single angle coordinate, two patterns suffice. For measurement of both angular coordinates, at least three patterns are needed.
6. The word “patterns” is used rather than “beams” because it is more general, as will be explained in Section 2.3.
7. The reference to lobe switching and conical scanning is not essential to the definition of monopulse but is included to emphasize the distinction between simultaneous and sequential receiving patterns (see Section 1.2).

¹ The comparison can always be expressed in terms of a complex ratio, which includes both an amplitude and a phase difference. Thus if two signals are $a_1 \exp(j\phi_1)$ and $a_2 \exp(j\phi_2)$ their complex ratio is $(a_1/a_2) \exp[j(\phi_1 - \phi_2)]$.

2.2 APERTURES AND ILLUMINATION FUNCTIONS

The word *aperture* (from the Latin *apertus*, open) means literally an opening. The use of this word in connection with electromagnetic radiation comes from classical optics, where it means an opening in an opaque screen. When the screen is illuminated from behind by a plane wave, the aperture acts as a radiating surface, forming a radiation (or diffraction) pattern. By extension, an aperture has come to mean any radiating surface, or any bounded surface that can be treated as if it were the source of radiation.

For a given antenna, the aperture is not unique. Any surface surrounding the antenna can be chosen arbitrarily as the aperture provided the fields and currents over the entire surface are taken into account [3]. The choice is made for analytical convenience in such a way that the fields and currents are negligible outside of a bounded area. In the case of a reflector-type antenna or an array antenna, the customary practice is to consider the aperture to be a surface (usually plane) bounded by the edge of the reflector or the edges of the array.

An *illumination function* (or aperture function), in transmission, describes the amplitude and phase of the applicable polarization component of the electromagnetic field at each point in the aperture as a function of its position. In reception, the illumination function describes the amplitude and phase weights applied to the contribution of the arriving wave to each element of the aperture in order to form the desired pattern. In a reflector-type antenna the illumination function is determined by the design of the reflector, feed system, and any power dividers, combiners, or hybrids that are used. In an array it is determined by amplitude and phase control of each element.

2.3 PATTERNS, LOBES, AND BEAMS

The terms antenna pattern, lobe, and beam have overlapping but somewhat different meanings.

For transmission, the *antenna pattern* describes the variation of the applicable polarization component of the electromagnetic field as a function of angle from a reference axis, as received at an observation point that varies in angle but remains at a constant range in the far field of the antenna. For reception, the antenna pattern describes the variation of the signal received by the antenna from a source having the applicable polarization and located at a constant range in the far field, as a function of the angle of the source from a reference axis. The antenna pattern can be calculated from a knowledge of the illumination function, including the aperture over which it extends. In the physical-optics method of analysis (approximate, but adequate for most purposes) the antenna pattern is calculated by Fourier transformation of the illumination function, provided the aperture is a

plane surface and the pattern is expressed in sine space (see Section 2.8 and Chapter 7 for an explanation of sine space).

In many measurements or calculations of antenna patterns, only amplitude (or power) is of interest. However, for a full analysis of some of the subtle aspects of monopulse, the phase as well as the amplitude of the pattern must be taken into account.

A *lobe*, in a general sense, is a rounded projection or protuberance. When applied to an antenna pattern, it means a portion of the pattern between adjacent nulls or between adjacent pronounced dips. An interferometer pattern may have many lobes of nearly equal amplitude, but the common type of pattern in radar is one that has a single major lobe (mainlobe) and a number of much smaller minor lobes (sidelobes). The mainlobe in such cases is also called a *beam*.

To summarize the distinctions among the three terms:

1. Pattern is the general term describing the variation of a transmitted field or received signal as a function of angle.
2. A lobe is a portion of a pattern between nulls or minima.
3. If a pattern has a single principal lobe, much larger than the other lobes, the principal lobe is also called a beam.

Figure 1.6 can serve as an illustration of the use of these terms. All the curves except the one marked d/s are antenna patterns. The main portions of the two individual squinted patterns and of the sum pattern can also be called beams or lobes (or mainlobes, when necessary to distinguish them from the sidelobes). The difference pattern is not usually called a beam, since it does not have a single predominant lobe. The main part of it is sometimes called a dual lobe or a split lobe.

The curve d/s , the ratio of the difference to the sum, is not an antenna pattern but rather a nonlinear function of two patterns.

The receiving patterns of a reflector-type antenna (at a specified frequency) are not determined uniquely by the shape and size of the reflector(s)² and by the locations of the feed horns. They depend also on the points in the radar at which the outputs are taken, and what transformations, if any, have occurred between the feed horns and the outputs.

To illustrate this point, consider the parabolic reflector with four-horn feed used as an illustration in Section 1.3. If an output were taken from the waveguide connected to one of the horns, it would form a beam squinted in a direction opposite to that of the displacement of the horn from the focus. Four such outputs (i.e., four beams) could be formed simultaneously. The antenna patterns in this case would be the patterns of the squinted beams. On the other hand, if the waveguides are interconnected by RF hybrid junctions to form a sum and two differences, and if the outputs are taken after the hybrids, then the antenna patterns are those of the sum and differences.

² The plural applies in Cassegrain antennas and certain other antennas having more than one reflector.

It is with these considerations in mind that the general term “patterns” rather than the more restricted term “beams” is used in the definition of monopulse given in Section 2.1. Thus, the comparisons can be between component beams (e.g., the squinted beams in Section 1.3), between the sum and differences, or between the members of any set of simultaneous patterns, whether formed directly or obtained as combinations of other patterns.

In this book antenna patterns always represent voltage, not power, unless otherwise specified. The pattern is sometimes measured directly, or it can be calculated from the illumination function through the Fourier transform. A calculation for a rectangular aperture in the azimuth plane takes the form

$$f(u) = \int_{-0.5}^{0.5} g(x) \exp(j2\pi xu) dx \quad (2.1)$$

where f is the voltage gain of the pattern, $u = (w/\lambda) \sin \theta$, θ is the azimuth angle in radians, $g(x)$ is the illumination function, and x is the horizontal coordinate, normalized to the aperture width w . The function $g(x)$ is usually normalized so that in transmission the total power on the aperture is unity:

$$\int_{-0.5}^{0.5} |g(x)|^2 dx = 1 \quad (2.2)$$

When that is done, the voltage $f(u)$ from (2.1) is normalized to the maximum voltage available from a uniformly illuminated aperture.

Forms equivalent to (2.1) for circular or elliptical apertures may be found in antenna texts.

2.4 SUM AND DIFFERENCE PATTERNS

In the baseline monopulse radar used as an illustration in Section 1.3, it is obvious why the sum and difference patterns are so called—they are obtained by addition and subtraction of the individual beam patterns produced by the four horns. It must be pointed out, however, that the patterns that were added or subtracted are not quite the same as those that would be obtained from the individual horns if the other horns were missing. They are not even the same as the outputs of the individual horns in the four-horn cluster unless all four horns are properly terminated. The patterns are affected by mutual coupling; therefore, they should be considered as members of a group rather than as patterns standing alone.

There are cases in which the interpretation of sum and difference patterns is not so obvious. For example, there is a type of monopulse design in which a single multimode feed horn [4, 5], together with suitable waveguide couplings, produces

simultaneous patterns similar to the sum and difference patterns of the baseline system. Even though these patterns are produced directly, without addition or subtraction, it is common practice to call them sum and difference patterns, or to use the initial letters of sum and difference as symbols.

Another example is a five-horn monopulse feed system consisting of a central horn surrounded by four other horns. The central horn is used for a *reference pattern* (and also for a transmitting pattern) and the outputs of the outer horns are combined in pairs to obtain two difference signals. The reference pattern is often called the sum pattern even though there is no summing, because it serves the same purpose as the sum pattern in the baseline system.

In a corporate-fed array antenna any desired set of patterns can be formed in the feed structure, within the physical limitations of the antenna. The “sum” and “difference” patterns are usually formed directly rather than by the addition and subtraction of outputs of individual beams; in fact, outputs of the individual beams may not be available anywhere in the system. In a physical sense the individual beams are fictitious, but mathematically it is always possible to decompose the “sum” and “difference” patterns into a set of individual beams.

We will use the term *component patterns* or *component beams* to describe a set of patterns, whether they exist physically or not, such that their sum and differences are identical to the given set of “sum” and “differences.”

The term “sum pattern” could be replaced by the more general “reference pattern,” which would include not only patterns actually obtained by summing but also directly formed patterns that have similar form and serve the same purpose. The term “reference pattern” is in fact sometimes used, as in the case of the five-horn feed mentioned above, but the term “sum pattern” is quite prevalent. There is no corresponding general term to replace “difference pattern.”

An alternative pair of terms is “even pattern” and “odd pattern.” These terms are descriptive and general, and they are especially useful in the mathematical analysis of patterns and illumination functions, but they are not as widely used.

By common usage, therefore, “sum” and “difference” are employed in a generalized sense. Even when they are not literally correct they can be rationalized by conceiving of component beams—actual or fictitious—which if added and subtracted would produce the given sum and difference patterns.

To illustrate, consider monopulse in one angular coordinate only. Let s and d represent the so-called sum and difference voltages and let v_1 and v_2 represent voltages from the (possibly fictitious) component beams. Then

$$s = (v_1 + v_2)/\sqrt{2} \quad (2.3)$$

$$d = (v_1 - v_2)/\sqrt{2} \quad (2.4)$$

The summing and differencing are usually done by a microwave device called a hybrid junction which accepts v_1 and v_2 as inputs and produces outputs s and d . The reason for the factor $\sqrt{2}$ is that, assuming the use of passive lossless devices to form the sum and differences, the power out must equal the power in. When the sum and differences are formed from four beams, the factor is 2 instead of $\sqrt{2}$.

Given any s and d , we can define component beam voltages v_1 and v_2 by inverting (2.3) and (2.4), regardless of whether v_1 and v_2 actually exist physically (i.e., are measureable) anywhere in the system:

$$v_1 = (s + d)/\sqrt{2} \quad (2.5)$$

$$v_2 = (s - d)/\sqrt{2} \quad (2.6)$$

In two-coordinate monopulse we can assume that there are four unknown component beams. Given the sum and two differences, the three equations (1.1) to (1.3) are not sufficient to determine the four component beams uniquely.³ However, it does not matter whether the solution is unique or not. The individual beams will not be used in any quantitative analysis but only as a concept to support the use of the terms sum and difference.

2.5 SUM AND DIFFERENCE NOTATION

In most of the past literature on monopulse, the Greek letters Σ and Δ have been used to represent sum and difference voltages. These symbols have been used for the most part as voltage magnitudes, whereas in much of the analysis presented in this book the complex (phasor) nature of the voltage is essential. In some of the more recent monopulse literature, the Latin capital letters S and D have been used to designate phasor sum and difference voltages, but they may cause confusion because the capital letter S is commonly used to represent signal *power*.

Hence we will use small letters s and d to designate sum and difference phasor voltage (that is, complex envelopes). However, symbols Σ and Δ will be used to identify sum and difference channels or output ports. Thus the conventional practice of symbolizing the output ports of a hybrid junction by Σ and Δ will be followed, but the voltages appearing at these ports will be denoted by s and d .

³ In forming the sum and differences, a fourth output $(B + C) - (A + D)$ becomes available as a by-product. This output, called the quadrupolar signal, the diagonal difference, or the double difference, is usually terminated in a dummy load and not used. If this pattern is known in addition to the other three, there is enough information to solve uniquely for A , B , C , and D . Alternatively, the symmetry of the four component beams can be invoked to make the solution unique.

2.6 ERROR SIGNALS

The original use of monopulse was in closed-loop, mechanically steered tracking radars. The servomechanism that drives the antenna requires as its input an error signal (in each coordinate) representing the difference between the target direction and the antenna pointing direction. When the two directions coincide, the error signal is zero. If read-outs from the mechanical rotation of the pedestal shafts are used as the sole indication of target direction, then the error signal really does represent the error in the angle output of the radar.

In other situations error signals do not represent errors in the radar's output data, but rather a means of obtaining or refining estimates of target direction. For example, some monopulse radars use an *error correction* technique, as explained in Section 1.3. This consists of a closed tracking loop with the shaft positions providing coarse angle estimates and the residual error signals providing corrections to the shaft position errors. There are other radars (or radar operating modes) in which the servo loop is not closed at all. Instead the beam axis is pointed in a pre-programmed or precomputed direction that in general does not coincide with the target direction (although the target must be within the beam), and the open-loop monopulse error signal is used as a measure of the target direction relative to the known axis direction. Thus there can be an error signal without any error in the radar's data output.

In some cases the error signal can be zero when there is actually a large error in the indicated target position. For example, in the case of target glint, unresolved targets or multipath, a closed-loop tracker may faithfully follow the apparent target direction (thus nulling the error signal), but that direction may differ greatly from the true direction of the desired target.

To prevent confusion, the monopulse output that provides an indication of target direction relative to the axis direction will be called *normalized difference signal* (where applicable), or more generally the *monopulse processor output*. The word *error* will be reserved for use in the sense of the difference between the radar's indicated angle and the true angle.

2.7 COMPLEX SIGNAL REPRESENTATION AND COMPLEX ENVELOPES

Complex notation for alternating currents, voltages, and electromagnetic field quantities is in common use and will be employed extensively in this volume in analyzing radar signals and noise. A brief review will be given here.

The word "complex" is used here in the mathematical sense of having a real part and an imaginary part. Thus a complex number z can be written as

$$z = x + jy \quad (2.7)$$

where

$$\begin{aligned} x &= \operatorname{Re}(z) = \text{real part of } z \\ y &= \operatorname{Im}(z) = \text{imaginary part of } z \end{aligned} \quad (2.8)$$

and

$$j = \sqrt{-1} \quad (2.9)$$

In mathematics and physics the symbol i is used to denote imaginary quantities. The equivalent symbol j is more common in engineering applications.

The conventional method of representing a complex quantity graphically is to plot the real and imaginary parts as the horizontal and vertical coordinates, respectively, of a point in the *complex plane*, as illustrated in Figure 2.1.

There is a well-known mathematical relationship, Euler's formula:

$$\exp(j\phi) = \cos \phi + j \sin \phi \quad (2.10)$$

a proof of which is found in any elementary textbook on complex functions. Thus

$$\cos \phi = \operatorname{Re}[\exp(j\phi)]$$

and

$$\sin \phi = \operatorname{Im}[\exp(j\phi)] \quad (2.11)$$

In this book, complex notation will be used mainly for voltage or electric field strength, never for power.

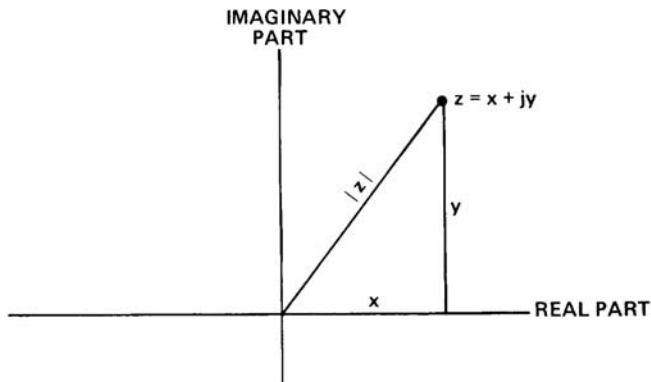


Figure 2.1 Real and imaginary parts of complex quantity.

Consider a sinusoidal voltage $v(t)$ with amplitude a , radian frequency ω , and phase ϕ :

$$v(t) = a \cos(\omega t + \phi) \quad (2.12)$$

According to (2.11), this can be written as

$$v(t) = a \operatorname{Re} \left\{ \exp \left[j(\omega t + \phi) \right] \right\} \quad (2.13)$$

In common practice the symbol $\operatorname{Re}(\)$ is omitted and equation (2.13) is shortened to

$$v(t) = a \exp \left[j(\omega t + \phi) \right] \quad (2.14)$$

It must be kept in mind that setting a real quantity such as an instantaneous voltage $v(t)$ equal to a complex expression, as in (2.14), is a kind of shorthand. Only the real part of the complex expression actually represents the voltage.

A complex quantity representing a voltage (or an electric field strength) is also called a *phasor*. It may be represented graphically by a line with length proportional to the amplitude and an angle with respect to a reference line equal to the phase angle. It is also sometimes called a *vector* voltage, but the term phasor is preferred (see definition of *phasor* in [1, p. 819]).

The advantage of the complex shorthand notation is not apparent from a comparison of (2.12) and (2.14)—the first one in fact looks simpler—but in the analysis of modulation, frequency translation, or other processing, the mathematical manipulations are greatly simplified by the complex notation. In particular, complex notation makes it possible to express carrier waveforms, modulation, frequency translations, and other operations as separable factors.

An example will illustrate the advantage of complex notation and at the same time will help to resolve a point of confusion that sometimes arises as to when the imaginary part must be retained and when it is to be discarded or ignored. Let the sinusoidal voltage in (2.12) be amplitude-modulated by a time-varying multiplier $a_m(t)$ and simultaneously phase-modulated by a time-varying phase shift $\phi_m(t)$. The resulting modulated voltage, $v_r(t)$ is

$$v_r(t) = a a_m(t) \cos \left[\omega t + \phi + \phi_m(t) \right] \quad (2.15)$$

To put this into complex form, we express the modulation as a complex quantity $m(t)$:

$$m(t) = a_m(t) \exp \left[j\phi_m(t) \right] \quad (2.16)$$

and multiply it by the complex form of $v(t)$, given by (2.14), to obtain

$$v_r(t) = v(t) \exp[j(\omega t + \phi)] a_m(t) \exp[j\phi_m(t)] \quad (2.17)$$

which can be combined thus:

$$v_r(t) = a a_m \exp\left\{j\left[\omega t + \phi + \phi_m(t)\right]\right\} \quad (2.18)$$

The real part of (2.18) is the same as (2.15). This confirms that the complex notation yields the correct result. The big advantage of the complex form, for our purpose, is shown by (2.17); the final voltage can be expressed as (the real part of) the product of the carrier voltage $v(t)$ expressed in complex form and a *complex modulation envelope* (or simply *complex envelope*) $m(t)$ that includes both amplitude and phase.

The information content of a signal (except for its frequency or Doppler shift) is in the complex envelope, not in the carrier; because of this fact, we will be able to simplify much of the subsequent analysis by dealing only with the complex envelope and omitting the carrier (which should be understood but need not be written). This convenient means of separating the carrier and the envelope is not possible when real notation is used, as in (2.15).

Whenever complex notation is used for a physical quantity that is inherently real, such as an instantaneous voltage, only the real part has physical meaning; the imaginary part is to be ignored. "Instantaneous" voltage means the value of the voltage at each instant within a cycle, not merely the amplitude of the envelope. In (2.14), $v(t)$ is an instantaneous voltage, and so is $v_r(t)$ in (2.17) and (2.18).

However, when a real, instantaneous voltage is written in complex form as the product of two or more complex factors, it is *not* permissible to drop the imaginary part of any individual factor. Thus in (2.17) it would not be correct to drop the imaginary part of $v(t)$ or the imaginary part of $m(t)$. Only the imaginary part of the product, $v_r(t)$, is to be dropped.

In (2.16), $m(t)$ was expressed in terms of its amplitude $a_m(t)$ and its phase $\phi(t)$. Alternatively, $m(t)$ can be expressed in terms of its real and imaginary parts I and Q respectively, usually called the in-phase and quadrature modulation components:

$$m(t) = I(t) + jQ(t) \quad (2.19)$$

In speaking of a complex modulation envelope we do not necessarily mean that we actually start with a carrier and modulate it, in the same way that voice signals modulate a carrier in radio. However, the received signals and noise in radar can be represented as if they resulted from a carrier modulated by a complex

signal, of which the amplitude and phase correspond respectively to the amplitude and phase modulation of the carrier.

While the carrier oscillates at RF, the modulation envelope varies much more slowly. According to Shannon's sampling theorem [6], if the signal is limited to a bandwidth W , complex samples of the envelope (i.e., samples of I and Q) at intervals $1/W$ are sufficient to reconstruct the complex envelope—that is, to determine its value at every instant. Typically in a radar,

$$W \approx 1/\tau \quad (2.20)$$

where τ is the pulse width (actual width of a simple pulse or compressed width of a coded pulse), and can also be regarded as the time duration of a range cell. A useful approximation, therefore, is to regard the real and imaginary parts of the modulation envelope (I and Q) as being confined to an effective bandwidth of about the reciprocal of the pulse length. The amplitude and phase can have much wider bandwidths, since they are nonlinear functions of I and Q . However, they can be reconstructed indirectly from amplitude and phase samples at intervals $1/W$ by converting the samples to I and Q , reconstructing I and Q , and then converting the reconstructed I and Q back to amplitude and phase.

The complex envelope remains unchanged upon frequency conversion from RF to IF provided the local-oscillator frequency is below the RF. If the local-oscillator frequency is above the RF, the phase of the complex envelope is inverted; in other words the IF complex envelope in this case is the complex conjugate of the RF complex envelope.

The complex envelope will be encountered repeatedly in this book, usually referred to simply as “complex voltage” or “phasor voltage,” with the tacit understanding that it is to be regarded as modulating a carrier. This concept is meaningful in radar because most radar signals and noise can be considered narrowband in the sense that the bandwidth seldom exceeds 10% of the RF center frequency (i.e., 5% on each side), and is usually much less.

A more comprehensive treatment of complex signal representation can be found in [7].

2.8 ELEVATION, AZIMUTH, AND TRAVERSE

The basic mathematical relations presented in this section apply to both mechanically and electronically steered antennas, but the discussion and illustrations apply primarily to the former. The application to electronically steered arrays requires further elaboration, to be presented in Chapter 7 and Section 8.3.

Target direction from a land-based radar is usually expressed in the angular coordinates of azimuth and elevation, and if the radar uses a mechanically steered

antenna, those are also the usual coordinates of mechanical rotation; they are not the same as the pair of angular coordinates in which the monopulse radar senses target direction.

When a radar is mounted on a ship or other moving surface platform, the same relationships hold provided the deck rather than the horizontal surface is used as the reference. The conversion from moving deck coordinates to fixed coordinates involves additional geometry but does not affect the basic relationship between the monopulse sensing coordinates and the servo drive coordinates. In airborne or missile-borne radar, a reference plane that includes the longitudinal axis and is horizontal when that axis is at zero elevation is used, and angles from this plane are called pitch (corresponding to elevation) and yaw (corresponding to azimuth from the nose).

In order to present the relationships and show how the monopulse sensing coordinates are converted to servo drive coordinates, we will confine our attention to land-based radars. In the usual design of a mechanically rotatable antenna mount, there are either one or two axes of rotation. (Three-axis mounts have also been built for special applications.) If there is one axis, it is usually vertical. The angle of rotation about the vertical axis is azimuth. The vertical axis is therefore called the azimuth axis.⁴

If there are two axes of rotation, the usual design is called an azimuth-elevation (frequently abbreviated as az-el) mount, and is illustrated in Figure 2.2. The lower axis (the azimuth axis) is vertical, and azimuth is defined as in the single-axis case. The portion of the mount that rotates on that axis carries a horizontal axis (the elevation axis), and the angle of rotation about that axis is elevation, measured upward from horizontal. The antenna itself (the reflector) is mounted so that its axis (the *beam axis* or the *boresight axis*) is perpendicular to the elevation axis. The drawing is simplified in order to make the azimuth axis, elevation axis, and boresight axis visible. The counterpoise is a massive solid piece added so that the part of the structure that rotates in elevation will have its center of gravity on the elevation axis. Omitted from the drawing are a number of other components such as the drive motors, antenna feed assembly, and waveguides. Photographs of an actual monopulse antenna and its mount are shown in Chapter 4.

The following simple analogy aids in visualizing azimuth and elevation: If the antenna were placed at the center of the earth with its azimuth axis aligned with the earth's axis of rotation, azimuth and elevation would correspond to longitude and latitude respectively.

The natural coordinate system for a planar aperture, however, is sine space (also called cosine space when referring to the complementary angles). Planar

⁴ On a ship the corresponding axis is perpendicular to the deck and the angle of rotation is called deck azimuth or train.

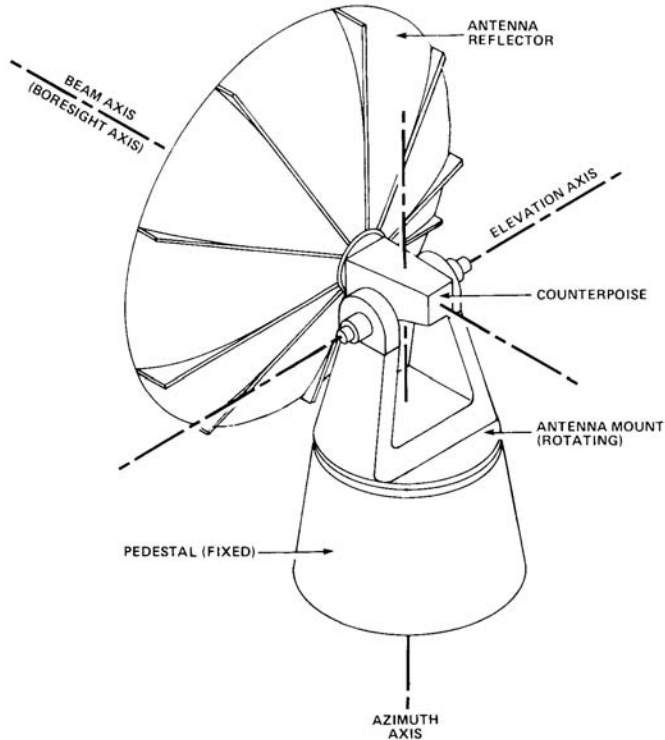


Figure 2.2 Axes of a mechanically steerable antenna.

apertures can be interpreted to include not only arrays but also the apertures of reflector antennas.⁵

Let α , β , and γ be the angles that a given direction makes with the positive x , y , and z axes, respectively, and let u , v , and w be their respective cosines:

$$u = \cos \alpha = \sin \alpha' \quad (2.21)$$

$$v = \cos \beta = \sin \beta' \quad (2.22)$$

$$w = \cos \gamma = \sin \gamma' \quad (2.23)$$

⁵ The following discussion assumes that the illumination in the aperture plane, for the pattern under consideration, has uniform or uniformly tapered phase. This is not quite true in a reflector antenna, but it is a close representation.

where α' , β' , and γ' are the complements of α , β , and γ respectively. The u - v - w coordinate system is called either sine space or cosine space, depending on the point of view.

Because $u^2 + v^2 + w^2 = 1$, we can write

$$1 - w^2 = u^2 + v^2$$

or

$$\sin^2 \gamma = \sin^2 \alpha' + \sin^2 \beta' \quad (2.24)$$

The geometric interpretation of these angles is as follows: α' is the angle between the given direction and the x - z plane; β' is the angle between the given direction and the x - z plane; γ is the angle off broadside (of an array) or off axis (of a reflector antenna).

In array antennas that can be steered electronically, angles α and β and their complements have no standardized names. They are usually identified simply by symbols such as those used here, either in angle space or in sine space. In reflector antennas, however, α' is called the traverse angle and β' is loosely called the elevation angle (relative to the antenna axis elevation). The latter is an approximation, exact only when the traverse angle is zero.

In a reflector antenna the traverse and elevation normalized difference signals are zero when α' and β' are zero and are approximately proportional to α' and β' respectively when those angles are small. In an array that can be steered electronically, the normalized difference signals are approximately proportional respectively to the u and v components of the deviation of the given direction from the beam pointing direction in sine space.

Let A be the azimuth of a given direction relative to the antenna pointing direction. Angle A is measured clockwise in the horizontal plane from the projection of the axis (the broadside direction or boresight axis) to the projection of the given direction. Let E be the elevation of the given direction measured upward from the horizontal plane, and let E_a be the elevation of the aperture normal. E_a is called the tilt angle in the case of an array or the axis elevation angle in the case of a reflector antenna. The relations between these quantities and angles α' and β' are [8]:

$$\sin \alpha' = \sin A \sin E \quad (2.25)$$

$$\sin \beta' = \sin E \cos E_a - \cos E \sin E_a \cos A \quad (2.26)$$

Equation (2.25) can be inverted:

$$\sin A = \alpha' \sec E \quad (2.27)$$

which for small A is approximated by

$$A \approx \alpha' \sec E \quad (2.28)$$

Note that (2.27) and (2.28) are independent of the elevation of the antenna axis. Equation (2.28) is the basis of the “secant correction” in mechanically steered tracking radars. The monopulse traverse output is approximately proportional to α' but the servo requires an input approximately proportional to A in order to maintain proper loop gain. The conversion is accomplished by generating a multiplying factor proportional to the secant of the antenna elevation angle E_a . This is not quite the same as the secant of the target elevation E demanded by (2.28), but since $E - E_a$ is usually only a fraction of a degree and since the servo input need not be exactly proportional to A , the approximation suffices at elevation angles up to about 85° ($\sec 85^\circ = 11.5$). The secant correction is done by a secant-wound potentiometer in some radars and by computer in others.

The more exact equation, (2.27), may appear puzzling in one respect. As the target approaches the zenith, $\sec E$ approaches infinity. If α' is not equal to zero, then $\sin A$ must also approach infinity, but $\sin A$ cannot exceed 1 in magnitude. The seeming paradox is resolved by noting that as $E \rightarrow 90^\circ$, the possible target locations are confined to a decreasing cone that shrinks to a vertical line (which is in the y - z plane). Hence as $E \rightarrow 90^\circ$, $\alpha' \rightarrow 0$. When $E = 90^\circ$, A is indeterminate.

If $A = 0$, then (2.26) reduces to

$$\begin{aligned} \sin \beta' &= \sin E \cos E_a - \cos E \sin E_a \\ &= \sin(E - E_a) \end{aligned}$$

or

$$E = E_a + \beta' \quad (2.29)$$

Hence the target elevation equals the antenna elevation plus β' if the target traverse is zero, and for small values of A this is still a good approximation, since $\cos A \cong 1$ when A is small. However, if E is close to 90° , A tends to grow large, and the approximation breaks down. The exact equation for E in terms of α' and β' is obtained by eliminating A from (2.25) and (2.26). The result is

$$\sin E = \cos E_a \sin \beta' + \sin E_a \sqrt{1 - \sin^2 \alpha' - \sin^2 \beta'} \quad (2.30)$$

The distinction between azimuth and traverse is sometimes explained (as it was in Chapter 1) by saying that they are measured in the horizontal plane and the slant plane respectively. Although this statement is imprecise, its simplicity makes

it useful in visualizing the relationship, at least in a gross manner. To make the statement more precise insofar as traverse is concerned, one must specify that:

1. The slant plane is the one perpendicular to the vertical boresight plane and containing the line of sight to the target, and
2. The traverse angle is measured from the intersection of that slant plane with the vertical boresight plane.⁶

Figure 2.3 illustrates the geometrical relations expressed by (2.27). The line labeled "beam axis" in the diagram refers to a mechanically steered antenna. A more general designation would be "normal to the antenna aperture." Thus in the case of an electronically steered array that line represents the broadside direction.

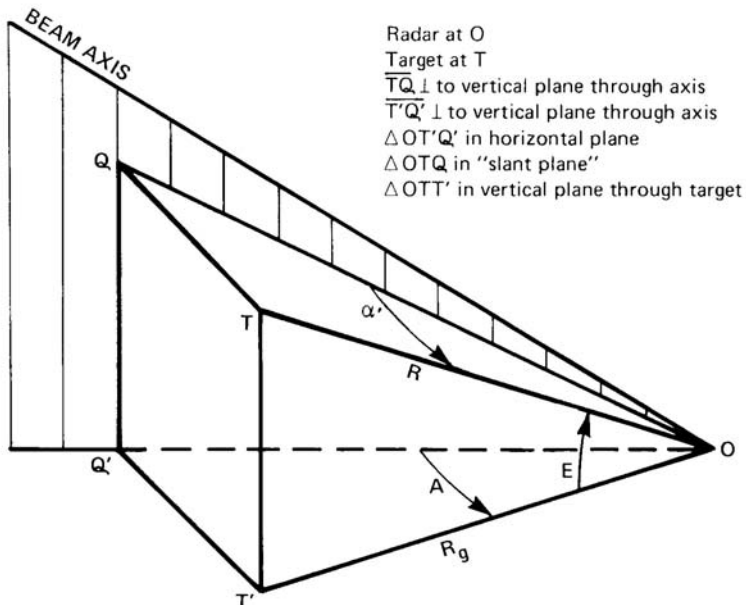


Figure 2.3 Geometrical relations among angles: azimuth (A), elevation (E), and traverse (α').

Figure 2.4 shows how a square in sine space, centered at the boresight direction, maps into az-el coordinate space, at various values of the boresight elevation E_a . The corners of the square in array coordinates are $\pm 1^\circ$ in traverse (α') and $\pm 1^\circ$ in antenna-coordinate elevation (β'), as in Figure 2.4(a). The center of the square is the boresight direction. Figure 2.4(b) shows the corresponding areas in az-el space for antenna boresight elevations of 0° , 60° , and 75° . The coordinates of the corners of these three areas are as shown in Table 2.1.

⁶ The vertical boresight plane is the vertical plane containing the antenna boresight or broadside axis.

At 0° boresight elevation the az-el area differs by a negligible amount from a square with corners at $(\pm 1^\circ, \pm 1^\circ)$. As the boresight elevation increases, the area becomes elongated in azimuth while the elevation remains equal to β' at the center and only slightly less than β' at the edges.

If a target passes close to the zenith, the azimuth rate tends to become extremely high. No matter how exact the conversion from the natural α' , β' coordinates of the monopulse outputs to az-el, track may be lost because the servo drive is unable to keep up with the target azimuth rate.

The azimuth and elevation of a target relative to the antenna normal are the differences between the azimuths and elevations respectively of the target and antenna normal referred to fixed geographical coordinates, usually north and horizontal. If target direction and antenna normal direction are interchanged, their relative azimuth and elevation are merely reversed in sign.

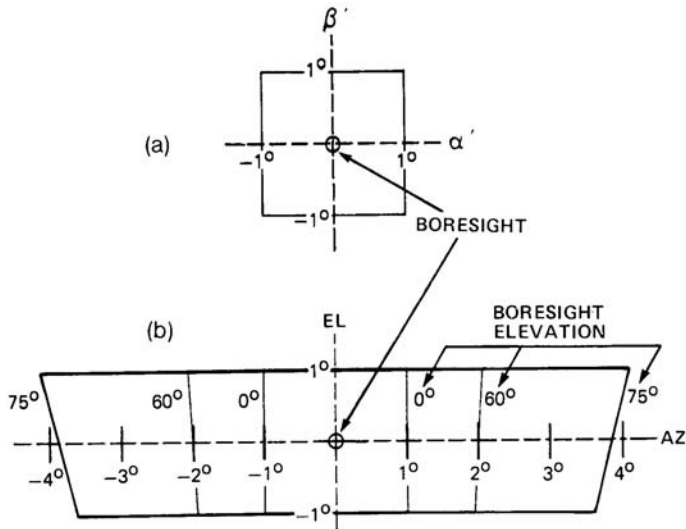


Figure 2.4 Coordinate conversions from α' - β' to azimuth-elevation. (a) $\pm 1^\circ$ square in α' - β' space. (b) Transformation into az-el space for boresight elevation angles of 0° , 60° , and 75° .

Table 2.1 Conversion to Az-El Space

<i>Az-El Coordinates of Corners (degrees)</i>		
E_a	Upper Corners	Lower Corners
0°	$(\pm 1.00, 1.00)$	$(\pm 1.00, -1.00)$
60°	$(\pm 2.06, 0.98)$	$(\pm 1.94, -1.01)$
75°	$(\pm 4.13, 0.97)$	$(\pm 3.62, -1.03)$

Traverse and antenna-coordinate elevations (β'), on the other hand, are defined only in the coordinate system determined by the antenna orientation and cannot be transformed to a different coordinate system (e.g., a different antenna orientation) by simple addition. If target direction and antenna normal direction are interchanged, the new traverse and antenna-coordinate elevation are *not* obtained by merely reversing the signs, although in many cases a close approximation may be obtained in that manner.

References

- [1] IEEE Standard 100, *The Authoritative Dictionary of IEEE Standards Terms*, 7th ed., New York: IEEE Press, 2000.
- [2] H. T. Budenbaum, "Monopulse Automatic Tracking and the Thermal Bound," *Convention Record of IRE First National Convention on Military Electronics*, June 17–19, 1957, Session 20, pp. 387–392.
- [3] S. Silver, *Microwave Antenna Theory and Design*, Vol. 12 of MIT Radiation Laboratory Series, New York: McGraw-Hill, 1949. Reprint, CD-ROM edition, Norwood, MA: Artech House, 1999 (see pp. 158–160).
- [4] J. H. Dunn, D. D. Howard, and K. B. Pendleton, "Tracking Radar," Chapter 21 of *Radar Handbook*, M. I. Skolnik, (editor-in-chief), New York: McGraw-Hill, 1970 (see pp. 21-18–21-21).
- [5] P. J. Mikulich et al., "High-Gain Cassegrain Monopulse Antenna," *IEEE G-AP International Antenna Propagation Symposium Record*, Boston, MA, September 1968.
- [6] C. E. Shannon, "A Mathematical Theory of Communication," *Bell Syst. Tech. J.*, Vol. 27, July 1948, pp. 379–423; October 1948, pp. 623–656.
- [7] H. Urkowitz, *Signal Theory and Random Processes*, Dedham, MA: Artech House, 1983 (see Chapter 3).
- [8] W. H. VonAulock, "Properties of Phased Arrays," *Proc. IRE*, Vol. 48, No. 10, October 1960, pp. 1715–1727 (see Eq. (42)).

Chapter 3

The Monopulse Output as a Complex Ratio

In this chapter we extend the concepts introduced in Chapters 1 and 2 and formulate general principles and equations that will be used later in classifying and analyzing various specific types of monopulse.

3.1 GENERAL PRINCIPLES

All monopulse processors are intended to produce outputs that depend only on ratios, not absolute values, of signal voltages. Any sensitivity that they have to absolute values is due to design compromises or equipment imperfections.

In a general sense, the ratio of two voltages means their *complex ratio*. The phasor voltages (complex envelopes) of a monopulse difference d and sum s can be expressed as¹

$$d = |d| \exp(j\delta_d) \quad (3.1)$$

$$s = |s| \exp(j\delta_s) \quad (3.2)$$

where δ_d and δ_s are phase angles relative to any arbitrary reference. The complex ratio is

$$\frac{d}{s} = \left| \frac{d}{s} \right| \exp[j(\delta_d + \delta_s)] = \left| \frac{d}{s} \right| \exp(j\delta) \quad (3.3)$$

¹ A pair of vertical bars enclosing a symbol for a complex quantity indicates the *amplitude*, *magnitude*, or *absolute value* of the quantity. A corresponding mathematical term is *modulus*.

where δ is the relative phase:

$$\delta = \delta_d - \delta_s \quad (3.4)$$

The phasor relationships are illustrated in Figure 3.1. Thus the complex ratio has a magnitude equal to the ratio of the magnitudes of the two voltages and a phase equal to their relative phase or phase difference.

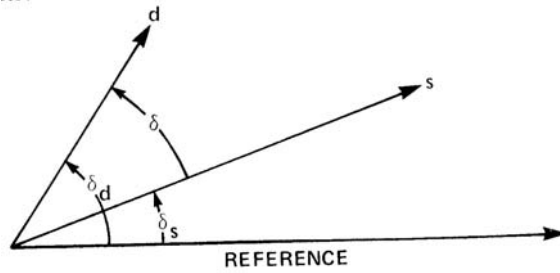


Figure 3.1 Sum and difference phasors.

The complex ratio of the difference voltage in each coordinate to the sum voltage contains essentially all the information about the target direction that is available from the received monopulse signals. Theoretically, additional information may be contained in the ratio of the unused diagonal difference voltage to the sum voltage. Section 15.2 discusses the diagonal difference voltage and shows that the information it contributes is unimportant for most practical purposes.

The equivalent of d/s could be obtained in other ways. For example, if d and s are the difference and sums of voltages v_1 and v_2 from two individual beams or from two pairs of beams, then

$$d = (v_1 - v_2) / \sqrt{2} \quad (3.5)$$

and

$$s = (v_1 + v_2) / \sqrt{2} \quad (3.6)$$

so that

$$\frac{d}{s} = \frac{v_1 - v_2}{v_1 + v_2} = \frac{1 - v_2/v_1}{1 + v_2/v_1} \quad (3.7)$$

Hence, by measuring the complex ratio v_2/v_1 we could calculate d/s or vice versa. The two ratios contain equivalent information, and other relevant ratios can be formed from linear combinations of the voltages.

However, d/s is the most widely used form of monopulse ratio and it is analytically convenient. It is logical to regard it as the fundamental monopulse ratio. When other signal voltage ratios or associated quantities are encountered, we will show how they are related to d/s .

Voltage amplitude ratios and relative phases are not necessarily measured or computed directly. Equivalent information can be derived indirectly. For example, the equivalent of the amplitude ratio is obtained in some radars by taking the difference of the outputs of logarithmic amplifiers; the tangent or some other function of the relative phase angle may be measured instead of the angle itself. Alternatively, the I (in-phase) and Q (quadrature-phase) components of the difference and sum signals relative to a common reference oscillator can be produced and the real and imaginary parts of d/s can be computed from those components.

3.2 RELATIVE PHASE OF DIFFERENCE AND SUM

In the description of the baseline radar model used for illustration in Section 1.3, it was stated that the relative phase δ of d and s is 0° or 180° . For brevity, “in-phase” will be interpreted to include both 0° and 180° . The in-phase condition applies to many monopulse radars, but in others the relative phase of d and s is $\pm 90^\circ$ (quadrature phase) depending on the type of antenna, feed system, and microwave combiners that form the sum and difference.

For $\delta = 0^\circ, 180^\circ$, and $\pm 90^\circ$, the values of $\exp(j\delta)$ in (3.3) are 1, -1 , and $\pm j$, respectively. It might appear, therefore, that d/s is pure real or pure imaginary and that there is no need to treat it as a complex quantity. As a matter of fact, the usual monopulse processor extracts only the real or imaginary part, depending on the type of monopulse.

However, the in-phase or quadrature-phase relationship of d and s is an idealization. In practice, d and s can have any relative phase because of noise, interference, multipath, unresolved targets (including a single target with multiple scattering points), or nonideal design, construction, and alignment [1, 2]. Thus, even when d/s is supposedly real, it can have a significant imaginary part (or vice versa) under certain conditions. To analyze the effects of these factors and to understand certain techniques that have been proposed to improve performance, the ratio d/s must be treated as a complex quantity.

We will refer to the in-phase or quadrature-phase relationship of d and s under ideal conditions as the *nominal* phase relationship.

3.3 SOME USEFUL RELATIONSHIPS AND FORMULAS

Invoking Euler’s formulas (2.8), we can express (3.3) in the form

$$\frac{d}{s} = \frac{|d|}{|s|} \exp(j\delta) = \frac{|d|}{|s|} \cos \delta + j \frac{|d|}{|s|} \sin \delta \quad (3.8)$$

Thus, the real and imaginary parts of d/s are

$$\operatorname{Re}(d/s) = \frac{|d|}{|s|} \cos \delta \quad (3.9)$$

and

$$\operatorname{Im}(d/s) = \frac{|d|}{|s|} \sin \delta \quad (3.10)$$

Referring to Section 1.3 and Figure 1.1, we see that the baseline radar model described there produces only the real part (or in-phase component) of the complex ratio d/s . Circuits that perform this operation will be described in Chapter 8. The imaginary part (or quadrature component) could also be extracted, if it were needed, by adding another channel to the monopulse processor for each angular component. The added channel would work in the same way except that either the d or s input voltage would be shifted by 90° . Normally the imaginary part is not used because ideally the target contributes only to the real part, while the imaginary part is due to noise or other disturbances. Similarly, in radars that produce d and s in nominal quadrature phase, only the imaginary part of d/s is normally processed. Because of practical constraints, the actual output of a monopulse processor is usually not exactly the real or imaginary part of d/s , but an approximation.

The complex ratio d/s can also be expressed in “ I and Q ” form. The I and Q components of the difference signal, denoted by d_I and d_Q , are the in-phase and quadrature components relative to a reference oscillator at the signal frequency (usually at IF). From (3.1) and Figure 3.1, we have

$$d_I = |d| \cos \delta_d = \operatorname{Re}(d) \quad (3.11)$$

$$d_Q = |d| \sin \delta_d = \operatorname{Im}(d) \quad (3.12)$$

Similarly, from (3.2), the in-phase and quadrature components of s are

$$s_I = |s| \cos \delta_s = \operatorname{Re}(s) \quad (3.13)$$

$$s_Q = |s| \sin \delta_s = \operatorname{Im}(s) \quad (3.14)$$

Note that this representation involves the phases of d and s relative to a common reference oscillator, not relative to each other.

From (3.11) and (3.12),

$$d = \text{Re}(d) + j \text{Im}(d) = d_I + jd_Q \quad (3.15)$$

and from (3.13) and (3.14),

$$s = \text{Re}(s) + j \text{Im}(s) = s_I + js_Q \quad (3.16)$$

The *complex conjugate* of a complex quantity has the same real part, and the negative of the imaginary part. Referring to (3.16), the complex conjugate of s , denoted by s^* , is

$$s^* = s_I - js_Q \quad (3.17)$$

Multiply the numerator and denominator of d/s by s^* to obtain

$$\begin{aligned} \frac{d}{s} &= \frac{ds^*}{ss^*} = \frac{(d_I + jd_Q)(s_I - js_Q)}{(s_I + js_Q)(s_I - js_Q)} \\ &= \frac{d_I s_I + d_Q s_Q + j(d_Q s_I - d_I s_Q)}{s_I^2 + s_Q^2} \end{aligned} \quad (3.18)$$

Thus

$$\text{Re}(d/s) = \frac{d_I s_I + d_Q s_Q}{s_I^2 + s_Q^2} \quad (3.19)$$

and

$$\text{Im}(d/s) = \frac{d_Q s_I - d_I s_Q}{s_I^2 + s_Q^2} \quad (3.20)$$

In some radars, the I and Q components of d and s are extracted and digitized, then $\text{Re}(d/s)$ or $\text{Im}(d/s)$ is computed by (3.19) or (3.20).

If the phase of the reference oscillator were changed, all four of the quantities d_I , d_Q , s_I , and s_Q would change, but in such a way that $\text{Re}(d/s)$ and $\text{Im}(d/s)$, as computed by (3.19) and (3.20), would remain invariant.

Although all monopulse processors produce a ratio, some of them do so by means of a device known as a “product detector,” implying multiplication. In the receivers preceding the product detector, the sum voltage is operated upon by

AGC, which causes the voltage gain to vary as $1/|s|$, so that the sum voltage out of the receiver is proportional to $s/|s|$; in other words, the sum voltage amplitude is held constant while phase is preserved. The same AGC voltage that acts on the sum channel also controls the gain of the difference channel, so that the difference receiver output is proportional to $d/|s|$. The product detector accepts the voltages from the sum and difference receivers and produces an output proportional to the product of their amplitudes and the cosine of their relative phase angle. That is, after adjustment of the scale factor,

$$\text{Product detector output} = \frac{|s|}{|s|} \frac{|d|}{|s|} \cos \delta = \frac{|d|}{|s|} \cos \delta \quad (3.21)$$

which is the real part of d/s , as expressed in (3.9).

In practice, an ordinary AGC circuit will not hold the sum voltage at a constant level on each pulse, as is assumed in (3.21). This means that the product-detector output, which ideally should be independent of signal voltage, will vary to some degree with signal voltage, and the scale factor in the equation will vary accordingly. For closed-loop tracking the effect of this variation is minor, since the null direction is unchanged and the change in servo loop gain is usually small. However, in radars that use the error signal to determine the angular position of the target relative to the beam axis, other methods of obtaining the result expressed by (3.21), described in Chapter 8, are preferred.

References

- [1] S. M. Sherman, "Complex Indicated Angles Applied to Unresolved Targets and Multipath," *IEEE Trans. on Aerospace and Electronic Systems*, Vol. AES-7, No. 1, January 1971, pp. 160–170.
- [2] J. T. Nessmith and S. M. Sherman, "Phase Variations in a Monopulse Antenna," *Record of IEEE International Radar Conference*, Washington, D.C., April 21–23, 1975, pp. 354–359.

Chapter 4

Components Used in Monopulse

Many types of components are common to radars in general, including monopulse radars. Certain components, however, are either unique to monopulse or are designed and used in a special way for monopulse, or with more demanding requirements. Principal components of these types are discussed and illustrated in this chapter. Omitted from this chapter, however, are monopulse processors. Because of their importance and the multiplicity of forms that they can take, they are treated separately in Chapter 8.

4.1 ANTENNA MOUNTS

Antenna mounts of mechanically steered monopulse radars are basically no different from those of other mechanically steered radars, but the requirements in many cases are more severe. Antenna mounts are subject to several mechanical sources of angular error (see Section 7.4).

Because monopulse is capable of higher angular accuracy than other methods of radar angle measurement and tracking, the units must be designed and built to more demanding specifications in order not to limit the attainable accuracy. The boresighting and alignment procedures must be more painstaking and provisions must be made for adjustments where needed.

Many different types of mounts have been devised [1], ranging from a single axis of rotation to three or even four axes, but in the large majority of radars either single-axis or two-axis mounts are used. The single axis is usually azimuth. (These terms were defined in Section 2.8.) A single-axis mount obviously does not permit closed-loop tracking in both coordinates but monopulse can be used for closed-loop tracking in azimuth or open-loop measurements in elevation, or both. Open-loop azimuth monopulse can also be used in a search radar scanning me-

chanically in azimuth. The monopulse provides a fine measure of target angle (“beam splitting”) to supplement the relatively coarse angle indication obtained from the basic search mode.

Most land-based tracking radars, including monopulse trackers, have elevation-over-azimuth two-axis mounts, illustrated in simplified form in Figure 2.2. The monopulse outputs provide measures of traverse (α') and antenna-coordinate elevation (β'), which are related to the azimuth and elevation angles by equations given in Section 2.8.

As pointed out in Chapter 1, monopulse is capable of a higher data rate than sequential lobing and therefore is better suited to tracking of rapidly moving and accelerating targets. High angular rates and accelerations are not necessarily those of the target itself; they can occur because of the coordinate conversion from antenna coordinates to azimuth and elevation, as explained in Section 2.8. In order to utilize the superior data-rate capability of monopulse, the mounts must have sufficiently powerful drives to follow the target motion.

To carry signals and power between fixed equipment and a rotating antenna, it is necessary to use rotating joints, sliprings, wind-up cables, or similar devices. With monopulse this requirement is somewhat more demanding than with sequential lobing because there are usually three receiving channels in monopulse and only one in sequential lobing. The antenna rotation must not disturb the amplitude and phase balance of the three channels or introduce distortion. For this reason, the monopulse receivers are often mounted on the antenna, so that their RF inputs need not be passed through rotating or flexing transmission lines.

Although elevation is defined only up to 90° (the zenith), in some antenna mounts the antenna can be plunged—that is, rotated in elevation through the zenith down to the horizon on the opposite side. Plunging is used as an aid in bore-sighting and alignment. If the antenna is to track correctly when plunged, the polarity of the azimuth drive must be reversed.

Most mounts also allow the antenna to be rotated below horizontal to small negative elevation angles in order to track targets that are lower than the antenna.

The photographs in Figures 4.1 and 4.2 are two views of the antenna and mount of the AN/FPS-16 monopulse tracking radar. The basic structure is the same as in the simplified sketch, Figure 2.2, but the actual equipment has a more extensive antenna support structure and additional components such as drive motors, antenna feed assembly, and waveguides.

4.2 ANTENNAS

An *antenna* is the portion of a radar that radiates power from the transmitter into space or collects power from an incoming wave, to be transferred to a receiver. It can be described as a device that provides coupling or impedance matching be-



Figure 4.1 AN/FPS-16 antenna, side view. (Figure courtesy RCA.)

tween the transmitter and space or between space and the receiver. A single antenna can be shared by one or more transmitters and one or more receivers. Monopulse is concerned primarily with reception. Some of the antenna terminology had its origin in transmission but by reciprocity it applies to reception as well.

Three main categories of antennas used in monopulse radar (as well as in other radars) are lenses, reflectors, and arrays, and each category can be divided into various types. The principal distinction between monopulse antennas and similar antennas used for other purposes is the nature of their feeds. Although the feeds are really part of the antennas, they will be described separately in the next subsection.

The remainder of this section pertains primarily to mechanically scanned antennas, but components and techniques used in monopulse arrays are also discussed. Monopulse in array systems is described in Chapter 7.

4.2.1 Lens Antennas

Lens antennas of various types have been built [2, 3]. One type is constructed of dielectric material, in which the phase velocity is less than in air. Such lenses are

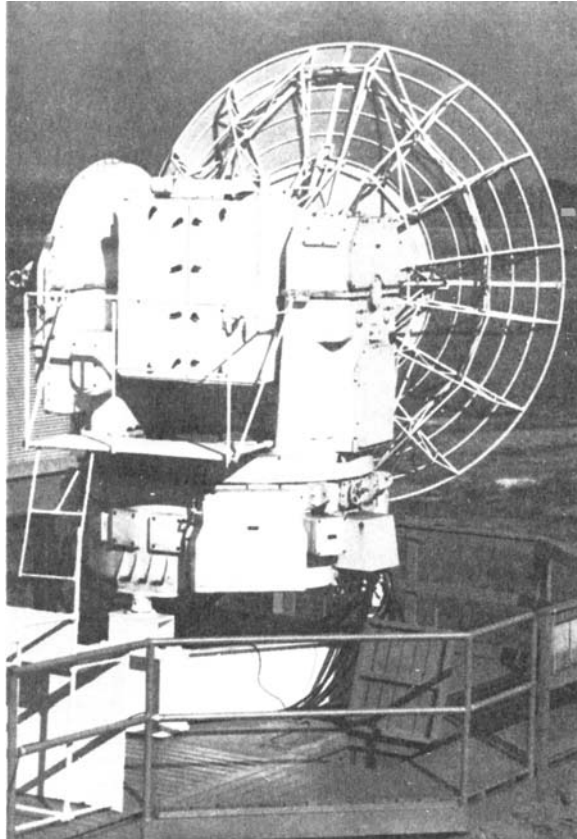


Figure 4.2 AN/FPS-16 antenna, rear view. (Figure courtesy RCA.)

similar to optical lenses. Since the usual purpose of a microwave lens in reception is to cause a wave from a distant source (essentially a plane wave) to converge at the feed in the focal plane, the dielectric lens is a convex figure of revolution, as illustrated in cross section in Figure 4.3(a).

Another type of lens antenna is the metal-plate lens [4], illustrated in cross section in Figure 4.3(b), composed of plates parallel to the E-vector, spaced so that the phase velocity in the waveguides formed by adjacent pairs of plates is considerably greater than in air. To produce convergence, the lens must therefore be concave. Although the plates run in only one dimension, the converging effect is two-dimensional if the surface is concave in both dimensions. Because the phase velocity is a strong function of frequency, the useful bandwidth is small.

In both parts of Figure 4.3 a single feed horn is shown in order to illustrate the action of the lens. A lens used for amplitude-comparison monopulse would have

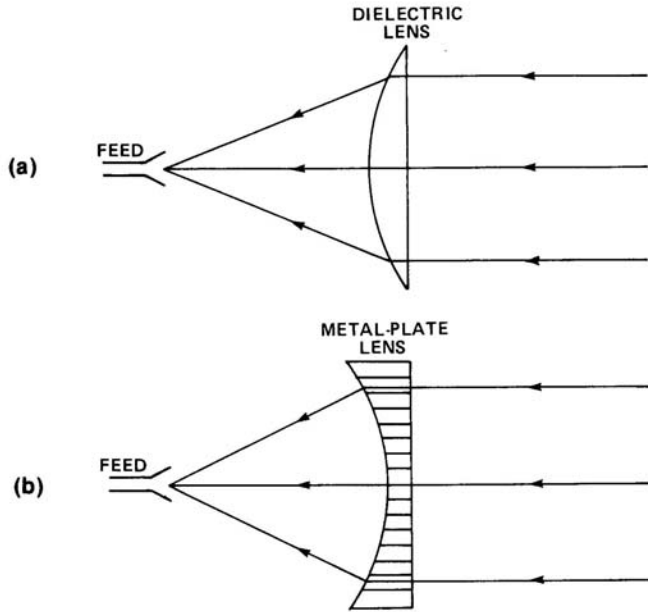


Figure 4.3 Lens antennas: (a) dielectric lens; and (b) metal-plate lens.

multiple feed horns in the focal plane, displaced from the axis. If lenses were to be used for phase-comparison monopulse, there would be multiple lenses side by side, each with a single feed horn.

To reduce the thickness and weight of dielectric or metal-plate lenses, they can be “stepped” or “zoned.” Progressing from the thinnest part of the lens, the thickness increases within each zone as in the basic lens, but at the zone boundaries the thickness is decreased in successive steps of one wavelength, causing phase steps of 360° across the aperture. These steps theoretically have no effect, since 360° is equivalent to 0° . However, such lenses are narrowband, since the one-wavelength steps must be matched to a particular frequency. Furthermore, the steps cause some shadowing and discontinuity, resulting in energy loss and increased sidelobes.

Still another type of lens antenna is the constrained metal lens [5], which consists of waveguides, or of metal plates perpendicular to the E-vector, connecting the inner and outer faces. The phase velocity is approximately the same as in air, with little frequency sensitivity, permitting operation over a wider frequency band than the metal-plate lens described above. The converging effect is achieved by arranging the lengths and orientations of the guides so that the wave in each guide follows an indirect path between corresponding points on the two faces, with longer length at the center than at the edges.

4.2.2 Single-Reflector Antennas

Although lens antennas have some advantages and have been used in monopulse systems, reflector antennas are more common in mechanically steered monopulse radars. Typically the reflector surface is a paraboloid constructed of aluminum, steel, or metal-coated plastic. It is colloquially called a “dish.” If different beam-widths in the two dimensions are desired, the surface is still a paraboloid but the contour of the edges may be an ellipse instead of a circle. The reflecting surface may be perforated or constructed of mesh in order to reduce weight and wind loading.

Figure 4.4 shows a cross section of a paraboloidal reflector (any section parallel to the axis is a parabola), and traces the paths of rays arriving parallel to the axis. According to geometrical optics, the rays, after reflection, would all converge at the focal point, producing an infinite power density at that point. Geometrical optics, however, is only an approximation. The power is actually distributed in a diffraction pattern in the vicinity of the focal point with maximum (but finite) density at that point [6]. If the wave arrives at an angle to the axis, the point of maximum power density is displaced from the axis in the opposite direction.

A disadvantage of this type of antenna is that the feed, including its waveguides and support structure, is in front. The blockage thus created causes some loss in power, an increase in sidelobes, and an error in monopulse angle measurement. A lens antenna, in contrast, suffers no blockage by the feed, although it has other disadvantages mentioned in Section 4.2.1. However, progress in the science and technology of feed design over the years has resulted in more compact feeds for reflector antennas, reducing the blockage problem.

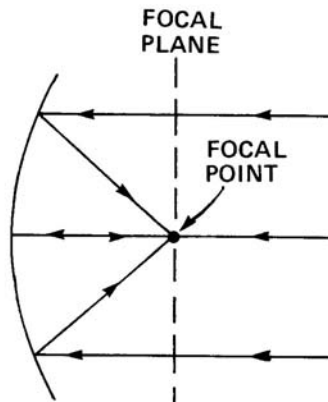


Figure 4.4 Paraboloidal reflector.

4.2.3 Cassegrain (Double-Reflector) Antennas

The Cassegrain antenna is the microwave analog of the optical technique named after its inventor and long used in optical telescopes. It is illustrated in Figure 4.5. The main reflector is a paraboloid and the subreflector is a hyperboloid. One of the two foci of the hyperboloid is coincident with the focus of the paraboloid. The feed is placed at the other focus of the hyperboloid, which is at, or slightly in front of, the main reflector. According to the approximate ray-tracing method of geometric optics, a plane wave arriving in the axial direction would be concentrated at that focal point, but more refined analysis shows that there is a diffraction pattern with peak intensity at the focal point.

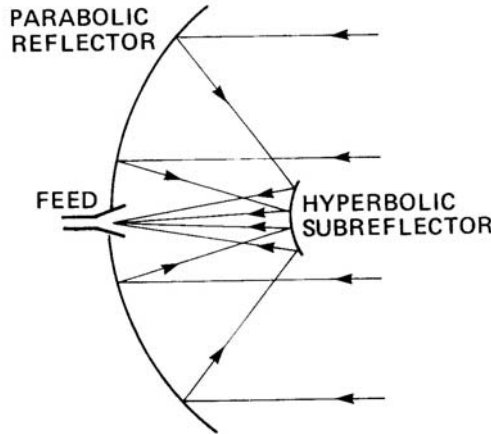


Figure 4.5 Cassegrain antenna.

The advantages of a Cassegrain antenna over a single-reflector antenna are a more compact antenna structure and reduction of length of transmission lines to the feed. These features are especially useful in large monopulse antennas, since the cluster of feed horns and associated hybrid junctions and waveguides tends to be bulky and heavy. If placed in front of the reflector, such feeds are difficult to support adequately to prevent excessive deflection due to angular acceleration and gravity. In the Cassegrain configuration the only component that needs to be supported in front of the main reflector is the subreflector, which is lighter than the feed assembly and is positioned closer to the main reflector. However, because of blockage by the subreflector, the Cassegrain design is ordinarily not advantageous in antennas having a beamwidth greater than about 1° .

4.2.4 Polarization-Twisting Reflector Systems

Blockage by the subreflector can be overcome or reduced, and the use of Cassegrain antennas can be extended to beamwidths greater than 1° , with a technique called *polarization twisting*. This has been used in some applications, limited to antennas designed for a single polarization. One form of this technique [3] will be described in terms of transmission; by reciprocity, the same principle holds in reception. Supposed vertical polarization is desired. Then the feed horns are designed for horizontal polarization. The subreflector is composed of a grating of horizontal wires laid out to form a hyperbolic contour (see Figure 4.6). The grating is almost as effective as a continuous hyperbolic surface in reflecting the horizontally polarized radiation from the horns back toward the main reflector.

The main reflector has the usual parabolic shape, but in addition there is a grating of wires placed one-quarter wavelength in front of the surface. These wires are oriented at 45° from horizontal. The horizontally polarized wave from the subreflector can be decomposed into two equal, orthogonally polarized components, one parallel to the 45° wires and the other perpendicular to the wires. The wires reflect the parallel component but are essentially transparent to the perpendicular component, which is reflected from the main reflector surface with an additional half-wavelength two-way path length. Thus a 180° difference in the relative phase of the two components is introduced, and their resultant is converted from horizontal to vertical polarization. The horizontal subreflector wires are

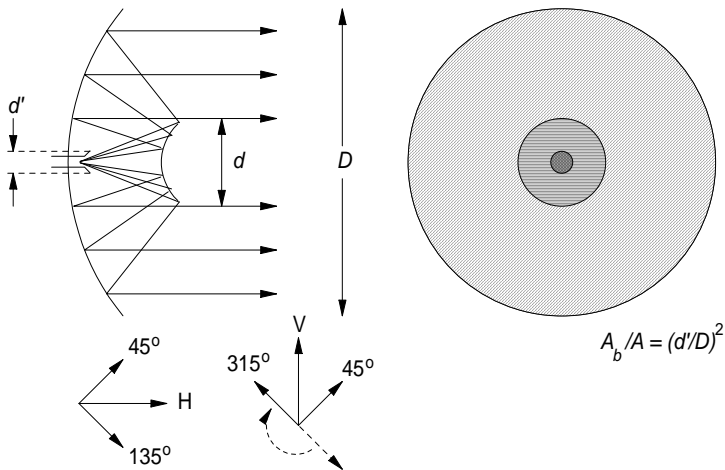


Figure 4.6 Geometry of polarization-twisting Cassegrain system. The wire subreflector does not block rays reflected from the main reflector, leaving as a blocked area only that of the feed horn (diameter d'). The blockage of the main reflector is thus characterized by the fraction $A_b/A = (d'/D)^2$.

transparent to the vertically polarized wave and therefore cause very little blockage. There are other versions of this design, one of the objectives being to decrease the frequency-dependence in order to permit broadband operation.

The principle of polarization twisting has also been applied in a class of antennas in which the feed illuminates the concave side of a fixed parabolic reflector composed of wires parallel to the feed polarization vector, supported by a low-loss dielectric material (Figure 4.7). The paraboloid reflects the wave back to a planar twist reflector whose center is near the feed aperture. The planar reflector rotates the polarization by 90° and directs the wave back toward the paraboloid, which is now transparent because the wires are perpendicular to the polarization vector. The beam can be scanned over a wide angle by mechanical rotation of the planar reflector while the feed and the parabolic reflector remain fixed. Advantages of this design are that the planar reflector has much less rotational inertia than a conventional antenna, and no RF joints are required, since the feed remains stationary. Although this type of antenna differs from the classical Cassegrain design, it is considered to belong to the Cassegrain family because it uses two reflectors.

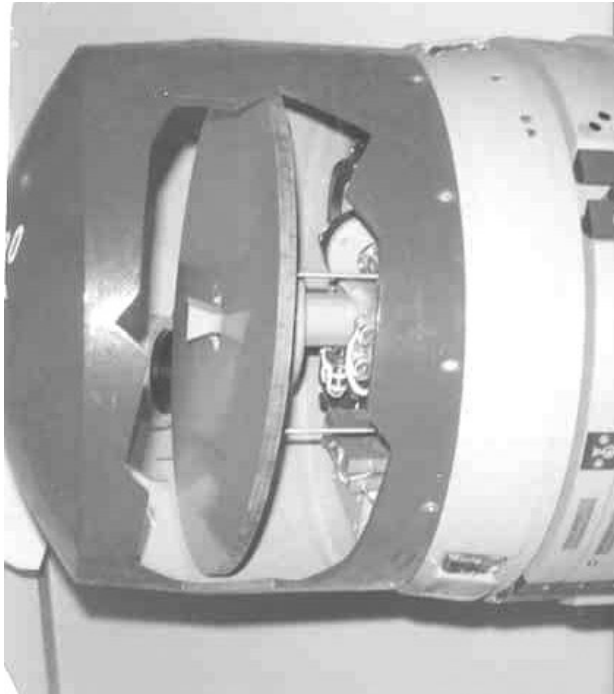


Figure 4.7 Polarization twisting dual-reflector system used in Mirage aircraft. The beam is scanned by tilting the polarization-rotating planar reflector that is pivoted near the feed horn. Push rods that control tilt can be seen to the right of the planar reflector.

4.3 FEEDS

A *feed* is that part of an antenna that distributes power from the transmitter to the main aperture (a lens, reflector or array) in a desired manner and collects the power captured by the aperture with some desired weighting for transfer to a receiver. Two general classes of feeds are distinguished:

1. An *optical* or *space* feed radiates power to (or receives power from) the main aperture, through open space. The desired amplitude and phase distribution over the area of the aperture is achieved by the combination of the geometry and the radiation pattern of the feed.
2. A *constrained* (or *corporate*) feed distributes power from the transmitter to the elements of the aperture, or combines the power received by the antenna elements, through waveguides or transmission lines. The desired amplitude and phase distribution is achieved by power dividers or combiners, transmission line lengths, and phase shifters.

Dipoles, waveguide horns, and other types of space feeds are used in lens and reflector antennas. In monopulse, horns are most often used. They are essentially waveguides with flared ends.

In particular, a widely used type of feed in amplitude-comparison monopulse consists of a cluster of four feed horns, offset symmetrically from the focus, as illustrated in Figure 1.3. Figure 1.3(b) is a view looking into the aperture of the four feed horns, which are labeled A, B, C, and D to correspond with the squinted beams shown in Figure 1.4. The upper horns produce the lower beams. The size of the horns is exaggerated for clarity in Figure 1.3. The dimensions of a horn aperture are of the order of a wavelength, while the diameter of a reflector is typically tens of wavelengths and may exceed 100 wavelengths. The waveguides leading from the horns could be connected to individual receivers but instead they are usually connected to a device called a comparator that forms the sum and two differences of the voltages of the horns. The sum and the differences then go to receivers.

The square shape of the horns shown in Figure 1.3(b) does not necessarily portray the actual construction, but is a customary diagrammatic representation. Figure 4.8 is a photograph looking into the aperture of the feed of the AN/FPS-16 radar. The horns are rectangular rather than square, designed for vertical polarization. At first glance it appears that there are only two horns but closer inspection reveals four. In earlier feed designs the horizontal septum¹ and the vertical septum came flush to the front surface. However, the vertical septum acted as a short for the vertical E-field, causing a null. Thus, the E-field distribution across the feed aperture for the sum pattern was approximately as in Figure 4.9(a), whereas the

¹ A septum is a dividing wall or partition. In this case it is the dividing wall between adjacent pairs of waveguides.

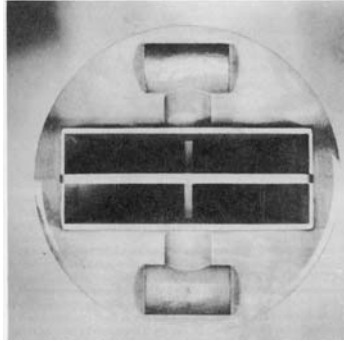


Figure 4.8 AN/FPS-16 feed, front view.

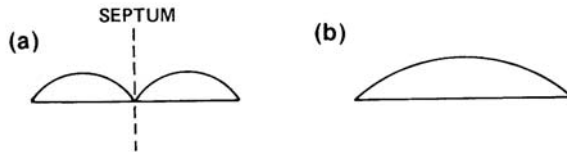


Figure 4.9 Strength of E-field versus distance across feed aperture: (a) with vertical septum extending to horn aperture; and (b) desired distribution.

desired distribution is as shown in Figure 4.9(b). The null at the center reduced the sum-pattern efficiency and increased the sidelobes. In the later design the performance was greatly improved by cutting the vertical septum back so that it does not extend all the way to the aperture, as can be seen in Figure 4.8. The resulting field distribution more nearly resembles that of Figure 4.9(b).

The circular metal plate surrounding the feed aperture, including the raised bosses above and below the horns, is designed to achieve the desired field distribution and impedance matching as well as to provide an integral feed structure.

The reference point of a feed horn is not the center of its aperture but the phase center, which is generally slightly behind the aperture plane. When feeds are installed, their positions are adjusted while monitoring the electrical outputs so that the phase centers are at the correct locations.

When the radar is in use, the feed aperture is normally not visible because it is covered with a small plastic radome to protect the interior from the environment. For the photograph in Figure 4.8 the radome was removed. Figure 4.10 shows another view of the feed horn assembly of Figure 4.8, this time from the side and rear. The horn apertures seen in Figure 4.9 are at the left, hidden from view in this picture, but the waveguide can be seen. The bottom pair of waveguides are curved in order to make them longer than the top pair by a quarter wavelength, as required for the inputs to the hybrids (not included in this part of the equipment) which produce the sum and difference signals.

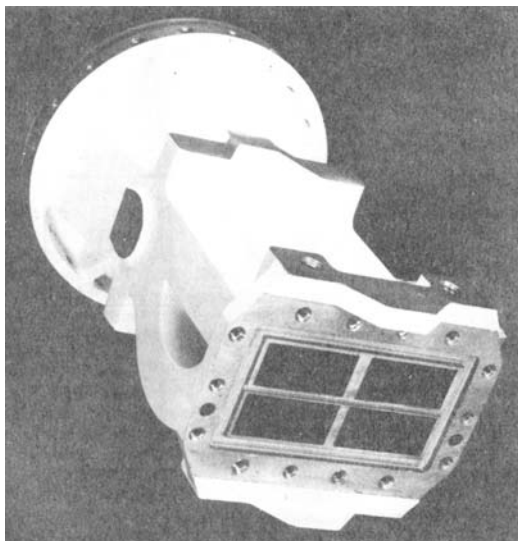


Figure 4.10 AN/FPS-16 feed, rear view.

The remainder of the antenna feed assembly, not shown, is joined to the end of the piece shown in Figure 4.10. It consists essentially of the comparator, the device that accepts the inputs from the horns via the four waveguides and converts them to the sum signal and the two difference signals (see Section 4.4).

The four-horn feed is capable of excellent performance but even with the best design it does not approach the theoretically optimum feed characteristics. Because it cannot optimize the sum and difference patterns independently, it must compromise.

Another type of feed, illustrated in Figure 4.11, has five horns. The center one is used for transmission and for reception of a reference signal that serves the

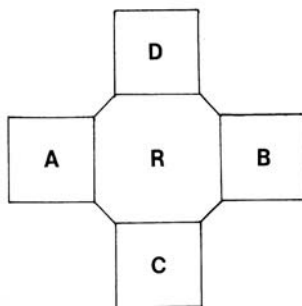


Figure 4.11 Five-horn monopulse feed.

same function as the sum signal in four-horn monopulse.² One difference signal is derived from the left and right outer horns and the other from the top and bottom horns.

Other horn configurations include a 12-horn feed, multimode, multilayer feeds, and a single-horn multimode feed. The advantages and limitations of the various types of amplitude-comparison monopulse feeds will be discussed in Chapter 6.

Phase-comparison monopulse, which has been mentioned but not yet discussed in detail, uses a cluster of four side-by-side lenses or reflectors rigidly connected to form a single antenna. Each lens or reflector has a single feed at its focus.

4.4 DEVICES FOR FORMING SUMS AND DIFFERENCES

In a monopulse radar antenna having multiple feeds, the sum and difference signals, or rather linear combinations of the feed outputs, are formed using certain passive microwave devices. Usually these are four-port devices with two input ports and two output ports, each output voltage being a different linear combination of the two input voltages. The same or similar devices are also used for other radar functions, such as power division or combining, but here we will concentrate on monopulse functions.

There are several forms of these devices. The nomenclature is not completely standardized [7–16] but two major categories (each having a number of subcategories) are usually recognized: *hybrid junctions* and *directional couplers*. These categories overlap.

The principal forms of the various devices will be described and illustrated, their electrical characteristics will be explained and compared, and their graphic symbols will be shown. The way in which these devices are interconnected to form the comparator in two-coordinate monopulse will be illustrated.

The particular versions of the various devices that will be illustrated are those used in waveguide systems. Corresponding versions also exist for coaxial-cable and stripline systems.

4.4.1 Hybrid Junctions

In a hybrid junction (often called simply “hybrid”) with properly matched terminations, a signal entering either of the two input ports is divided equally in power (but not necessarily in the same phase) between two output ports and does not appear at all at the other input port. Furthermore, when two signals having the

² In subsequent discussions the term “sum pattern” or “sum voltage” will be interpreted as including the reference pattern or voltage provided by a separate horn.

proper relative phase are applied simultaneously to the respective input ports, the two outputs are proportional to their sum and their difference. The required relative phase of the two inputs depends on the specific type of hybrid junction. It is usually either 0° or 90° . Likewise the sum and difference outputs may be in phase or in quadrature.

In microwave terminology, the name “hybrid” was first applied to the magic-T junction described below because it is a combination of the E-plane and H-plane T junctions.³ By extension the same name has also come to be applied to other types of junctions that perform the same function.

Magic-T Junction

Figure 4.12 illustrates one type of hybrid junction known as a *magic-T* (or magic-Tee). A signal input at port 1 divides equally between ports 3 and 4 but does not appear at port 2 because waveguide 2 cannot support that propagation mode. A signal input at port 2 divides equally between output ports 3 and 4 but will not appear at port 1. Hence, if the waveguide sections comprising the hybrid junction have the proper lengths and if inputs are applied simultaneously to ports 1 and 2, their sum will appear at one of the output ports and their difference at the other. By reciprocity, input and output ports can be interchanged.

In “folded” versions of the magic-T, the shape is modified without changing the electrical characteristics. For example, arms 3 and 4 may be folded upward or downward to be parallel to arm 2 or they may be folded forward to be parallel to arm 1.

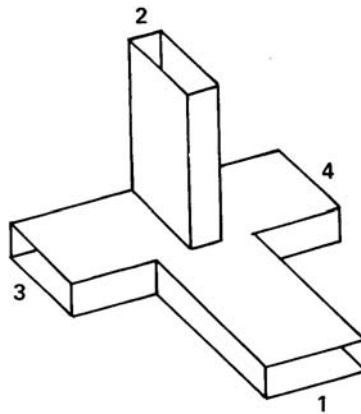


Figure 4.12 Magic-T hybrid junction.

³ Another explanation is that the word was carried over from hybrid coils that perform an analogous function in telephone circuits.

If the two inputs are in-phase, the sum and difference outputs will also be in phase. ("In-phase" includes phase opposition, which can be regarded as the same phase with sign reversal of the amplitude.)

In this device, as in the others that will be discussed, the output phase differs from that of the input phase because of the delay in propagation through the device, but this difference is immaterial in our application. Only the relative phase of the two inputs and the relative phases of the two outputs are of interest.

Theoretically, the behavior of this device is not frequency sensitive; therefore, it can work over a wide frequency band.

If v_1 and v_2 are the input voltages at ports 1 and 2, the output voltages at ports 3 and 4 are

$$v_3 = \frac{1}{\sqrt{2}}(v_1 + v_2) \quad (4.1)$$

and

$$v_4 = \frac{1}{\sqrt{2}}(v_1 - v_2) \quad (4.2)$$

The equations for v_3 and v_4 may have to be interchanged, depending on the polarity convention of the inputs, but in either case one output is proportional to the sum and the other to the difference. The reason for the factor $1/\sqrt{2}$ is that the total power out must equal the total power in (ignoring a small loss in the device). Squaring both sides of (4.1) and (4.2) and adding, we obtain

$$v_3^2 + v_4^2 = v_1^2 + v_2^2 \quad (4.3)$$

If (4.1) and (4.2) are solved for v_1 and v_2 , the resulting equations are the same with v_3 and v_4 replaced by v_1 and v_2 and vice versa. Inputs and outputs can be interchanged.

Hybrid Ring ("Rat-Race") Junction

The *hybrid ring junction* (also called a circular hybrid or a *rat-race*) is illustrated in Figure 4.13. A signal input at port 1 reaches output port 4 by two separate paths (clockwise and counterclockwise), which have the same pathlength, $3\lambda_g/4$, where λ_g is the wavelength in the guide. The two branch signals therefore reinforce at port 4. The same input signal reaches port 3 through paths having lengths $\lambda_g/4$ and $5\lambda_g/4$, differing by one wavelength. Therefore, reinforcement also occurs at port 3. On the other hand, the two path lengths from 1 to 2 differ by one-half wavelength; therefore cancellation occurs and there is no output at port 2.

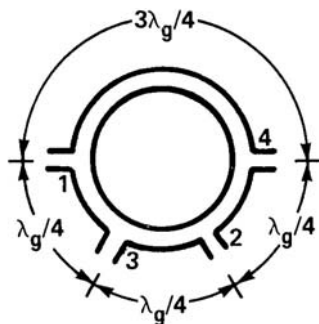


Figure 4.13 Hybrid ring junction (rat-race).

Similarly an input at port 2 will produce equal outputs at 3 and 4 but none at port 1. If signals of the same phase are entered simultaneously at 1 and 2, they reach output 3 in the same phase and they reach 4 in opposite phases. Therefore, the outputs at 3 and 4 are the sum and difference of the two inputs. The sum and difference outputs are in phase with each other. By reciprocity, input and output ports can be interchanged.

Since the phase relationships depend on the lengths of the waveguide sections, they are strictly correct at only one frequency. Therefore, this device can be used only over a limited frequency band.

The input-output relations for this device are the same as for the magic-T, as given by (4.1) and (4.2).

4.4.2 Directional Couplers

In general, a *coupler* is a device that taps off some fraction of the power flowing through a primary waveguide or transmission line into a secondary waveguide or line. The ratio of the primary input power to the power diverted to the secondary output is called the coupling factor, or simply the coupling, usually expressed in dB. For example, in a 20-dB coupler, 1/100 of the input power appears at the secondary output. In some radar applications, such as tapping off a portion of the transmitter power for measurement or monitoring or as a reference signal for the receiver, only weak coupling is needed. Couplers that are of particular interest in monopulse, however, have a coupling factor of 2 and are called 3-dB couplers. In 3-dB couplers the primary and secondary outputs are equal in power.

A coupler has three or more ports—two for the primary path and one or more for secondary paths. The couplers used in monopulse have four ports.

A *directional coupler* is one that produces an output at a given secondary port when power flows through the primary port in one direction and not in the other. A four-port directional coupler produces an output at one or the other of the two secondary ports, depending on the direction of power flow in the primary path.

A typical design of a directional coupler is shown in simplified form in Figure 4.14. It consists of contiguous primary and secondary waveguides with holes or slots in the common wall, causing a portion of the power to pass from one waveguide to the other. In the device illustrated, there are two holes spaced a quarter wavelength apart. An input at port 1 provides an output at port 3 having the power of the input minus the power diverted to the secondary (lower) waveguide. Each hole launches a pair of waves in the secondary waveguide, one traveling to the right and the other to the left. The waves from the two holes reinforce toward the right, producing an output at 4, but because of the quarter-wavelength separation (traversed twice by one of the waves) they cancel toward the left, producing zero output at 2. An input in the reverse direction at port 3 produces outputs at 1 and 2 but not at 4.

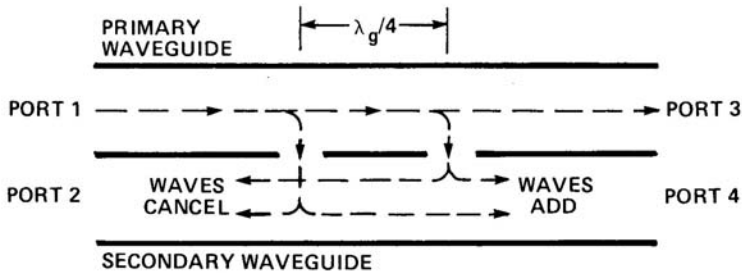


Figure 4.14 Two-hole directional coupler.

A type of coupler of particular importance in monopulse (and also in other radar applications) is the *3-dB directional coupler*. Referring again to Figure 4.14, an input at port 1 splits equally in power, half appearing at port 3 and half at port 4, with no output at port 2. By symmetry, primary and secondary waveguides are interchangeable, as are the input and output ports. The 3-dB directional coupler therefore has the same functional characteristics as a hybrid junction, and is usually regarded as a subset of the latter.

A four-port directional coupler of any coupling factor has the following inherent phase characteristic when all the ports have matched terminations: If an input is applied to one port, the two outputs are in phase quadrature with each other. Thus, in a 3-dB directional coupler if input voltage v_1 is applied at port 1, the outputs at ports 3 and 4 are $v_1/\sqrt{2}$ and $\pm jv_1/\sqrt{2}$, respectively (ignoring a propagation phase delay common to both, which does not affect their relative phase). The reason for the plus-or-minus sign is that the secondary output may either lead or lag the primary output by 90° , depending on the coupler construction [15, 17]. In a side-wall coupler, the common wall in which the holes are placed is the narrow wall of the waveguides; in this type the secondary output lags

by 90° . In a top-wall coupler the common wall is the broad one; here the secondary output leads by 90° . (The phase lead may be regarded as a combination of a 90° phase lag and a reversal of the E-field vector on passing through the opening between the two guides.) In monopulse, either or both types of coupler may be used. The choice is governed largely by which type lends itself better to a compact design of the microwave assembly.

If inputs v_1 and v_2 are applied simultaneously to ports 1 and 2, the outputs of ports 3 and 4 are

$$v_3 = (v_1 \pm jv_2)/\sqrt{2} \quad (4.4)$$

$$v_4 = (\pm jv_1 + v_2)/\sqrt{2} \quad (4.5)$$

The same sign (plus or minus) of the quadrature terms applies to both equations.

If it is desired to obtain the sum and difference of v_1 and v_2 , the phase of one of them must be shifted 90° before the input. Suppose v_2 is delayed 90° by a phase shifter preceding the input. Then the output to port 2 of the coupler is

$$v_2' = -jv_2 \quad (4.6)$$

Taking the positive sign in (4.4) and (4.5), we obtain modified outputs:

$$v_3' = (v_1 + jv_2')/\sqrt{2} = (v_1 + v_2)/\sqrt{2} \quad (4.7)$$

$$v_4' = (+jv_1 + v_2')/\sqrt{2} = j(v_1 - v_2)/\sqrt{2} \quad (4.8)$$

These outputs are proportional to the sum and difference but they are in phase quadrature. Depending on the further combining or processing that is to be done, these outputs may be used as they are or one of them may be phase shifted by 90° to bring them into phase alignment.

Because of this phase characteristic, this device is sometimes called a *quadrature phase coupler*, *90° coupler*, *quadrature hybrid*, or *90° hybrid*.

As in the other devices described in the preceding sections, there is a phase delay due to propagation of the wave through the coupler, over and above the phases that appear in (4.7) and (4.8), but since this delay does not affect the relative phase of the two outputs, it can be ignored for our purpose.

Because the behavior of this device depends on the size and spacing of the holes, it is frequency-sensitive. By using more than two holes, or by using slots instead of holes, the frequency-sensitivity can be reduced and the device can be designed to work over a useful frequency band.

4.4.3 Comparators

Any one of the devices described in the preceding sections, which we will lump under the general name of hybrids, can be used to obtain the sum and difference of two inputs. In a lens or reflector antenna designed for monopulse in both angular coordinates there are at least four feed horns.⁴ A sum and two differences (one for each coordinate) must be obtained, and this cannot be done with a single hybrid. Several hybrids in tandem and in parallel are required. The whole assemblage of hybrids, phase shifters (if needed), and waveguide sections that convert signals from the individual feed horns into a sum and two differences is called a *comparator*. The comparator does not really compare anything, but it provides means for indirect comparison of the signal from the individual feed horns.

Figure 4.15 is a schematic diagram of an illustrative comparator of a monopulse tracking radar with a four-horn feed. The horns, labeled A to D, are arranged as shown at top center. (The lower horns produce the upper beams illustrated in Figure 1.3 and the upper horns produce the lower beams.) The four input lines labeled A to D at the left are the signals obtained from the corresponding horns. Four hybrids are used. The details of the interconnections may differ from one radar to another but the general arrangement is usually similar to that shown in the figure.

The ports of each hybrid in Figure 4.15 are labeled 1 to 4 corresponding to those in Figure 4.14. The hybrids in this example are 3-dB directional couplers (quadrature hybrids), which produce outputs $v_3 = v_1 + jv_2$ and $v_4 = jv_1 + v_2$ when the inputs are v_1 and v_2 .

In order to obtain sums and differences from hybrids 1 and 2 it is necessary to shift one of the inputs by 90° , as mentioned in the preceding section. The phase shifts shown in the lines B and C may be obtained by phase shifters or by differential line lengths. All electrical lengths of waveguides at corresponding points in the various paths are equal except where a quarter-wavelength difference is deliberately used to obtain the phase shifts shown in lines B and C.

The outputs of the comparator are shown at the right. They are the sum, the traverse difference, and the elevation difference, and a fourth output proportional to $[(A - B) - (C - D)]$, sometimes called the “double difference,” the “second difference,” or the “quadrupolar signal.” By rearranging the terms in the form $[(A + D) - (B + C)]$, this signal can be viewed as the difference between the two diagonal sums, and it will therefore be referred to as the “*diagonal difference*.” This output is normally unused and is terminated in a matched dummy load. It will be discussed further in Section 15.2.

⁴ It is possible to get two-coordinate monopulse with only three feed horns, but this is not normally a practical design.

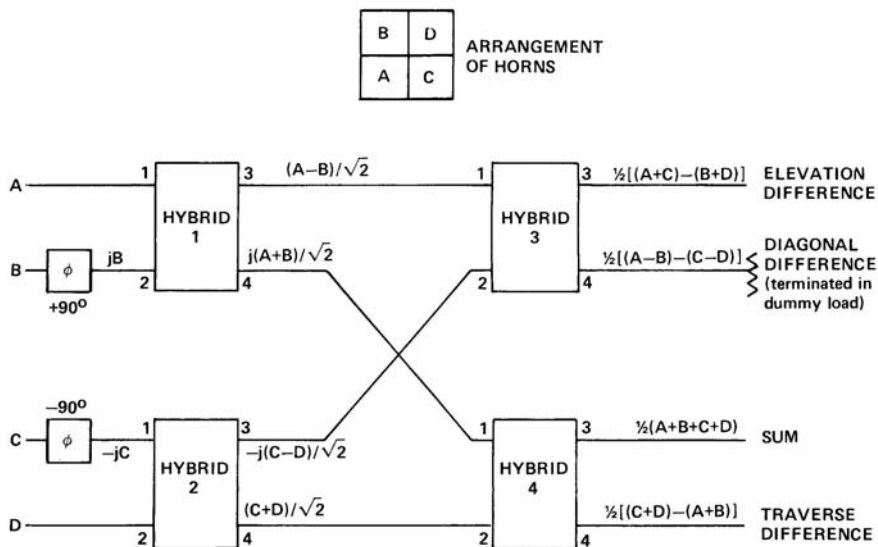


Figure 4.15 Comparator for four-horn monopulse feed using quadrature hybrids.

The outputs shown in Figure 4.15 assume lossless components. Small losses are present in the physical devices and should be taken into account in the gain and loss budget. If the components were perfectly lossless, the total output power would equal the total input power, as can be verified by squaring and adding the input voltages and squaring and adding the output voltages. The special case of four equal inputs (target on the boresight axis) is easy to check. Call the input voltage at each port v . Then

$$A = B = C = D = v \quad (4.9)$$

The total input power is

$$A^2 + B^2 + C^2 + D^2 = 4v^2 \quad (4.10)$$

In this case all the outputs are zero except the sum, whose power is

$$\frac{1}{4}(A + B + C + D)^2 = \frac{1}{4}(4v)^2 = 4v^2 \quad (4.11)$$

In actual designs the hybrids comprising the comparator are placed close together and the comparator is placed close to the feed horns to form a single com-

pact assembly. Compactness is important for two reasons: to minimize blockage when the feed assembly is in front of the reflector, and to make the waveguide lengths short in order to minimize phase differences in the different paths due to inability to match the path lengths exactly. In addition, light weight is desirable in order to minimize mechanical deflection of the feed assembly due to gravity or acceleration.

4.4.4 Other Methods of Obtaining Monopulse Sum (or Reference) and Differences

The comparator described in the preceding section is for a four-horn feed. Some monopulse radars have a five-horn feed, and other feed arrangements have been designed with as many as twelve horns. With four horns it is possible, by proper design and placement of the horns, to optimize either the sum pattern or the difference patterns but not both, since they are interdependent. With more horns there is greater independence and it is possible to achieve more nearly optimum sum and difference patterns simultaneously. Optimum patterns are those that represent the best compromise (for a particular system) among sum-pattern gain and beamwidth, monopulse sensitivity, and sidelobe levels.

A simplified sketch of a five-horn feed was shown in Figure 4.11. The traverse difference is obtained from the left and right horns, A and B, and the elevation difference is obtained from the top and bottom horns, C and D. The comparator contains only two hybrid junctions, one for each difference signal. The center horn R produces the transmitted beam and also provides the reference signal for monopulse reception. The reference pattern has the same general shape as the sum pattern in a four-horn monopulse and the reference signal is used in the same way as the sum signal. Because of this analogy, a receiver or processor channel carrying the reference signal is often identified by the same symbol Σ that is used for a sum channel.

An experimental twelve-horn feed, designed by MIT Lincoln Laboratory, gave a closer approximation of ideal sum and difference patterns but required a complicated comparator with numerous hybrids (Chapter 21 of [10]). At the other extreme, monopulse patterns can be obtained from a multimode feed with a single horn by using symmetrical (even) waveguide modes to produce the “sum” signal and antisymmetrical (odd) modes to produce the “difference” signals [18, 19]. The sum and differences require no addition or subtraction and therefore no hybrids of the types described previously. However, since they are carried by different modes in the same waveguide, special microwave circuits are needed to extract them as separate inputs to their respective receiver channels.

In the discussion so far, it has been tacitly assumed that only a single linear polarization is used. If dual linear polarization is required, microwave devices (e.g., certain forms of the magic-T) are used to separate the two polarizations. The comparator for forming the sum and differences is the same as for a single polari-

zation. If only one polarization at a time is needed, a switch is used to select the signals of the desired polarization as inputs to the comparator. If both polarizations are to be used simultaneously, two comparators are needed. However, if the two linear polarizations are combined at RF to form right or left circular, but not both simultaneously, a single comparator suffices.

In array antennas different methods are used to obtain the sum and the differences. In some cases the array is divided into four quadrants, in each of which the elements are summed to form a single output from each quadrant. The outputs of the four quadrants correspond to the outputs of the four feed horns in a lens or reflector phase-comparison antenna. Most arrays, however, are not designed in this way; there are no available outputs of component beams corresponding to those in a space-feed-type antenna. These issues will be discussed further in Chapter 7.

4.4.5 Graphical Symbols

In Figure 4.15 rectangular boxes labeled Hybrid 1, Hybrid 2, and so forth were used to identify the hybrid junctions. It is more customary, however, to use graphical symbols for various types of hybrids [20, 21]. Some of the more common symbols used in monopulse circuit diagrams are shown next. They are subject to minor variations by different users. Most of the symbols bear some resemblance to the devices they represent. In some technical literature the symbols are used more or less interchangeably, the choice being based on convenience of drawing or simply user preference, on the grounds that all of the devices are functionally equivalent. The preferred practice, however, is to use the appropriate symbol if the specific type of hybrid junction is known. If it is not desired to specify a particular type of hybrid junction, a simple box with an appropriate label, such as “3-dB hybrid” or simply “hybrid,” may be used.

In the symbol drawings given below, the input labels v_1 and v_2 are not part of the symbol but have been added to aid in identifying the input ports and relating them to those shown in Figures 4.11 to 4.13. The output ports are usually marked Σ for sum and Δ for difference, with appropriate subscripts if needed. In these drawings, letters Σ and Δ are used only to identify the output ports or channels, not the signal voltages, which are represented by the letters s and d .

Two versions of the symbol for a magic-T hybrid are shown in Figure 4.16. The three-dimensional version has a rough resemblance to the device itself as shown in Figure 4.11, with inputs entering the two in-line waveguides (shown lying in a horizontal plane), the sum emerging from the horizontal output waveguide, and the difference emerging from the vertical waveguide. The actual physical connections need not conform to this stylized symbol. The connections may be interchanged in various ways, and the magic-T structure may be modified so that it has a different shape while continuing to behave in the same way.

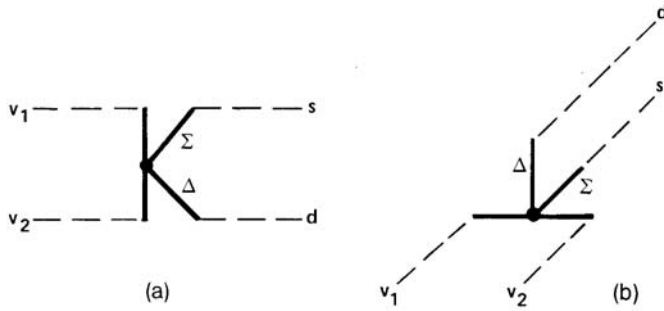


Figure 4.16 Magic-T symbols: (a) flat version; and (b) three-dimensional version. (Dashed lines added to show input and output connections.)

The three-dimensional version of the magic-T symbol can aid in visualizing interconnections of multiple hybrids. Figure 4.17 represents the same comparator

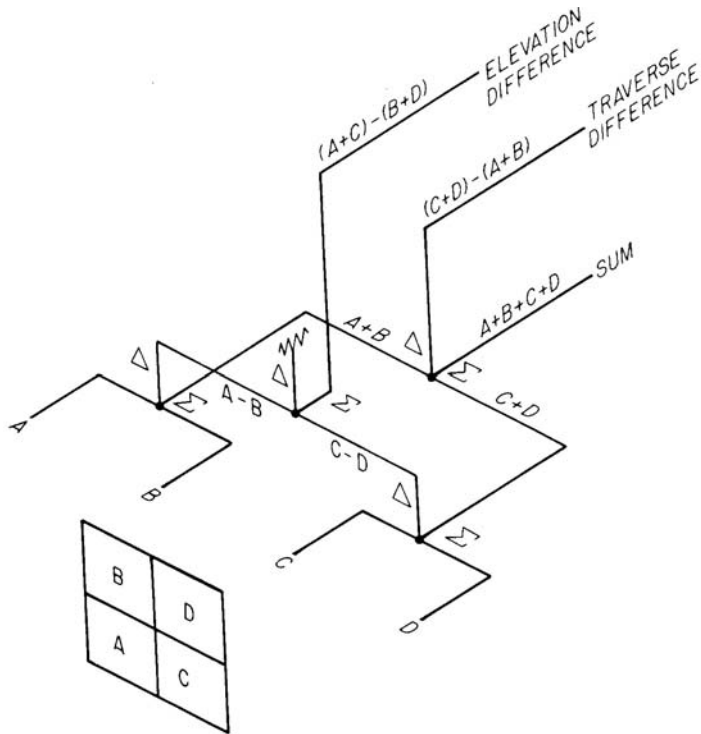


Figure 4.17 Comparator for four-horn monopulse feed using magic-T hybrids (factors of $1/\sqrt{2}$ and $1/2$ omitted).

network as in Figure 4.15 with the 90° hybrids replaced by magic-T hybrids.⁵ The 90° phase shifts in lines B and C are not needed with the magic-T.

Figure 4.18 is a symbol for a hybrid ring junction. The symbol may be rotated to any orientation and ports may be interchanged in various ways. However, input and output ports must alternate, and the Σ port must always be the one midway between the two input ports.

Figure 4.19 shows the usual symbol for a 3-dB directional coupler (quadrature hybrid), sometimes drawn with arrowheads at both ends of the two diagonals. When the two input voltages are in quadrature phase, the outputs will be sum and difference, also in quadrature phase. The positive or negative sign depends on the particular design, as explained previously.

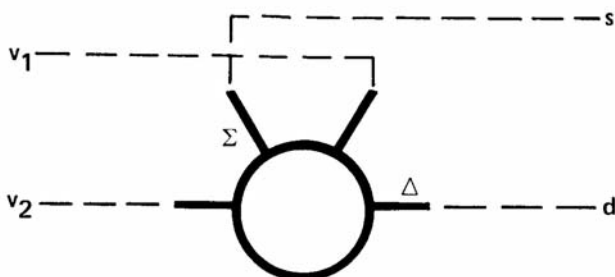


Figure 4.18 Symbol for hybrid ring junction (dashed lines are added to show input and output connections). Letter symbols same as for magic-T.

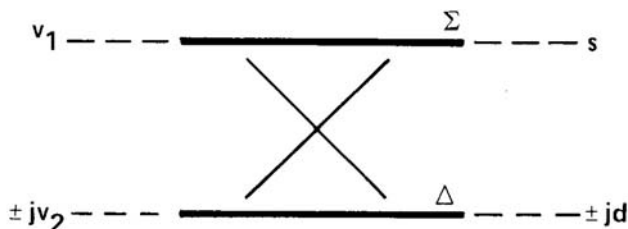


Figure 4.19 Symbol for 3-dB directional coupler (dashed lines added to show input and output connections). Letter symbols same as for magic-T.

4.5 RECEIVERS

In the receivers of the sum and difference channels, the radio frequency (RF) voltages from the microwave combining network are converted to intermediate fre-

⁵ The factors of $1/\sqrt{2}$ and $1/2$ are omitted from Figure 4.17 to avoid crowding.

quency (IF) by mixing with the output of a local oscillator, then amplified and filtered at IF. The filter is matched to the radar pulse. This means that ideally the filter transfer function is the complex conjugate of the pulse voltage spectrum. In practice this characteristic is approximated, so that the filter bandwidth is roughly equal to the reciprocal of the duration of the transmitted pulse (if simple pulses are used) or of the compressed pulse (if coded pulses are used).

Because the sum and differences have been formed by stable passive devices preceding the receivers, the boresight direction is more stable than if the sum and differences were formed after the receivers. A null difference signal at the input to a receiver produces a null output even if the receiver gain or phase drifts. However, a null is never perfect; because of imperfections in the RF devices the difference has a residual voltage in quadrature phase with the sum. This residual voltage, when combined with phase imbalance between sum and difference receivers, causes an angle error. Furthermore, when off-axis angle measurements are made, amplitude imbalance in the receiver channels produces an angle error that increases with angle off axis. Hence, although the RF sum-and-difference approach is less susceptible to receiver-drift errors than if sum and difference were formed after the receivers, it is not totally immune. For precise angle tracking or measurement, it is important that the three receiver channels *track* one another in gain and phase. By tracking, we mean that once the gains and phases have been equalized, they must remain equal (within tolerable limits) with the passage of time until the next calibration, and over an adequate range of input levels, temperatures, and frequency within the tuning band of the radar.

Some monopulse radars use pilot pulses, injected at the front end of the receivers, to maintain the amplitude and phase matching. Disparities among the three receivers are automatically detected and corrected by adjustable attenuators and phase shifters or in the computation of the monopulse output if done by computer.

In some monopulse radars the receivers must maintain their performance over a very wide dynamic range of signal levels. This requirement and means for meeting it are discussed in Chapter 8.

References

- [1] W. M. Cady, M. B. Karelitz, and L. A. Turner, (eds.), *Radar Scanners and Radomes*, Vol. 26 of MIT Radiation Laboratory Series, New York: McGraw-Hill, 1948. Reprint, CD-ROM edition, Norwood, MA: Artech House, 1999 (see Figure 4.1, p. 106).
- [2] J. R. Risser, "Dielectric and Metal-Plate Lenses," Chapter 11 of *Microwave Antenna Theory and Design*, S. Silver, (ed.), Vol. 12 of MIT Radiation Laboratory Series, New York: McGraw-Hill, 1947. Reprint, CD-ROM edition, Norwood, MA: Artech House, 1999.
- [3] M. I. Skolnik, *Introduction to Radar Systems*, 3rd ed., New York: McGraw-Hill, 2001 (see p. 664).
- [4] W. E. Kock, "Metal-Lens Antennas," *Proc. IRE*, Vol. 34, No. 11, November 1946, pp. 828–836.

- [5] W. E. Kock, "Path-Length Microwave Antennas," *Proc. IRE*, Vol. 37, August 1949, pp. 852–855.
- [6] J. H. Dunn, D. D. Howard, and K. B. Pendleton, "Tracking Radar," Chapter 21 of *Radar Handbook*, M. I. Skolnik, (editor-in-chief), New York: McGraw-Hill, 1970 (see Figures 12 and 13).
- [7] C. G. Montgomery, R. H. Dicke, and E. M. Purcell (eds.), *Principles of Microwave Circuits*, Vol. 8 of MIT Radiation Laboratory Series, New York: McGraw-Hill, 1948. Reprint, CD-ROM edition, Norwood, MA: Artech House, 1999.
- [8] N. Marcuvitz, (ed.), *Waveguide Handbook*, Vol. 10 of MIT Radiation Laboratory Series, New York: McGraw-Hill, 1951. Reprint, CD-ROM edition, Norwood, MA: Artech House, 1999.
- [9] P. A. Matthews and I. M. Stephenson, *Microwave Components*, London: Chapman and Hall, 1968.
- [10] M. I. Skolnik, (editor-in-chief), *Radar Handbook*, Chapter 8 by G. P. Kefalas and J. C. Wiltse and Chapter 21 by J. H. Dunn, D. D. Howard, and K. B. Pendleton, New York: McGraw-Hill, 1970.
- [11] J. A. Staniforth, *Microwave Transmission*, New York: John Wiley & Sons, 1972.
- [12] H. E. Thomas, *Handbook of Microwave Techniques and Equipment*, Englewood Cliffs, NJ: Prentice-Hall, 1972.
- [13] T. Laverghetta, *Microwave Measurement and Techniques*, Dedham, MA: Artech House, 1976.
- [14] IEEE Standard 100, *The Authoritative Dictionary of IEEE Standards Terms*, 7th ed., New York: IEEE Press, 2000, (see pp. 526–527, 315).
- [15] *Microwave Associates Cast Components* (booklet), Burlington, MA: Microwave Associates, 1978.
- [16] S. Y. Liao, *Microwave Devices and Circuits*, Englewood Cliffs, NJ: Prentice-Hall, 1980.
- [17] H. E. Schrank and C. H. Grauling, Jr., "Phase Relationships in Short-Slot Hybrid Couplers," *Proc. IRE*, Vol. 47, No. 11, November 1959, p. 2017.
- [18] D. D. Howard, "Single Aperture Monopulse Radar Multi-Mode Antenna Feed and Homing Device," *1964 IEEE International Conv. Military Electronics, Conf. Proc.*, September 14–16, 1964, pp. 259–263.
- [19] P. Mikulich, R. Dolusic, C. Profera, and L. Yorinks, "High Gain Cassegrain Monopulse Antenna," *IEEE G-AP International Antenna and Propagation Symp. Record*, September 1968, pp. 375–382.
- [20] IEEE Standard 315-1975, "Graphic Symbols for Electrical and Electronics Diagrams," New York: The Institute of Electrical and Electronics Engineers, 1975 (also identified as American National Standard ANSI Y32.2-1975).
- [21] *Microwave Symbols and Definitions*, (booklet) Burlington, MA: Microwave Associates, 1978.

Chapter 5

Amplitude-Comparison and Phase-Comparison Classification

In the early days of monopulse radar the terms amplitude comparison and phase comparison provided a clear, useful distinction between two basic classes of monopulse, differing unmistakably in principle of operation and in the physical construction of the antenna. However, with the increased variety and sophistication of modern radars, it is not always obvious whether a particular radar should be classified as amplitude comparison or phase comparison, or even if those terms retain significance in describing the radar. With minor exceptions,¹ monopulse radars designed since 1960 have used microwave comparators to form sum and difference patterns s and d , and subsequent circuits form a *normalized difference signal* d/s , regardless of the antenna configuration and the relative phase of the d and s voltages produced by the antenna. The important characteristics of the antennas are the sum-channel gain and beamwidth, the difference-channel slope at the axis, and the sidelobe structure of the two patterns.

This chapter gives the IEEE definitions of amplitude- and phase-comparison monopulse, and examples of reflector antennas in which the distinction is obvious. It is shown that the two classes are essentially equivalent in theory but differ in design and in practical performance. Both types are compared with the optimum monopulse antenna characteristics derived in 1952 by Kirkpatrick [1, 2], with respect to sum-channel gain, difference slope, and sidelobe levels. This comparison shows why the amplitude-comparison monopulse approach has predominated in tracking radar. The discussion here, concentrated on reflector or lens antennas, will be extended to array antennas in Chapter 7.

¹ The notable exception is the stacked-beam 3-D surveillance radar, in which elevation estimates are made by direct comparison of signal amplitudes in adjacent beams.

5.1 DEFINITIONS AND EXAMPLES

5.1.1 Definitions

The *Authoritative Dictionary of IEEE Standards Terms* [3] gives the following definitions:

Amplitude-comparison monopulse.

A form of monopulse in which the angular deviation of the target from the antenna axis is measured as the amplitude ratio of the target as received by two antenna patterns. The patterns may be a pair of beams displaced on opposite sides of the antenna axis or a difference-channel beam having odd symmetry about the axis and a sum beam having even symmetry. In the latter case the ratio may have positive and negative values (0° or 180° phase shift, or in some cases $+90^\circ$ and -90°). Distinguished from phase-comparison monopulse, in which the relative phase of the two patterns carries the information on target displacement.

Phase-comparison monopulse.

A form of monopulse employing receiving beams with different phase centers, as obtained, for example, from side-by-side antennas or separate portions of an array.

Note: The information on target displacement from the antenna axis appears as a relative phase between the signals received at the two phase centers.

Note that amplitude-comparison monopulse is defined as using either a pair of beams squinted to each side of the axis or a pair with even and odd symmetry about the axis, while phase-comparison monopulse is defined in terms of separate aperture regions with different phase centers. The term “phase center” used in differentiating between the two classes of monopulse requires further explanation, which will be given in Section 5.2. We can then examine the distinction between the two classes more comprehensively.

5.1.2 Interpretation

The names *amplitude comparison* and *phase comparison*, although appropriate in the early days of monopulse, are no longer truly descriptive, and are not to be interpreted literally. Modern monopulse radars actually do not measure the amplitudes and phases of the radar returns in individual beams (that is, the outputs of the individual feed horns) and then compare them. First of all, as already explained, the individual beam outputs may not be readily accessible for measurement. In fact, some types of antennas, such as reflectors with single, multimode feed horns, and many arrays, do not produce voltages associated with the individual component beams, but form “sum” and “difference” voltages directly.

Even when the component beam outputs are available, they would have to be connected to individual receivers for frequency conversion, filtering, and amplification before amplitude or phase measurements could be made. Near the boresight axis (usually the region of primary interest) the amplitudes and phases would be

nearly equal and angle information would reside in differences that are small compared to the individual measurements. Mismatches or drifts in the gains or phase shifts of the individual receiver channels would cause serious errors in the boresight and in the angle estimation in general, as was learned in early monopulse development.

Therefore, the usual practice in both amplitude- and phase-comparison monopulse is to do the comparison in an indirect manner, which consists of forming differences (one for each angular coordinate) at RF by means of stable passive devices known as *comparators* (Section 4.4), before any active devices have acted on the signals. The comparator is generally placed as close as possible to the feed horns in a single, compact assembly, in order to minimize variations or distortions due to long transmission lines. Thus the use of the difference voltages instead of the individual beam voltages produces a null that remains much more stable in direction (the boresight direction) than if the differencing were done after the receivers, because a null input to a receiver produces a null output even if the receiver drifts.

In addition to a difference voltage for each of the two angular coordinates, the comparator produces a sum voltage (obtained by summing the outputs of the two component beams, when these are formed in the antenna). The function of the sum voltage (besides detection and range measurement) is to *normalize* the difference voltage. Normalization means forming the ratio (Chapter 3) of the difference to the sum in order that the monopulse output be a function only of target angle, not of the strength of the echo.

After the sum and difference voltages are amplified by the receivers, they become the inputs to the monopulse processor (Chapter 8), which produces the normalized monopulse output (often called the error signal) that indicates target angle from the boresight axis. Although the formation of sum and difference voltages before the receivers greatly reduces boresight shift, mismatch or drifts in the receiver will still cause errors on off-axis angle measurements. Therefore, to maintain constant tracking-loop gain or to make accurate off-axis measurements, care must be taken in maintaining a good match in both gain and phase of receivers.

Confusion in describing the type of monopulse can be avoided by adhering to the convention that the names amplitude comparison and phase comparison pertain only to the nature of the antenna patterns, regardless of whether the processing that follows involves amplitude or phase measurements or both. Even with this convention, confusion in terminology can arise because the use of certain RF devices makes it possible to transform one class into what appears to be the equivalent of the other [4]. As pointed out in Section 2.3, the patterns of an antenna are not unique; they depend on the point in the system at which they are measured. However, the two classes can still be defined unambiguously. In array antennas with constrained feeds the distinction is not important because any given set of sum and difference patterns (within the physical limitations of the antenna) can be produced by either class of monopulse, whereas in space-fed antennas

there is a significant difference between sum patterns obtainable from the two classes.

The analysis and descriptions that follow apply to single-coordinate monopulse or to either angular coordinate in two-coordinate monopulse. The off-axis angle coordinate is denoted by θ , which is replaced by A for azimuth or E for elevation. The aperture coordinate x and width w , applying to azimuth, are replaced by y and height h for elevation.

5.1.3 Optimum Monopulse

In an early analysis of monopulse antenna design and performance, Kirkpatrick [1] developed the theory of the optimum monopulse antenna, defined as one that would produce the highest possible accuracy in an environment where thermal noise was the only factor interfering with target measurement. This theory is summarized here to provide a background against which to describe amplitude- and phase-comparison monopulse antennas.

Kirkpatrick described first a number of methods by which an even (sum) and an odd (difference) pattern could be obtained and processed for angular measurement of targets. He noted that there was a well established result [5, p. 177] that the maximum gain G_0 obtainable for a given aperture area results from applying a uniform illumination function g_0 over that area:

$$g_0(x, y) = 1, \quad |x| \leq w/2, \quad |y| \leq h/2 \quad (5.1)$$

where w and h are the width and height of the aperture, and x and y are the corresponding aperture coordinates. This choice gives an optimum sum power gain

$$\begin{aligned} G_0 &= \frac{4\pi wh}{\lambda^2} \quad \text{for a rectangular aperture} \\ &= \left(\frac{\pi D}{\lambda} \right)^2 \quad \text{for a circular aperture} \end{aligned} \quad (5.2)$$

where λ is the wavelength and D is the diameter of a circular aperture. For an elliptical aperture, the product wh of the two axes replaces D^2 in (5.2). Kirkpatrick noted the absence of a criterion in the literature to evaluate odd patterns. He chose to use the voltage slope of the odd far field, on the beam axis, as the figure of merit of the direction-finding properties of the antenna. The normalized azimuth difference illumination function then takes the form

$$g_{d0}(x) = 2\sqrt{3}x, \quad |x| \leq w/2; \quad g_{d0}(y) = 1, \quad |y| \leq h/2 \quad (5.3)$$

where the constant in $g_{d0}(x)$ results in unity total illumination power on the aperture. In the elevation plane, h and y replace w and x in (5.3). It should be noted that this relationship for the difference illumination does not specify the relative phase of g_0 and g_{d0} , which can be in-phase or in quadrature.

The pattern voltage corresponding to uniform illumination g_0 can be calculated using (2.1), rewritten here for the sum azimuth pattern as

$$s(u) = \int_{-0.5}^{0.5} g_0(x) \exp(j2\pi xu) dx \quad (5.4)$$

where the angle $u = (w/\lambda) \sin \theta$ and θ is azimuth angle from the axis. In elevation the same expression is used with h and y replacing w and x , and θ representing elevation. The closed form for this pattern can also be found in standard antenna texts as

$$s(u) = \text{sinc}(u) \equiv \frac{\sin u}{u} \quad (5.5)$$

The optimum difference pattern $d(u)$ is found by replacing $g_0(x)$ with $g_{d0}(x)$ in (5.4). The optimum sum and difference illumination functions for a rectangular aperture are shown in Figure 5.1(a), plotted with respect to an aperture coordinate normalized to the width (or height) of the aperture. The corresponding antenna patterns are shown in Figure 5.1(b), plotted as a function of a normalized angle $\theta' = \theta/\theta_{bw}$ normalized to sum beamwidth θ_{bw} . The difference pattern resulting from (5.4) is in phase with the sum pattern, assuming that a hybrid comparator without phase shift (e.g., a magic-T) is used to form the s and d beams from the in-phase individual beams formed from the aperture.

Kirkpatrick's choice of difference slope as the performance measure for direction finding was used by Hannan [6], who normalized the slope to the optimum sum voltage gain, defining a *relative difference slope* as

$$K \equiv \frac{1}{\sqrt{G_0}} \left. \frac{d}{du} d(u) \right|_{u=0} \quad \text{normalized volts per } (w/\lambda) \times \text{radian} \quad (5.6)$$

Here the difference (odd) pattern is denoted by $d(u)$. The word *relative* refers to the normalization to ideal sum voltage gain. Skolnik [7], Barton [8], and others adopted K as an important measure of monopulse antenna performance.²

² Kirkpatrick's slope is defined using a derivative with respect to a normalized angle $\alpha = 2\pi(w/\lambda)\theta = 2\pi u$, and is not normalized to sum-channel voltage gain. Taking into account the angle u and gain normalization, his expressions agree with (5.6).

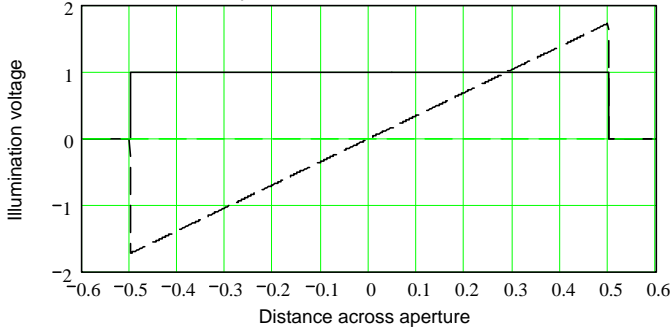
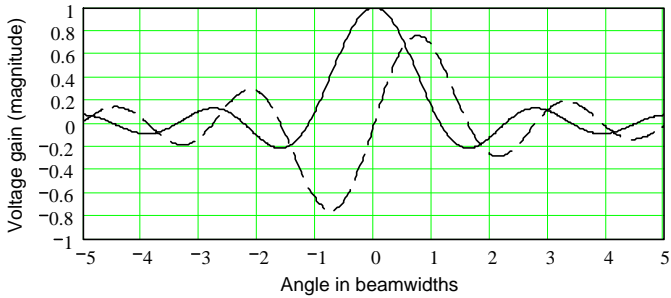
(a) Sum and difference illumination functions $g_0(x)$ and $jg_{d0}(x)$ (b) Sum and difference antenna patterns $s(\theta')$ and $d(\theta')$

Figure 5.1 (a,b) Sum and difference illumination functions and patterns of optimum rectangular monopulse antenna. Plotted pattern voltages are normalized to the peak sum-channel voltage gain, and angle is normalized to the half-power beamwidth θ_{bw} of the sum pattern.

The relative slope K , expressed in normalized volts per $(w/\lambda) \times$ radian, is an absolute measure of the monopulse antenna sensitivity to deviations of the target from the axis, and its evaluation requires knowledge of the aperture dimensions, the wavelength, and the illumination functions or antenna patterns. For the optimum difference illumination function $g_{d0}(x)$ in the horizontal plane, the relative difference slope is given by

$$\begin{aligned}
 K_0 &= \frac{\pi w}{\sqrt{3}\lambda} = 1.814 \frac{w}{\lambda} \quad \text{for a rectangular aperture} \\
 &= \frac{\pi D}{2\lambda} = 1.571 \frac{D}{\lambda} \quad \text{for a circular aperture}
 \end{aligned} \tag{5.7}$$

For an elliptical aperture, the horizontal axis w will replace D in (5.7). In the vertical plane, (5.7) applies with the aperture height h replacing the width w .

The *difference slope ratio* describes the antenna performance relative to that of the optimum monopulse antenna of the same dimensions. It is defined [6] as

$$K_r \equiv \frac{K}{K_0} \quad (5.8)$$

A further normalization to the actual sum-channel beamwidth θ_3 and gain G_m [8, p. 274] results in the *normalized monopulse slope*, defined as

$$k_m \equiv \frac{\theta_{bw}}{\sqrt{G_m}} \frac{d}{d\theta'} d(\theta') \bigg|_{\theta'=0} = \frac{\theta_{bw}}{\sqrt{\eta_a}} K \quad \text{normalized volts per beamwidth} \quad (5.9)$$

where η_a is the aperture efficiency and $\theta' = \theta/\theta_3$ is the angle measured in beamwidths rather than in (w/λ) radians. For the optimum antenna, we find:

Efficiency η_a :	1.000
Beamwidth θ_{bw} :	$0.886\lambda/w$
Monopulse slope k_m :	1.606

The normalized monopulse slope k_m can be evaluated from measured antenna patterns even when parameters such as illumination function, aperture shape and dimensions, and wavelength are not known. It is more convenient than K for use in expressions for tracking error, as will be found in Chapter 10.

The sidelobe levels of the optimum monopulse antenna, shown in decibel form over an extended angular region in Figure 5.2, have maximum values of -13.3 dB for the sum channel and -10.7 dB for the difference channel. The sidelobe levels remain above -30 dB even beyond ± 10 beamwidths from the axis, and are excessive for a practical radar operating in a realistic environment containing clutter or jamming.

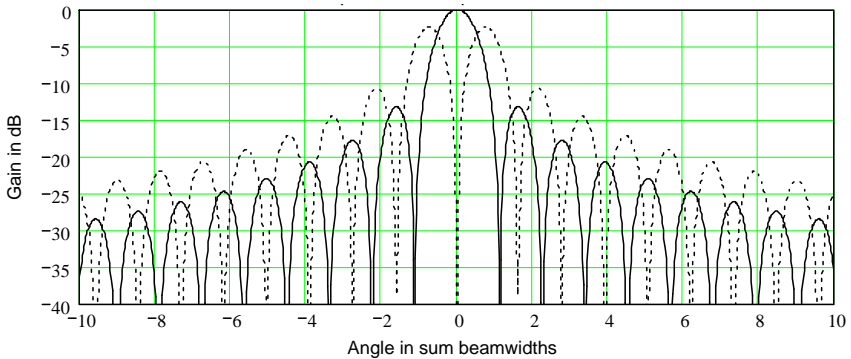


Figure 5.2 Patterns of optimum rectangular monopulse antenna on decibel scale.

Although unsuitable for practical use, and unfeasible with space-fed antennas, the characteristics of the optimum monopulse antenna are useful as a reference in evaluating practical antenna designs, which may be compared to the optimum as a measure of performance. Kirkpatrick presented plots of the patterns and tables of relative slopes K for a number of difference illumination functions. In practice, the need to reduce sidelobes and the physical limitations of horn illumination functions for reflector and lens antennas dictate departures from the optimum illumination functions shown in Figure 5.1(a). This will be shown in the next sections for examples of amplitude- and phase-comparison monopulse.

5.1.4 Amplitude-Comparison Monopulse Antenna Example

With Kirkpatrick's theory as a background, we can now evaluate an example of the conventional amplitude-comparison monopulse radar using a horn-fed reflector. Many radars such as the AN/FPS-16, illustrated in Figures 4.1 and 4.2, have antenna patterns similar to those produced by a rectangular aperture with illumination functions for the azimuth sum and difference channels given by

$$g(x) = \sqrt{2} \cos(\pi x), \quad |x| \leq 0.5, \text{ sum channel} \quad (5.10)$$

$$g_d(x) = -j7.8239x \cos x, \quad |x| \leq 0.5, \text{ difference channel} \quad (5.11)$$

The constants in these equations result in unity illumination power on the aperture, and the factor $-j$ in g_d places the difference voltage pattern d in-phase with s , with positive on-axis slope. These functions and the resulting antenna patterns are shown in Figure 5.3. The illumination functions represent those of an optimum rectangular monopulse antenna to which a cosine taper has been applied in both sum and difference channels for sidelobe reduction. The cosine taper is also assumed to be applied to the orthogonal angle coordinate. As with the optimum monopulse, the difference pattern is the negative of the first derivative of the sum pattern, and is in-phase with the sum pattern.

The application of cosine taper reduces the antenna performance relative to that of the optimum antenna (Table 5.1).

Table 5.1 Comparison of Optimum and Cosine Tapered Apertures

<i>Parameter</i>	<i>Optimum Taper</i>	<i>Cosine Taper</i>
Aperture efficiency η_a	1.000	0.657
Beamwidth θ_{bw}	$0.886 \lambda/w$	$1.189 \lambda/w$
Difference slope K	1.814	1.334
Difference slope ratio K_r	1.000	0.736
Monopulse slope k_m	1.606	1.957

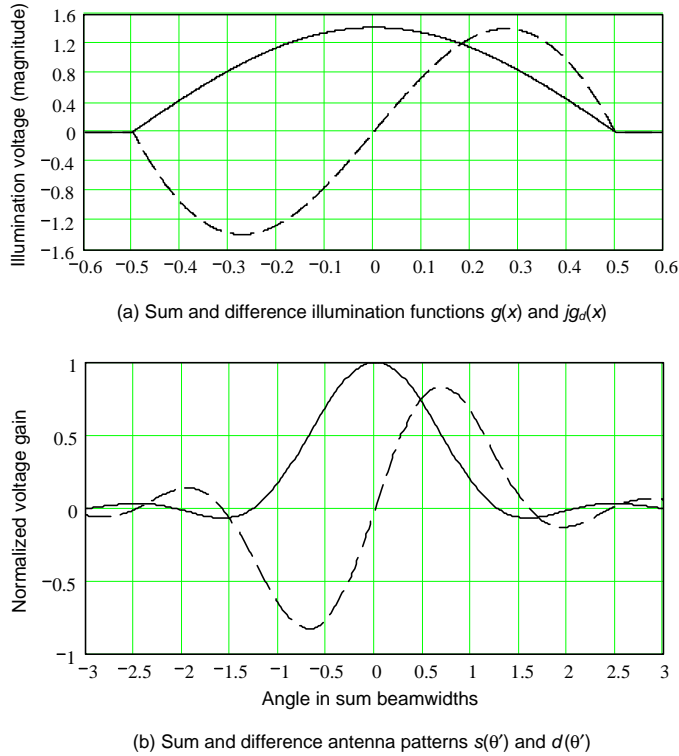


Figure 5.3 (a,b) Sum and difference illumination functions and patterns of cosine tapered rectangular monopulse antenna. Plotted pattern voltages are normalized to the peak sum-channel voltage gain, and angle is normalized to the half-power beamwidth of the sum pattern.

The sum beamwidth of a circular reflector or lens, as found in radars such as the AN/FPS-16, is, of course, greater than for a rectangular antenna with the same width, but the slope values apply to both rectangular and circular apertures.

The increase in k_m from the optimum-antenna value of 1.606 results from the normalization factors in (5.9), where the increased beamwidth and decreased efficiency cause the ratio $\theta_{bw}/\sqrt{\eta_a}$ to increase more rapidly than the decrease in K . The larger value of k_m does not indicate better monopulse performance than that of the optimum antenna, because when measurement error is calculated from k_m the larger beamwidth and smaller efficiency appear in the error equation as factors that increase the error (see Chapter 10).

The cosine taper reduces the first sidelobes from -13.3 dB to -23.1 dB for the sum channel and from -10.7 dB to -18.9 dB for the difference channel. Sidelobe levels on a decibel scale are shown in Figure 5.4. Beyond four beamwidths from

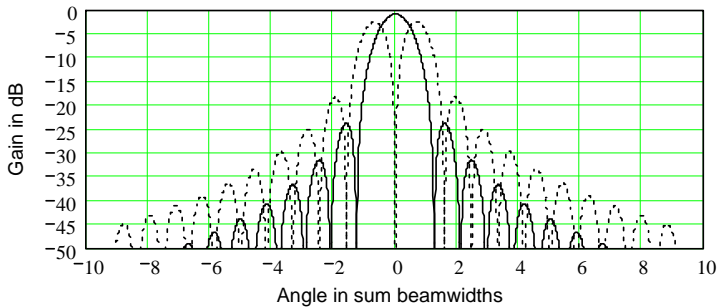


Figure 5.4 Patterns of amplitude-comparison monopulse antenna on decibel scale.

the axis the levels fall below -30 dB even for the difference channel. These patterns are typical of those found in many deployed radars that use reflector or lens antennas, and the tapered illumination functions shown in Figure 5.3 can be approximated using feed horns of the types described in Chapter 4.

5.1.5 Phase-Comparison Monopulse Antenna Example

A phase-comparison reflector antenna consists of a cluster of four reflectors side by side in a square or cloverleaf arrangement, joined together at their edges to form a rigid assembly. Each reflector has a single feed horn. Figure 5.5 shows an artist's sketch of an early experimental phase-comparison antenna built by the General Electric Company. The sum and difference illumination functions and beam patterns of such a system are similar to those shown in Figure 5.6.

A characteristic of phase monopulse antennas that use reflectors or lenses is the null in the center of the sum illumination function, caused by the use of separate portions of the aperture to create widely spaced phase centers. The result is

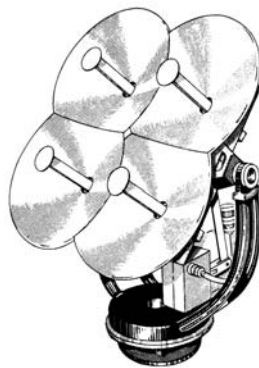


Figure 5.5 Phase-comparison monopulse antenna (General Electric Co.).

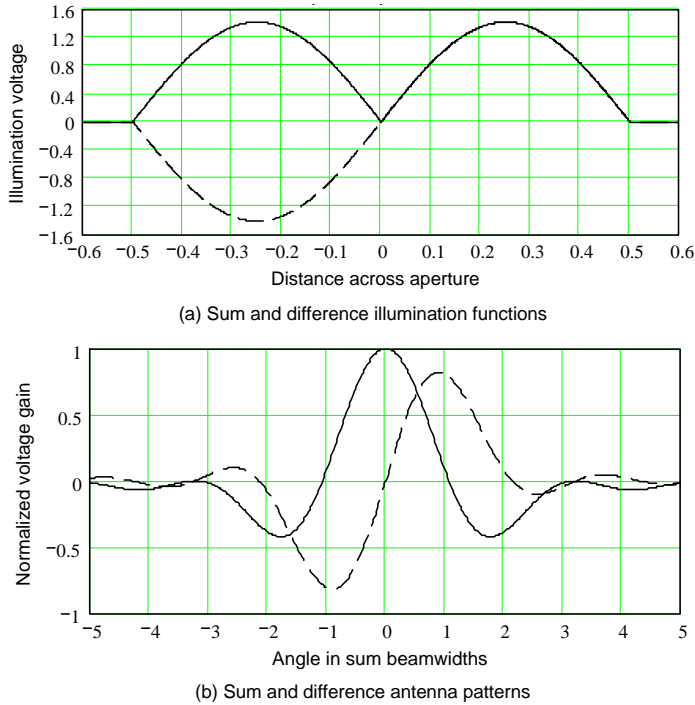


Figure 5.6 (a,b) Illumination functions and patterns of phase-comparison monopulse antenna with cosine taper on each half of the aperture.

very high sum-channel sidelobes: -7.5 dB for the first sidelobes in the case shown. The extent of these high sidelobes is shown in Figure 5.7. The sum-channel sidelobes are above -40 dB within ± 10 beamwidths. The difference-channel sidelobes are relatively small, being comparable to those of the cosine-tapered amplitude-comparison monopulse antenna (Figure 5.4). Characteristics of the modeled phase-comparison monopulse antenna are compared to the optimum antenna in Table 5.2.

In practice, although the experimental system shown in Figure 5.5 was apparently built and tested, there is no indication of application of such an antenna in a production radar. A phase-comparison monopulse radar was included in a ballistic missile guidance system designed by General Electric, but did not reach production status. An experimental combination phase-amplitude-comparison radar, the AN/APG-25(XN-2), was discussed in a paper by General Electric authors [9]. It apparently satisfied the development requirements of the Navy contract, although production did not follow. No other references to deployed phase-comparison

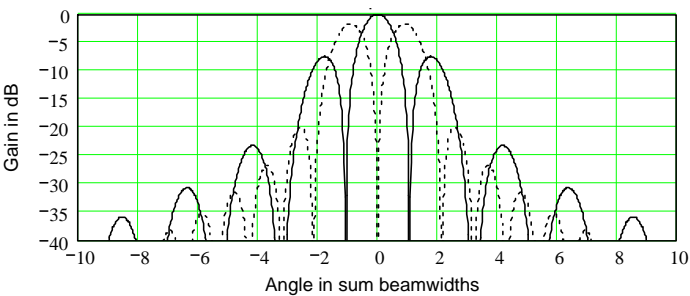


Figure 5.7 Patterns of phase-comparison monopulse antenna on decibel scale.

Table 5.2 Comparison of Optimum and Phase-Comparison Monopulse		
Parameter	Optimum Taper	Phase Comparison
Aperture efficiency η_a	1.000	0.657
Beamwidth θ_{bw}	$0.886 \lambda/w$	$0.931 \lambda/w$
Difference slope K	1.814	1.273
Difference slope ratio K_r	1.000	0.702
Monopulse slope k_m	1.606	1.463

monopulse systems using reflectors or lenses have appeared. Phased array applications of phase-comparison monopulse are discussed in Chapter 7.

5.2 PHASE FRONTS, PHASE CENTERS, AND RELATED CONCEPTS

Since the term *phase center* enters into the definitions of amplitude- and phase-comparison monopulse, and also will be referred to elsewhere, it will be defined here. First, it is necessary to understand the meaning of a *phase front*. Although both of these terms seem easy to grasp intuitively, there are subtleties that sometimes lead to misunderstanding. Phase front and phase center are most easily explained initially in terms of transmission. The interpretation for reception and for radar targets will then be given.

5.2.1 Transmitting Antennas

A phase front of a radiating antenna is any surface along which the phase of the radiated field is constant. In physical terms, imagine an instrument capable of measuring the phase of the radiation field at any point, without disturbing the field. The phase reference could be provided, in concept, by a long flexible cable of fixed length connected between the transmitter and the instrument. The abso-

lute phase of this reference is immaterial, as long as it is unaffected by the flexure or motion of the cable as the instrument is moved around.

If the instrument is moved along any path on a phase front, it will register constant phase. If amplitude is measured at the same time, it will, in general, be found to vary along the phase front. There may be points or curves on the phase front on which the amplitude is zero. When a path passes through such a point or curve, there is an amplitude null, and usually (but not necessarily, as a later example will show) a 180° phase reversal, causing a discontinuity in the phase front.

The direction of the normal to a phase front at a given point is sometimes referred to as the *direction of propagation* of the waves.

A given antenna may produce two or more simultaneous radiation patterns, such as monopulse sum and difference patterns. Each pattern has its own set of phase fronts. For a particular pattern, one and only one phase front can be drawn through any specified point in the radiation field.

The phase center is the center of curvature of a phase front. If the radiating source were an isotropic point radiator, the phase fronts would be spherical and the phase center would be at the radiator. Such a radiator is possible only for scalar (e.g., acoustic) fields, not for the vector fields of electromagnetics, although it is sometime useful for reference.

The existence of a fixed phase center is not limited, however, to an idealized point radiator. A physical radiating aperture may or may not have a fixed phase center (in the far field), depending on the aperture illumination function. A fixed phase center implies that the phase fronts are spherical or that they are composed of spherical segments having a common center, separated by jumps of one-half wavelength where the pattern passes through nulls and the phase jumps 180° . Such a case is illustrated in Figure 5.8. The rays (normals to the phase front) all intersect at a common point, the phase center.

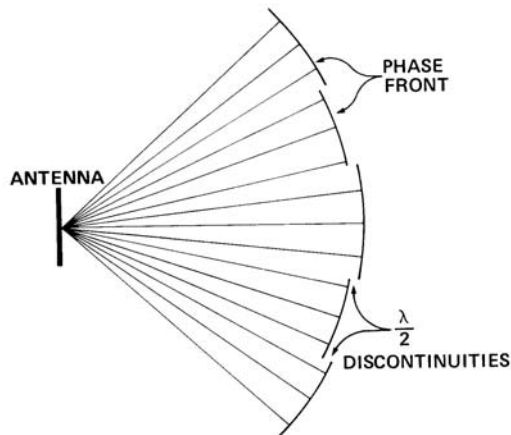


Figure 5.8 Illustration of fixed phase center.

In many cases the phase fronts are not spherical, but one can define a *local phase center* as the center of curvature at any point on a phase front. This means that any small portion of the phase front is approximated by a spherical phase front originating at the local phase center. The location of the local phase center will vary with the direction of the point of measurement from the source (and also with range if not in the far field), and this variation generally will have a component perpendicular as well as parallel to the antenna aperture plane. Figure 5.9 illustrates this situation. The phase front is not quite spherical; therefore the normals do not intersect at a common point. However, if only a small area of the phase front is considered, the points of intersection of rays from that area will lie within a small region that shrinks to a point. The point of intersection of the infinitesimal bundle of rays is the local phase center. It can also be described as the center of the osculating sphere, defined as the sphere that is tangent to the phase front and has the same curvature at the point under consideration.

Thus, over any small area through which the wave radiated by the antenna passes, the electromagnetic field is nearly the same as if it came from a point source at the local phase center. As the angle of observation changes, the amplitude, phase, and position of the apparent source may change also.

In many cases there is not even a local phase center, as defined above, because the phase front has different curvatures in different planes. Even so, it is sometimes useful to apply the concept of a phase center in a specified plane, defined as the center of curvature in that plane.

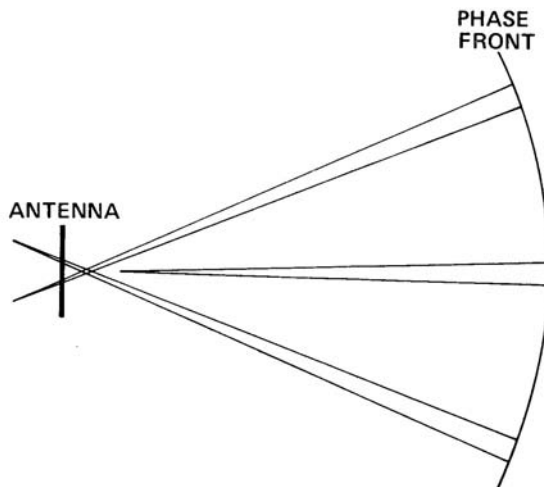


Figure 5.9 Illustration of local phase centers.

5.2.2 Receiving Antennas

To apply the concept of phase fronts and phase centers to a receiving antenna, imagine an external radiating source moving along a surface that maintains constant phase of the signal in a receiver connected to the antenna. If that surface is a sphere or consists of spherical segments having a common center, then the geometric center is the phase center. If the surface is not a sphere, the center of curvature at any point, in a particular plane, is the local phase center in that plane.

Two patterns of the same antenna (such as sum and difference) may differ in phase (by 90° , for example) and still have the same phase center. In such a case, phase fronts of the two patterns drawn through the same point will coincide geometrically but will have different phases. Stated another way, phase fronts of the two patterns, for the same specified phase, will be displaced from each other but will have a common phase center. The phase difference is accounted for by a difference in phase of the source (or receiving beamformer), not by a displacement of the phase center location.

5.2.3 Targets

The concept of a phase center can be applied also to a radar target. When a target reradiates power incident on it from a radar, it produces a radiation pattern in the same manner as a transmitting antenna, characterized by phase fronts and a phase center. In the case of a target, we are interested in that part of the phase front that is intercepted by the receiving antenna. As the target changes its orientation relative to the line of sight from the radar, its phase front changes and the antenna intercepts different portions of it. Except for certain special shapes (of which the sphere is a familiar example), the location of the target phase center as seen by the radar varies as a function of target aspect angle.

The phase of the apparent source located at the phase center of a target depends not only on the range of the target but also on its shape and composition. Assuming perfect reflectivity and monostatic operation, the phase center of a sphere having a radius much larger than a wavelength is very close to the leading edge, with essentially zero phase shift contributed by the target. For a flat plate at normal incidence, it is at the center, with a 90° phase advance contributed by the target. For the tip of a cone at nose-on incidence, long enough to remove the base from the range resolution cell containing the tip, the phase center is at the tip, with a 90° phase lag contributed by the tip.

For some purposes such as analysis of angular glint, it is sufficient to know the angular location (not the range) of the phase center. This is simply the direction normal to the phase front.

5.2.4 An Example: Phase Fronts of a Two-Element Source

The following simple example will illustrate some of the properties of phase fronts and phase centers. It is worded in terms of a transmitting antenna consisting of two discrete radiating elements but would apply equally well to a receiving antenna of the same configuration, or to the reradiated wave from a target having two scattering points, illuminated from a fixed direction relative to the target axis.

The left half of Figure 5.10 (adapted from [10] but computed and plotted independently) shows electromagnetic phase fronts emanating from a pair of sources having equal amplitudes, 180° relative phase, and a separation of three wavelengths. The successive phase fronts differ in phase by 2π radians. Each source is assumed to be a dipole having its polarization vector perpendicular to the plane of the figure and an isotropic radiation pattern in the plane of the figure. The resultant phase fronts were plotted by theory. The outmost phase front (discussed in Section 5.2.5) was computed for infinite distance but plotted at a short distance in order to be visible in the figure.

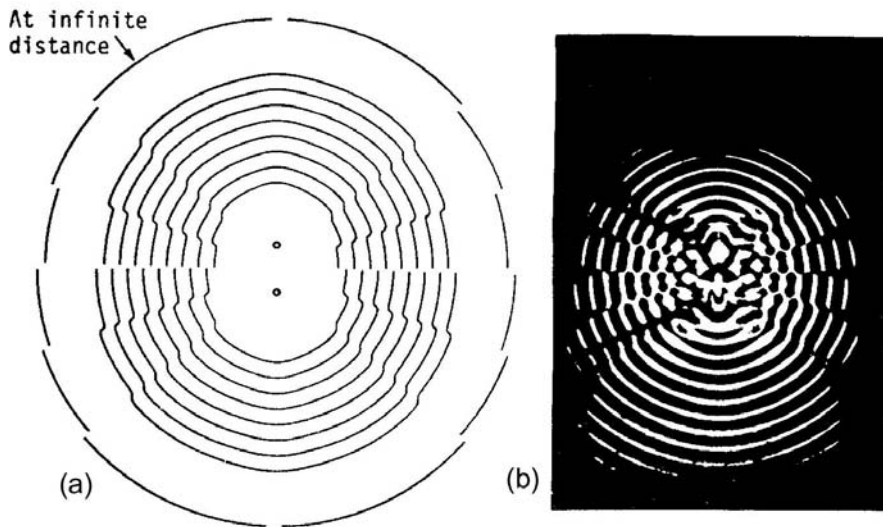


Figure 5.10 Theoretical and experimental phase fronts from two sources spaced three wavelengths apart, with equal amplitude but 180° out of phase. (a) Theoretical plot. (b) Photograph of waves in a ripple tank with same source conditions (NRL).

Physical verification is provided by the phase fronts in the right half of Figure 5.10 (taken from [10]) produced by water waves photographed in a ripple tank³ with corresponding sources. The scales of the electromagnetic and water-wave fronts have been normalized to their respective wavelengths. Under the assumed conditions the equations for propagation of the electromagnetic waves and water waves are essentially the same.

The fields E_1 and E_2 contributed by the two sources are

$$E_1 = C \frac{\exp(-j2\pi R_1/\lambda)}{R_1} \quad (5.12)$$

$$E_2 = -C \frac{\exp(-j2\pi R_2/\lambda)}{R_2} \quad (5.13)$$

where C is a constant that includes the amplitude of the sources, λ is the wavelength, and R_1 and R_2 are the distances from the respective sources to the point where the field is being measured. The resultant field is the sum of E_1 and E_2 . These equations assume that R_1 and R_2 are much greater than λ ; otherwise the equations include higher-order terms.

Along the horizontal centerline there is complete cancellation because $R_1 = R_2$; the field strengths contributed by the individual sources are equal in amplitude and opposite in phase. The phase fronts have a discontinuity of one-half wavelength in crossing that line. At any point where the pathlength difference $R_1 - R_2$ is a nonzero multiple of a wavelength, the two components are out of phase but not exactly equal in amplitude because $R_1 \neq R_2$. Therefore the resultant amplitude has a minimum but not a complete null. The phase front at such a point has a “kink”—that is, an abrupt change in direction—but not a discontinuity. The smooth portions of the curves between the kinks are not exactly circular.

It has been pointed out [10] that a tracking radar tends to align its axis along the normal to the phase front. Thus, if the two sources in Figure 5.10 were radar targets and if a tracking radar were located at one of the kinks, the tracking radar would point in a direction outside the angular span of the pair of targets, on the side of the stronger (i.e., the closer) target. This result is also found by other methods of analysis and has been confirmed by experiment.

5.2.5 Simplification at Large Distances

In the usual radar situation we are interested in distances much greater than those shown in Figure 5.10. As the distance increases, the kinks become more abrupt,

³ A ripple tank is a flat tank filled with liquid and illuminated so that the peaks of the wavefronts emanating from vibrating acoustic sources appear bright.

and in the limit they become discontinuities, as shown in the outermost phase front of the figure. The resultant field can then be expressed in a simple analytic form. The ratio of the distances from the two sources to a field point approaches unity and in the denominators of (5.12) and (5.13) we can set

$$R_1 = R_2 = R \quad (5.14)$$

where R is the distance from the midpoint of the two sources to the field point. We cannot, however, ignore the range difference in the exponents, since it is in the order of a wavelength and therefore affects the relative phase.

The lines from the two sources to a distant field point are essentially parallel, as shown in Figure 5.11. The distances are

$$R_1 = R - \frac{3\lambda \sin \theta}{2} \quad (5.15)$$

and

$$R_2 = R + \frac{3\lambda \sin \theta}{2} \quad (5.16)$$

where θ is measured from the normal to the line between the two sources. Com-

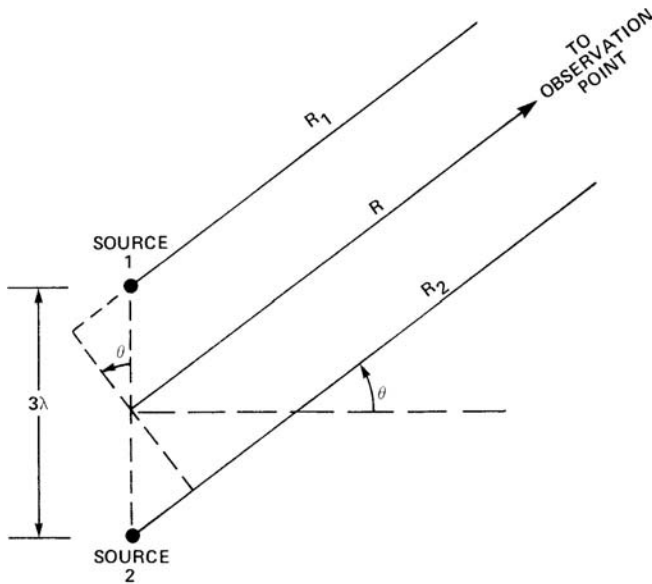


Figure 5.11 Geometry for analysis of resultant field.

binning these equations with (5.12) and (5.13), we obtain

$$\begin{aligned} E &= E_1 + E_2 = \frac{C}{R} \exp(-j2\pi R/\lambda) 2j \sin\left(\frac{2\pi}{\lambda} \frac{3\lambda}{2} \sin\theta\right) \\ &= j \frac{2C}{R} \exp(-j2\pi R/\lambda) \sin(3\pi \sin\theta) \end{aligned} \quad (5.17)$$

This equation shows that the condition for constant phase is that R be constant, except at the discontinuities that occur at those values of θ where the amplitude function $\sin(3\pi \sin\theta)$ passes through zero and changes sign. Figure 5.12 is a plot of this function. The discontinuities occur at $\theta = 0, \pm 19.5^\circ, \pm 41.8^\circ$, and at the supplementary (with respect to 180°) values of θ . At $\theta = \pm 90^\circ$ in the far field there is a null but not a change in sign; hence, there is a “hole” in the phase front but not a discontinuity. The far-field phase front is composed of circular pieces. The phase center is at the midpoint between the two sources. The field is equivalent to that of a single source at the phase center, having 90° or -90° phase relative to the upper actual source when the $\sin(3\pi \sin\theta)$ factor in (5.17) is positive or negative respectively. At a discontinuity there is no jump in the *location* of the phase center but a 180° jump in the *phase* of the equivalent source located at the phase center.

In the general far-field case (not limited to the example used above) the position, amplitude, and phase of the equivalent source at the phase center depend on direction only, not on the distance of the observation point from the antenna. All phase fronts intersecting a particular ray (which is a straight line in the far field) have a common center of curvature at the points of intersection.

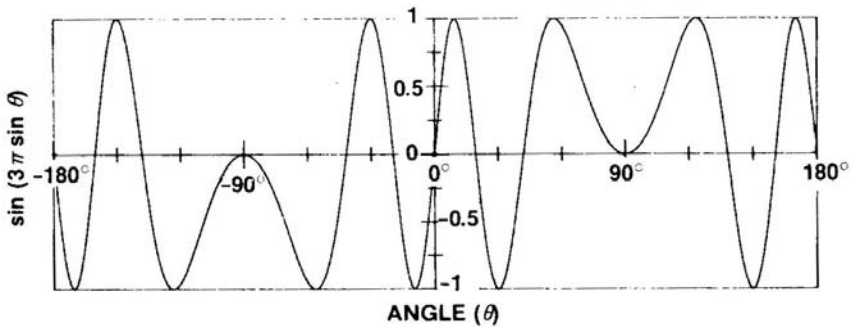


Figure 5.12 Normalized far-field amplitude versus angle.

5.2.6 Phase Centers of Array Antennas

Consider an electronically steered planar array, symmetrical in each coordinate, with constant phase illumination (for a broadside⁴ beam) or uniformly tapered phase illumination (for an off-broadside beam). It will be shown that the sum and difference patterns of such an array have a common phase center at the geometric center of the aperture. However, the component beams (usually fictitious) into which the sum and difference beams can be decomposed may have different phase centers.

The proof that follows presupposes some knowledge of electronically steered arrays and familiarity with the sine-space coordinate system described in Section 2.8. Further information on electronically steered arrays for monopulse will be found in Chapter 7.

Let the plane of the array be the x - y coordinate plane, as in Section 2.8, with the x -axis horizontal and the origin at the center. Consider even (symmetrical) amplitude illumination in either coordinate, say x , as required for the sum pattern:

$$a_e(x) = a_e(-x) \quad (5.18)$$

and uniformly tapered phase for steering the pattern. If the phase at the center is taken as the zero reference, the phase function ϕ_{st} for steering is odd:

$$\phi_{st}(x) = -\phi_{st}(-x) \quad (5.19)$$

The subscript in (5.18) identifies a_e as an even function and distinguishes it from an odd amplitude function that will be considered later. No subscript is needed to indicate whether ϕ is even or odd, since only odd phase functions will be considered. However, a distinction is made between the steering phase ϕ_{st} in (5.19) and the phase ϕ_{ar} of the arriving wave.

Let α_{st} be the steering angle measured from the positive x -axis. Then

$$\phi_{st}(x) = -k u_{st} x \quad (5.20)$$

where

$$k = 2\pi/\lambda \quad (5.21)$$

and

$$u_{st} = \cos \alpha_{st} \quad (5.22)$$

Now consider a distant point source or target at angle α_{ar} and range R from the center of the array. The phase of the wave arriving at point x on the array is

⁴ Broadside is defined as normal to the array face.

$$\phi_{ar}(x) = ku_{ar}x - kR \quad (5.23)$$

where

$$u_{ar} = \cos \alpha_{ar} \quad (5.24)$$

The net phase of the signal received at point x after the steering phase shift is applied is

$$\phi(x) = \phi_{st}(x) + \phi_{ar}(x) = k\Delta u x - kR \quad (5.25)$$

where

$$\Delta u = u_{ar} - u_{st} = \cos \alpha_{ar} - \cos \alpha_{st} \quad (5.26)$$

Hence Δu is the deviation of the target direction from the steering direction in sine space. When the target is on the axis in the steered direction, $\Delta u = 0$.

The sum signal received by the array is

$$s = \frac{1}{R} \exp(-jkR) \int_{-w/2}^{w/2} a_e(x) \exp(jkx\Delta u) dx \quad (5.27)$$

where w is the extent of the array in the x -direction. In (5.27) a constant factor outside the integral, which is a function of wavelength, has been omitted, since it has no effect on the final result. The equation can be rewritten, using (5.25), as

$$\begin{aligned} s &= \frac{1}{R} \exp(-jkR) \int_{-w/2}^{w/2} a_e(x) \exp(jkx\Delta u) dx \\ &= \frac{1}{R} \exp(-jkR) \int_{-w/2}^{w/2} a_e(x) [\cos(kx\Delta u) + j \sin(kx\Delta u)] dx \end{aligned} \quad (5.28)$$

Since $a_e(x)$ is even, only the cosine term contributes to the integral, which reduces to

$$s = \frac{1}{R} \exp(-jkR) \int_{-w/2}^{w/2} a_e(x) \cos(kx\Delta u) dx \quad (5.29)$$

The integral is real, and the phase is determined by the exponential factor outside the integral. The consideration for constant phase is constant R , and since R is measured from the center of the array, the phase center is at the phase center of the array and the phase fronts consist of spherical segments interrupted by half-wavelength jumps at nulls of the integral (i.e., nulls of the pattern). The same result is obtained in the y -direction.

Now consider an odd (antisymmetric) illumination function, as required for a difference pattern:

$$a_o(x) = -a_o(-x) \quad (5.30)$$

The reversal at the center is regarded as a sign reversal of the amplitude rather than as a 180° phase jump. The steering phase function is odd as before. If a_o is substituted for a_e in (5.28), only the sine term contributes to the integral. The difference signal received by the array is

$$d = \frac{1}{R} j \exp(-jkR) \int_{-w/2}^{w/2} a_e(x) \sin(kx\Delta u) dx \quad (5.31)$$

The integral is real. The j factor outside the integral indicates 90° phase, but this is constant. The only *variation* of phase is due to R . Constant R produces constant phase. Just as in the case of even illumination, the phase center for odd illumination is at the center of the array and the phase fronts are portions of spheres.

The difference illumination for each coordinate is even in one coordinate and odd in the other. The phase center is still at the center of the array and the phase fronts are portions of spheres, as in the previous cases.

The integrals in (5.29) and (5.31) can be replaced by summations of the contributions of elements of the array, provided these contributions include the element pattern. The results, however, remain the same as far as the phases of s and d are concerned. The same analysis can be applied to the orthogonal coordinate by replacing x by y and α by β .

In deriving (5.29) and (5.31) it has been assumed that the beamforming networks that combine the element outputs to form s and d introduce no phase shift (though in practice they may). On this assumption, s and d are seen to be in-phase. The effect of the phase relationship between s and d on the classification of monopulse as amplitude comparison or phase comparison will be discussed in Section 5.3.

Another assumption that has been made is that the illumination phase is constant or uniformly tapered. This is not generally exactly true, because an array is composed of individual elements (e.g., dipoles, slots, horns, or open-ended waveguides), which produce small “ripples” in the phase front. As long as the elements are all alike, the sum and difference patterns still have a common phase center, but that phase center may shift slightly from the geometric center of the aperture as a function of steering angle. The shift may have components both parallel and normal to the array plane. Even in the broadside direction the phase center need not be exactly in the front surface of the array.

5.2.7 Phase Centers of Reflector Antennas

The analysis just presented for array antennas actually applies more generally to any planar aperture with even or odd amplitude illumination and constant or uniformly tapered phase. Therefore, it might appear to apply to the sum and difference patterns of a reflector antenna if the plane of the rim is regarded as the aperture plane. Since all rays going from the focus to the plane by way of the reflector surface have the same length, it follows that by geometric optics a point source or infinitesimal dipole source at the focus will produce a plane wave front across the aperture plane. However, a physical feed is a distributed source, and geometric optics is only an approximation. It has been shown by more refined analysis [11] that the phase center of the sum pattern in the axial direction is on the axis of symmetry but generally does not lie in the aperture plane; it may be slightly behind the plane or in front of it. The displacement from the aperture plane depends on the ratio of the focal length to diameter of the paraboloid and on the feed characteristics. In general, because of polarization, the phase center has different locations in the two principal planes. Furthermore, the phase center is not fixed but varies with the direction of arrival.

An analysis of the phase center for odd illumination does not appear to have been reported in the literature. However, it has been established experimentally that in properly adjusted amplitude-comparison monopulse the sum and difference voltages maintain a very nearly constant relative phase (namely 0°) over the half-power beamwidth of the sum pattern. For larger angular deviations from the axis the relative phase departs from that value [12]. From these observations one can deduce that the sum and difference patterns of a reflector antenna, within the useful width of the sum beam, have very nearly the same phase center, generally not exactly in the aperture plane and not exactly on the axis except for the axial direction of arrival.

5.3 DISTINGUISHING BETWEEN PHASE- AND AMPLITUDE-COMPARISON MONOPULSE

5.3.1 Reflector Antenna Examples

We now apply the discussion of antenna phase centers to the reflector-type monopulse antennas discussed in Sections 5.1.4 and 5.1.5. The amplitude-comparison example was chosen to represent the four-horn type of feed described for the AN/FPS-16 in Chapter 4. The receiving beams mentioned in the definition of amplitude-comparison monopulse are defined in Section 5.1.4 as sum and difference beams. Hence their phase centers are coincident. We can, however, derive from the sum voltage s and the difference voltage d , using (2.3) and (2.4), the individual

component beam patterns v_1 and v_2 that would produce the sum and difference patterns. Repeating those equations here with angle θ' in beamwidths, we have:

$$v_1(\theta') = \frac{s(\theta') + d(\theta')}{\sqrt{2}} \text{ right beam} \quad (5.32)$$

$$v_2(\theta') = \frac{s(\theta') - d(\theta')}{\sqrt{2}} \text{ left beam} \quad (5.33)$$

The factor $1/\sqrt{2}$ is included to make the output power equal to input power. Since s and d are real, v_1 and v_2 have the same phases but their amplitude ratio varies with target angle, being unity on the monopulse axis. These patterns are shown in Figure 5.13. The beams have been normalized to the peak gain of the sum beam, and plotted in angle normalized to the sum beamwidth θ_{bw} . The half-power width of the individual beams is $0.859 \theta_{bw}$ and the peak amplitudes are 0.941. The first sidelobes are asymmetrical, the larger being -10 dB and the smaller -18.8 dB below the peak gain. Such patterns are consistent with those of a reflector illuminated by a closely spaced pair of horns near the focal point. The relationship to the actual AN/FPS-16 antenna will be discussed in Chapter 6.

The phasors v_1 and v_2 and the corresponding s and d are drawn in Figure 5.14 for a target to the right of the axis, at an arbitrary phase angle to emphasize that only their relative phase (0°), not their absolute phase, is relevant. The phases of v_1 and v_2 will remain equal at all target angles even though that phase may vary with target angle. This means that the two patterns must have a common phase center or a common local phase center at all angles. The reversal of the difference voltage on passing through its null can be treated mathematically as a 180° jump.

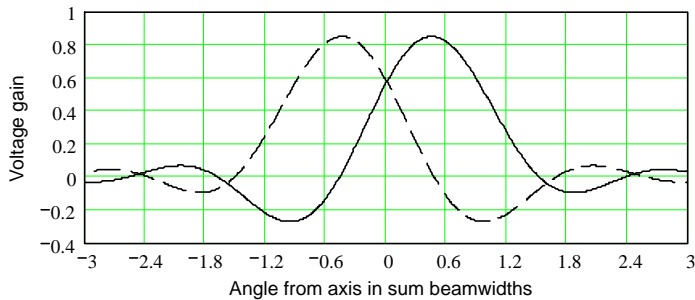


Figure 5.13 Individual squinted beam amplitudes versus angle for amplitude-comparison monopulse antenna discussed in Section 5.1.4.

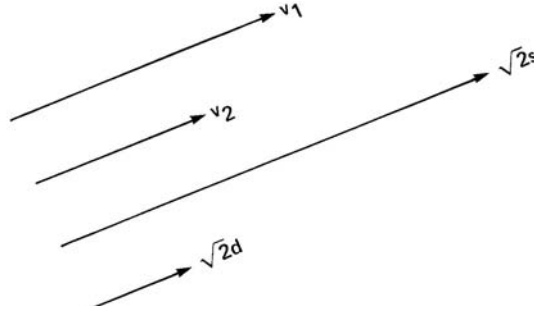


Figure 5.14 Phase relationships in amplitude-comparison monopulse.

The same phase relationship also applies to five-horn amplitude comparison, since the reference pattern has the same phase center as the squinted patterns. That is, the reference and difference voltages are in quadrature. More generally, the 90° phase relationship applies to any antenna with a single main reflector (including a Cassegrain antenna) with any number of feed horns clustered about the focus. This category is broad enough to include, for example, a twelve-horn feed or a single-horn multimode feed.

Turning now to the phase-comparison example, v_1 and v_2 have the same amplitude at all target angles but their phase difference varies with target angle, being zero on the monopulse axis. Equations (5.32) and (5.33) are now modified to replace the voltage d with jd , placing it in quadrature with s . The two amplitude patterns, shown in Figure 5.15(a), are overlaid on each other, but the phases shown in Figure 5.15(b) are exactly opposite each other, varying linearly with the sine of off-axis angle. As a result, in Figure 5.16, phasors v_1 and v_2 have equal amplitudes but different phases, diverging by equal amounts, in opposite directions from the sum phasor s . Since the relative phase of the beams whose outputs are v_1 and v_2 varies with angle, they must have different phase centers.

In phase-comparison monopulse the phase of s is always the average of phases of v_1 and v_2 . In the far field, therefore, the phase center of s is half way between the phase centers of v_1 and v_2 . The phase center of d is at that same midpoint, since d differs from s in phase by 90° . The phase fronts of the d pattern are displaced by one-quarter wavelength from those of the s pattern but they have the same center of curvature. Since d is in quadrature with s as a result of (5.31) with the odd illumination function, the monopulse comparator must maintain the input phase relationships at its outputs.

Thus it would appear that one could distinguish between the two classes of monopulse simply by computing or measuring the relative phase of the difference and sum at the comparator output: 0° for amplitude comparison and 90° for phase comparison.

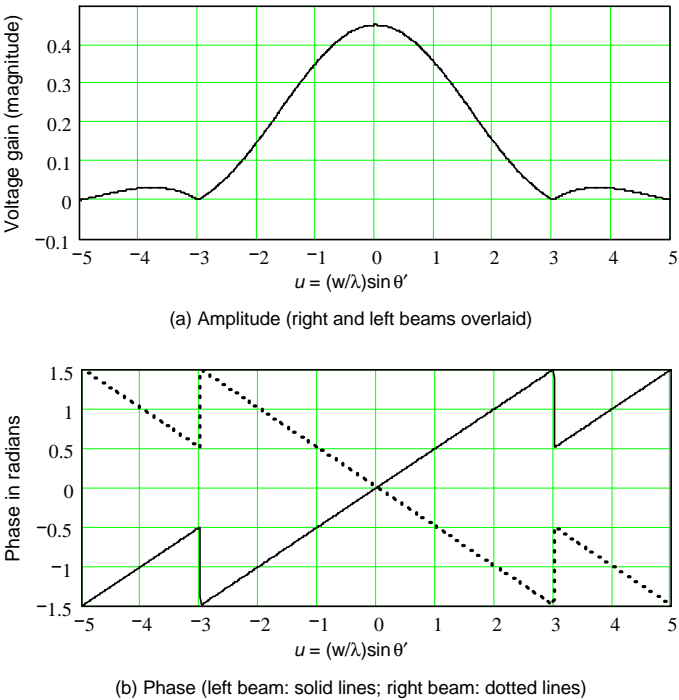


Figure 5.15 (a, b) Amplitude and phase versus target angle θ' for individual beams in phase monopulse versus angle from axis.

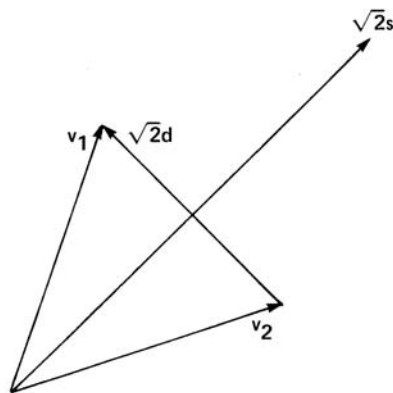


Figure 5.16 Phase relationships in phase-comparison monopulse.

However, such a distinction requires more specific wording to avoid ambiguity. The preceding explanation, including the phase diagrams, is based on (2.1), (2.2), (5.32), and (5.33). Those equations assume that the sum and difference are produced by a device such as a magic-T or circular hybrid (Section 4.4.1), which has in-phase outputs (s and d) when the inputs (v_1 and v_2) are in phase. If a directional coupler is used instead (Section 4.4.2), the situation is reversed, because the outputs have 90° relative phase when the inputs are in phase, and vice versa. Furthermore, a 90° relative phase shift may be introduced deliberately for some reason by a phase shifter at a point in the system following the comparator.

Hence the distinction between the two classes can be expressed in either of the following ways:

1. If an observer did not know the design of the antenna but had access to the inputs v_1 and v_2 to the hybrid and plotted their angular patterns, he could identify phase comparison by the fact that as the angle of a distant source or target varies, v_1 and v_2 would have equal amplitude but variable relative phase. He could identify amplitude comparison by the fact that the amplitude ratio of v_1 and v_2 would vary but their relative phase would remain constant at 0° or 90° , depending on the type of hybrid and the relative lengths of transmission lines. If the antennas had a five-horn feed, the reference-horn voltage would also have a constant phase and a variable amplitude relative to v_1 and v_2 but the observer would not need this information.
2. If the observer did not have access to the inputs to the hybrid but only to the sum and difference at the output of the hybrid or at some later point in the system, he would not be able to distinguish the two classes of monopulse unless he knew the characteristics of the hybrid and any other intervening components. Knowing these characteristics, he could make the classification by referring the observed voltages back to the inputs to the hybrid and noting the distinction described above. Or he could determine whether, in the absence of any 90° phase shift introduced by the hybrid, the sum and difference voltages at the hybrid output would have zero or 90° relative phase, and thus he would classify the monopulse as amplitude comparison or phase comparison, respectively.

The 0° or 90° phase of s and d in all the preceding discussion is the *nominal* phase, obtained under ideal conditions when the target is off the boresight axis. (When the target is on boresight, d is zero and the relative phase is undefined.) Under practical conditions the relative phase between s and d deviates from the nominal value because of noise, system imperfections, and other sources of disturbance. The deviation is usually small but can become quite large under certain

conditions. Unresolved targets or multipath, for example, can cause the relative phase of s and d to have any value.

Whether the nominal relative phase of s and d is 0° or 90° is of no importance as far as operation of the radar is concerned. By means of phase shifters the relative phase can be transformed to the other value if the monopulse processor requires it, or an equivalent transformation can be accomplished in a processor that uses digitized I and Q components by interchanging these components.

5.4 DISTINCTION BASED ON RELATIVE PHASE OF ILLUMINATION FUNCTIONS

It has been proved in Section 5.3.1 that in amplitude-comparison and phase-comparison monopulse, the relative phases of the sum and difference voltages, as they leave the comparator, are 0° and 90° respectively. A fact that sometimes causes confusion, however, is that the relative phase of the sum and difference aperture illumination functions is just the opposite, namely 90° in amplitude comparison and 0° in phase comparison. The proof that follows is for the illumination as a function of the x -coordinate in the aperture plane. The same proof would apply to the y -coordinate.

In amplitude comparison the two squinted beams correspond to uniform phase tapers in opposite directions across the aperture. At a point x in the aperture, the illumination phase factor due to a traverse squint angle α'_{sq} is $\exp(\pm jkxu_{sq})$, where $k = 2\pi/\lambda$ and $u_{sq} = \sin \alpha'_{sq}$. (Traverse angle, denoted by the symbol α' , was defined in Section 2.8.) The plus sign is for one squinted beam and the minus sign is for the other. The illumination amplitude $a_e(x)$ is an even function of x . Hence

$$\begin{aligned} \text{Sum illumination} &= a_e(x) \left[\exp(jkxu_{sq}) + \exp(-jkxu_{sq}) \right] \\ &= 2a_e(x) \cos(kxu_{sq}) \end{aligned} \quad (5.34)$$

$$\begin{aligned} \text{Difference illumination} &= a_e(x) \left[\exp(jkxu_{sq}) - \exp(-jkxu_{sq}) \right] \\ &= j2a_e(x) \sin(kxu_{sq}) \end{aligned} \quad (5.35)$$

Equations (5.34) and (5.35) show that the two illumination functions are in phase quadrature at each point in the aperture plane.

To confirm that the resultant sum and difference voltages are in phase, we must consider an off-axis target, since the difference voltage is zero on axis. Let the traverse angle of arrival (target angle) be α'_{ar} . The contribution of an element dx of the aperture to each squinted beam is $a_e(x) \exp[jkx(u_{ar} \pm u_{sq})]dx$. Then

$$\text{Contribution to the sum} = 2a_e(x) \exp(jkxu_{ar}) \cos(kxu_{sq}) dx \quad (5.36)$$

$$\text{Contribution to the difference} = j2a_e(x) \exp(jkxu_{ar}) \sin(kxu_{sq}) dx \quad (5.37)$$

The resultant sum and difference voltages are calculated by integrating (5.36) and (5.37), making use of the relation

$$\exp(jkxu_{ar}) = \cos(kxu_{ar}) + j \sin(kxu_{ar}) \quad (5.38)$$

Since the integral is taken between symmetrical limits, odd terms drop out and the integrals reduce to

$$\text{Sum voltage} = 2 \int a_e(x) \cos(kxu_{ar}) \cos(kxu_{sq}) dx \quad (5.39)$$

$$\text{Difference voltage} = -2 \int a_e(x) \sin(kxu_{ar}) \sin(kxu_{sq}) dx \quad (5.40)$$

Both (5.39) and (5.40) are real. Therefore the sum and difference voltages are in phase. For an array antenna the resultant voltages can be expressed as summations rather than integrals, with the same result.

5.5 DISTINCTION BASED ON SUM AND DIFFERENCE PATTERNS

A question arises as to whether there is anything in the *shape* of the sum and difference patterns (rather than just their relative phase) that distinguishes the two classes of monopulse. In theory, as will be illustrated later, if a given pair of sum and difference patterns is obtained from an amplitude-comparison antenna, the identical pair of sum and difference patterns (except for a 90° change in their relative phase) can be obtained from a phase-comparison antenna, and vice versa. However, because of the physical constraints of reflector and lens antennas, those designed for amplitude comparison do not produce quite the same sum and difference patterns as those designed for phase comparison. For example, the latter class usually gives a larger slope of the difference-to-sum ratio versus angle (which is desirable) but higher sum pattern sidelobes [13]. The reason for the higher sidelobes can be seen qualitatively in Figures 5.3(a) and 5.6(a), which plot the sum illumination voltages across the antenna aperture for amplitude comparison and phase comparison. In a reflector antenna the illumination amplitude has a natural taper, which is maximum at the center of each aperture and falls off at the edges, as illustrated. The cusp (slope discontinuity) in phase comparison produces

large sidelobes in the sum pattern, since the pattern has a Fourier-transform relationship with the illumination function.

5.6 APPARENT CONVERSION OF ONE CLASS TO THE OTHER

An apparent conversion from amplitude comparison to phase comparison or vice versa can be effected [4] by a passive microwave device such as a 3-dB directional coupler (Section 4.4.2). When used for this purpose, the device is not part of the comparator. A 3-dB directional coupler splits the power from each of the two input ports equally between the two output ports but shifts the phase of one input signal by $\pm 90^\circ$ at one output port and of the other input signal by $\pm 90^\circ$ at the other output port. The positive or negative sign depends on the particular construction of the coupler. If the inputs are v_1 and v_2 , the outputs are

$$v_3 = (v_1 \pm jv_2)/\sqrt{2} \quad (5.41)$$

$$v_4 = (\pm jv_1 + v_2)/\sqrt{2} \quad (5.42)$$

In Figure 5.17 the inputs v_1 and v_2 shown have the same phases but different amplitudes, as in amplitude comparison. The outputs have the same amplitude but different phases, as in phase comparison.

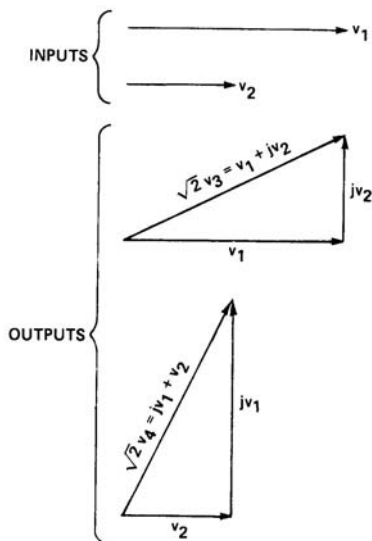


Figure 5.17 Output phasors of 3-dB directional coupler when inputs are in phase.

Conversely, the same kind of device can effect an apparent conversion from phase comparison to amplitude comparison. If the inputs have equal amplitude but different phases, the outputs will have equal phases but different amplitudes. To prove this statement, let the two inputs have equal amplitude but different phases ψ_1 and ψ_2 . Assume the positive sign for the 90° phase shift. As shown in Figure 5.18(a), v_3 is the resultant of v_1 and jv_2 , the latter being represented by the dashed phasor equal in amplitude to v_2 , but advanced 90° in phase. Since v_1 and jv_2 are equal in amplitude, their resultant v_3 bisects the angle between them. Therefore the phase of v_3 is $(\psi_1 + \psi_2 + \pi/2)/2$. In Figure 5.18(b), v_4 is the resultant of jv_1 and v_2 , and its phase is $(\psi_1 + \pi/2 + \psi_2)/2$. Hence, v_3 and v_4 have the same phase. It is obvious from the figure that their amplitudes, in general, are unequal.

Although these examples illustrate how a 3-dB coupler, or an equivalent device or circuit, appears to convert amplitude comparison to phase comparison or vice versa, there need not be any ambiguity in the classification if it is based on the “raw” component voltages v_1 and v_2 before the conversion.

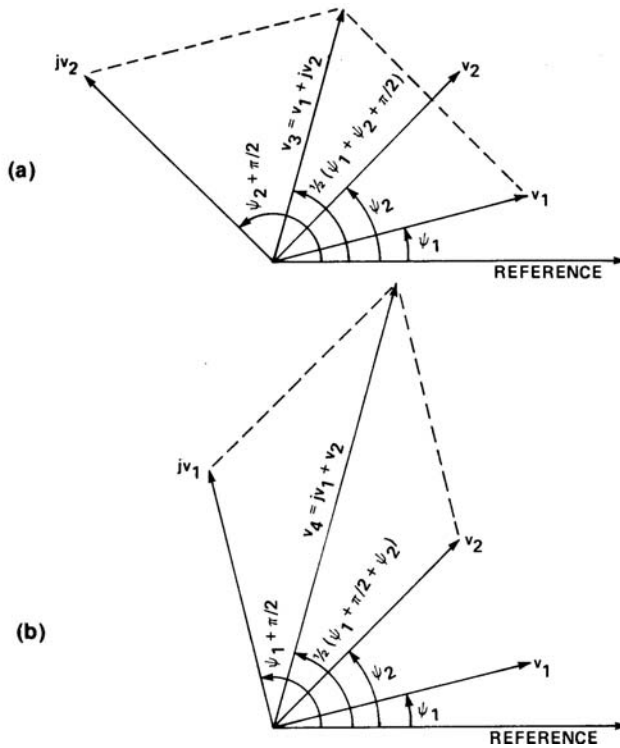


Figure 5.18 Transformation from phase comparison to amplitude comparison. (a) $v_3 = v_1 + jv_2$.

(b) $v_4 = jv_1 + v_2$.

5.7 SUMMARY OF AMPLITUDE-COMPARISON AND PHASE-COMPARISON CLASSIFICATION

Confusion in usage of the terms amplitude comparison and phase comparison can be avoided by adhering to the convention that these names refer to the receiving antenna, not to the monopulse signal processing. In this connection, “antenna” is interpreted to include not only the radiating structure but also all of the components needed to provide the antenna pattern outputs. The two classes can be distinguished by any of four equivalent criteria, as summarized in Table 5.3.

Table 5.3
Distinctions Between Amplitude Comparison and Phase Comparison

Class	Construction (Lens or Reflector Antennas*)	Component Beams	Relative Phase of <i>s</i> and <i>d</i>	
			Voltages	Aperture Illuminations
Amplitude Comparison	Single lens or main reflector with multiple feed horns	Squinted beams Single phase center Amplitude ratio varies with angle, being unity on axis	0°	90°
Phase Comparison	Multiple side-by- side lenses or reflectors, each with single feed horn	Parallel beams Same amplitude pattern Different phase centers Relative phase varies with angle, being 0° on axis	90°	0°

* Applies also to space-fed arrays or reflectarrays acting essentially as lenses or reflectors.

The first distinction (physical construction) is applicable only to space-fed antennas, which include lenses or reflectors and also certain types of arrays that act like lenses or reflectors.

The second distinction (nature of component beams) applies to space-fed antennas and some arrays, in which the component beams exist physically in the sense that there are points in the system where voltages corresponding to those beams exist, even if they are not readily accessible for measurement. If the component beams do not exist physically, they can still be calculated as fictitious beams, which would produce the given sum and difference if added and subtracted.

The third distinction (relative phase of sum and difference voltages) assumes that the comparator that produces the sum and difference *s* and *d* is of a type that does not introduce any relative phase shift between them, or that any phase shift that the comparator does introduce is “subtracted out” before making the classification.

The fourth distinction (relative phase of sum and difference aperture illuminations) is derived from the third (or vice versa) by a mathematical transformation. It is sometimes helpful in determining the classification of a given array radar.

In the third and fourth distinctions, “reference” can be substituted for “sum” in those antennas that generate a reference pattern, for example by means of a separate feed horn.

In a constrained-fed array, any sum and difference patterns that can be produced by amplitude comparison can also be produced by phase comparison and vice versa. In space-fed antennas the sum and difference patterns obtainable from the two classes are very similar but differ to some degree in monopulse slope and sidelobe levels.

An apparent conversion from amplitude comparison to phase comparison or vice versa can be effected by applying a 90° phase shift to the sum or difference voltage (or by interchanging I and Q if the processing is digital), or by passing the component beam voltages through a 3-dB directional coupler before the comparator. However, such conversion need not create any ambiguity if the classification is based on the voltages before the conversion.

References

- [1] G. M. Kirkpatrick, “Final Engineering Report on Angular Accuracy Improvement,” General Electric Electronics Laboratory, Syracuse, NY, Contract D.A. 36-039-sc-194, August 1, 1952. Reprinted in *Radars*, Vol. 1, *Monopulse Radar*, D. K. Barton, (ed.), Dedham, MA: Artech House, 1974.
- [2] G. M. Kirkpatrick, “Aperture Illumination for Radar Angle-of-Arrival Measurements,” *Trans. IRE Professional Group on Aeronautical and Navigational Electronics*, Vol. PGAE-9, September 1953, pp. 20–27.
- [3] IEEE Standard 100, *The Authoritative Dictionary of IEEE Standards Terms*, 7th ed., New York: IEEE Press, 2000.
- [4] D. R. Rhodes, *Introduction to Monopulse*, New York: McGraw-Hill, 1959. Reprint, Dedham, MA: Artech House, 1982.
- [5] S. Silver (ed.), *Microwave Antenna Theory and Design*, Vol. 12 in MIT Radiation Laboratory Series, New York: McGraw-Hill, 1949, p. 177. Reprint, CD-ROM Edition, Norwood, MA: Artech House, 1999.
- [6] P. W. Hannan, “Optimum Feeds for All Three Modes of a Monopulse Antenna,” *IRE Trans. on Antennas and Propagation*, Vol. AP-9, No. 5, September 1961, pp. 444–461. Reprinted in *Radars*, Vol. 1, *Monopulse Radar*, D. K. Barton, (ed.), Dedham, MA: Artech House, 1974.
- [7] M. I. Skolnik, *Introduction to Radar Systems*, 3rd ed., New York: McGraw-Hill, 2001.
- [8] D. K. Barton, *Radar System Analysis*, Englewood Cliffs, NJ: Prentice-Hall, 1964. Reprint, Dedham, MA: Artech House, 1976.

- [9] W. Hausz and R. A. Zachary, "Phase-Amplitude Monopulse System," *IRE Trans. on Military Electronics*, Vol. MIL-6, No. 2, April 1962, pp. 140–146. Reprinted in *Radars*, Vol. 1, *Monopulse Radar*, D. K. Barton, (ed.), Dedham, MA: Artech House, 1974.
- [10] D. D. Howard, "Radar Target Angular Scintillation in Tracking and Guidance Systems Based on Echo Signal Phase Front Distortion," *Proc. of the National Electronics Conf.*, Vol. XV, October 1959, pp. 840–849.
- [11] D. Carter, "Phase Centers of Microwave Antennas," *IRE Trans. on Antennas and Propagation*, Vol. AP-4, No. 4, October 1956, pp. 597–600.
- [12] J. T. Nessmith and S. M. Sherman, "Phase Variations in a Monopulse Antenna," *Record of IEEE International Radar Conference*, Washington, D.C., April 21–23, 1975, pp. 354–359.
- [13] H. W. Redlein, Jr., *A Unified Viewpoint for Amplitude and Phase Comparison Monopulse Radars*, Wheeler Laboratories, Report 845, March 16, 1959.

Chapter 6

Optimum Feeds for Space-Fed Amplitude-Comparison Monopulse Antennas

Although the basic principle of amplitude-comparison monopulse is easy to grasp, the design of the antenna and feed for optimum performance is a highly specialized task. The “optimum” is not absolute; it depends on the system application and requirements, and usually is a compromise among various performance objectives and practical constraints. This chapter will outline criteria for optimization in relation to feed configuration and parameters.

The advantages and disadvantage of three basic space-fed antenna types—lens, single reflector, and Cassegrain—are discussed in Chapter 4. To these we may add the space-fed array, which acts essentially as a lens or reflector. The general principles of feed optimization apply to any of these antenna types but for the sake of concreteness and numerical examples, a single-reflector antenna will be assumed. Where the considerations in optimization of feeds for lenses differ from those for reflectors, that will be noted.

6.1 NATURE OF OPTIMIZATION

Consider first an antenna designed to produce only a sum (reference) pattern, using only a single feed horn. The smaller the feed aperture, the broader its radiation pattern toward the reflector, resulting in more power wasted in spillover beyond the edges of the aperture, and therefore reduced gain. The larger the feed aperture, the more directive the feed radiation pattern. The increased directivity reduces spillover but if carried to excess it effectively illuminates only the inner portion of the reflector; thus the full aperture of the reflector is not utilized efficiently and gain is reduced. Another factor that must be considered is the presence of the feed in front of the reflector; the larger the feed, the more blockage and the larger the resulting reduction in gain. (This consideration is absent in optimization of a lens

antenna.) Taking all these effects into account, the maximum-gain feed size can be determined.

However, maximum gain is accompanied by high sidelobes. The sidelobes can be reduced at the expense of some sacrifice in gain by making the feed size somewhat larger than that required for maximum gain. This process must not be carried beyond the point where the decrease in sidelobes from spillover is offset by the increase in sidelobes from blockage.

Upon balancing these conflicting factors it is found [1, 2] that in most cases the optimum feed aperture size is one that tapers the reflector illumination by about 10 or 11 dB from the center to the edge, or somewhat more if extremely low sidelobes are desired. As will be noted in Section 6.9, the use of multimode or corrugated horns better optimizes the illumination function and may permit different taper values.

In a monopulse feed the problem of optimization is more complicated, since the sum and two difference patterns have to be considered. For the sum pattern the usual objective is maximum on-axis gain¹ consistent with sidelobe requirements. For each difference pattern the objective is maximum on-axis slope, again consistent with sidelobe requirements. Hannan [3] analyzed this problem and derived the optimum aperture sizes for sum and difference feeds if each could be controlled independently. Although the exact numbers² depend somewhat on the desired trade-off between gain (or slope) and sidelobes, the difference-feed aperture in the coordinate of interest should be about twice as wide as the sum-feed aperture. (The aperture in each case refers to the entire cluster of horns that produce the sum or difference pattern, not to each horn.) The sum and difference feed apertures should be continuous (without gaps); therefore they must overlap. Hannan proposed several feed designs intended to approach optimum performance more closely than is possible with the basic four-horn feed.

The twelve-horn feed, to be discussed in Section 6.9, comes closest to the theoretical optimum but is complicated to build. The four-horn feed, which remains the most common, has overlapping sum and difference apertures, since they are composed of the same horns, but the apertures have the same width rather than the optimum 2:1 width ratio. In the early five-horn feed, on the other hand, the difference-feed aperture is nearly three times the width of the sum-feed aperture, and furthermore it has a gap in the center, since it cannot overlap the sum feed. By multimode operation and other techniques of shaping the feed aperture illumination, the four-horn and five-horn feeds can be made more efficient than the basic configuration would indicate. But although such feeds are capable of excellent performance, they cannot achieve simultaneous, independent optimization of sum

¹ In some cases the objective is minimum beamwidth, which is not quite equivalent to maximum gain.

² Hannan's results are expressed in terms of normalized feed dimensions, which must be multiplied by the wavelength and by twice the f/D ratio to obtain the physical dimensions.

and difference patterns. They can, however, be optimized in the sense of achieving the most effective compromise within their physical constraints.

Particular attention will be given to the four-horn feed, which is of special interest because of its long and widespread use. The feed optimization will be explained and illustrated in terms of the squint angle of the component beams, rather than in terms of feed sizes, as in Hannan's analysis. The two methods of analysis are essentially equivalent but the squint-angle method permits the use of a simplified, approximate model, which is easier to handle mathematically and perhaps easier to interpret physically. It will be shown that the optimized parameters of this model agree closely with those of a widely used precision monopulse radar. Other types of feeds will also be discussed.

6.2 f/D RATIO

One of the parameters to be selected is the ratio of focal length to antenna diameter, known as the f/D ratio. The required diameter is determined by the specifications for gain and angular resolution of the sum pattern, leaving the focal length selectable. Since the feed is located at the focus, it is desirable to make the focal length short in order to alleviate the problem of rigidly supporting the feed in front of the reflector. On the other hand, small f/D poses difficulty in designing a feed with a wide enough radiation pattern, uniform phase, and low cross-polarization to provide proper illumination of the reflector. A large f/D means a shallow reflector, which is less sensitive to cross-polarization; but the disadvantage, in addition to the increased difficulty of supporting the feed, is that it requires a narrower width of the feed radiation pattern to prevent excessive spillover of the reflector illumination. This in turn means a larger feed aperture, which increases the blockage and also increases the weight of the feed, thereby further aggravating the feed support problem. A large f/D also increases the reaction of the reflector on the feed, which causes impedance mismatch.³

In considering blockage and mechanical support, it must be remembered that a multihorn feed assembly, including the comparator, is larger and heavier than a single-horn nonmonopulse feed used, for example, in a communications antenna.

Typical compromise values of f/D are in the range of 0.3 to 0.5 for single-reflector antennas. For example, the AN/FPS-16 instrumentation radar has a single paraboloidal reflector with $f = 127$ cm (50 inches), $D = 366$ cm (12 feet), and $f/D = 0.35$. In the AN/FPQ-6 radar, which has a Cassegrain antenna, the f/D ratio of the main paraboloidal reflector is 0.3 but because of the Cassegrain configuration the effective f/D ratio is 1.6.

³ The opposite would be true if the feed design remained constant while f/D increased. However, in order to maintain the same illumination taper across the reflector (usually about -10 dB at the edges), the feed directive gain must increase with f/D , and this increases the reaction.

6.3 EFFECT OF SQUINT ANGLE IN A FOUR-HORN FEED

In the conventional four-horn feed, described and illustrated in Chapters 1 and 4, the horns are paired so that for each coordinate they act as two horns. Radars using four-horn feeds are in wide use and perform very well. However, with this horn arrangement it is not possible to optimize the sum pattern and the difference patterns independently, so a compromise must be reached.

Here we will illustrate the limitation of four-horn monopulse by a simple model. The variable to be adjusted for optimization is the squint angle, which is a function of the spacing of the horn centers. We will assume that each squinted beam is formed with cosine illumination (see Section 5.1.4), producing the patterns plotted in Figure 6.1, and that if the squint angle is varied, each squinted beam undergoes an angular shift but remains unchanged otherwise. The cosine illumination model gives a good fit to patterns produced by simple horn illuminations over angular regions out to the first sidelobes. The assumption that the squinted pattern remains unchanged in width, height, and phase may be questioned, because as the squint angle is varied the coupling between the feed horn changes, causing a change in the patterns. However, at squint angles near or greater than the optimum, the coupling is weak. The objective here is only to illustrate the existence of an optimum compromise and to obtain rough numerical values. Yet in spite of the crudeness of the model, the calculated results are found to be remarkably close to those derived from measured patterns of the AN/FPS-16 monopulse radar.

Let v_1 and v_2 be the voltages from the two pairs of horns which produce the squinted beams, and from which the sum and difference in one angular coordinate are to be formed. The squinted beams have the patterns assumed in the model:

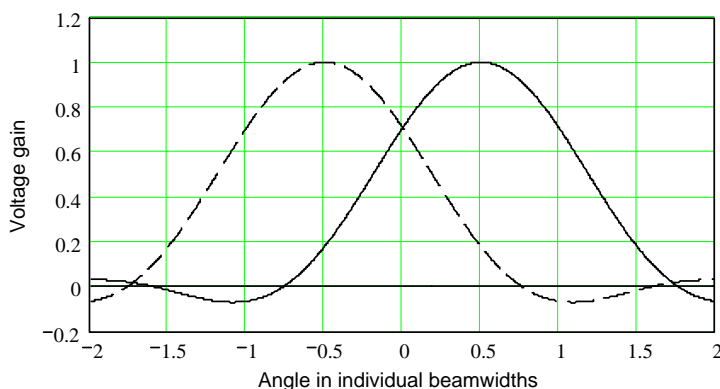


Figure 6.1 Squinted beam patterns v_1 (solid curve) and v_2 (dotted curve) produced by feed with cosine illumination with squint angle $\theta_{sq} = 0.5$ beamwidths.

$$v_1 = \frac{\cos\left[\pi K_\theta (\theta - \theta_{sq})\right]}{1 - \left[2K_\theta (\theta - \theta_{sq})\right]^2} \quad (6.1)$$

$$v_2 = \frac{\cos\left[\pi K_\theta (\theta + \theta_{sq})\right]}{1 - \left[2K_\theta (\theta + \theta_{sq})\right]^2} \quad (6.2)$$

where θ is the target angle from the boresight axis in one coordinate, θ_{sq} is the squint angle in the same coordinate, and $K_\theta = 1.19$ is the beamwidth constant for cosine illumination.⁴ In these equations the unit of θ and θ_{sq} is the half-power beamwidth of the squinted beams rather than of the sum beam, the latter being the more usual unit but less convenient for our present purposes. The quantity in brackets is in radians. The beamwidth constant is chosen so that v_1 and v_2 equal 0.707 when $\theta - \theta_{sq}$ and $\theta + \theta_{sq}$ equal 0.5 (the half-power point).

The sum and difference voltage patterns are

$$s = (v_1 + v_2) / \sqrt{2} \quad (6.3)$$

$$d = (v_1 - v_2) / \sqrt{2} \quad (6.4)$$

The factor $1/\sqrt{2}$ arises from the fact that in a passive hybrid (assumed lossless, with all ports terminated in matched impedances) total output power equals total input power.

Figure 6.2 shows plots of the sum and difference for various squint angles. The ordinates are normalized to the peaks of the squinted beams. (In the model the peak voltage of a squinted beam is assumed to be independent of the squint angle.)

In all these plots the field strength of the echo wave arriving at the antenna is assumed constant in amplitude. Only the squint angle differs from one curve to another. The curves for $\theta_{sq} = 0.3$ are of doubtful validity because of appreciable coupling at such a small squint angle; they are included only to illustrate the trend.

The unit of target angle on the abscissa scale in Figure 6.2 is the half-power beamwidth of each squinted beam, which in the beam model described above is assumed to be constant, independent of squint angle. The choice of this unit of angle is convenient for our purpose but it must be remembered that it differs from

⁴ In the exact pattern, the quantities in parentheses in (6.1) and (6.2) are the sine of the target angle \pm the sine of the squint angle. However, for angles not exceeding a few degrees the sines are closely approximated by the angles themselves.

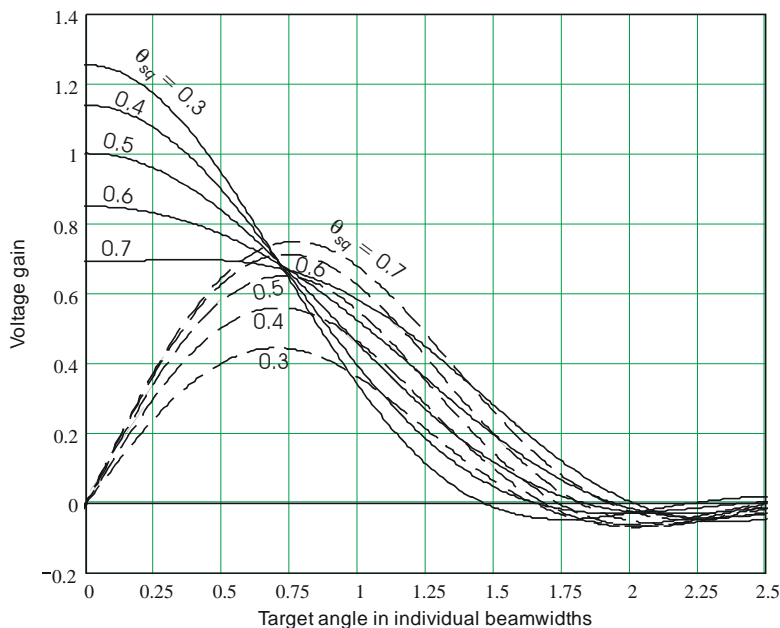


Figure 6.2 Sum and difference of a pair of squinted $(\sin x)/x$ beams. Solid and dashed curves represent sum and difference respectively, θ_{sq} = squint angle, normalized to beamwidth of squinted beams.

the conventional definition of the term “beamwidth,” which when used without qualification refers to the sum pattern. The sum pattern beamwidth does of course vary with squint angle.

Figure 6.2 shows that the on-axis sum beam voltage decreases with increasing squint angle. When $\theta_{sq} = 0.5$, the peak of the sum beam equals the peak of each squinted beam. For $\theta_{sq} > 0.68$, the on-axis voltage changes from a maximum to a minimum between two peaks. The plots also show that the sum-pattern beamwidth increases with increasing squint angle. Therefore, to maximize sum-pattern gain and resolution the squint angle should be small.

The difference pattern, on the other hand, has a small slope on axis when the squint is small, and this means poor sensitivity. The difference slope increases with squint angle until it reaches a maximum when $\theta_{sq} = 0.68$ (the same squint angle at which the sum changes from a maximum to a minimum). This suggests that a large squint angle (i.e., about 0.7) is optimum for good difference pattern, at least for targets on or near boresight.

Hence, it is not possible to optimize both the sum and difference patterns with a four-horn feed. One criterion for the optimum compromise is described in the Section 6.4.

6.4 OPTIMIZATION OF SQUINT ANGLE

The criterion for optimization depends on the radar function that is to be optimized. If detection sensitivity is of paramount importance and angular accuracy is secondary, then the squint angle should be as small as possible. (If angle measurements were not needed at all, the two horns would coalesce into one and the squint angle would be zero.)

Here we will assume that angular accuracy for targets on or near the axis, rather than detection sensitivity, is to be optimized. Consider first the case where the sum beam is used for both transmission and reception and the target is passive (i.e., one that merely scatters or reradiates the power incident on it) rather than active (i.e., a beacon). Although a squint angle of 0.68 maximizes the difference slope (Section 6.3), it will be shown that this is not the optimum. Instead, the optimum squint angle is the one that maximizes the product of on-axis difference slope and on-axis sum voltage.

In Chapter 10 the following approximate formula is derived for the single-pulse error due to thermal noise, for a steady target on or near the axis:

$$\sigma_{\theta} = \frac{\theta_{bw}}{k_m \sqrt{2S/N_d}} \quad (6.5)$$

where

- σ_{θ} = standard deviation of angle error, in the same units as θ_3 ;
- θ_{bw} = sum-pattern 3-dB beamwidth;
- k_m = normalized monopulse slope (defined more fully below);
- S = sum-signal power;
- N_d = average noise power in difference channel.

Since the unit of angle for θ and θ_{sq} used in the preceding sections is the beamwidth of the squinted beams, the same unit will be used here for σ_{θ} and θ_{bw} . The sum beam is wider than the squinted beam; therefore the ratio of θ_{bw} to individual beamwidth is greater than unity.

Let s_o be the on-axis sum voltage and let k_d be the on-axis difference slope on any of the plots in Figure 6.2, normalized to the peaks of the squinted beams. (This form of normalization is not essential but is chosen for consistency with Section 6.3.) The normalized monopulse slope k_m is the ratio of k_d to the maximum on-axis sum voltage s_o , expressed in terms of the sum half-power beamwidth; that is,

$$k_m = \frac{k_d \theta_{bw}}{s_o} \quad (6.6)$$

Thus the slopes k_d and k_m differ in two ways: they are normalized to the peak of the squinted beam and the peak of the sum beam, respectively, and the unit of

angle is the beamwidth of a squinted beam and the beamwidth of the sum beam, respectively.

By convention, the term *monopulse slope* (sometimes called “error slope”) means k_m unless otherwise indicated. In general it is the slope of the difference pattern at angle θ , in volts per sum-pattern beamwidth, divided by the sum voltage at angle θ , in volts. The units of k_m are usually expressed as volts per volt per beamwidth. Usually k_m is not exactly constant as θ varies over $\pm\theta_{bw}/2$, but varies somewhat with θ ; here we are concerned with the on-axis value.

To minimize the angle error σ_θ in (6.5) we must maximize $k_m \sqrt{S}/\theta_{bw}$. The on-axis sum power S is proportional to s_o^4 if the sum pattern is used both for transmission and reception, as it normally is in radar. Hence, the figure of merit to be maximized is

$$\frac{k_d \theta_{bw}}{s_o} \frac{s_o^2}{\theta_{bw}} = k_d s_o \quad (6.7)$$

which is the product of the difference slope k_d and the sum voltage, both on axis.

Figure 6.3 is a plot of the figure of merit $k_d s_o$ versus squint angle. The maximum occurs at a squint angle of 0.453 beamwidth of the squinted beams. With this squint angle, $s_o = 1.067$, $k_d = 1.32$, $\theta_{bw} = 1.263$ times the individual beamwidth, and the crossover point is 2.44 dB down from the peak of each squinted beam. The squint angle can also be expressed as 0.453/1.263 or 0.358 sum-pattern beamwidth. The normalized monopulse slope k_m is 1.635.

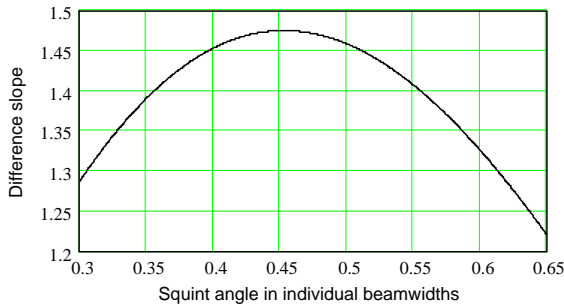


Figure 6.3 Angular accuracy performance index $k_d s_o$ as a function of squint angle θ_{sq} .

The illumination functions that result from beams generated with optimum squint are shown in Figure 6.4. The difference illumination matches closely that for the cosine-tapered optimum monopulse, as shown in Figure 5.3(a). The sum illumination closely matches the function $\sqrt{8/3} \cos^2(\pi x)$, giving very low sidelobes (≈ -34.5 dB) with relatively low illumination efficiency: $\eta_x = 0.640$. The

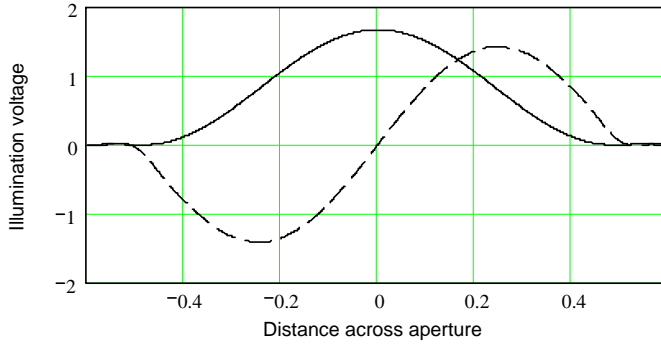


Figure 6.4 Illumination function for sum (solid curve) and difference (dashed curve), for beams with optimum squint angle.

total aperture efficiency, if the illumination in the y coordinate is $\cos(\pi y)$, is $\eta_a = 0.519$.

6.5 COMPARISON WITH MEASURED PATTERNS

It is interesting to compare the numbers derived from this simplified model with those derived from pattern measurements of an operational monopulse radar. The AN/FPS-16 instrumentation radar will be used as an example.

The sum and difference patterns are known directly from measurements. Because the outputs of the individual feed horns are not normally accessible, the squinted beam patterns are not measured directly, but they can be inferred from the sum and difference patterns. The squinted patterns include the effects of mutual coupling among the horns. They are not quite the same as the patterns that would be obtained from each horn or pair of horns if the others were removed, but those patterns are of no interest for our purpose, since the coupling is always present.

The following empirical formulas have been found to be close approximations of the measured sum and difference patterns⁵ of the AN/FPS-16 over the angular region encompassing most of the main lobe of the sum pattern [4]:

$$s = \cos^2(1.14\theta) \quad (6.8)$$

$$d = \frac{1}{\sqrt{2}} \sin(2.28\theta) \quad (6.9)$$

⁵ Patterns are normally plotted in dB, but were converted to voltage for this purpose.

In these equations θ is the off-axis angle normalized to the 3-dB beamwidth of the sum pattern, and the quantities in parentheses are in radians. The coefficients 1.14 and 2.28 in these equations differ slightly from the 1.18 and 2.36 in corresponding equations given in [5]. The discrepancy is the result of rounding and conversion in [5] of the numbers given in [4], which are in degrees. The coefficients used in equations (6.8) and (6.9) above are consistent with [4] and give the correct half-power value $s = 1/\sqrt{2}$ when $\theta = 0.5$.

Given the sum and difference voltages s and d , the squinted beam voltages v_1 and v_2 are obtained from the equations derived in Section 2.4:

$$v_1 = (s + d)/\sqrt{2} \quad (6.10)$$

$$v_2 = (s - d)/\sqrt{2} \quad (6.11)$$

In elevation, for example, v_1 is obtained by summing the outputs of the lower pair of horns and v_2 is obtained in the same way from the upper pair.

All four of the voltages in the equations above are phasors (i.e., complex) in general, but in pure amplitude comparison they have the same phase.⁶ Since absolute phase is arbitrary, they will be treated as real quantities. In an actual radar the phases differ slightly because of the physical separation of the horns [6], but within the half-power beamwidth of the sum pattern this effect is negligible.

Figure 6.5 shows the sum and difference patterns computed by (6.8) and (6.9) and squinted patterns computed by (6.10) and (6.11). The negative half of the difference pattern has been inverted in order to condense the vertical scale. The abscissa scale unit is now the conventional beamwidth of the sum pattern rather than the beamwidth of the squinted patterns. The following points are of interest:

1. The squint angles are ± 0.426 beamwidth (of the sum beam).
2. The peak of each squinted beam is down 0.3 dB from the peak of the sum beam.
3. The crossover point of the squinted beams is 2.7 dB down from their peaks.
4. The normalized monopulse slope k_m is 1.62.
5. The half-power width of each squinted beam is 0.88 times the half-power width of the sum pattern. That is, $\theta_3 = 1/0.88 = 1.14$.

The crossover must always be 3 dB below the peak of the sum beam, because at that point $v_1 = v_2$ and $s = (v_1 + v_2)/\sqrt{2} = \sqrt{2}v_1 = \sqrt{2}v_2$. Therefore the 0.3 dB in item 2 and the 2.7 dB in item 3 contain redundant information, since they must total 3 dB.

⁶ A 180° phase reversal is regarded as the same phase with a sign reversal of the amplitude.

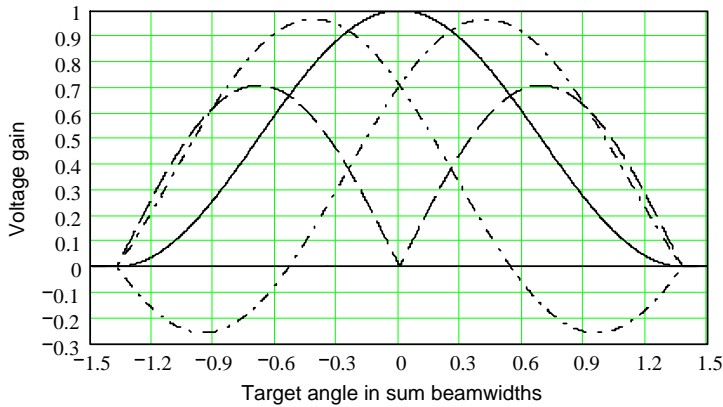


Figure 6.5 Patterns of sum (solid curve), magnitude of difference (dashed curve), and squinted beams (dot-dashed curves) of AN/FPS-16 radar.

Table 6.1 compares the parameters of the AN/FPS-16 model with those of two optimized analytical models. The close agreement with the squinted-beam model may be partly fortuitous but it does suggest that the AN/FPS-16 feed design is close to optimum for a four-horn feed, and that the truncated septum (see Section 4.3) may produce performance exceeding that of the optimum simple four-horn design. In Section 6.8 it will be shown that the optimum squint angle is not much less than the squint angle that causes the coupling between the feed horns to vanish. This fact tends to justify the use of the simplified analytical model in which coupling is ignored.

Table 6.1 Comparison of Pattern Parameters

<i>Parameter</i>	<i>AN/FPS-16 Model</i>	<i>Squinted Beam Model</i>	<i>Cosine Tapered Monopulse</i>
θ_3 (ref.: squinted beamwidth)	1.14	1.26	—
Squint angle (ref.: sum beamwidth)	0.418	0.358	—
s_o (ref.: squinted beam peak)	1.035 (0.3 dB)	1.067 (0.57 dB)	—
Crossover (ref.: squinted beam peak)	2.7 dB	2.44 dB	—
Sum sidelobes (ref.: sum peak)	None	-34.5	-23.0
η_a (aperture efficiency)	0.50*	0.54	0.657
k_m (V/V/beamwidth of sum beam)	1.618	1.635	1.96
K (relative difference slope)	1.144	0.952	1.334
K_r (difference slope ratio)	0.631	0.525	0.736

* Assumed aperture efficiency for AN/FPS-16.

Thus, the four-horn feed, even when using optimum beam squint, falls below the potential performance for a given aperture with illumination taper formed by a more complex feed system.

6.6 BEACON OPERATION

For tracking of a beacon or transmitting source, the transmission-pattern gain of the radar antenna has no effect on accuracy, except that if the beacon is a transponder, the radar must transmit enough power to interrogate it. On the left side of (6.7), therefore, the factor s_o^2 in the numerator is replaced by s_o and the right side of the equation is simply k_d . Hence to minimize angular error the unnormalized on-axis slope should be maximized. This condition, according to the model plotted in Figure 6.2, would require a squint angle $\theta_{sq} = 0.68$. The radar cannot be simultaneously optimized for accurate tracking of skin targets and beacon targets. It is usually more important to optimize for skin tracking.

6.7 COMPARISON OF BEAM SQUINT ANGLE AND FEED OFFSET ANGLE

The squint angle of the beam produced by an offset feed horn is not quite the same as the off-axis angle of the line from the vertex of the paraboloid to the center of the horn. This fact is demonstrated by the AN/FPS-16 radar used in the previous example. The focal length of the AN/FPS-16 antenna (Figure 4.1) is about 127 cm (50 inches). The vertical offset of the horn centers from the paraboloid axis is 0.98 cm (0.386 inch). Thus the feed offset angle in elevation is 0.44° , or when normalized is about 0.37 times the sum beamwidth θ_{bw} , which is about 1.2° . This compares with the squint angle $0.418\theta_{bw}$, a factor of 1.13 greater than the horn offset angle. According to [7–10] the beam squint angle is a little less (in a ratio of about 0.85) than the feed offset angle,⁷ whereas in the present case it is greater. However, the results in the cited references were derived for a single offset feed. The discrepancy in the present case is probably due to mutual coupling among the multiple feed horns.

In traverse the geometric offset angle of the centers of the horns is 0.86° or about 0.72 beamwidth. However, by the design of the feed system, including truncation of the vertical septum at a point behind the feed aperture and generation of higher-order modes, the illumination at the feed aperture has been shaped so that the effective electrical centers of the horns are closer to the axis than the geomet-

⁷ The ratio of the beam squint angle to the feed offset angle is called *beam deviation factor*.

ric centers. The result is that the squint angle is about the same in traverse as in elevation.

6.8 EFFECT OF SQUINT ANGLE ON NORMALIZED DIFFERENCE PATTERN

Figure 6.6 shows plots of the normalized difference signal d/s as a function of the angle θ from the axis, for three different squint angles θ_{sq} . For the special case $\theta_{sq} = 0.421$ (in squinted beamwidths) the plot is a straight line, assuming that the squinted patterns are exactly those produced by cosine illumination. With this value of θ_{sq} all the off-axis sum and difference nulls coincide. It can be shown that with $\theta_{sq} = 0.421$ the two squinted beams are orthogonal, which means that their coupling is zero. For $\theta_{sq} < 0.421$ the plot curves upward. If this plot were extended to the right, it would become infinite at the first sum null, which occurs before the first off-axis difference null. For $\theta_{sq} > 0.421$ the plot curves downward. If extended to the right, it would pass through zero at the first off-axis difference null, which occurs before the first sum null. The particular values of θ_{sq} chosen for the plots, besides 0.421, are 0.453 (the optimized value derived in Section 6.4 for minimum angular error) and an arbitrary value of 0.400. The slopes of the three

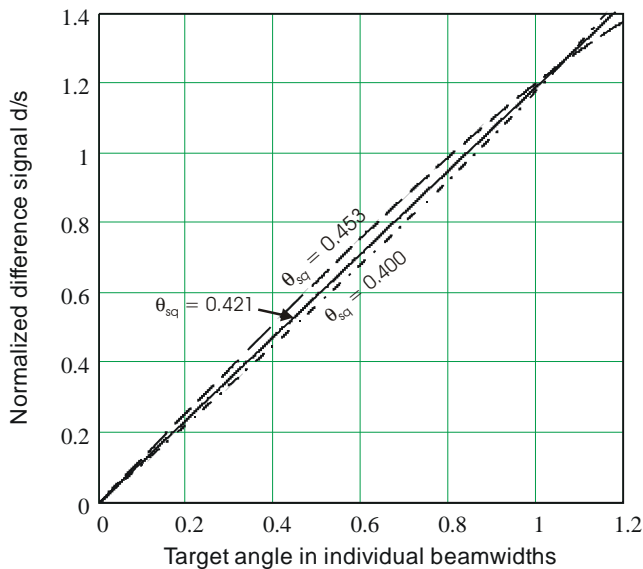


Figure 6.6 Normalized difference signal versus angle for three values of squint (measured in individual beamwidths).

curves at the origin are not to be interpreted as a figure of merit in themselves. As explained above, slope must be considered in combination with the sum-signal voltage gain, unless the radar is operating in a beacon or receive-only mode.

The usual shape of the normalized difference pattern is concave upward, like the bottom curve in Figure 6.4. The actual output of a monopulse radar follows such a curve over a moderate range of angles (usually over the sum-pattern beamwidth), then starts to saturate because of dynamic range limitations in receivers or in the processor.

6.9 OTHER FEED CONFIGURATIONS

In a five-horn feed such as the one used in the AN/FPQ-6 radar, shown schematically in Figure 4.12, the central horn R provides a reference signal that serves the same function as the sum signal in a four-horn feed; it is used for transmission as well as reception. The difference signals in traverse and elevation are obtained from the left and right horns A and B and from the lower and upper horns C and D respectively. The four outer horns are used only for reception.

Both four-horn and five-horn feeds have been used successfully. Each has certain advantages and disadvantages.

The five-horn feed has more degrees of freedom than the horn-horn feed but still does not permit independent optimization of sum and difference patterns. Although the aperture dimensions of the individual horns can be chosen somewhat independently, the *spacing* of the outer horns depends on the dimensions of the central horn, since the horns cannot physically overlap. Either the squint angle is larger than optimum for the difference pattern (while in the four-horn feed it is smaller than optimum) or the reference horn is smaller than optimum for the sum pattern. Therefore a compromise is necessary.

The five-horn feed has an advantage in that the reference pattern is produced by a single horn and requires no hybrids. This simplifies the RF hardware, reduces losses and troublesome adjustments, and simplifies the transmission of high powers through the feed. The five-horn feed also has some advantages over the four-horn feed when dual polarization is required, because of the smaller number of hybrids. On the other hand, the feed itself is a more complicated structure (compared to a four-horn feed) and is generally larger in size, causing more blockage (in a reflector system).

An alternate version of a five-horn feed uses a dielectric-loaded center horn. This permits a reduction in size of the center horn while maintaining its directivity, thus bringing the outer horns closer together and improving the difference patterns. A disadvantage is that the dielectric has some loss. Care must be taken to ensure that this loss, even though small (of the order of a tenth of a dB), does not cause excessive heating of the dielectric. The AN/MPS-36 is an example of a radar that uses this type of feed, with boron nitride as the dielectric.

A configuration that approaches the theoretical goal of simultaneous optimization of the sum and difference patterns is the experimental 12-horn feed design by Lincoln Laboratory [11] and discussed by Hannan [3]. It is shown schematically in Figure 6.7. All unused outputs of the hybrids are terminated in matched dummy loads, omitted from the diagram. The twelve-horn feed is equivalent in effect to a five-horn feed with overlapping horns. To see the equivalence, compare Figure 6.7 with the illustration of a five-horn feed in Figure 4.11. The correspondence is as shown in Table 6.2.

The 12-horn feed was reported to give near-optimum performance, but because of the complexity of the feed and comparator it has not been adopted for general use in U.S. systems.

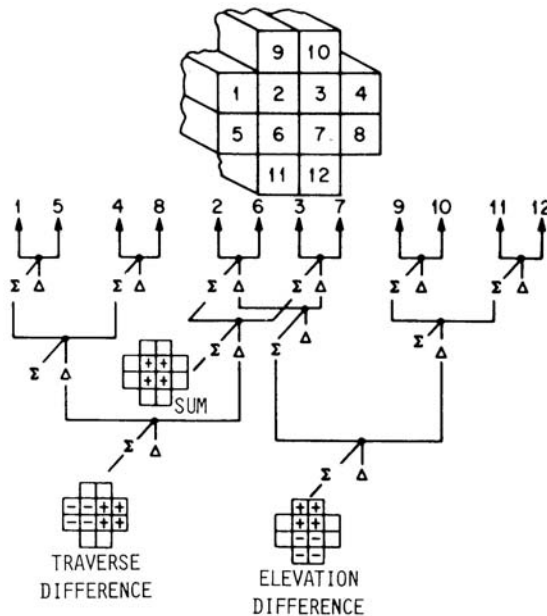


Figure 6.7 Twelve-horn monopulse feed (Lincoln Laboratory).

Table 6.2 5-Horn and 12-Horn Correspondence

5-Horn Feed (Figure 4.11)	12-Horn Feed (Figure 6.7)
R	2 + 3 + 6 + 7
A	1 + 2 + 5 + 6
B	3 + 4 + 7 + 8
C	6 + 7 + 11 + 12
D	9 + 10 + 2 + 3

The foregoing discussions and illustrations of feed systems and comparators have assumed the use of a single polarization. If dual linear or circular polarization is used, the arrangement is similar but somewhat more complicated. The horns are usually square or circular for equal reception of both components. RF devices are needed to extract the two polarization components and process them either simultaneously or by switching.

The use of multiple modes of waveguide propagation (known as multimode operation) has already been mentioned. It is analogous to the use of harmonic frequency components added to a fundamental frequency to shape a waveform by Fourier synthesis. The sum signal is composed of even modes; the difference signal in each coordinate is composed of modes that are odd in that coordinate and even in the other. The mode synthesis permits flexibility in the shaping of the feed aperture illumination even though the physical dimensions are fixed. Besides its use in optimized four-horn feeds, it has been used or proposed in certain special feed configurations in which a single feed horn produces both a sum and difference pattern in one coordinate [12] or a sum and both difference patterns [13–15]. The horn aperture has the width needed for the optimum difference pattern but the sum-pattern illumination is concentrated near the center so that in effect it occupies only about half the physical dimension. This type of feed is theoretically capable of closely approaching simultaneous optimization of sum and difference patterns, but control of the higher-order modes over a broad frequency band is a difficult design problem.

One of the feed configurations proposed by Hannan [3], and used successfully in radars such as the Nike Hercules tracker, combines multimode operation in one coordinate with physical aperture control in the other coordinate. It consists of four parallel, contiguous, rectangular horns joined by common walls in their long dimension (Figure 6.8). For the purpose of description, let the horns be numbered sequentially. The difference pattern in the coordinate of polarization (the short dimension of each horn) is obtained from $(1 + 2) - (3 + 4)$ and the reference is obtained by $(2 + 3)$. This conforms to Hannan's rule that the feed aperture should be about twice as wide for the difference as it is for the reference. In the long dimension, multimode shaping of the horn aperture illumination is done in such a way that the odd component (for the difference) uses the entire aperture while the even component (for the reference) is mostly concentrated in the central portion, effectively using one-half of the physical aperture.

Hannan presented data on the relative performance of four-horn, twelve-horn, and the four-horn multimode feed, showing that the last option provided greater sum-channel gain, largely the result of lower spillover loss, and significantly greater monopulse sensitivity. Measured by the sum-channel aperture efficiency η_a and the difference slope ratio K_r (averaged between azimuth and elevation coordinates), the values for the three options were listed in Table 6.3.

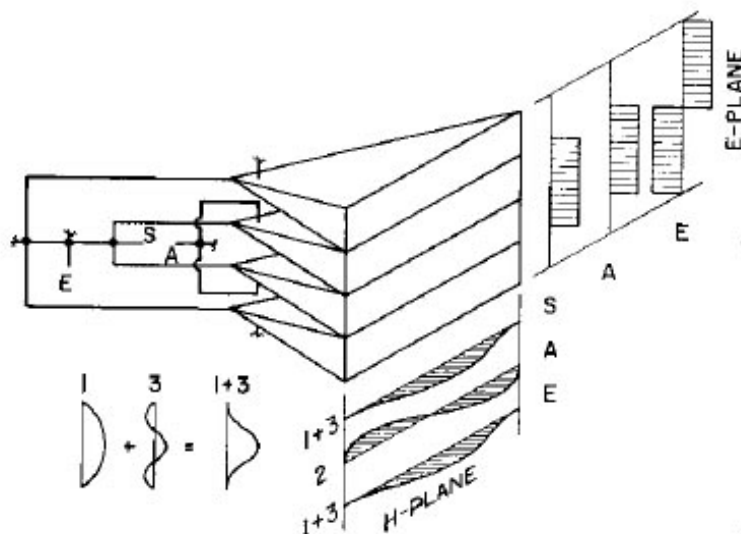


Figure 6.8 Four-horn multimode monopulse feed. (From: [3]. © 1961, IEEE. Reprinted with permission.)

Table 6.3 Efficiency and Difference Slope Ratio of Different Feeds

Feed Type	Efficiency η_a	Relative Difference Slope K_r
Four-horn	0.58	0.50
Twelve-horn	0.58	0.69
Four-horn multimode	0.75	0.78

Further development based on Hannan's four-horn multimode feed was performed during the 1970s, leading to the five-horn multimode feed for the Patriot fire control radar, shown in Figure 6.9. Three center horns now provide the sum and azimuth difference patterns, the former using the central portions of these horns. The elevation difference pattern is provided by the central portions of the upper and lower pairs. In its original design the Patriot radar was to use two transmitters, selected by steering the focal point of the lens array to one of the transmitting horns located beside the monopulse receiving horn stack. This so-called "space duplexing" provision eliminates the loss of a high-power duplexer that would otherwise be required, and makes possible a simpler, low-power monopulse horn stack.

More detailed information on optimized design of monopulse feeds can be found in [3] and in [11–16], several of which are reprinted in [17].

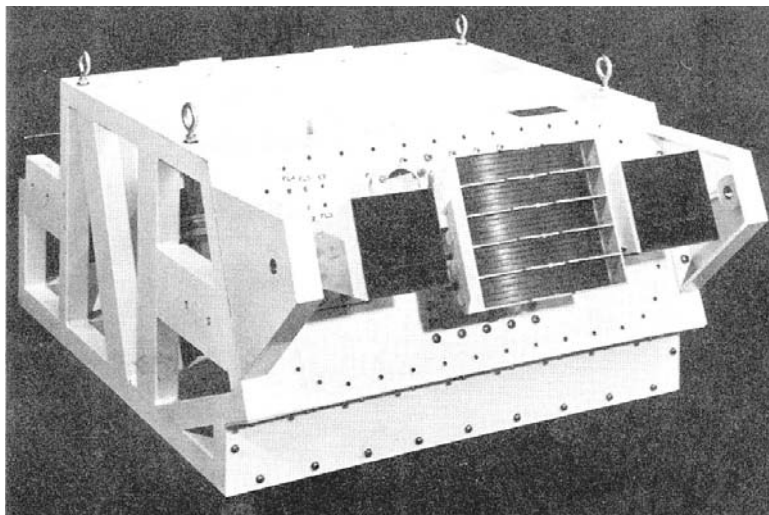


Figure 6.9 Five-layer multimode monopulse feed for the Patriot fire control radar. Either of the separate horns, beside the receiving feed, can be selected for transmitting by focusing the array on it. (Figure courtesy of Raytheon Company.)

Another modern development in feed horn design is the corrugated horn [18]. For a single pencil beam or monopulse reference beam this type of horn gives improved efficiency with low sidelobes. It has found use in satellite communication antennas and other systems where the monopulse performance requirements are modest or where monopulse is not needed at all. However, it is difficult to adapt for high-performance monopulse operation.

The ultimate in independent optimization of sum and difference patterns is an array antenna with amplitude weighting of each element, independently tailored for sum signal and two difference signals. Such optimization is possible with the Lopez feed discussed in Chapter 7, and with digital beamforming systems in which received signals from each radiating element are converted to digital form.

6.10 SUMMARY OF FEED OPTIMIZATION

It has been shown theoretically that for optimization of space-fed amplitude-comparison monopulse antennas the effective feed dimension in each coordinate must be about twice as large for the difference pattern as for the sum (reference) pattern. In a feed with four horns in a conventional square (or rectangular) arrangement this requirement cannot be met; either the sum or difference pattern can be optimized but not both simultaneously. The simplified analysis that has been presented illustrates how optimization of the sum and difference patterns imposes

conflicting requirements, and shows how a compromise is reached. If minimum angular error on skin targets is the objective, the best compromise is one that maximizes the product of on-axis sum voltage and on-axis difference slope. The analysis ignores such factors as impedance matching and feed coupling, besides using an inexact model for the squinted beams. Nevertheless the results agree closely with the monopulse characteristics of the AN/FPS-16 instrumentation radar, as inferred from measured patterns. Although not theoretically optimum, the conventional four-horn feed has practical advantages and has been used successfully in many radars.

A five-horn feed provides somewhat greater flexibility but still requires a compromise, since it is also incapable of simultaneous optimization of reference and difference patterns. A 12-horn feed, using the four central horns for the reference, and the central horns plus four additional horns in each coordinate for the two differences, can come close to simultaneous optimization at the expense of considerable complexity in the feed and comparator. Separation of the transmitting and receiving horns, using polarization screens or switching the focal point of a space-fed lens between separate horns (space duplexing), allows the monopulse horn to be designed in more compact form for low-power operation and also eliminates the need for a high-power duplexer with its associated loss.

The use of higher-order waveguide modes in combination with the fundamental modes makes it possible to shape the illumination to reduce the effective aperture width for the sum pattern while using the full aperture for the difference pattern, and thus approach the optimum more closely. This principle has been used to improve the performance of conventional four-horn feeds. A further step toward optimization is a feed devised by Hannan consisting of four horns in a stacked rather than square arrangement; for the E-plane patterns the inner two horns are used for the reference and all four are used for the difference, while the desired H-plane illumination is obtained by multimode operation within each horn. The addition of a fifth horn to the stack allows somewhat better performance in the elevation coordinate. By use of multimode techniques it is even possible to produce near-optimum reference and difference patterns with a single feed horn. However, broadband control of the various modes is difficult.

References

- [1] C. C. Cutler, "Parabolic-Antenna Design for Microwaves," *Proc. IRE*, Vol. 35, No. 11, November 1947, pp. 1284–1294.
- [2] J. W. Crompton, "On the Optimum Illumination Taper for the Objective of a Microwave Aerial," *Proc. IEE*, Vol. 101, Pt. 3, November 1954 (also ASTIA Document AD 12,571).
- [3] P. W. Hannan, "Optimum Feeds for All Three Modes of a Monopulse Antenna: Part I, Theory and Part II, Practice," *IRE Trans. on Antennas and Propagation*, Vol. AP-9, No. 6, September 1961, pp. 444–454 (Part I); pp. 454–461 (Part II).

- [4] A. F. George and A. S. Zamanakos, "Multiple Target Resolution of Monopulse vs. Scanning Radars," *Proc. National Electronics Conf.*, Vol. XV, October 12–14, 1959, pp. 814–823.
- [5] D. K. Barton, *Radar System Analysis*, Englewood Cliffs, NJ: Prentice-Hall, 1965. Reprint, Dedham, MA: Artech House, 1976 (see p. 272).
- [6] J. T. Nessmith and S. M. Sherman, "Phase Variations in a Monopulse Antenna," *Record of the IEEE 1975 International Radar Conf.*, Washington, D.C., April 21–23, 1975, pp. 354–359.
- [7] S. Silver, *Microwave Antenna Theory and Design*, Vol. 12 of MIT Radiation Laboratory Series, New York: McGraw-Hill, 1947. Reprint (CD-ROM edition), Artech House, 1999 (see pp. 487–488).
- [8] Y. T. Lo, "On the Beam Deviation Factor of a Parabolic Reflector," *IEEE Trans. on Antennas and Propagation*, Vol. AP-8, No. 3, May 1960, pp. 347–349.
- [9] S. S. Sandler, "Paraboloidal Reflector Patterns for Off-Axis Feed," *IRE Trans. on Antennas and Propagation*, Vol. AP-8, No. 4, July 1960, pp. 368–379.
- [10] J. Ruze, "Lateral Feed Displacement in a Paraboloid," *IEEE Trans. on Antennas and Propagation*, Vol. AP-13, No. 5, September 1965, pp. 660–665.
- [11] L. J. Ricardi and L. Niro, "Design of a Twelve-Horn Monopulse Feed," *IRE Conv. Record*, Pt. 1, 1961, pp. 49–56.
- [12] P. W. Hannan and P. A. Loth, "A Monopulse Antenna Having Independent Optimization of the Sum and Difference Modes," *IRE Conv. Record*, Pt. 1, 1961, pp. 57–60.
- [13] D. D. Howard, "Single Aperture Monopulse Radar Multimode Antenna Feed and Homing Device," *1964 IEEE Military Electronics Conv.*, September 14–16, 1964, pp. 259–263.
- [14] P. Mikulich, R. Dolusic, C. Profera, and I. Yorinks, "High Gain Cassegrain Monopulse Antenna," *IEEE G-AP International Antenna Symp. Record*, September 1968, pp. 375–382.
- [15] J. H. Dunn, D. D. Howard, and K. B. Pendleton, "Tracking Radar," Chapter 21 of *Radar Handbook*, (M. I. Skolnik, editor-in-chief), New York: McGraw-Hill, 1970 (see pp. 21-18–21-20).
- [16] G. M. Kirkpatrick, "Final Engineering Report on Angular Accuracy Improvement," General Electric Co. Electronics Laboratory, Syracuse, NY, August 1, 1952.
- [17] D. K. Barton, (ed.), *Radars*, Vol. 1, *Monopulse Radar*, Dedham, MA: Artech House, 1974.
- [18] A. W. Love, "Horn Antennas," Chapter 15 of *Antenna Engineering Handbook*, R. C. Johnson, (ed.), New York: McGraw-Hill, 1984.

Chapter 7

Monopulse in Array Antennas

In the preceding chapters most of the specific examples and illustrations of monopulse have been drawn from systems using reflector or lens antennas in which the beam is steered by mechanical rotation. It has been pointed out, however, that the principles and techniques of monopulse are not limited to those types of antennas. In particular, monopulse has been implemented in various ways in array antennas. Some preliminary comments about monopulse in array antennas were presented in Sections 5.2.6 and 5.8.

The subject of array antennas is very broad and is treated extensively in the technical literature (see, for example, [1–6]). Array antennas can be steered either mechanically or electronically in either or both coordinates. Combinations of mechanical and electronic steering are common. A brief general summary will be given in Section 7.1. The remainder of the chapter will treat particular aspects of the subject that pertain to monopulse, with emphasis on the differences between monopulse in array antennas and in mechanically steered reflector or lens antennas. The space-fed array antenna, which combines many of the features of mechanically steered reflector or lens antennas with the ability to scan electronically, will be discussed as a special case.

7.1 PRINCIPLES OF OPERATION

A voltage pattern of an antenna is approximately equal to the Fourier transform of the aperture illumination function¹ from which it was produced (see Sections 2.2, 2.3, 5.1.3, and 5.2.6). In a space-fed reflector or lens antenna the illumination function is determined by the design of the feed, the f/D ratio, and any power

¹ Also called the aperture distribution function or simply the aperture function.

dividers, combiners, or hybrids used in forming the pattern. This applies equally to mechanically and electronically scanned reflectors and lenses.

In array antennas using constrained (or *corporate*) feeds, however, the illumination function is formed directly in the aperture plane by control of the amplitudes and phases of the excitation coefficients of the individual radiating *elements* of the array. The elements are usually a set of identical radiators such as dipoles, open ends of waveguides, slots in waveguides, or horns. For reasons of economy or design simplification, with some sacrifice in performance, the elements are sometimes grouped into *subarrays*. The amplitude is then uniform within each subarray but differs from one subarray to the next. Phase control is still exercised over the individual elements. To avoid needless repetition, the word “element” will be used hereafter to include subarrays as well, except where a distinction is being made.

In airborne radars and missile seekers, the antenna often takes the form of a lightweight flat-plate array of slotted waveguides that is mounted on a gimbal assembly for mechanical steering in pitch and yaw. In this case the illumination function is determined by the network that couples the waveguides to the common feed point and by the size and orientation of the slots in the waveguide walls. The steering of the beam is entirely mechanical. Monopulse is commonly used in such airborne arrays.

In surveillance radars a monopulse antenna may take the form of horizontal slotted waveguides or rows of dipoles with constrained feed networks, stacked vertically and fed through a vertical power-dividing network that may contain phase shifters or a frequency-sensitive network for electronic steering in elevation. The monopulse network is usually applied only in the elevation coordinate, mechanical scanning being used to cover 360° in azimuth. Examples will be shown in Chapter 14.

Electronic scan in both coordinates requires phase control of each individual element. The pattern direction is steered by imposing an appropriate linear phase progression from element to element along the aperture in the desired direction. The element amplitudes are set at values that will produce the illumination function for the desired pattern shape. These amplitudes are usually fixed by the feed network, and therefore the pattern shape remains approximately invariant in sine space (but not in angle space) as the beam direction changes. To control the phase function for steering requires the ability to change the phases of the individual elements, and an antenna with this capability is commonly called a *phased array* or *electronically scanned array* (ESA). The term *electronic scanning* seems to imply that the beam motion follows a regular pattern, and *electronic steering* might be more appropriate for the irregular and arbitrary beam motions that are actually used in most cases.

The most recent development in array antennas is the *active electronically scanned array* (AESA), in which each element of the array includes the final power amplification stages of a distributed transmitter and the first, low-noise

amplifier (LNA) stages of the receiver, as well as the phase shifter. The constrained feed networks for transmission and receiving (including monopulse networks) can then be implemented more simply, as the network loss appears only in the excitation signal input to the modular amplifiers and the outputs of the receiving LNAs, where it has negligible effect on the system performance. While the aperture illumination for transmitting is usually uniform, to take advantage of the saturated power output of the element amplifiers, it is also possible to adjust this power electronically for individual elements to control the transmit illumination function. In other respects, at least with regard to monopulse performance, the operation of the AESA is similar to that of the ESA.

There are three principal methods of electronic steering:

1. *Phase steering* by electronically controlled changes in the setting of a variable phase shifter in the feed line of each element.
2. *Time-delay steering* by electronically controlled changes in the setting of a variable time-delay device in the feed line of each element or subarray.
3. *Frequency steering* by changes in frequency. In series-fed arrays designed for frequency steering, the incremental pathlength that the wave travels between successive elements causes a frequency-dependent phase increment that is sufficient to steer the beam over the desired scan sector.

An array antenna may use different methods of steering in the two angular coordinates; for example, frequency steering in one coordinate and phase steering in the other. When steering electronically in only one coordinate, a phase shifter or other controllable device is used at each row or column, rather than at the individual element. When time-delay steering is used, it is often applied to subarrays, rather than to individual elements, which then have their own phase shifters.

Two simultaneous receiving patterns (a sum and a difference) are needed for monopulse in a single angular coordinate and three (a sum and two differences) are needed in two-coordinate monopulse. The sum and difference patterns (as well as the transmitting pattern) are all steered in the same direction and therefore they use the same settings of the element phases, but different amplitude weights.

The methods of distributing power to, and collecting power from, the elements are divided into two major categories: *space feeds* (also called *optical feeds*) and *constrained feeds* (also called *corporate feeds*). These were defined in Section 4.3. Examples of each will be given below.

The main advantage of array antennas is their ability to change beam direction rapidly, without inertia. Disadvantages include complexity, cost, and limitation of the electronic scan sector to about $\pm 60^\circ$ from broadside (normal to the array face).

The choice among the various types of monopulse processors, several of which will be described in Chapter 8, is theoretically independent of the type of

antenna used, and therefore that chapter applies equally well to array antennas. For operational reasons, however, certain combinations are unsatisfactory. For example, a multifunction radar that uses an array antenna for short dwells in various directions (perhaps only one pulse per dwell) must have a processor that provides instantaneous normalization rather than a slow-acting processor using AGC.

7.2 ARRAY COORDINATES

The most convenient coordinate system in which to express patterns of a planar array is sine space. The coordinate system was defined and explained in Section 2.8. The sine-space coordinates (u, v) of a specified direction are $u = \sin \alpha'$ and $v = \sin \beta'$ where α and β are the angles measured from normal to the x -axis and the y -axis, respectively, with the x -axis usually horizontal. Equivalent expressions for u and v are $u = \cos \alpha$ and $v = \cos \beta$, where the primes indicate the complementary angles (measured from the x -axis and the y -axis, respectively).

When a pattern of an array is steered away from broadside by a linear phase function while the amplitude function remains unchanged, the pattern broadens and becomes distorted in angle space. When plotted in sine space, however, with the axis shifted to the beam steering direction, the pattern remains nearly invariant, and the same is true of the monopulse calibration function, since it is the ratio of nearly invariant difference and sum patterns. The monopulse outputs for the two coordinates are functions of $\Delta u = \cos \alpha - \cos \alpha_{st}$ and $\Delta v = \cos \beta - \cos \beta_{st}$, where the subscript st designates the steering direction.

The channels that carry the difference signals for the two coordinates are often denoted by the symbols Δ_{az} and Δ_{el} , but it is understood that the respective coordinates are not really azimuth and elevation. The first coordinate is more properly called traverse; the second will be identified in this chapter as “elevation” for lack of a generally recognized correct name. A simple way to avoid the nomenclature problem is to label the two difference channels d_α and d_β (or Δ_α and Δ_β), with the understanding that the signals they carry are responsive to the respective components of the sine-space deviations, not angular deviations, of the target direction from the beam steering direction.

7.3 ARRAYS WITH SPACE FEEDS

The most common use of space feeds is in mechanically steered reflector and lens antennas, as discussed in earlier chapters and illustrated in Figures 4.1–4.3. In an analogous way they are used in certain types of array antennas that serve the same purpose as reflectors and lenses and in addition have the capability of rapid beam steering.

A lens-type array, illustrated in Figure 7.1(a), has radiating elements on the opposite parallel faces, coupled by electronically controlled phase shifters. A reflector-type array (or *reflectarray*), illustrated in Figure 7.1(b), has radiating elements on one face; each element is connected to a short-circuit termination through a phase shifter. The short circuit reflects the incoming wave back in the opposite direction. Since each phase shifter is traversed twice, it is set for half the desired phase shift. The phase shifter for the reflectarray must be reciprocal, in order to produce the desired phase shift in the round-trip path to and from the short circuit. This contrasts with the lens array, where nonreciprocal phase shifters can be used with their magnetic field reversed between transmission and reception of each pulse. The feed for a space-fed array can be any of the types of monopulse feeds described in previous chapters, such as a four-horn feed.

As in the case of an optical reflector or lens, an array acting as a reflector or lens converts the curved phase front from the feed into a plane wave front in

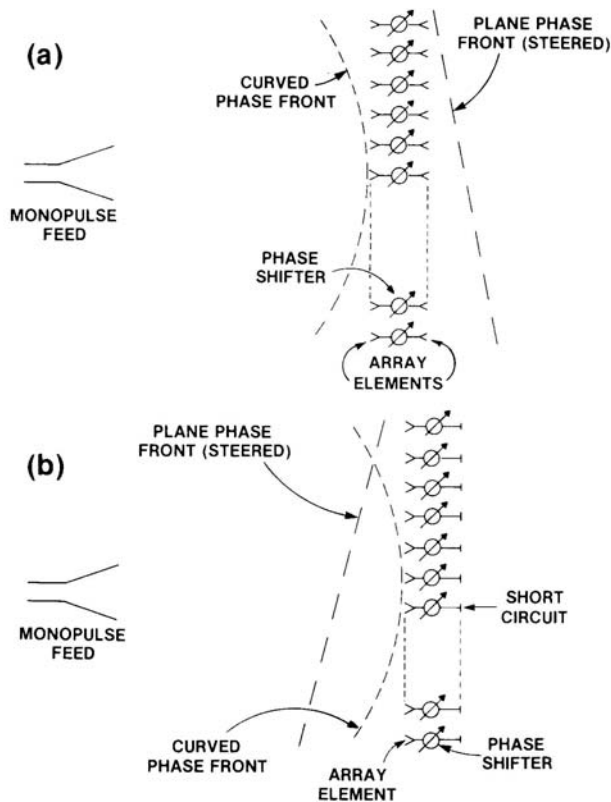


Figure 7.1 Space-fed array antennas: (a) lens; and (b) reflector.

transmission and does the reverse in reception, as shown in Figure 7.1. The conversion is accomplished by the appropriate phase function introduced by the phase shifters. Added to that phase function are the linear phase tapers needed to steer the beam to the desired direction in each coordinate. The illumination amplitude function is determined by the feed, as in the case of physical lens and reflector antennas, and the monopulse is classified as amplitude comparison, as defined in Chapter 5.

Several types of space-fed lens phased arrays have been produced in quantities. These systems combine mechanical steering of the scan field and electronic steering within that field, typically an azimuth sector of 90° to 120° and an elevation sector from the horizon to near zenith. The radars are used in fire control for land-based air and missile defense systems. The lens is a circular or elliptical planar array of passive phase-shifting elements, fed by a multihorn, multimode monopulse horn cluster evolved from those used previously in metal-plate lens and reflector antennas. The lens has uniform mechanical thickness, and by careful matching of the planar array structure and elements to the air on both sides of the lens the losses encountered in metal-plate and other lens types can be held to satisfactorily low levels. Each phase shifter is controlled electronically to provide both the focusing and the steering phase components. The monopulse features, components and performance are similar to those in mechanically steered systems.

An example of a space-fed lens array is the Russian system shown in Figure 7.2, known under its NATO name Tombstone. The array uses circularly polarized Faraday rotator phase shifters, in which right-hand circular polarization (RHCP) is



Figure 7.2 Tombstone space-fed lens array used in Russian SA-20 SAM system.

transmitted and left-hand circular polarization (LHCP) is received (or vice versa) after reflection from the target with a single bounce. These phase shifters are reciprocal, since the transmitted RHCP is shifted by the same amount as the received LHCP traveling in the opposite direction. The feed system, shown in Figure 7.3, supports this mode of operation with separate, linearly polarized transmitting and receiving feeds and a polarization screen. The transmitting horn in this case is horizontally polarized, and is located at the bottom of the sketch, directed upwards toward a planar reflecting screen oriented at a 45° angle to the lens axis and consisting of horizontal wires. After being reflected from these wires, and prior to reaching the array, the emissions pass through a polarizing grid (located beneath a plastic radome at the lower left of Figure 7.2) that converts the waves to RHCP. The phase shifters are set to convert the RHCP spherical wave from the transmitting horn into a plane wave directed to the desired angle in space.

Single-bounce reflection from the target converts the received wave to LHCP. This is focused by the lens and is converted by the polarizing grid to vertical polarization, which passes directly through the 45° screen of horizontal wires to the vertically polarized receiving feed. The eight-horn monopulse feed forms a sum pattern from the two center horns, elevation difference from the center, upper, and lower horns, and traverse difference from the center and side horns, using multi-mode techniques to optimize the sum and both difference patterns. The resulting illumination is similar to that of the 12-horn feed shown in Figure 6.7. The system needs no high-power duplexer, since the polarizing grid and 45° reflecting screen isolate the receiving feed from the transmission. A succession of Russian and Chinese fire control radars use this antenna technique, which requires the phase-shifters to be reset only when a change in beam position is required, rather than before and after each transmitted pulse. This is an important property of the array, as it permits transmission of high-PRF waveforms without the expenditure of time

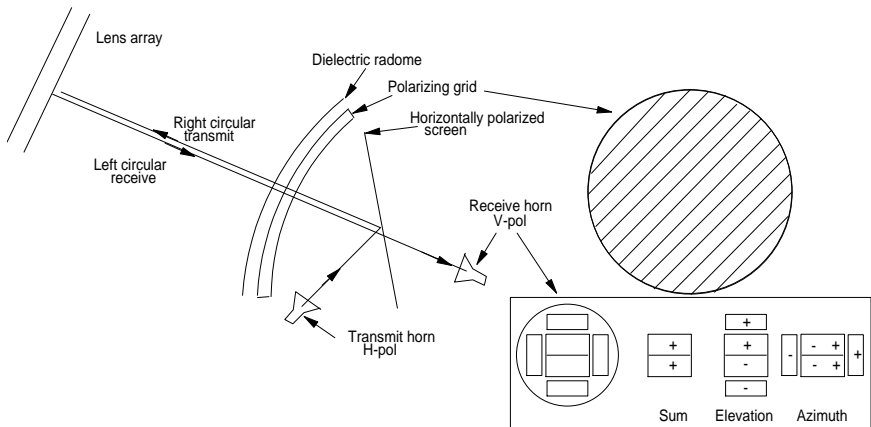


Figure 7.3 Method of feeding the Flap Lid lens array.

and control power to switch the phase shifters at twice the PRF, as would be necessary if they were not reciprocal.

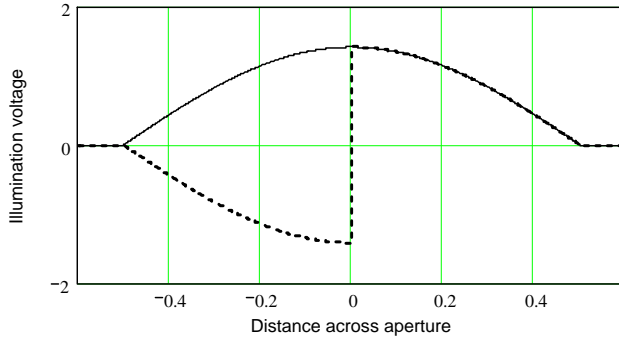
7.4 ARRAYS WITH CONSTRAINED FEEDS

In a constrained feed, power is distributed to, and collected from, the elements by waveguides or transmission lines (constrained within the walls or outer conductors). An advantage of array antennas with constrained feeds is the high degree of control that they permit in the design of illumination amplitude functions to obtain desired patterns. In addition, they have no spillover and no blockage, although they may have significant loss in the feed network. Simultaneous optimization of the sum and difference patterns is possible, in contrast to the compromise that is usually necessary in reflector or lens antennas (see Chapter 6). This does not mean that optimization is necessarily fully achieved in the design of an array antenna; for economy and design simplification some compromises are often made, but optimization can be approached more closely than in reflector or lens antennas.

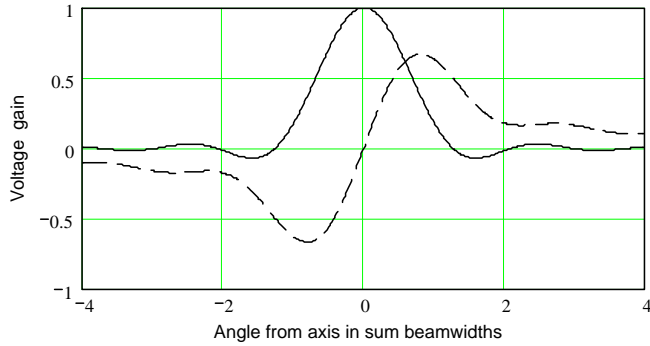
7.4.1 Constrained-Fed Arrays Divided into Quadrants or Subarrays

A simple method of obtaining monopulse operation is to split the array into symmetrical quadrants. The outputs of the elements in each quadrant are summed to produce four signals that are then combined to form a sum and two differences. Figure 7.4(a) shows a cosine sum illumination and a difference illumination formed in a quadrant-split array. The discontinuity at the center of the difference illumination causes high sidelobes in the corresponding difference pattern, shown in Figure 7.4(b). These sidelobes extend many beamwidths each side of the axis, accepting interference (jamming, clutter, multipath reflections) that can greatly increase the tracking error. A plot of the patterns in decibel form, covering ± 15 beamwidths from the axis, is shown in Figure 7.5. The difference sidelobes remain above -30 dB throughout this sector, falling away slowly at larger angles.

The need to compromise between sum and difference channel performance can be eased by dividing the aperture into more than two modules in each coordinate, at the expense of additional hybrids and couplers. One approach to reducing the center discontinuity is to subdivide each quadrant of the array into subarrays, and use a more complicated network to adjust separately the sum and difference coupling to these subarrays. The waveguide network behind a flat-plate waveguide antenna then appears more like that shown in Figure 7.6. Within each subarray, the power-splitting network can be implemented in stripline or printed structure not visible in this photograph.



(a) Illumination functions: sum (solid curve); difference (dashed curve)



(b) Antenna patterns: sum (solid curve); difference (dashed curve)

Figure 7.4 (a, b) Illumination functions and patterns of quadrant-split monopulse array using cosine sum illumination.

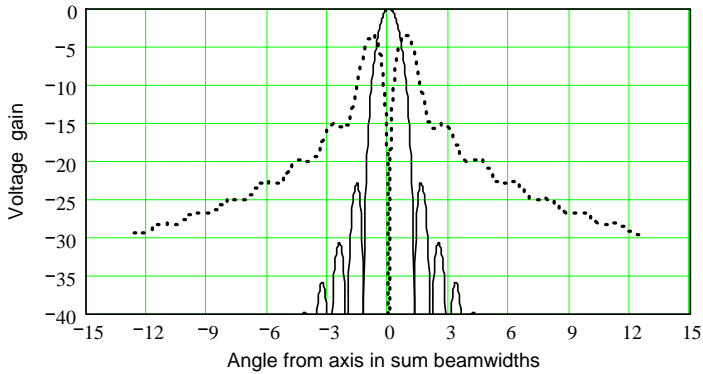


Figure 7.5 Decibel plot of antenna patterns for quadrant-split monopulse array.

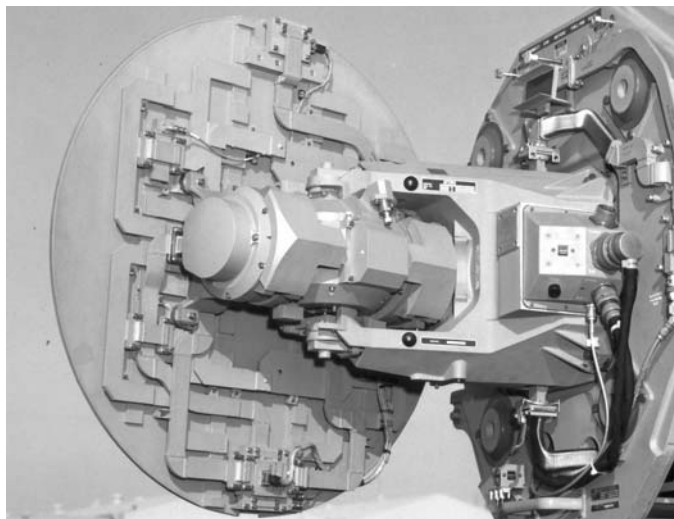


Figure 7.6 Power-dividing network for flat-plate waveguide array with subarrays.

7.4.2 Constrained-Fed Arrays with Independent Illuminations

Two monopulse feed arrangements will be shown that permit essentially independent shaping of sum and difference patterns so that each can be optimized. The first is illustrated in simplified form in Figure 7.7. An example of its use is in the AN/SPY-1A radar [7]. Figure 7.7(a) shows one column of the array. Each symmetrical pair of elements is connected to a hybrid that yields the sum and difference of the pair. The sums of all pairs are added with an appropriate set of weights in the column sum combiner to produce the column sum, and the differences of the pairs are added with a different set of weights in the column difference combiner to produce the column difference.

Figure 7.7(b) shows how the sum and difference signals of the entire array are formed. The column sums from all the columns are combined in symmetrical pairs, each pair being connected to a hybrid that yields their sum and difference. The sums and differences of all the column sum pairs go to the array sum combiner and the α (traverse) difference combiner respectively, where they are added with independent sets of amplitude weights to obtain the array sum voltage s and the traverse difference voltage d_α . Likewise, the column differences from all the columns are combined in symmetrical pairs, each pair being connected to a hybrid that produces their sum and difference. The difference is terminated in a dummy load. The sums of all the column difference pairs are added with appropriate weights in the “elevation” combiner to obtain the “elevation” difference voltage d_β for the entire array.

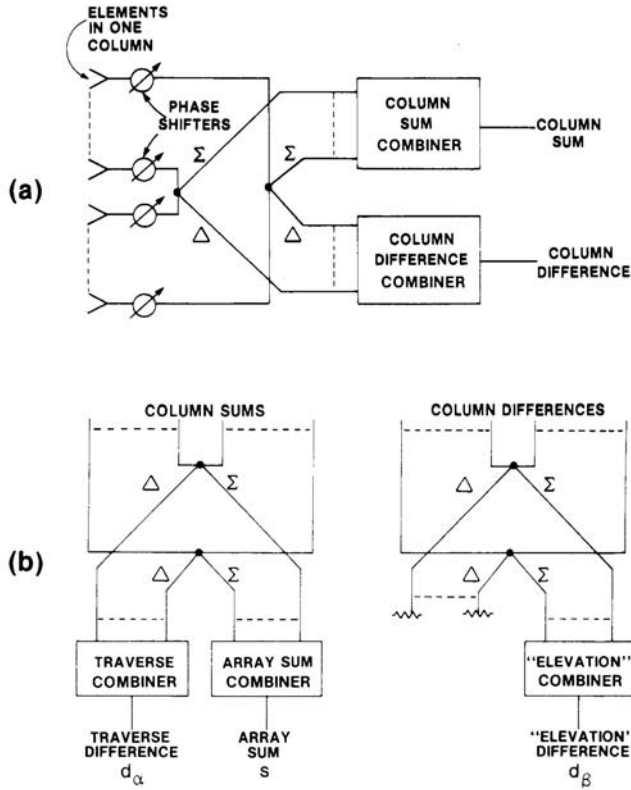


Figure 7.7 Array with nearly independent sum and difference illuminations: (a) formation of column sum and difference; and (b) formation of array sum and differences.

Because different sets of amplitude weights are used in the different combiners shown in Figure 7.7, the aperture amplitude distributions can be tailored independently for the sum and the two differences to obtain nearly optimized patterns. In the arrangement shown in that figure the independence is not complete because the sum and traverse difference share the same weighting within each column. However, this dependence imposes very little penalty on performance, since the optimum weighting within each column is nearly the same for the sum and traverse difference. Completely independent amplitude distributions for the sum and the two differences can be obtained at the price of additional complexity.

A second method of optimizing both sum and difference illuminations is the Lopez feed, described in [8] and shown in Figure 7.8. Each element is coupled to both the primary and the secondary line, shown in Figure 7.8(a). The primary feed line and couplers are designed to handle the full transmitter power and produce

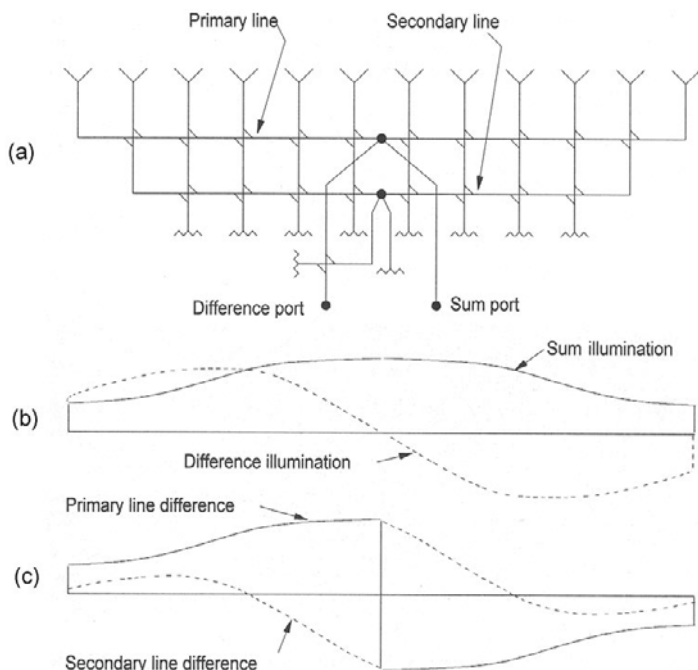


Figure 7.8 Lopez feed: a dual-ladder network for separate optimization of sum and difference excitation of a linear array: (a) dual-line network; (b) desired illumination functions; and (c) illumination functions produced by primary and secondary lines. (After: [8].)

the desired sum illumination function shown in Figure 7.8(b). The difference port of the hybrid at the center of the primary line would produce the center discontinuity, as in Figure 7.8(c) and in Figure 7.4(a). The coupling to the secondary line modifies each element's coupling to the difference port, canceling the discontinuity in the difference illumination and producing the desired smooth difference illumination function shown in Figure 7.8(b).

The examples discussed here and in Section 7.4.1 are intended only to illustrate the variety of ways in which monopulse can be implemented in arrays with constrained feeds. Other examples can be found in the cited references.

7.4.3 Efficient Illumination Tapers for Phased Arrays

A corporate feed that permits independent control of illumination functions for sum and differences can implement tapers such as those defined by Taylor [9, 10] and Bayliss [11], that combine low sidelobes with narrow beamwidth and high efficiency. Patterns using the "Taylor \bar{n} taper" have the property that the first \bar{n} sidelobe peaks on each side of the main lobe are all equal to a specified level. The

parameter \bar{n} is related to the ratio of beam-axis power gain to peak sidelobe power gain SLPR by

$$\bar{n} = \text{floor}[2A + 0.5] \quad (7.1)$$

where $A = (1/\pi) \cosh^{-1} \sqrt{\text{SLPR}}$ and the function $\text{floor}(x)$ is the first integer below x . The first $\bar{n} - 1$ zeroes in the pattern on each side of the main lobe are located at angles

$$\begin{aligned} z_n &= \pm \bar{n} \sqrt{\frac{A^2 + (n - 0.5)^2}{A^2 + (\bar{n} - 0.5)^2}}, \quad n \leq \bar{n} \\ &= \pm n, \quad \bar{n} < n \end{aligned} \quad (7.2)$$

and the pattern is

$$s(u) = \text{sinc}(\pi u) \prod_{n=1}^{\bar{n}-1} \frac{1 - (u/z_n)^2}{1 - (u/n)^2} \quad (7.3)$$

Sidelobes beyond $\bar{n} - 1$ on each side fall off with increasing u . For example, for $\text{SLPR} = 1,000 = 30 \text{ dB}$, $\bar{n} = 3$, and the pattern is shown in Figure 7.9(a). One method of establishing the difference-channel illumination function $g_d(x)$ is to weight the sum illumination function $g(x)$ by the linear-odd function, producing the function $g_d(x) = xg(x)$ and a pattern that is the derivative of the sum pattern with respect to angle, as shown in Figure 7.9(b). Note that the first difference-pattern sidelobes using this method are 10 dB higher than those of the sum pattern and fall off steadily with off-axis angle. In order to hold the maximum difference-pattern sidelobes to the same level as those of the sum pattern, it would be necessary to base the difference illumination function on a sum taper with lower sidelobes than those of the actual sum pattern (-40 dB , in this case).

Plots of sum and difference patterns and illumination functions, and tables listing the beamwidth factors, efficiencies, and difference slopes for several sidelobes levels are presented in [12]. For the patterns shown in Figure 7.9, the values are as in Table 7.1 (where the aperture efficiency assumes equal tapers in the two coordinates).

Similar results are obtained for the Taylor circular-aperture tapers and the Bayliss taper. The latter is a difference-channel taper designed to maximize slope, for a given sidelobe level with the circular aperture.

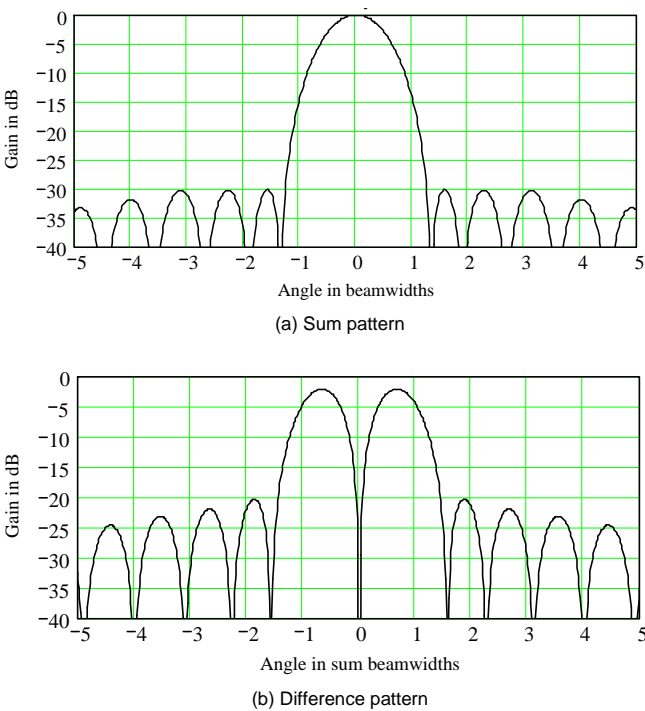


Figure 7.9 (a) Sum and (b) difference patterns for Taylor taper, $G_s = -30$ dB, $\bar{n} = 3$.

Table 7.1 Typical Taylor Array Parameters

Sidelobe level:	-30 dB
Aperture efficiency η_a :	0.738
Beamwidth θ_{bw} :	$1.118 \lambda/w$
Difference slope K :	0.506
Difference slope ratio K_r :	0.918
Monopulse slope k_m :	1.195

7.5 CLASSIFICATION AS AMPLITUDE OR PHASE COMPARISON

Chapter 5 discussed the classification of monopulse radars as amplitude comparison or phase comparison, based on the convention that the distinction resides in the antenna (including the feed system and the comparator or beamformer), not in the processing that follows.

In a reflector or lens antenna the distinction is obvious from the physical construction. By analogy, the space-fed arrays described in Section 7.3 are all seen to belong to the amplitude-comparison class.

In constrained-fed arrays the distinction is usually not evident from the external physical appearance, but requires knowledge of the feed and beamformer. The first array described in Section 7.4.1 is divided into four quadrants to produce monopulse operation. This type of array is equivalent to the four-reflector antenna shown in Figure 5.5 and is likewise classified as phase comparison. The classification of the first array described in Section 7.4.2 (and illustrated in Figure 7.7) can be determined by either of the criteria listed in the last two columns of Table 5.1, namely the relative phase of the sum and difference voltages or the relative phase of the sum and difference aperture illuminations. The relative phase in each case is interpreted on the assumption that the hybrids and combiners are of types that introduce no relative phase shift (see Section 4.4). Since the steering phase affects the sum and difference equally, it can be ignored, so the analysis is simplified by assuming broadside (unsteered) patterns.

Consider first a single column of the array, as in Figure 7.7(a). When the array is receiving a plane wave from a distant target which is off-axis in "elevation," any symmetrically located pair of elements will deliver voltages like those labeled e_1 and e_2 in Figure 7.10. The sum and difference phasors in the figure are reduced in length by a factor of $\sqrt{2}$, for the reason explained in Section 2.4. Voltages e_1 and e_2 have equal amplitudes but different phases. Their phase difference is proportional to the distance of the pair of elements from the center, but the sum voltage of any pair always has the phase that would be obtained from an element located at the center of the column. The difference voltage of the pair differs in phase by 90° from the sum. Since the sums of all the pairs have equal phase and the differences of all pairs have equal phase, the column sum and the column difference are in phase quadrature.

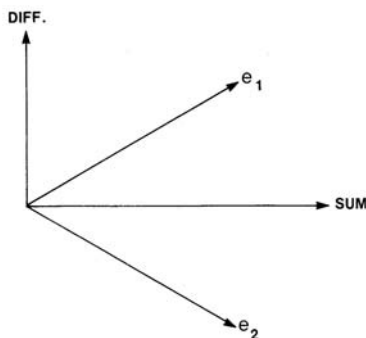


Figure 7.10 Phase relationships of a symmetrical pair of elements, their sum, and their difference.

with the aid of Figure 7.7(b), it is found that when the target is off-axis in both coordinates, the d_α and d_β difference voltages are in phase quadrature with the sum voltage s . According to the next-to-the-last column in Table 5.3, this type of array is therefore classified as phase comparison.

The same conclusion is reached by examining the relative phase of the sum and difference illumination functions. This is most easily visualized by assuming transmission and invoking reciprocity for reception. Examination of Figure 7.7 shows that if the same transmitter were connected in turn to each of the three ports s , d_α , and d_β , the aperture illumination would have the same phase in all three cases (180° phase being regarded as 0° phase with a change in sign of the amplitude). The last column of Table 5.3 again leads to the phase-comparison classification.

There is an interesting difference, however, between this example of phase-comparison monopulse and that of the four-reflector cluster shown in Figure 5.5. In the reflector antenna the illumination for each of the component beams (from which the sum and differences are obtained) is limited to one quadrant, with no overlap except for a small amount of spillover between the reflectors. In the array antenna the component beams do not exist physically; that is, there are no points in the system where their voltages are present. However, their illumination functions can be derived mathematically by addition and subtraction of the known sum and difference illumination functions and division by $\sqrt{2}$, as with the pattern voltages in (2.3) and (2.4). In an example, the sum and difference illuminations are assumed to be a cosine function and a full-cycle sine function, respectively. The relative scales of the sum and difference illuminations are such that the total sum and difference powers are equal. The resulting illumination functions for the fictitious component beams are shown in Figure 7.11. They show that the illumination functions of the component beams overlap, and in fact each one extends

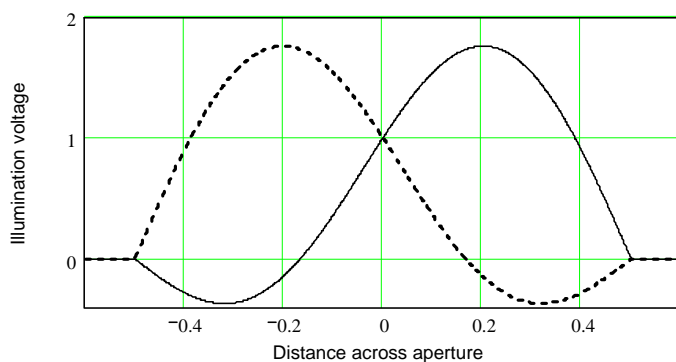


Figure 7.11 Derived illumination functions for fictitious component beams in phase monopulse array: beams from right side (solid curve) and left side of aperture (dashed curve).

over the entire array aperture. They produce the same amplitude patterns but with different phase centers. Actual illumination functions may differ from those assumed in Figure 7.11 but will generally be similar in form.

Usually the amplitude-comparison or phase-comparison classification of a constrained-fed array is a matter of academic rather than practical interest. More important descriptors are the method of steering, the angular coverage, the specific type of feed, the type of elements, and the sum and difference illumination functions. The amplitude- or phase-comparison classification can be ambiguous unless the users of these terms adhere to a common set of definitions and criteria such as those presented in Chapter 5. Thus, the classification is not affected by the type of processor or by any operation subsequent to the formation of the sum and difference.

7.6 SPECIAL TYPES OF ARRAYS

Although mechanical and electronic steering have been treated separately, they are sometimes combined in hybrid arrangements. For some applications rapid electronic steering is needed only over a narrow electronic sector at any one time, and that sector can be centered in any required direction by slower, less agile mechanical steering or mechanical scanning of the entire array. Such a combination can be simpler and cheaper than all-electronic steering over a wide angle. Another arrangement consists of mechanical rotation of the array in azimuth combined with electronic steering or scanning in elevation. (Even when the array is designed for electronic steering in only one coordinate, it can have monopulse in both coordinates.) It is also possible to feed a mechanically steered reflector with a small array (in lieu of a horn feed) for rapid steering over a small angle from the reflector axis. In such hybrid arrangements the monopulse techniques are essentially the same as in other array antennas. The required coordinate conversions (usually to azimuth and elevation) may be either simpler or more complicated than in fixed arrays, depending on the configuration.

Monopulse operation is not limited to planar arrays. It can be implemented, for example, in circular or conformal arrays. The coordinate system described in Section 7.2 does not apply to nonplanar arrays. The coordinate system and the phase function needed to “flatten” the curves phase front must be worked out for each configuration.

References

- [1] W. H. Von Aulock, “Properties of Phased Arrays,” *Proc. IRE*, Vol. 48, No. 10, October 1960, pp. 1715–1727. Reprinted, *Significant Phased Array Papers*, R. C. Hansen, (ed.), Dedham, MA: Artech House, 1973.

- [2] R. C. Hansen, *Microwave Scanning Antennas*, Vols. I–III, New York: Academic Press, 1964.
- [3] R. C. Johnson, (ed.), *Antenna Engineering Handbook*, New York: McGraw-Hill, 1993.
- [4] R. C. Hansen, *Phased Array Antennas*, New York: John Wiley & Sons, 1998.
- [5] R. J. Mailloux, *Phased Array Antenna Handbook*, Norwood, MA: Artech House, 2005.
- [6] J. Frank and J. D. Richards, “Phased Array Radar Antennas,” Chap. 13 in *Radar Handbook*, M. I. Skolnik, (editor-in-chief), 3rd ed., New York: McGraw-Hill, 2008.
- [7] R. M. Scudder and W. H. Sheppard, “AN/SPY-1 Phased Array Antenna,” *Microwave J.*, May 1974, pp. 51–55.
- [8] A. R. Lopez, “Monopulse Networks for Series Feeding an Array Antenna,” *IEEE Trans. Antennas and Propagation*, Vol. 16, No. 4, July 1968, pp. 436–440.
- [9] T. T. Taylor, “Design of Line-Source Antennas for Narrow Beamwidth and Low Sidelobes,” *IRE Trans. Antennas and Propagation*, Vol. AP-3, No. 1, January 1955, pp. 16–18.
- [10] T. T. Taylor, “Design of Circular Apertures for Narrow Beamwidth with Low Sidelobes,” *IRE Trans. Antennas and Propagation*, Vol. AP-8, No. 1, January 1960, pp. 17–22.
- [11] E. T. Bayliss, “Design of Monopulse Antenna Difference Patterns with Low Sidelobes,” *Bell System Tech. J.*, Vol. 47, No. 5, May-June, 1968, pp. 623–650.
- [12] D. K. Barton and H. R. Ward, *Handbook of Radar Measurement*, Englewood Cliffs, NJ: Prentice-Hall, 1969. Reprinted, Dedham, MA: Artech House, 1984.

Chapter 8

Monopulse Processors

The monopulse processor is that portion of a monopulse radar that operates on the voltages derived from the simultaneous antenna patterns to produce the monopulse outputs. This chapter deals with the functions, properties, and design characteristics of monopulse processors.

It is difficult to categorize the many types of monopulse processors, since endless variations exist or are possible. We will define an *exact* processor, which will serve as a baseline reference, and then describe several practical types of processors. The names used to identify them have been chosen somewhat arbitrarily, since the names are not standardized. Examples of specific radars that use or have used some of these types of processors will be mentioned where appropriate.

Most of the practical processors produce outputs essentially identical to those of an exact processor when operating on signals from a point target in the clear, not too far from the beam axis, at a high signal-to-noise ratio. However, they differ in their responses to large angular deviations from the axis and in errors caused by low signal-to-noise ratio, external interference, and unresolved targets, including the special cases of multipath and single-target glint. Therefore, in analyzing or simulating monopulse performance under those conditions, the modeling should be based on the characteristics of the processor actually used rather than assuming an exact processor, as is often done.

In the diagrams of the various processors only a single angle channel will be shown. Unless it is otherwise stated, it is to be understood that if monopulse is used in both angular coordinates, a corresponding processor must be added for the other coordinate.

Two-coordinate monopulse normally requires three receiver channels. However, descriptions will be given of special forms of monopulse reported in the technical literature (although not necessarily adopted for practical use) that require only two channels or a single channel.

8.1 FUNCTIONS AND PROPERTIES OF MONOPULSE PROCESSORS

The voltages on which the monopulse processor operates may be those of the component beams (for example, the squinted beams in amplitude-comparison monopulse) or the sum and difference voltages, usually the latter. The word “sum” is used here in a broad sense to include a reference voltage used in place of a sum. In designing a monopulse processor to operate on the sum and difference voltages, it makes no difference whether those voltages are obtained from an amplitude-comparison or phase-comparison antenna, except that it may be necessary to insert a 90° relative phase shift (or interchange I and Q components) as explained in Chapter 5. It also does not matter whether the antenna uses a lens, a reflector, or an array.

It is not always possible to draw a sharp line separating the monopulse processor from other portions of the radar, since some functional components may overlap and share common hardware. The monopulse processor usually follows the receivers, but sometimes the receivers are part of the processing function. The monopulse processor in turn is often considered part of the signal processor. In some cases the monopulse processing is done by a computer, which also performs other radar functions. The monopulse processor is therefore identified by function and not necessarily by separate hardware.

The monopulse outputs are a pair of voltages or digital numbers related to the two angular components of the target direction relative to the beam axis. The relationship is represented by a calibration function (sometimes called the “discriminator curve”) by which each monopulse output can be converted into a corresponding angle estimate.

The monopulse output for each angular coordinate is used in either or both of the following ways: (1) as an input to a servo that drives the antenna mechanically or steers the pattern electronically toward a null in the monopulse output, or (2) as an open loop indication of the off-axis target angle (with the appropriate scale factor or calibration function). In (1) the target direction is indicated by the mechanical shaft rotation angles obtained from synchro, potentiometer, or digital read-outs; or in the case of electronic steering the target direction is taken to be the direction of the beam steering orders. In (2) the target direction angle in each coordinate is the sum of the corresponding beam-axis angle, obtained as in (1), and the angle of the target from the beam axis.

One characteristic of a monopulse processor is of fundamental importance: the output should depend on the complex ratio (that is, the amplitude ratio or phase difference, or both) of the voltages derived from the antenna, not on their absolute magnitudes or phases. This characteristic is necessary in order to make the output dependent only on the angle of the target, not on its range or radar cross section. The process of obtaining a ratio (called *normalization*) is a nonlinear operation. No processor does it perfectly. One of the main differences among various kinds of monopulse processors is the method and accuracy of normalization. Note

that the nonlinear nature of this essential step in obtaining monopulse outputs requires that any Doppler filtering needed to remove clutter from the receiver outputs must be performed in the sum and difference channels before normalization. Otherwise the nonlinearity of the process will degrade the signal-to-clutter ratio relative to what would be obtained with linear Doppler processing.

There are other properties of monopulse processors that usually are desirable and may or may not be essential, depending on the application. Among them are the following:

1. The output for each angular coordinate should be an odd function of angular deviation (or sine-space deviation in the case of an electronically steerable array) from the beam axis. That is, equal target deviations to the left and right or above and below the axis should produce equal and opposite outputs. Since the property is inherent in the difference-to-sum antenna pattern ratio in most cases, the processor merely is required to preserve it. Lack of odd symmetry would cause difficulty in the closed-loop response characteristics, and would make open-loop calibration more complicated.
2. The monopulse output should be very nearly proportional to off-axis angle (or sine-space deviation) for small angles. Since this property is inherent in the difference-to-sum voltage ratio in most cases, the processor merely is required to preserve it.
3. The processor should maintain its performance over a wide dynamic range of input signal strength. This property is important in applications where accuracy must be maintained while radar cross sections and ranges of targets may vary widely.
4. The output for each angle coordinate should be as nearly independent as possible of the target angle in the other coordinate. In practice the antenna often produces minor interaction or cross-talk between the two off-axis components. This may require two-dimensional calibration. The processor should not contribute additional cross-talk.
5. The angular error due to thermal noise should be as small as possible. Some processors have the smallest possible value of error, which is determined by the antenna pattern and the signal-to-noise ratio. Others have larger errors.
6. The angular error due to external interference, multipath, or undesired targets in the same resolution cell as the desired target should be as small as possible. Various types of processors differ in their errors due to these causes even though they may give identical outputs for a single target in a clear environment.

For closed-loop null tracking, where the antenna axis is usually close to the target direction and angle estimates are obtained from the shaft rotation angle

read-outs, relatively crude monopulse calibration suffices. This consists only of determining the monopulse slope and adjusting the servo loop characteristics accordingly to obtain proper dynamic response. If electrical correction signals (the residual monopulse outputs) are used to refine the angle estimates, the calibration must be more accurate but usually it still is within the linear range. In multifunction array-radar operation, targets may be one-half beamwidth or more off axis and the calibration must include the nonlinearity.

One of the main problems in the design of a practical processor is normalization, which means the division (or equivalent process) needed to produce the ratio $|d|/|s|$. Accurate normalization is especially difficult if the division is done by analog processing.

If normalization is done digitally, any desired accuracy can be achieved in the division process itself (except when s approaches zero), depending on the number of bits used; the accuracy is then limited by other factors, such as the analog-to-digital (A/D) converters, amplitude matching of the receiver channels, and so forth. The signal strength may vary over tens of dB or even 100 dB or more, and maintaining the desired accuracy over such a wide dynamic range is one of the problems. Phase tracking of the receiver channels must also be maintained, since the cosine of the difference-to-sum relative phase is a factor in the monopulse output. Obtaining the desired accuracy of normalization imposes accuracy requirements not only on the processor itself but also on the receivers, A/D converters, and any other devices that operate on the signals.

8.2 RANGE GATING

In a pulsed radar the echoes from the target whose direction is being tracked or measured arrive at a time corresponding to the target range. All other ranges contribute only noise, clutter, or unwanted returns from other targets. To enable the monopulse processor to reject extraneous echoes and noise and to operate only on echoes received from the desired target, a range tracking loop keeps a range gate (time gate) centered on the desired target. A gate whose width is matched to the transmitted pulse is used as a matched filter following a wideband receiver. When matched filtering for the pulse occurs earlier in the receiver, a short sampling strobe is used to create an effective range gate whose width is equal to the width of the receiver impulse response, and that width preceding the strobe can be considered as the "range gate." Only signals from the receiver output during the gate are passed on to the monopulse processor. If there is AGC, it also responds only to outputs within the gate. The position of the gate provides measurement of target range. The range gating feature is not unique to monopulse but is needed in all angle-tracking pulsed radars.

In radars with doppler processing, a "velocity gate" formed by a filter that tracks the target doppler shift provides resolution in that coordinate, replacing or

supplementing the range gate. The range gate is not needed in continuous-wave radar or in a passive (receive-only) monopulse system such as one used for receiving signals transmitted or relayed from Earth satellites. A radar that normally transmits and receives may also have a receive-only mode. For example, it has been demonstrated that a radar can track the sun passively in angle (for boresighting) by using the radio-frequency radiation from the Sun [1, 2]. Military radars often have a “track-on-jam” mode for angular location of noise jamming sources. In such applications the signals are received in all range cells. In the following sections, where the term “range gate” is used, it should be understood that the discussion also applies to a velocity gate.

With an electronically steered array it is possible to track several targets on a time-shared basis, since the beam direction can be switched almost instantly to each target in turn. Each target has its own range gate. With a reflector antenna only one target at a time can be tracked in angle, but it is possible to provide additional range gates, each with appropriate normalization circuits, in which other objects within the beam can be observed at the same time. From their monopulse outputs their angular positions relative to the beam axis can be measured.

8.3 ANGULAR COORDINATES FOR MONOPULSE CALIBRATION

If the antenna has a planar aperture with constant-phase illumination (approximately true of the sum and difference in a reflector antenna) or uniformly tapered phase illumination (true of the sum and difference in an electronically steered array), then the natural angular coordinates (that is, the coordinates in which the patterns are expressed most simply) are those denoted by α' and β' in Section 2.8. More specifically, the pattern equations are functions of Δu and Δv , defined by

$$\Delta u = u - u_{st} \quad (8.1)$$

$$\Delta v = v - v_{st} \quad (8.2)$$

$$u = \sin \alpha' \quad (8.3)$$

$$v = \sin \beta' \quad (8.4)$$

$$u_{st} = \sin \alpha'_{st} \quad (8.5)$$

$$v_{st} = \sin \beta'_{st} \quad (8.6)$$

In these equations, all angles are measured from “broadside” (the normal to the aperture). The subscript *st* indicates the direction to which the beam axis is steered in an electronically steerable array and the letters without subscripts refer to the

target direction. In a reflector antenna the beam usually is not steerable relative to the aperture normal, so $u_{st} = v_{st} = 0$.

In a reflector antenna that has a beamwidth no greater than a few degrees, it makes little difference whether the normalized difference signal is expressed as a function of the angle coordinates (α', β') or sine-space coordinates (u, v) , since they are nearly equal. Angle α' for this type of antenna is called traverse (or traverse “error”) and is approximately the azimuth deviation of the target from the beam axis, multiplied by the cosine of the target elevation angle. Angle β' usually is called elevation “error,” although that name is not exactly correct; it is approximately equal to the elevation angle of the target from the beam axis when α' is small and is exactly equal to that deviation when $\alpha' = 0$.

In an electronically steered array, angles α' and β' have no standardized names, although they are sometimes loosely referred to as “azimuth error” and “elevation error” for lack of better names. Since the beam axis direction may differ widely from the aperture normal direction, the exact relations given in (2.25) and (2.26) must be used to relate α' - β' coordinates to azimuth-elevation coordinates.

If the sum and difference patterns of an electronically steered array were plotted as functions of the angular deviation from the beam steering direction (that is, $\alpha' - \alpha'_{st}$ or $\beta' - \beta'_{st}$) the patterns would broaden as the steering angle increased; therefore, a different monopulse calibration function would be needed for each different steering angle. When the patterns are plotted as functions of *sine-space* deviation Δu or Δv , the patterns remain essentially invariant with the steering angle except that both patterns decrease in amplitude as the steering angle increases (as a result of the element pattern). Since this applies equally to sum and difference patterns, the monopulse calibration remains essentially invariant with the steering angle. Thus the use of sine-space coordinates for monopulse calibration and target tracking provides a great advantage in electronically steered arrays but not in reflector antennas.

8.4 EXACT MONOPULSE PROCESSOR

In Chapter 5 it was shown that depending on the type of antenna and comparator, the relative phase between the sum and difference signals from an off-axis target has a nominal value of either 0° or 90° , so that the ratio d/s is nominally either pure real or pure imaginary. The nominal value, however, applies only to a point target with no noise, clutter, multipath, or interference, and to a radar with no imperfections. It was pointed out in Chapters 3 and 5 (and will be explained further in Chapter 9) that in practice the relative phase between s and d is not confined to 0° or 90° and that therefore the ratio d/s is complex in general.

To avoid having to deal separately with the cases of 0° and 90° nominal relative phase, we will assume hereafter that it is 0° (the reversal of the difference voltage on crossing the axis being treated as a change in sign of the amplitude rather than as a 180° phase jump). For radars in which the nominal relative phase is 90° it is only necessary to interchange reals and imaginaries (or sines and cosines) in the equations, or to introduce a 90° phase shift in the appropriate circuits. As will be shown in Chapter 12, it makes a difference whether such a phase change is introduced in the RF or IF portions of the receiver (but that does not affect the material in this chapter).

Since it usually is not possible to predict the specific deviations of the relative phase from its nominal value under the variety of conditions of operation, the radar is designed for the nominal relative phase.

We arbitrarily define an *exact* monopulse processor as one that produces the real part of the complex ratio perfectly for each angle coordinate. This does not mean necessarily that such a processor (if it existed) would be better, for every application, than an inexact processor or one designed for a different type of output, but it serves as a reference with which practical processors can be compared. All monopulse processors are inexact to some degree because of equipment or alignment imperfections, finite dynamic range, and other limitations, or because they are designed for a different type of output. For some radars rough approximations suffice, permitting simplification of equipment and reductions in cost.

The output of the exact processor is

$$\operatorname{Re}(d/s) = \frac{|d|}{|s|} \cos \delta \quad (8.7)$$

where δ is the phase of the difference relative to the sum. The output is the magnitude ratio of the difference to the sum, multiplied by the cosine of their relative phase. In other words, it is the component of the difference that is in phase with the sum, divided by the magnitude of the sum.

If it is desired to obtain the imaginary as well as the real part of d/s (that is, the quadrature-phase as well as the in-phase component of the normalized difference signal), a second monopulse processor can be added, using the same inputs but with one of them shifted 90° . If both processors are exact, their outputs form the complex ratio of d/s . The imaginary part is

$$\operatorname{Im}(d/s) = \frac{|d|}{|s|} \sin \delta \quad (8.8)$$

The derivation of (8.7) and (8.8) was given in Chapter 3.

The usual practice is to process the real part and ignore the imaginary part. The rationale is that the target contributes only to the real part while noise, interference, and clutter contribute equally to the real and imaginary parts. Hence, by using the real part only, the angular accuracy in the vicinity of the null is improved by the equivalent of a 3-dB increase in signal-to-noise ratio. Furthermore, since the cosine factor changes sign on crossing the axis, it provides sense as well as magnitude of the angular deviation from the axis.

The imaginary part, although not normally used, contains information that may be useful in certain special applications, particularly to detect the presence of unresolved targets or multipath and to reduce the resulting errors. Such possible applications will be discussed in Chapter 9.

The fact that the exact processor, by definition, follows (8.7) exactly does not mean that it would yield the exact location of the target. The output is subject to errors due to noise, imperfections in other components or in calibration, and external causes.

8.5 PROCESSOR USING PHASES AND LINEAR AMPLITUDES OF s AND d

One obvious approach to monopulse processing, illustrated in Figure 8.1 for one angle channel, is to measure the amplitudes of the sum and difference signals at the outputs of linear receiver channels, measure their phase difference (or their phases individually, and subtract), digitize these measurements, then compute the monopulse output by (8.7). The relative phase δ in that equation is the difference-voltage phase δ_d minus the sum-voltage phase δ_s . The imaginary part of d/s , if needed, is obtained the same way except that the cosine is replaced by the sine.

This is a straightforward approach to an exact processor in concept but it may impose severe demands on the dynamic range of the receivers, A/D converters,

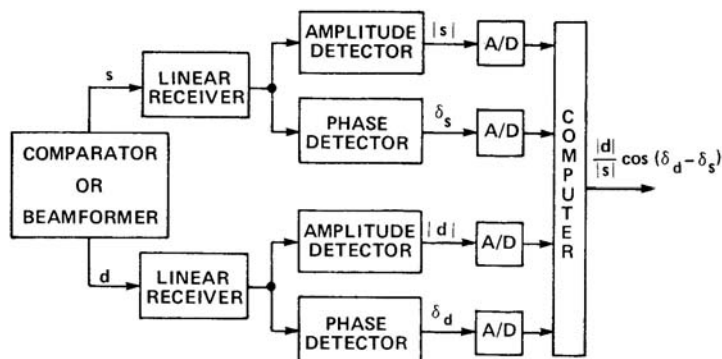


Figure 8.1 Processor using phase and linear amplitudes of s and d .

and phase detectors in order to perform properly over the required dynamic range of signals. Furthermore, the mathematical operations indicated by (8.7), if performed on every pulse, may place a sizable load on the computer, if many pulses are exchanged with the target.

Dynamic range of monopulse receivers, mentioned briefly in Section 4.5, needs further explanation. A distinction is made between *instantaneous* and *expanded* dynamic range. The instantaneous dynamic range of linear operation of a receiver is the range over which the output voltage remains proportional to the input voltage on each pulse. This dynamic range is inversely proportional to the bandwidth of the receiver and it depends also on the degree of care (and expense) devoted to the design. For typical receiver bandwidths of the order of a megahertz, a 60-dB linear dynamic range of IF output is well within the state of the art, and 70 or 80 dB is achievable with very sophisticated and painstaking design. However, the limiting factor in amplitude measurement is the envelope detector, which typically has a linear dynamic range of less than 30 dB. For some monopulse applications an instantaneous dynamic range of 30 dB or less is adequate, but other applications require linear operation on signal strengths that vary over a much larger dynamic range.

An *expanded* (or *total*) dynamic range can be obtained by the use of automatic gain control (AGC) or switchable attenuators, or both, to keep the signal level within the "window" of instantaneous dynamic range. Analog AGC is relatively slow-acting and will cause errors in normalization when a target is off axis and is fluctuating in amplitude from pulse to pulse. Switchable attenuators are usually preferable. The problem is to know when to switch. If the target is being tracked continuously or during a dwell of several pulses, the amplitude of each pulse in the sum channel indicates whether the signal strength is approaching, or has reached, a point where switching is required. The switching is not retroactive to the pulse on which the measurement was made, so there is a possibility that the pulse preceding the switching will yield bad data. However, this is unlikely except perhaps on the first pulse of a dwell. The instantaneous dynamic range (without switching the attenuators) is usually adequate to accommodate pulse-to-pulse cross-section fluctuations of any one target at constant range.¹ The attenuators are needed because of the increased dynamic range requirement imposed by the changing range of any one target and by different ranges and average cross sections of various targets. In continuous track on any one target the attenuators are unlikely to need frequent switching.

However, in an electronically steerable multifunction array system that performs interleaved track (and sometimes search) on multiple targets of various cross sections and at various ranges, there may be only one pulse or a few pulses

¹ There are of course exceptions. For example a large, rapidly rotating cylindrical target can exhibit a very brief and very large specular "flash" as it passes through the broadside orientation with respect to the radar line of sight.

during a dwell on each target, and the interval between dwells on any one target is longer than the interpulse interval in a radar that tracks a single target continuously. Such a system cannot afford to risk bad data on the first pulse of a dwell; the normalization must be accurate on every pulse. One method of obtaining a quasi-instantaneous expanded dynamic range is to pass the sum and difference signals through equal delay lines before they enter the monopulse processor. Meanwhile the approximate amplitude of the *undelayed* sum signal is sensed and the attenuators are switched if necessary to place the signal within the linear dynamic range window. The attenuators in the sum and difference channels must be very accurately matched (or pilot pulses must be used to compensate for mismatch) and the attenuator switching time must be shorter than the delay time.

The computational load can be reduced in some applications by averaging the sum and difference amplitudes and their phase difference over several pulses before doing the computation indicated by (8.7). If the primary mission of the radar is to track the target in order to obtain data for refined postmission analysis, real-time averaging permits an adequate data rate for tracking. Pulse-by-pulse postmission analysis then can be done provided the pulse-by-pulse data are recorded during the mission.

Generally speaking, the phase-and-linear-amplitude approach is not the preferred method for accurate monopulse measurements over a wide dynamic range, especially if the radar must track rapidly fluctuating targets or perform interleaved tracks on multiple targets. For such uses other methods of processing, such as I and Q (Section 8.6) or phase and logarithmic amplitude (Section 8.7) should be considered.

8.6 PROCESSOR USING I AND Q

It was shown in (3.19) that another way of expressing the real part of d/s is

$$\operatorname{Re}(d/s) = \frac{d_I s_I + d_Q s_Q}{s_I^2 + s_Q^2} \quad (8.9)$$

where d_I , d_Q , s_I , and s_Q are the in-phase and quadrature components of the difference and sum signals at baseband. Figure 8.2 is a simplified diagram showing one angle channel. The I and Q components are obtained by mixing the difference and sum voltages with the output of a reference oscillator (local oscillator) at the signal frequency and also with a 90° phase-shifted output of the same oscillator. The four components are digitized and the calculations indicated by (8.9) are performed by computer. The receivers are linear and the dynamic-range design requirements are similar to those described in Section 8.5. The imaginary part of d/s , if needed, is obtained in a similar manner by using (3.20).

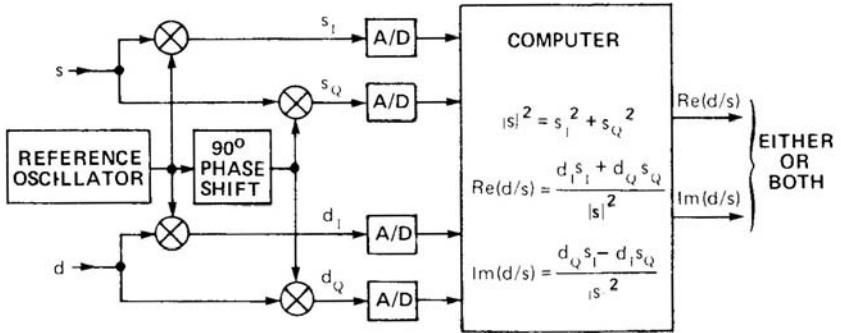


Figure 8.2 Processor using I and Q .

The absolute phase of the local oscillator that provides the common phase reference is immaterial. If it were changed, all four of the I and Q components would change but there would be no change in the computed real and imaginary parts of d/s indicated by (3.20) and (8.9).

One advantage of I and Q processing is that it uses synchronous (phase-sensitive) detectors, which are capable of a much wider dynamic range than the envelope detectors used in linear amplitude processing (Section 8.5). Another advantage that it has over phase-and-linear-amplitude (or log-amplitude) processing is that the spectral content of the I and Q signals is confined to the IF bandwidth, while that of amplitude, log amplitude, and phase can extend over a much wider frequency band, as explained in Section 2.7. For example, when the complex envelope of the IF signal passes through a null, I and Q vary smoothly while the amplitude has a cusp, log amplitude goes to $-\infty$, and phase jumps by 180° . Hence, channels that carry those three functions require wider bandwidth than do channels carrying I and Q , for comparable fidelity of reproduction.

8.7 PROCESSOR USING PHASES AND LOGARITHMIC AMPLITUDES OF s AND d

This type of processor is similar to the type that uses phase and linear amplitude, except that it uses IF logarithmic amplifier-detectors for the sum and differences. An example of its use can be found in the Target Resolution and Discrimination Experiments (TRADEX) radar [3]. TRADEX is a reflector-type tracking radar used for phenomenology measurements.

There are various forms of logarithmic amplifiers [4–7], all using some form of nonlinear circuit element either in the forward signal path or in a feedback path. It is possible to design a true logarithmic amplifier with IF output amplitude proportional to the logarithm of the IF input amplitude [8]. For most radar applica-

tions, however, a logarithmic IF output is not needed, but rather a logarithmic *detected* (i.e., IF envelope) output. Although this can be obtained by putting a detector after a true IF logarithmic amplifier, there is an easier and more stable design, which is called more properly a logarithmic amplifier-detector.

The usual configuration of an IF logarithmic amplifier-detector is illustrated in Figure 8.3. It consists of a series of cascaded IF amplifier stages, the detected outputs of the individual stages being summed. Each amplifier stage limits at a certain level. If the limiting were abrupt, the final output would be a piecewise-linear approximation to a logarithmic function; actually the limiting is not abrupt, and the corners of the linear segments are not sharp but rounded. The more stages there are, the more closely a logarithmic characteristic can be approached. It may be necessary to insert delay lines (not shown in the diagram) between the detectors and the summing amplifier to compensate for amplifier interstage delays; the first stage requires the longest delay and the last stage none.

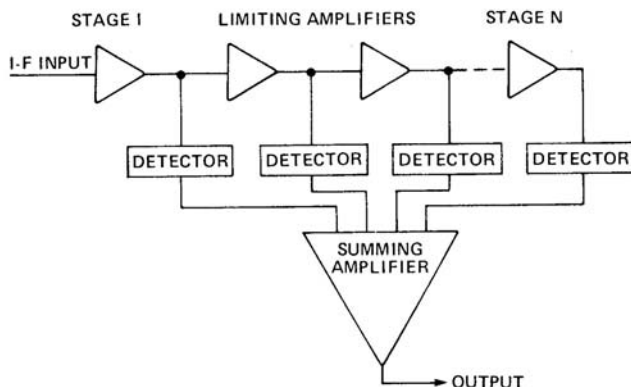


Figure 8.3 Typical IF logarithmic amplifier-detector.

Figure 8.4 is a simplified diagram showing how these devices are used in monopulse processing. A well-designed logarithmic amplifier-detector can have a dynamic range of about 80 dB with less than one decibel departure from a logarithmic characteristic. In addition to increasing the dynamic range of the analog portion of the system, this type of processor extends the effective dynamic-range capability of the A/D converters, since each incremental bit represents a fixed number of dB rather than volts.

The amplitude ratio of the difference to the sum is obtained, in concept, by subtracting the respective logarithmic outputs and taking the antilogarithm. In practice, since the devices are not perfectly logarithmic or perfectly stable, their input-output responses should be calibrated periodically and the computer should use the actual calibration functions rather than take the antilogarithm. In this way the error can be reduced to as little as 0.1 dB (about 1% error in amplitude ratio),

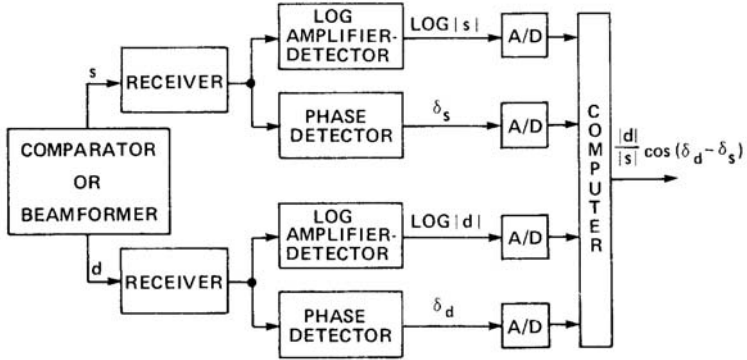


Figure 8.4 Typical IF logarithmic amplifier-detector.

depending on the elapsed time since the last calibration. The phases are used in the same way as in the processor that uses linear amplitude.

As a target approaches the null direction, the log of the difference voltage becomes an increasingly large negative number, which might appear to pose a severe problem in dynamic range at the low end. However, since the ability to measure small signal voltages is limited by noise, the low end of the dynamic range need not be much below the average noise level.

8.8 PROCESSOR USING DOT-PRODUCT DETECTOR WITH AGC

Assume a multiplying device that produces the instantaneous product of two input voltages. Let the input voltages be a sum and a difference at IF:

$$s(t) = |s| \cos(\omega t + \delta_s) \quad (8.10)$$

$$d(t) = |d| \cos(\omega t + \delta_d) \quad (8.11)$$

The symbols $s(t)$ and $d(t)$ represent instantaneous voltages as distinguished from the phasor (complex envelope) voltages s and d . The other symbols are ω for the IF radian frequency, t for time, and δ_s and δ_d for the sum and difference phase. The product is

$$s(t)d(t) = |s||d| \cos(\omega t + \delta_s) \cos(\omega t + \delta_d) \quad (8.12)$$

By the use of a trigonometric identity for the product of two cosines, this becomes

$$s(t)d(t) = \frac{1}{2}|s||d|\left[\cos(2\omega t + \delta_d + \delta_s)\cos(\omega t + \delta_d) + \cos(\delta_d - \delta_s)\right] \quad (8.13)$$

If the double-frequency (2ω) component is filtered out, there remains the component

$$\left[s(t)d(t)\right]_f = \frac{1}{2}|s||d|\cos\delta \quad (8.14)$$

where the subscript f denotes the output after filtering and $\delta = \delta_d - \delta_s$.

Such a multiplying device, with associated filter, is called a *product detector*, a *dot-product detector*, a *synchronous detector*, or a *phase-sensitive detector*.² The name dot-product detector is derived from an analogy with vector algebra. Let \mathbf{A} and \mathbf{B} be two vectors making an angle μ . Their “dot-product” (scalar product) is

$$\mathbf{A} \cdot \mathbf{B} = |\mathbf{A}||\mathbf{B}|\cos\mu \quad (8.15)$$

which has the same form as (8.14).

In order to make the output of a product detector, given by (8.14), equivalent to that of an exact monopulse processor, (8.7), it must be divided by $|s|^2$. (The factor of $1/2$ can be ignored, since the scale factor is determined by calibration.)

Division by $|s|^2$ is often accomplished by automatic gain control (AGC) derived from the sum channel and controlling both the sum and difference channels, as illustrated in Figure 8.5. The AGC acts to keep the sum voltage at a constant amplitude, which we can call unity; in other words, the sum channel input to the dot-product detector is not s but $s/|s|$, which has unit amplitude and the same variable phase as s . Since the same AGC also controls the gain of the difference channel, the difference-channel input to the dot-product detector is $d/|s|$. If now in (8.14) we replace d by $d/|s|$ and s by $s/|s|$, and ignore the factor $1/2$, we obtain as the monopulse processor output

$$\frac{|s|}{|s|} \frac{|d|}{|s|} \cos\delta = \frac{|d|}{|s|} \cos\delta \quad (8.16)$$

Hence a perfect dot-product detector with perfect AGC would be a form of exact processor.

During the time between transmitted pulses both s and d are varying because of noise, clutter echoes, and target echoes. The rate of variation is determined by

² It is sometimes also called a phase detector, but this name is ambiguous, since it can also mean an amplitude-insensitive circuit for measuring phase. The same device can be used for either function, but the method of use and the associated circuits are different.

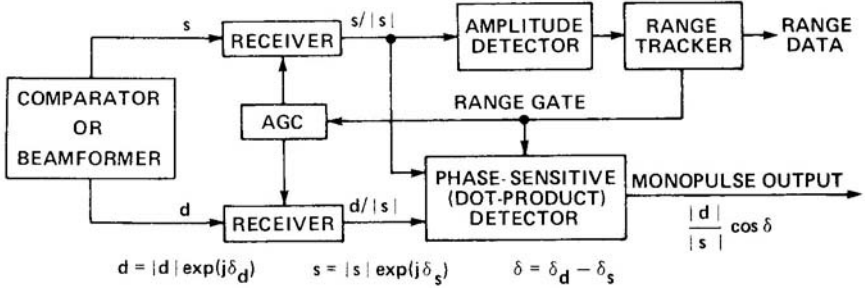


Figure 8.5 Processor using dot-product detector with AGC.

the IF bandwidth, which in most cases is approximately the reciprocal of the pulse duration (meaning the duration of the compressed pulse if pulse coding is used). The circuits are arranged so that the AGC voltage is derived only from the sum signal within the range tracking gate after range lock-on has occurred.

Ideally the AGC should act instantaneously so as to keep every sum pulse at exactly the same magnitude. In practice, the AGC usually has a time constant. If the target cross section varies during that time, as it often does, the AGC cannot follow the variation, and therefore the normalization (the division of $|d|$ by $|s|$) is not perfect. Nevertheless, it is possible to maintain close track because when the target is close to the tracking axis, d is close to zero and the imperfect normalization has only a second-order effect on the tracking-loop behavior. In other words, a modulated null is still a null. If, however, there is a dynamic lag because of inability of the servos to keep up with high angular rates or accelerations, the d is nonzero and its modulation due to imperfect AGC and target amplitude scintillation causes an angular error [9, 10].

In deriving the equations in this section an instantaneous multiplier was assumed. A perfect analog multiplier does not exist, but the same effect can be achieved or approximated by other nonlinear devices. For example, let $s(t)$ and $d(t)$ be added and then operated on by an instantaneous square-law device (not a square-law detector). The result is $[s(t) + d(t)]^2$. Similarly, let $s(t)$ and $d(t)$ be subtracted and then operated on by an identical square-law device. The result is $[s(t) - d(t)]^2$. Now let the output of the second square-law device be subtracted from the output of the first. The result is $4s(t)d(t)$, which is the same as (8.13) except for an unimportant scale factor. After filtering, the desired output is obtained as in (8.14).

8.9 AN APPROXIMATE DOT-PRODUCT DETECTOR

The circuit shown in simplified form in Figure 8.6 is used as an “error detector” in some monopulse radars. It is not a true dot-product detector, but gives an adequate approximation to it under conditions normally encountered in a tracking radar. Its attractiveness lies in its simplicity.

The device consists essentially of a pair of rectifiers arranged in a bridge. The inputs are normalized (by AGC) IF sum and difference signals $s/|s|$ and $d/|s|$, which are added in the same phase on one side of the bridge and in opposite phase on the other side. The resulting voltages are rectified separately with opposite polarity and then added, so that the result is actually subtraction. The output of the device, denoted here by x' , is given by

$$2x' = \frac{|s+d|}{|s|} - \frac{|s-d|}{|s|} = \left| 1 + \frac{d}{s} \right| - \left| 1 - \frac{d}{s} \right| \quad (8.17)$$

The factor 2 on the left side of the equation (or $\frac{1}{2}$ on the right side) is an arbitrary scale factor chosen for convenience in expressing the relations to be derived.

Let x be the real part of d/s ; this would be the output of an exact processor as defined in Section 8.4, meaning a perfect dot-product detection. Let y be the imaginary part of d/s . If desired, y could be obtained by another perfect dot-product detector with one of its inputs shifted by 90° . Then complex d/s is expressed by

$$\frac{d}{s} = x + jy \quad (8.18)$$

With this substitution, (8.17) becomes

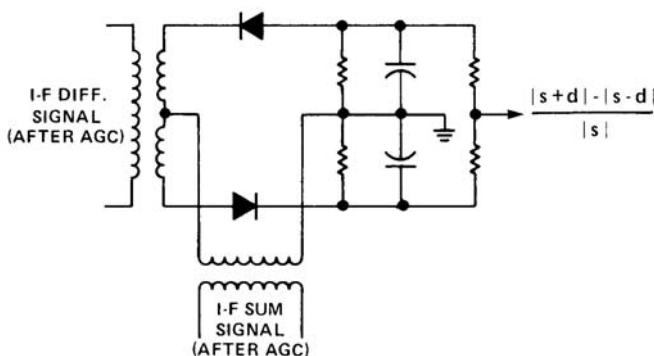


Figure 8.6 Typical IF logarithmic amplifier-detector.

$$\begin{aligned}
 2x' &= |1 + x + jy| - |1 - x - jy| \\
 &= \sqrt{(1+x)^2 + y^2} - \sqrt{(1-x)^2 + y^2}
 \end{aligned}
 \tag{8.19}$$

Consider the idealized case $y = 0$ (a point target in the clear, with no noise, interference, or clutter, no phase imbalances between channels, etc.). Assuming furthermore that $|x| \leq 1$, which means that the target lies between angular limits that usually approximate the half-power points of the sum pattern, (8.19) reduces to

$$\begin{aligned}
 2x'_{|x|>1, y=0} &= |1+x| - |1-x| = (1+x) - (1-x) = 2x \\
 \text{or} \\
 2x'_{|x|>1, y=0} &= x
 \end{aligned}
 \tag{8.20}$$

If $y = 0$ and $|x| > 1$ (target outside of the half-power beamwidth), then (8.19) reduces to

$$\begin{aligned}
 2x'_{|x|\leq 1, y=0} &= \pm(1+x) \pm(1-x) = \pm 2 \\
 \text{or} \\
 2x'_{|x|\leq 1, y=0} &= \pm 1
 \end{aligned}
 \tag{8.21}$$

in which the sign of the right-hand side is the sign of x .

Figure 8.7 compares the output of the approximate processor with that of an exact processor, x , using as an example the antenna patterns of the AN/FPS-16 radar modeled empirically by (6.8) and (6.9) and plotted in Figure 6.4. The dashed and solid curves are for the exact and approximate processors, respectively. Since all curves have odd symmetry about the origin, only the positive halves are shown.

One pair of curves, labeled $\delta = 0^\circ$, is plotted for the ideal case discussed above, in which $y = 0$ and the relative phase between the sum and difference, $\delta = \tan^{-1}(y/x) = 0$. For this case the two processors produce the same output up to the points where $x' = \pm 1$. Beyond those points the output of the exact processor continues to increase (theoretically to infinity, but in practice restricted by the dynamic range of the equipment³) while the output of the approximate processor limits abruptly at $x' = \pm 1$. The limiting effect is inherent in this type of "error detector," over and above any saturation that may occur in amplifiers or other components. The angular region of operation before limiting occurs is approximately the sum-pattern beamwidth, which is adequate for most applications; it can be extended if desired by reducing the gain of the difference channel. Ordinarily the target is not more than one-half beamwidth off axis except perhaps during acquisi-

³ Note, here and subsequently, that when the processor is implemented digitally in a computer, a division by zero may cause problems other than simple saturation of an analog circuit.

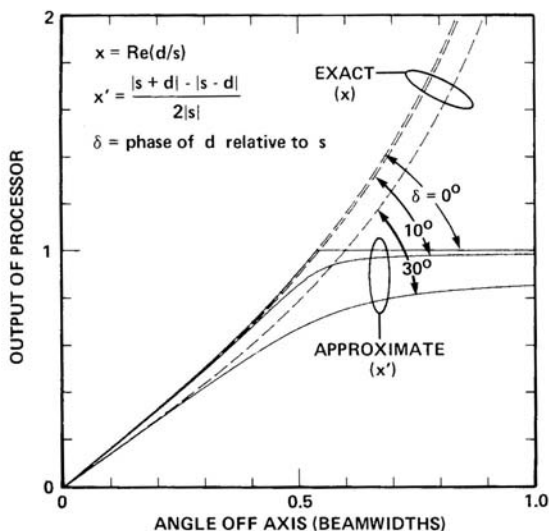


Figure 8.7 Outputs of approximate dot-product processor and exact processor for three values of relative phase.

tion. If lock-on in acquisition occurs when the target is in the saturated region (less likely because the signal is weaker), the servo drive signal still has the correct polarity but the loop gain is reduced until the unsaturated region is reached.

In general, the relative phase δ between the sum and the difference is not zero as assumed in the idealized case. For example, postcomparator phase imbalance between the sum and difference receiver channels causes a nonzero value of δ , which reduces x by the factor $\cos \delta$ and introduces a y -component proportional to $\sin \delta$. The other two pairs of curves in Figure 8.7 are for illustrative phase imbalances of 10° and 30° . The dashed curves for these cases were obtained by reducing the dashed curve for $\delta = 0^\circ$ by the factor $\cos \delta$. The solid curves were computed by (8.19), x being the ordinate of each of the respective dashed curves at the same abscissa and y being calculated by $y = x \tan \delta$. A 30° imbalance is larger than allowed by most monopulse radar specifications but easily can occur or be exceeded if a radar is not properly designed and maintained. A more typical specified value is 10° . When $\delta \neq 0^\circ$, the exact and approximate processor curves are tangent on the axis but deviate elsewhere. The approximate processor output approaches an asymptotic limit equal to $\cos \delta$. For small angles the exact and approximate processors are essentially equivalent, but the phase imbalance causes both of them to have reduced tracking sensitivity (reduced slope) and to incur errors in off-axis angle measurements, especially in the case of the approximate processor.

These curves illustrate one of the reasons why specifications usually require that the phase unbalance be kept low, even if a near-perfect processor is used. Another reason is that post-comparator imbalance in combination with pre-comparator phase imbalance (manifested by a finite null depth in the difference pattern) causes a boresight shift (see Section 10.4.1).

A nonzero value of y can be due to causes other than circuit phase imbalance. As will be shown in Chapters 9 and 11, it can be caused by unresolved targets, including the special cases of multipath and single-target glint. Unresolved targets not only introduce a quadrature component but also distort the in-phase component. Under such conditions the relationships of x and x' to each other and to the target angle are more complicated than in the case of circuit imbalance and cannot be represented by a simple family of curves like those shown in Figure 8.7, because as the antenna pointing direction changes, so do the relative illuminations of the targets in the resolution cell.

However, the relationship between the exact and approximate dot-product outputs can be shown parametrically for any values of x and y due to any causes. Suppose a second device identical to the one described above were added, operating on the same inputs, s and d , but with one of them shifted 90° . Then just as the first device gives an approximation of the real part of d/s , $x' \equiv x = \text{Re}(d/s)$, the second would give an approximation of the imaginary part, $y' \equiv y = \text{Im}(d/s)$. Interchanging x and y in (8.19) we obtain

$$2y' = \sqrt{(1+y)^2 + x^2} - \sqrt{(1-y)^2 + x^2} \quad (8.22)$$

When x and y are both small, they are closely approximated by x' and y' , but the deviation increases with increasing values of x and y . Figure 8.8 illustrates the distortion produced by this type of processing as compared with the outputs of exact processors, such as those using perfect dot-product detectors. Because of symmetry, it suffices to show one quadrant. In this figure y' is plotted versus x' as various constant values are assigned to x while y is varied (solid curves) and vice versa (dashed curves). If there were no distortion, the result would be a square grid. Note that x' , y' , and their resultant $|x' + jy'|$ cannot exceed 1, no matter how large x and y become. The distortion is unimportant in many applications, but if necessary it can be reduced by reducing the gain of d relative to s , thus reducing the values of x and y proportionately.

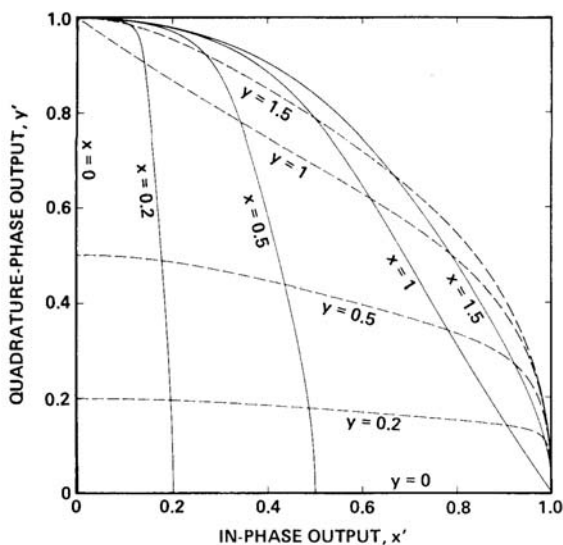


Figure 8.8 Relation between in-phase and quadrature-phase outputs of exact processors (x and y) and approximate dot-product processors (x' and y').

8.10 NONCOHERENT PROCESSOR USING SUM AND DIFFERENCE OF $|v_1|$ AND $|v_2|$

This type of processor, which can be used only in amplitude-comparison monopulse, forms the sum and difference of the voltages from the component beams after they are individually detected rather than at RF. Because it ignores phase, it is sometimes called noncoherent monopulse. One application of this form of monopulse processing is in a search radar transmitting a fan beam which is narrow in azimuth and broad in elevation, with two or more simultaneous receiving beams, narrow in both coordinates, stacked in elevation (the so-called *stacked-beam 3-D radar*). Each adjacent pair of receiving beams provides the v_1 and v_2 inputs needed for interpolation of target elevation between the beam-axis elevations.

Consider a pair of squinted receiving beams, as illustrated in Figure 5.13, and assume that the transmitted beam is wide enough to illuminate targets in both receiving beams. One could measure the amplitudes of voltages v_1 and v_2 obtained from the two beams after detection, calculate their ratio, and convert this ratio to the angle of offset from the axis by means of a known calibration function. But this ratio has a value of 1 on the axis; it lacks the desired property of being zero on the axis and having odd symmetry off axis.

In the technique described here, the desired property is obtained by adding and subtracting the voltages after amplitude detection, and taking the ratio of their

difference to their sum. A simplified block diagram is shown in Figure 8.9. The function indicated by the divider block in the figure can be accomplished by digitizing the two inputs and using a computer for the division. An alternative method is to derive an AGC voltage from $|v_1| + |v_2|$ and feed it back to control the gains of the v_1 and v_2 channels. In that case no actual division is needed, since the $|v_1| - |v_2|$ voltage is in effect divided by $|v_1| + |v_2|$ by the AGC, thus providing the desired output.

The behavior of this processor is the same as that of an exact processor when the off-axis angle is not too large and v_1 and v_2 have their nominal relative phase of 0° . Let x and x' be the outputs of the exact and noncoherent processors, respectively. Then

$$x' = \frac{|v_1| - |v_2|}{|v_1| + |v_2|} \quad (8.23)$$

If v_1 and v_2 have 0° relative phase, the absolute sign can be omitted and the output can be written, using (2.3) and (2.4), as

$$x' = \frac{v_1 - v_2}{v_1 + v_2} = \frac{d}{s} \quad (8.24)$$

If v_1 and v_2 have 0° relative phase, so do s and d . The output of an exact processor in that case would be

$$x = \text{Re}(d/s) = \frac{d}{s} \quad (8.25)$$

Under the assumed conditions, therefore, the noncoherent processor has the same output as the exact processor.

When v_1 or v_2 is zero (a condition that occurs at roughly one-half the sum beamwidth off-axis), the processor output is unity. At larger angles, where either

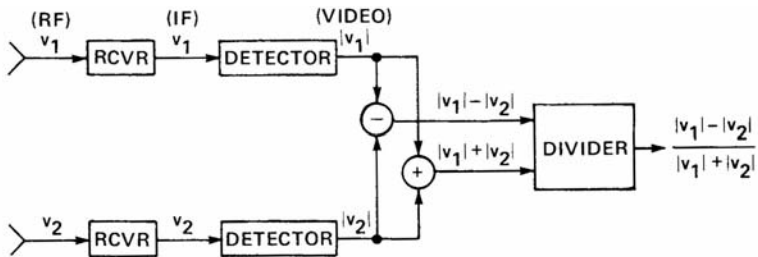


Figure 8.9 Processor using sum and difference of $|v_1|$ and $|v_2|$.

v_1 or v_2 changes sign after passing through zero (i.e., goes into a sidelobe of a squinted beam), the behavior of the noncoherent processor is anomalous. The relative phase of v_1 and v_2 is then 180° and

$$x' = \frac{|v_1| - |v_2|}{|v_1| + |v_2|} = \frac{v_1 + v_2}{v_1 - v_2} = \frac{s}{d} = \frac{1}{x} \quad (8.26)$$

Figure 8.10 compares the output of this processor (solid curve) with that of an exact processor (dashed curve), using as an example the antenna patterns of the AN/FPS-16 radar plotted in Figure 6.4 and assuming the nominal condition of 0° relative phase. The figure is plotted only for positive angles, since the curves have odd symmetry. Up to the point where $x' = x = 1$, the two processors produce the same output. Beyond that point the output of the exact processor continues to increase, theoretically to infinity but in practice limited by the dynamic range of the processor; on the other hand, the output of the noncoherent processor decreases. Thus, any given output is ambiguous, since it corresponds to more than one angle. However, in a null tracking system, in which the antenna axis follows the target closely, the ambiguity is not a problem. In the acquisition mode, even if lock-on occurs when the target is in the anomalous region, the monopulse output has the correct sign to cause the servos to drive the antenna in the direction of the null. The servo loop gain is reduced, but it regains its normal value as soon as the transition point (where $d/s = 1$) is crossed. Not unless acquisition occurred in the first sidelobe would the monopulse output have the wrong sign, which would drive the antenna away from the target, but acquisition in that region is unlikely because of the weak signal.

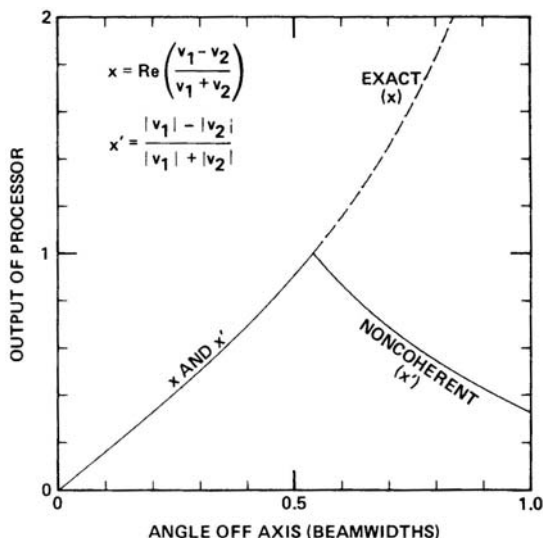


Figure 8.10 Outputs of noncoherent processor using $|v_1|$ and $|v_2|$ and exact processor, for 0° relative phase.

An advantage of this processor is that the receiver channels need not be matched in phase. On the other hand, amplitude (gain) imbalance between the channels causes a shift in the boresight axis, whereas this is not the case in receivers that operate on the sum and difference. The shift can be reduced by using pilot pulses to monitor the imbalance or by commutating (alternating) the inputs and outputs of the receiver channels. At angles well off boresight, this processor is *less* sensitive to amplitude imbalance than is a sum-and-difference processor. For example, when either v_1 or v_2 is zero, one channel carries no signal and its gain does not matter; the ratio of the difference to the sum is unity despite the gain imbalance.

Even though the output of the noncoherent processor is insensitive to phase shifts in the receiver channels, it is subject to error due to external factors, such as multipath, which distort the amplitude and phase distribution of the arriving wave. A phase taper of the arriving wave across the aperture causes unequal amplitudes of v_1 and v_2 . These distortions are explained in Chapter 9. The exact processor also gives an erroneous output under these conditions but the errors of the two processors are not the same, since one depends on the coherent (phasor) sum and difference and the other on the noncoherent sum and difference.

8.11 PROCESSOR USING $s + d$ AND $s - d$

Since $v_1 = (s + d)/\sqrt{2}$ and $v_2 = (s - d)/\sqrt{2}$, as shown in (2.3) and (2.4), any processing that can be done with v_1 and v_2 , as in the preceding section, can also be done with $s + d$ and $s - d$ instead. This means forming s and d by an RF comparator in the usual way, then combining them at RF or IF to obtain $s + d$ and $s - d$, which are then processed. This may seem like a roundabout method compared with taking v_1 and v_2 directly from the feeds, but it is advantageous in some two-coordinate monopulse systems, such as the one described in Section 8.14.

Since the sum voltage exists at a point preceding the $s + d$ and $s - d$ hybrids, it is available for detection (acquisition). By connecting a duplexer at that point, the sum pattern is made available also for transmission. A noncoherent processor using $|s + d|$ and $|s - d|$ can be used in both amplitude- and phase-comparison monopulse, whereas the one using $|v_1|$ and $|v_2|$ described in the Section 8.10, is limited to amplitude comparison. To use this processor in phase-comparison monopulse, either d or s must be phase-shifted 90° before adding and subtracting them, since they emerge from the comparator in phase quadrature.

Although a noncoherent processor using $|s + d|$ and $|s - d|$ is insensitive to phase imbalance in the receiver channels, it is subject to error due to phase imbalance between the s and d channels arising from components between the comparator output and the point where s and d are combined before entering the receiver. That path should therefore be kept as short as possible. Figure 8.11 compares the

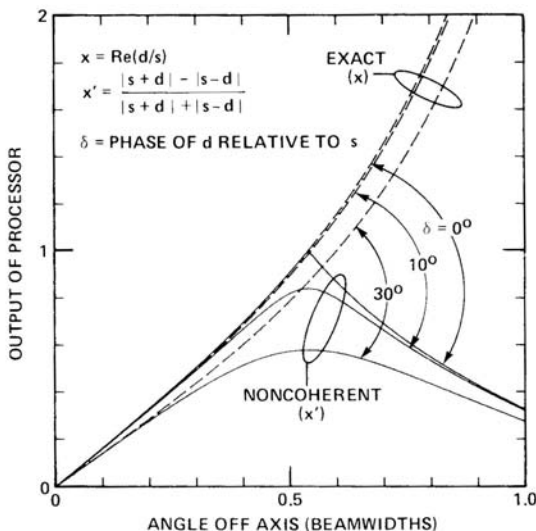


Figure 8.11 Outputs of noncoherent processor using $|s + d|$ and $|s - d|$ and exact processor, for three values of relative phase.

output x' of such a processor (solid curves) with the output x of an exact processor (dashed curves) as a function of angle, again using as an example the antenna patterns of the AN/FPS-16 as modeled by (6.8) and (6.9) and plotted in Figure 6.4. Three pairs of curves are shown, for a phase imbalance δ of 0° , 10° , and 30° between s and d before they are combined to form $s + d$ and $s - d$. The pair of curves for $\delta = 0^\circ$ is identical to the curves in Figure 8.10. All three dashed curves are the same as in Figure 8.7 since they represent the output of the exact processor. For $\delta = 10^\circ$ the solid curve deviates only slightly from the dashed curve. For $\delta = 30^\circ$ there is considerable deviation, and the slope of both the solid and dashed curves at the origin is appreciably reduced from its nominal value.

8.12 PROCESSOR USING LOG $|v_1|$ AND $|v_2|$

In this type of monopulse processing the component voltages v_1 and v_2 go to receivers with logarithmic amplifier-detectors such as the ones described in Section 8.7. In place of v_1 and v_2 , the equivalent voltages $s + d$ and $s - d$ may be used. The logarithmic outputs are subtracted to produce the monopulse output. Figure 8.12 is a simplified diagram. The logarithmic amplifier-detectors may be considered part of the receivers but are drawn separately in the figure for clarity.

The output can be written in mathematical form as

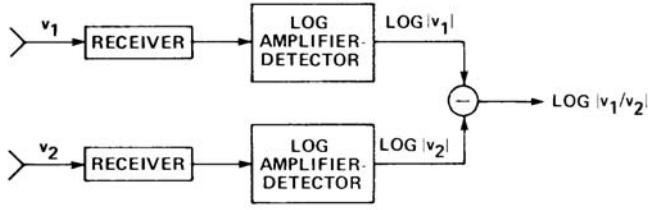


Figure 8.12 Processor using $\log |v_1| - \log |v_2|$.

$$K (\ln |v_1| - \ln |v_2|) = K \ln (|v_1|/|v_2|) = K \ln (v_1/v_2) \quad (8.27)$$

where K is a scale factor that depends on the particular circuits. In this equation and in those that follow, the logarithms are written to base e rather than base 10 to simplify the analysis. A change of base merely amounts to a change in the scale factor.

The output has the desired characteristic of odd symmetry, with a null on the axis. Since phase is not used, this is another example of a noncoherent technique.

Equation (8.27) can be expressed in terms of the sum and difference voltages even if those voltages do not exist physically in the radar; the output can be written as

$$K (\ln |v_1| - \ln |v_2|) = K \ln \frac{|s+d|}{|s-d|} = K \ln \frac{|1+d/s|}{|1-d/s|} \quad (8.28)$$

Assume first that d and s have the nominal phase relationship of 0° (or 180°), making d/s real, and that $|d/s| \ll 1$. Then we can approximate (8.28) by using the first term of the series expansion of a logarithmic function:

$$1 + d/s \approx d/s \quad (8.29)$$

$$\ln(1 - d/s) \approx -d/s \quad (8.30)$$

and therefore, since we assume d/s to be real,

$$\ln |1 + d/s| = \ln(1 + d/s) \approx d/s \quad (8.31)$$

$$\ln |1 - d/s| = \ln(1 - d/s) \approx -d/s \quad (8.32)$$

The result is

$$\ln |v_1/v_2| \approx 2d/s \quad (8.33)$$

Hence, except for the scale factor of 2, which can be included in the coefficient K , the output of this processor is approximately the same as that of an exact processor when d/s is real and small, which is the case for a point target close to the axis in a clear environment.

To illustrate the action of this processor in another way, assume that the squinted beams have Gaussian patterns. (At small angles there is little difference between a Gaussian beam, a $(\sin x)/x$ beam, and a typical squinted beam all with the same beamwidth.) The Gaussian voltages are

$$v_1 = \exp \left[-1.386 (\theta - \theta_{sq})^2 \right] \quad (8.34)$$

$$v_2 = \exp \left[-1.386 (\theta + \theta_{sq})^2 \right] \quad (8.35)$$

where θ is the angle off boresight and θ_{sq} is the squint angle, both in beamwidths of the squinted beams. The coefficient 1.386 is chosen so that v_1 and v_2 have the value $1/\sqrt{2}$ (half power) when $\theta - \theta_{sq}$ and $\theta + \theta_{sq}$ both have the value 0.5.

Substituting (8.34) and (8.35) in (8.27), we obtain

$$K \ln |v_1/v_2| = -1.386 (\theta - \theta_{sq})^2 + 1.386 (\theta + \theta_{sq})^2 = K' \theta \theta_{sq} \quad (8.36)$$

where K' is a scale factor equal to $5.544K$.

Hence with the Gaussian squinted beam model and 0° relative phase this type of processor would produce a monopulse output, according to (8.36), which is exactly proportional to angle off axis. (The output of an exact processor with the same beam model would be a nonlinear function of angle, although nearly linear at small angles.) A truly Gaussian beam model is not physically realizable, and is used here only for illustration. Whatever the actual patterns are, this processor behaves essentially like an exact processor at small angles but deviates from it as the angle increases or when the relative phase is other than 0° .

Figure 8.13 compares the output of this processor (solid curve) with that of an exact processor (dashed curve), using again the antenna patterns of the AN/FPS-16 radar as an example and assuming exactly 0° relative phase. The fact that the curves differ is not important in itself, since it merely means that the two processors require different calibration functions for conversion of monopulse output to angle. However, when $v_2 = 0$ (i.e., $d/s = 1$), at an angle a little beyond the half-power point, the processor output theoretically becomes infinite, although in practice it is limited by the dynamic range of the circuits. At small angles, however, as in null tracking, satisfactory operation can be obtained.

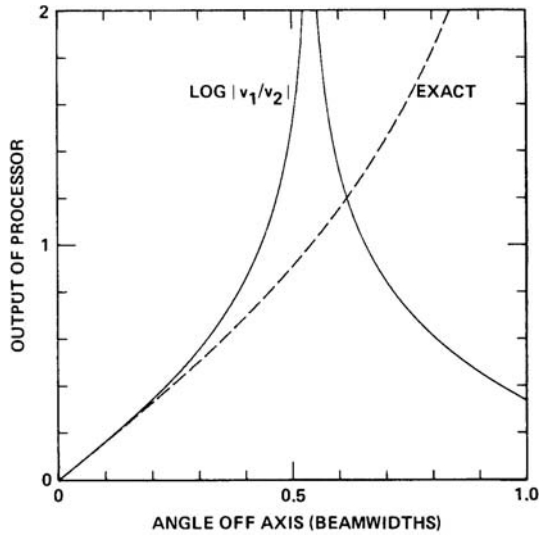


Figure 8.13 Outputs of $\log |v_1/v_2|$ processor and exact processor versus angle.

To make the comparison with an exact processor more general, allow d/s to be complex and not necessarily small, and let the beams have any physically realizable shape. Then

$$d/s = x + jy \quad (8.37)$$

where x and y are the real and imaginary parts, respectively, which would be the outputs of in-phase and quadrature-phase exact processors. Substituting (8.37) in (8.28), with the scale factor omitted, we obtain

$$\begin{aligned} \ln |v_1/v_2| &= \ln \frac{|1+x+jy|}{|1-x-jy|} = \frac{1}{2} \ln \frac{|1+x+jy|^2}{|1-x-jy|^2} \\ &= \frac{1}{2} \ln \frac{(1+x)^2 + y^2}{(1-x)^2 + y^2} \end{aligned} \quad (8.38)$$

This is to be compared with the output of an exact processor, which is simply x . The calculation of x and y under external conditions that disturb the nominal 0° relative phase will be discussed in Chapter 9.

An advantage of this type of processor is that it does not require phase matching of the receiver channels. Another advantage is that it gives instantaneous nor-

malization. A potential disadvantage is its susceptibility to boresight error due to gain imbalance between the receiver channels, but this error can be largely eliminated by use of pilot pulses or by commutation of inputs and outputs of the receiver channels on every other pulse.

8.13 PROCESSOR USING $s \pm jd$

In this technique the sum and difference voltages s and d are formed by the comparator in the usual way and then combined to form $s + jd$ and $s - jd$, as shown in Figure 8.14. These two voltages are hard-limited to keep their amplitudes constant while preserving their phases. Their relative phase, denoted by $2\phi_0$, is then measured by a phase detector.⁴ An optional additional step is to take the tangent of half their relative phase angle. Either the angle itself or the tangent can be used as the monopulse output, since they provide equivalent information with different calibration functions. For ease of comparison with an exact processor it will be assumed that the tangent function is used.

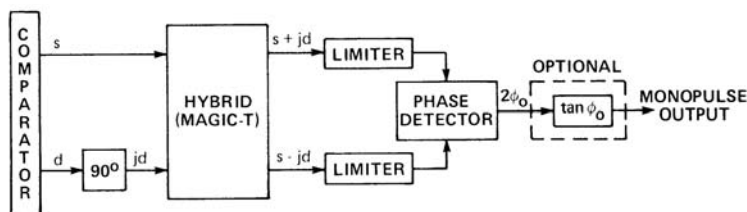


Figure 8.14 Processor using $s \pm jd$.

The reason for hard-limiting the inputs to the phase detector is that otherwise the output would depend not only on the relative phase but on the amplitudes of the two inputs. The limiting of $s + jd$ and $s - jd$ makes their amplitudes constant while preserving their phases, and thus makes the phase detector output a function of their relative phase only.

In Figure 8.14 it is assumed that s and d are initially in phase, as they are (under ideal conditions) in amplitude-comparison monopulse using magic-Ts or other phase-preserving hybrids in the comparator. In the diagram, d is then phase-shifted 90° to produce jd , and a phase-preserving hybrid such as a magic-T produces the sum and difference of s and jd . Alternatively, the 90° phase shift can be applied to s instead of to d . Still another variation is to use a quadrature hybrid (a

⁴ A phase detector must be distinguished from a phase-sensitive detector. The former responds to the relative phases of two inputs; the latter responds to their dot-product. Certain physical devices can be used for either function, but the method of use is different.

3-dB directional coupler, Section 4.4.2) in place of a magic-T and to insert the 90° phase shift in one of the outputs rather than in one of the inputs.

This type of processor provides instantaneous normalization. It is especially useful in a radar system that is not dedicated to continuous tracking of a single target but must maintain interleaved tracks of several targets of different signal strengths. Under these conditions, automatic gain control is too slow to normalize the difference signal. Another useful feature of this processor is that it cannot be saturated by very strong signals (as some of the other processors can), since it amplitude-limits the signals. This type of processor was used in the missile site radar of the Sentinel and Safeguard ballistic-missile defense systems, designed and deployed in the 1970s. That radar was designed to perform a closed-loop track on one target while measuring the relative positions of several other targets within the same beam.

Figure 8.15 illustrates the phasor relationships, assuming that s and d are initially in phase. The $\pm j$ factor rotates the d phasor $\pm 90^\circ$. The phase angle $2\phi_0$ between $s + jd$ and $s - jd$ is related to the normalized difference signal by the equation

$$\tan \phi_0 = \frac{d}{s} \quad (8.39)$$

The subscript in the symbol ϕ_0 is a reminder that (8.39) is correct only when d and s have 0° relative phase, in which case the processor acts like an exact processor. To obtain an angle estimate, d/s can be computed by (8.39) from the measurement of $2\phi_0$, and converted to angle offset by a calibration function, or the calibration can be expressed directly as a relation between the phase-detector output and the angle offset.

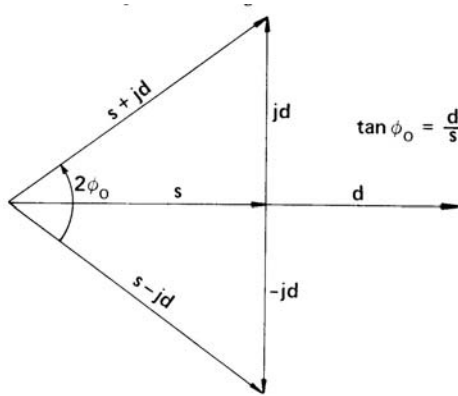


Figure 8.15 Phasor diagram of $s \pm jd$ when s and d are in phase.

If the radar is designed for phase comparison instead of for amplitude comparison, or if the comparator uses quadrature hybrids, d and s are already in phase quadrature when they emerge from the comparator. In that case the processing is the same except that d and s are added and subtracted without the 90° phase shift shown in Figure 8.14.

Instead of using both $s + jd$ and $s - jd$, either one can be used in combination with s alone, since the relative phase between s and either $s + jd$ or $s - jd$ is ϕ_0 . The phasor diagram for that case is simply the upper or lower half of Figure 8.15.

However, as has already been pointed out, the relative phase between d and s generally will deviate to some extent from the nominal value of 0° because of imperfections within the radar and because of external factors such as multipath. Let the actual phase of d relative to s be δ . Then in place of Figure 8.15, the phasor diagram is as shown in Figure 8.16. Let ϕ_1 be the phase of $s + jd$ relative to s and let ϕ_2 be the phase of s relative to $s - jd$. Then

$$\tan \phi_1 = \frac{|d| \cos \delta}{|s| - |d| \sin \delta} \quad (8.40)$$

By dividing numerator and denominator by $|s|$ and using (3.9) and (3.10), we can write the same equation in the form

$$\tan \phi_1 = \frac{|d/s| \cos \delta}{1 - |d/s| \sin \delta} = \frac{\operatorname{Re}(d/s)}{1 - \operatorname{Im}(d/s)} \quad (8.41)$$

Similarly,

$$\tan \phi_2 = \frac{|d/s| \cos \delta}{1 + |d/s| \sin \delta} = \frac{\operatorname{Re}(d/s)}{1 + \operatorname{Im}(d/s)} \quad (8.42)$$

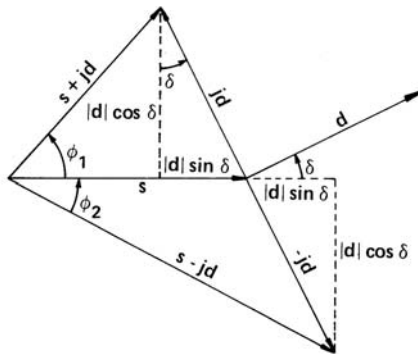


Figure 8.16 Phasor diagram of $s \pm jd$ when s and d have relative phase δ .

The output of an exact processor would be $|d/s| \cos \phi$ or its equivalent, $\text{Re}(d/s)$.

These last two equations show that both $\tan \phi_1$ and $\tan \phi_2$ are different from the output of an exact processor (except when $\phi = 0^\circ$ or 180°), one being larger and the other smaller, depending on the sign of $\sin \phi$. Therefore some form of averaging generally will produce an output closer to that of an exact processor than will $\tan \phi_1$ or $\tan \phi_2$ alone. One form of averaging might be to measure ϕ_1 and ϕ_2 separately and average their tangents. A simpler form of averaging, requiring less equipment, is the one already described above and shown in Figure 8.14. It consists of measuring the phase angle between $s + jd$ and $s - jd$, which is $\phi_1 + \phi_2$, and computing the tangent of half of that angle (that is, the tangent of the average of ϕ_1 and ϕ_2).

Figure 8.17 compares the output of the processor shown in Figure 8.14, namely $\tan[(\phi_1 + \phi_2)/2]$, and the output of an exact processor, as functions of angle. As in the comparisons presented in earlier sections, the antenna patterns of the AN/FPS-16 radar modeled by (6.8) and (6.9) and plotted in Figure 6.4 have been used for illustrative purposes in making the computations. When s and d have the same phase, the two processors produce the same output, plotted in the curve labeled $\delta = 0^\circ$. When $\delta = 30^\circ$, the outputs differ, although not drastically. Curves for $\delta = 10^\circ$, plotted in corresponding figures for some of the other processors described in this chapter, are omitted from Figure 8.17 because they are barely distinguishable from the curves for $\delta = 0^\circ$.

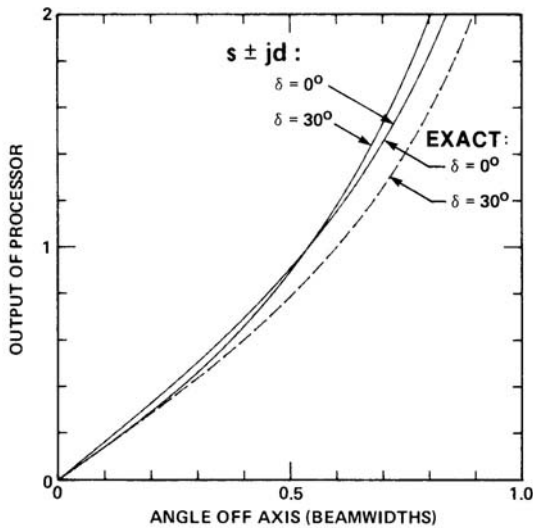


Figure 8.17 Outputs of $s \pm jd$ processor and exact processor for two values of relative phase.

In this type of system it is essential that the range gate be restricted to the region where the received pulse voltage is near its peak value. If there is any extension of the gate beyond this region, the amplitude-limiting action will cause the noise within that extension to be passed to the output at the same level as the signal plus noise during the pulse. Thus, if the gate is twice as wide as the signal pulse, the maximum effective signal-to-noise ratio will be unity even if the signal-to-noise ratio during the pulse approaches infinity. This comment applies to angle measurement, not necessarily to detection and range tracking, which may operate on a separate sum channel not subjected to amplitude-limiting.

8.14 TWO-CHANNEL MONOPULSE USING $s + d$ AND $s - d$

One disadvantage of ordinary two-coordinate monopulse is the need for three carefully matched receiver channels. Various methods have been proposed to reduce the number of receiver channels. Usually a sacrifice in data rate or in some other aspect of performance is necessary, but for certain types of use the sacrifice may be unimportant.

A practical two-channel system has been described by Chuff, Huland, and Noblit [11], and further details and variations have been given by Noblit [12]. Besides reducing the number of receiver channels, this system provides “graceful degradation” by operating as a form of conical scan or lobe switching when one of the two channels fails. However, the data rate is lower than in three-channel monopulse at the same pulse repetition rate, and in certain versions of the system the S/N ratio is somewhat lower.

Figure 8.18 is a simplified diagram of the basic version of the technique as described in [11]. The sum signal and the traverse and elevation difference signals are formed by a comparator in the usual way. The two difference signals are injected in space quadrature (i.e., at orthogonal polarizations) into a microwave resolver consisting of a circular waveguide with a motor-driven hook-shaped probe at the other end rotating at an angular rate ω_r . The resolver output is amplitude modulated by the probe rotation. This modulated difference signal, labeled d_m in the figure, is proportional to the traverse difference signal d_{tr} times the cosine of the rotation angle $\omega_r t$ plus the elevation difference signal d_{el} times the sine of that angle.

The output of the resolver becomes an input to a hybrid junction, the other input being the sum signal s from the comparator. This hybrid produces outputs proportional to $s + d_m$ and $s - d_m$. Voltages $s + d_m$ and $s - d_m$, still at RF, now go to separate receivers, the IF outputs of which are added and then video-detected to provide the sum signal for AGC, detection, and ranging. The AGC is applied to both receiver channels for normalization.

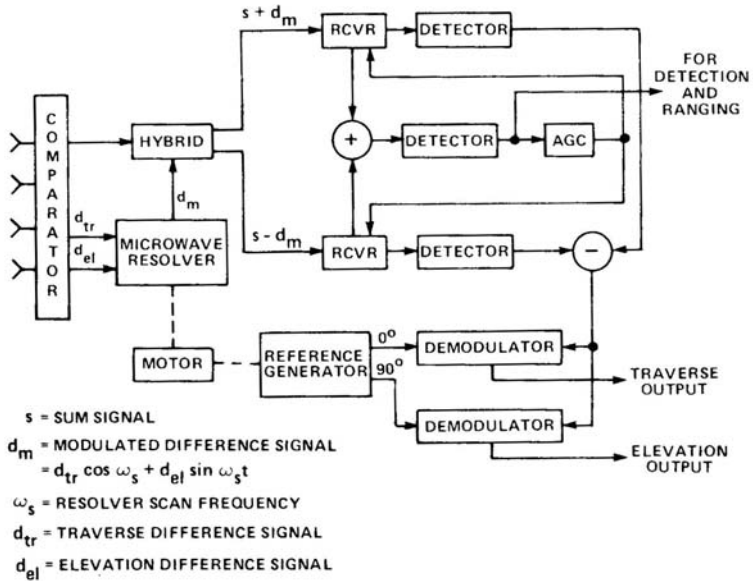


Figure 8.18 Two-channel monopulse using a microwave resolver. (After: Chubb, Hulland, and Noblit [11, 12].)

The IF outputs of the two receivers are also separately video-detected and then subtracted, thus canceling the sum signal and leaving only the normalized difference signal.

The normalized difference signal at this point is a succession of pulses (or “boxcarred” pulses) with a sinusoidal envelope. The amplitude of the envelope is approximately proportional to the vector angular displacement of the target from the boresight axis and the phase of the envelope depends on the ratio of the traverse and elevation components. This signal goes to a pair of demodulators (synchronous detectors). The other input to each of the demodulators is a reference voltage from a voltage generator driven by the same motor that drives the rotating probe. The reference-voltage input to one of the demodulators is phase-shifted by 90° . The outputs of the demodulators, after filtering, are the normalized traverse and elevation difference signals. Omitted from this diagram are steps such as boxcar generation, amplification, and filtering. The data rate is no greater than twice the rotation rate of the resolver.

Some simplification can be gained by adding $s + d_m$ and $s - d_m$ at video (after detection) rather than at RF to obtain the sum signal for detection, ranging, and AGC, but there is a loss due to noncoherent addition. The amount of this loss depends on the signal-to-noise ratio but is typically less than 1 dB.

In one variation of this technique, the microwave resolver is replaced by a switching arrangement that causes d_m to cycle through the sequence $+d_{tr}$, $+d_{el}$, $-d_{tr}$, $-d_{el}$ on successive pulses at the pulse repetition frequency. This “modulated” (switched) difference signal d_m is added to and subtracted from s as in the basic method described above, to provide inputs to the two receiver channels. The outputs are added and subtracted to obtain the sum signal and the commutated difference signal. The latter is acted upon by another synchronous switch (the demodulator) to separate the traverse outputs on pulses 1 and 3 from the elevation outputs on pulses 2 and 4 and to reverse the sign of the outputs during pulses 3 and 4. Thus, the traverse and elevation are obtained from alternate pulses rather than simultaneously. This type of system found application in monopulse radar such as the AN/MPS-36 and AN/TPQ-27.

When the switched version of this technique is used in a four-horn monopulse system, the successive combinations of $s + d_m$ and $s - d_m$ are equivalent to forming simultaneous receiving patterns corresponding to the left and right pairs of beams on the odd-numbered pulses and the top and bottom pairs on the even-numbered pulses. Thus, the technique has some similarity to ordinary (non-monopulse) lobe switching as described in Section 1.2, but with three important advantages over the latter: (1) the data rate is twice as high, one-half the pulse repetition frequency rather than one-fourth; (2) errors due to target amplitude fluctuation at or near the switching cycle frequency are avoided; and (3) the transmitting path (not shown in the diagram) is through the sum channel and therefore does not reveal the rate or even the existence of switching, unless mismatch within the comparator-resolver network allows modulation to leak into the sum channel. If the switching cycle can be detected by a hostile interceptor, it makes the system more vulnerable to jamming. In monopulse antennas using five or more horns the patterns of $s + d_m$ and $s - d_m$ are similar to those in four-horn monopulse, although the relationship to the patterns of the individual beams is somewhat more complicated.

The microwave-resolver version of the technique resembles conical scan, but with the same advantages as in the switched version (in this case the data rate is twice the scan frequency while in conical scan it equals the scan frequency).

If one of the two receiver channels fails in either of the two versions, monopulse operation is no longer possible but the radar continues to operate in a lobe-switching or conical-scan mode on reception and to transmit the sum pattern.

Since ordinary AGC is relatively slow, faster-acting alternatives can be used if the application requires accurate normalization on every pulse. One is to use AGC only to keep the signals within the dynamic range of the receivers, then digitize the outputs of the two channels and perform the normalization (division) by computer. Another is to use logarithmic amplifier-detectors in the $s + d_m$ and $s - d_m$ channels for normalization, as described in Section 8.12, instead of linear amplifiers with AGC.

As explained in Sections 8.10 and 8.11, this system in any of the versions described is insensitive to phase imbalance of the receiver channels.⁵ However, it is sensitive to the relative phase of the s and d_m , as explained in Section 8.11. Hence, the signals $s + d_m$ and $s - d_m$ should be formed at the earliest possible point and the phase imbalance between s and d_m preceding that point should be kept low.

8.15 PHASE-AMPLITUDE MONOPULSE

This technique [13] provides two-coordinate monopulse with only two feed horns, one hybrid junction, and two receiver channels. Two reflectors, positioned side by side in a rigid assembly, furnish phase-comparison monopulse in traverse. The feeds are placed a little above and below the foci of their respective reflectors, producing a pair of squinted beams that furnish amplitude-comparison monopulse in elevation. (The two coordinates could, of course, be interchanged by rotating the antenna assembly 90° .)

Figure 8.19 is a simplified block diagram. The hybrid junction produces the sum and difference of the two feed-horn outputs. As explained in Section 5.4, the amplitude-comparison and the phase-comparison components of the difference signal are respectively at 0° and 90° phase relative to the sum signal. Hence, they are carried in a single receiver channel, ideally without any coupling between the two coordinates. The other receiver channel carries the sum signal. Normalization is accomplished by AGC or other means.

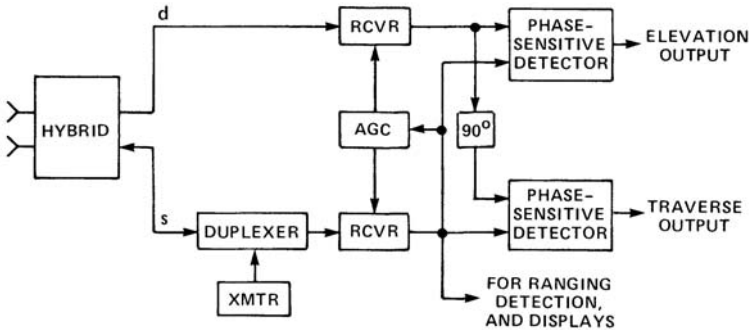


Figure 8.19 Phase-amplitude monopulse system. (After: Hausz and Zachary [13].)

⁵ This statement is not exactly true if $s + d_m$ and $s - d_m$ are added coherently (after amplification but before detection) to obtain the sum signal; in that case a phase imbalance decreases the sum signal slightly.

The combined difference signal and the sum signal out of the receiver channels are then split equally to become inputs to two phase-sensitive detectors, one of the inputs having first undergone a 90° phase shift. The two phase-sensitive detectors provide the traverse and elevation monopulse outputs.

To achieve the simplification offered by this type of system, certain sacrifices are necessary. Because of the smaller number of degrees of freedom available in a feed having only two horns, the tracking accuracy index (the product of sum voltage gain and difference slope; see Section 6.4) cannot equal that obtainable with a larger number of horns.

Another disadvantage is that phase imbalance between the sum and difference channels causes traverse-elevation coupling; as a result, when the antenna axis is displaced from the target, the servos tend to drive it toward the target in a spiral rather than a straight path. Even without phase imbalance in the receiver channels, serious coupling can occur in a situation where the difference signal contains an appreciable quadrature-phase component due to external factors such as multipath. In normal monopulse, multipath reflections from the surface can make elevation tracking of a low-angle target erratic or even impossible, but traverse tracking can still be maintained with relatively little deterioration. In phase-amplitude monopulse, the traverse channel would respond to the quadrature-phase component of the elevation difference signal due to multipath, causing large errors in both angular coordinates.

The description of phase-amplitude monopulse has been included here for historical completeness, since there appears to have been no application of this antenna and processing technique other than in the initial developments by General Electric Company in the 1960s. These included the experimental airborne radar described in [13] and a subsequent radar proposed for guidance of the Atlas ballistic missile.

8.16 MULTIPLEXED MONOPULSE RECEIVERS

One approach to minimizing receiver complexity and lack of accurate gain and phase tracking among the three receiver channels is to combine the sum and difference signals, either at RF or after conversion to IF, by time-multiplexing. Leonov and Fomichev [14, Section 7.6] discuss this approach, among several multiplexing methods. A simplified diagram of the RF-delay multiplexing system is shown in Figure 8.20. A delay is applied to d before summing with s at the input to the mixer. After amplification and detection, a compensating delay is applied to s before subtraction at the output. Normalization is performed by subtracting the two outputs of the logarithmic amplifier-detector, after they have been realigned in time.

The authors note that the RF-delay method has two drawbacks: (1) targets separated by less than two pulsewidths cannot be resolved, as they will overlap as

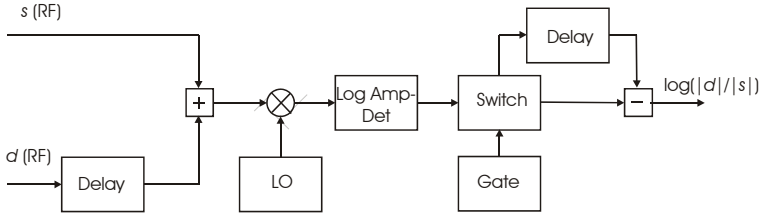


Figure 8.20 Processor using RF time-delay multiplexer. (After: Leonov and Fomichev [14].)

a result of the time delay in the processor, and (2) the system is vulnerable to jamming from a pair of pulses separated by the processor delay.

A similar process can be used with the first delay at IF, after downconversion. Mixers and IF preamplifiers must be duplicated (or triplicated, for a two-coordinate system), but a single log amplifier-detector provides most of the receiver gain in a common path.

Frequency multiplexing is another approach to minimizing receiver hardware and errors caused by poor gain and phase tracking. This approach is discussed in [14] and its application to homing seekers is described in [15]. In the seeker application, where Doppler processing is required, a linear main IF amplifier, controlled by sum-channel AGC, is used. Normalization results from the use of the common, gain-controlled main IF amplifier. Each channel must have its mixer and a bandpass amplifier-filter, but most of the gain comes from the main IF amplifier, whose gain or phase variations are applied identically to all three channels. The multiplexed output is separated using bandpass filters before being applied to phase-sensitive detectors to extract the two monopulse outputs.

A similar multiplexing technique called the single-channel monopulse processor (SCAMP) is described in [16]. The system actually uses three channels, frequency-multiplexed into a main IF amplifier and demultiplexed with bandpass filters. A simplified block diagram is shown in Figure 8.21, for a single angular coordinate. The sum and difference voltages are formed in the usual way and converted from RF to two closely spaced IFs f_s and f_d by mixing with separate local oscillators, and are then summed and amplified in the wideband main amplifier followed by a hard limiter. The sum and difference signals are then separated by two bandpass filters tuned to their respective frequencies.

It is shown in [17], using results of an analysis presented in [4], that when two signals at different frequencies are added and hard-limited, the bandpass-filtered output at the frequency of the stronger signal (the sum in this case) has a constant amplitude proportional to the limit level and independent of the original signal strength, and the bandpass-filtered output at the frequency of the weaker signal (the difference in this case) has an amplitude proportional to the ratio of the two original signal amplitudes. In other words, the limiting serves to normalize the difference to the sum. The sum voltage may be given additional amplification

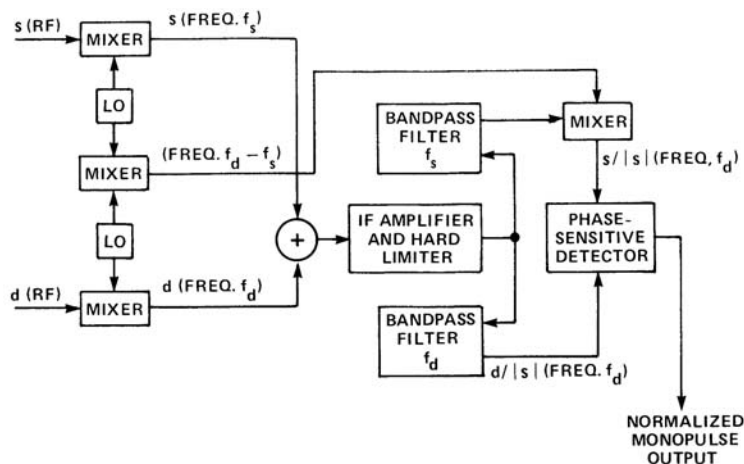


Figure 8.21 “Single-channel” monopulse processor. (After: Rubin and Kamen [17].)

before adding it to the difference voltage in order to ensure that it is always the larger of the two, within the usable portion of the beam.

After the sum and difference signals are separated by filtering, the sum is converted to the same frequency as the difference (or vice versa) by mixing with a signal of frequency $f_d - f_s$ derived by mixing of the two local oscillators. After this conversion the sum and difference have the same relative phase that they had at RF. The two signals are then applied as inputs to a phase-sensitive detector to obtain the monopulse output.

A cross-modulation problem in the SCAMP processor is discussed by Naval Research Laboratory engineers in [18], where it is pointed out that even though the spectra of the three input signals may not overlap, cross-modulation between these signals can manifest itself as a serious error in the directional information in the system. When the sum channel is assigned to the center frequency of the multiplexed combination, an intolerable level of cross-modulation between azimuth and elevation channels occurs in the limiter. The effect can be ameliorated but not eliminated when the sum channel is assigned to one of the end positions in the combination. Another caution from the NRL authors is that narrowband filters for each of the three IF channels (not shown in Figure 8.21) should be used prior to limiting, in order to minimize the effect of any broadband noise and interference passed through the RF circuits and mixers. This requirement implies that matching IF preamplifiers, preceding these filters, should precede the summing of the three channels shown in the figure, in order to minimize the effects of loss in the filters. Similar problems can be anticipated in other frequency-multiplexing processors, unless the main IF amplifier operates in the linear mode.

8.17 CONOPULSE

Monopulse, in principle, is free of errors due to target amplitude fluctuation, but usually requires three receiver channels. Conical scan, on the other hand, needs only a one-channel receiver but is subject to errors caused by target amplitude fluctuation.

A hybrid system called *conopulse*, which uses two receiver channels, has been proposed by Peebles and Sakamoto [19–21], who state that the basic concept goes back to 1958 or earlier but had received little attention in the prior open literature. It includes not only a special form of processing but also a unique method of two-coordinate angle tracking with only two beams. The authors describe and analyze different versions of the system.

The same technique had been discussed in a 1964 Russian radar text [22, p. 537], under the name *scan with compensation*. It was discussed there as a possible alternative to “instantaneous amplitude comparison” (monopulse) as a means of reducing the error due to target fluctuation, and also providing immunity against jamming.

One implementation suggested by Peebles and Sakamoto is shown in the simplified block diagram of Figure 8.22. The antenna produces a pair of squinted beams, from which a sum and difference are obtained. The difference signal is normalized by instantaneous AGC (IAGC) derived from the sum channel and acting on both the sum and difference, and by a phase-sensitive detector having the gain-controlled sum signal as its other input. The pair of squinted beams is rotated about the antenna axis (for example, by rotating the feed assembly), causing the normalized difference signal to be modulated in accordance with the magnitude and direction of the angular displacement of the target from the antenna axis. A pair of phase-sensitive detectors extracts the in-phase and quadrature components of the modulation relative to a sinusoidal voltage at the scan frequency. These components indicate the two orthogonal components of target displacement from the antenna axis, and are used as inputs to the angle servos if closed-loop me-

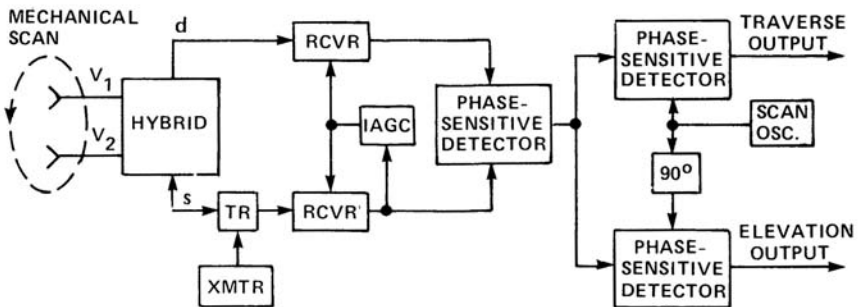


Figure 8.22 One possible form of conopulse system. (After: Sakamoto and Peebles [19].)

chanical angle tracking is done. The data rate is limited to that of the conical scan. This technique is seen to have some similarity to the microwave-resolver technique described in Section 8.14.

The normalization made possible by the use of two simultaneous beams eliminates the errors of conventional conical scan due to target fluctuation (assuming that the normalization is perfect). The advantages of conopulse over ordinary monopulse are the reduction in the number of receiver channels from three to two and the reduction of the feed from four horns to two, accompanied by simplification of the comparator. On the other hand, the necessity of rotating the beam pair (preferably without polarization rotation) poses a difficult design problem.

8.18 SUMMARY OF MONOPULSE PROCESSORS

The monopulse processor operates on the voltages derived from the antenna to produce the normalized monopulse output. The voltages on which it operates may be those of the individual component beams, but usually they are the sum (or reference) and a difference in each angular coordinate. The sum and difference emerge from the comparator at a nominal relative phase of either 0° or 90° , depending on the type of antenna and comparator. To avoid having to treat the two cases separately, we adopt the convention that the relative phase is 0° , with the understanding that if it is actually 90° , it can be converted to 0° by a phase shift or by an equivalent step in the processing.

As a standard for comparison, an exact processor has been arbitrarily defined as one that produces an output described in various equivalent ways:

- The real part of the complex ratio of the difference to the sum: $\text{Re}(d/s)$;
- The difference-to-sum magnitude ratio multiplied by the cosine of the difference-to-sum relative phase: $|d/s|\cos\delta$;
- The component of the difference that is in phase with the sum, divided by the magnitude of the sum: $(|d|\cos\delta)/|s|$.

Alternatively, an exact processor can be used to produce the imaginary part of the complex ratio d/s (equivalent to $|d/s|\sin\delta$) if either the difference or the sum is phase-shifted by 90° before processing. Unless otherwise stated, however, the output of the exact processor is understood to be the real part.

Various types of monopulse processors are in use. Some approach the performance of the exact processor, limited only by finite dynamic range, quantization (if the processing is digital), and imperfections in equipment performance or calibration. Others are designed to act like exact processors only when the imaginary part is zero and the magnitude ratio $|d/s|$ does not exceed unity. Still others produce an output that deviates from that of the exact processor under all condi-

tions but approximates it closely enough when the off-axis angle is small and the imaginary part is zero.

The choice among the processors depends on the type of use and the accuracy required of the radar. Generally speaking, the more closely a processor is designed to approach an exact processor the more expensive it tends to be and the more care it requires in design and calibration. In many radars designed for continuous closed-loop tracking of one target at a time, close to the axis, a simpler processor suffices.

In analyzing or simulating the performance of a monopulse radar, the characteristics of the processor used in that radar should be taken into account rather than assuming an exact processor. The difference can be significant if the target is not close to the axis or if there is a nonzero imaginary part of d/s due to unresolved targets, multipath, or misalignment within the radar. The responses to noise and interference may also differ.

Table 8.1 compares the various processors described in this chapter with an exact processor. In this comparison, each processor is assumed to work perfectly in accordance with its basic concept; in other words, errors due to finite dynamic range, quantization, and imperfections in equipment, alignment, or calibration are ignored, leaving only those deviations from an exact processor that are inherent in the method of processing. All the processors that operate on a sum and difference can be used either with amplitude-comparison or phase-comparison antennas. The processors that operate on the amplitudes of the component beam voltages are limited to amplitude comparison.

The processors listed in the table normally require three receiver channels for two-coordinate monopulse. In Sections 8.14 to 8.17 special techniques have been described that can reduce the number of channels to two, or even to one. Each of these techniques imposes either design difficulties or some sacrifice in performance, such as reduced data rate or signal-to-noise ratio. Of those techniques, the switched version of the one described in Section 8.14 is in practical use in some radars, the sacrifice in data rate being an acceptable trade-off for simpler design. The frequency multiplexing technique discussed in Section 8.16 has been applied to homing seekers, of which several thousand have been produced in the United States. The other special techniques do not appear to have found application.

In selecting a monopulse processor design, compatibility with other signal-processing functions in the system must be considered. If Doppler filtering is to be done, for example, it requires linear processing up to the point where the clutter has been filtered out. Therefore it is not directly compatible with monopulse processors that include nonlinear operations such as logarithmic amplification or amplitude limiting. In order to do Doppler filtering in systems using such monopulse processors it is necessary to provide linear channels in parallel.

Table 8.1 Comparison of Monopulse Processors

<i>Processor Using</i>	<i>Section</i>	<i>Equivalent to Exact Processor under the Following Conditions (assuming perfect operation)</i>	<i>Application to Amplitude or Phase Comparison</i>
Phases and amplitudes of s and d	8.5	All conditions	Both
I and Q	8.6	All conditions	Both
Phases and log amplitudes of s and d	8.7	All conditions	Both
Dot-product detector with AGC	8.8	All conditions	Both
Approximate dot-product detector	8.9	$\delta = 0^\circ, d/s \leq 1$	Both
$(v_1 - v_2)/(v_1 + v_2)$	8.10	v_1 and v_2 in phase, target in mainlobe of both squinted beams	Amplitude comparison
$(s + d - s - d)/(s + d + s - d)$	8.11	$\delta = 0^\circ, d/s \leq 1$	Both
$\log v_1 - \log v_2 $	8.12	Not equivalent, but close approximation if v_1 and v_2 are in phase and target is close to axis	Amplitude comparison
$s \pm jd$	8.13	$\delta = 0^\circ$, all values of $ d/s $	Both

References

- [1] Mehuron, W. O., "Passive Radar Measurements at C-Band Using the Sun as a Noise Source," *Microw. J.*, Vol. 5, No. 4, April 1962, pp. 87–94.
- [2] J. T. Kennedy and J. W. Rosson, "The Use of Solar Radio Emission for the Measurement of Radar Angle Errors," *Bell Sys. Tech. J.*, Vol. XLI, No. 6, November 1962, pp. 1799–1812.
- [3] J. T. Nessmith, "New Performance Records for Instrumentation Radar," *Space/Aeronautics*, December 1962, pp. 86–93. Reprinted in *Radars*, Vol. 1, *Monopulse Radar*, D. K. Barton, (ed.), Dedham, MA: Artech House, 1974.
- [4] S. N. Van Voorhis, (ed.), *Microwave Receivers*, Vol. 23 of MIT Radiation Laboratory Series, New York: McGraw-Hill, 1948, pp. 583–606. Reprint, CD-ROM ed., Norwood, MA: Artech House, 1999.
- [5] J. Croney, "A Simple Logarithmic Receiver," *Proc. IRE*, Vol. 39, No. 7, July 1951, pp. 807–813.
- [6] S. J. Solms, "Logarithmic Amplifier Design," *IRE Trans. on Instrumentation*, Vol. I-1, No. 3, December 1959, pp. 91–96.
- [7] S. N. Rubin, "A Wideband UHF Logarithmic Amplifier," *IEEE J. Solid-State Circuits*, Vol. 1, No. 2, December 1966, pp. 74–81.
- [8] B. Loesch, "A True Logarithmic IF Amplifier," *IEEE Trans. Aerospace and Electronic Systems*, Vol. AES-9, No. 5, September 1973, pp. 660–664.
- [9] J. H. Dunn and D. D. Howard, "The Effects of Automatic Gain Control Performance on the Tracking Accuracy of Monopulse Radar Systems," *Proc. IRE*, Vol. 47, No. 3, March 1959, pp. 430–435.
- [10] D. D. Howard, "Predicting Target-Caused Errors in Radar Measurements," *IEEE Eascon-76 Record*, September 26–29, 1976, pp. 30A–30-H.
- [11] C. F. Chubb, B. L. Hulland, and R. S. Noblit, "Simplified Monopulse Radar Receiver," U.S. Patent No. 3,239,836, March 8, 1966.
- [12] R. S. Noblit, "Reliability Without Redundancy from a Radar Monopulse Receiver," *Microwaves*, December 1967, pp. 56–60.
- [13] W. Hausz and R. A. Zachary, "Phase-Amplitude Monopulse System," *IRE Trans. on Military Electronics*, Vol. MIL-6, No. 2, April 1962, pp. 104–146. Reprinted in *Radars*, Vol. 1, *Monopulse Radar*, D. K. Barton, (ed.), Dedham, MA: Artech House, 1974.
- [14] A. I. Leonov and K. I. Fomichev, *Monoimpul'snaya Radiolokatsiya, (Monopulse Radar)*, Moscow: Radio i Svyaz, 1984. Translation, Norwood, MA: Artech House, 1986.
- [15] A. Ivanov, "Improved Radar Designs Outwit Complex Threats," *Microwaves*, April 1976, pp. 54–71. Reprinted, *Radar Electronic Counter-Counter-Measures*, S. L. Johnston, (ed.), Dedham, MA: Artech House, 1979, pp. 457–462.
- [16] W. B. Davenport, Jr., and W. L. Root, *An Introduction to the Theory of Random Signals and Noise*, New York: McGraw-Hill, 1958, p. 288.
- [17] W. L. Rubin and S. K. Kamen, "SCAMP—A New Ratio Computing Technique with Application to Monopulse," *Microwave J.*, December 1964, pp. 83–90. Reprinted in *Radars*, Vol. 1, *Monopulse Radar*, D. K. Barton, (ed.), Dedham, MA: Artech House, 1974.

- [18] J. E. Abel, S. F. George, and O. D. Sledge, "The Possibility of Cross Modulation in the SCAMP Signal Processor," *Proc IEEE*, Vol. 53, No. 3, March 1965, pp. 317–318c.
- [19] H. Sakamoto and P. Z. Peebles, Jr., "Conopulse Radar," *IEEE Trans. on Aerospace and Electronic Systems*, Vol. AES-14, No. 1, January 1978, pp. 199–208.
- [20] P. Z. Peebles, Jr. and H. Sakamoto, "On Conopulse Radar Theoretical Angle Tracking Accuracy," *IEEE Trans. on Aerospace and Electronic Systems*, Vol. AES-16, No. 3, May 1980, pp. 399–402.
- [21] P. Z. Peebles, Jr. and H. Sakamoto, "Conopulse Radar Angle Tracking Accuracy," *IEEE Trans. on Aerospace and Electronic Systems*, Vol. AES-16, No. 6, November 1980, pp. 870–874.
- [22] P. A. Bakut and G. P. Tartakovskiy, *Problems in Statistical Radar Theory*, Moscow: Soviet Radio, Vol. 1, 1963, Vol. 2, 1964. Translation, Foreign Technology Division, Wright-Patterson Air Force Base, June 28, 1966, DDC document AD 645,755.

Chapter 9

Response to Unresolved Targets

In the preceding chapters it has been assumed that only a single target, confined to one point in angle space (or sine space) is present. Situations occur, however, in which the signals acted upon by the monopulse processor come not from a single target but from two or more unresolved targets. Even a single target may have multiple scattering points, which are equivalent to multiple unresolved targets. Multipath can also be treated as a special case of unresolved targets, in which the image or images produced by reflection from the ground or sea are equivalent to additional targets within the resolution cell. A jammer within the same beam as a target has the same effect as an unresolved target.

When targets are unresolved, the radar produces a single angle indication based on the composite sum and difference signals. In general, the angle indicated by the radar does not correspond to the angle of any of the unresolved targets or scattering points. It wanders as the relative amplitudes and phases of the targets change because of amplitude fluctuation, relative motion, or other causes. Sometimes the indicated angle is even outside of the angular span that the targets subtend at the radar. The errors can be large enough to cause loss of track. Similar effects occur in measurement of range and Doppler, but here we are concerned only with angle.

Unresolved targets cause a change in the relative phase of the difference voltage d and the sum (or reference) voltage s , so that even if all other conditions are ideal (no noise, no equipment imperfections, and so forth) the ratio d/s is no longer pure real or pure imaginary, but complex.

In addition to causing errors in angle measurement, unresolved targets affect detection, which the radar must accomplish before it can track. The strength of the sum signal fluctuates as the relative phases of the targets vary. Averaged over all phases, the combined power is the sum of the powers received from the individual targets, but part of the time the instantaneous combined power is less than that of the desired target alone. Detection probability may be seriously degraded. Since

the effect of unresolved targets (particularly multipath) on detection is common to all radars and is amply treated in the general radar literature, it will not be pursued here.

This chapter will first review the monopulse response to a point target, then analyze the response to two unresolved point targets (after defining “unresolved targets” more fully). The two-target problem is not uncommon in real life and both the mathematics and the physical concepts are readily manageable. For three targets, the mathematics of a deterministic analysis (i.e., one in which the positions, amplitudes, and phases of the targets are specified) becomes considerably more complicated, and for more than three targets it becomes impractical. However, the physical insight gained from the two-target analysis aids in interpreting the multitarget problem. For any number of targets, a statistical analysis with target amplitudes and phases as random variables can be performed, and this sometimes provides more useful information than a deterministic analysis.

In the usual situation, the radar is tracking or attempting to track one of the targets, and the presence of another target (or source of radiation) in the same resolution cell causes errors in measurements of the primary target. A number of ideas have been proposed and investigated as ways to reduce these errors and possibly obtain information about the angular location of both targets. Some of those approaches are informative from a theoretical viewpoint but appear to have limited or questionable practical use. They are discussed in this chapter because they may be effective in certain special applications, or if not, it is useful to understand the reason. In any case, they provide insight into the fundamental limitation of any electromagnetic measuring system in a situation of this kind, namely distortion of the electromagnetic wave front arriving at the receiving antenna, as illustrated by an example in Chapter 5. An understanding of this topic is needed for error budgeting when specifying realistic performance standards for a proposed radar and in designing a radar to meet those standards.

When the ratio d/s is complex, we can regard its real and imaginary parts as if they were due to a complex target angle, known as a *complex indicated angle*. The two parts are related to the phase and amplitude gradients, respectively, of the arriving wave across the antenna aperture. Certain techniques using both the real and imaginary parts have been proposed to detect “contamination” of the monopulse output due to the presence of unresolved targets, and to deduce further information about them. In theory it is possible to use the complex values of d/s to determine the locations of two unresolved targets, but there are practical difficulties and limitations.

The following assumptions are made initially to simplify the analysis. The effects of removing these assumptions will be examined later.

1. The sum and difference voltages from a single point target emerge from the comparator at 0° (or 180°) relative phase, so that the monopulse ratio d/s is real. For radars in which the relative phase is

90° (d/s is pure imaginary), the results are easily modified by interchanging reals and imaginaries (in-phase and quadrature-phase components) or by a 90° rotation when dealing with plots in the complex plane. The assumption that d/s is pure real (or pure imaginary) applies only to a single target, not to unresolved targets.

2. The monopulse processor is an exact processor as defined in Section 8.4. That is, its output is normally the real part of the ratio d/s , but another identical processor can be added, with one of its inputs shifted by 90° , to measure the imaginary part also, if desired. Because of the variety of types of “inexact” processors, their responses to unresolved targets will not be presented, but the procedure for analyzing and computing their responses will be outlined.
3. The normalized difference signal for a single target is proportional to its angle. The property of proportionality to angle is independent of the assumption of an exact monopulse processor. A typical response of an exact processor as a function of angle can be seen in either the d/s curve of Figure 1.6 or the equivalent dashed curve labeled $\delta = 0^\circ$ in Figure 8.7. Those curves are based on the patterns of the AN/FPS-16 radar but most monopulse radars exhibit a d/s curve of similar shape. The slope is generally not constant but increases somewhat with angle. For directions close to the axis, the on-axis tangent straight line gives a close fit. Over a wider angular region, say between the half-power points, the curve can be approximated by a best-fit straight line of somewhat greater slope, passing through the origin. In the operation of a radar for off-axis measurements, the actual curve should be used unless the angles are small. However, for purposes of error analysis a straight-line approximation usually suffices. Should it be found necessary to use the actual curve, the results derived for straight-line response can be modified by a procedure described later in this chapter.
4. The response in each angular coordinate is independent of the target location in the other coordinate provided that the amplitude ratios and relative phases of the returns from the individual targets are specified for the actual locations. This assumption is usually justified in error analysis even though coupling between the coordinates may require two-dimensional calibration in the actual operation of the radar.
5. Noise and other sources of error (except the error caused by unresolved targets) are ignored.

9.1 REVIEW OF MONOPULSE RESPONSE TO A POINT TARGET

A *point target* is one that appears to the radar to be concentrated at a point in angle space (or in sine space). It need not be confined to a single point in range¹; however, if it has appreciable extent in range, rotation of the body may convert the range extent to lateral extent, so that it no longer appears as a point target.

Most targets of interest have multiple scattering points. These are usually points of discontinuity of silhouette area, or its derivatives, as a function of range along the target extent. Discontinuities include leading and trailing edges. Generally the scattering points are not at exactly the same angle from the radar. Each scattering point makes its own contribution to the sum and difference signals, and the complete target therefore affects the radar in the same way as a cluster of unresolved point targets, causing angular wander known as glint (which will be discussed more fully in Chapter 10). Hence, most targets are not true point targets. As a practical matter, however, a target may be considered to be a point target if the angle that it subtends at the radar (in each coordinate) is small compared to the angular measurement errors of the radar due to other causes. At sufficiently long range every target looks to the radar like a point target. Although the amplitude of its echo may fluctuate because of interference among the scattering points as their relative phases change, the amplitude fluctuation does not affect angle measurements by a monopulse radar.

In accordance with the assumptions made above, the monopulse output in either angular coordinate (traverse or elevation), in the absence of noise or other sources of error, is

$$\frac{d}{s} = k_m \theta \quad (9.1)$$

where d/s is the normalized difference signal in the selected coordinate, θ is the angle off axis in that coordinate expressed in beamwidths (of the sum beam), and k_m is the slope of the monopulse response curve versus angle in the same coordinate, expressed in volts per volt per beamwidth (see Section 6.4). The choice of the beamwidth as the unit of angle is convenient because then k_m has roughly the same value (≈ 1.6) in many monopulse radars. The values of k_m in the two coordinates need not be equal, but they are usually close. In making computations for a particular radar, absolute angular units (degrees or milliradians) may be substituted provided angle and slope are in consistent units.

The radar produces the monopulse ratio d/s and divides it by the known slope k_m to obtain the *indicated angle*, denoted by θ_i :

¹ The term “point target” is sometimes also applied to a target confined to a single point in range. In the present context the term refers only to angle.

$$\theta_i = \frac{1}{k_m} \frac{d}{s} = \theta \quad (9.2)$$

which means that the radar is designed to yield an indicated angle equal to the actual geometric angle of a single target under ideal conditions.

9.2 THE MEANING OF UNRESOLVED TARGETS

There is no need in this book for a general definition of resolution, various versions of which are in existence. Instead we need merely define what is meant here by *unresolved targets* in the specific context of angle measurement: targets are unresolved if an angle measurement cannot be made on each target without significant error due to the presence of others. “Significant error” can be defined by quantitative criteria where needed. To be resolved, the targets must be sufficiently separated in at least one coordinate (traverse, elevation, range, or Doppler) to make their interference with each other’s measurements negligible.

Note that in order to be unresolved, targets must be closely spaced in *all* coordinates, not just angle. As a rule of thumb, targets are often called unresolved if they are within the same *resolution cell* having nominal dimensions of the beam-width, the pulse length, and the Doppler filter bandwidth (if Doppler is used); but they may cause mutual interference and therefore be unresolved in the sense defined here even if their separations are greater, since resolution cells with sharp boundaries are fictitious. Even if they are sufficiently separated to be recognized and measured by the radar as individual targets, there may be enough overlap to cause errors in the angle measurements. In the usual case, however, the radar fails to recognize that there is more than one target in the cluster, and reports a detection and a set of measurements as if there were only one target.

Resolvability depends of course not only on the targets, but on the characteristics of the radar, including the type of processing.

9.3 SUPERPOSITION AS AN APPROXIMATION

It is commonly assumed that superposition applies to the electromagnetic fields scattered by multiple targets, but strictly speaking that is not true; in solving a boundary-value problem it is not correct simply to add the electromagnetic fields obtained by considering one part of the boundary (that is, one target) at a time, as if the others were not present. The incident field at each target is modified by the scattered fields from the other targets. A less rigorous but easier way of expressing the same idea is in terms of “multiple-bounce” reflections (from one target to another, one or more times, then back to the radar).

However, in most practical situations with which we are concerned, the multiple-bounce contributions are negligible and we can assume that superposition applies. The following example will illustrate the fact that the error in this assumption is typically very small, although it can be significant under some unusual conditions.

Consider two isotropic targets (targets that radiate or scatter an incident plane wave uniformly in all directions). Let their radar cross sections be σ_a and σ_b and let their separation be R_{ab} . The transmitted radar power captured and reradiated by the first target is proportional to σ_a . Similarly, the transmitted radar power captured and reradiated by the second target is proportional to σ_b ; of this power, the first target captures and reradiates a fraction $\sigma_a/(4\pi R_{ab}^2)$. Hence, the ratio of double-bounce power (radar to second target to first target to radar) to single-bounce power (radar to first target to radar) that the first target reradiates back to the radar is

$$\frac{\sigma_a \sigma_b}{4\pi R_{ab}^2} \div \sigma_a = \frac{\sigma_b}{4\pi R_{ab}^2} \quad (9.3)$$

For a numerical example, let $\sigma_b = 1 \text{ m}^2$ and $R_{ab} = 10\text{m}$. Then the double-bounce power is 31 dB below the single-bounce power, making it negligible for most applications.

For a particular instantaneous geometry it is the electromagnetic fields, not the powers, that are additive. Thus in this example the ratio of the double-bounce field to the single-bounce field, equal to the square-root of the power ratio in (9.3), is 0.028, and the relative phase may have any value, depending on the positions of the two bodies. The resultant power may therefore be larger or smaller than the single-bounce power alone. Averaged over all possible phases, however, the resultant power is the sum of the two individual powers. Hence, the average apparent cross section of the first target is increased by the factor 1.0008 by the double-bounce contribution.

In a similar manner, we can compute the triple-bounce power contribution (radar to first target to second target to first target to radar) as a fraction of the double-bounce contribution. This fraction is $\sigma_a/(4\pi R_{ab}^2)$, which will usually be an insignificant correction to the already negligible double-bounce contribution.

Since the designations “first target” and “second target” are arbitrary, the same type of analysis applies to the other target if σ_a and σ_b are interchanged.

While this method of rough calculation is intended only for an order-of-magnitude illustration, it gives results that are in reasonable agreement with the results of a more rigorous analysis of the radar backscatter from two unresolved spheres [1]. If the radar cross section of each of two unresolved targets is much smaller than the square of the distance between them (say, by a factor of 100), then multiple-bounce effects can be ignored and superposition can be assumed. This is the usual situation in two-target problems, and our analysis will therefore

be based on superposition. This means that the resultant signal voltages received from two or more unresolved targets are calculated by phasor addition of the voltages that would have been received from the individual targets if the others were not there.

However, one should be aware that superposition applied to multiple radar targets is only an approximation, which should be used with caution if the square of the distance between two targets is not much larger than the radar cross section of the larger target.

9.4 THE TWO-TARGET PROBLEM

In the single-target case the sum and difference voltages s and d are in phase and the normalized difference signal d/s is real. In the case of unresolved targets, however, s and d may have any relative phase and their ratio is therefore complex.

To demonstrate this fundamental point in a simple way [2, 3], consider two unresolved targets at different angles within the beam and confine attention to one angular coordinate at a time. In the phase diagram, Figure 9.1, s_a and d_a are the monopulse sum and difference signals from the first target, and s_b and d_b the corresponding signals from the second target. Though the two targets are in the same range resolution cell, in general their ranges are not exactly equal and there will be some phase difference between s_a and s_b . Even if the ranges are equal, there may be a phase difference because of different backscatter phase characteristics of the two targets. The total sum signal is the resultant s . Suppose, for illustration, that the two targets are on opposite sides of the beam axis, the first target being on the side that causes d_a to be in phase with s_a ; then d_b is in phase opposition to s_b . The total difference signal d is the resultant of d_a and d_b .

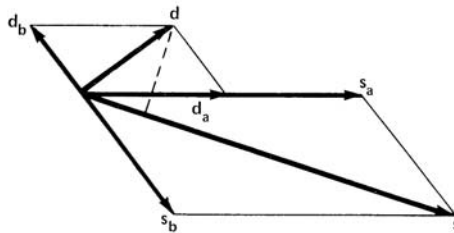


Figure 9.1 Sum and difference phasors for two unresolved targets.

It is clear from Figure 9.1 that, in general, d has a component in phase quadrature with s , shown by the dashed line, as well as an in-phase component. In other words, the ratio d/s is complex. It is easy to see also that if s_a and s_b are 180°

out of phase and nearly equal in magnitude, the ratio d/s can become very large. The foregoing result is not confined to cases where the two targets lie on opposite sides of the beam axis—it is quite general.

To express the result mathematically, let θ_a and θ_b be the angular displacements of the two targets from the axis in the selected coordinate. Then from (9.1)

$$d_a = k_m \theta_a s_a \quad (9.4)$$

$$d_b = k_m \theta_b s_b \quad (9.5)$$

The resultant indicated angle is

$$\theta_i = \frac{1}{k_m} \frac{d}{s} = \frac{1}{k_m} \frac{d_a + d_b}{s_a + s_b} = \frac{\theta_a s_a + \theta_b s_b}{s_a + s_b} \quad (9.6)$$

This equation says that the indicated angle θ_i is a weighted average of the actual angles of the targets, with weighting proportional to their respective sum-signal contributions. However, the weighting is complex, since s_a and s_b have difference phases in general, and the end result is not readily apparent without further analysis.

Let

$$s_b/s_a = pe^{j\phi} \quad (9.7)$$

where

$p = gr$ = amplitude ratio of sum-signal returns from the two targets;

g = ratio of antenna sum-pattern voltage gains in the directions of the two targets;

r = ratio of backscatter voltage coefficients of the two targets (the square root of the ratio of their radar cross sections);

ϕ = relative phase of the sum-signal returns from the two targets.

The ratios g and r and the relative phase ϕ are arbitrarily defined to refer to the second target (at angle θ_b) relative to the first (at angle θ_a), not vice versa. The quantity g means the two-way voltage gain ratio in the usual case of passive radar targets. In the case of active sources or beacons, g refers to the one-way voltage gain, r is the ratio of the strengths (voltages) of the sources, and ϕ is their relative phase. Both g and r are defined as non-negative and real, and therefore the same is true of p .

Dividing the right-hand side of (9.6) through by s_a and using (9.7), we obtain

$$\theta_i = \frac{\theta_a + pe^{j\phi}\theta_b}{1 + pe^{j\phi}} \quad (9.8a)$$

An equivalent form of the same equation expresses the result in terms of the angular midpoint θ_{mid} and angular separation $\Delta\theta$ of the two targets:

$$\theta_i = \theta_{\text{mid}} - \frac{\Delta\theta}{2} \frac{1 - pe^{j\phi}}{1 + pe^{j\phi}} \quad (9.8b)$$

where

$$\theta_{\text{mid}} = \frac{\theta_a + \theta_b}{2} = \text{angular midpoint};$$

$$\Delta\theta = \theta_a - \theta_b = \text{angular separation}.$$

The equation can also be written in a third form that equates the indicated angle to the true angle of the first target, θ_a , plus an error term; this form is convenient for determining the error in measuring the angle of a particular target:

$$\theta_i = \theta_a + \Delta\theta \frac{pe^{j\phi}}{1 + pe^{j\phi}} \quad (9.8c)$$

Since (9.8a), (9.8b), and (9.8c) are all equivalent, they will be referred to collectively as (9.8) except when a distinction among the three versions is being made. The choice of the particular version to be used is a matter of convenience of analysis, computation, or plotting in each case.

9.5 THE COMPLEX INDICATED ANGLE

The quantity θ_i on the left-hand side of (9.8) has been named the *complex indicated angle* or simply the *complex angle* [2, 3]. When $p = 0$ (second target removed), the right-hand side of the equation reduces to θ_a and the indicated angle equals the geometric angle, as expected. When p is infinite (first target removed), the indicated angle reduces to θ_b . When $\theta_a = \theta_b$ (both targets at the same angle in the coordinate under consideration), the indicated angle equals the geometric angle regardless of the amplitudes and phases of the two targets. However, in general the indicated angle is a complex quantity.

Since the monopulse processor is normally designed to extract only the real part of the indicated angle, the usual method of analysis of the two-target problem is to deal only with the real part of (9.8). This is obtained by multiplying numerator and denominator of the fraction in the appropriate version of (9.8) by $1 + pe^{-j\phi}$ (remembering that $e^{\pm j\phi} = \cos\phi \pm j \sin\phi$), and then collecting the real terms on the right-hand side. The results can be expressed in various equivalent forms. Starting

successively with (9.8a), (9.8b), and (9.8c), the corresponding expressions for the real part are, respectively,

$$\operatorname{Re}(\theta_i) = \frac{\theta_a + p \cos \phi (\theta_a + \theta_b) + p^2 \theta_b}{1 + 2p \cos \phi + p^2} \quad (9.9a)$$

$$\operatorname{Re}(\theta_i) = \theta_{\text{mid}} - \frac{\Delta\theta}{2} \frac{1 - p^2}{1 + 2p \cos \phi + p^2} \quad (9.9b)$$

$$\operatorname{Re}(\theta_i) = \theta_a + \Delta\theta \frac{p \cos \phi + p^2}{1 + 2p \cos \phi + p^2} \quad (9.9c)$$

Although the imaginary part is normally ignored, it is available for measurement if needed. Its physical significance and possible uses will be discussed later. The imaginary part, obtained from any version of (9.8), is

$$\operatorname{Im}(\theta_i) = \Delta\theta \frac{p \sin \phi}{1 + 2p \cos \phi + p^2} \quad (9.10)$$

The relative phase δ between the sum and difference signals has the following relation to the real and imaginary parts:

$$\tan \delta = \frac{\operatorname{Im}(\theta_i)}{\operatorname{Re}(\theta_i)} = \frac{p \sin \phi}{\theta_a + p \cos \phi (\theta_a + \theta_b) + p^2 \theta_b} \quad (9.11)$$

The mathematical expressions are more compact when written in complex form. Any one of the three versions of the complex equation (9.8) is equivalent to a pair of equations composed of one part of the versions of (9.9) for the real part and (9.10) for the imaginary part. Although decomposition into real and imaginary parts becomes necessary when numerical computations are needed, the complex form often facilitates mathematical operations and plotting. It also facilitates analysis of the effects of imperfections such as amplitude and phase imbalances in the radar equipment.

To examine the nature of the complex indicated angle as a function of the target parameters, define the auxiliary quantity w :

$$w = p e^{j\phi} \quad (9.12)$$

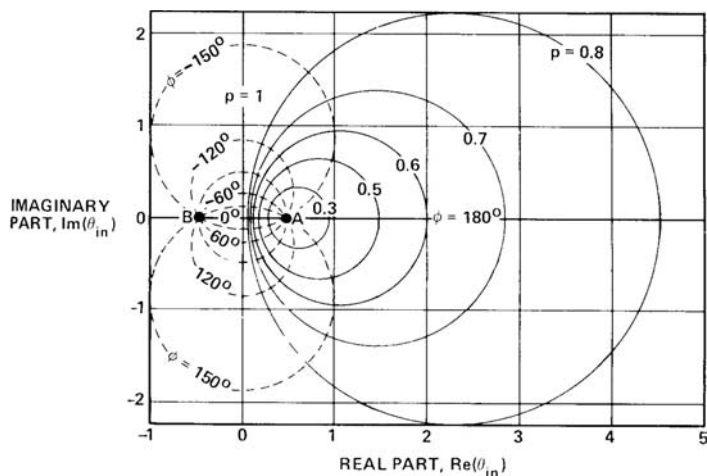
Substituting in (9.8a):

$$\theta_i = \frac{\theta_a + \theta_b w}{1 + w} \quad (9.13)$$

Both θ_i and w are complex. If θ_a and θ_b are held constant, (9.13) shows that θ_i is composed of a linear function of w divided by another linear function of w . In the theory of functions of a complex variable this is known as a bilinear transformation of w , and it has the property (see any textbook on functions of a complex variable) that straight lines and circles in the w -plane are transformed into straight lines and circles in the θ_i -plane. The straight lines occur as special cases, equivalent to circles of infinite radius.

If the relative phase ϕ of the two targets is varied while their amplitude ratio p and their angles θ_a and θ_b are held constant, w traces out a circle of radius p centered on the origin in the w -plane, and the bilinear transformation transforms this into a circle in the θ_i -plane. Different values of p produce a family of circles in the θ_i -plane.

The circles for several values of the amplitude ratio p are drawn in solid lines in Figure 9.2. The figure has been normalized by putting the origin at the midpoint of θ_a and θ_b and taking $\theta_a - \theta_b$ as the unit of angle. In other words, the complex quantity being plotted is a normalized indicated angle θ_{in} , which can be written, with the aid of (8.8b), as



Normalized so that origin is at angular midpoint and unit of angle is angular separation of the targets. First target at A, second target at B.

Figure 9.2 Complex indicated angle for two targets (in one coordinate).

$$\theta_{in} = \frac{\theta_i - \theta_{mid}}{-\Delta\theta} = \frac{1}{2} \frac{1 - pe^{j\phi}}{1 + pe^{j\phi}} \quad (9.14)$$

The arbitrary choice of the negative sign before $\Delta\theta$ is convenient for plotting.

These curves are easy to plot, once it is recognized that they must be circles and that their centers must lie on the real axis because the substitution of $-\phi$ for ϕ reverses the sign of the imaginary part without affecting the real part. The two points of intersection of each circle with the real axis are easily calculated by substituting $\phi = 0$ (left intersection) and $\phi = \pi$ (right intersection). To plot each circle, take the midpoint between the two intersections as the center and half the distance between them as the radius. The same circles could be obtained (but with much more labor) by plotting $\text{Im}(\theta_i)$ versus $\text{Re}(\theta_i)$ point by point with ϕ as the implicit variable, using (9.9) and (9.10).

The circles for $p < 1$ lie on the side closer to the first target (the one designated by the subscript a). The circles for $p > 1$ lie on the side closer to the second target. Reciprocal values of p produce pairs of circles that are symmetrical with respect to the imaginary axis. The circle for $p = 1$ degenerates into the imaginary axis. The circles for $p = 0$ and ∞ degenerate into points A and B representing the first and second target, respectively. If ϕ varies at a uniform rate, the motion of the corresponding point on the θ_{in} circle is *not* uniform; it is slow when ϕ is near 0° and rapid when ϕ is near 180° .

If the amplitude ratio p is varied while the relative phase angles are held constant, w traces out a straight line in the w -plane, which transforms into a circle in the θ_r -plane (or θ_{in} -plane). Different values of ϕ produce a family of constant- ϕ circles, orthogonal to the constant- p family. These are drawn as broken circles in Figure 9.2. Each broken circle is composed of two arcs, one above the real axis and the other below, differing in phase by 180° . For $\phi = 0^\circ$ the arc (of infinite radius) is the part of the real axis between A and B, and for 180° it is the remainder of the real axis.

It must be remembered that Figure 9.2 pertains to a single angle coordinate. If that coordinate is traverse, the vertical coordinate in the figure represents the imaginary part of the indicated traverse angle, not the indicated elevation angle. The same set of normalized curves would apply also to elevation.

If the amplitude ratio, the relative phase, and the angles of the two targets relative to the beam axis are known, Figure 9.2 can be used to read off the complex indicated angle in the following manner. Normalize the scale by letting unit distance on the real and imaginary axes represent the angular separation of the two targets in the coordinate under consideration. Shift the origin to the left or right until the distances from the origin to points A and B representing the first and second targets equal their respective normalized angles from the axis. The intersection of the appropriate p circle and ϕ circle is the value of the complex indicated

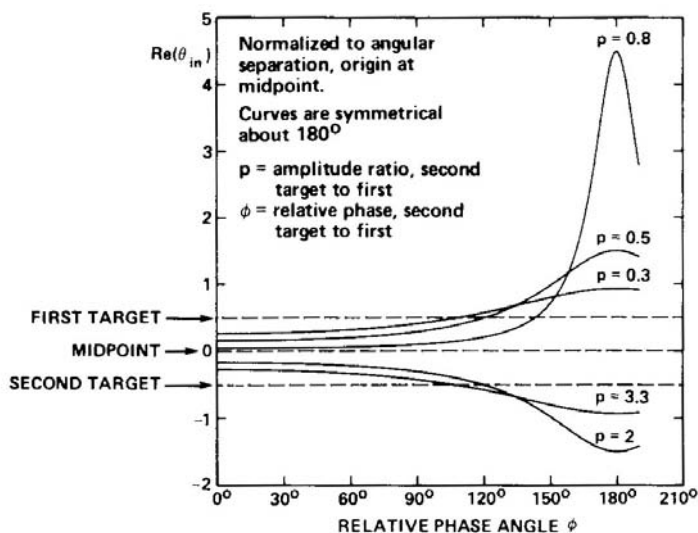


Figure 9.3 Real part of complex angle versus relative phase for two unresolved targets.

angle in normalized form. To remove the normalization, multiply by the angular separation of the two targets.

If d/s is linear with angle as assumed, a shift in beam pointing angle relative to the two targets would mean simply a horizontal shift of the origin by a corresponding amount in Figure 9.2 if p remained constant. The fact is, however, that as the beam direction changes, there is a change in the sum-pattern voltage-gain ratio g defined under (9.7), causing a change in p . Therefore the correct value of p for the actual beam position must be used.

Figure 9.3 shows plots of $\text{Re}(\theta_{in})$, the real part of the normalized indicated angle, as a function of ϕ for different values of p , computed by (9.9b) and normalized by (9.14). The form of these curves could have been visualized by examination of Figure 9.2. Since the curves are symmetrical about 180° , only the left halves are shown.

Equation (9.9b) and Figure 9.3 are the same as equations and curves derived or reproduced in various papers and books in the radar literature (see, for example, [4, p. 87; 5, p. 169]). It is interesting to note that the families of curves have a simpler form (circles) when plotted in the complex plane. The complex plots also help to visualize the effect of phase imbalance between the sum and difference channels due to imperfections in the radar. The effect is a rotation of Figure 9.2 about a point representing the axis, by an angle equal to the phase imbalance, causing coupling between the real and imaginary parts.

By setting $\text{Re}(\theta_i) > \theta_a$ in (9.9c), it is found that the fraction of the time that the indicated angle lies outside of the angular span of the two targets is $(\cos^{-1}p)/\pi$. For example, if $p = 0.5$, the fraction is $1/3$.

It is emphasized that Figures 9.2 and 9.3, and the equations on which they are based, represent *open-loop* monopulse response, obtained when the antenna axis is held fixed. In the normal *closed-loop* tracking mode, the antenna beam moves in order to null out the real part of the indicated angle. As it does so, the amplitude ratio of the targets changes. Closed-loop response will be discussed in a later section.

9.6 PHYSICAL INTERPRETATION

It has been stated [6] that any tracking radar, not only monopulse, tends to align its axis in the direction of the normal to the phase front. This is a useful rule if properly interpreted and qualified. In monopulse terms, it means that the real part of the indicated angle in each angular coordinate becomes zero when the antenna aperture plane² is aligned with the arriving phase front. This is true in the case of a plane wave, as from a distant point target. However, unresolved targets distort the arriving phase front, making it nonplanar, and also cause amplitude variations over the phase front. It is not possible to align the aperture plane with a nonplanar phase front. The sum and difference signals result from integration of the phasor contributions (amplitude and phase) of the arriving wave to each element of area of the aperture, weighted by the aperture illumination functions of the sum and difference patterns respectively. A tracking radar therefore tends to align its axis with the normal to the “weighted-average” phase front, and this is generally not the same as the normal to the actual phase front at the center of the aperture. Two monopulse tracking radars, one amplitude comparison and the other phase comparison, will align their axes with the normals to their respective weighted-average phase fronts, but the two directions may differ somewhat because of the difference in the aperture illumination functions.

When the axis points in the direction that nulls the real part of the indicated angle, there remains in general an imaginary part.

When the axis points in other than the null direction, both the real and imaginary parts of the indicated angle depend in a rather complicated way on the amplitude and phase distribution of the arriving wave across the aperture [2, 7]. However, two special cases of arriving wave are easy to analyze [7] if it is assumed that the sum and difference illumination functions have constant phase over the aperture:

² In an electronically steerable array, the aperture plane in this context is interpreted as the “steered plane” rather than the plane of the physical array.

1. *Uniform amplitude, linear phase taper (tilted plane wave)*: The indicated angle is pure real and equal to the angle of the normal to the phase front.
2. *Constant phase (plane phase front normal to beam axis)*: linear amplitude taper: The indicated angle is imaginary and proportional to the amplitude taper normalized to the amplitude at the center.

In these two special cases, the real part of the indicated angle is due to phase taper and the imaginary part is due to amplitude taper. In general, however, the two effects are not separable; the real and imaginary parts depend on both the phase and amplitude distributions of the arriving wave, and these are functions of the off-axis angles, amplitudes, and phases of the unresolved targets.

Although an exact processor ideally responds only to the real part, phase imbalance between the radar sum and difference channels causes some of the imaginary part to couple into the real part and thus affect the monopulse output. Imbalance occurs to some degree not only in receivers but also in antenna patterns. In a reflector-type amplitude-comparison antenna, for example, the sum and difference patterns have slightly different phase centers [8] and their illumination functions do not have exactly constant phase over the aperture; although the effect is negligible for targets near the axis, it may cause significant distortion of the relative phase when one or the both targets are near or beyond the edge of the beam.

The imaginary part is also of interest because some types of monopulse processors, as explained in Chapter 8, do not respond purely to the real part of d/s but to a nonlinear combination of real and imaginary parts. Both parts should be taken into account when analyzing performance on unresolved targets.

9.7 MEASUREMENT OF THE IMAGINARY PART (QUADRATURE-PHASE) COMPONENT

Since an exact processor, as defined in Section 8.4, responds to the component of the difference signal that is in phase with the sum signal and measures the real part of the indicated angle, the imaginary part can be measured by another exact processor. For example, if the real part is obtained from a dot-product detector as described in Section 8.8, the imaginary part can be obtained from another dot-product detector in parallel with the first, with the same inputs except that one of them (sum or difference) is phase-shifted 90° . To measure the real and imaginary parts in both angular coordinates, four such processors would be needed. If the processor is of a type that uses a computer to obtain $\text{Re}(d/s)$ from measurements of amplitude and phase of the sum and difference signals (see Section 8.5 or 8.7), the imaginary part is obtained without additional hardware by replacing cosines by sines in the computations. If the processor computes the real part from I and Q measurements by (8.9), it can also compute the imaginary part by (3.20).

Although an exact processor is an idealization, some of the practical processors described in Chapter 8 approach the performance of an exact processor, limited only by finite dynamic range and by errors due to equipment imperfections, quantization, and calibration.

The theoretical circular plots shown in Figure 9.2 have been verified experimentally. In one experiment a monopulse radar was modified with an extra dot-product detector to measure the traverse quadrature output in addition to the in-phase output. The outputs of the two processors were connected to the inputs of an X - Y plotter. Two beacon horn antennas were attached to the top of a boresight tower, at the same elevation but separated in traverse by a fraction of the radar beamwidth. The horns were pointed toward the radar and pulsed by a signal generator, with pulse synchronization obtained from the radar. A variable phase shifter and variable attenuator were inserted in the line to one of the beacon antennas. The radar was allowed to lock onto the beacon pulses in range but the antenna was fixed, with the servos disabled, to inhibit tracking in angle. By varying the phase while holding the attenuation constant and vice versa, circles like those in Figure 9.2 were obtained.

Some processors are not designed to work as exact processors even if the equipment and calibration were perfect. Under limited conditions, however, they may produce the same output as an exact processor, or a close approximation to it. For example, the approximate dot-product detector described in Section 8.9 has an output that is equal to the real part when the imaginary part is 0 and the real part is between -1 and 1 . Otherwise the output is a nonlinear function of both the real and imaginary parts of the indicated angle, in accordance with (8.19). A second identical device connected to the same inputs (s and d), with one of the inputs phase-shifted 90° , would produce a corresponding output with the real and imaginary parts interchanged, as shown in (8.22). By inverting the pair of simultaneous equations, the real and imaginary parts can theoretically be computed from the outputs of the two processors. However, because of the saturation effect illustrated in Figures 8.7 and 8.8, the solutions may become indeterminate or inaccurate when the real or imaginary part is large.

Similar comments apply to noncoherent processors using the sum and difference of $|v_1|$ and $|v_2|$ (see Section 8.10) or $|s + d|$ and $|s - d|$ (see Section 8.11). In those cases solutions can be ambiguous because of the reversal of the curves plotted in Figures 8.10 and 8.11.

The preceding two paragraphs do not imply any deficiency in such "inexact" processors. They have advantages of simplicity and moderate cost. They have been used extensively in some monopulse radars and have given excellent performance in the application for which they are designed, namely closed-loop tracking of single targets close to the axis. However, they are not the preferred choice in applications requiring accurate off-axis measurements over the entire beam or measurements of the imaginary as well as the real parts when the indicated angle is complex.

9.8 EFFECT OF LOCAL-OSCILLATOR FREQUENCY

In radar receivers the signals from the antenna at radio frequency (RF) are usually converted to an intermediate frequency (IF) by mixing with the voltage from a local oscillator (LO). The LO is offset in frequency from the RF so that the difference frequency equals the desired IF. The LO frequency can be either above or below the RF.

If the LO frequency is below the RF, the sum and difference signals have the same relative phase at IF as at RF. If the LO frequency is above the RF, a relative phase ϕ at RF changes to $-\phi$ at IF. This change has no effect on the real part, but it changes the sign of the imaginary part; thus Figure 9.3 is unchanged but in Figure 9.2 the phases of the broken circular arcs above and below the real axis are interchanged. The effect on multipath response curves is discussed in Section 11.12.

9.9 DETECTION OF PRESENCE OF UNRESOLVED TARGETS

Since a single target produces little or no imaginary part of the indicated angle, the presence of an imaginary part exceeding a threshold can theoretically be used as an indication that more than one target is present [2]. The threshold must be set so that the probability of false alarms from noise, clutter, and other interference does not exceed some specified value. The information from a threshold crossing may be used for target analysis or counting, or to discard a “contaminated” measurement that may do more harm than a missing measurement.

An analysis of this technique [9] has shown that at moderate signal-to-interference ratios the single-pulse discrimination between a single target and multiple targets is poor, but that the reliability of discrimination can be raised to a useful level by integrating the imaginary part (quadrature component) from several independent pulses. It was also found that the probability of correct discrimination was higher for steady targets than for fluctuating targets. As an example, with two independent Swerling Case 2 targets of equal average cross section,³ separated by one-quarter beamwidth and producing a combined average signal-to-interference ratio of 24 dB, the analysis showed that integration of five pulses gave a detection probability of 0.9 (probability of recognizing the presence of more than one target) with a threshold such that the false-alarm probability was 0.17 (probability of declaring the presence of more than one target when there was actually only one). With steady targets under the same conditions the corresponding probabilities were 0.95 and 0.01.

Another approach, intended for use in multiple-beam antennas, has been described in [10]. Recognizing that the interference from unresolved targets or mul-

³ A Swerling Case 2 target has a negative exponential distribution of radar cross section (Rayleigh distribution in amplitude), fluctuating independently from pulse to pulse.

tipath creates an imaginary part of what otherwise would be a real ratio, it uses a generalized likelihood-ratio test to detect the presence of such interference in order to reject contaminated angle measurements.

9.10 MEAN AND VARIANCE OF INDICATED ANGLE

Sometimes it is of interest to know the mean of the indicated angle if it is averaged over many measurements while the relative phase ϕ varies linearly as a function of time or randomly with uniform distribution. Linear variation of phase with time may be the result of a constant range-rate differential between the two targets or RF stepping from pulse to pulse, assuming that the reflection phase characteristics of the individual targets remain constant. Random variation of relative phase can occur because of random changes in the orientations or the range differential of the targets, or because of pseudo-random pulse-to-pulse frequency agility of the radar.

Assume at first that the amplitude ratio and off-axis angles of the two targets remain constant during the averaging time. For the real part, the average of the fraction $(1 - p^2)/(1 + 2p\cos\phi + p^2)$ in (9.9b), obtained by integrating⁴ it from $\phi = 0$ to $\phi = 2\pi$ and dividing by 2π , is 1 if $p < 1$ and -1 if $p > 1$. Substituting these values in (8.8b), we obtain the result that the mean of the indicated angle is θ_a if $p < 1$ or θ_b if $p > 1$; in other words, the mean equals the angle of the stronger target [11]. If $p = 1$ the mean is the midpoint, but this is an academic case because the probability of exact equality is zero.

The mean of the imaginary part is zero, as can be seen by inspection of (9.10) or Figure 9.2.

Although calculation of the mean by taking the definite integral of the real part is straightforward under the assumed conditions, it becomes awkward or impractical when the amplitude ratio p is not constant or when there are more than two targets (this case will be examined later). A more powerful method, better suited for those cases, is complex integration. We will apply it first to the simple case already treated, with constant amplitude ratio, to illustrate its use and show that it yields the expected result.

For this purpose it is convenient to start with the complex equation (8.8c). The mean is:

$$\overline{\theta}_i = \theta_a + \frac{\Delta\theta}{2\pi} \int_0^{2\pi} \frac{pe^{j\phi}}{1 + pe^{j\phi}} d\phi \quad (9.15)$$

Define a complex variable w as in (9.12) and take its differential:

⁴ This definite integral can be found in various published tables.

$$w = pe^{j\phi} \quad (9.16)$$

$$dw = jpe^{j\phi} d\phi \quad (9.17)$$

Then

$$\overline{\theta}_i = \theta_a + \frac{\Delta\theta}{2\pi} \int_C \frac{1}{j} \frac{dw}{1+w} \quad (9.18)$$

The letter C represents the contour of integration in the complex plane. In the case of constant amplitude ratio, the contour is a counterclockwise circle of radius p centered at the origin.

If $p < 1$, the contour of integration does not enclose or intersect with the point $w = -1$. Therefore the integrand has no singularities within or on the contour, and according to the Cauchy-Goursat theorem [12], the integral is zero. This means that both the real and imaginary parts are zero. Hence, if $p < 1$, the mean is equal to θ_a , the angle of the stronger target.

If $p > 1$, the contour is a circle that encloses the singular point $w = -1$. According to the Cauchy integral formula [12], if w_o is any point in the complex plane, the integral of $f(w)/(w - w_o)$ around a contour that encloses w_o is $j2\pi f(w_o)$. In our case $w_o = -1$, $f(w) = 1/j$, and $f(w_o) = 1/j$. Therefore (9.18) reduces to

$$\overline{\theta}_i = \theta_a + \frac{\Delta\theta}{2\pi} j2\pi \frac{1}{j} = \theta_a + \Delta\theta = \theta_b \quad (9.19)$$

Here again the result agrees with that obtained by real integration.

The advantage of complex integration, however, is that the contour need not be restricted to a circle but may be any closed path. Thus, the amplitude ratio p may vary. As long as the contour does not enclose the point $w = -1$ (a condition that allows $p > 1$ except when $\phi = 180^\circ$), the mean indicated angle is θ_a . Similarly, if $p > 1$ when $\phi = 180^\circ$, the mean indicated angle is θ_b . If the amplitude ratio and the relative phase vary in such a way that the contour must make n circuits around the origin in order to close, the contributions of the individual circuits to the Cauchy integral (± 1) are summed and the sum divided by n .

If both the amplitude ratio and the relative phase vary randomly and independently, we assume that the contour closes if the averaging time is long enough. If two such targets have constant angles relative to the beam axis and if their amplitudes vary in such a way that one remains stronger than the other, then the mean indicated angle over all relative phases is the angle of the stronger target. If one target is not always the stronger, then the mean indicated angle is the weighted mean of the individual angles of the two targets, the weighting being the fraction of the time each target is stronger than the other. If the targets conform to

the standard analytical models of fluctuating targets such as the Swerling models and if their average signal strengths are specified, those fractions can readily be calculated. It has been shown, for example, that for two independent targets with Rayleigh distributions of amplitude (negative exponential distributions of power) and uniform distributions of phase, the average indicated angle is the “power centroid”—that is, the average of the two target angles weighted by their respective powers [13]. This type of amplitude distribution characterizes (by definition) Swerling Case 1 and Case 2 targets and is a reasonable model for noise jammers. Hence, the result applies to two such targets, two jammers, or one of each in the same resolution cell.

The single-target monopulse output is not exactly proportional to angle, as has been assumed. Nevertheless the results derived above are still correct provided the averaging is done on the measurements of normalized monopulse output before conversion to angle rather than converting each measurement to angle and then averaging. The results still depend, however, on the assumption of an exact processor, one that measures $\text{Re}(d/s)$. Furthermore, the results apply only to open-loop measurements or to closed-loop tracking with a long time constant, since it is assumed that the beam axis remains fixed relative to the angular positions of the targets during the averaging time.

The variance of the indicated angle (the mean-squared deviation of the indicated angle from its mean) has been analyzed [14]. For a constant amplitude ratio the real and imaginary parts have the same variance:

$$\text{Var}[\text{Re}(\theta_i)] = \text{Var}[\text{Im}(\theta_i)] = \frac{p^2 (\Delta\theta)^2}{2(1-p^2)} \quad (9.20)$$

In this equation p is interpreted as the amplitude ratio of the weaker target to the stronger, so $p < 1$. If one target is much weaker than the other ($p \ll 1$), the variance is approximately $p^2(\Delta\theta)^2/2$. If $p = 1$, the variance according to (9.20) is infinite, but this result is academic because the limited dynamic range of the radar circuits keeps the variance finite, and in any case the probability of maintaining exactly equal amplitudes during the observation time is zero.

For variable p , as in the case of fluctuating targets, the result of (9.20) must be averaged over p^2 , the power ratio, in accordance with the appropriate probability density. If neither target is always the stronger, the variance must be referenced to the mean indicated angle, calculated as above. The variance is computed for each target when it is the stronger of the two, multiplied by the fraction of the time when it is the stronger, and the two partial results are added.

In practice, the result of averaging will generally not be exactly equal to the mean as derived above, even if the assumptions of constant target angles and linearly or randomly varying relative phase are valid and even if noise and other er-

rors are ignored. One reason is that the measurements are sampled (on individual pulses or dwells) rather than continuous; the analytical results are changed if the integral in (9.15) is replaced by a summation. Another is that the theoretical results are based on averaging over an integer number of cycles in the case of linearly varying relative phase or over an infinite time in the case of either linearly or randomly varying phase. Neither of these conditions is fulfilled in practice.

9.11 WEIGHTED MEAN OF INDICATED ANGLE

The mean derived in the preceding section was unweighted; that is, all measurements of the indicated angle were given equal weight. In this section we consider the effect of weighting each measurement by the ratio of the sum-signal power during that measurement to the total of the sum-signal powers during all the measurements.

Consider the real part of the indicated angle, as given by (9.9a). The denominator is the sum-signal power normalized to the power of the first target alone. This could be converted to absolute power by multiplying it by the power of the first target. The numerator would then have to be multiplied by the same number, leaving the value unchanged. Therefore we can assign a value of unity to the power of the first target.

For purposes of analysis we assume that the measurements are continuous rather than sampled and that the target angles relative to the axis are constant during the averaging time. Initially, we assume also that the amplitude ratio p is constant. The weighted mean of the real part over the relative phase ϕ , from (8.9a), is

$$\overline{\text{Re}(\theta_i)_{wp}} = \frac{\int_0^{2\pi} [\theta_a + p \cos \phi (\theta_a + \theta_b) + p^2 \theta_b] d\phi}{\int_0^{2\pi} [1 + 2p \cos \phi + p^2] d\phi} \quad (9.21)$$

The subscript wp signifies that the weighting is in proportion to power (of the sum signal) on each measurement.

Since the integral of $\cos \phi$ over a cycle is zero, the result is

$$\overline{\text{Re}(\theta_i)_{wp}} = \frac{\theta_a + p^2 \theta_b}{1 + p^2} \quad (9.22)$$

This is the “power centroid” of the two targets. The result applies to all values of p , whether < 1 or > 1 . The factor p^2 is the ratio of radar cross sections of the targets multiplied by the ratio of antenna power gains in the two directions (one-way

or two-way gain, depending on the mode of operation of the radar). If there is any Doppler discrimination, this may also affect the value of p^2 . The range-dependent effect is usually negligible, since the ranges of two unresolved targets are normally nearly equal.

The mean of the imaginary part, whether weighted or unweighted, is zero. This can be seen by noting that the integral of $\sin\phi$ in (9.10) is zero when taken over a cycle.

If p^2 varies because of target cross-section fluctuations, independently of the variation of ϕ , the power centroid derived in (9.22) can be averaged over p^2 with the appropriate probability density function.

The power-weighted average on n pulses can be written as:

$$\overline{\text{Re}(\theta_i)_{wp}} = \frac{\sum_{k=1}^n \frac{|d_k|}{|s_k|} |s_k|^2 \cos \delta_k}{\sum_{k=1}^n |s_k|^2} \quad (9.23)$$

A brute-force method of computation would be to form the monopulse output $|d_k/s_k| \cos \delta_k$ on each pulse, multiply it by $|s_k|^2$, sum the products for the n pulses, and divide by the summation of sum-signal powers for the n pulses. However, the computation can be reduced by simplifying the numerator:

$$\overline{\text{Re}(\theta_i)_{wp}} = \frac{\sum_{k=1}^n |d_k| |s_k| \cos \delta_k}{\sum_{k=1}^n |s_k|^2} \quad (9.24)$$

For example, consider the I and Q processor described in Section 8.6, which computes each single-pulse output by (8.9). To compute the power-weighted average, the division of the numerator by the denominator on each pulse is omitted. Instead, the numerators are computed for each pulse and summed over the n pulses and the same is done for the denominators. Then the quotient of the two summations is computed.

The comments in the preceding section pointing out why an average obtained in a practical situation can be expected to differ from the theoretical apply also to weighted averaging.

9.12 POSSIBILITY OF DETERMINING ANGLES OF UNRESOLVED TARGETS

The question arises whether measurement of both the real and imaginary parts of the indicated angle would provide enough information to solve for the individual angles of two unresolved targets. Having measured $\text{Re}(\theta_i)$ and $\text{Im}(\theta_i)$, we wish to use (9.10) and one of the forms of (9.9) to solve for θ_a and θ_b (the angles of the first and second targets respectively), keeping in mind that θ_{mid} and $\Delta\theta$ are related to θ_a and θ_b by the definitions under (9.8b). For each angular coordinate we have two equations but four unknowns: θ_a , θ_b , p (the amplitude ratio of the two targets), and ϕ (their relative phase). Therefore a solution based on a single pulse (or single measurement derived from a train of pulses) is impossible if the measurement is made in only one angular coordinate.⁵

If we make simultaneous measurements in both angular coordinates, we have four equations but six unknowns: θ_a and θ_b , in traverse and in elevation, a common value of p , and a common value of ϕ . Again a solution is impossible.

The fact that the primary interest is in the target angles rather than their amplitude ratio or relative phase does not help, since the solutions are not separable.

In addition to the sum and two difference signals, monopulse radars that use a four-horn feed have an unused by-product of the comparator, the diagonal difference (see Section 4.4.3), which is terminated in a dummy load. It might appear that measurement of the in-phase and quadrature components of this signal, normalized to the sum, could provide the additional equations needed for a solution. It will be shown in Section 15.2, however, that this signal is not useful, because it has zero or low sensitivity to target direction in the vicinity of the beam axis and along the traverse and elevation principal planes.

Therefore in the general case of two arbitrary targets and with a conventional configuration of monopulse antenna patterns, a single-pulse solution is impossible. This statement still leaves open the possibility of a single-pulse solution in special cases of specular multipath where there are known relationships between a low-angle target and its image; this case will be discussed in Chapter 11.

The next question to be examined is whether measurements made on two or more successive pulses⁶ would make a solution possible. It will be shown that in theory a solution can be obtained with as few as two pulses. To provide independent equations either the radar parameters or the target parameters must change between pulses in such a way that the additional number of independent measurables exceeds the additional number of unknowns.

⁵ This statement applies to the usual form of monopulse in which two antenna patterns are available in each coordinate—either a sum and difference or a pair of component patterns. It does not necessarily apply to special configurations that provide more than two patterns.

⁶ The word “pulse” is to be interpreted here as either a single pulse or a train of pulses from which a single set of measurements is made.

Various types of changes are possible between pulses—for example, a change in beam pointing direction, frequency, or polarization of the radar, or some change in the targets. The method described here is based on a change in relative phase ϕ during the interval, due to relative motion of the two targets while their other parameters remain constant. This method is presented as an illustration of the potentially useful information in the imaginary part of the indicated angle, but because of errors and limitations, which will be discussed, the possibility of its practical application is limited to certain restricted conditions.

To illustrate the changes produced by relative target motion, suppose that the radar has a wavelength of 10 cm and that during the interval between pulses, say 0.01s, the range difference of the two targets changes by 1 cm. Then the change in ϕ is 72° , while θ_a and θ_b in each angular coordinate can usually be considered constant over such a short interval. This is true even if the target directions are changing rapidly (but not relative to each other), provided the antenna beam is moving with them, since angles are measured with respect to the beam axis. For steady or slowly fluctuating targets, the target amplitude ratio p may also be considered constant.

If the relative phase is changing at a steady rate, there is a Doppler difference, which amounts to 1 m/s in this particular case. It might be argued that there is already a known solution for this type of problem, namely resolution of the two targets by Doppler filtering. However, the average rate of change of relative phase may be too small to permit Doppler resolution of the targets by a particular radar, or the radar may not be equipped to do Doppler resolution. Furthermore, the pulse-to-pulse change may be random or transient rather than steady, so that Doppler resolution is impossible. For example, two aircraft attempting to maintain a constant separation may have zero relative Doppler shift on the average, but random perturbations in their positions will produce pulse-to-pulse changes in relative phase. The method to be described applies to random as well as uniform phase changes.

There are five unknown quantities (for one angular coordinate) that must be calculated from the data obtained on the two pulses: the two target angles θ_a and θ_b , the relative phases ϕ_1 and ϕ_2 , and the target amplitude ratio p . To determine these unknowns, there are five measured quantities available from the two pulses: x_1 , y_1 , and x_2 , y_2 , the real and imaginary parts of the indicated angles measured on the first and second pulses respectively, and the ratio r_p of received powers of the two pulses. The solution is obtained through the following procedure.

Let x_c represent the x -coordinate of the center of the circle and ρ the radius. Then the circle satisfies two equations:

$$\begin{aligned}(x_1 - x_c)^2 + y_1^2 &= \rho^2 \\ (x_2 - x_c)^2 + y_2^2 &= \rho^2\end{aligned}\tag{9.25}$$

Solving for the circle parameters x_c and ρ we obtain

$$x_c = \frac{x_2^2 - x_1^2 + y_2^2 - y_1^2}{2(x_2 - x_1)} \quad (9.26)$$

$$\rho = \sqrt{(x_1 - x_c)^2 + y_1^2} \quad (9.27)$$

Then, we express from (9.8a) the points x_0 and x_{180} where the circle intersects the real axis ($\phi = 0^\circ$ and 180°) in terms of the target angles and amplitude ratio:

$$\begin{aligned} x_0 &= \frac{\theta_a + p\theta_b}{1 + p} \\ x_{180} &= \frac{\theta_a - p\theta_b}{1 - p} \end{aligned} \quad (9.28)$$

From (9.28) another pair of equations relates x_c and ρ to the target angles and amplitude ratio

$$\begin{aligned} x_c &= \frac{\theta_a - p^2\theta_b}{1 - p^2} \\ \rho &= \frac{p(\theta_a - \theta_b)}{1 - p^2} \end{aligned} \quad (9.29)$$

These expressions permit us to express the target angles in terms of the circle parameters and the unknown amplitude ratio p :

$$\theta_a(p) = x_c - p\rho \quad (9.30)$$

$$\theta_b(p) = x_c - \frac{\rho}{p} \quad (9.31)$$

Using (9.9a), the two phase angles can now be expressed in terms of the circle parameters and the unknown amplitude ratio p :

$$\cos[\phi_{1,2}(p)] = \frac{\theta_a(p) - x_{1,2} + [\theta_b(p) - x_{1,2}]p^2}{[2x_{1,2} - \theta_a(p)x_{1,2} - \theta_b(p)x_{1,2}]} \quad (9.32)$$

The power ratio r is a function of p and the phase angles:

$$r = \frac{|s_2|^2}{|s_1|^2} = \frac{1 + 2p \cos \phi_2 + p^2}{1 + 2p \cos \phi_1 + p^2} \quad (9.33)$$

Thus, all five unknowns can be expressed in terms of four measured quantities and the unknown p . The final step uses the root-finding process available in common mathematical programs (e.g., Mathcad) to solve for p , from which the other unknowns can be calculated:

$$p = \text{root}_p (R_p - r_p) \quad (9.34)$$

where R_p is the measured power ratio, r_p is the value obtained from (9.33), and the notation $\text{root}_p(\cdot)$ denotes the value of p for which $(\cdot) = 0$.

For a numerical example, suppose the measured real and imaginary parts on the two pulses are

$$x_1 + jy_1 = 0.09 + j0.13$$

$$x_2 + jy_2 = 0.34 + j0.22$$

and suppose the sum-signal power ratio on the two pulses is

$$R_p = |s_2|^2 / |s_1|^2 = 0.35$$

The circle parameters are found from (9.26) and (9.27) as:

$$x_c = 0.278, \quad p = 0.229$$

The root-finder, using (9.34), gives

$$p = 0.415$$

From this, the target off-axis angles are given by (9.30) and (9.31) as

$$\theta_a = 0.183, \quad \theta_b = -0.272$$

and the signal phase angles are

$$\phi_1 = 1.305 = 74.1^\circ, \quad \phi_2 = 2.542 = 145.3^\circ, \quad \phi_2 - \phi_1 = 1.241 = 71.1^\circ$$

The units of θ_a and θ_b are the same as those of x_1 , y_1 , and x_2 , y_2 . For example, these quantities may be in degrees or beamwidths, or they may be left in the form of monopulse voltage ratios without conversion to angles.

There is another value of p that satisfies (9.33), namely the reciprocal of the value shown in (9.34). However, when the reciprocal value is substituted in (9.30) and (9.31), it merely interchanges θ_a and θ_b . Therefore the solution is unique, at least in this example.

Examination of the sensitivity of this procedure to small errors in measurement of the indicated angles shows that a change in any one real or imaginary part by 0.01 causes the target off-axis angles to change by ≈ 0.02 , for the situation represented by the example values, with 71° phase shift between the two pulses. Random noise with rms level 0.01 in all five measurements would presumably cause rms errors of ≈ 0.04 in the target angles. This indicates that the two-target measurement, even with near-optimum phase change between the two pulses, requires about 12 dB more signal-to-noise ratio to preserve the accuracy available with only one target. Such an increase is consistent with theory of resolution improvement [15], which showed that a 2:1 improvement in resolution is available at the expense of about 10 dB in signal-to-noise ratio, but that further increase requires much stronger signals.

Two points that are closely spaced in the x -coordinate will give a less accurate solution than points that are widely spaced. When the two points have the same x -coordinate, however, there are several sources of error:

1. Thermal noise will generally cause more error for angle estimation of two unresolved targets than for one target.
2. The assumption that the two targets maintain not only the same amplitude ratio but also the same absolute amplitude on the two pulses, as required by (9.33), is not generally realistic; pulse-to-pulse amplitude fluctuations may cause serious errors. However, the assumption is valid if the interpulse interval is short.
3. Phase and amplitude imbalance in the sum and difference channels, as well as imperfect normalization and processing, will cause errors in measurement of x_1 , y_1 , and x_2 , y_2 . There will also be errors in measurement of the sum-signal power ratio $|s_1|^2/|s_2|^2$. In order to derive useful results it would be necessary to design and maintain the equipment to tighter tolerances than are normally required.
4. A real-life target is generally not a point target but has multiple scattering points whose relative phases vary with motion of the target. This variation causes not only amplitude fluctuation but also angular wander of the apparent location (known as glint) of each target, contrary to the assumption that the target angles are constant during each interpulse period. Unless the angular extent of each tar-

get is small compared with the angular separation of the two targets or the glint is only slowly varying, there may be appreciable error.

5. The solution is based on the assumption that no more than two targets are present. If there is only one, the correct results are still obtained, because then (disregarding noise) $x_1 = x_2$, $y_1 = y_2$, and $|s_1|^2/|s_2|^2 = 1$, which gives the correct angle for the first target and zero amplitude for the second. If, however, more than two targets are present, the results will be erroneous.

The method described does not depend, however, on the assumption that the monopulse output is linear with angle. The values of x_1 , y_1 , and x_2 , y_2 used in the solution should be the monopulse ratios in "raw" form, before conversion to angle. The solution will be the monopulse ratios of the individual targets. Conversion to angles of those targets, using the actual calibration function, is the final step.

Results could be improved to some extent by using several pulses rather than two, but not if pulse-to-pulse amplitude fluctuations of the targets are the limiting source of error. Some advantage might also be gained from the fact that simultaneous measurements in both angular coordinates would provide more measurables than unknowns and thus overdetermine the solution. The second coordinate has two additional unknowns, the angles θ_a and θ_b of the two targets in that coordinate, but it gives four additional measurables, x_1 , y_1 , and x_2 , y_2 .

Theoretically, therefore, the use of both the real and imaginary parts of the indicated angle on two or more pulses offers the possibility of determining the individual angles of two arbitrary targets that are unresolved in the usual sense. From a practical standpoint, however, any potential applications appear to be limited to steady or slowly fluctuating targets (not more than two), high signal-to-noise ratios, and very accurate equipment.

9.13 INFORMATION DERIVABLE FROM REAL PART

It has been shown [11] that partial information about two unresolved targets is theoretically derivable from monopulse measurements on two pulses, under the same conditions as in the preceding section, but without requiring the imaginary part of the monopulse ratio. The measurements consist of the real part on each pulse and the ratio of the powers of the two pulses. The information that can be deduced from the two pulses consists of the angular midpoint of the two targets in each coordinate and the slope of the line joining them.

As in the preceding sections, for each angular coordinate we denote the real parts by x_1 and x_2 , the ratio of the sum-signal powers by $|s_2|^2/|s_1|^2$, the angular midpoint by θ_{mid} , and their angular separations by $\Delta\theta$. From (9.9b),

$$x_1 = \theta_{\text{mid}} - \frac{\Delta\theta}{2} \frac{1-p^2}{|s_1|^2} \quad (9.35)$$

$$x_2 = \theta_{\text{mid}} - \frac{\Delta\theta}{2} \frac{1-p^2}{|s_2|^2} \quad (9.36)$$

The solution for θ_{mid} is

$$\theta_{\text{mid}} = \frac{x_2 |s_2|^2 / |s_1|^2 - x_1}{|s_2|^2 / |s_1|^2 - 1} \quad (9.37)$$

This equation gives the angular midpoint in each coordinate when the measured values of x_1 , x_2 , and $|s_2|^2/|s_1|^2$ are inserted.

Furthermore, subtraction of (9.35) from (9.36) gives

$$x_2 - x_1 = \frac{\Delta\theta}{2} (1-p^2) \left(\frac{1}{|s_1|^2} - \frac{1}{|s_2|^2} \right) \quad (9.38)$$

This equation applies separately to traverse and elevation. On the right-hand side the values of p , s_1 , and s_2 are the same in both coordinates but the values of $\Delta\theta$ are different. Designating the two coordinates by subscripts tr and el , we obtain

$$\frac{\Delta\theta_{el}}{\Delta\theta_{tr}} = \frac{(x_2)_{el} - (x_1)_{el}}{(x_2)_{tr} - (x_1)_{tr}} \quad (9.39)$$

which is the slope of the line joining the two targets.

This method is subject to the same kinds of errors as the two-pulse solution for the individual target angles (described in the preceding section), but probably to a lesser extent, since fewer unknowns and fewer measurements are involved.

Going a step further, it was shown in Section 9.10 that the result of averaging the real part of the indicated angle over many pulses is to indicate the angle of the stronger target, provided that during the averaging time, (1) the angles of the two targets relative to the radar axis are constant, (2) the relative phase of the two targets is uniformly distributed from 0 to 2π , and (3) the target amplitudes remain constant or vary in such a way that one target is always stronger than the other.

The angle of the stronger target in combination with the midpoint angle also determines the angle of the weaker target. However, the conditions imposed on the targets and the errors discussed in Section 9.10 restrict the practical usefulness of this method.

9.14 REMOVAL OF INITIAL ASSUMPTIONS

At the beginning of this chapter four assumptions were made in order to simplify the analysis. The effects of removing these assumptions will now be examined and it will be shown that the analysis is still basically valid but may require some refinements.

The first assumption was that the sum and difference voltages from a single point target have 0° (or 180°) relative phase. In practice there may be a small phase difference, due to inherent characteristics of the antenna or to imperfections in components or alignment. A 90° relative phase occurring in some radar designs, as explained in Chapter 5, is of no concern. Since it is predictable, it can be removed by a phase shifter, or the equivalent transformation can be accomplished in the processing. Our concern is with smaller, residual phase deviations. The complex-plane loci of constant amplitude ratio and constant relative phase of the two targets are still circles, as in Figure 9.2, but the points representing the two targets are displaced from the real axis and the centers of the circles deviate to some extent from the real and imaginary axes respectively. If the difference-to-sum relative phase characteristics of the radar are known (the phase will generally vary as a function of off-axis angle), they can be taken into account in the analysis with a little more labor. Or for the purposes of error analysis, the effect of a specified phase deviation can be calculated.

The second assumption was that the monopulse processor is an exact processor measuring the real part of d/s , and that if the imaginary part is also desired, it is obtained from an additional, identical processor with one of the inputs shifted by 90° . As explained in Chapter 8, many processors are not of the "exact" type. They may perform in a nearly equivalent manner when tracking a single target close to the axis but may differ greatly in their response to unresolved targets or even to single targets near or beyond the edge of the beam. In some cases their outputs can be converted by computation to the equivalent of the outputs of exact processors. For example, a pair of approximate dot-product processors (see Section 8.9), with one input to one of them shifted by 90° , can produce a pair of outputs from which $\text{Re}(d/s)$ and $\text{Im}(d/s)$ can be calculated. However, when such processors operate in their saturation region, the lost information cannot be recovered. The two-target response of any type of processor can be analyzed by using equations such as those derived in Chapter 8, but generally the analysis is more complicated and the results cannot be expressed in a simple, normalized, parametric form as they can for an exact processor. For this reason many published analyses have been based on the implicit assumption of an exact processor; while they are useful, they should be used with this limitation in mind.

The third assumption was that the normalized difference signal from a single target is proportional to its angle off axis, so that conversion from normalized difference signal to angle or vice versa requires only multiplication or division by a

constant factor. This assumption simplifies physical interpretation, but is not necessary. It can easily be removed in the following way. Wherever the symbols θ_a and θ_b occur in equations, they are to be interpreted not as the off-axis angles of the first and second target respectively, but as their respective normalized difference signals. Thus, if the angles are given, they should be converted to normalized difference signals by means of the known calibration function for the particular radar, and then entered in the equation. Conversely, if θ_a and θ_b are unknowns for which solutions are being sought, the solutions are to be interpreted as normalized difference signals, which are then converted to angles. The same rules apply to the indicated angle θ_i , and to any other symbols in the equations that represent angles. When the target angles and the indicated angles are small, the assumption of proportionality is usually safe. It should be kept in mind, however, that the indicated angle can be larger than either of the target angles. If the purpose of analysis is error budgeting, a best-fit linear approximation to the calibration function usually suffices.

The fourth assumption was that the response in each angular coordinate is independent of the target location in the other coordinate. In practice the cross-coupling is not always negligible in the actual operation of the radar, but it can generally be ignored in analyzing errors due to unresolved targets (as distinguished from analyzing single-target errors due directly to the coupling). If necessary, two-coordinate calibration can be used.

9.15 EXTENSIONS OF MONOPULSE TECHNIQUES AND FUNDAMENTAL LIMITATIONS

Various techniques other than conventional monopulse have been investigated for the purpose of determining the individual angles of targets that are unresolved in the usual sense [16–20]. These techniques differ from conventional monopulse in that they require more than two simultaneous antenna receiving patterns in each angular coordinate. They can be regarded as extended forms of monopulse, since they make use of complex ratios of simultaneously received patterns. The patterns may be obtained from multiple feed horns or feed connections in a reflector antenna, or from individual elements or groups of elements (subarrays) in an array. The use of simultaneous signals from individual elements or subarrays is known generally as *aperture sampling*.

With the additional information available from more than two patterns it is theoretically possible to obtain a solution from a single pulse, thus avoiding the error due to target amplitude fluctuation in the two-pulse method described in Section 9.12. However, the other sources of error still apply. The lower bound of

single-pulse error due to thermal noise⁷ has been analyzed and plotted in parametric form [21]. The results shown that as the angular separation of two targets decreases below a beamwidth (while they are unresolved in range and Doppler), there is a sharp increase in the signal-to-noise ratio required for individual angle estimates of specified accuracy from a single pulse. As a rule of thumb, resolution can be considered lost when the standard deviation of error on either target exceeds the separation between the targets; at typical signal-to-noise ratios this condition occurs when the separation is only a little less than a beamwidth.

In addition to thermal-noise errors, there are of course other errors, such as those due to the equipment.

Another limitation of single-pulse two-target angle estimation is that it is based on the assumption that the number of targets is exactly two. There is an error not only when there are more than two targets but also when there is only one. In the latter case the estimator, programmed to extract the locations of two targets from the measurements (when in fact there is only one), will do so, but both estimated angles may be much farther from the true angle than if the estimator were programmed to interpret the measurements as if they were due to a single target.

The preceding comments apply to single-pulse estimation. Improvement may be obtained by the use of multiple pulses, either by averaging or smoothing the estimates obtained from each pulse or by combining the raw single-pulse measurements in some way before forming an estimate.

The lower bound of thermal-noise error mentioned above does not apply directly to the two-pulse method of angle estimation described in Section 9.12. The sensitivity of that method to noise was analyzed only approximately, but was found to require about 12 dB increase in signal-to-noise ratio to preserve the accuracy achievable with a single target.

9.16 CLOSED-LOOP TRACKING

The analysis presented in the earlier sections pertains to the *open-loop* monopulse response to unresolved targets. The direction of the antenna beam axis has been assumed to remain fixed, so that only the open-loop indicated angle (relative to the beam axis) varies as a result of changes in the relative phase, amplitude ratio, and/or angular locations of the targets.

In *closed-loop* tracking the analysis is more complicated. As the antenna beam moves in order to null out the real part of the indicated angle, it changes the relative illumination of the two targets. As a result, the values of g , p , and possibly

⁷ The lower bound is determined by the Cramér-Rao inequality, derived from estimation theory. With a given antenna aperture, no form of processing can have a smaller error or necessarily have an error as small as the lower bound.

ϕ , all defined in (9.7), vary as the beam axis moves, even if the targets remain fixed in absolute position and constant in radar cross section and phase. Hence, the closed-loop tracking angle is generally not the same as the open-loop indicated angle.

To calculate the tracking equilibrium direction of the beam requires an iterative type of solution using knowledge of the antenna patterns and the monopulse processor characteristics. The solution is obtained by searching for the beam axis direction that nulls the real part of the indicated angle. Depending on the angular separation of the targets and their relative amplitude and phase, there may be only one stable equilibrium direction or there may be two, with an unstable equilibrium between them.⁸ At unstable equilibrium the slope of the monopulse response versus angle has the wrong sign, so that a displacement of the beam axis produces an output that drives the beam farther away from that direction rather than back toward it.

If the antenna is mechanically steerable, the problem is further complicated by the fact that the antenna cannot respond instantaneously. In a typical situation where the target positions, amplitudes, and/or phase are changing (the phases are likely to change most rapidly), the dynamic characteristics of the entire servo loop must be taken into account. Because the results depend on so many factors, including the time-dependent target behavior, they cannot be presented in any simple normalized form analogous to the open-loop equations and curves of Sections 9.4 and 9.5.

An analysis of this problem, using the characteristics of one specific radar (including its antenna patterns, monopulse processor, and servo loop) has been published [22]. Results are given for various angular separations, amplitude ratios, and relative phases of two unresolved targets. The same kind of analysis can be adapted to other radars. For most monopulse tracking radars the results are qualitatively similar. Both analysis and experience have demonstrated that under some conditions the antenna can oscillate erratically, sometimes causing loss of track.

9.17 MORE THAN TWO TARGETS

If the number of unresolved targets exceeds two, a deterministic analysis of monopulse response (with position, amplitude, and phase of each target specified) can still be carried out by straightforward extension of the analysis presented in Sections 9.4 and 9.5. However, the mathematics becomes increasingly complicated as the number of targets increases [2, 3]. The usefulness of such an analysis is limited, since the positions, amplitudes, and phases of the targets at any instant

⁸ There may be additional equilibrium directions in the sidelobe region (even when there is only one target) but these are usually not a problem. Because they produce a smaller signal strength, the radar is unlikely to lock on them.

are not likely to be known. Parametric plots of the form of Figures 9.2 and 9.3 could be made, but they would comprise multiple families of curves because of the increased number of parameters.

The inverse problem of solving for the angles of the individual targets, given a set of measurements either from one pulse or from multiple pulses, not only involves laborious mathematics but appears academic in view of the difficulty of obtaining useful accuracy for even two targets. Extension of the method described in Section 9.12 to three targets, for example, would require measurements of the complex indicated angle and of sum-signal amplitude ratios on six pulses, yielding 17 equations in 17 unknowns [2].

A statistical rather than deterministic analysis of the multiple-target problem is usually more tractable and more useful. The statistical behavior of the monopulse response to independent unresolved targets is most conveniently analyzed by assuming the targets to be infinite in number. The results are found to give a close approximation for as few as five or six roughly equal targets, and they indicate at least the qualitative trends for as few as three.

The statistical behavior of the monopulse output for a target complex consisting of an infinite number of independent scatterers of equal cross section, uniformly spaced along a line perpendicular to the radar line of sight and within the radar beam, has been analyzed [2, 23]. The percentage of the time that the indicated angle lies outside the angular span of the target complex was calculated as 13%. A corresponding analysis for an infinite number of independent scatterers of equal strength uniformly spaced over a circular area showed that the direction indicated by the radar would lie outside the circle 20% of the time.

In both of these analytical cases the target model is artificial and the radar performance is idealized. Nevertheless the analytical results are in reasonable agreement with experimental measurements, which have shown that for complex targets such as ships and aircraft the indicated direction can lie outside of the physical extent of the target 10% to 20% of the time [24]. Many measurements of angular wander (angle noise) have been made on a variety of aircraft [25]. Expressed in terms of lateral distance at the range of the target, the standard deviation is found to be proportional to the radius of gyration (in the coordinate of interest) of the distribution of radar cross sections of the reflecting areas of the target. For most aircraft the standard deviation has been found to be between $0.15L$ and $0.25L$ (L being the projected width of the target in the coordinate of interest), depending on the distribution of major scattering areas such as engines, wing tanks, and the like. For a small single-engine aircraft, viewed nose-on, the standard deviation can be as low as $0.1L$; for a large aircraft with outboard engines and possibly wing tanks, or an aircraft viewed from the side, it can be as much as $0.3L$. A somewhat higher standard deviation is obtained in the worst case, in which the target complex consists of a formation of two unresolved aircraft.

The derivation of the average indicated angle given in Section 9.10 for two targets can be extended to any number of targets, distributed in any manner.

Analysis by contour integration in the complex plane shows that if the amplitude of one target is always greater than the sum of the amplitudes of the others, the average is the angle of that target. Another interesting finding [13] is that for any number, arrangement, and strengths of independent targets and/or jammers all having independent Rayleigh-distributed amplitudes and uniformly distributed phases (i.e., Swerling Case 1 or Case 2 targets and/or noise jammers), the average indicated angle is the “power centroid”—that is, the average of the angles of the individual targets or jammers weighted by their respective average powers. That is an extension of the corresponding result for two targets stated in Section 9.10.

9.18 NONINDEPENDENT TARGETS

In the preceding sections the targets were allowed to be arbitrary and independent. However, when the unresolved targets are scattering points on a single rigid body, they are not independent. Their positions, motions, and amplitudes are related. Their relative phases depend on the configuration of the body and on its orientation relative to the radar line of sight, and can change only in accordance with changes in orientation. Furthermore, if the body is free of external forces except gravity (as in the case of a satellite), there are physical constraints on its translational and rotational motion.

A satellite or other long-range target subtends such a small angle at the radar that it is essentially a point target, and monopulse measurements can reveal little or nothing about its configuration. However, if its orientation relative to the radar line of sight changes in a regular manner, so do the relative phases of the scattering points, causing the resultant amplitude and phase of the echo signal to fluctuate. In such cases a great deal of information about the size, shape, and rotation of the body can often be deduced from analysis of the time history of the sum-signal amplitude, with or without phase, over some period of time (usually on the order of seconds or minutes) during which the orientation of the body relative to the line of sight is changing in a regular way [26, 27]. Such methods of analysis are called by various names, including *radar signature analysis*, *target recognition*, and *space object identification*.

The primary value of monopulse in such an application lies in its ability to keep the beam axis pointing very close to the target direction and its freedom from radar-imposed modulation (such as the modulation imposed by conical scan). As a result, the observed modulation is known to be caused entirely by the target and can be analyzed accordingly.

Another situation in which unresolved targets are not independent is that of specular multipath. In that case the reflecting surface produces an image of a physical target, so that the target and image act like a pair of unresolved targets, which are related in amplitude, phase, and location according to the geometry and

electromagnetic characteristics of the reflecting surface. Multipath is discussed in Chapter 11.

References

- [1] J. H. Bruning and Y. T. Lo, "Electromagnetic Scattering by Two Spheres," *Proc. IEEE*, Vol. 56, No. 1, January 1968, pp. 119–120.
- [2] S. M. Sherman, "Complex Indicated Angles in Monopulse Radar," Ph.D. Dissertation: University of Pennsylvania, December 1965. Reprinted in *Radars*, Vol. 4, *Radar Resolution and Multipath Effects*, D. K. Barton, (ed.), Dedham, MA: Artech House, 1975.
- [3] S. M. Sherman, "Complex Indicated Angles Applied to Unresolved Targets and Multipath," *IEEE Trans. on Aerospace and Electronic Systems*, Vol. AES-7, No. 1, January 1971, pp. 160–170.
- [4] D. K. Barton, *Radar System Analysis*, Englewood Cliffs, NJ: Prentice-Hall, 1964. Reprinted: Dedham, MA: Artech House, 1976.
- [5] M. I. Skolnik, *Introduction to Radar Systems*, 2nd ed., New York: McGraw-Hill, 1980.
- [6] D. D. Howard, "Radar Tracking Angular Scintillation in Tracking and Guidance Systems Based on Echo Signal Phase Front Distortion," *Proc. National Electronics Conf.*, Vol. 15, 1959, pp. 840–849. Reprinted in *Radars*, Vol. 4, *Radar Resolution and Multipath Effects*, D. K. Barton, (ed.), Dedham, MA: Artech House, 1975.
- [7] D. D. Howard, J. T. Nessmith, and S. M. Sherman, "Monopulse Tracking Errors Due to Multipath: Causes and Remedies," *IEEE Eascon '71 Conf. Record*, Washington, D.C., October 6–8, 1971, pp. 175–182 (see Appendix).
- [8] J. T. Nessmith, and S. M. Sherman, "Phase Variations in a Monopulse Antenna," *IEEE 1975 International Radar Conf. Record*, Washington, D.C., April 21–23, 1975, pp. 354–359.
- [9] S. J. Asseo, "Detection of Target Multiplicity Using Monopulse Quadrature Angle," *IEEE Trans. on Aerospace and Electronic Systems*, Vol. AES-17, No. 2, March 1981, pp. 271–280.
- [10] R.. J. McAulay and T. P. McGarty, "Maximum-Likelihood Detection of Unresolved Radar Targets and Multipath," *IEEE Trans. on Aerospace and Electronic Systems*, Vol. AES-10, No. 6, November 1974, pp. 821–829.
- [11] R. S. Berkowitz and S. M. Sherman, "Information Derivable from Monopulse Radar Measurements of Two Unresolved Targets," *IEEE Trans. on Aerospace and Electronic Systems*, Vol. AES-7, No. 5, September 1971, pp. 1011–1013. Reprinted in *Radars*, Vol. 4, *Radar Resolution and Multipath Effects*, D. K. Barton, (ed.), Dedham, MA: Artech House, 1975.
- [12] R. V. Churchill, *Complex Variables and Applications*, New York: McGraw-Hill, 1960, pp. 106, 118.
- [13] I. Kanter, "Varieties of Average Monopulse Responses to Multiple Targets," *IEEE Trans. on Aerospace and Electronic Systems*, Vol. AES-17, No. 1, January 1981, pp. 25–28.

- [14] S. J. Asseo, "Effect of Monopulse Signal Thresholding on Tracking Multiple Targets," *IEEE Trans. on Aerospace and Electronic Systems*, Vol. AES-10, No. 4, July 1974, pp. 504–509.
- [15] G. J. Buck and J. J. Gustincic, "Resolution Limitations of a Finite Aperture," *IEEE Trans. on Antennas and Propagation*, Vol. AP-15, No. 3, May 1967, pp. 376–381. Reprinted in *Radars*, Vol. 4, *Radar Resolution and Multipath Effects*, D. K. Barton, (ed.), Dedham, MA: Artech House, 1975.
- [16] G. E. Pollon and G. W. Lank, "Angular Tracking of Two Closely Spaced Radar Targets," *IEEE Trans. on Aerospace and Electronic Systems*, Vol. AES-4, No. 4, July 1968, pp. 541–550. Reprinted in *Radars*, Vol. 4, *Radar Resolution and Multipath Effects*, D. K. Barton, (ed.), Dedham, MA: Artech House, 1975.
- [17] T. P. McGarty, "The Effect of Interfering Signals on the Performance of Angle of Arrival Estimates," *IEEE Trans. on Aerospace and Electronic Systems*, Vol. AES-10, No. 1, January 1974, pp. 70–77.
- [18] F. G. Willwerth and I. Kupiec, "Array Sampling Techniques for Multipath Compensation," *Microwave J.*, June 1976, pp. 37–39.
- [19] T. Thorvaldsen, "Maximum Entropy Spectral Analysis in Antenna Spatial Filtering," *IEEE Trans. on Antennas and Propagation*, Vol. 28, No. 4, July 1980, pp. 556–560.
- [20] B. H. Cantrell, W. B. Gordon, and G. V. Trunk, "Maximum Likelihood Elevation Angle Estimates of Radar Targets Using Subapertures," *IEEE Trans. on Aerospace and Electronic Systems*, Vol. AES-17, No. 3, March 1981, pp. 213–221.
- [21] J. R. Sklar and F. C. Schweppe, "On the Angular Resolution of Multiple Targets," *Proc. IEEE*, Vol. 52, No. 9, September 1964, pp. 1044–1045. Reprinted in *Radars*, Vol. 4, *Radar Resolution and Multipath Effects*, D. K. Barton, (ed.), Dedham, MA: Artech House, 1975.
- [22] M. R. Ducoff, "Closed-Loop Angle Tracking of Unresolved Targets," *1980 IEEE International Radar Conf. Record*, Washington, D.C., April 28–30, 1980, pp. 432–437.
- [23] R. H. Delano, "A Theory of Target Glint or Angular Scintillation in Radar Tracking," *Proc. IRE*, Vol. 41, No. 12, December 1953, pp. 1778–1784.
- [24] D. K. Barton and H. R. Ward, *Handbook of Radar Measurement*, Englewood Cliffs, NJ: Prentice-Hall, 1969. Reprint: Dedham, MA: Artech House, 1984, p. 167.
- [25] J. H. Dunn and D. D. Howard, "Target Noise," Chapter 28 of *Radar Handbook*, M. I. Skolnik, (ed.), New York: McGraw-Hill, 1970, pp. 28-8–28-15.
- [26] D. K. Barton, "Sputnik II as Observed by C-Band Radar," *IRE National Conv. Record*, Part 5, March 23–26, 1959.
- [27] C. Brindley, "Target Recognition," *Space/Aeronautics*, June 1965.

Chapter 10

Monopulse Angle Errors

Monopulse, along with all other angle-measuring systems, is subject to errors from various sources. Certain types of errors are singled out for particular attention in other chapters of this book:

- Errors due to inexact methods of monopulse processing were pointed out and illustrated in portions of Chapter 8.
- Errors due to unresolved targets were treated in Chapter 9.
- Multipath is another special case, in which the target and its reflections from the surface are equivalent to unresolved targets; this usually becomes the dominant error at low target angles. It is treated separately in Chapter 11.
- Intentional interference (ECM) is a significant source of error in military radar systems. This is discussed in Chapter 12, along with methods of reducing the effects (ECCM).

The present chapter analyzes types of error not covered in other chapters, and presents practical formulas, analytical methods, and other useful information.

Errors in radar angle measurement of target coordinates can be classified in several ways:

1. Into bias and random errors, or more completely by their spectra or correlation functions.
2. By their causes, into radar-dependent, target-dependent, and propagation errors.
3. By their point of origin in the system, into tracking errors (deviations from the beam axis or measured off-axis angle), and errors in translating that angle into the coordinate system of the system that uses the data output.

The spectral properties of error are of critical importance if the target position data are to be differentiated into velocity and acceleration components, since a

fixed bias has little effect on the derivatives of the data, while time-varying errors can appear with multiplying factors that depend on the position error spectrum.

The angle error sources commonly encountered in radar are listed in Table 10.1. Those components pertaining specifically to monopulse angle measurement are listed in boldface in the table, and discussed here or in Chapters 11 and 12.

Table 10.1 Sources of Angle Error

<i>Class of Error</i>	<i>Bias Components</i>	<i>Noise Components</i>
Radar-dependent tracking errors	Boresight axis setting and drift Normalization errors Servo unbalance and drift Torque from wind and gravity	Thermal noise Clutter Multipath (Chapter 11) Jamming (Chapter 12) Servo noise Torque from wind gusts Deflection of antenna during acceleration
Target-dependent tracking errors	Dynamic lag	Glint Dynamic lag variation Scintillation or beacon modulation Cross-polarized response
Radar-dependent translation errors	Pedestal leveling Azimuth alignment Orthogonality of axes Pedestal flexure from gravity Pedestal flexure from solar heating	Bearing wobble Data gear nonlinearity and backlash Data take-off nonlinearity and granularity Pedestal deflection during acceleration Phase shifter error
Propagation errors	Average tropospheric refraction Average ionospheric refraction	Irregularities in tropospheric refraction Irregularities in ionospheric refraction
Apparent errors (in test instrumentation)	Stability of telescope or reference instrumentation Stability of film base or emulsion Optical parallax	Vibration or jitter in reference instrument Film transport jitter Reading error Granularity error Variation in parallax

10.1 ERROR DUE TO NOISE

Noise is the dominant source of angular error (or loss of track) under conditions of low signal-to-noise ratio, usually at long ranges. Thermal noise is internally generated in all receivers, and other noise can also come from external sources. As mentioned in Section 1.4, one of the advantages of monopulse over sequential scan is that the monopulse radar has less angular error due to noise, compared to other radar types having the same transmitted power and antenna size.

In this chapter the analytical approach to the calculation of noise errors is described and practical formulas are derived.

10.1.1 Analytical Model

We wish to determine the error in an estimate of target angle due to noise. Since the fundamental monopulse output in each angular coordinate is the ratio d/s in that coordinate, we first determine the error in d/s and then the conversion to angle error.

The analysis begins with the assumption of an exact monopulse processor, defined in Section 8.4 as a processor that produces exactly the real part of the complex difference-to-sum ratio, and optionally the imaginary part if needed. (This definition does not require that the output be a linear function of angle.) The effects of other conditions are then considered. The analysis is carried out for a single pulse; for a multiple-pulse estimate the single-pulse standard deviation in general is divided by the square root of the number of pulses, but in some cases correlation from pulse to pulse does not permit such a reduction.

In analyzing the error due to noise, we assume a point target—that is, a target with a single scattering point. The error due to multiple scattering points on a target, called glint, is treated in Section 10.5.1.

Let s and d represent the noise-free sum and difference phasor voltages (complex envelopes, as explained in Section 2.7 of Chapter 2), and let n_s and n_d represent the additive phasor noise voltages in the respective channels. Then the noise-corrupted sum and noise voltages are

$$s' = s + n_s \quad (10.1)$$

$$d' = d + n_d \quad (10.2)$$

Under conditions such as multipath, unresolved targets, or a target with glint, d and s will generally differ in phase, and their ratio must be treated as a complex quantity. For a single point target, as assumed here (and assuming no phase distortions in the radar) the analysis is simplified because d and s have 0° or 180° relative phase and the noise-free monopulse ratio d/s is real.¹

10.1.2 Noise Statistics

The receiver-generated sum noise and difference noise are random variables, statistically independent of each other since they come from separate receivers. In some cases, however, there may be a correlated noise component. This may come from an external source such as a jammer or from a source within the radar such

¹ As pointed out previously, in some monopulse radars d and s emerge from the comparator with 90° relative phase. It is assumed here that one of them is shifted 90° to bring them into phase alignment. If not, the results are the same except that the reals and imaginaries are interchanged.

as the local oscillator. To allow for the possibility of correlation, we write n_s and n_d each as the sum of two components:

$$n_s = n_{su} + n_c \quad (10.3)$$

$$n_d = n_{du} + cn_c \quad (10.4)$$

where n_{su} and n_{du} are the uncorrelated components and n_c and cn_c are the respective correlated components. The coefficient c means that the correlated noise component may not be equal in the sum and difference channels; it may have different values—positive or negative, even complex—depending on the source and on other factors. The correlated noise is statistically independent of the uncorrelated noise components.

The noise voltages are treated as complex quantities. The real and imaginary parts of each noise component have independent Gaussian distributions with zero mean and equal variance.²

If n_c comes from an external point source such as a single jammer, then the coefficient c is real (positive or negative) and equal to d/s for a nonjamming target at the same location. If n_c comes from the local oscillator, c is presumably also real because the local oscillator feeds the same voltage (including noise) to the sum and difference channels, assuming that the circuits are properly matched.

From (10.3) and (10.4), we obtain for the noise-corrupted monopulse ratio

$$\frac{d'}{s'} = \frac{d + n_{du} + cn_c}{s + n_{su} + n_c} \quad (10.5)$$

Let $\epsilon_{d/s}$ denote the error in the monopulse ratio:

$$\epsilon_{d/s} = \frac{d'}{s'} - \frac{d}{s} \quad (10.6)$$

By use of (10.5) this reduces to

$$\epsilon_{d/s} = \frac{n_{du} - (d/s)n_{su} + (c - d/s)n_c}{s + n_{su} + n_c} \quad (10.7)$$

² The variance of a random variable is the mean squared deviation from the mean value. The square root of the variance is the standard deviation.

The quantity $\epsilon_{d/s}$ is generally complex. If only the real part is of interest, as is usually the case, (10.7) can be separated into its real and imaginary parts and the latter can be ignored in the remainder of the analysis. The mathematical expressions for the real part, however, are more complicated than those for the complex quantity. Therefore the method chosen here is to work with complex quantities until it actually becomes necessary to extract the real part for the final result. This also makes it possible to obtain information about the imaginary part, should it be needed.

10.1.3 Conversion of Voltages to Powers

The analysis so far has involved sum, difference, and noise voltages. Antenna patterns, however, are usually plotted as power versus angle, and formulas used in calculating errors due to noise (as well as those used in calculating detection probability and other performance characteristics) are most conveniently expressed in terms of power, particularly signal-to-noise power ratios. The conversion from voltage equations to power equations is done in the following manner.

As noted in the preceding subsection, the real and imaginary parts of each noise component have independent Gaussian distributions with zero mean and with equal variance. Let N_s , N_{su} , N_d , N_{du} , and N_c represent the variance of each real part and each imaginary part of the respective noise components. The variance of the sum noise n_s , for example, is the sum of the variances of its real and imaginary parts, namely $2N_s$. Since $|n_s|$ is the *envelope amplitude* (not the rms value) of an IF voltage, the average electrical power of the sum noise is half of $2N_s$, or simply N_s . Similarly the average electrical power of each of the other noise components is N with the appropriate subscript.³

The sum-signal power, represented by the symbol S , is the square of the rms voltage amplitude, which is one-half of the square of the voltage amplitude. Thus

$$S = |s|^2 / 2 \quad (10.8)$$

These relationships will be used in later sections.

10.1.4 Conversion from d/s Error to Angular Error

As explained in Section 2.8, directional coordinates for mechanically steerable antennas are expressed in terms of angles. For fixed array antennas, directions are expressed in array coordinates (sine space). The following derivations are pre-

³ The power is the square of the rms voltage divided by an appropriate load resistance. Assuming that the load resistance is the same in both channels, it cancels out when power ratios are taken, and can therefore be ignored.

sented in angle space, but they can be applied to fixed array antennas by substituting sine space coordinates for angle space coordinates.

It is shown in Section 15.1 that it is possible to design sum and difference patterns producing a monopulse ratio proportional to the sine of the off-axis angle and thus very nearly proportional to the angle itself out to several degrees. However, patterns generally are not designed to have this property unless there is a specific need for it, because it requires some sacrifice of other desirable characteristics.

A typical curve of the monopulse ratio versus off-axis angle, like the one plotted in Figure 1.6, has a shape resembling a tangent function. In the main lobe it goes from negative infinity at the first sum-pattern null on one side of the axis to positive infinity on the other side. The values are repeated in the sidelobes and therefore the conversion from monopulse ratio to angle is theoretically ambiguous. In normal practice, however, the indicated angle is interpreted as being within the main lobe, and since the target is also presumed to be within the main lobe, the angle error cannot exceed the null-to-null width of the main lobe. Furthermore, in some systems a measured monopulse ratio greater than a specified limit (corresponding, say, to a little more than one-half beamwidth from the axis) is either discarded as being erroneous or is truncated to the limiting value.

Thus, even if the equipment could produce an infinite monopulse ratio, the corresponding angle estimate could not be infinite. Therefore the rms value of the angle error is finite and its maximum possible value is of the order of the beamwidth.

For purposes of error analysis, the nonlinear function d/s versus angle can be linearized about the target angle provided the deviation θ of the target direction from the boresight direction is small compared to the beamwidth. Then the angle error as a fraction of the beamwidth is obtained by dividing the error in the monopulse ratio by the monopulse slope:

$$\frac{\epsilon_\theta}{\theta_{bw}} = \frac{\epsilon_{d/s}}{k_m}, \text{ or } \epsilon_\theta = \frac{\theta_{bw} \epsilon_{d/s}}{k_m} \quad (10.9)$$

In these equations ϵ_θ and $\epsilon_{d/s}$ are the errors in angle and monopulse ratio respectively, θ_{bw} is the one-way 3-dB beamwidth of the sum pattern in the same units as ϵ_θ , and k_m is the monopulse slope in volts/volt/beamwidth; that is, the slope of the curve of d/s versus angle in beamwidths. Since $\epsilon_{d/s}$ is complex in general, ϵ_θ is also complex. Normally, however, ϵ_θ is interpreted to mean only the real part.

The value of k_m that should be used is the slope at the target angle. If the target is off axis, this may differ considerably from the slope at boresight. In the AN/FPS-16 radar, for example, the d/s ratio, obtained from (6.8) and (6.9), is

$$\frac{d}{s} = \sqrt{2} \tan(1.14\theta) \quad (10.10)$$

and the slope is

$$k_m(\theta) = \frac{\theta_{bw}}{s(0)} \left| \frac{d}{d\theta} d(\theta) \right| = 1.14\sqrt{2}\theta_{bw} \sec^2(1.14\theta) \quad (10.11)$$

where the absolute value is used to express the slope as a positive number. On the boresight axis ($\theta = 0$) the slope is 1.62 volts/volt/beamwidth. At one-half beamwidth off axis it is 1.42 volts/volt/beamwidth.

10.1.5 Bias in Monopulse Ratio

Although each of the noise variables has a circular normal distribution with zero mean value, the mean value of the resulting error is not zero. Correlated noise has a “pulling” effect similar to that of an unresolved second target, and uncorrelated sum noise also contributes a bias that can be significant at low signal-to-noise ratios.

The bias in the monopulse ratio d/s is the average of $\epsilon_{d/s}$ over the distributions of the noise variables. The contribution of n_{du} to the error, from (10.7), is given by $n_{du}/(s + n_{su} + n_c)$. If this is averaged over the distribution of n_{du} while the other two noise variables are held constant, the result is zero by symmetry, and since this is true for all combinations of values of the other variables, we conclude that the uncorrelated component of the difference noise does not contribute to the bias:

$$\text{Bias due to } n_{su} = 0 \quad (10.12)$$

In determining the contributions of n_{su} and n_c to the bias, the analysis is simplified and insight is gained by first treating each one separately as if the other were absent. (The presence or absence of the uncorrelated difference noise does not matter.) Consider first the correlated component n_c . The error it produces, again referring to (10.7), with n_{du} and n_{su} set equal to zero, is

$$\epsilon_{d/s} = \frac{(c - d/s)n_c}{s + n_c} = \frac{(c - d/s)(n_c/s)}{1 + n_c/s} \quad (10.13)$$

Comparing this with the analysis in Section 9.10 for the bias due to an unresolved second target, we find that if $|n_c/s| < 1$, the average error over uniformly distributed phase is zero, and if $|n_c/s| > 1$, the average is $c - d/s$. The latter is the differ-

ence of the monopulse ratios of the jammer (or equivalent noise source) and the target, which is approximately proportional to their angular separation. The bias due to correlated noise is $c - d/s$ multiplied by the fraction of the time that $|n_c|$ exceeds $|s|$.

Since n_c has a circular normal distribution, its magnitude has a Rayleigh distribution with probability density function given by

$$p(|n_c|) = \frac{|n_c|}{N_c} \exp\left(-\frac{|n_c|^2}{2N_c}\right) \quad (10.14)$$

The probability (fraction of the time) that $|n_c|$ exceeds $|s|$ is the integral of the probability density function from $|s|$ to infinity:

$$P(|n_c| > |s|) = \int_{|s|}^{\infty} p(|n_c|) d|n_c| = \exp\left(-\frac{|s|^2}{2N_c}\right) \quad (10.15)$$

$$\text{Bias due to } n_c \text{ alone} = \left(c - \frac{d}{s}\right) \exp\left(-\frac{S}{N_c}\right) \quad (10.16)$$

where N_c is the average power of the correlated component of sum noise n_c . This is equivalent to the result obtained in [1, Eq. (40)], for a steady target and an external point source of noise at angles that produce monopulse ratios d/s and c respectively. If the source is at the same angle as the target, it causes no error. Otherwise, there is a “pulling” effect approximately proportional to the angular separation and inversely proportional to the exponential of the ratio of signal power to average noise power. Note that the bias is less than predicted by the power-weighted centroid approximation sometimes employed. For example, if the signal power and noise power are equal, that approximation gives a bias of half the separation, while (10.15) gives a bias of 0.37 times the separation.

If either c or d/s happens to be complex, the mean of the monopulse ratio is complex and the bias is complex. Only the real part is used unless some special application requires both the real and imaginary parts.

Returning now to (10.7), we examine the effect of the uncorrelated sum noise n_{su} , on the assumption that n_c is zero (but n_{du} need not be zero). This is analyzed in the same way as n_c , the only difference being in the coefficient. The result is

$$\text{Bias due to } n_{su} \text{ alone} = -\left(\frac{d}{s}\right) \exp\left(-\frac{S}{N_{su}}\right) \quad (10.17)$$

where N_{su} is the average power of the uncorrelated component of sum noise n_{su} .

In system error analysis the internally generated sum and difference noises are usually assumed to be uncorrelated, on the grounds that any correlated component that they may have is presumably negligible. In this case the bias is given by (10.17). For a target on the axis, d/s is zero and the bias is therefore zero, as expected because of symmetry. For a target at an angle where $d/s = \pm 1$ (a little more than one-half beamwidth from boresight), with a signal-to-noise power ratio of 10, the bias according to (10.17) is less than 5 ± 10^{-5} volt/volt, which is entirely negligible. At a signal-to-noise ratio of 4 = 6 dB, the bias is 0.018 volt/volt, or about 0.01 beamwidth, which may not be negligible. At a signal-to-noise ratio of 1 = 0 dB, the bias is 0.37 volt/volt, or about one-sixth of a beamwidth.

Equations (10.16) and (10.17) are useful in understanding and calculating the effects of either n_c or n_{su} alone when the other is absent or negligible, but they are not additive when both are present. The exact result for the total bias has been worked out by Kanter [2]:

$$\begin{aligned} \text{Total bias} &= \left(\frac{cN_c}{N_s} - \frac{d}{s}\right) \exp\left(-\frac{S}{N_s}\right) \\ &= \left(\rho \sqrt{\frac{N_d}{N_s}} - \frac{d}{s}\right) \exp\left(-\frac{S}{N_s}\right) \end{aligned} \quad (10.18)$$

Here N_s is the total sum-channel noise power and ρ is the correlation coefficient between the sum- and difference-channel noise. Note that the uncorrelated component of the difference-channel noise does not affect the bias.

10.1.6 Exact Solution for Probability Density Function of d/s

The desired measure of error is the root-mean-squared (rms) value: the combined effect of the mean error (bias) and the standard deviation from the mean. In contrast to the simple, exact formula for the bias, given by (10.18), there is no exact formula for the standard deviation of the noise-corrupted monopulse ratio; in fact the standard deviation does not exist, mathematically speaking. An exact expression for the probability density function (pdf) of the noise-corrupted monopulse ratio was derived by Kanter [2]. His analysis is general enough to cover a steady target anywhere in the beam, unequal noise powers in the sum and difference channels, any degree of correlation between sum channel and difference channel,

and any signal-to-noise ratio. He showed that the distribution has a bias (as shown in the preceding subsection), that it is skewed (asymmetric), and that in theory it has infinite standard deviation. His results apply not only to single-pulse estimates but also to the average of n “looks” or pulses. Even for single-pulse estimates the equation by which the pdf is computed is rather complicated.

The reason for the infinite standard deviation is that for large values of the ratio the pdf falls off as the inverse third power of the ratio. When the pdf is multiplied by the square of the ratio and integrated over infinite limits in order to calculate the variance, the integrand falls off only as the reciprocal of the ratio and the integral increases as the logarithm of the ratio.

In lieu of the standard deviation it is possible to define an alternate measure of spread such as the standard deviation of a Gaussian distribution that fits the actual distribution in some sense. For example, a Gaussian random variable lies between the “one-sigma” values (one standard deviation above and below the mean) with probability 0.68 and in each tail of the distribution with probability 0.16. For the actual noise error distribution one can define an “equivalent sigma” as half the interval within which the integral of the pdf is 0.68. This definition permits the limits to “slide” as long as they bound an area of 0.68 under the pdf curve, so an additional constraint must be imposed. Because the distribution is skewed, whichever interval is chosen cannot satisfy more than one of the following conditions: symmetrical limits above and below the mean; equal area, 0.34, between the mean and each limit; or equal area in each tail. The “equivalent sigma” will vary with the choice of interval. Furthermore, the result will be different if, for example, the “equivalent sigma” is redefined as one-fourth of an interval in which the probability is 0.95, corresponding to the interval between the “two-sigma” points in a Gaussian distribution. Kanter chose as a measure of spread, for comparison with the standard deviation computed by an approximate formula, one-half the interval containing an area of 0.68, placed so as to give an area of 0.16 in each tail.

In actual practice, the standard deviation of the monopulse ratio cannot be infinite. The measured values of the monopulse ratio are always finite because of the finite dynamic range of the equipment and computations. Even if infinite values of the monopulse ratio were possible, they would not correspond to infinite angles. As explained in Section 10.1.4, the standard deviation of the angle error is finite and its maximum possible value is of the order of the beamwidth.

Although the exact analysis does not yield a practical formula for the standard deviation, the measure of spread adopted by Kanter does agree well, at high signal-to-noise ratios, with the approximate formula for standard deviation, as illustrated by a set of comparative curves included in the paper. Thus, the exact solution serves as a partial check. In addition, it leads to the simple exact formula for the bias given in (10.18).

10.1.7 First-Order Approximation for $S/N \gg 1$

Experience has shown that fairly simple approximate formulas usually are adequate for performance prediction provided they are properly interpreted and used. In their simplest form, based on a first-order approximation, they are in close agreement with the exact calculation at high signal-to-noise ratios (above about 10 dB). By inclusion of second-order terms they can be used also for lower signal-to-noise ratios approaching 0 dB.

In (10.7) divide the numerator and denominator by s and let v (with appropriate subscripts) denote the normalized noise variates: $v_{du} = n_{du}/s$, and so forth. Then

$$\epsilon_{d/s} = \frac{v_{du} - (d/s)v_{su} + (c - d/s)v_c}{1 + v_{su} + v_c} \quad (10.19)$$

The first-order approximation is based on the assumption that the signal-to-noise ratio in the sum channel is so high that the amplitude of the total sum-channel noise consisting of its correlated and uncorrelated components, is (almost always) much less than the amplitude of the sum signal, and therefore the noise terms in the denominator of (10.7) can be neglected, so that

$$\epsilon_{d/s} = \frac{n_{du}}{s} - \frac{d}{s} \frac{n_{su}}{s} + \left(c - \frac{d}{s} \right) \frac{n_c}{s} \quad (10.20)$$

Conversion of (10.20) to a more usable formula involves a number of relationships and algebraic steps, the details of which are omitted here but can be outlined as follows.

1. Each of the three noise variates has zero mean, and therefore $\epsilon_{d/s}$ has zero mean. Because of the assumption of high S/N ratio, the bias (Section 10.1.5) does not appear in this approximation. (It does, however, appear in the higher-order approximation discussed later.)
2. The symbols s , d , and n (with appropriate subscripts) represent voltage amplitudes. To obtain the desired formula each voltage amplitude is converted to average power, which is one-half of the mean squared voltage amplitude, as shown in Section 10.1.3.
3. Since each noise variate has a circular normal distribution, the entire complex error $\epsilon_{d/s}$ has a circular normal distribution, and because the three noise components are uncorrelated with one

another, the sum of the mean squared values of the terms on the right side of (10.20) is the mean squared value of $\epsilon_{d/s}$.

4. Although (10.20) applies even if c and d/s are complex, they are real under normal conditions and are treated as such.
5. In the conversion from voltages to powers the quantity in parentheses, $(c - d/s)$, is squared and expanded. Correlated and uncorrelated sum-noise powers N_{su} and N_c are added and expressed as total sum-noise power N_s . Similarly, the difference-noise power components N_{du} and $c^2 N_c$ are added and expressed as N_d .

Equation (10.20) then becomes:

$$\sigma_{d/s}^2 = \frac{N_d}{2S} + \left(\frac{d}{s}\right)^2 \frac{N_s}{2S} - \frac{d}{s} \frac{cN_c}{S} \quad (10.21)$$

where $\sigma_{d/s}$ is the rms value of the error in the monopulse ratio. It is seen that the error consists of three components: a first-order noise term inversely proportional to the ratio S/N_d of signal to difference-channel noise, a term for off-axis measurement inversely proportional to the ratio S/N_s of signal to sum-channel noise, and an off-axis correlated noise term inversely proportional to the ratio $S/(cN_c)$ of signal to correlated noise.

Taking the square-root of both sides of (10.21) and rearranging, we obtain:

$$\sigma_{d/s} = \frac{1}{\sqrt{2S/N_d}} \left[1 + \left(\frac{d}{s}\right)^2 \frac{N_s}{N_d} - 2 \frac{d}{s} \frac{cN_c}{N_d} \right]^{1/2} \quad (10.22)$$

If the correlated noise is from a jammer, it will typically be much larger than the signal; in that case, these equations do not apply, since they assume a high S/N ratio. The jamming problem is treated in Chapter 12. If the correlated noise is from the local oscillator, it is essentially equal in the matched sum and difference channels, which means that $c = 1$; the uncorrelated noise power is also equal in both channels. Therefore $N_s = N_d = N$, and (10.22) is simplified to

$$\sigma_{d/s} = \frac{1}{\sqrt{2S/N}} \left[1 + \left(\frac{d}{s}\right)^2 - 2 \frac{d}{s} \frac{N_c}{N} \right]^{1/2} \quad (10.23)$$

Again, three noise components are present, two of which appear only for off-axis targets.

In practice, the internally generated correlated noise (from the local oscillator, for example) is not normally measured separately but is considered small enough to be simply included as part of the receiver noise. Then the last term in (10.23) can be omitted.

A further simplification can be made when the tracking is known to be on or near boresight; the entire bracketed quantity can then be considered equal to 1 and omitted, leaving only the first-order noise term.

The final step is to convert the error $\epsilon_{d/s}$ to angle error as explained in Section 10.1.4. Equation (10.23) then becomes

$$\sigma_{\theta} = \frac{\theta_{bw}}{k_m \sqrt{2S/N}} \left[1 + \left(\overline{k_m} \frac{\theta}{\theta_{bw}} \right)^2 - 2\overline{k_m} \frac{\theta}{\theta_{bw}} \frac{N_c}{N} \right]^{1/2} \quad (10.24)$$

and as before, the last term inside the brackets is normally omitted. The bar over k_m indicates the average value from boresight to the target angle.

Equation (10.24), with or without the last term, is a commonly used formula. In other literature it has been derived in a simpler manner by adopting the necessary assumptions and approximations at the outset. The more complete derivation given here shows the contributions of the individual noise components and permits application to nonstandard conditions—for example, if the sum and difference noises are known to be unequal. In particular, it should be noted that the S/N inside the radical is the ratio of sum-signal power to *difference*-channel noise.

It is often convenient to express in separate equations the on-axis and off-axis error components. The first-order noise error for on-axis tracking becomes

$$\sigma_{\theta a} = \frac{\theta_{bw}}{k_m \sqrt{2S/N_d}} \quad (10.25)$$

A second error component for off-axis measurement is found as

$$\sigma_{\theta b} = \frac{\theta}{\sqrt{2S/N_s}} \sqrt{1 - \frac{s}{d} \frac{2cN_c}{N_s}} \quad (10.26)$$

These two components are combined in rss fashion for off-axis targets:

$$\sigma_{\theta} = \sqrt{\sigma_{\theta a}^2 + \sigma_{\theta b}^2} \quad (10.27)$$

In the absence of an external point source of noise it is usually assumed that the correlation is zero, on the grounds that the local oscillator and mixers are presumably designed to contribute very little noise, and external noise from a distributed source such as the sky is essentially uncorrelated in the sum and difference channels. Furthermore, even if there is some correlation, it adds a term to the mean squared error when the target is on one side of the axis and subtracts the same term when the target is at the same angle on the other side, so that the overall mean squared error is the same as without correlation.

10.1.8 Higher-Order Approximation for $S/N > 1$

Returning to (10.21) we now assume that the sum-channel signal-to-noise ratio is not high enough to justify neglecting the noise terms in the denominator, but high enough to allow the assumption that the ratio of sum-noise amplitude to sum-signal amplitude is (almost) always less than unity:

$$|v_s| = |v_{su} + v_c| < 1 \quad (10.28)$$

The fraction $1/(1 + v_s)$ can then be expanded to

$$\frac{1}{1 + v_s} = 1 - v_s + \dots \quad (10.29)$$

Using only these first two terms of the expansion and substituting in (10.19) with $v_s = v_{su} + v_c$, we obtain the following approximate equation for the error (the approximation symbol will be omitted):

$$\epsilon_{d/s} = [v_{du} - (d/s)v_{su} + (c - d/s)v_c](1 - v_{su} - v_c) \quad (10.30)$$

Each noise variate is decomposed into its real and imaginary parts, and after all multiplications are carried out, the real terms are collected. The resulting expression is then squared and averaged. The mean square value equals the variance because the mean of each term before squaring is zero. The procedure is similar to that described in the preceding section except that the real part of the error now includes higher-order terms containing cross-products and squares of the noise variates. The following relations are used in deriving the average:

1. Mean-square noise voltages are given by

$$\begin{aligned}
\overline{v_{du}^2} &= \frac{N_{du}}{2S} \\
\overline{v_{sui}^2} &= \overline{v_{suq}^2} = \frac{N_{su}}{2S} \\
\overline{v_{ci}^2} &= \overline{v_{cq}^2} = \frac{N_c}{2S}
\end{aligned} \tag{10.31}$$

2. The mean product of independent random variables is the product of their means; for example,

$$\overline{v_{du}^2 v_{sui}^2} = \overline{v_{du}^2} \overline{v_{sui}^2} = (0) \left(\frac{N_{su}}{2S} \right) = 0 \tag{10.32}$$

$$\overline{v_{du}^2 v_{sui}^2} = \overline{v_{du}^2} \overline{v_{sui}^2} = \frac{N_{du} N_{su}}{4S^2} \tag{10.33}$$

$$\overline{v_{sui}^2 v_{suq}^2} = \frac{N_{su}^2}{4S^2} \tag{10.34}$$

3. The third moment of a zero-mean Gaussian random variable is zero; for example,

$$\overline{v_{ci}^3} = 0 \tag{10.35}$$

4. The fourth moment of a zero-mean Gaussian random variable is three times the square of its variance; thus,

$$\overline{v_{ci}^4} = \overline{v_{cq}^4} = \frac{3N_c^2}{4S^2} \tag{10.36}$$

The variance of $\text{Re}(\epsilon_{d/s})$, if c and d/s are real, is

$$\begin{aligned}
\sigma_{d/s}^2 &= \frac{N_d}{2S} \left(1 + \frac{N_s}{S} \right) + \frac{c^2 N_c^2}{2S^2} + \left(\frac{d}{s} \right)^2 \frac{N_s}{2S} \left(1 + \frac{2N_s}{S} \right) \\
&\quad - \frac{d}{s} \frac{cN_c}{S} \left(1 + \frac{2N_s}{S} \right)
\end{aligned} \tag{10.37}$$

The product cN_c can be expressed in the equivalent form $\rho\sqrt{N_d N_s}$. If the higher-order noise terms are dropped, (10.37) reduces to (10.21).

As an example of the contribution of the higher-order terms, consider a target approximately on axis, equal noise powers in both channels ($N_d = N_s = N$). Then

$$\sigma_{d/s}^2 = \frac{N}{2S} \left(1 + \frac{N}{S} \right) \quad (10.38)$$

or

$$\sigma_{d/s} = \frac{\sqrt{1 + N/S}}{\sqrt{2S/N}} \quad (10.39)$$

If the signal-to-noise ratio is 10 dB ($N/S = 0.1$), the second-order term increases the variance by 10% and the standard deviation by about 5%, which is not usually significant in an error analysis. However, if the signal-to-noise ratio is only 3 dB, the second-order term increases the variance by 50% and the standard deviation by 22%.

If the target is near the edge of the beam, where $|d/s| \approx 1$, then instead of (10.38) we have

$$\sigma_{d/s}^2 = \frac{N}{2S} \left(1 + \frac{N}{S} \right) + \frac{N}{2S} \left(1 + \frac{2N}{S} \right) = \frac{N}{S} \left(1 + 1.5 \frac{N}{S} \right) \quad (10.40)$$

Inclusion of the $1.5N/S$ term in this case increases the standard deviation by 7% and 32% at 10 dB and 3 dB signal-to-noise ratio respectively.

The low-signal-to-noise correction factor $1 + N/S$ in (10.38) for the on-axis case appears also elsewhere in the radar literature, explained in a somewhat different manner. In [3] it is called an “AGC factor,” referring to the fact that in a system where AGC provides the monopulse normalization, the AGC responds to signal plus noise in the sum channel rather than to signal alone.

Although (10.37) is a better approximation than (10.21) because the expansion is carried out to second-degree noise terms, it still rests on the assumption that the ratio of sum-noise amplitude to sum-signal amplitude is always less than unity. The error due to neglect of the tails of the distribution, where noise amplitude exceeds signal amplitude, increases with decreasing signal-to-noise ratio. At 5-dB signal-to-noise ratio, noise exceeds signal only 4% of the time; at 3-dB, 14% of the time; and at 0 dB, 37% of the time. The validity of the formula at 0 dB or below becomes questionable, and should be verified by analysis or simulation using the characteristics of the actual system, including the monopulse ratio as a function of angle.

The expressions for error in the d/s ratio using the higher-order approximation are converted to angular error in the same way as in Section 10.1.7, substituting

$$\frac{d}{s} = \frac{k_m}{\theta_{bw}} \theta \quad \text{and} \quad \sigma_{d/s} = \frac{k_m}{\theta_{bw}} \sigma_\theta \quad (10.41)$$

Thus, (10.39) can be written as

$$\sigma_\theta = \frac{\theta_{bw} \sqrt{1 + N/S}}{k_m \sqrt{2S/N}} \quad (10.42)$$

10.1.9 Multiple-Pulse Estimates

The preceding analyses have considered only the single-pulse monopulse estimates of target position. In most monopulse applications, however, the estimates are averaged over n pulses:

$$n = f_r t_o = \frac{f_r}{2\beta_n} \quad (10.43)$$

where f_r is the pulse repetition frequency and $t_o = 1/2\beta_n$ is the averaging time, β_n being the (one-sided) noise bandwidth of the tracking loop.

In the absence of correlated noise components, the variance of the n -pulse average is simply $1/n$ times the single-pulse value. This relationship is correct for the case in which the noise is generated in components within the separate sum- and difference-channel receivers, or in the outside environment by sources that are spread over the mainlobes of the sum and difference patterns, giving uncorrelated sum and difference components. For this case, the n -pulse error can be expressed from (10.24) by setting $c = 0$ and inclusion of the factor n within the radical in the denominator:

$$\sigma_\theta = \frac{\theta_{bw}}{k_m \sqrt{2nS/N}} \left[1 + \left(\frac{\theta}{k_m \theta_{bw}} \right)^2 \right]^{1/2} \quad (10.44)$$

$$\sigma_\theta \approx \frac{\theta_{bw}}{k_m \sqrt{2nS/N}} \quad \text{for targets near the axis} \quad (10.45)$$

Presence of a correlated noise component, however, causes the bias error given by (10.18), and additional noise components from (10.24) and (10.37) that are not reduced by the n -pulse averaging. Correlated noise can be introduced by the common local oscillator or by an external source within a narrow angle in space. We will see this effect when considering noise jamming (Chapter 12), and also in errors caused by clutter (see Section 10.2).

For high S/N , the tracking-loop bandwidth β_n is held constant at a design value β_{n0} by the monopulse processor, using, for example, AGC and a dot-product detector (Section 8.8). The bandwidth is reduced, however, when the single-pulse signal-to-noise ratio S/N approaches unity. Two factors reduce the loop gain at low S/N : the normalization method in the receiver fails to hold constant the sum signal into the processor that forms $|d/s|$, and the useful signal in that processor is further suppressed by the presence of noise [4, pp. 467–472]. The loop bandwidth varies with reduced S/N :

$$\beta_n = \frac{\beta_{n0}}{\left(1 + \frac{N}{S}\right)^2} \quad (10.46)$$

The result is that the number of pulses integrated increases, causing the output noise to level off according to

$$\sigma_\theta = \frac{\theta_{bw}}{k_m \sqrt{(1 + S/N)(f_r/\beta_{n0})}} \quad (10.47)$$

as S/N drops to and below zero. Loss of track occurs not as a result of a large increase in noise error as predicted by (10.44), but rather by failure of the loop to follow target dynamics (see Section 10.3). This can be observed in actual operation of a mechanically steered monopulse radar, where the random antenna motion after disappearance of the target is limited to a small fraction of the beamwidth.

10.1.10 Fluctuating Targets

If the target fluctuates, the sum-signal power S (which is proportional to the target cross section) is a random variable. For a single-pulse angle estimate the preceding angle-error equations still would be correct if the value of S on that pulse were used. However, the value of S on each pulse is unknown; only the average value is assumed to be known or specified, and the error formula must be expressed in terms of the average of S . It turns out that the standard deviation of the error for a fluctuating target generally is larger than for a steady target having the same average cross section, although if multiple-pulse averaging is performed with proper

weighting the fluctuating target error approaches that of the steady target as the number of pulses is increased.

The effect of fluctuation on any of the errors derived in previous sections can be calculated by expressing the error variance as

$$\sigma_{\theta}^2 = \frac{K(\theta)}{S} \quad (10.48)$$

where $K(\theta)$ for the case represented by (10.42), for example, is

$$K(\theta) = \frac{\theta_{bw}^2 (1 + N/S)}{2k_m^2/N} \quad (10.49)$$

It is then assumed that only pulses whose power reaches some threshold T are processed for angle measurement. The resulting error is found as

$$\sigma_{\theta f}^2 = K(\theta) \frac{\int_T^{\infty} \frac{1}{S} p(S) dS}{\int_T^{\infty} p(S) dS} \quad (10.50)$$

where $p(S)$ is the pdf of the signal power. The denominator normalizes the variance to the fraction of the pulses that exceed the threshold. (If $T = 0$, the denominator is unity.) Dividing (10.50) by (10.48) gives the ratio of the fluctuating-target variance to the steady-target variance, if the average signal power is the same for both cases. We can apply this procedure to the most common models [5] for target fluctuation.

The pdf of signal power S for a wide variety of fluctuating targets can be represented by the chi-square distribution

$$p(S, K) = \frac{K}{(K-1)!} \left(\frac{SK}{\bar{S}} \right)^{K-1} \exp \left(-\frac{SK}{\bar{S}} \right) \quad (10.51)$$

where K is the number of duo-degrees of freedom and \bar{S} is the average of S . The values $K = 1$ and 2 correspond to the Swerling Cases 1 and 3, respectively:

$$p(S, 1) = \frac{1}{\bar{S}} \exp \left(-\frac{S}{\bar{S}} \right) \text{ for Swerling Case 1} \quad (10.52)$$

$$p(S, 2) = \frac{4S}{\bar{S}} \exp\left(-\frac{2S}{\bar{S}}\right) \text{ for Swerling Case 3} \quad (10.53)$$

The results of the integration (10.50) are shown in Figure 10.1. The Case 1 error increases steadily as the threshold drops below the average signal power, while for Case 3 the error levels off at $\sqrt{2}$ times the steady-target error. Basically, the improvement in accuracy as average signal increases for the fluctuating target does not keep pace with that for a steady target.

Connolly in [6] compared the steady-target error normalized to the beam-width, to that for Case 1 targets, as a function of \bar{S}/N . His curves can be reproduced in Figure 10.2, using (10.50) with the assumption that the threshold to accept a pulse for measurement is set at a level $T = \bar{S}N/(\bar{S} + N)$, which varies from 0 for $\bar{S} \rightarrow 0$ to N for $\bar{S} \gg N$. Figure 10.2 also shows values for $K = 2$ (Case 3) and $K = 4$, which could be obtained if two independent samples of Case 4 or four independent samples of Case 2, obtained by time or frequency diversity, were averaged in forming the d/s ratio. That amount of averaging reduces the error to very near the steady-target value.

It is only recently that monopulse radars have been deployed that actually form measurements on a single pulse, and the possible penalty in tracking Case 1 targets can be significant. By using frequency diversity to obtain independent target samples and applying an AGC or other process that normalizes the d/s ratio over more than one pulse this penalty can be avoided, providing time is available to transmit and receive more than one pulse per beam dwell.

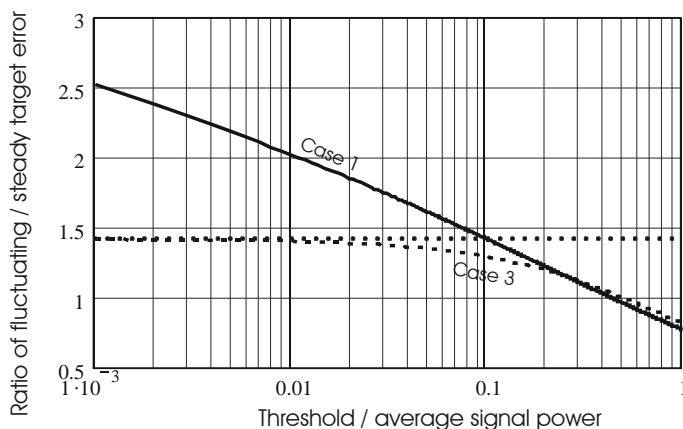


Figure 10.1 Ratio of error standard deviation: fluctuating/steady targets, as a function of threshold setting for acceptance of a measurement.

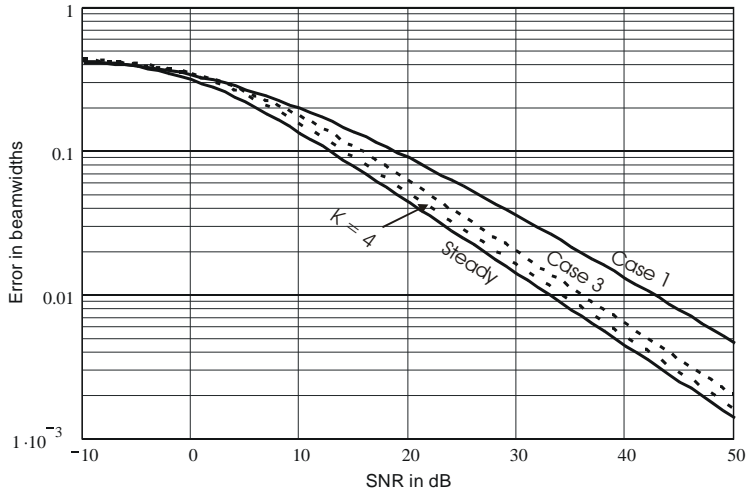


Figure 10.2 Angle error standard deviation for fluctuating and steady targets, as a function of average signal-to-noise ratio, for $k_m = 1.6$.

The “ I and Q ” type of processor described in Section 8.6 is an example in which averaging may be applied. For a single-pulse angle estimate this processor performs the arithmetic indicated by (8.9) to obtain the monopulse ratio. The numerator in the fraction in that equation is the “dot-product” of the difference and the sum; the denominator is the sum-signal power. For a weighted average the weight given to each pulse is equal to the sum-signal power of the pulse divided by the summation of the sum-signal powers of all the pulses. Hence, the numerator of the weight cancels the denominator of the monopulse ratio. The multiple-pulse estimate turns out to be simply the sum of all the numerators divided by the sum of all the denominators, which avoids the division process on each pulse. This result is then converted to an angle estimate by means of the monopulse calibration function.

An analog counterpart is the processor described in Section 8.8, consisting of a dot-product detector operating on each pulse and a relatively slow AGC, in which the time constant is chosen to correspond to the desired length of the multiple-pulse dwell. The AGC should not be slower than the servo response, which in turn must be a compromise between noise and lag errors. In effect, the servo filter sums (averages) the dot-products and the AGC filter sums (averages) the pulse powers, and the AGC action divides the first sum by the second. The result is analogous to that described above for the “ I and Q ” processor.

As the number of pulses used in the pulse-power-weighted averaging is increased, the standard deviation of error of a fluctuating target with a specified average cross section approaches that of a steady target with the same cross sec-

tion, provided the same number of pulses is used in both cases. The same error formulas that apply to a steady target, such as (10.24) or (10.42), can then be used for fluctuating targets by substituting \bar{S} for S and inserting the factor n (the number of pulses) under the square-root sign.

In practice, the weighting actually achieved is not quite the same as the optimum weighting, because instead of being proportional to signal power it is proportional to signal-plus-noise power. Similarly, if there is a threshold, it acts on the signal plus noise rather than on signal alone as the analysis assumes. Hence, the results are not exactly as described above. However, if the pulse-to-pulse fluctuation is due mainly to the target cross section variation rather than to noise, as is normally true at large or moderate \bar{S}/N ratios this approximation has only slight effect.

To calculate the bias error for single-pulse angle estimates on a fluctuating target, start with the steady-target bias formula (10.18) but regard S as a random variable rather than a constant. Multiply the right-hand side of (10.18) by the pdf of S and integrate. If there is a threshold power level T , the integral is from T to infinity, and it must be divided by the integral of the pdf between the same limits. As a simple example, consider a Swerling Case 1 or Case 2 target, for which the pdf is given by (10.52). This pdf is the same as that of noise except that in the case of noise the average signal power \bar{S} is replaced by the average noise power N . For $T = 0$, the following result is obtained after conversion to angle:

$$\text{Bias of single pulse estimate (no threshold)} = \frac{\theta_{bw}}{k_m} \frac{cN_c/N_s - d/s}{\bar{S}/N_s + 1} \quad (10.54)$$

Comparison of (10.54) with (10.18) shows that the fluctuating target has a larger bias than a steady target at the same (average) cross section at the same angle. A uniformly weighted average estimate from n pulses has the same bias as for a single pulse. If averaging could be done over multiple pulses yielding independent samples, with ideal weighting proportional to signal power, the bias would be reduced; the formula would be

$$\text{Bias of } n\text{-pulse weighted average estimate} = \frac{\theta_{bw}}{k_m} \frac{cN_c/N_s}{\left(\bar{S}/N_s + 1\right)^2} \quad (10.55)$$

In practice, however, the weighting of each pulse can be made proportional to signal-plus-noise power but not to signal power alone. When this fact is taken into account in the analysis [7], the bias of the power-weighted average is found to be the same as the single-pulse bias given by (10.54).

10.1.11 “Inexact” Monopulse Processors

The analysis has assumed that the output of the monopulse processor is exactly equal (or proportional) to the real part of the monopulse ratio. Some of the practical processors described in Chapter 8 follow this behavior very closely; others approximate it only at high signal-to-noise ratios, real values of d/s , and target angles not too far from the axis. Where these conditions are not met, a more detailed analysis or simulation may be required, using the equations developed in Chapter 8 for each processor.

10.1.12 Closed-Loop Versus Open-Loop Operation

The equations developed in this chapter have been based on open-loop operation; that is, it has been assumed that the beam pointing direction does not change in response to the indicated off-axis angle. The target angle is estimated by converting the measured monopulse ratio to an angle and adding that angle to the known pointing angle of the beam axis. The error is the deviation of the indicated angle from the true angle.

In closed-loop operation a servo uses the monopulse ratio as an error signal and attempts to null it by causing the beam axis to point toward the target. The error in that case is the deviation of the beam axis from the true target direction. As the beam moves relative to the target, the signal power and monopulse slope change, so the error in beam pointing direction is not exactly the same as the open-loop error. At high signal-to-noise ratios the difference is usually so slight that the open-loop formulas can be applied also to closed-loop operation, provided the appropriate value of n (number of pulses effectively averaged by the servo time constant) is inserted, as discussed in Section 10.1.9. At low signal-to-noise, changes occur in the monopulse slope and servo loop characteristics and must be taken into account [3, 8].

10.2 ERRORS DUE TO CLUTTER

Clutter is normally assumed to originate from scatterers that are broadly distributed in one or both angular coordinates. Surface clutter is distributed in azimuth over the entire main-lobe region of the sum and difference patterns; precipitation clutter or chaff is distributed over the elevation patterns as well, except for tracking near the lower or upper altitude limits of the clutter.

10.2.1 Random Error from Clutter Distributed Across the Beam

When the clutter is uniformly distributed over the angular extent of the main difference lobes, or over two or more sidelobes, the clutter in the sum channel is uncorrelated with that in the difference channel. Denote the rms clutter error on a single measurement sample by $\sigma_{\theta c1}$, where the subscripts identify angle error from clutter on a single pulse. The equation for the rms value of the monopulse ratio d/s is the same as for uncorrelated thermal noise error (10.37) with noise powers N_s and N_d replaced by the corresponding clutter powers. Including the second-order terms that allow for low sum-channel signal-to-clutter ratios S/C_s , we find:

$$\sigma_{\theta c1} = \frac{\theta_{bw}}{k_m \sqrt{2S/C_d}} \sqrt{1 + \frac{C_s}{S} + \left(\frac{d}{s}\right)^2 \frac{C_s}{C_d} \left(1 + \frac{2C_s}{S}\right)} \quad (10.56)$$

where C_s is clutter power in the sum channel, C_d is clutter power in the difference channel, and d/s is the monopulse ratio corresponding to an off-axis target. The fraction preceding the large radical in (10.56) represents the first-order clutter error. The product of that error and the second term in the radical is the second-order error component. The product of first-order error and the third term in the large radical is the off-axis error component, including its first- and second-order components. Clutter powers in this expression are evaluated after any Doppler processing, which must be applied by linear circuits with identical response in the sum and difference channels.

When tracking a target near the beam axis, the terms in (10.56) that include d/s may be neglected to obtain an expression for first- and second-order clutter errors:

$$\sigma_{\theta ca1} = \frac{\theta_{bw}}{k_m} \sqrt{\frac{C_d}{2S} \left(1 + \frac{C_s}{S}\right)} \quad (10.57)$$

where the subscript on σ denotes the angle error from clutter for the on-axis, single-pulse case, similar to the on-axis noise error $\sigma_{\theta a}$ in (10.25).

Unlike thermal noise, clutter echoes are characterized by a correlation time that may extend over many successive pulses, so the number of independent clutter samples is reduced from $n = f_r t_o$ given by (10.43) to a value n_i given in Section 10.2.2. The clutter error of (10.57) is reduced by a factor $\sqrt{n_i}$ with averaging over the time constant of the tracking loop, resulting in an averaged error, for C_d uncorrelated with C_s , given by

$$\sigma_{\theta_{can}} = \frac{\theta_{bw}}{k_m} \sqrt{\frac{C_d}{2Sn_i} \left(1 + \frac{C_s}{S}\right)} \quad (10.58)$$

The ratio of clutter power in the difference channel to that in the sum channel is normally $\approx 0.63 = -2$ dB, which is the ratio of integrals of the product of sum and difference power patterns $s^2(\theta)d^2(\theta)$ to the two-way sum power pattern $s^4(\theta)$. An exception is in elevation measurement with precipitation or chaff clutter, where C_d at the output of Doppler processor may exceed C_s because of the broader clutter spectrum produced by wind shear in the elevation difference pattern. For clutter in the sidelobes, the ratio of difference- to sum-channel power is usually greater than unity because of higher difference sidelobes.

In off-axis measurement, the terms that include d/s in (10.56) increase the error in clutter, as was also the case with thermal noise. The single-pulse off-axis clutter error can be considered as the rss sum of $\sigma_{\theta_{ca1}}$ from (10.57) and an off-axis error component given by

$$\sigma_{\theta_{cb1}} = \frac{\theta_{bw}}{k_m} \frac{d}{s} \sqrt{\frac{C_s}{2S} \left(1 + \frac{2C_s}{S}\right)} = \theta \sqrt{\frac{C_s}{2S} \left(1 + \frac{2C_s}{S}\right)} \quad (10.59)$$

where θ (assumed $< 0.5\theta_{bw}$) is the off-axis angle of the measured target. Because the second-order term in (10.59) is not reduced by averaging, the expression for the averaged off-axis error component is

$$\sigma_{\theta_{ctn}} = \frac{\theta_{bw}}{k_m} \frac{d}{s} \sqrt{\frac{C_s}{2S} \left(\frac{1}{n_i} + \frac{2C_s}{S}\right)} = \theta \sqrt{\frac{C_s}{2S} \left(\frac{1}{n_i} + \frac{2C_s}{S}\right)} \quad (10.60)$$

This is added in rss fashion to the averaged on-axis error from (10.58).

10.2.2 Number of Independent Clutter Samples

The sum-channel output $s + c_s$ is used as a reference in phase-sensitive detection of the difference-channel clutter c_d (after any Doppler processing of both channels). The clutter correlation time in each channel is

$$t_c = \frac{\lambda}{2\sqrt{2\pi}\sigma_v} \quad (10.61)$$

where λ is the wavelength and σ_v is the rms velocity spread resulting from internal motion, beam scanning, and (for precipitation or chaff) wind shear. Hence the number of independent clutter samples available for averaging over the time constant of the tracking loop may vary, depending on the relative target-to-clutter velocity, between limiting values:

$$1 + \frac{t_o}{t_c} \leq n_i \leq f_r t_o = \frac{f_r}{2\beta_n} \quad (10.62)$$

where $t_o = 1/2\beta_n$ is the time constant of the tracking loop.

For example, consider an X-band radar tracking a target over land clutter, with the following characteristics:

- Wavelength $\lambda = 0.03\text{m}$;
- PRF $f_r = 300\text{ Hz}$;
- Servo bandwidth $\beta_n = 3\text{ Hz}$;
- No Doppler processing.

A typical velocity spread for land clutter, $\sigma_v \approx 0.5\text{ m/s}$, gives, from (10.61), a clutter correlation time $t_c = 12\text{ ms}$ at the radar input. The averaging time for a loop bandwidth $\beta_n = 3\text{ Hz}$ is $t_o = 0.167\text{ s}$, setting the lower limit of n_c at 15. The upper limit is $f_r t_o = 50$, resulting in $15 \leq n_i \leq 50$. It should be kept in mind that the correlation time of clutter residue is reduced by Doppler processing, and may fall below the pulse repetition interval $1/f_r$, in which case the upper limit for n_i applies.

When the radar uses pulse-to-pulse frequency agility, the number of independent clutter samples is

$$n_i = \text{lesser of } \left[(1 + \tau \Delta_f), f_r t_o \right] \quad (10.63)$$

where τ is the pulsewidth and Δ_f is the agile bandwidth, and it is assumed that the clutter density is uniform over the range resolution cell width $\tau c/2$, where c is the velocity of light.

10.2.3 Random Error from Clutter at a Specific Angle in the Beam

Surface clutter in a given range gate appears at a fixed elevation angle located below the tracking axis, either in the mainlobe region or in one of the lower sidelobes. In this case C_s and C_d are mutually correlated. The variance of single-pulse error for correlated sum and difference clutter is found from (10.37) by replacing noise terms with clutter and converting to angle error:

$$\sigma_{\theta c1}^2 = \left(\frac{\theta_{bw}}{k_m} \right)^2 \left[\frac{C_d}{2S} \left(1 + \frac{2C_s}{S} + \left(\frac{d}{s} \right)^2 \frac{C_s}{C_d} \right) - \frac{d}{s} \frac{cC_c}{S} \left(1 + \frac{2C_s}{S} \right) \right] \quad (10.64)$$

where the factor $cC_c = \sqrt{C_d C_s}$ for completely correlated clutter.

For a radar tracking a target near the beam axis, the terms in (10.64) that include d/s can be neglected, leading to

$$\sigma_{\theta c1} = \frac{\theta_{bw}}{k_m} \sqrt{\frac{C_d}{2S} \left(1 + \frac{2C_s}{S} \right)} \quad (10.65)$$

Temporal averaging over n_i clutter samples reduces the first-order term in (10.65) but the correlation between sum- and difference-channel clutter does not permit reduction of the second-order term, leading to

$$\sigma_{\theta can} = \frac{\theta_{bw}}{k_m} \sqrt{\frac{C_d}{2S} \left(\frac{1}{n_i} + \frac{C_s}{S} \right)} \quad (10.66)$$

The significance of (10.66) was first appreciated when a monopulse radar using wideband frequency agility with large n_i was found to have a larger than expected error component in tracking at low elevation angle over land clutter. Consider a tracking radar with the following characteristics:

- Beamwidth $\theta_{bw} = 1.7^\circ = 30$ mrad;
- PRF $f_r = 2000$ Hz;
- Servo bandwidth $\beta_n = 3$ Hz;
- Error slope $k_m = 1.6$;
- Pulsewidth $\tau = 1$ μ s;
- Agile bandwidth $\Delta f = 500$ MHz.

The potential number of independent clutter samples in frequency is $\Delta f \tau = 500$, but from (10.62) the maximum number of samples is $n_{if} = 333$ for samples uncorrelated from pulse to pulse. Assume a track over land clutter with $S/C = S/C_d = 10$ and complete correlation. The single-sample error from (10.57) is $\sigma_{\theta c1} = 4.4$ mrad. Mistakenly applying (10.58), on the assumption of uncorrelated clutter, leads to a reduction factor of 18 from averaging, giving $\sigma_{\theta can} = 0.24$ mrad, essentially all from the first-order term. However, the actual error from (10.66) is $\sigma_{\theta can} = 1.3$ mrad, more than five times as large, resulting from the second-order term having no reduction from averaging.

Correlation between sum- and difference-channel clutter normally occurs in elevation measurement over surface clutter in a particular range gate, which is concentrated at a single elevation angle below the target. The same expression applies to azimuth tracking when there is a dominant discrete scatterer offset in azimuth from the target.

10.2.4 Bias Error Due to Clutter

Correlated clutter also causes a bias error ϵ_c in the measurement, similar to that from noise as given in (10.18):

$$\begin{aligned}\epsilon_{\theta c} &= \frac{\theta_{bw}}{k_m} \left(\frac{cC_d}{C_s} - \frac{d}{s} \right) \exp \left(-\frac{S}{C_s} \right) \\ &\approx \frac{\theta_{bw}}{k_m} \frac{cC_d}{C_s} \exp \left(-\frac{S}{C_s} \right) \quad \text{for a target near the axis}\end{aligned}\tag{10.67}$$

Using parameters from the preceding example, the error is less than 1 μrad , but bias can become significant for $S/C_s < 4 = 6 \text{ dB}$.

10.3 DYNAMIC LAG ERROR

One of the advantages listed in Section 1.4 for monopulse radar is the increased data rate provided by angle measurements on each received pulse, as compared to sequential scanning methods. The data rate is one of the factors that establish the bandwidth of the angle tracking loops of a tracking radar. That bandwidth in turn controls the dynamic lag error in following a target with given velocity and acceleration.

10.3.1 Tracking-Loop Error Coefficients

The dynamic lag error consists of components corresponding to the velocity, acceleration, and higher derivatives of the measured coordinate. In azimuth A ,

$$\epsilon_{\text{lag}} = \frac{\dot{A}}{K_v} + \frac{\ddot{A}}{K_a} + \frac{\dddot{A}}{K_3} \dots\tag{10.68}$$

Similar expressions apply to the elevation coordinate. The *error coefficients* K_v , K_a , K_3 , ... are determined by the open- and closed-loop frequency response of the

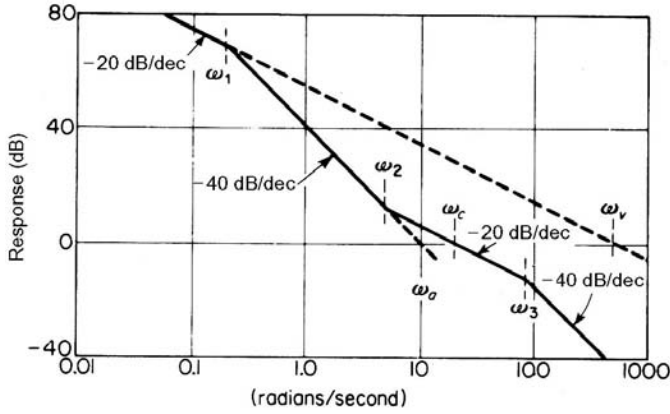


Figure 10.3 Typical open-loop response of first-order servo with single integration [3, p. 296].

tracker servo loop in the coordinate under consideration (see, for example, [3, pp. 295–301]). Figure 10.3 shows the open-loop servo response of a typical antenna servo. High gain at low frequencies is necessary to overcome torque disturbances and lag in following high-velocity targets. A region with a slope of -20 dB/decade, extending about two octaves each side of the unity-gain crossover, is necessary to provide stability.

The locations of break points in the open-loop response (at ω_1 , ω_2 , ω_3) control the error coefficients and closed-loop bandwidth. The velocity error coefficient is the intersection of the low-frequency -20 -dB/decade slope with the 0-dB gain axis at $\omega_v = 500$ rad/s, giving $K_v = 500 \text{ s}^{-1}$. The intersection of the -40 -dB/decade slope at mid-frequency with the 0-dB gain axis at $\omega_a = 10$ rad/s gives $K_a = \omega_a^2 = 100 \text{ s}^{-2}$. The second -20 -dB/decade slope crosses the 0-dB gain axis at $\omega_c \approx 2\omega_a = 20$ rad/s (or 3.2 Hz), and the noise bandwidth β_n of the servo is typically about twice this value: $\omega_n = 4\omega_a = 40$ rad/s, giving $\beta_n = 40/2\pi = 6.4$ Hz in this case.

There is no upper limit to the velocity error coefficient K_v , but the practical value is limited by the duration of the transient when tracking is initiated. The acceleration error constant is limited by the closed-loop servo bandwidth β_n :

$$K_a = \omega_a^2 = \left(\frac{2\pi}{4} \beta_n \right)^2 = 2.5 \beta_n^2 \quad (10.69)$$

The acceleration term normally dominates the lag error, and higher-order terms can be neglected (although they may be calculated using expressions in [3] if necessary).

Consider a target flying at a ground range $R = 30$ km with velocity $v_t = 300$ m/s and acceleration $a_t = 20$ m/s², both in the horizontal plane and normal to the line of sight. For $\beta_n = 3$ Hz, $K_a = 22.5$, and $K_v = 300$ and the azimuth lag error is

$$\begin{aligned}\epsilon_{\text{lag}} &= \frac{1}{K_v} \frac{v_t}{R} + \frac{1}{K_a} \frac{a_t}{R} = \frac{1}{300} \frac{300}{30,000} + \frac{1}{2.5 \times 3^2} \frac{10}{30,000} \\ &= (33 + 30) \times 10^{-6} \text{ rad} = 0.063 \text{ mrad}\end{aligned}$$

This error seems very small, but the lag would be a significant contributor to error in a precision instrumentation radar with a specified total error < 0.1 mrad.

10.3.2 Pass-Course Problem

The angular rate and acceleration of a target in radar (spherical) coordinates depend on the target dynamics and its range from the radar. The classic *pass-course* problem is illustrated in Figure 10.4. The target travels at a constant velocity v_t

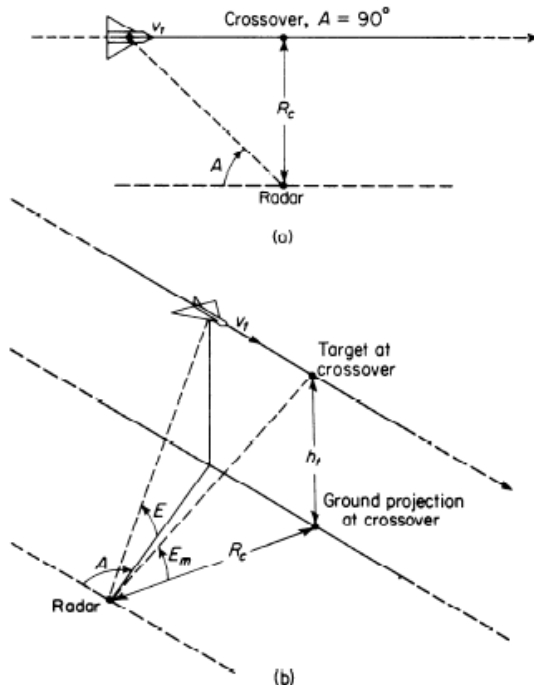


Figure 10.4 Geometry of pass-course problem: (a) ground projection of flight path; and (b) pass course with target in level flight [4, p. 460].

along a path whose closest approach to the radar (the *crossover point*) is at a ground range R_c . The azimuth rate is

$$\omega_{az} = \dot{A} = \frac{v_t}{R} \sin A = \frac{v_t}{R_c} \sin^2 A \quad (10.70)$$

The azimuth acceleration for a constant-velocity target is

$$\dot{\omega}_{az} = 2 \left(\frac{v_t}{R} \right)^2 \sin^3 A \cos A \quad (10.71)$$

To this “geometric” acceleration will be added any component of actual target acceleration normal to the ground projection of the radar-target line. The maximum geometric acceleration occurs at $A = 60^\circ$ and 120° , where

$$\dot{\omega}_{az} = \pm \frac{3\sqrt{3}}{8} \left(\frac{v_t}{R_c} \right)^2 \quad (10.72)$$

For example, a subsonic aircraft flying at a constant velocity $v_t = 300$ m/s along a path with crossover range $R_c = 10$ km will have maximum azimuth rate $\omega_{az} = 0.03$ rad/s at crossover, and maximum acceleration of ± 0.000585 rad/s². A radar with the same servo response assumed in the earlier example would incur lag error components of 0.1 mrad in velocity and 0.026 mrad in acceleration.

Tracking-loop bandwidths of 3 Hz, as in the examples above, are normally available in conical scanning radars as well as in monopulse, so there is no special monopulse advantage in these examples. However, in tracking targets with higher accelerations, such as antiair missiles that may accelerate at $20g = 196$ m/s², the error for $\beta_n = 3$ Hz would be 0.9 mrad at $R = 10$ km. A bandwidth of 9 Hz reduces this to 0.1 mrad, but such bandwidth is not available with the usual conical-scan frequency of 30–60 Hz.

As noted in Section 10.1.9, the servo loop bandwidth is reduced from its design value (available at high S/N ratio) as S/N drops below about 6 dB. The bandwidth reduction causes the output noise to level off as S/N drops below unity, as indicated by (10.47). The dynamic lag component from target velocity, however, varies as $1/\beta_n$, and that from acceleration as $1/\beta_n^2$, or as $(1 + N/S)^4$. The result is loss of track on dynamic targets for $S/N < 0$ dB.

10.4 RADAR-DEPENDENT ERRORS

Table 10.1 listed sources of error that are dependent on the radar design. These are described in [4], and those that are specific to monopulse radars will be discussed here. Stability of the monopulse boresight axis is a major factor in bias error.

10.4.1 Monopulse Network Effects on the Boresight Axis

Boresight errors caused by faulty implementation of the monopulse networks and receivers are discussed in [8, pp. 208–210]. The monopulse comparator, receivers and processor are represented by the block diagram shown in Figure 10.5, where d_1 and d_2 are network errors before and after the comparator.

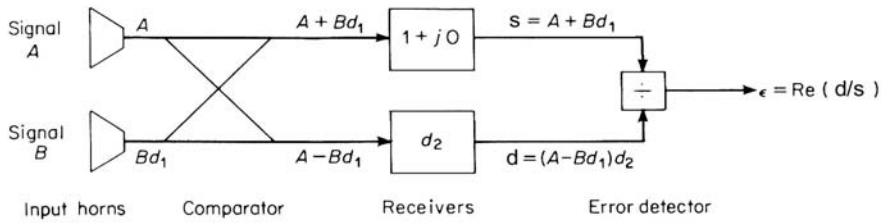


Figure 10.5 Monopulse network error. (After: [8, p. 208].)

The precomparator errors, between the input horns (or array elements) and the comparator, change that portion of the sum-channel response from unity to:

$$d_1 = 1 + a_1 + j\phi_1 \quad (10.73)$$

where a_1 is the amplitude error and ϕ_1 is the phase error in radians, both for convenience assigned to the B signal source. Postcomparator errors, between the comparator and the error detector, change that portion of the difference-channel response from unity to

$$d_2 = 1 + a_2 + j\phi_2 \quad (10.74)$$

where a_2 and ϕ_2 the amplitude and phase errors, assigned to the difference channel. All errors are assumed small relative to unity gain and one radian phase. The comparator is often described in terms of the depth G_n of the monopulse null, defined as

$$G_n \equiv \left| \frac{s}{d} \right|_{\theta=0}^2 \quad (10.75)$$

Figure 10.6 shows the vector voltages s and d formed with precomparator errors.

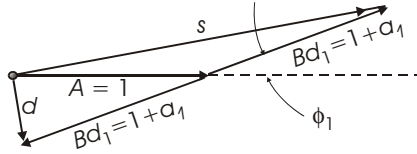


Figure 10.6 Precomparator error effect on monopulse sum and difference signals.

Expressing s and d in terms of signals $A = 1$ and $Bd_1 = (1 + a_1)\angle\phi_1$, we find

$$\begin{aligned}
 G_n &= \left(\frac{s}{d} \right)_{\theta=0}^2 = \left(\frac{A + Bd_1}{A - Bd_1} \right)^2 \\
 &= \frac{1 + (1 + a_1)^2 - 2(1 + a_1)\cos(\phi_1)}{1 + (1 + a_1)^2 - 2(1 + a_1)\cos(\pi - \phi_1)} \approx \frac{4(1 + a_1)}{\sin^2 \phi_1} \approx \frac{4}{\phi_1^2}
 \end{aligned} \tag{10.76}$$

where in the final approximation we set $\cos\phi_1 \approx 1 - (\sin^2\phi_1)/2$ and $\sin\phi \approx \phi$, assuming $\phi \ll 1$, and omit second-order terms containing a_1^2 and $a\sin\phi_1$. A null depth of 35 dB, for example, requires $\phi_1 \leq 0.036 \text{ rad} = 2^\circ$, a requirement that can be met with refined feed design.

The bias error in the normalized monopulse ratio d/s at boresight can be found using the values of d and s from (10.76), and can be expressed as

$$\epsilon_{d/s} = \text{Re} \left(\frac{d}{s} \right)_{\theta=0} = \frac{-a_1}{2} - \frac{a_1 a_2}{2} + \frac{a_1^2}{4} + \frac{\phi_1 \phi_2}{2} + \frac{\phi_1^2}{4} + \dots \tag{10.77}$$

where terms of order higher than two are neglected. From this we can express the error in boresight angle as

$$\epsilon_\theta = \frac{\theta_{bw}}{k_m} \left(\frac{-a_1}{2} - \frac{a_1 a_2}{2} + \frac{a_1^2}{4} + \frac{\phi_1 \phi_2}{2} + \frac{\phi_1^2}{4} + \dots \right) \tag{10.78}$$

The network errors will also change the normalized monopulse slope to a new value given by

$$k_m' = k_m \left(1 + a_2 + \frac{a_1^2}{4} - \phi_1 \phi_2 - \frac{3\phi_1^2}{4} \right) \quad (10.79)$$

Normally the feed system in a mechanically steered radar is adjusted physically to place the RF null at an angle normal to the aperture plane with the receivers carefully adjusted to obtain $a_2 = \phi_2 = 0$. This requires a displacement of the null by the angle

$$\epsilon_{\theta 0} = \frac{\theta_{bw}}{k_m} \left(\frac{-a_1}{2} + \frac{a_1^2}{4} + \frac{\phi_1^2}{4} \right) \quad (10.80)$$

Having made this adjustment, any subsequent shifts in receiver gain or phase will introduce a bias error given by

$$\epsilon_{\theta r} = \epsilon_{\theta} - \epsilon_{\theta 0} = \frac{\theta_{bw}}{k_m} \left(\frac{\phi_1 \phi_2}{2} - \frac{a_1 a_2}{2} \right) = \frac{\theta_{bw}}{k_m} \left(\frac{\phi_2}{\sqrt{G_n}} - \frac{a_1 a_2}{2} \right) \quad (10.81)$$

Keeping in mind that a_2 is the allowable departure from unity of the ratio of the two receiver gains and ϕ_2 is their relative phase, this expression defines the allowable gain and phase tracking tolerances of the receivers for a given boresight error. The tolerance is inversely proportional to the corresponding precomparator error.

Receiver gain and phase tend to vary as a function of signal level, temperature of the receiver enclosure, and power supply voltages. Assuming that the resulting errors vary slowly, randomly and independently during a tracking operation, with rms values σ_{a2} and $\sigma_{\phi 2}$, the rms tracking error is

$$\sigma_{\theta r} = \frac{\theta_{bw}}{2k_m} \left(\sqrt{(\phi_1 \sigma_{\phi 2})^2 + (a_1 \sigma_{a2})^2} \right) \quad (10.82)$$

For example, assume the following antenna and comparator parameters:

- $\theta_{bw} = 20$ mrad;
- $k_m = 1.6$;
- $a_1 = 0.04$;
- $\phi_1 = 0.04$ rad;
- Allowable error $\sigma_{\theta r} = 0.002\theta_{bw} = 0.04$ mrad.

Setting equally strict tolerances on receiver gain and phase, we find $\sigma_{a2} = 0.113$, corresponding to 0.93 dB and $\sigma_{\phi2} = 0.113 \text{ rad} = 6.5^\circ$. Any other combination holding $\sigma_{a2}^2 + \sigma_{\phi2}^2 \leq 0.026$ would suffice.

Depending on the operating conditions and the allowable errors, it may be necessary to incorporate into the receivers a *pilot pulse* control loop. This technique monitors the gain and phase errors by inserting into couplers at the input to the two receivers, at a time outside the target tracking range gate, pulses of equal phase whose equal amplitudes approximate those of the signal being tracked. Output errors are measured and corrected continuously with controlled gain and phase-shift elements.

10.4.2 Boresight Axis Shift with Radar Frequency

If the electrical axis of the radar is stable over long periods of time, the accuracy with which it can be collimated (adjusted to match the mechanical axis) is dependent primarily upon the care and patience that are exercised in calibration. Comparisons of the electrical axis with boresight telescope observations on visible targets can be made over a period of time and over a range of operating conditions such that noise components of error are averaged to very low values. This process is especially accurate if photographic or TV readings are taken from the telescope while a point-source target is being tracked at relatively high elevation angle, where multipath and propagation errors are minimized. The residual errors are caused by drift components that change between calibrations. These can be the result of variation in several operating parameters of the radar and of environmental factors such as uneven heating of the radar components. In a complete error analysis, the variation in position of the axis must be determined as a function of the following:

1. Frequency of operation within the radar band;
2. Tuning of the system (center IF frequency);
3. Phase or gain variations in the receiver;
4. Signal strength;
5. Temperature or intensity of solar (thermal) radiation.

These factors introduce differential gain or phase variations that shift the axis according to (10.77) and (10.82). When these effects are known, it is possible to devise calibration and collimation procedures, and to estimate the errors remaining in the radar output at various times after calibration.

Electrical lengths and mismatches in the RF system change as the radar carrier frequency is tuned over the operating band, introducing precomparator errors as represented by (10.73). For example, consider the experimental curve of Figure 10.7, which represents the shift in position of the null point in the RF difference pattern of the AN/FPS-16 as its operating frequency varies over a 10% band. No RF tuning elements are included in the antenna system, so this error can be re-

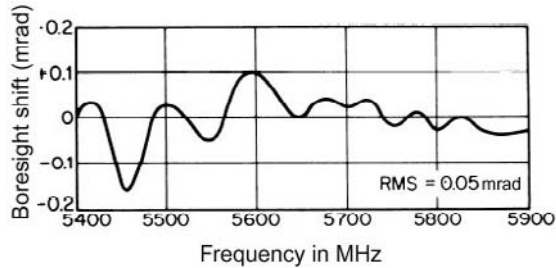


Figure 10.7 Typical boresight shift versus RF tuning [3, p. 537].

duced only by collimation at the frequency to be used, or by applying a calibration curve in data processing. Assuming that many different frequencies are used in the period between collimations, and that no calibrations are applied to correct for the shift, the error can be expressed as the rms value of the curve shown, or about 0.05 mrad. This presumes that the frequency chosen for collimation gives an error near zero.

When the operating frequency is different from that used in collimation, errors ϵ_{el} in elevation and ϵ_{az} in traverse angle will appear. These errors vary slowly with postcomparator gain and phase errors, so over a track they may be represented by their rms values σ_{θ_r} , according to (10.82). The azimuth error ϵ_{az} will be equal to the traverse bias ϵ_{tr} , at low elevation angles, but will increase as the target rises in elevation:

$$\epsilon_{az} = \epsilon_{tr} \sec E \quad (10.83)$$

Although the azimuth error becomes infinite at zenith, the traverse error is constant.

The electrical boresight also varies with phase changes between the IF stages of sum and difference receivers as the downconverted signal at intermediate frequency shifts from that at which the radar was collimated. These receiver errors are represented by (10.74), and illustrated in Figure 10.8, which shows the sensitivity of the AN/FPS-16 radar to IF excursions (tuning error). Assuming that collimation is done with the system properly tuned, the shift in the tracking axis may be estimated for any operating condition that leads to tuning error by assigning to the tuning error a probability distribution and calculating the rms value of the corresponding error from this figure. The tuning error may arise from Doppler shift, drift in the transmitting frequency of a beacon, or uncorrected drifts in the radar oscillators.

Expressing the curve for boresight error as a function of IF frequency, $\Delta(f_{IF})$, the rms error can be found by assuming that the tuning error is normally distributed with a standard deviation σ_{IF} . The rms boresight error is then

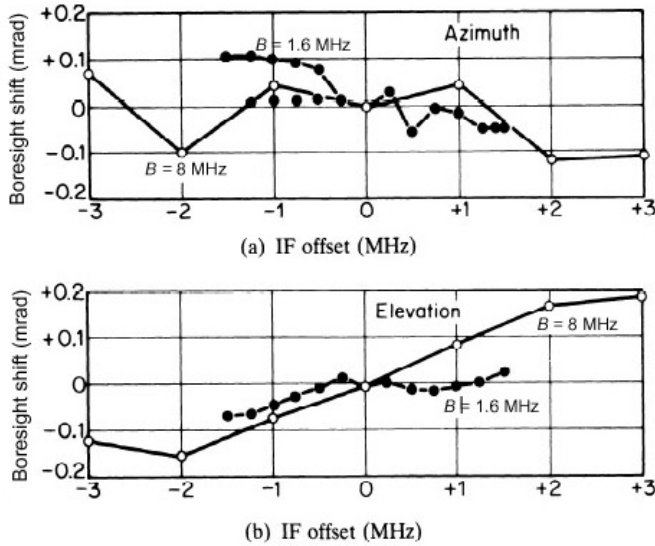


Figure 10.8 (a,b) Typical boresight shift versus IF tuning [3, p. 538].

$$\sigma_{\theta IF} = \sqrt{\frac{1}{2\pi\sigma_{IF}} \int_B \Delta_{IF}^2 \exp\left(-\frac{f^2}{2\sigma_{IF}^2}\right) df} \quad (10.84)$$

10.4.3 Polarization Effects

Antennas are designed to respond to input waves having a particular polarization (e.g., vertical), and there is always one orthogonal polarization (or cross-polarization) for the antenna (e.g., horizontal). The antenna patterns for a cross-polarized input will differ from those for the intended polarization, and targets that scatter both polarizations when illuminated by the radar transmission will generate spurious responses at the antenna output.

Cross-polarized responses of a reflector antenna, known as Condon lobes, are an inherent result of curvature of the reflector, and increase with decreased f/D ratio. Cross-polarized response in a circular array results primarily from interaction of edge currents with elements on the periphery, but it can also be caused in any array by imperfect construction or orientation of elements themselves. Figure 10.9 shows typical s and d voltage patterns for the intended polarization, and s_c and d_c for the cross-polarization.

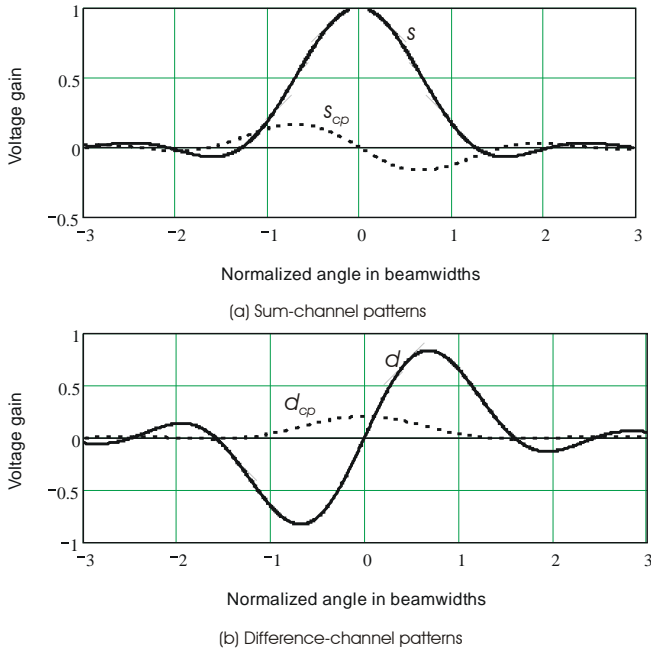


Figure 10.9 (a, b) Monopulse patterns for intended and orthogonal (cross) polarizations [9, p. 405].

The normalized monopulse output for a target near the axis, in the presence of a cross-polarized component, is

$$\frac{d'}{s'} = \frac{ed + e_{cp}d_{cp}}{es + e_{cp}s_{cp}} \approx \frac{d}{s} + \frac{d_{cp}}{s} \sqrt{\frac{\sigma_{cp}}{\sigma}} = \frac{d}{s} + \epsilon_{cp} \quad (10.85)$$

where $e = k\sqrt{\sigma}$ is the target field scattered at the intended polarization, σ is the radar cross section of the target, k is a constant, $e_{cp} = k\sqrt{\sigma_{cp}}$ is the cross-polarized field for cross-polarized cross section σ_{cp} , and ϵ_{cp} is the error caused by cross-polarization. The polarization interference component in the d channel is $I_{cp} = \sigma_{cp}d_{cp}^2$, and the rms error, for σ_{cp} having random phase relative to σ , is

$$\sigma_{\theta} = \frac{\theta_{bw} d_{cp} / s}{k_m \sqrt{2\sigma/\sigma_{cp}}} \quad (10.86)$$

The cross-polarized target cross section for many targets averages about -6 dB relative to the intended polarization. Then, for a cross-polarized difference-pattern response -30 dB relative to the sum-pattern response at the intended polarization, ($d_{cp}/s = 0.032$) and $k_m = 1.6$, we find

$$\sigma_\theta = \frac{\theta_{bw} \times 0.032}{1.6\sqrt{8}} = 0.007\theta_{bw}$$

When higher tracking precision is required on a target with typical cross-polarized RCS, the cross-polarized response of the antenna must be reduced below -30 dB.

10.5 TARGET-DEPENDENT NOISE ERRORS

10.5.1 Glint Error

Glint is defined [10] as

The inherent component of error in measurement of position and/or Doppler frequency of a complex target due to interference of the reflection from different elements of the target. *Notes:* 1. Glint may have peak values beyond the target extent in the measured coordinate. 2. Not to be confused with scintillation error.

Since it is inherent in the target, glint affects all types of angle measurement systems, including monopulse. It will be discussed here because it bears on the choice of normalization method and time constant used in monopulse systems.

The glint from a two-element source was discussed in Sections 5.2.4 and 5.2.5. The target consisting of two equal point sources is a special case not often encountered in practical radar applications. The more general case of multiple fluctuating sources has been analyzed in [11]. Let ϵ be the glint, normalized to one-half the target span L in the plane of measurement. The glint is described by a Student distribution with two degrees of freedom

$$W(\epsilon) = \frac{\mu}{2(1 + \mu^2 \epsilon^2)^{3/2}} \quad (10.87)$$

where μ is a parameter measuring the concentration of target scatterers about the centroid. The minimum value $\mu = 1$ applies to the two-point target, where all scattered energy comes from the extremities of the target. Larger values of μ characterize targets with scatterers more narrowly distributed about the centroid, as shown by solid curves in Figure 10.10.

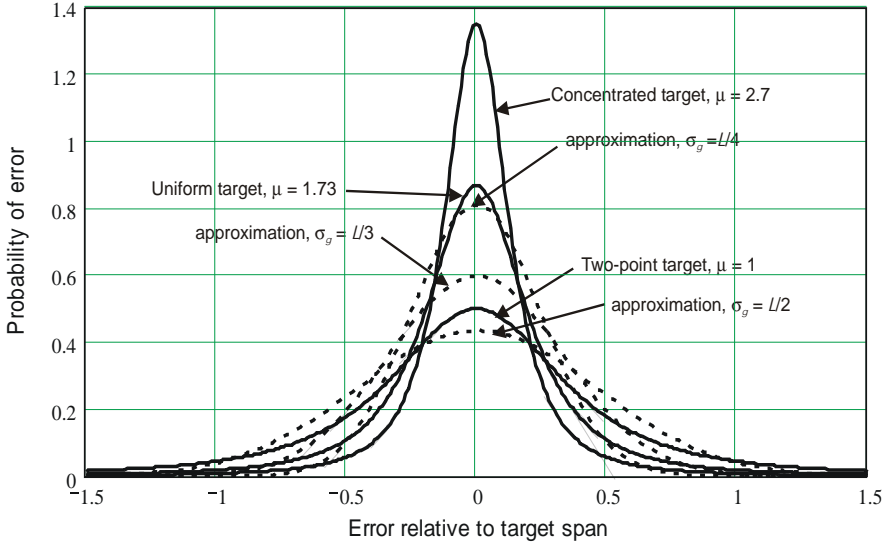


Figure 10.10 Distributions of glint for different degrees of scatterer concentration [11, p. 100].

The variance of the Student distribution is infinite, and observations of actual targets show large spikes in the monopulse output corresponding to minima of the sum-channel signal amplitude s . The probability that the measured position lies beyond the target span can be matched by a normal distribution with a standard deviation σ_g expressed as some fraction of the target span L . Approximations are shown as dashed lines in the figure, showing standard deviations between $\sigma_g = 0.25L$ (for a concentrated target, $\mu = 2.7$), $\sigma_g = 0.33L$ (for uniform scatterer distribution, $\mu = \sqrt{3}$), and $\sigma_g = 0.5L$ (for a two-point target, $\mu = 1$).

The error expressed in terms of the target span L may be converted to an angle error σ_{θ_g} in radians, for a target at range R , using

$$\sigma_{\theta_g} = \frac{\sigma_g}{R} \quad (10.88)$$

where σ_g and R are in the same units.

The single-pulse glint error in practical monopulse systems can be limited or reduced using any of the following methods, all but (1) requiring multiple pulses:

1. Saturation in the normalization or processing circuits;
2. Normalization of the difference signal d with respect to a sum signal \bar{s} averaged over several pulses (e.g., slow AGC);
3. Averaging the monopulse ratio d/s over several pulses;

4. Selecting the monopulse outputs having the largest values of s ;
5. Combining 3 or 4 with pulse-to-pulse frequency agility.

Results of options 2 and 3 depend on the spectrum of the glint and the averaging time used. A typical glint spectrum is given in [12]:

$$N(f) = \sigma_{\theta_g}^2 \frac{2B_n}{\pi(B_n^2 + f^2)} \quad (10.89)$$

where $N(f)$ is the power density per Hz, σ_{θ_g} is the rms angular glint error, B_n is the noise bandwidth of the spectrum, and f is frequency (both in Hz). Values of B_n at X-band are given as 1 Hz for small aircraft and 2.5 Hz for larger aircraft. Spectra for the two bandwidths are shown in Figure 10.11.

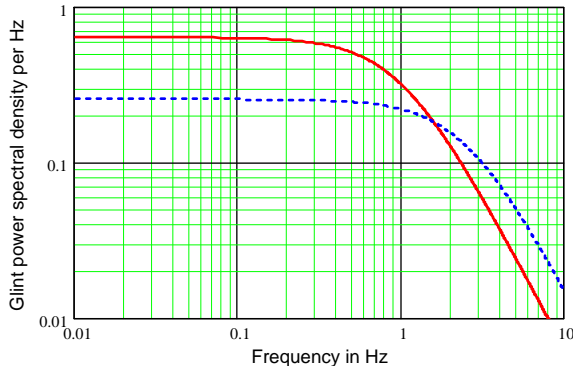


Figure 10.11 Typical glint spectra for aircraft observed at X-band: $B_n = 1$ Hz (solid line), $B_n = 2.5$ Hz (dashed line).

Averaging the sum signal before normalization, method 2, has been shown to reduce thermal noise error on fluctuating targets (see Section 10.1.8), by avoiding deep minima in the denominator of the monopulse ratio $(d + n_d)/(s + n_s)$ that cause spikes to appear in the output. A similar advantage is obtained with regard to glint error and high S/N ratio when d/\bar{s} is used in tracking fluctuating targets.

Considering the 6.4-Hz noise bandwidth of the servo whose open-loop transfer functions were shown in Figure 10.1, little smoothing reduction of glint would be available. Reducing that bandwidth to $\beta_n = 1$ Hz would reduce the glint error by a factor of two, at the risk of increased dynamic lag error.

In [13] it was found that option 4 combined with frequency agility gave the lowest error, with σ_{θ_g} varying as $1/n$ for $1 \leq n \leq 4$ and with only small reductions for additional pulses.

Disadvantages accompany each of the glint-reduction options listed above. The nonlinear operation inherent in 1 can cause bias errors, since the positive and negative spikes that occur with low s do not necessarily have the same shape and duration. Averaging in 2 and 3, or selection of one or a few widely-separated pulses in 4 reduces the ability of the monopulse system to maintain a constant error slope on fluctuating targets, producing scintillation error when the tracking axis lags the position of a fast-moving target (see Section 10.5.2). The selection of the best process for controlling glint depends on the radar and target parameters and the radar application.

10.5.2 Scintillation Error

The term *scintillation* is applied in the radar context to the fluctuations of target amplitude that cause errors in tracking or measurement. The *scintillation error* is defined [10] as

Error in radar-derived target position or Doppler frequency caused by interaction of the scintillation spectrum with frequencies used in sequential measurement techniques *Note:* Not to be confused with glint.

This definition describes the first component of scintillation error discussed in [3, pp. 289–290], where scintillation components at frequencies near the lobing frequency introduce error in sequential lobing systems. The definition omits a second error component that appears in both sequential scan and monopulse tracking, as presented in [12, 14]. This second component results from scintillation components within the bandwidth of the servo that modulate the off-axis error voltage on targets whose dynamics cause the track to lag the target. It is analyzed in detail in [3, pp. 290–293].

The scintillation power spectrum for a typical aircraft target is [14]:

$$A^2(f) = \frac{0.12B}{B^2 + f^2} \quad (10.90)$$

where $A^2(f)$ is the spectral density in (fractional modulation)²/Hz, B is the half-power bandwidth, and f is frequency in Hz. Values of B vary from 1.0 Hz to 2.5 Hz, larger values applying to targets with scatterers widely spread over the target span. The fractional modulation, found as the square root of the integral of (10.90) over all frequencies, is 0.43 times the mean echo signal voltage.

The object of the AGC is to suppress the target scintillation spectrum $A(f)$ over the response band of the servo. That suppression is described by the *scintillation error factor* $Y_s(f)$, defined as the ratio of signal scintillation voltage spectrum after AGC relative to that of the target scintillation at the receiver input. This factor can be written in terms of the open-loop AGC response Y_a and the closed-loop servo response Y_c :

$$Y_s(f) = \frac{Y_c(f)}{|1 + Y_a(f)|} \quad (10.91)$$

The voltage spectrum of the scintillation at the receiver output is then

$$A_o(f) = A(f)Y_s(f) \quad (10.92)$$

The resulting scintillation power is the integral of scintillation output power spectrum

$$\sigma_s^2 = \int_0^\infty A_o^2(f) df = \int_0^\infty A^2(f) Y_s^2(f) df \quad (10.93)$$

The rms scintillation error in angle is the product of the rms output scintillation voltage and the off-axis error Δ_θ :

$$\sigma_{\theta s} = \sigma_s \Delta_\theta \quad (10.94)$$

Use of a normalization such as AGC with a time constant longer than the servo time constant ($Y_s = 1$) allows the full scintillation spectrum to modulate the lag error. Thus $\sigma_s \approx 0.4\Delta_\theta$ for a servo bandwidth greater than the scintillation bandwidth, $\beta_n > B$.

As the AGC time constant is reduced to approach the pulse repetition interval (fast AGC), the scintillation error factor Y_s is reduced, allowing only a fraction of the target scintillation to modulate the lag error and thereby reducing the scintillation error. With instantaneous (single-pulse) normalization and high S/N the output signal s from the receiver is held constant ($Y_s = 0$ over the servo bandwidth) and the scintillation error disappears.

The interaction of AGC response with tracking error is analyzed using the transfer functions of the AGC and servo loops, illustrated in Figures 10.12 and 10.13, for slow and fast AGC systems. In each part of the figures, the input and output scintillation spectra are plotted along with the functions Y_a , Y_c , and Y_s as defined above.

The slow and fast AGC systems have noise bandwidths of 2 Hz and 8 Hz respectively. The slow AGC open-loop gain falls through 0 dB at 1.3 Hz, and is unable to suppress the scintillation components at the upper end of the servo bandwidth, allowing the output to rise slightly above the input spectrum in that region. The output scintillation voltage for slow AGC is 0.32 (reduced only slightly from the value 0.41 for input scintillation within the servo bandwidth). The fast AGC

open-loop gain falls through 0 dB at 5 Hz, and is more successful, reducing the output scintillation voltage to 0.16.

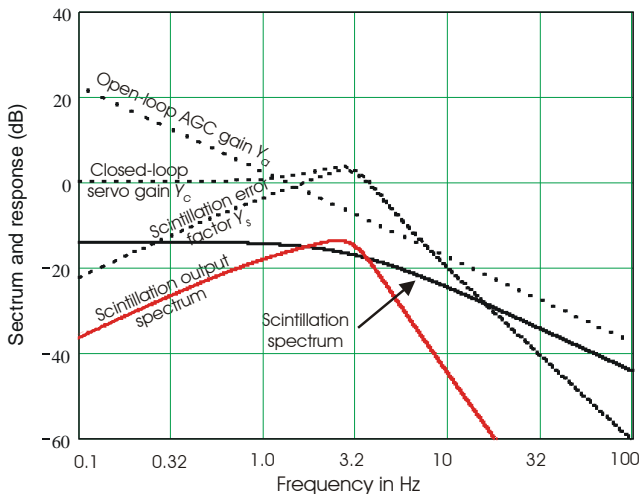


Figure 10.12 Frequency response of AGC and servo loop, scintillation spectra and scintillation error factor, versus frequency, for slow (2-Hz) AGC system.

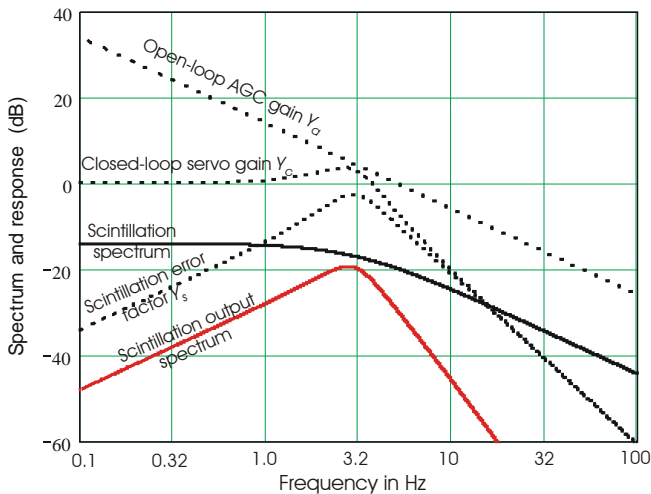


Figure 10.13 Frequency response of AGC and servo loop, scintillation spectra and scintillation error factor, versus frequency, for fast (8-Hz) AGC system.

References

- [1] I. Kanter, "Varieties of Monopulse Responses to Multiple Targets," *IEEE Trans. on Aerospace and Electronic Systems*, Vol. AES-17, No. 1, January 1981, pp. 25–28.
- [2] I. Kanter, "The Probability Density Function of the Monopulse Ratio for N Looks at a Combination of Constant and Rayleigh Targets," *IEEE Trans. on Information Theory*, Vol. IT-23, No. 5, September 1977, pp. 643–648.
- [3] D. K. Barton, *Radar System Analysis*, Englewood Cliffs, NJ: Prentice-Hall, 1964; reprint, Dedham, MA: Artech House, 1976.
- [4] D. K. Barton, *Modern Radar System Analysis*, Norwood, MA: Artech House, 1988.
- [5] P. Swerling, "Probability of Detection for Fluctuating Targets, *RAND Corp Res Memo RM-1217*, March 17, 1954; reprinted: *IRE Trans. on Information Theory*, Vol. IT-6, No. 2, April 1960, 269–308; reprinted: *Detection and Estimation*, S. S. Haykin, (ed.), Stroudsburg, PA: Halstad Press, 1976, 122–158.
- [6] T. E. Connolly, "Statistical Prediction of Monopulse Errors for Fluctuating Targets," *IEEE International Conf. Radar-80*, Washington, D.C., April 28–30, 1980, pp. 458–463.
- [7] I. Kanter, "Multiple Gaussian Targets: The Track-on-Jam Problem," *IEEE Trans. on Aerospace and Electronic Systems*, Vol. AES-13, No. 6, November 1977, pp. 620–623.
- [8] D. K. Barton and H. R. Ward, *Handbook of Radar Measurement*, Englewood Cliffs, NJ: Prentice-Hall, 1969. Reprint, Dedham, MA: Artech House, 1984.
- [9] D. K. Barton, *Radar System Analysis and Modeling*, Norwood, MA: Artech House, 2005.
- [10] IEEE Standard 100, *The Authoritative Dictionary of Standard Terms*, 7th ed., New York: IEEE Press, 2000.
- [11] R. V. Ostrovityanov and F. A. Basalov, *Statistical Theory of Extended Radar Targets*, Dedham, MA: Artech House, 1985.
- [12] J. H. Dunn and D. D. Howard, "The Effects of Automatic Gain Control Performance on the Tracking Accuracy of Monopulse Radar Systems," *Proc. IRE*, Vol. 47, No. 3, March 1959, pp. 430–435.
- [13] J. M. Loomis and E. R. Graf, "Frequency-Agile Processing to Reduce Radar Glint Pointing Error," *IEEE Trans. on Aerospace and Electronic Systems*, Vol. AES-10, No. 6, November 1974, pp. 811–820.
- [14] D. D. Howard, "Tracking Radar," Chapter 9 in *Radar Handbook*, 3rd ed., M. I. Skolnik, (ed. in chief), New York: McGraw-Hill, 2008.

Chapter 11

Multipath

Multipath is defined [1, p. 714] as the propagation of a wave from one point to another by more than one path. When multipath occurs in radar, it usually consists of a direct path and one or more indirect paths by reflection from the surface of the Earth (land or sea) or from large man-made structures. At frequencies below 40 MHz it may also include more than one path through the ionosphere.

If the reflection surface is flat or smoothly rounded, the multipath is *specular* (mirror-like); if the surface is irregular, the multipath is *diffuse*. When the mean contour of the surface is smooth but the surface is perturbed by small-scale irregularities, both specular and diffuse components (also called the coherent and incoherent components respectively) are present.

If, as is usually the case with low-angle targets over a reflecting surface, there is not enough separation in angle, range, or Doppler to resolve the direct and reflected wave, then specular multipath is equivalent to a special case of unresolved targets, and much of the analysis in Chapter 9 is applicable. In the case of multipath, however, the “targets” are not independent but are related according to the geometry and electrical characteristics of the reflecting surface.

Specular multipath causes erratic elevation tracking (which sometimes includes complete loss of track) at target elevations within a beamwidth of the horizon, and causes significant elevation error even at target elevations a few beamwidths above the horizon. The theory is well known and has been confirmed by a large amount of experimental and operational data. The effects are deterministic in the sense that if the pertinent radar characteristics, reflection-surface characteristics, and multipath geometry are specified, the results can be computed. Results can also be expressed statistically (e.g., in the form of rms error) if they are to apply to a specified range of conditions or if the parameters cannot be specified exactly.

Diffuse multipath effects are somewhat noise-like (although they are correlated over many successive pulses) and can be treated only statistically, since they

are caused by irregularities over the entire surface, the exact contour of which is unknown and can vary unpredictably with time (as in the case of waves on water or wind-swept vegetation on land). Since the 1970s much serious attention has been devoted to the theoretical analysis of diffuse multipath as it affects radar. The major work on this subject by Beckmann and Spizzichino [2] has been extended [3, 4] to develop a theoretical model that can be used as a basis for calculating the errors. The difficulty of the analysis has necessitated some approximations. Experimental confirmation is also difficult. The data available appear consistent with the models, although not conclusive. It is known, however, that although diffuse multipath can be a significant item in the error budget, it is not serious enough to disrupt tracking. Its main effect is in elevation but it also causes a slight error in azimuth (as well as errors in range and Doppler that are not considered here). Diffuse multipath will be discussed in Section 11.14.

Multipath effects are not limited to monopulse but are similar in all angle-measuring and tracking techniques.¹ However, the method of analysis, the quantitative results, and possible remedies differ somewhat. The discussion that follows applies specifically to monopulse.

11.1 FLAT-EARTH SPECULAR MODEL

We will first consider specular reflection from the surface of the Earth and will assume initially that the surface is flat and horizontal. The geometry is shown in Figure 11.1. The distance to the target is assumed to be so great that the rays from the target to the radar and from the target to the point of reflection² on the surface can be considered parallel. The reflected ray reaching the radar is equivalent to a ray from the image, which is below the surface at a location symmetrical to that of the target.

Let E and E_0 be the elevation angles (measured from horizontal) of the target and the beam axis respectively. Because of errors caused by multipath, E and E_0 will generally not be equal. The elevation angle of the image is $-E$.

The flat-Earth model gives a reasonable approximation over water or over flat, level land surfaces when the reflection point is not too far from the radar. In cases where Earth's curvature must be taken into account, the monopulse aspect of the analysis is basically the same but the surface reflection coefficient may be reduced by a divergence factor (convex-mirror effect) [5] and the geometry becomes somewhat more complicated. Finite target distance (rays not parallel) may also have to be taken into account; this complicates the geometry only slightly.

¹ Multipath also produces analogous effects in range and Doppler, but here we are concerned only with angle.

² The reflection is from the entire surface but can be treated by geometric optics as if it were from a single point.

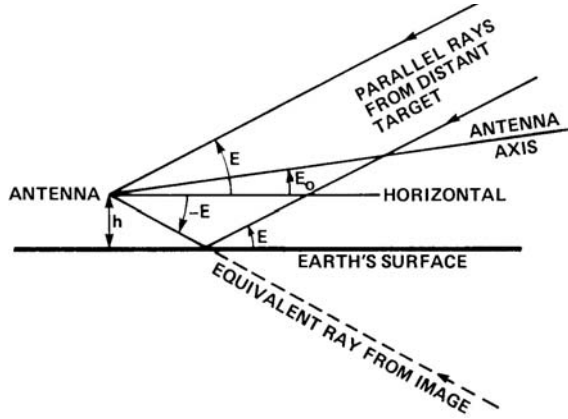


Figure 11.1 Geometry of target and image, flat-Earth approximation.

To relate the multipath problem to that of two unresolved targets treated in Chapter 9, we use the same symbols θ_a and θ_b to represent the angles of the target and the image respectively relative to the beam axis. Then

$$\theta_a = E - E_0 \quad (11.1)$$

$$\theta_b = -E - E_0 \quad (11.2)$$

Substitution of these equations into (9.8b) gives the complex indicated angle:

$$\theta_i = -E_0 + E \frac{1 - pe^{j\phi}}{1 + pe^{j\phi}} \quad (11.3)$$

of which the real and imaginary parts are

$$x = \text{Re}(\theta_i) = -E_0 + E \frac{1 - p^2}{1 + 2p \cos \phi + p^2} \quad (11.4)$$

$$y = \text{Im}(\theta_i) = -E \frac{2p \sin \phi}{1 + 2p \cos \phi + p^2} \quad (11.5)$$

Recall from the definitions under (9.7) that p , the amplitude ratio of the reflected signal to the direct signal, is the product of g and r , where g is the ratio of antenna sum-pattern voltage gain in the direction of the image to that in the direction of the target, and r is the ratio of voltage coefficients of the image and the

target. The voltage ratio g is a function of E and E_0 . The image-to-target amplitude ratio r is equal to the magnitude of the surface reflection coefficient provided the target scatters isotropically; the value of r is between 0 and 1. Most physical targets are not isotropic scatterers, but they can usually be assumed to be isotropic over the small differential angle between the direct ray and the reflected ray leaving the target.³ On this assumption, r is a function of E only.

The relative phase ϕ has two components:

$$\phi = \phi_s + \phi_p \quad (11.6)$$

where ϕ_s is the phase of the surface reflection coefficient and ϕ_p is due to the geometric path-length difference between the direct and reflected rays. From Figure 11.1 it is seen that

$$\phi_p = -4\pi(h_a/\lambda)\sin E \quad (11.7)$$

where h_a is the height of the phase center of the antenna above the surface and λ is the wavelength. Both ϕ_s and ϕ_p are functions of E alone. If the antenna sum pattern has an appreciable phase variation as a function of angle, this may also contribute to the relative phase ϕ , but this contribution is usually small and will be ignored.

The ratio of the reflected field strength to that reaching the surface from the target is given by the magnitude ρ_0 of the Fresnel reflection coefficient (Figure 11.2), which is a function of the complex dielectric constant of the surface and the wavelength, polarization, and grazing angle of the incident ray [2–5]. At grazing angles below 10° , ρ_0 is lower for vertical polarization than for horizontal, and most tracking radars are vertically polarized to minimize multipath error. At a grazing angle known as the pseudo-Brewster angle, between 6° and 25° depending on the surface material, the magnitude of ρ_0 reaches a minimum value that is near zero for microwaves. The reflections are small enough, within a small sector about this angle, to have minimal effect on tracking. For narrow-beam radars, however, the most serious multipath errors occur below this sector. Grazing angles typically used in examples of multipath errors are near 1° , at which angle Figure 11.2 shows that $\rho_0 \geq 0.75$ for all surface types and polarizations.

The specularly reflected multipath component r is the product of ρ_0 and a *specular scattering factor* ρ_s :

$$r = \rho_0 \rho_s \quad (11.8)$$

³ However, the instantaneous reflected signal can occasionally exceed the direct signal (that is, $r > 1$) because the target (or radiating source) is not perfectly isotropic or because of diffuse reflection components adding to the specular.

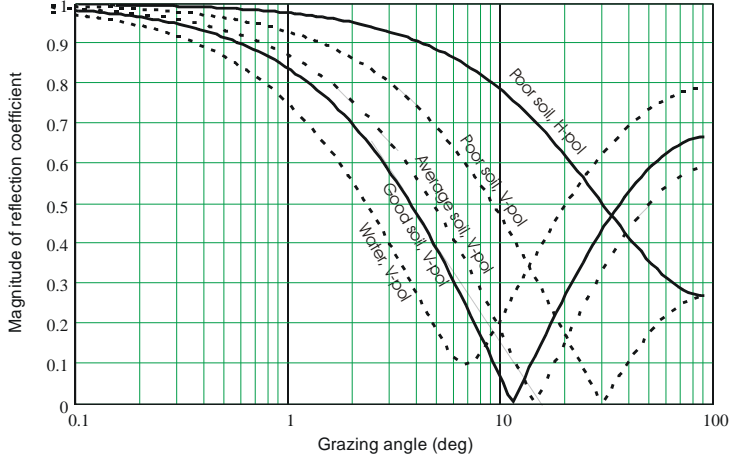


Figure 11.2 Magnitude of Fresnel reflection coefficient ρ_0 versus grazing angle.

where the latter has been derived [2, 6] on the basis of a simplified model having a Gaussian distribution of surface height and negligible shadowing:

$$\rho_s = \exp \left[-2 \left(\frac{2\pi\sigma_h \sin \psi}{\lambda} \right)^2 \right] \quad (11.9)$$

Here σ_h is the standard deviation of surface height, ψ is the grazing angle, and λ is the electromagnetic wavelength. For the geometric model considered here, namely a flat horizontal surface and a target at infinite distance, the grazing angle equals the target elevation angle E . When this model is not adequate (for example, when Earth's curvature must be taken into account), the two angles differ.

Experimental measurements of specular reflection from a rough surface show reasonable agreement with (11.8) and (11.9). As the grazing angle approaches zero, both ρ_0 and ρ_s approach unity and the phase of the reflection coefficient approaches 180° , for all polarizations. These values are often used in worst-case analyses of specular multipath at very low angles.

Since the target and the image are at the same azimuth angle and at elevation angles of E and $-E$, respectively, they are also at the same traverse angle, according to (2.25). Even when the image elevation is not exactly $-E$ (because of Earth's curvature, for example), the cosines of E and $-E$ are so close to unity at small angles that for practical purposes the traverse angles of the target and image can be considered equal. Therefore, in (9.8c), $\Delta\theta = 0$ and the indicated traverse angle equals the target traverse angle, unaffected by multipath. This is not true, how-

ever, if the radar is on a tilted platform such as the deck of a ship or if it is situated over a land surface that has a cross-range component of slope. Because of geometric coupling in that case, multipath will have some effect on traverse as well as elevation. Traverse-elevation “cross-talk” in the radar antenna or circuitry may also contribute to traverse error due to multipath. Additional causes of traverse multipath error are irregularities in the surface and diffraction of reflection from trees or from the sides of man-made structures in the vicinity of the radar.

11.2 EFFECT ON DETECTION

In addition to its effect on angle measurement, multipath has a well known effect on detection [5]. Figure 11.3 illustrates the effect of multipath on typical monopulse sum voltage in elevation. Since such a pattern typically has a beamwidth of a few degrees at most (less than 1° in some cases), the vertical scale of the figure has been expanded for clarity. The lobing is due to interference between the direct and reflected waves, which are alternately in phase and out of phase as the elevation varies. In the horizontal direction there is a null because the target and the image have the same elevation, the same amplitude, and 180° relative phase. The ratio of the free-space beamwidth to the multipath lobe spacing (that is, the number of lobes within the free-space beamwidth) is approximately equal to twice the height of the antenna phase center above the reflecting surface divided by the diameter (or vertical dimension) of the antenna. In Figure 11.3 there are about five lobes within the half-power beamwidth; therefore the antenna phase-center height must be about 2.5 times its diameter.

The difference pattern also has an interference lobing structure due to multipath. This affects the elevation angle measurements (which depend on the complex ratio of the difference to the sum) but does not affect detection.

The effect of multipath on detection is not of primary interest in connection with monopulse but it does have indirect relevance. First of all, it is necessary to detect a target in order to track it or measure its angular location. Second, when the target is in or near a null its sum-channel signal strength is low and this means

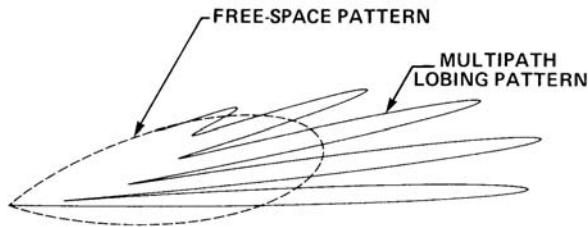


Figure 11.3 Effect of multipath on sum pattern.

a large error in elevation measurement due to thermal noise, although this is likely to be overshadowed by the error due to the unresolved-target effect.

11.3 EFFECT ON CLOSED-LOOP ELEVATION TRACKING

A closed-loop tracker attempts to point the beam in a direction that nulls the real part of the indicated angle. The effect of multipath on closed-loop tracking is the same as that of two unresolved targets, discussed in Section 9.16. Motion of the beam from an off-null direction toward the null direction changes the amplitude ratio of the target and image. Therefore the null direction is generally not the same as the direction indicated by the open-loop monopulse output when the beam is pointed off null.

To calculate the tracking equilibrium direction (i.e., the null direction) for a given target elevation angle requires an iterative solution using knowledge of the antenna height, the antenna patterns, the monopulse processor characteristics, and the amplitude and phase of the surface reflection coefficient. Depending on the conditions, there may be one stable equilibrium direction or there may be two (not counting possible equilibrium directions in the sidelobes). If there are two stable equilibrium directions, there is an unstable equilibrium direction between them. At an unstable point the monopulse response curve passes the zero axis with a slope of the wrong sign, which drives the beam away from the null rather than toward it.

Figure 11.4 illustrates the problem of closed-loop elevation tracking in multipath. A flat earth was assumed and an analytical model of typical sum and difference patterns was used in the calculations. An exact monopulse processor (as defined in Section 8.4) was assumed. The reflection coefficient is unity at 0° target elevation and decreases with increasing elevation angle.

Plotted horizontally is the true elevation angle of the target. Plotted vertically is the null direction, which is the same as the beam pointing direction if the target varied slowly enough to allow the servo loop to reach equilibrium at each point. The upper dashed line at 45° is the direction in which the beam would point if the image were absent and the lower dashed line is the corresponding direction if the image were present without the target.

In the upper half of the curve (the part above zero elevation) the radar is tracking the target, with perturbations caused by the image. The upper peaks occur when the target and image signals are in phase opposition. The lower peaks occur when they are in phase. The variation in relative phase is due mainly to path-length difference as a function of elevation angle, and to a lesser extent to variation of the phase of the reflection coefficient as a function of grazing angle.

The lower part of the figure, consisting of a series of disjointed closed curves, shows the locus of a pair of other null directions. The solid portion of each loop is stable and is due to tracking of the image, with perturbations by the target, rather

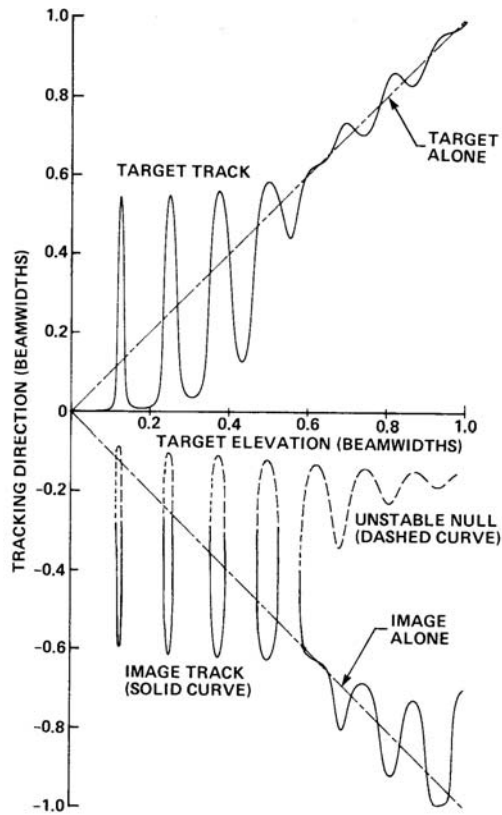


Figure 11.4 Closed-loop tracking in multipath.

than vice versa. The dotted portion of each curve is unstable; if the antenna were pointed in that direction, a slight deflection would cause it to move toward one of the stable null directions. In analyzing radar tracking behavior against a target flying at a specified constant altitude, it is sometimes useful to plot the null directions as functions of target range rather than elevation angle [7]. If the target is approaching or receding at a specified constant speed, the horizontal scale can also be expressed in terms of time, so that the dynamic behavior can be analyzed.

Consider a radar with a mechanically steered antenna tracking a target that is approaching at a constant low altitude. The target elevation angle is near zero at long range and it increases as the target approaches. The oscillations in the beam-pointing direction sometimes become quite violent, and the inertia of the antenna can carry it from the upper stable direction to the lower one, if a lower stable null exists at the moment. This phenomenon, known as “nose-diving,” has often been

observed in practice. The track may then transfer back to the upper null or it may be lost altogether.

Figure 11.5 illustrates the multipath phenomenon in another way, for the same set of conditions used in plotting Figure 11.4. With the target elevation held constant, the open-loop monopulse output (real part) is plotted versus beam elevation angle. Curves are plotted for several values of target elevation angle in the vicinity of the second peak in Figure 11.4 to demonstrate the sensitivity to relative phase in the vicinity of 180° . If the loop is closed, the downward closings of the zero axis are stable tracking directions, and the upward crossings, where they exist, are unstable nulls. The slopes are the opposite of those shown in earlier chapters because the beam axis elevation is varying while target elevation is constant, rather than vice versa. Comparison of Figures 11.4 and 11.5 shows why there are two stable tracking directions for some target elevations and only one for others.

The nulls that have a slope of the correct sign are stable in the sense that a displacement of the beam axis from the null produces a restoring force toward the null. The servo response, however, is generally not the same as it is for a single target without multipath. The forward gain is proportional to the slope of the zero crossing; this slope can be higher or lower than the normal single-target slope, shown by the dashed line in Figure 11.5. The closed-loop tracking performance

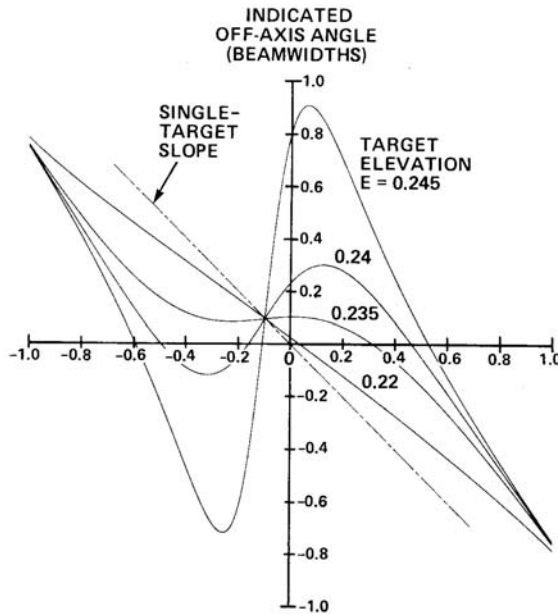


Figure 11.5 Open-loop indicated off-axis angle versus beam elevation angle for fixed values of target elevation angle.

will vary accordingly. Referring to Figure 10.3, the open-loop frequency response of the servo is designed to have a region of 6-dB/octave slope extending for at least one, and preferably two octaves, each side of the unity-gain point. This preserves stability of the closed-loop operation by providing an adequate margin from the prohibited 180° phase shift at unity gain. If the open-loop gain varies by more than a factor of two above or below its design value, as a result of varying monopulse response slope, the servo approaches instability and tends to oscillate at a frequency near that at which the response crosses unity gain. This can lead to loss of track on low-angle targets above a reflecting surface.

The closed-loop tracking behavior shown in Figure 11.4 is intended only for illustration, since it is based on a particular set of conditions and some simplifying assumptions. The behavior of a specific radar (e.g., the amplitudes and spacing of the oscillations) will of course depend on the characteristics and geometry of the radar, the reflecting surface, and the target. For a more refined analysis it is usually necessary to take Earth's curvature into account unless the reflection point is close to the radar. Not only the sum and difference patterns of the antenna but also the type of monopulse processor used may have a decided effect. A more subtle factor is that the sum and difference signals for a point target in the clear are not exactly in phase as assumed, either because of the inherent characteristics of the feed [8] or because of imbalance in transmission lines and receivers. Even a small phase difference can cause the actual behavior to differ from the theoretical [9], because it couples a portion of the imaginary part of the monopulse output (which can be quite large) into the real part.

Although the computations for Figure 11.5 omit these complicating factors, and are based on only one particular set of parameters, it has been amply confirmed by experiments and actual operation that the oscillatory behavior exhibited in the figure is at least qualitatively typical and that it seriously degrades or prevents normal tracking of low-angle targets in multipath. Even at target elevation angles up to a few beamwidths above the horizon, multipath constitutes a significant item in the system error budget, but only within a beamwidth of the horizon does it become severe enough to disrupt tracking.

11.4 TYPES OF MULTIPATH REMEDIES

A number of remedial techniques have been developed or proposed to alleviate the low-angle tracking problem, some of which will be described in this chapter. Additional discussions of the various techniques are available elsewhere [3, 8, 10, 11], with summaries of their advantages and limitations and estimates of their accuracies and of the lowest angles at which they can operate.

The various remedies differ in the degree of sophistication, in the types of applications to which they are suited, and in effectiveness. They are not necessarily mutually exclusive; some of them can be used in combination. No technique

yields the same elevation accuracy that is attainable in the absence of multipath, but the errors can be reduced and tracking can be extended to a lower angle than would be possible otherwise.

Some of the techniques do not attack the multipath problem directly, but by selection of the radar design or operating parameters such as beamwidth, sidelobe level, polarization, or servo bandwidth, they attempt to mitigate the effects of multipath while continuing to operate in a normal mode. Other techniques require special modes of operation such as a “low-E mode,” designed to reduce multipath errors, but they still base their elevation estimates or tracking on the assumption that only one target (without multipath) is present. The most sophisticated techniques do not merely treat multipath as a disturbance but actually take it into account in their tracking loops or in their open-loop calibration functions; if the multipath conformed exactly to the model on which each such technique is based (i.e., pure specular reflection), there would be no multipath error.

In the Sections 11.5–11.13, only the effects of specular multipath are considered quantitatively. In Section 11.14 the characteristics of diffuse multipath and its effects on each of the mitigation techniques is discussed.

11.5 BEAM PATTERN DESIGN

Two design features that are of obvious benefit are narrow elevation beamwidth and low sidelobes, but the extent to which they can be implemented is limited by other system considerations.

Reduction of the elevation beamwidth permits tracking to a lower angle. However, it requires an increase in antenna size or an increase in frequency, either or both of which may conflict with other system constraints. Increased antenna size also means an increased cost. A radar operating at two frequencies sharing the same antenna [11, 12] permits high-angle tracking at a frequency that is optimum for that purpose, and low-angle tracking at a second frequency in a higher band that produces a narrower beamwidth. Sole reliance on the higher band (e.g., K_a -band) may be inconsistent with achieving the detection ranges required under unfavorable atmospheric conditions.

Low sidelobes do not help when the image is in the mainlobe, as in the left-hand part of Figure 11.4. However, when the target elevation is high enough to put the image in the close-in sidelobes, where the elevation error is still significant (although not disruptive), sidelobe control can give substantial reduction of the error not only from specular multipath but also from diffuse multipath and clutter, besides having other possible system benefits. On the other hand, reduced sidelobes are obtained at the price of reduction in gain and widening of the beam, increasing the elevation sector within which the more serious disruption of tracking can occur.

11.6 RANGE AND DOPPLER RESOLUTION

The reflected signal travels a longer path than the direct signal, so it is possible in theory to resolve them in range; since the pathlength difference changes as the target approaches or recedes, it is possible in theory to resolve the signals in Doppler. In practice, however, the differences in range and Doppler are usually too small for resolution.

Unless the radar is operating in a one-way mode (receiving signals from a beacon or transponder), multipath affects both the transmitting and receiving paths, and therefore a single transmitted pulse will produce *three* (not two) received pulses. Figure 11.6(a) shows the transmitted waveform arriving at the target. It consists of the direct pulse *D* and the pulse *R* reflected from the surface. In this example, it is assumed that the two pulses are separated by more than the pulse length, so they are resolvable. An illustrative value of 0.75 is used for the ratio of the amplitude of the reflected pulse to that of the direct pulse. This ratio includes the effects of the reflection coefficient and the antenna elevation pattern. Figure 11.6(b) shows the waveform arriving at the receiving antenna. It consists of three pulses. The first pulse *DD* follows the direct path in both directions, and if it is resolved in range from the others it yields the correct target angle. The third pulse *RR* follows the reflected path in both directions. Its amplitude is $(0.75)^2$ or about 0.56 times the amplitude of the first pulse in this example, and it yields the image angle. The middle pulse *DR + RD* is the sum of the direct-reflected and the reflected-direct contributions of equal amplitude and phase; hence, it has 1.5 times the amplitude of the first pulse in this example. Since it consists of one component arriving from the direction of the target and another of equal amplitude arriving from the direction of the image, its indicated angle is midway between target and image. (Because the Earth is curved, the target-image midpoint lies above the surface.)

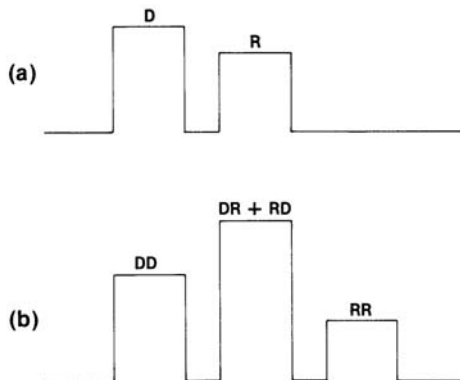


Figure 11.6 Direct and reflected pulses: (a) at target; and (b) at receiving antenna.

A corresponding set of three pulses is received in the difference channel. Their relative amplitudes and phases depend on their angles of arrival as well as on the factors that determine the sum-channel amplitudes.

Hence if range resolution is to be used to separate the image from the target, not only must the bandwidth be wide enough, but a methodology must be developed to recognize the three pulses as belonging to the same target. The first pulse is the desired one, but if it has a low signal-to-noise ratio it may not be detected; the second pulse, which can have a higher amplitude than the first, might be the first pulse detected, giving an erroneous angle indication. The multiplicity of pulse returns is compounded by the fact that a typical target is not a point scatterer but has several distinct scattering points. Hence the echo from a typical target such as an aircraft may have a string of overlapping triplets of pulses. Only the first of these scatterers may be resolvable from multipath returns, and if this comes from the nose of the aircraft (possibly a radome tip) it is unlikely to be detectable by itself. As a result, even the highest available range resolution is unlikely to provide a measurement free of multipath error.

The one-way pathlength difference ΔR between the direct and reflected rays is

$$\Delta R = \frac{2h_a h_t}{R} \quad (11.10)$$

where h_a and h_t are the altitudes of the radar antenna phase center and of the target respectively, above the reflecting surface, and R is the target range. For example, let $h_a = 20\text{m}$, $h_t = 100\text{m}$, and $R = 10\text{ km}$. Then

$$\Delta R = 0.4\text{m}$$

The range resolution must be sufficient to resolve the *one-way* pathlength difference, which is the interval between the first and second pulses and between the second and third. In the present example, a bandwidth of about 800 MHz would be required in order to resolve the three pulses from a single scattering point illustrated in Figure 11.6(b).

Equation (11.10) shows that increasing the antenna altitude aids range resolution of multipath, but for surface-based radars it is not usually possible to obtain enough height to make range resolution a useful tool against multipath, especially when coping with targets that fly lower than the 100-m altitude used in the example. However, if the radar is airborne or situated on a mountain or cliff overlooking a flat surface, range resolution can be effective, or can at least reduce the degree of overlap of the direct and reflected pulses and therefore reduce the error.

The rate of change of the pathlength difference is obtained by differentiating (11.10), assuming that the target is approaching or receding at a constant altitude over a flat earth:

$$\frac{d(\Delta R)}{dt} = -\frac{2h_a h_t}{R^2} \frac{dR}{dt} \quad (11.11)$$

Using the same numbers as in the previous example, and assuming $dR/dt = -200$ m/s, we obtain

$$\frac{d(\Delta R)}{dt} = 0.008 \text{ m/s}$$

The Doppler difference Δf between the first and second pulses and between the second and third pulses is

$$\Delta f = \frac{d(\Delta R)}{dt} \frac{1}{\lambda} \quad (11.12)$$

where λ is the wavelength. Note that the usual factor of two in the numerator, for conversion of range rate to Doppler, is missing here since we are dealing with one-way effects. If the wavelength is 0.03m (X-band), for example, we obtain

$$\Delta f = (0.008 \text{ m/s}) / (0.03\text{m}) = 0.27 \text{ Hz}$$

This is the Doppler difference between DD and $DR + RD$ components. Such a small frequency difference is not resolvable in most practical applications. It would require a coherent integration time of ≈ 4 s, which could not be used in a dynamic situation. Even if Doppler resolution of 0.27 Hz could be accomplished, there is another fundamental reason why it would not be effective against complex targets such as aircraft. Because of the modulation caused by rotational and vibrational perturbations in flight, such a target does not have a sharply defined Doppler frequency but rather a Doppler spectrum. Typical Doppler spreads of aircraft (expressed in m/s so they can be converted to Doppler frequency for any given radar frequency) are 0.04–1.8 m/s [13]. According to (11.11), the mean range-rate difference in our example is only 0.008 m/s. Hence, the spectra of the target and image would almost completely overlap and Doppler resolution would be impossible.

Although Figure 11.6 shows that a single transmitted pulse produces four components of the received signal as a result of multipath (DD , DR , RD , and RR), it is only necessary to consider two components in the usual case where path-length difference is much less than the range resolution of the radar. In such a case the pair of pulses illuminating the target, as shown in Figure 11.6(a), coalesce into a single pulse that is the resultant of the two contributions. In monopulse reception, it is then necessary only to consider the one-way direct and reflected contri-

butions to the sum and difference voltages. This conclusion is based on the assumption that the target scatters isotropically over the small angular interval between the direct and reflected rays. Rare cases can occur in which a target has such a strongly directional scattering pattern that this assumption is not valid, and in such cases all four contributions should be considered. These cases can be recognized as occurring when the target scatterers have a spread Δh in height such that

$$\frac{\lambda}{\Delta h} < \frac{1}{4} \frac{2h_a}{R} \quad (11.13)$$

where $\lambda/\Delta h$ is the elevation width of each lobe of the directional scattering pattern, $2h_a/R$ is the elevation angle between the antenna and its image, as viewed from the target, and the constant $1/4$ ensures that the reflected field from the target will illuminate the antenna and its image with essentially the same field strength.

11.7 SMOOTHING AND AVERAGING

Smoothing of the elevation fluctuations (for example, by reducing the loop bandwidth) is beneficial if the fluctuations are rapid, as in a case where the radar site is high above the reflecting surface and the target is approaching or receding at high speed. A similar effect is obtained in open-loop measurements by averaging over several pulses. In many cases, however, the fluctuations are too slow to allow any benefit from smoothing or averaging. The value $\Delta f = 0.27$ Hz derived from (11.12) in our earlier example is the frequency at which the multipath error varies, and smoothing over some multiple of $1/\Delta f = 3.75$ s is not generally permissible in radar tracking applications.

Pulse-to-pulse frequency changing ("frequency agility") can speed up the fluctuations, since the spacing of the error cycles illustrated in Figure 11.4 is inversely proportional to the radar's carrier frequency. However, to produce any substantial benefit (e.g., to convert an error maximum to an error minimum in Figure 11.4) a very wide frequency band is required, especially in the lowest multipath lobes. The one-way pathlength difference given by (11.10) is equal to the radar wavelength times the number of the null (starting with zero at the horizon). To change the first null to a peak would thus require that the frequency be reduced to $1/2$ or increased to $3/2$ of the value that produced the null. The required band is comparable to the bandwidth needed to resolve the target from the image in range. In our previous example, that range difference, from (11.10) was $\Delta R = 0.4$ m (corresponding approximately to the 13th null from the horizon), and the bandwidth required for resolution is 750 MHz. The use of frequency agility for multipath reduction is similar to its application to reduction of target glint [14], where a simulation showed that basing the angle estimate on the single pulse having the

largest sum-signal amplitude gave less error than that obtained by averaging several pulses.

11.8 “LOW-E” MODES

One method that is used to prevent violent oscillations in elevation tracking of low-angle targets is to disable the elevation tracking loop and keep the beam at a fixed elevation when the indicated angle drops below a specified value (usually ≈ 0.75 beamwidth). Thus, as long as the target is within the beam and the signal is strong enough, track is maintained in range and traverse. There are several forms of this method, known generically as “low-E” modes.

In the simplest low-E mode the radar provides no information about target elevation, the rationale being that it is better to forgo the elevation information, which is erroneous anyway, than to risk complete loss of track. In some applications the range and traverse information is useful in itself. If the target is approaching the radar at constant altitude, the expectation is that it will eventually reach an elevation angle that permits a transition to full track.

Some applications require prediction of future position of the target. If the target is known to be of a type that flies at a constant low altitude and if elevation information from the radar is either unavailable or of poor quality, it is sometimes helpful to insert a “most probable” constant altitude for use in the prediction equation. The prediction error due to incorrect altitude may be much less than the error that would result from fictitious high rate of change of altitude.

While the radar is operating in a low-E mode, the open-loop elevation monopulse output can be measured and used for crude estimation of target elevation if desired. In any case, it is monitored to determine, either by the operator’s judgment or by a prescribed logic, when the elevation has increased sufficiently to permit switching to closed-loop tracking. Similarly, observation of the closed-loop tracking behavior determines when to switch to the low-E mode.

Figure 11.7 is a plot of open-loop indicated elevation in the low-E mode, for the same radar and multipath parameters used in Figures 11.4 and 11.5, with a constant beam axis elevation $E_0 = 0.75$ beamwidth. The indicated elevation is obtained by converting the open-loop output to an off-axis angle (using the single-target calibration) and adding that angle to the known elevation of the beam. Comparison of Figures 11.4 and 11.7 shows that at target elevation angles below 0.6 beamwidth the open-loop errors are smaller than the closed-loop errors. The reason is that the low-E mode places the image on the steep underside of the sum beam and thus reduces the ratio of image amplitude to target amplitude. Besides reducing the error, the main advantage is immunity to loss of track caused by antenna oscillations. At target elevation angles a little higher than 0.6 beamwidth the low-E mode offers no advantage and at still higher elevation angles it becomes inferior to closed-loop tracking. The specific results will vary, of course, with the

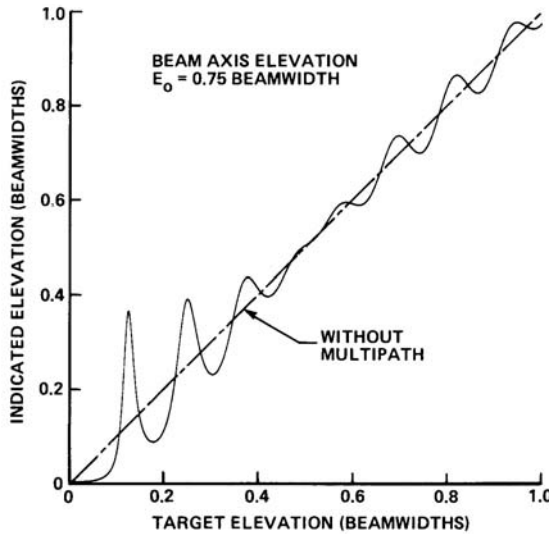


Figure 11.7 Open-loop indicated elevation versus true target elevation in low-E mode, beam axis elevation fixed at 0.75 beamwidth.

parameters of the radar and the reflecting surface and with the geometry of a particular radar installation, but it is generally true that although the low-E mode is not a “cure” for multipath, it reduces errors and prevents loss of track at very low target elevation angles.

If the antenna is an electronically steered array, it is not subject to mechanical oscillations, and the beam pointing position can easily be inhibited from going below the horizon. Nevertheless a low-E mode can still be useful because it reduces elevation errors.

Omitted from the computations for Figure 11.7 is the error in making open-loop angle measurements, due to the difficulty of maintaining accurate off-axis calibration. As a rough rule of thumb, this error is typically 10% of the indicated off-axis angle unless special self-calibration techniques or other stabilizing features are incorporated in the radar to reduce it. The open-loop calibration error reduces the advantage of the low-E mode, but only to a minor extent.

The optimum beam elevation angle must be determined by analysis or simulation for each radar. Against very low targets, the error is minimized by a beam elevation angle that puts the target and image near the steepest part of the underside of the sum beam. Unfortunately, this reduces the signal-to-noise ratio and increases the thermal-noise error. In a typical low-angle situation, however, multipath is the dominant source of error, and thermal noise is only a secondary consideration.

11.9 OFFSET-NULL TRACKING

Another technique that gives some reduction of multipath errors is closed-loop tracking with the patterns modified so that the elevation difference-pattern null is offset from the peak of the sum pattern. This can be done by adding a portion of the sum voltage to the elevation difference voltage, as described by David and Redlein [15, 16]. An equivalent effect can be obtained by inserting a voltage offset in the servo, or a numerical offset if the loop includes a computer. To see the equivalence, note that the modified difference signal is $d + Ks$, where d and s are the original difference and sum signals and K is a constant. Then the modified monopulse ratio is

$$\frac{d + Ks}{s} = \frac{d}{s} + K \quad (11.14)$$

which is the original monopulse ratio plus an offset K . Modification of the difference pattern in the antenna feed system is the preferred approach, because an offset voltage in the servo tends to cause rapid loss of track when signal fading opens the track loop or reduces its gain significantly. In most radars, a standard maintenance or operating procedure is to adjust for zero bias in the servo input by observing and setting to zero rate the drift in antenna position when only noise is present at the input.

The offset null puts the direction of the sum-pattern peak above the direction of the difference-pattern null. The steep fall-off of the underside of the sum pattern gives increased rejection of the image contribution relative to the target contribution. The offset can be a fixed amount or it can be continuously variable in accordance with the indicated elevation to provide a smooth transition rather than an abrupt change between normal track and offset-null track.

Figure 11.8 illustrates the improvement obtained by offset-null tracking at the lowest elevation angles, using the same parameters as in Figure 11.4 but with the null displaced downward from the sum-pattern peak by 0.5 beamwidth. The spurious nulls in the vicinity of the image direction, shown in the lower half of Figure 11.4, are omitted from Figure 11.8. They are still present but are further removed from the primary null directions; for this reason and because the amplitude of the oscillations is reduced, “nose-diving” is unlikely to occur.

11.10 ELEVATION PATTERNS HAVING A SYMMETRICAL RATIO

In contrast to conventional monopulse patterns, in which the ratio of the difference to the sum is an odd function of angle, a technique devised by White [17] uses a pair of elevation patterns whose ratio is an *even* (symmetrical) function of angle, parabolic in shape, with a null on the axis. The axis elevation angle is held

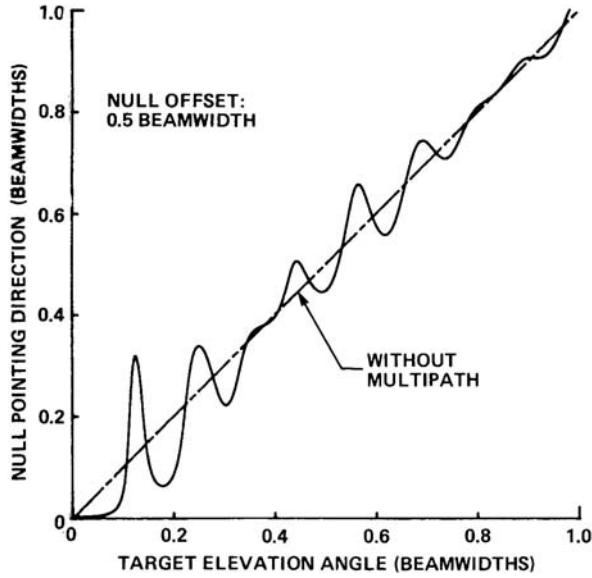


Figure 11.8 Offset-null tracking in multipath.

fixed and open-loop elevation measurements are made while normal tracking is maintained in range and traverse.

The symmetrical ratio means that if the axis is pointed horizontally,

$$\frac{F_B(E)}{F_A(E)} = \frac{F_B(-E)}{F_A(-E)} \quad (11.15)$$

where E is elevation angle, $F_A(E)$ is the “A pattern,” and $F_B(E)$ is the “B-pattern.”

Let p and ϕ be the amplitude ratio and relative phase of the image to the target, as before, and let v_A and v_B be the voltages derived from the two patterns. Then if the desired target is at elevation angle E and the image is at $-E$, as in Figure 11.1,

$$\frac{v_A}{v_B} = \frac{F_B(E) + pe^{j\phi}F_B(-E)}{F_A(E) + pe^{j\phi}F_A(-E)} \quad (11.16)$$

From (11.15)

$$F_B(-E) = F_A(-E) \frac{F_B(E)}{F_A(E)} \quad (11.17)$$

Upon substituting (11.17) into (11.16) and dividing the numerator and denominator by $F_A(E)$, we can write

$$\frac{v_B}{v_A} = \frac{F_B(E)}{F_A(E)} \quad (11.18)$$

which is the same as it would be for the target alone, unaffected by multipath. Target elevation is obtained by taking the ratio of the two voltages, v_B/v_A , and converting it to angle by use of the known free-space calibration function.

Under ideal conditions this technique gives a true solution; it yields the correct target elevation on a single pulse (provided the ratio is computed on each pulse), with no multipath error. Of course under practical conditions it cannot have the same accuracy in multipath that a conventional monopulse radar can achieve in free space, but it can give useful information measurements in the low-angle region, not obtainable from conventional tracking.

Sources of error include deviation of the reflecting surface from the assumed model and imperfect symmetry of the pattern ratio. Because of the shallow slope of the pattern ratio at very low angles, the thermal noise error in that region is larger than in conventional monopulse in free space.

Figures 11.9(a) and (b) are examples of two different pairs of A and B patterns having ratios that are parabolic functions of elevation angle [private communication with W. D. White, 1983]. The symmetry constraint is imposed only on the ratio, not the individual patterns, which are deliberately designed to be weaker on the negative elevation side in order to minimize errors due to deviation from the assumed reflection geometry, as well as from surface clutter and diffuse multipath. These particular patterns are synthesized by superimposing three component beams, each of which has the shape that is characteristic of a uniformly illuminated line source, namely $[\sin(\pi\theta Y/\lambda)]/(\pi\theta Y/\lambda)$, where θ is the elevation angle measured from the axis of each component beam and Y is the vertical dimension of the antenna.⁴ The quantity λ/Y is known as the *standard beamwidth*. The choice as to which pattern pair is better depends on factors such as target elevation and surface roughness. There is considerable flexibility in the design of pattern pairs having a symmetrical ratio but different individual characteristics.

⁴ To be more rigorous, θ should be replaced by its sine, but for small angles there is negligible difference.

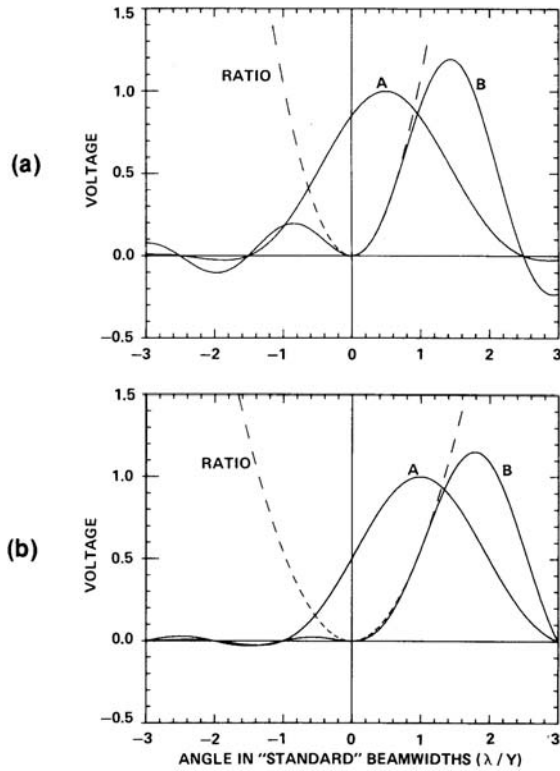


Figure 11.9 (a, b) Two examples of elevation patterns with symmetrical ratio. Parameters of patterns are given in Table 11.1.

In these two examples the A and B patterns are composed of three adjacent beams separated by the standard beamwidth and combined with different weights. Table 11.1 lists the elevation angles of the component beams and the weights used in superimposing them to form the A and B patterns. The total power in the B pattern (sum of the squares of the weights) is the same as in the A pattern.

Pointing the axis of symmetry horizontally is based on the assumptions of a flat Earth and infinite target range, but these assumptions are not necessary. For a flat Earth and finite target range the axis can be programmed in accordance with the measured range to point at the target-image midpoint, which is a point on the surface approximately at the range of the target. Curved-Earth geometry could also be taken into account in programming the axis pointing direction. In that case, however, at any given range the target-image midpoint varies somewhat with target elevation, and as a result there is no axis direction that can maintain the desired target-image symmetry exactly.

Table 11.1 Synthesis of Patterns with Symmetrical Ratio

<i>Pattern Pair</i>	<i>Beam</i>	<i>Elevation*</i>	<i>A Weight</i>	<i>B Weight</i>	<i>Ratio v_A/v_B</i>
Figure 11.9(a)	1	-0.5	0.5000	0.13206	$1.0564 E^2$
	2	+0.5	1.0000	0.26413	
	2	+1.5	0.5000	1.18861	
Figure 11.9(b)	1	0.0	0.5000	0.00000	$0.54772 E^2$
	2	+1.0	1.0000	0.54772	
	3	+2.0	0.5000	1.09545	

* Elevation is in units of standard beamwidth.

Although this technique uses patterns unlike conventional sum and difference patterns, it falls under the broad definition of monopulse given in Chapter 2 because it bases its angle estimate on the ratio of voltages derived from simultaneous receiving beams.

The principle of a symmetrical monopulse ratio has also been applied in a different way by Dax [18, 19]. Instead of a special pair of patterns like those in Figure 11.9, this technique uses sum and difference patterns like those of conventional monopulse but with an important modification. Normally a plot of the monopulse ratio is concave upward, as in the bottom curve of Figure 6.6; if extended to the right, it becomes infinite⁵ at the first sum-pattern null, which occurs before the first off-axis difference-pattern null. In the modified patterns the off-axis difference null occurs before the sum null, and a plot of the ratio is convex upward, as in the top curve of Figure 6.6. If extended to the right the curve reaches a peak and then decreases, passing through zero. Between the on-axis null and the off-axis null, the curve has approximate symmetry.

Figure 11.10 is an illustrative plot of the sum and difference patterns and their ratio. The negative angle where the ratio has its peak value is the axis of symmetry, which is programmed to point in the direction that bisects the angle between target and image. The required elevation angle of the axis of symmetry is computed approximately as the negative of the ratio of antenna height to target range. Thus, the target and image are at symmetrical angles, and their individual monopulse ratio is the same as that of the target alone. The target elevation angle is estimated by means of the single-target calibration function.

⁵ In practice it is limited, of course, to a finite value by the nature of the monopulse processor or by the finite dynamic range of the components. Furthermore, the nulls are never complete; there is always some residual voltage, which prevents the infinite ratio.

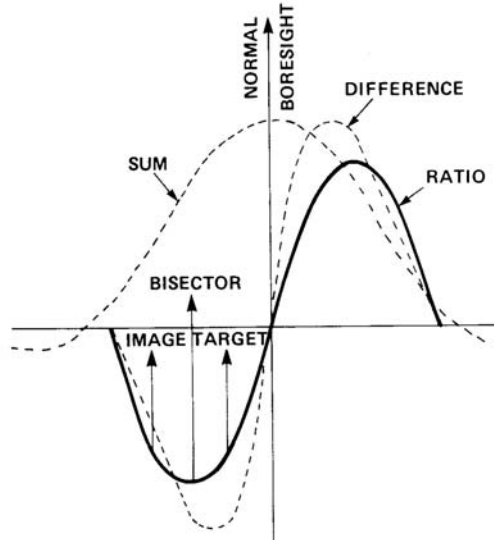


Figure 11.10 Off-axis symmetrical ratio technique. (After: Dax [20].)

11.11 DOUBLE-NUL TRACKER

This is a closed-loop tracking technique devised by White [17, 20]. The difference pattern has not only a primary null (which in the case of a reflector antenna is along the mechanical axis), but also a second null at a lower elevation angle. A single control loop steers the primary null toward the target direction and at the same time offsets the second null downward from the first by an angle computed by the laws of reflection from a level surface, so that the second null is directed at the image. Although this technique differs from conventional monopulse, it falls under the broad definition of monopulse given in Section 2.1, since it makes use of simultaneous receiving patterns.

The theory and implementation of this technique are explained in [17]. A nonmathematical explanation given in [20] begins with a conceptual description of a maximum-likelihood estimator (MLE) designed on the idealized assumption of a perfectly smooth and level reflecting surface. Such a surface creates a specular image at an angle having an exactly known relationship to the target angle. The MLE based on this assumption would give equal weights to the target and the image contributions. If the ideal conditions actually existed, the estimator would be totally immune to the multipath elevation errors that occur in conventional tracking systems. However, it would be excessively sensitive to deviations from the ideal conditions. The deviations usually encountered are clutter and diffuse

multipath because the surface is not perfectly smooth, and displacement of the specular image because the surface is not perfectly level.

In order to reduce the errors caused by the nonideal conditions, the actual design is a “tempered” double-null tracker, similar in concept to the MLE except that the patterns are designed to have a smaller response at negative than at positive elevation angles. This modification retains the theoretical immunity to specular multipath error under ideal conditions, and under practical conditions it substantially reduces the errors caused by the nonideal reflecting surface. The price paid for this improvement is a reduction in error slope sensitivity compared with the MLE, resulting in somewhat higher thermal-noise error. This technique requires some additional complexity in the feed and processing compared with conventional monopulse.

The closed-loop operation requires a loop settling time. Hence, it is intended for continuous track, not for single-pulse or short-dwell operation. The technique has been implemented in a reflector antenna, using a feed that provides six pencil beams arranged in three horizontal pairs stacked in elevation. The traverse sum and difference are obtained by combining the left and right members of the pairs in hybrids. The elevation patterns are generated by a weighted combination of the outputs of the three pairs. Tests in which a monopulse radar could be operated either in its normal tracking mode or in the double-null tracking mode on low angle targets are reported to have shown smooth tracks in the double-null mode, with marked reduction in elevation error and complete freedom from the “nose-diving” (abrupt transition from target track to image track) occasionally encountered in the normal tracking mode.

11.12 USE OF THE COMPLEX INDICATED ANGLE

The concept of a complex indicated angle was introduced in Section 9.5. It was pointed out that although the monopulse ratio due to a single target is nominally real, unresolved targets cause the ratio to be complex; the real and imaginary parts can be interpreted to correspond to the real and imaginary parts of a complex angle. Normally only the real part is used but the imaginary part, when it exists, also contains information.

Since multipath is a special case of unresolved targets, it produces an indicated angle that is complex in general. For the simple flat-Earth geometry shown in Figure 11.1, the real and imaginary parts x and y are given by (11.4) and (11.5). In the ordinary low-E mode (Section 11.8), E_0 is held fixed and target elevation can be estimated from the open-loop measurement of the real part x , together with the known elevation angle of the beam axis, producing the type of result illustrated in Figure 11.6.

In the complex-indicated-angle version of the low-E mode [21], the beam elevation is held constant and both x and y , the real and imaginary parts of the open-loop indicated angle, are measured. Measurement of the imaginary part requires some additional processing and computation (Section 9.7) but no change in the antenna patterns. If y is plotted against x as the target elevation angle varies, the resulting curve is a sort of spiral with a moving center, as illustrated in Figure 11.11. (In the absence of multipath the plot would simply be that of a point moving along the x -axis.) In part (a) of the figure the parameters are the same as those used in plotting Figures 11.4 and 11.7, including the same ratio of antenna height to antenna vertical dimension, namely 4. In part (b) the parameters are also the same except that the ratio has been reduced from 4 to 2. The encircled points on the spirals and the adjacent numbers indicate increments of 0.1 beamwidth in target elevation. In plotting these spirals it has been assumed that the local-oscillator frequency is below the radar frequency. If it is above the radar frequency, the phases are inverted, causing the spirals to be turned upside down.

The reason the behavior illustrated in the figure can be understood by recalling from Section 9.5 that if the relative phase of two targets is varied while their amplitude ratio and their angles remain constant, the locus of the complex indicated angle is a circle like one of the solid circles in Figure 9.2. In the multipath case the relative phase of the target and image varies with the target elevation angle, producing the loops seen in Figure 11.11. The loops are not circular for two

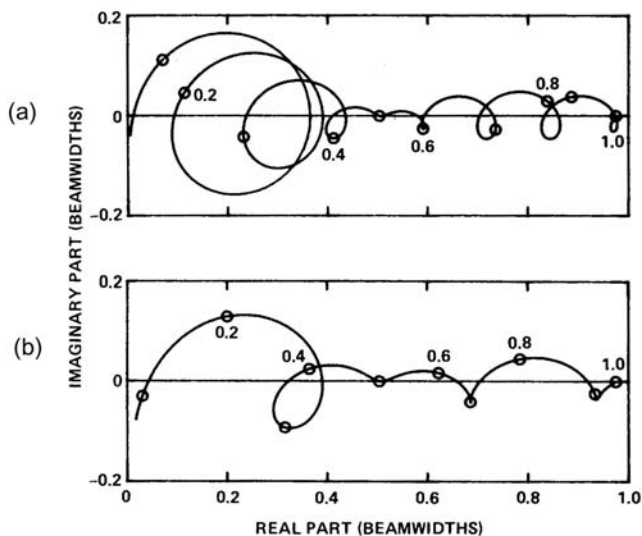


Figure 11.11 Complex indicated angle in multipath. Beam axis elevation = 0.75 beamwidth. Ratio of height of antenna phase center to antenna vertical dimension: (a) 4 and (b) 2. Numbers at circled points on spiral are target elevation angles in beamwidths.

reasons: the ratio of image amplitude to target amplitude decreases with increasing target elevation, causing the loops to become progressively smaller (except when the image enters the sidelobes), and the increasing target elevation relative to the beam axis causes the center of the loops to move in the positive direction.

Since every point on the spiral corresponds to a particular elevation angle (ignoring the ambiguities, which will be discussed later), it should be possible in theory, once the spiral has been plotted for a particular radar installation (with an X - Y plotter, for example), to use it as a two-dimensional calibration curve or look-up table to determine the elevation angle of a target from the measurements of x and y . The calibration spiral could be computed, but since the reflection characteristics of the surface are not generally known with sufficient accuracy, it is preferable to obtain the calibration spiral from measurements on a test target whose elevation angle at each instant is determined by some independent means which is not subject to multipath error. Although a flat Earth was assumed in order to simplify the computations for Figure 11.11, there is no need for this assumption in plotting an actual calibration spiral, whether by theory or measurement. When Earth's curvature is taken into account, the spiral will have the same general form as in Figure 11.11 but will differ in detail. The exact shape will also depend, of course, on the specific parameters of the radar and the characteristics of the surface.

In describing this technique, it was stated above that the beam elevation is held constant. If constant elevation were referred to the horizontal, the calibration spiral would vary somewhat with target range, requiring different spirals for different ranges. To eliminate all but second-order range-dependence, the beam axis should be kept instead at a fixed elevation above the *effective horizon direction*. This is defined as the direction from the antenna to the point on the surface directly below the target unless that point is beyond the horizon, in which case the effective horizon direction is the same as the true horizon direction—that is, the direction of the ray from the antenna tangent to the Earth's surface. The effective horizon direction is the zero reference because it is the direction where target and image merge, and in general it is approximately midway between the target and the image directions. Thus, the required beam elevation angle when operating in this mode varies with target range but it is easily computed from the known antenna height and the measured range.

Because of noise, drifts, measurement errors, time-varying diffuse multipath, and changes in reflection characteristics of the surface, the measured point will generally fall near, but not actually on the spiral. Pulse-to-pulse fluctuations can be reduced by smoothing but some deviation from the spiral will remain. The procedure for making the elevation estimate is illustrated in Figure 11.12, using an enlarged portion of the spiral drawn in Figure 11.10(a). Point A represents the true elevation and A' is the measured point after smoothing. The elevation estimate is based on A'' , which is the point on the spiral closest to the measured point. The arc AA'' represents the error.

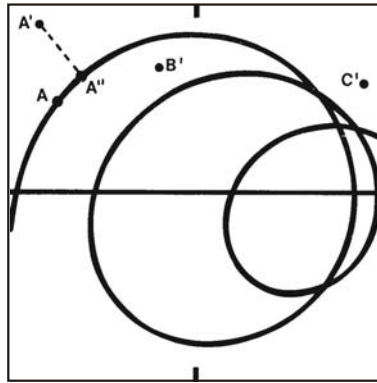


Figure 11.12 Estimation procedure and ambiguities in calibration-spiral technique.

Errors due to noise and to changes in the surface reflection coefficient, using the estimation procedure just described, have been investigated by simulation [22]. Provided that any ambiguities that occurred were resolved, it was found that noise errors were smaller, on the average, than noise errors with normal monopulse in free space when the comparison was made at the same actual signal-to-noise ratio. The reason is that the radar and its image below the surface act as an interferometer, which has greater angular sensitivity than the radar alone. Another form of explanation is that the multipath expands the calibration scale, since the length of the spiral curve is greater than the length along the real axis between the same end-point angles.

It was found in the same investigation that changes in the surface reflection coefficient by as much as 50% caused only moderate errors. The explanation lies in the fact that a change in the reflection coefficient makes the loops of the spiral expand or contract, so that each point on the spiral shifts in a direction that is primarily perpendicular to the curve at that point, rather than tangential. The perpendicular component of shift causes no error.

One problem that is evident is that there are ambiguities where the curve crosses itself or where loops lie close together. The ambiguity problem, however, is less serious when both x and y are used than when x alone is used. Suppose that in the low-E mode using measurements of x only, as in Figure 11.7, a reading is obtained that lies anywhere in the range of 0.24 to 0.36 beamwidth. In Figure 11.7, a line drawn horizontally at any coordinate in that range intersects the curve at five points, yielding five possible values for true elevation. The same result can be illustrated in Figure 11.11(a), which is based on the same parameters and the same mode of operation as Figure 11.7. The x -coordinate of any point on the spiral is the same as the coordinate of the point in Figure 11.7 at the same target elevation. Therefore corresponding to the horizontal line in Figure 11.7, draw a vertical line in Figure 11.11(a) at a horizontal position anywhere between 0.24 and

0.36 beamwidth and note that it intersects the spiral at five points, producing a five-fold ambiguity if only x is measured. If, however, both x and y are measured, each pair of values of x and y unambiguously identifies one point on the spiral, except for a two-fold ambiguity at points where the curve crosses itself. Comparison of Figure 11.11(a, b) shows that the lower the antenna height, the fewer are the ambiguities.

However, the ambiguity problem is aggravated by noise, changes in reflection coefficient, and other perturbations. For example, if a measurement falls at a point such as B' or C' in Figure 11.12, there is an ambiguity even if the closest point on the spiral is not a point where the spiral crosses itself, because the measured point may lie closer to the wrong arc than to the right one. As already pointed out and illustrated in Figure 9.10, low antenna height alleviates the problem if other system requirements permit the choice.

There are several possible ways of resolving the ambiguities that remain after advantage is taken of smoothing and the lowest antenna height permitted by other system requirements. The simplest way, if enough time is available, is to observe the time history of the target, either continuously or by a series of discrete observations, as its complex indicated angle moves along part of a spiral, preferably through an entire loop. The trace that it makes will identify the correct arc. This method imposes an initial delay, but once the correct arc is identified, the target can be followed without further delay.

Other possible methods of resolution of ambiguities include diversity in frequency, antenna boresight angle, or antenna height. Frequency diversity, for example, consists of making calibration spirals at two different frequencies, separated by 5% to 10%, within the tuning band of the radar. The ambiguous regions on the second spiral are displaced from those on the first. Later, when measurements are made on an unknown target, the same two frequencies are used in rapid succession and the measurements are compared with the respective calibration spirals. Details of such a procedure and of an experimental program have been reported [23]. The radar was an AN/FPS-16, a C-band radar with a 3.66-m (12-ft) reflector at a height of 9.9m (32.5 ft), the target was a beacon that was raised and lowered by an elevator on a boresight tower, and the reflecting surface was asphalt. Both frequency diversity and boresight diversity reduced the number of ambiguities, and the time history method was able to eliminate ambiguities altogether if enough time was allowed.

The calibration-spiral technique is not suitable for use over terrain whose contour or reflection characteristics vary with azimuth, because this would require a large number of different calibration spirals, of the same order as the number of beamwidths in the azimuth coverage sector. Even if coverage is limited to a narrow azimuth sector, irregular terrain will cause an irregular spiral, which may make calibration impractical and may aggravate the ambiguities.

The most promising type of application of the complex-angle calibration-spiral technique is with a land-based antenna overlooking water (so that the mean

surface contour is regular and independent of azimuth), with a low height-to-diameter ratio (to minimize ambiguities), and at a low frequency (to reduce diffuse relative to specular multipath). A brief series of tests was conducted on the TRADEX radar at Kwajalein, overlooking the Pacific Ocean and operating at 1.32 GHz with an elevation beamwidth of 11.4 mrad [24]. The diameter of the parabolic antenna is 25.6m (84 ft) and the height of the phase center above mean sea level is 26.2m (86 ft). The in-phase component of the normalized difference signal, used for normal tracking, is obtained in the manner shown in Figure 7.4. To obtain the quadrature component it is only necessary to compute an additional output, without hardware modification, using the sine instead of the cosine of the relative phase.⁶

Figure 11.13 shows the results of one of the tests. The dashed curve is a calibration spiral obtained from measurements on a metal sphere dropped from high altitude and observed as it fell through the multipath region into the ocean. The solid curve is the spiral obtained from a reentry body about 90 minutes later as it fell at approximately the same range and azimuth. The “true” elevations of both the sphere and the other body were obtained from another source whose errors were small compared with the uncorrected multipath errors of TRADEX. Before plotting, the measurements were smoothed by means of a sliding average to reduce the effects of noise and diffuse multipath. Since the reentry body descended more rapidly than the sphere, the smoothing necessary to reduce its noise fluctua-

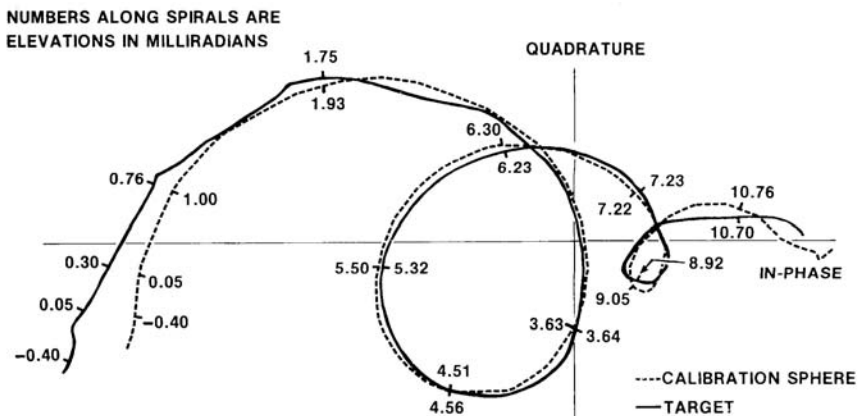


Figure 11.13 TRADEX complex-angle spirals.

⁶ The reference to sines and cosines in this book (including Figure 7.4) are in accordance with the convention that the nominal phase between the sum and difference signals is 0°. In TRADEX it is actually 90° because of the type of comparator used, and therefore sines and cosines are interchanged.

tions to an acceptable level also “shrank” the spiral, but by simply enlarging the resulting spiral by an appropriate scale factor a good fit to the calibration spiral was obtained, as seen in the figure. It may be possible to avoid the shrinkage and the need for compensatory enlargement by using a more sophisticated smoothing algorithm.

Although the elevation calibration is essentially continuous, only a few points are marked on the calibration spiral, to illustrate the trend. They are indicated by the tick marks on the calibration spiral, labeled with the elevation in mrad. To determine the agreement between the two spirals, these tick marks are extended to the closest points on the reentry-body spiral, and those points are labeled with the corresponding elevations obtained from the independent source. The agreement is quite close down to about 1 mrad. Part of the error, especially at low angles, is contributed by the independent calibration source.

Thus, it appears that the complex-angle calibration-spiral technique is capable of accurate elevation estimates down to very low elevations, but the conditions under which it can be used practically are rather restricted, and the necessity of generating calibration spirals and of resolving possible ambiguities imposes an additional operating burden. The radar must have accurate normalization so that the monopulse output will be independent of signal strength, and its open-loop calibration must also be stable. TRADEX meets these requirements but many monopulse radars do not, especially those designed only for closed-loop tracking of targets near the axis.

The calibration-spiral technique is not the only method that has been proposed for the use of complex-angle monopulse to combat multipath. One method [25] requires two or more pulses and is similar in some respects to the two-target solution described in Section 9.12, but differs in two ways: rather than wait for the relative phase between target and image to change as a result of target motion, the frequency is varied from pulse to pulse by an amount sufficient to change the relative phase but not the target-image amplitude ratio; and instead of measuring the ratio of resultant amplitudes of successive pulses to obtain enough measurements to equal or exceed the number of unknowns, the number of unknowns is reduced by using the known or assumed geometric relation between target and image.

Still another approach is based on the principle that if the image-to-target relative phase is held constant while their amplitude ratio varies, the locus in the complex plane is a circle like one of the dotted circles in Figure 9.2. These circles all intersect the real axis at points corresponding to the target and image angles. The image-to-target amplitude ratio depends on the surface reflection coefficient and the beam elevation angle. Hence the approach is to vary the beam elevation angle from pulse to pulse in order to obtain enough points to define the arc of a circle, which is then extrapolated to the real-axis intersection corresponding to the target angle. Although this approach has a sound theoretical basis, it requires that the sum and difference patterns have constant phase, which is generally not true in practice. The phase variation with angle is typically very small near the center of

the beam, but it can become appreciable as the target or image approaches the edge of the beam, especially in a reflector-type antenna. The error in the extrapolation can be quite large.

11.13 INDEPENDENT-TARGET METHODS

Of the techniques described so far, some base their target elevation estimates on the same calibration functions of tracking loops that are used for a target in free space—by ignoring the presence of the image they incur errors when multipath is present. Others take the image into account in determining target elevation but they do so on the assumption that the image angle is related to the target angle by the geometry of reflection from a flat horizontal surface or from a spherical surface. Therefore they are subject to error if, for example, the reflecting surface has an unknown slope. The only technique discussed so far that takes multipath into account without assuming a specific reflection geometry is the complex indicated angle, provided the calibration spiral is generated by means of a test target rather than by theoretical calculation. It can therefore be used over a sloping or an irregular surface. It is, however, subject to assumption that once the calibration spiral has been generated, the geometry and reflection characteristics of the surface remain reasonably stable.

In an effort to remove the limitations imposed by these assumptions, some investigators have attacked the multipath problem in a different way by treating the target and the image as two independent unresolved targets, with no assumption as to their relationship in amplitude, phase, or angle (except that they are separated by no more than a beamwidth or so).

When regarded in this way, the multipath problem is essentially the same as the general problem of two unresolved targets treated in Chapter 9 (particularly Section 9.15), except that the solution is needed only in the elevation coordinate. The discussion and references given in that chapter are therefore pertinent.

It was shown in Section 9.12 that with two patterns, producing one voltage ratio, a single-pulse solution for the locations of two independent targets is impossible even if both real and imaginary parts of the ratio are used, and that multiple-pulse solutions, although theoretically possible, have only a limited practical potential. The fact that the desired information is only the target angle, not the image angle, does not alleviate the problem, since the solution is not separable. All of the techniques discussed in the previous sections use just one pair of elevation patterns, which may be conventional sum and difference patterns, modified sum and difference patterns, or asymmetrical “A” and “B” patterns having a symmetrical ratio. Hence they are unable to obtain single-pulse solutions for two independent targets.

Therefore techniques have been proposed that use three or more simultaneous elevation patterns (the *multiple-beam* method), or three or more voltages derived

from individual elements or subarrays of an array antenna (the *aperture-sampling* method), to obtain sufficient information for a solution. Three beams or aperture samples (yielding two complex ratios) are necessary. A larger number can be used for overdetermination to improve accuracy. In addition to the general reference cited in Chapter 9, specific applications of these principles to multipath have been reported, including design approaches, analysis or simulation, and some testing [26–31].

The advantage of such methods is that they are immune to error resulting from surface slope that is unknown or that varies with time, season, or azimuth. They are also immune to changes in image angle due to variation in antenna height above sea surface as a result of tide or of platform motion, as on a ship. (The methods described in preceding sections can be compensated for tide, but knowledge of the tidal height is usually only approximate.)

However, the independent-target methods still rely on the assumption of a point target and a point image.⁷ Because they do not make use of a priori knowledge or assumptions about the geometric relations between target and image, as do the techniques described earlier, they depend more heavily on small differences among the sampled voltages or beam outputs. As a result, they have larger errors due to noise, diffuse multipath, imperfect knowledge of beam patterns (or element gains), and drifts in equipment calibration. They also require more complicated feeds or combining networks and more signal channels.

11.14 DIFFUSE MULTIPATH EFFECTS ON MONOPULSE

There have been numerous references in the preceding sections to diffuse multipath, and its potential for causing errors in tracking and in the various methods of alleviating the problems caused by specular multipath. In discussion of these methods, the word *image* is used frequently. It is appropriate to examine each such use, and to evaluate how the measurement would be affected if, instead of a well defined point reflection, the multipath arrived at the radar antenna from a region spread across an area of the surface with varying angles, amplitudes, and phases. In this section we will review the theory of diffuse multipath, obtain some quantitative measure of its power and distribution in space and frequency, and apply those data to determine its effect on radar measurement of low-altitude target angles.

⁷ In theory, a “straightforward extension” would make it possible to handle more than one image, resulting from multiple specular reflections from irregular terrain. However, each additional image adds three unknowns: angle, amplitude, and phase. In view of the difficulty of even a single-target-single-image solution with useful accuracy, such an extension appears remote.

11.14.1 Power of Specular and Diffuse Multipath Reflections

In Section 11.1 the Fresnel reflection coefficient ρ_0 of the surface was introduced to describe the amplitude of specular reflection relative to the direct signal from the target. Considering narrow-beam microwave systems, the region of interest is near 1° grazing angle where $0.75 < \rho_0 < 0.98$, the highest values applying to dry land surfaces or horizontal polarization on any surface.

The *specular scattering factor* ρ_s that modifies the reflection amplitude for other than smooth surfaces was defined in (11.9), showing its dependence on surface height deviation σ_h , wavelength λ , and grazing angle ψ . The surface area from which multipath reflections originate is known as the *glistening surface*, following the usage of Beckmann and Spizzichino [2]. We can describe the components of power on that surface, relative to the power reaching the radar directly from the target, as follows:

1. A fraction given by $1 - \rho_0^2$ is absorbed in a thin volume at or just below the surface;
2. A fraction ρ_0^2 is reflected;
3. A fraction $\rho_0^2 \rho_s^2$ is in the specular reflection;
4. A fraction $\rho_0^2 (1 - \rho_s^2)$ remains to be apportioned between “diffuse” (or “quasi-specular”) reflection and a wide-angle scattered component that includes backscattered and bistatic clutter.

The *Rayleigh criterion* for a “rough” surface is that the ratio $(\sigma_h \sin \psi) / \lambda$ is greater than $1/8$, which from (11.9) gives $\rho_s < 0.3$. When $(\sigma_h \sin \psi) / \lambda = 1/15$, normally considered a relatively smooth surface, the specular and diffuse components have equal powers $= \rho_0^2 / 2$. For a typical grazing angle $\psi = 1^\circ$, this situation corresponds to an rms height deviation $\sigma_h = 3.8\lambda$, or 0.11 m at X-band. Thus, even at low grazing angles, the presence of significant diffuse scattering is almost universal at X-band, and very common at S-band as well.

Integration of the backscatter and other wide-angle scattered power, using currently accepted models, shows those components to represent a very small fraction (typically 2–3%) of the nonspecular reflected power. Since this is less than the uncertainty in the value of ρ_0^2 , it can be neglected and the reflected power that is not in the specular ray can be assigned to the diffuse component $\rho_0^2 \rho_d^2$, where $\rho_d \approx \sqrt{1 - \rho_s^2}$ is the *diffuse scattering factor*. The diffuse power is reflected from small, tilted facets of the surface and is confined to a narrow *forward scatter* sector surrounding the specular ray. The surface is described as having a normal distribution of facet slopes with angular standard deviation $\beta_0 / \sqrt{2}$ relative to the mean surface, and the angular spread of diffuse scattering from any small area can

be described as a Gaussian beam with elliptical shape, having an elevation width (at the power level $1/e$ relative to its peak) given by $\pm 2\beta_0$ and an azimuth width $\pm 2\beta_0 \sin(\psi)$. Viewed from the radar antenna, the diffuse components arrive from the elliptical area on the surface, as shown in azimuth-elevation space in Figure 11.14(a).

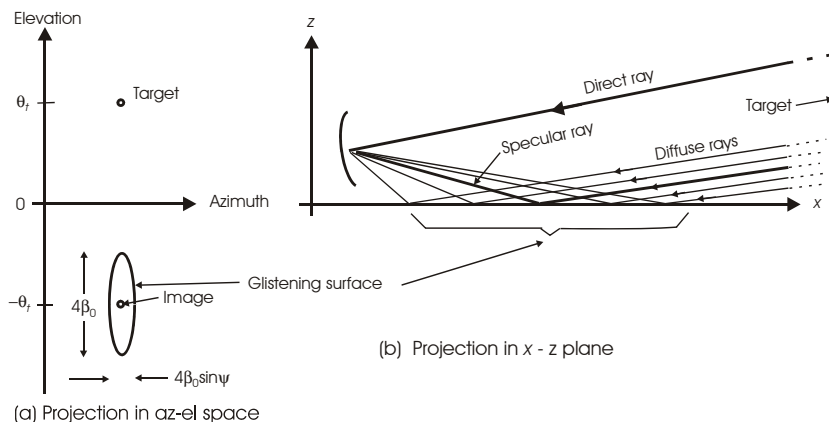


Figure 11.14 (a, b) Specular and diffuse reflections from partially rough surface for specular grazing angle $\psi > 2\beta_0$.

Typical values of the slope parameter β_0 for both land and sea surfaces are in the order of $0.05 \text{ rad} = 3^\circ$. For grazing angles below $2\beta_0$, the upper elevation limit of the glistening surface reaches the horizon, and an intensified region is formed just below the horizon. Modifications to the Beckmann and Spizzichino rough-surface scattering theory that adjust the diffuse power reaching the radar antenna for such low-angle situations are described in [4] and in [31, pp. 430–439].

Over land surfaces, a vegetation absorption factor ρ_v multiplies the Fresnel coefficient, reducing both multipath components. A model in [31, p. 287] provides an estimate of this effect, which will not be considered further here. It should be kept in mind, however, that results from tests run over vegetated terrain may not show the multipath effects that are encountered over barren terrain or the sea.

11.14.2 Distribution of Multipath in Elevation Angle

The effect on a null-tracking monopulse radar is analyzed using the distribution of multipath shown in Figure 11.15. The target appears as an impulse function with power S (normalized to unity as a reference for the multipath power) at elevation θ_t , and its specular image as a smaller impulse of power ρ_{s0}^2 at $-\theta_0 \approx -\theta_t$. The diffuse components have a continuous density extending downward from the horizon. The density has a peak between the horizon and the specular component, and decreases with depression angle. The integral of this density is equal to the total diffuse power $\rho_0^2 \rho_d^2$. In the case shown, the target elevation angle is ≈ 0.7 beamwidth, and the lower difference-channel lobe peaks just below the horizon, with its null near the specular image but with substantial response in the region of maximum diffuse intensity. The specular component of multipath error corresponds to the low value shown in Figure 11.4 for this target elevation.

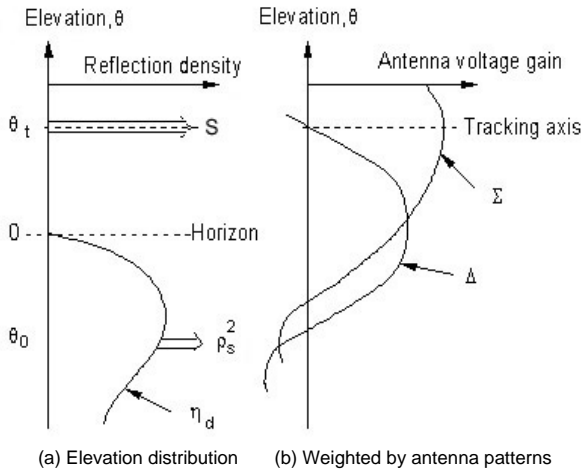


Figure 11.15 (a) Distribution of multipath components and (b) antenna weighting versus elevation for closed-loop tracking. (After: [31].)

11.14.3 Multipath Error for Closed-Loop Tracking

The multipath error for a monopulse radar is calculated separately for specular and diffuse components. The target power S in the sum channel is the product of the sum power gain Σ^2 and the normalized target power on the axis at θ_t . The specular multipath interference I in the sum channel is the product of ρ_s^2 and the value of Σ^2 at the specular angle θ_0 . The difference-channel interference I_d is the product of ρ_s^2 and the value of Δ^2 at the specular angle. The interference terms replace the corre-

sponding random noise terms in (10.39) or clutter terms in (10.57) to give the specular component of multipath error:

$$\sigma_{\theta} = \frac{\theta_{bw}}{k_m} \sqrt{\frac{I_d}{2S} \left(1 + \frac{I}{S} \right)} \quad (11.19)$$

Unless a strong specular component enters the main difference lobe, the sum-channel interference-to-signal ratio I from multipath is small, and the final term in (11.19) can be neglected. Once a strong specular component enters the main difference lobe, the nose-diving phenomenon begins, and error increases rapidly beyond the value given in (11.19).

The diffuse multipath density, weighted by the sum and difference pattern power gains, is integrated over elevation to find interference power components I and I_d for use in calculation of the diffuse multipath error, again using (11.19). The specular and diffuse errors are combined in rss fashion to find total multipath error.

A typical plot of error for an X-band monopulse radar in closed-loop tracking with a beamwidth $\theta_{bw} = 26 \text{ mrad} = 1.5^\circ$, operating over a calm sea (state 2) with roughness $\sigma_h = 0.11 \text{ m}$, has been calculated using the multipath prediction procedure of [31], and is shown in Figure 11.16. At target elevation angles above $1.5\theta_e$ the specular component is negligible, and the diffuse component is below $0.01\theta_{bw}$. As the target descends below $1.5\theta_e$ the diffuse component increases toward $0.04\theta_{bw}$ and the specular component in the first sidelobe rises to $0.02\theta_{bw}$. When the target elevation is $0.5\theta_{bw}$ the “nose-diving” phenomenon appears, and the error abruptly increases to an indeterminate value, reflecting the instability and probable loss of track. This corresponds to the appearance of the first severe dip in tracking angle and the presence of a stable image track curve in Figure 11.4.

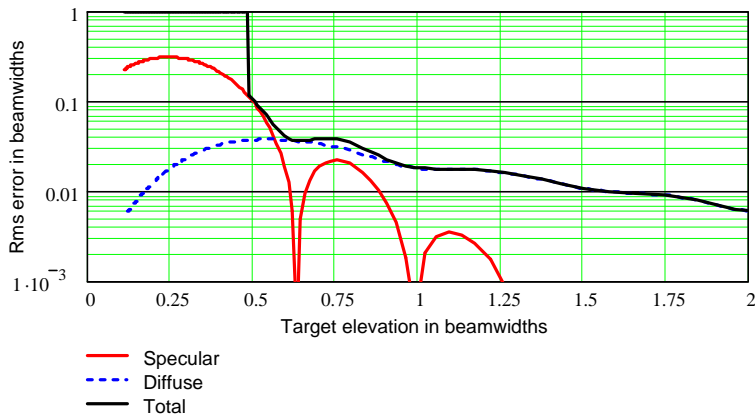


Figure 11.16 Typical elevation multipath error versus target elevation in closed-loop monopulse track.

11.14.4 Effect of Range or Doppler Resolution and Smoothing

In Section 11.6 the use of range or Doppler resolution to reduce multipath error was discussed, and it was concluded that neither offered a practical solution, at least for surface-based radars, because of the small displacement of the specular component in these coordinates. This is illustrated in Figure 11.17 for a radar antenna at $h_a = 20\text{m}$ and a target at $R = 20\text{ km}$, $h_t = 100\text{m}$, flying inbound at 300 m/s . The specular reflection accompanies the peak in diffuse reflection at 0.2-m range delay (relative to the direct ray), and is at the frequency $f_s = 0.12\text{ Hz}$ in Doppler.

The ineffectiveness of smoothing, discussed in Section 11.7, also applies to the diffuse multipath, which in our example appears primarily at frequencies between 0.085 Hz and 0.14 Hz . Smoothing times in excess of 10 seconds would be required to reduced the diffuse multipath, and such times are inconsistent with target dynamics.

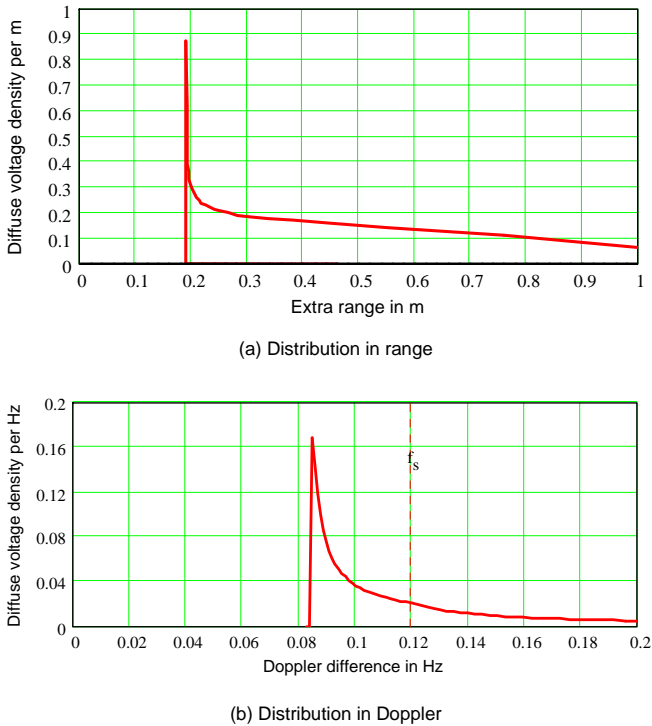


Figure 11.17 (a) Range and (b) Doppler distribution of diffuse multipath components [31].

11.14.5 Low-E Mode

Section 11.8 discussed the use of a mode in which the antenna elevation is limited to an angle of ≈ 0.75 beamwidth when the indicated monopulse angle falls below that value. The multipath error for this mode is shown in Figure 11.18, for the same conditions as used in calculating Figure 11.16. The diffuse error remains essentially the same as for closed-loop tracking, but the specular error is limited, rising gradually at target elevations below $0.5\theta_{bw}$ to reach $\sigma_\theta = 0.4\theta_{bw}$ when the target is at $0.15\theta_{bw}$. The error is large enough that the elevation data becomes useless at target elevations below $\approx 0.3\theta_{bw}$. These results are consistent with the addition of a diffuse component to the errors illustrated in Figure 11.7.

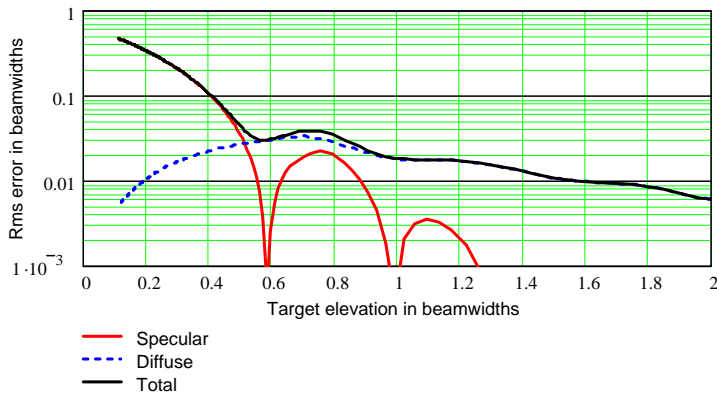


Figure 11.18 Low-E mode monopulse elevation multipath error versus target elevation.

11.14.6 Offset-Null Tracking

The offset-null technique described in Section 11.9 avoids nose-diving and reduces the specular error component. Because the difference pattern continues to track the target in this method, the diffuse multipath will be received with essentially the same strength as in the conventional closed-loop tracker, as shown in Figure 11.16. The over-all effect closely matches the data shown in Figure 11.18 for the low-E mode.

11.14.7 Diffuse Multipath in Patterns Having a Symmetrical Ratio

The special antenna elevation patterns shown in Figure 11.9 are designed to produce the same monopulse output ratios for sources above and below the horizon, eliminating error caused by the specular image. The pattern pair of Figure 11.9(a)

has substantial response in both the A and B patterns to diffuse reflections in the region from the horizon to $-1.5\theta_A$, where θ_A is the beamwidth of the A pattern. This response is reduced in the pattern pair of Figure 11.9(b), at the expense of lower sensitivity to the target signal.

By integration of the diffuse multipath density over these patterns, the error in the symmetrical-ratio system can be found, as shown in Figure 11.19. The pattern pair of Figure 11.9(b) reduces this diffuse multipath error substantially at target elevation angles above $\approx 0.7\theta_A$. However, in the presence of diffuse multipath the technique does not reduce the error below the level seen in Figure 11.18 for the low-E mode using conventional monopulse patterns and is somewhat less accurate below $0.7\theta_A$. Given the additional complexity of creating the patterns and merging the symmetrical-ratio method with normal tracking at higher elevation angles, there seems to be little reason to adopt this technique.

The same problem appears in the double-null tracking technique described in Section 11.11. The high-density diffuse reflection occurs just below the peak value of the ratio plotted in Figure 9.10, and its random phase relative to the direct and image response causes a large elevation error to appear at the output.

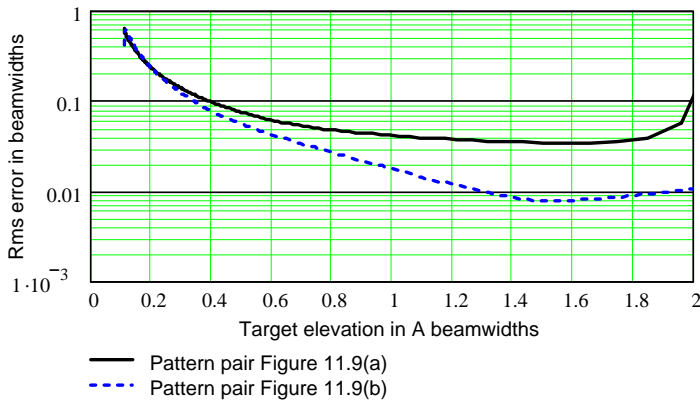


Figure 11.19 Symmetrical-ratio monopulse elevation multipath error versus target elevation.

11.14.8 Complex Indicated Angle with Diffuse Multipath

The use of complex indicated angles from a monopulse radar whose antenna has been fixed near $0.75\theta_{bw}$ was described in Section 11.12, and shown to have been effective in reducing multipath error from the sea surface, when applied to the TRADEX L-band radar at Kwajalein Island (see Figure 9.13). The conditions for that test can be approximated for the grazing angle of the first loop in the spiral plotted in that figure: $\psi \approx 4.5$ mrad, assuming a wavelength $\lambda = 0.23$ m and a sea

state 2 ($\sigma_h = 0.1\text{m}$). The resulting specular scattering factor is $\rho_s = 0.9983$, corresponding to a small diffuse component $\rho_d = 0.059$. Little difficulty from diffuse multipath would be expected.

Another experiment [32] used a K_u-band radar with an elevation beamwidth $\theta_e = 1.4^\circ = 24\text{ mrad}$, operating from an antenna height of 4.7m over a calm sea (state 1, $\sigma_h = 0.03\text{m}$) at ranges from 1 to 9 km, with the target elevation angle varying from 25 mrad to 3 mr. Frequency diversity over a 2-GHz band was used to obtain samples that varied in relative phase more rapidly than would have been the case at a fixed frequency. The signal processor used these samples with time averaging to calculate the derivative of the multipath phase with respect to range, and from that found the target altitude, given the known antenna height and wavelength, and the measured range. The method proved effective over the calm sea, but would obviously have encountered difficulty for sea states 2 and above.

A different situation arose when testing the same technique on a C-band AN/FPS-16 radar over desert terrain characterized by “boondocks” with an surface roughness $\sigma_n \approx 0.5\text{m}$. The elevation beamwidth is $\theta_{bw} = 1.2^\circ = 21\text{ mrad}$, and the radar installation at White Sands gives an antenna height $h_a = 12\text{m}$. When the target elevation is $0.5\theta_{bw} = 10.5\text{ mrad}$, the specular scattering factor is $\rho_s = 0.487$ and the corresponding maximum diffuse factor is 0.873. The result, taken from the final report on the contract that supported the experiment, is presented in [33] and appears in Figure 11.20. As the target flew out to ranges near 50 km, the grazing angle was reduced toward zero, and a larger specular component would be expected, reducing the diffuse component. One loop of the spiral can be discerned where the real part of the monopulse output is negative. There is little information to be obtained from the imaginary part of the complex angle over the remainder of the plot, although the real part shows the expected increase corresponding to higher elevation at short range. Although attributed in the report to a problem with the beacon being tracked, the data show the random variations expected in a diffuse multipath environment.

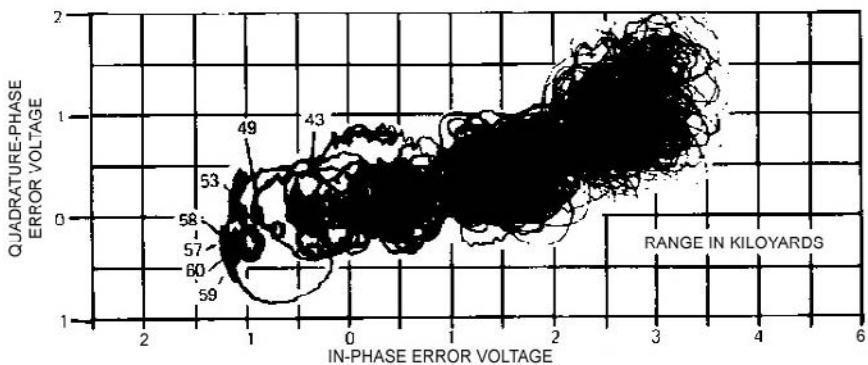


Figure 11.20 Complex indicated angle plot for the White Sands experiment.

These results confirm the judgment expressed in Section 11.12 that the complex-angle method is useful when applied to a low-sited, low-frequency antenna looking over water, in which case diffuse multipath is minimized.

11.14.9 Diffuse Multipath Effect on Independent-Target Methods

Multiple-beam and aperture-sampling solutions to the multiple-source (and multipath) problem were discussed briefly in Section 11.13, and several references were given. It was stressed that three or more beams or samples are required to solve for two targets (e.g., a point target and its specular image), and one additional beam or sample for each additional source. The sensitivity of these procedures to noise increases steeply as the angular separation of the sources decreases below one beamwidth.

As an example, in [34] a C-band aperture-sampled array and processing system was described that minimized both specular and diffuse multipath errors. The aperture-sampled sum and difference beam-forming network is preceded by a spatial filter with response shown in Figure 11.21, designed to minimize all response below the horizon. The thinned array of eight dipole elements had a total height $h = 28\lambda$, giving a standard beamwidth $\theta_0 = 1/28 = 0.036 \text{ rad} = 2.0^\circ$. This limited the slope of the high-pass spatial filter in the cutoff region near the horizon, but its inclusion minimized all the multipath components. Simulations showed significant reduction in the specular multipath error, accompanied by degradation in sum-channel signal-to-noise ratio up to 15 dB at target elevation of 0.1 beamwidth (target-image separation of 0.2 beamwidth).

Less successful was a four-element sampled-aperture array attached to a conventional shipboard X-band monopulse reflector radar, the AN/SPG-53A, and described in a conference paper [28]. The radar beamwidth is $\theta_{bw} = 20 \text{ mrad}$. Simulations presented in the paper showed that the normal monopulse tracking

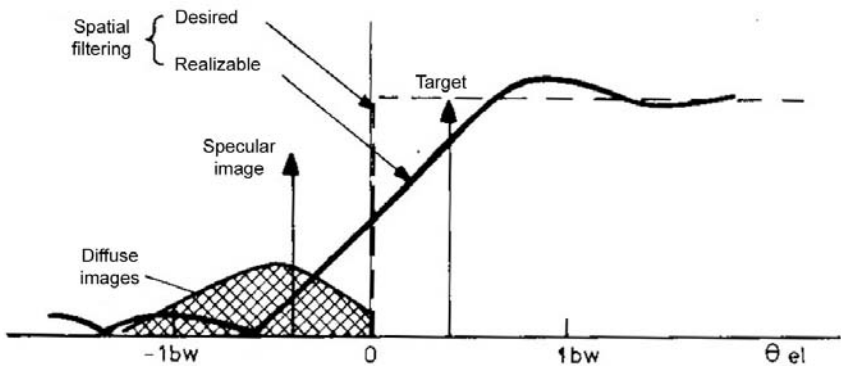


Figure 11.21 Distribution of signal inputs and response of spatial filter. (After: [34].)

error was $\sigma_\theta = 0.7\theta_{bw} - 0.9\theta_{bw}$ at target elevations between $0.125\theta_{bw}$ and $0.376\theta_{bw}$. With the array the rms errors were reduced to $\sigma_\theta < 0.1\theta_{bw}$ on a single-pulse measurement and $\sigma_\theta \approx 0.01\theta_{bw}$ after averaging of 100 pulses. The paper indicated that results of sea trials from Pacific Ocean operations would be presented at the conference. Those results turned out to show that the normal monopulse error in tracking below one beamwidth over the sea was $\sigma_\theta \approx 2$ mr, and that the errors using the aperture-sampling array were $\sigma_\theta \approx 2.5$ mr. It was concluded that the Pacific Ocean failed to conform to the smooth-surface model for specular multipath that was the basis of design.

The type of result found for the system of [28] characterizes most multiple-beam and aperture-sampling systems designed for multiple-target estimation, because the number of multipath sources in the actual operational environment cannot be known in advance, and exceeds the values for which practical systems can be designed.

11.14.10 Summary of Multipath Mitigation Methods

It is seen in this section that the several approaches to multipath mitigation yield consistent results:

1. Many methods provide protection against the nose-diving phenomenon that afflicts the closed-loop tracker over smooth surfaces.
2. None of the methods provide accuracy in the diffuse multipath environment that is significantly better than the fixed-beam low-E mode of a conventional monopulse radar, and some are subject to larger errors or total failure for other than pure specular multipath.

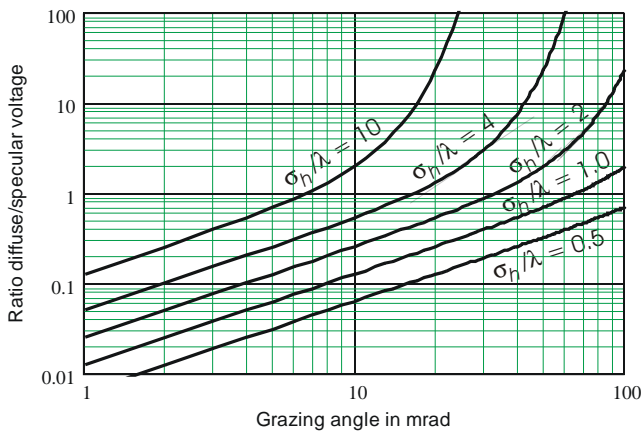


Figure 11.22 Ratio of diffuse to specular multipath voltage versus grazing angle, for different ratios of roughness/wavelength.

3. Use of a narrow elevation beam with vertical polarization is the fundamental approach to obtaining accurate elevation data.

The requirement for “pure specular” reflection can be interpreted using Figure 11.22, which shows the ratio ρ_d/ρ_s of diffuse to specular scattering factors. The diffuse component may generally be neglected if it is less than 1% of the specular, a ratio that is available only for very smooth surfaces at very low grazing angles (e.g., $\sigma_h/\lambda < 0.5$ at $\psi < 2$ mrad). It must be considered a serious source of error if it is greater than 10% (e.g., $\sigma_h/\lambda < 1.0$ at $\psi < 10$ mrad, or $\sigma_h/\lambda < 2$ at $\psi < 4$ mrad). For X-band radar ($\lambda = 0.03$ m), these values correspond to $\sigma_h < 1.5$ cm, 3 cm, and 6 cm, respectively, or to sea states 0, 1, and ≈ 1.5 . Test data confirm that the only method providing satisfactory reduction in multipath error is the complex-angle method, as applied to the low-sited L-band TRADEX radar over the Pacific Ocean [24] and the low-sited Ku-band radar over smooth water [32].

References

- [1] IEEE Standard 100, *The Authoritative Dictionary of IEEE Standard Terms*, 7th ed., New York: IEEE Press, 2000.
- [2] P. Beckmann and A. Spizzichino, *The Scattering of Electromagnetic Waves from Rough Surfaces*, Oxford, U.K.: Pergamon Press, 1963; reprint, Dedham, MA: Artech House, 1987.
- [3] D. K. Barton, “Low-Angle Radar Tracking,” *Proc. IEEE*, Vol. 62, No. 6, June 1974, pp. 687–704. Reprinted in *Radar*, Vol. 4, *Radar Resolution and Multipath Effects*, Dedham, MA: Artech House 1975.
- [4] D. K. Barton, “Low-Altitude Tracking Over Rough Surfaces, I: Theoretical Predictions,” *IEEE Eascon-79*, Washington, D.C., October 9–11, 1979, pp. 224–234.
- [5] D. E. Kerr, (ed.), *Propagation of Short Radio Waves*, New York: McGraw-Hill, 1947. Reprint, CD-ROM ed., Norwood, MA: Artech House, 1999.
- [6] W. S. Ament, “Toward a Theory of Reflection by a Rough Surface,” *Proc. IRE*, Vol. 41, No. 1, January 1953, pp. 142–146.
- [7] M. Calamia, et al., “Radar Tracking of Low-Altitude Targets,” *IEEE Trans. on Aerospace and Electronic Systems*, Vol. 10, No. 4, July 1974, pp. 539–544 (corrections, March 1975 issue).
- [8] J. T. Nessmith and S. M. Sherman, “Phase Variations in a Monopulse Antenna,” *Proc. IEEE International Radar Conf.*, Washington, D.C., April 21–23, 1975, pp. 354–359.
- [9] D. D. Howard, J. T. Nessmith and S. M. Sherman, “Monopulse Tracking Errors Due to Multipath,” *IEEE Eascon-71*, Washington, D.C., October 6–8, 1971, pp. 175–82. Reprinted in *Radars*, Vol. 4, *Radar Resolution and Multipath Effects*, D. K. Barton, (ed.), Dedham, MA: Artech House, 1975.
- [10] M. I. Skolnik, *Introduction to Radar Systems*, 3rd ed., New York: McGraw-Hill, 2001, pp. 172–176.

- [11] F. H. Thompson and F. A. Kittredge, *A Study of the Feasibility of Using 35 GHz and/or 94 GHz as a Means of Improving Low-Angle Tracking Capability*, Naval Research Laboratory Report 2249, May 1971. Reprinted in *Radars*, Vol. 4, *Radar Resolution and Multipath Effects*, D. K. Barton, (ed.), Dedham, MA: Artech House, 1975.
- [12] L. Klaver, "Combined X/K_a-Band Tracking Radar," *Proc. Mil. Microw. Conf.*, MM-78, London, October 25–27, 1978, pp. 146–156. Reprinted, *Radar Electronic Counter-Countermeasures*, S. L. Johnston, (ed.), Dedham, MA: Artech House, 1979, pp. 179–188.
- [13] F. E. Nathanson, *Radar Design Principles*, 2nd ed., New York: McGraw-Hill, 1991 (see Table 5.12, p. 196).
- [14] J. M. Loomis and E. R. Graf, "Frequency-Agility Processing to Reduce Glint Pointing Error," *IEEE Trans. on Aerospace and Electronic Systems*, Vol. AES-10, No. 6, November 1974, pp. 811–820. Reprinted in *Radars* Vol. 6, *Frequency Agility and Diversity*, D. K. Barton, (ed.), Dedham, MA: Artech House, 1977, pp. 385–396.
- [15] S. David and H. W. Redlein, "Extending the Low-Altitude Tracking Capabilities of Monopulse Radars by Antenna Pattern Modification," *Proc. 14 Annual Tri-Service Radar Symp.*, June 1968, pp. 589–609 (see unclassified abstract).
- [16] H. Redlein, *Modification of Monopulse Antenna Radiation Patterns for Low-Angle Tracking Improvement*, Wheeler Laboratories, Report 1506, March 10, 1969.
- [17] W. D. White, "Low-Angle Radar Tracking in the Presence of Multipath," *IEEE Trans. on Aerospace and Electronic Systems*, Vol. AES-10, No. 6, November 1974, pp. 835–852. Reprinted in *Radars*, Vol. 4, *Radar Resolution and Multipath Effects*, D. K. Barton, (ed.), Dedham, MA: Artech House, 1975.
- [18] P. R. Dax, "Accurate Tracking of Low-Elevation Targets over the Sea with a Monopulse Radar," *IEE Conf. Publ. No. 105, Int. Conf. on Radar—Present and Future*, London, October 23–25, 1973, pp. 160–165.
- [19] P. R. Dax, "Keep Track of That Low-Flying Attack," *Microwaves*, April 1976, pp. 36–53.
- [20] W. D. White, "Double-Null Technique for Low-Angle Tracking," *Microw. J.*, December 1976, pp. 35–38, 60.
- [21] S. M. Sherman, "Complex Indicated Angles Applied to Unresolved Radar Targets and Multipath," *IEEE Trans. on Aerospace and Electronic Systems*, Vol. AES-7, No. 1, January 1971, pp. 160–170. Reprinted in *Radars* Vol. 1, *Monopulse Radar*, D. K. Barton, (ed.), Dedham, MA: Artech House, 1977.
- [22] P. Z. Peebles, Jr., and L. Goldman, Jr., "Radar Performance with Multipath Using the Complex Angle," *IEEE Trans. on Aerospace and Electronic Systems*, Vol. AES-7, No. 1, January 1971, pp. 171–178. Reprinted in *Radars*, Vol. 4, *Radar Resolution and Multipath Effects*, D. K. Barton, (ed.), Dedham, MA: Artech House, 1975.
- [23] D. D. Howard, S. M. Sherman, D. N. Thomson and J. J. Campbell, "Experimental Results of the Complex Indicated Angle Technique for Multipath Correction," *IEEE Trans. on Aerospace and Electronic Systems*, Vol. AES-10, No. 6, November 1974, pp. 779–787.
- [24] S. M. Sherman and J. C. Spracklin, "Complex-Angle Monopulse Using the TRADEX Radar," *Proc. ARPA Low-Angle Tracking Symp.*, Washington, D.C., December 1976.
- [25] M. D. Symonds and J. M. Smith, "Multi-Frequency Complex-Angle Tracking of Low-Level Targets," *IEE Conf. Publ. No. 105, Int. Conf. on Radar—Present and Future*, Lon-

- don, October 23–25, 1973, pp. 166–171. Reprinted in *Radars*, Vol. 4, *Radar Resolution and Multipath Effects*, D. K. Barton, (ed.), Dedham, MA: Artech House 1975.
- [26] P. Z. Peebles, Jr., “Multipath Angle Error Reduction Using Multiple-Target Methods,” *IEEE Trans. on Aerospace and Electronic Systems*, Vol. AES-7, No. 6, November 1971, pp. 1123–1130. Reprinted in *Radars*, Vol. 4, *Radar Resolution and Multipath Effects*, (D. K. Barton, ed.), Dedham, MA: Artech House, 1975.
- [27] P. Z. Peebles, Jr., “Further Results on Multipath Angle Error Reduction Using Multiple-Target Methods,” *IEEE Trans. on Aerospace and Electronic Systems*, Vol. AES-9, No. 5, September 1973, pp. 654–659.
- [28] J. E. Howard, “A Low-Angle Tracking System for Fire Control Radars,” *IEEE 1975 International Radar Conf.*, Washington, D.C., April 21–23, 1975, pp. 412–417.
- [29] F. G. Willwerth and I. Kupiec, “Array Aperture Sampling Technique for Multipath Compensation,” *Microw. J.*, June 1976, pp. 37–39.
- [30] S. Haykin, J. Kesler and J. Litva, “Evaluation of Angle of Arrival Estimators Using Real Multipath Data,” *Proc. International Conf. on Acoustics, Speech and Signal Processing*, Boston, MA, April 14–16, 1983.
- [31] D. K. Barton, *Radar System Analysis and Modeling*, Norwood, MA: Artech House, 2005.
- [32] C. Eckersten and B.-O. Ås, “Radar Tracking of Sea-Skimmers, an Implementation of ‘Complex Angle,’” *IEE International Conf Radar-92*, Brighton, U.K., October 12–13, 1992, pp. 46–49.
- [33] D. K. Barton, “Radar Multipath,” *1976 Microwave Journal Microwave Engineers’ Handbook and Buyer’s Guide*, pp. 36–41.
- [34] P. Barton, et al., “Array Signal Processing for Tracking Targets at Low Elevation Angles,” *IEE International Conf. Radar-77*, London, October 25–28, 1977, pp. 318–322.

Chapter 12

Monopulse Countermeasures and Countercountermeasures

Deployment of monopulse radars for military use was accompanied by development and deployment of electronic countermeasures (ECM¹) equipment for use against them. A monopulse radar acquiring its target is subject to the same ECM techniques used against any type of radar, such as masking of the target by random pulses, noise jamming, or chaff. These common techniques are discussed here only briefly, except when monopulse offers a solution not available in other types of radar. Another class of ECM techniques developed to disturb the tracking of sequential lobing radars has little effect on monopulse tracking. Such techniques include self-protection jammers that rely on amplitude modulation to induce large errors in radars that use sequential lobing. They provide a strong, point-source signal that may actually improve monopulse tracking accuracy.

ECM techniques used specifically against monopulse radars are designed to break the lock of the angle tracking loop, or at least to induce large errors, either by increasing errors that are naturally present in monopulse radars or by exploiting faulty radar design, construction, or adjustment. The first type is known as *generic monopulse ECM*. The sources of angle error in monopulse radars are listed in Table 12.1, along with the corresponding ECM techniques. Sections of this book in which the errors have been discussed are listed. The present chapter discusses monopulse ECM techniques and their effects on tracking, as applicable to surface-based and airborne radars and homing seekers. Limitations of ECM techniques and radar counters (ECCM) to them are also discussed.

¹ Rather than the terms electronic attack (EA) and electronic protection (EP), recently coined by the electronic warfare community, we use here the traditional ECM and ECCM because they more clearly define the measures and counters applicable to monopulse, and are less likely to be replaced by yet another new set of terms needed to cover the diversity of military electronics.

Table 12.1 Natural Error Sources and Related ECM

<i>Natural Source</i>	<i>Chapter/Section</i>	<i>ECM Technique</i>
Thermal noise	Section 10.1	Noise jamming (stand-off or escort)
Unresolved targets	Chapter 9	Formation jamming, decoys
Clutter	Section 10.2	Chaff
Multipath	Chapter 11	Surface bounce, bistatic jamming
Glint	Section 10.5	Cross-eye
Cross-polarized response	Section 10.4	Cross-pol
Phase and amplitude imbalance	Section 10.4	Skirt- and image-frequency jamming Two-frequency jamming
Monopulse normalization	Chapter 8	Intermittent (AGC) jamming

Generic monopulse jamming techniques are listed in bold type.

The first section briefly discusses the use of jamming that masks the target echo, either to deprive the radar of range or Doppler data or to generate erroneous data in those coordinates. This is followed by a discussion of generic monopulse ECM techniques, listed in bold type in Table 12.1. A final section deals with ECM that is designed to exploit weaknesses in design or manufacture of the monopulse radar.

Much of the discussion in unclassified form is made possible by the published work of Leonov and Fomichev [1]. That book contained an entire chapter on “Interference Tolerance of Monopulse Radars,” in which both ECM and ECCM were discussed in detail, with copious references to both Russian and Western literature. We have made use of those discussions in the material that follows.

12.1 RANGE AND DOPPLER DENIAL AND DECEPTION

12.1.1 Range and Doppler Denial

Noise jamming is a robust ECM that can mask the target echo, preventing the radar from measuring range and Doppler shift of the target. When emitted from a jammer on the target (self-protection jamming) the jamming may provide a source of more accurate angle tracking in the track-on-jam or home-on-jam mode.

12.1.1.1 Track-on-Jam

The monopulse angle sensing system must produce outputs that accurately indicate the angle of arrival of the noise jamming, regardless of its bandwidth, spectral distribution, average power, amplitude distribution, and possible modulation. The spectral distributions of noise jammers vary widely, and may be generated by rapid sweeping of a narrowband signal over the band used by one or more radars.

Jammer noise amplitude distributions, often considered to be Gaussian, exhibit clipping of peaks or even hard limiting, introduced to increase the average power of the jammer transmitter. A monopulse radar that is intended to obtain angle data on jammers must preserve its angle sensing capability on “signals” that differ in many respects from the echoes of its own transmissions. This capability in a homing seeker is known as *home-on-jam*, and designers of homing seekers place a high premium on successful performance in this mode.

The jamming bandwidth may be wide enough to enter the monopulse receiving channels both at the frequency to which they are tuned for the target echo and at the image frequency (displaced by the IF from the local oscillator frequency, but on the opposite side from the echo). Many radar designs lack tunable RF preselectors that exclude inputs at the image frequency. Unless the phase shifts of the sum and difference receiver channels are matched in both the RF and IF stages, the image-frequency contribution to the d/s output of the monopulse processor may fail to assist in tracking, and in case of a 90° RF phase shift that is removed by a -90° IF phase shift, the contributions cancel, preventing measurement or tracking on the jammer. This problem was corrected in the design of the AN/FPS-16, not to provide track-on-jam but rather to permit passive tracking on the Sun [2]. Another solution is to use an IF that is high enough to place the image outside the band within which the radar can be tuned, allowing use of the more practical fixed-tuned RF preselector filters.

12.1.1.2 Weapon System Design

The purpose of most military monopulse radars (and all homing seekers) is to guide a weapon to the selected target. If the target has denied range and Doppler measurement, a fire-control solution must be used that directs the weapon on the basis of angle data alone. In the case of a homing missile, proportional navigation (or its modern Kalman-filter equivalent) can achieve adequate performance without range data (although approximate range-to-go information provides better end-game performance). Command guided missiles and gunfire control are more severely impacted by lack of range data. Triangulation from a separated radar is one method of obtaining approximate range on a jamming target.

12.1.2 Range and Doppler Deception

Deceptive repeater jammers are designed to capture the range or Doppler tracking loop and the AGC system of the radar. A deception pulse is superimposed on the target echo in the tracking gate. Its amplitude is increased to the point where the echo is suppressed, and the deceptive pulse (or spectrum, for a CW or pulsed Doppler radar) is then programmed to move away from the target position in range or Doppler. This is called range-gate pull-off (RGPO) or velocity-gate pull-off (VGPO). Both may be used simultaneously against pulsed Doppler radars. When

pull-off has been accomplished (as estimated by the jammer based on anticipated time constants of the AGC and range or Doppler tracking loops), the deceptive emission is discontinued, forcing the radar to reacquire the target. Rapid reacquisition by the radar tracker is possible when the radar beam still illuminates the target, so this jamming is usually combined with an angle deception technique to introduce an angular rate away from the target just before the deceptive emission is discontinued. If that rate is large enough, the radar may be forced to reacquire in angle as well as in range or Doppler, and during the required angle scan no tracking data are provided to the weapon. Angle deception is more effective when there is no target echo in the range or Doppler gate that selects inputs to the angle tracking loops.

Radar design to prevent effective RGPO/VGPO operation must provide either recognition that deception is occurring, permitting the established track to coast through the deception period, or rapid reacquisition after the deception cycle. Coordinated range and Doppler tracking and variation of AGC time constants makes deception more difficult. Avoiding angle deception as discussed in Sections 12.2 and 12.3, is a critical requirement, as is the ability to recognize the occurrence of angle deception. The use of monopulse information to detect the presence of unresolved targets (see Section 9.9) contributes to this ability if implemented in the radar.

12.1.3 Chaff Deception

Most modern monopulse radars have Doppler-based circuits (e.g., moving target indication or pulsed Doppler) to reject chaff and other clutter. Rejection is based on the difference between the target's radial velocity and that of the air mass in which airborne clutter is embedded. An aircraft self-protection technique, when under track by a weapon-control radar, is to release one or more chaff bursts while executing a turn that brings the aircraft radial velocity to zero (relative to the air mass). If the radar cross section of the chaff exceeds that of the target, the chaff echo may capture the radar track, allowing the target to move, unseen, out of the beam. The weapon system must recognize this event and reacquire the target to restore the needed guidance data.

The counter to chaff deception is to recognize the chaff deployment and to coast the range and angle tracks for a period long enough that the target becomes resolvable in at least one coordinate. This must be done even if the target performs further maneuvers to deviate from the coasting track. Since chaff comes to rest in the air mass almost instantly, linear track coasting is often sufficient, and addition of a quadratic term can extend the period in which the beam illuminates the target and can reacquire track.

As with active deception, the ability to recognize the occurrence of chaff deception is a critical requirement, along with use of monopulse information to detect the presence of unresolved targets (Section 9.9).

12.2 GENERIC MONOPULSE ECM

A monopulse jammer is generally carried by the target vehicle (self-protection ECM) or by the target vehicle in cooperation with others nearby. The equipment uses one or more deceptive jamming techniques, as distinguished from target masking. This class of ECM, known as generic monopulse ECM, exploits fundamental limitations of the angle sensing method that are inherent, to some extent, in all monopulse radars. Schleher notes in [3, p. 262]:

Some monopulse angular jamming techniques, such as skirt and image jamming and cross-polarized jamming, are designed to exploit weaknesses in the implementation of the monopulse radar. Other jamming techniques, such as cross-eye, terrain or ground bounce, and blinking or formation jamming, are designed to attack weaknesses fundamental to all monopulse tracking systems. In general, it is better to attack fundamental weaknesses than to rely on design weaknesses.

Designers of the generic monopulse ECM techniques seek to reproduce effects of natural sources of angle error, using emissions that increase the errors to the point where they may break lock of the angle tracking loops. The techniques may also attack the range tracking loop in order to suppress the target echo and achieve greater angle error than would be possible while competing with the echo.

12.2.1 Formation Jamming

It was established in Section 9.10 that the average tracking point of a monopulse radar, in the presence of two unresolved sources, lies on the stronger of the two sources. If both sources fluctuate in amplitude such that the stronger source shifts from one to the other, the tracking point shifts accordingly if the tracking loop response is fast enough to follow. If the shift occurs too rapidly for the loop to follow, the average tracking point lies at the power centroid of the sources, and this applies also to more than two rapidly fluctuating sources. Formation jamming exploits this relationship in any of three ways.

12.2.1.1 Multiple Continuous Noise Jammers

Noise jamming is a robust technique, in that it does not depend on detailed knowledge of the radar waveform and processing, and can be used simultaneously against more than one type of threat in the operating band. In the multiple-jammer approach, noise jammers, each delivering power to the radar that exceeds the target echo, are carried on two or more vehicles in formation within the width of the main difference lobes (approximately the width of the full sum mainlobe) and at approximately the same range. The radar tracking point in each angle coordinate then lies near the power centroid of the formation. Gunfire or a missile controlled by the radar track is directed toward the centroid rather than to any single target. Targets are protected if their linear separation, corresponding to the product of

range and the width across the lobes, exceeds the lethal diameter of the gunfire or missile warhead aimed at the centroid.

One limitation in this technique is that the linear extent of the formation must be scaled to the range from the radar, which may not be known to the attacking force, and cannot easily be measured with conventional on-board equipment such as radar warning receivers (RWRs). As the range decreases, the separation may become so narrow that it fails to provide protection. The proliferation of anti-air missiles using homing guidance, and including home-on-jam (HOJ) provisions, also discourages the use of continuous noise jamming. As the missile closes on the target formation, individual targets become resolvable and the missile homes accurately on a single jammer in the formation.

12.2.1.2 Multiple Blinking Noise Jammers

Use of a coordinated blinking strategy can overcome the limitations of the continuous-jamming technique. The jammers are turned on and off according to a pseudo-random schedule that abruptly shifts the tracking point from one to another target. By holding the tracking time on any single target to less than the time required to establish a track and compute new gun orders or a new missile aim point, accurate fire control is denied. In the case of a missile, the rapid changes in apparent target position may cause excessive acceleration commands that saturate the guidance loop and cause instability or even failure of missile structure. The induced errors are larger than for continuous jamming because the tracking point shifts from one side of the formation to the other, with possible overshoot in both directions depending on the loop characteristics. Loss of lock is possible and reacquisition is made difficult. The required spacing of jamming vehicles is similar to that in the continuous jamming technique.

12.2.1.3 Decoy Jammers

Towed decoys create false targets within the resolution cell occupied by the intended target of the monopulse radar. The decoy jammer can be either self-contained in the decoy capsule or it can amplify and emit signals generated on the protected aircraft and carried to the decoy over the tether. In either case the emission must be strong enough to capture the radar track and redirect the weapon (usually a missile) along a path that spares the aircraft. This imposes limits on the flight path of the aircraft relative to the radar and its associated weapon, on aircraft maneuvers, and on the length of the tether. The weapon must be redirected from the path to the target to one that avoids passing within fuzing range of the target. This generally requires that the tether length times the sine of the angle between the tether and the weapon trajectory exceed the fuzing range. Physical limitations on tether length usually guarantee that the decoy is unresolvable in angle from the target, and the jamming waveform is designed to prevent range resolution.

There is no specific monopulse counter to the towed decoy, but the weapon system can be designed to reduce its effectiveness by such measures as shaped trajectories and large warheads.

12.2.2 ECCM Against Formation Jamming

Monopulse radar counters to formation jamming include use of narrow beamwidth and adaptive nulling in array antennas. Narrow beamwidth is the primary monopulse ECCM against formation jamming. The narrow beam imposes a tight requirement on station-keeping in the jamming formation, and failure to meet the requirement may permit the radar to establish and maintain lock on a single target. At long ranges, where the station-keeping requirements are not difficult for the jammers to meet, the multiple-target tracking techniques discussed in Sections 9.12–9.17 may be used to impose more difficulty on the attacking formation. Adaptive nulling can be applied to array antennas, which can be designed to form one or more nulls, even within the mainlobes of the patterns. The null locations adapt to the angles of jammers that use high duty cycle emissions, as is the case with formation jamming. The literature describing adaptive nulling is extensive [4–6]. Most approaches to adaptive nulling require that multiple subarrays, if not individual elements of the array, pass their outputs through separate receivers into a beamforming processor, which calculates complex weights that are applied to the outputs before they are summed to produce the beam. In the case of monopulse radars, the sum and both difference patterns must be formed with adaptive weights, and constraints are imposed on the process to preserve monopulse angle estimation properties on the selected target.

12.2.3 Cross-Eye Jamming

The cross-eye jammer enhances the glint error already present in an extended target (see Section 10.5.1). Extreme errors can be generated if signals from two equal target sources arrive at the radar antenna in phase opposition (Figure 9.3). The tracking angle error ϵ_θ relative to the midpoint between the two sources is, from (9.8b) and (9.9b):

$$\epsilon_\theta = \frac{\Delta\theta}{2} \operatorname{Re} \left(\frac{1 - pe^{j\phi}}{1 + pe^{j\phi}} \right) = \frac{\Delta\theta}{2} \left(\frac{1 - p^2}{1 + 2p \cos \phi + p^2} \right) \quad (12.1)$$

where $\Delta\theta = L/R$ is the angle subtended by the two sources separated by a distance L at range R from the radar, p is the amplitude ratio of the two sources, and ϕ is their phase difference.

The cross-eye jammer attempts to create this situation from a single platform by radiating coherently related repeater signals from two separated antennas (e.g.,

on the wing-tips of an aircraft). If the null of the interferometer pattern created by these signals can be made to lie within the radar antenna, the sum signal s fades and the difference signal d is enhanced, generating a large error. The problem in implementing this jammer is that the interferometer null of the antenna pair must be positioned on the radar antenna for maximum effectiveness, and this requires that the two transmitted signals arrive at the radar with phase difference $\phi \approx 180^\circ$, as well as near-equality in amplitude ($p \approx 1$).

The magnitude of the error, and the tolerance in amplitude and phase to produce a given error, may be estimated from (12.1). For perfect antiphase sources ($\phi = \pi$ rad) the cross-range error $\epsilon_x = R\epsilon_\theta$ for a target span L at target range R is

$$\epsilon_x = \frac{L}{2} \left(\frac{1+p}{1-p} \right) \approx \frac{L}{1-p} \quad (12.2)$$

where the approximation assumes $p \approx 1$.

Assume as an example that an anti-air missile warhead has a nominal lethal radius of 15m, and that a miss distance of at least 60m from the center of the target aircraft is required to ensure its survival. For an aircraft with wingspan $L = 15$ m, assuming that the error is dominated by a cross-eye jammer, the cross-eye gain and phase tolerances can be specified as follows:

- If the phase between the two repeater outputs is exactly π rad, their amplitudes must be equal within ± 2.2 dB ($0.778 < p < 1.286$). The cross-eye null is pointed exactly at the center of the radar antenna and for $p = 0.778$ or 1.286 has a depth 12.2 dB below the sum of the two sources.
- If the amplitudes differ by 1.0 dB ($p = 0.891$ or 1.122), the phase difference ϕ must be within $\pi \pm 0.125$ rad ($180^\circ \pm 7.16^\circ$). It turns out that an amplitude ratio of 1.0 dB is near the optimum value, since for ratios nearer unity the error spike becomes narrower and the allowable phase error decreases. The null depth is 18.8 dB below the coherently added sum of the two sources. The spacing of wingtip antennas on the aircraft corresponds to $\Delta\phi = 2\pi L/\lambda$ radians of phase, or $1,000\pi$ radians at X-band. The tolerance in pointing the null is $(\pi - \phi)/\Delta\phi = \pm 40$ μ rad relative to the center of the radar antenna. If these tolerances can be held, and if the resulting cross-eye input to the sum channel exceeds the echo signal by a sufficient margin, the radar is subject to the error, and may lose lock as the error varies with variations in phase and amplitude.

More detailed analysis of the cross-eye jammer can be found in [7].

The cross-eye errors given by (12.1) and (12.2) are based on the assumption that the target echo signal is absent or very small relative to the cross-eye jamming

in the sum channel. This allows the denominator of (12.1) to approach zero (± 0.125) to produce a cross-range error $\epsilon_x = 4L$. According to [1, p. 259], effective cross-eye jamming must be 20 dB above the target echo. This can be reduced to 6 dB if range or Doppler deception is used to pull the tracking gate off the target echo.

Implementation of the cross-eye jammer is difficult, and practical methods are subject to both proprietary and classification restrictions. The basic method is shown in Figure 12.1. Each of the two antennas is connected through waveguide and a circulator to the input of one repeater amplifier and to the output of the other, so that signals received by each antenna are amplified and retransmitted through the other. If the paths between the two antennas were exactly equal, the retransmitted signals would add coherently at the radar, but a phase shift of 180° is placed in one path to place them in antiphase. Variation in the attitude of the aircraft does not disturb this 180° phase relationship, so all that is necessary is to maintain adequate antenna gain in the direction of the radar, approximate amplitude balance between the two retransmitted signals, and adequate gain to make the signals dominate the echo at the radar.

The cross-eye antenna outputs must be isolated from each other by a factor greater than the gain of the repeater amplifiers to avoid forming a self-excited oscillator. The total repeater gain G_{rep} can be defined as the ratio of its effective radiated power $P_j G_j$ in the direction of the radar to the input signal S_{rj} from the radar. Schleher [8] derived an expression for the effective radar cross section σ_e of a repeater:

$$\sigma_e = \frac{G_{rep} \lambda^2}{4\pi L_{pol}^2} \quad (12.3)$$

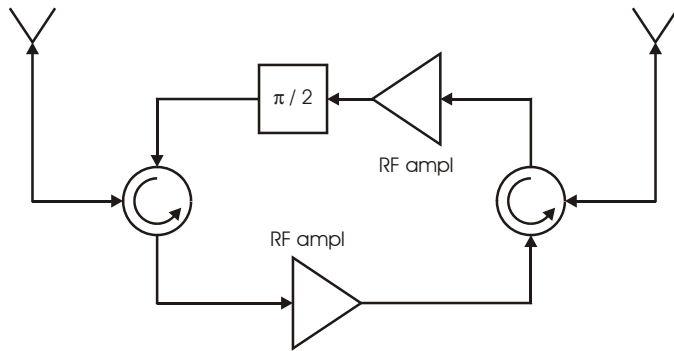


Figure 12.1 Basic cross-eye repeater configuration for jammer phase difference $\phi = 180^\circ$.

where $L_{pol} \geq 1$ is the one-way loss in jammer-to-radar coupling resulting from possible mismatched polarization of the jammer antennas. The repeater gain is expressed as the product of the antenna gains for transmitting and receiving and the electronic gain G_e of the amplifiers:

$$G_{rep} = G_{jr} G_{jt} G_e = G_j^2 G_e \quad (12.4)$$

where the transmitting and receiving gains G_{jr} and G_{jt} are assumed equal. Hence, the required electronic gain, to achieve the ratio $\sigma_e/\sigma = r_\sigma$ ($= 4$ to 100) required for effective jamming is

$$G_e = \frac{4\pi L_{pol}^2 \sigma}{G_j^2 \lambda^2} r_\sigma \quad (12.5)$$

As an example, assume the following parameters:

- Polarization mismatch $L_{pol} = 3$ dB;
- Target cross section $\sigma = 1$ m²;
- Jammer antenna gain $G_j = 6$ dB;
- Wavelength $\lambda = 0.03$ m;
- Required cross-section ratio $r_\sigma = 6$ dB (target echo pulled from tracking gate).

The required electronic gain is $G_e = 1.4 \times 10^4 = +41.4$ dB. In order to prevent self-oscillation, the product of electronic gain and coupling between antennas (and between isolated terminals of the circulator) must be less than unity, which in this case imposes difficult requirements on both the circulators and the antennas (including coupling through the aircraft structure). The problem may be solved by a combination of careful design and high-rate commutation (gating) that allows only one of the amplifiers to operate at a given instant.

12.2.4 Surface-Bounce Jamming

The problem of monopulse tracking in the presence of multipath at low elevation angles was discussed in Chapter 11. The low-angle target can increase the tracking error and potentially break the tracking loop by emitting jamming that is directed toward the surface, increasing the ratio p of reflected to direct signals in (11.3) and (11.4). When that ratio exceeds unity, the tracking point shifts from the target to its image. The geometry of surface-bounce jamming is shown in Figure 12.2.

Major problems in surface-bounce jamming are: to ensure that the signal emitted by the jammer sidelobe along the direct jammer-to-radar path, shown

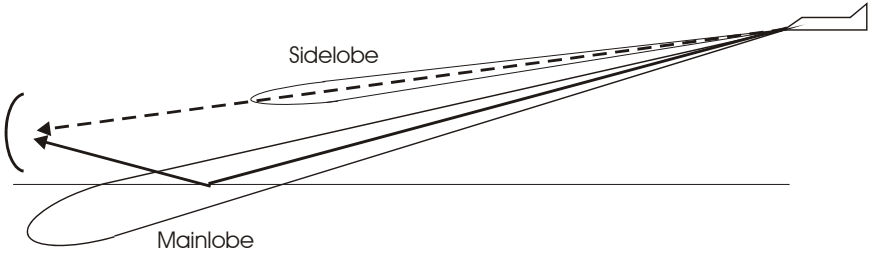


Figure 12.2 Geometry of surface-bounce jamming.

dashed in the figure, is a small fraction of that in the mainlobe directed to and reflected from the surface; and to redirect the radar mainlobe, which may be tracking the target before jamming begins, to the reflected image. The ratio p of reflected to direct signal voltage is

$$p = \rho \sqrt{G_{mlj} / G_{slj}} \quad (12.6)$$

Here G_{mlj} and G_{slj} are the jammer antenna mainlobe and sidelobe power gains and $\rho = \rho_0 \rho_v$ is the product of the Fresnel reflection coefficient of the surface (Figure 11.2) and a vegetation coefficient $\rho_v < 1$ applicable to most land surfaces. When the target elevation angle is less than $\approx 0.7\theta_{bw}$, the reflected jamming will lie within the radar antenna's mainlobe, and for $p > 1$ the track will then rapidly jump to the image angle (or to the angle of peak intensity of the glistening surface, if the reflection is predominantly diffuse). When the target elevation exceeds $0.7\theta_{bw}$ the radar can maintain angular resolution on the target, requiring a much larger reflected signal to cause transfer to the image.

The transfer to the image for targets above $0.7\theta_{bw}$ is made easier if strong diffuse reflection is present. As shown in Figure 11.15, diffuse reflections typically extend upwards from the image to the horizon, and a fraction of the diffuse power can enter the lower mainlobe of the difference pattern when the target is tracked at elevations as high as about $1.4\theta_{bw}$. In this case a ratio G_{mlj}/G_{slj} somewhat greater than would be required for a target below $0.7\theta_{bw}$ is necessary to transfer of the track from target to the underlying surface.

Monopulse radar counters to surface-bounce jamming include reduction in surface reflection coefficients from presence of vegetation and use of vertical polarization. Tracking over the sea, and over barren or snow-covered land, precludes reliance on absorption by vegetation. Exploitation of the drop in reflection coefficient for vertical polarization near the pseudo-Brewster angle (see Figure 11.2) has been a standard practice for minimizing multipath errors in tracking radars, and makes surface-bounce jamming more difficult, especially at elevation angles

above 1° . Some of the multipath remediation techniques described in Chapter 11 can reduce the effectiveness of surface-bounce jamming as well. They may prevent transfer of the track to the image, but as with natural multipath they can only reduce, not eliminate the error.

Surface-bounce jamming can be either noise jamming (with sufficient power to exceed the echo) or a repeater signal. The use of noise ensures that the radar cannot exploit the sum of repeater delay and reflection delay to perform a leading-edge track on the direct-path signal.

12.2.5 Bistatic Jamming

Surface-bounce is one form of bistatic jamming, but is limited to low-elevation targets. At high altitudes, reflection of jamming from chaff can be used to create angle errors in monopulse (as well as other) radars. The requirements for effective bistatic jamming from a chaff burst are discussed in [9, p. 502]. A chaff burst is illuminated by the mainlobe of the jammer on the protected target, while the jammer illuminates the radar directly only through sidelobes. For chaff with bistatic radar cross section σ_b at range R_1 from the radar and R_2 from the protected target, where the target is at range $R \approx R_1$ from the radar, the ratio of bistatic to direct jamming received by the radar is

$$\frac{J_b}{J_d} = \frac{\sigma_b G_{mlj}}{4\pi R_2^2 G_{slj}} \quad (12.7)$$

where G_{mlj} and G_{slj} are the jammer antenna mainlobe and sidelobe power gains. The requirement is that $J_b/J_d > 1$ at a range R_2 such that a weapon directed at the chaff reflection will spare the protected target.

As an example, assume the following parameters:

- $\sigma_b = 100 \text{ m}^2$;
- $R_2 = 500\text{m}$;
- $J_b/J_d = 2$.

The required jammer mainlobe-to-sidelobe ratio is $G_{mlj}/G_{slj} = 6.3 \times 10^4 = 48 \text{ dB}$. The bistatic jamming power must be strong enough to obscure the echo from the aircraft. For the parameters shown, the bistatic jamming power delivered to the radar is a factor $\sigma_b/(4\pi R_2^2) = 3 \times 10^{-5}$ times what would be delivered by the same jammer in a self-screening mode, using its mainlobe to illuminate the radar. Thus bistatic jamming requires about 45 dB more power than would be required for self-screening at the same range.

The advantage of the bistatic jamming mode, of course, is that it prevents target angle measurement by the track-on-jam technique. The disadvantage is that it requires dense chaff with large bistatic cross section within the jammer mainlobe

at a range not exceeding 500m. If the jammer mainlobe gain is 30 dB (assuming sidelobes at -18 dB), the corresponding beamwidth is 5° , and chaff of adequate cross section must lie within the $40\text{m} \times 40\text{m}$ cross-range width of the beam at 500m range from the aircraft. Assuming a roughly spherical chaff burst, the required density is $\approx 0.0024 \text{ m}^2/\text{m}^3$, much higher density than would be expected in an extended corridor of chaff. Hence, a succession of chaff packages would have to be launched from the aircraft to sustain the bistatic jamming. For this reason, bistatic jamming via chaff appears to be an unlikely threat to monopulse radars.

It has been suggested that corner reflectors or similar retroreflecting shapes, located on platforms launched from the protected aircraft, would overcome the limitations of chaff as sources of bistatic reflection. A problem with this approach is that the retroreflector concentrates its power in the direction of the source, rather than scattering it over a broad angular sector in which the victim radar might be located. In the case of an aircraft approaching a radar, a retroreflector towed behind the aircraft would be effective as long as the aircraft maintained its approach toward the radar. A triangular corner reflector with sides of length $a = 0.25\text{m}$ has a cross section $\sigma = 18 \text{ m}^2$ at X-band. The width of the reflected lobe is 4° , so the reflector-to-aircraft line would have to be maintained within $\pm 2^\circ$ of the aircraft-to-radar line to use it for bistatic jamming. For reasonable tether lengths this would violate the requirement that the weapon aimed at the reflector avoid passing the target within fuzing range.

12.3 EXPLOITATION OF RADAR FAULTS

Although the requirements for near-ideal monopulse operation are well known and technically achievable, most actual monopulse radars are forced to compromise on cost, weight, complexity, maintainability, and producibility of their component and subsystems. The result is to create opportunities for clever jamming techniques to degrade or deny the angle data needed in the military system, without investing in equipment that is successful against monopulse radars in general. The designers of this nongeneric ECM equipment have the burden of showing that the probability of successful jamming is high enough to justify investment in producing and installing the equipment in aircraft and other vehicles that are the targets of monopulse radars. This showing requires detailed information on the design features, production tolerances, and actual operation of the victim radars, obtained through intelligence or exploitation of actual equipment. The ability to program flexible emissions from digitally controlled ECM equipment and observe their effects on radar operation is an important factor in success. The ability of the radar designers to program flexible waveform generation, receiving, and processing equipment is similarly important in countering the ECM.

12.3.1 Cross-Polarized Jamming

The use of cross-polarized jamming (usually referred to as cross-pol) is sometimes considered a generic monopulse ECM technique, but since many modern monopulse radars have insignificant response to such jamming it is listed here as an exploitation of faulty design. The principle of angle deception by emitting a strong signal with polarization orthogonal to that used by the radar is well known and has been discussed in [1, pp. 238–253].

The effect of antenna response to a cross-polarized echo component was discussed in Section 10.4.3. A target component that is reflected to the radar aperture with polarization orthogonal to that for which the radar is designed is accepted with a small response by most antennas. The cross-polarized sum pattern for an antenna with symmetry about its center has a null on the axis with positive and negative lobes beside the null, similar to the usual difference pattern. The cross-polarized difference pattern has a lobe on the axis (Figure 10.9). The normalized monopulse output d'/s' in the presence of an input that includes a cross-polarized component e_{cp} is

$$\frac{d'}{s'} = \frac{ed + e_{cp}d_{cp}}{es + e_{cp}s_{cp}} \approx \frac{d}{s} + \frac{e_{cp}}{e} \frac{d_{cp}}{s} = \frac{d}{s} + \epsilon_{cp} \quad (12.8)$$

where e and e_{cp} are the field strengths in the intended- and cross-polarizations, d , s , d_{cp} , and s_{cp} are the difference and sum antenna voltage responses to those polarizations, ϵ_{cp} is the error term, and the approximation assumes $e_{cp}s_{cp} \ll es$. The error in angle is then

$$\sigma_{\theta} = \frac{\theta_{bw}}{k_m \sqrt{2}} \frac{e_{cp}}{e} \frac{d_{cp}}{s} \quad (12.9)$$

The polarized response ratio d_{cp}/s for typical monopulse antennas is -30 to -40 dB, near the antenna axis, so with $e_{cp}/e < 1$ the error is normally small.

The cross-pol jammer exploits the cross-polarized response of the monopulse antenna by transmitting to the radar a signal with polarization orthogonal to that for which the antenna is designed: $e_{cp} \gg e$. If this ratio overcomes the 30 to 40 dB cross-pol rejection of the antenna, the error from (12.9) reaches or exceeds half the beamwidth, and the track becomes unstable and may be lost.

When the cross-pol input is large, the term $e_{cp}s_{cp}$ in the denominator of (12.8) cannot be neglected. When it becomes large enough to dominate the input to both the sum and difference channels, the monopulse output d'/s' has a sharp peak that switches from positive to negative on the axis, establishing two null points near the half-power beamwidth. Depending on the relative phase of the d' and s' lobes,

these nulls may be stable track points or unstable points tending to force the antenna further off target.

Figure 12.3 shows the basic method of repeating a radar signal with orthogonal polarization. In the diagram, antennas accepting 45° and 135° linear polarizations are connected through circulators to a pair of RF amplifiers such that the 45° component is retransmitted at 135° and vice versa. Whatever the radar polarization, the repeated pulse is orthogonal to it. The problem of avoiding self-oscillation is similar to that of the cross-eye jammer, described in Section 12.2.3. The presence of a target echo with the intended polarization tends to overcome the jamming effect, so in this case also it is desirable to combine range or Doppler deception to pull the tracking gate off the target and leave pure cross-pol jamming as the input. The small response of the sum channel antenna to the cross-pol signal requires the range or Doppler deception process to use considerably higher power than would be required without cross-pol, but in a repeater that power level can be obtained without undue difficulty.

The basic monopulse radar counter to cross-pol jamming is minimization of the antenna cross-polarized response. In a parabolic reflector antenna, this response (the so-called Condon lobes) is caused by the curvature of the surface, and is reduced with higher f/D ratios. Cassegrain antennas using the polarization-twist technique (see Figure 4.6) are relatively immune to cross-pol jamming, because the polarization-sensitive subreflector fails to reflect the cross-pol component to the feed. A dual-polarization antenna option offers the ability to provide accurate tracking outputs on either polarization, but the complexity and cost of this approach has prevented its wide application.

Many monopulse airborne radar and seeker antennas use flat-plate antennas composed of slotted waveguides. Such an antenna would have reasonably pure polarization except for slot elements near the periphery, where there is interaction with the (usually circular) edge of the structure. Especially in seeker antennas that are relatively small, this creates significant cross-polarized response. The radome

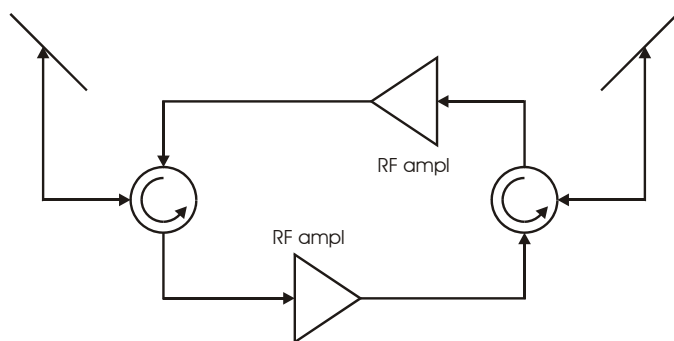


Figure 12.3 Basic cross-pol repeater configuration.

is also a source of cross-polarized response, especially in high-velocity missiles where a thick, elongated radome is necessary.

Surface-based phased-array antennas can be designed for low cross-polarized response, especially if they are large enough that only a small fraction of the elements are affected by proximity to the edges. The design described in Section 7.3, using circular polarized (CP) Faraday-rotator phase shifters with polarization duplexing has excellent immunity to cross-pol jamming. The array focuses incoming signals on the feed only if they have the correct sense of CP. In addition, signals of the wrong sense that do reach the duplexing grid are diverted into the path to the transmitter, rather than the receiver.

12.3.2 Exploiting Phase and Gain Imbalance

The effect of imbalance between sum- and difference-channel receivers has been discussed in Chapter 8 and Section 10.4.1. A phase imbalance causes the monopulse calibration curve for most types of processor to change, introducing errors in off-axis measurement. It also combines with comparator errors to introduce a bias error. These effects are normally small, but if the phase shift between channels approaches or exceeds about 45° the effect on servo loop gain can cause instability. In the limit, if the shift reaches 90° , the monopulse output drops to zero, and beyond that angle the sense of the error is reversed, introducing an unstable null on the axis. The target is then tracked on one of the opposite-slope nulls in the d/s curve, near the edge of the mainlobe.

A countermeasure technique that can introduce a 90° phase difference is *skirt-frequency jamming*, in which a repeater or other jamming source responds to illumination from the radar with a strong signal that is offset from the center frequency of the radar signal by an amount estimated to place the jamming at the edge of the receiver bandpass. Receiver gain and phase characteristics over the IF band are shown, for a typical response formed by multiple, stagger-tuned filters, in Figure 12.4. While the filters in the two channels are designed for identical phase and gain characteristics over most of the response, these may not be controlled carefully enough to retain their match in the skirt region, where phase changes rapidly with frequency. A jamming signal in that region may pass the sum and difference channels with relative phase that reaches 90° . The receiver response characteristics must be known for the jammer to exploit this problem, but it is possible for the jammer to probe the radar with different offset frequencies until a track disturbance is sensed, and then to use that frequency in subsequent jamming.

The basic radar counter to this technique is to design and fabricate the receiving filters to avoid approaching 90° phase difference anywhere in the response band of the filter. If this cannot be done, it is possible to place in each channel a narrow, single-tuned filter, centered within the bandwidth of the multiple filters,

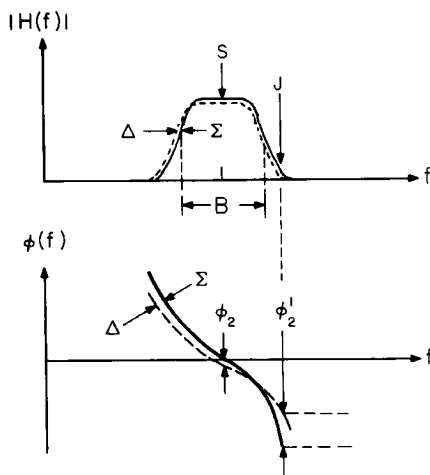


Figure 12.4 Skirt-frequency jamming.

whose phase varies only over $\pm 90^\circ$ over the band of significant response. Filters of this type maintain phase match between channels that is a small fraction of 90° . Modern radars using pulse compression are designed with complex filters that can retain their channel-to-channel match more accurately than the stagger-tuned filters used in earlier radars.

12.3.3 Exploiting AGC Response

A common normalization procedure in monopulse radar is to develop an AGC control voltage from the sum-channel output and use this to control the gains of all three receivers. While instantaneous AGC action is possible (using a time constant that is a fraction of the pulsewidth), it has been shown in Section 10.1.10 that such a response leads to increased tracking error on fluctuating targets, so an AGC that averages at least several pulses is often used instead. Such an AGC becomes vulnerable to a form of amplitude-modulated jamming sometimes called *intermittent jamming* (see Figure 12.5).

The diagram shows a jammer operating with about 40% duty cycle, the on-times selected to match the AGC response time. The voltages shown represent the envelopes of signal, noise, and jamming pulse trains. When the high-amplitude repeater jamming appears in the range gate of the receiver, whose gain has been set to place the target echo in the useful response range of the receiver, the receiver is driven into saturation. After one or two AGC time constants, the gain has been reduced so that useful track data are available on the jamming signal. At this time the jammer turns off, dropping the receiver output below the usable range. After another one or two time constants, the AGC has increased the gain to place

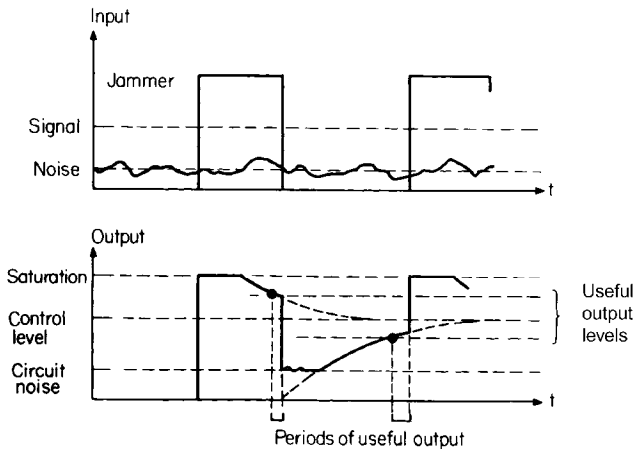


Figure 12.5 AGC jamming technique.

the target echo in the useful range, at which point the jammer turns on again to force saturation. If the jammer on and off times are correctly chosen relative to the AGC attack and recovery time constants, the periods of trackable outputs are reduced to the point where the angle tracking loops cannot function.

The radar counters to this type of jamming are to extend the dynamic range over which trackable outputs can be obtained, to use instantaneous AGC or logarithmic normalization and accept the resulting fluctuation errors, or to have available alternative time constants that can be selected to make the jamming less effective. The jammer designers or operators must have some knowledge of the AGC time constants in order to select the on and off time sequence of the jamming, and the effectiveness of AGC jamming is uncertain if this information is denied. When the radar uses a Doppler process (e.g., MTI) for clutter rejection, the receiver gains must normally remain fixed during the coherent processing interval of the Doppler circuits. Clutter rejection is compromised if gain variation is introduced during this interval, so a combination of active and passive jamming makes countercountermeasures more difficult.

12.3.4 Exploiting Image Response

The image-frequency jammer transmits a signal that is offset by the IF from the radar receiver's local oscillator, but on the opposite side from the radar transmission. The intent is to reverse the output polarity of the phase-sensitive error detector, creating an unstable null on the tracking axis. This technique is applicable when the sum and difference outputs of the comparator, with 90° relative RF phase, have been brought into phase equality with a 90° IF phase shift in either

receiver channel. A strong jamming input at the image frequency can then overcome the target error signal and force the tracking point to what is otherwise an unstable null near the edge of the mainlobe. Knowledge of the IF is required, but if this is unavailable the jammer can probe with a variable offset from the received radar frequency until it detects a track disturbance.

Radar counters to this technique include use of an RF preselector filter that excludes the image frequency from the input to the mixer, or placing the 90° phase shifter in the RF portion of one receiver, rather than at IF. The image-frequency output of the receivers then has the same phase as the normal output, allowing the radar to track as well on that response as on the target echo. This method was used in the AN/FPS-16 radar [9], where the comparator output phases were equalized with phase shifters in the RF portion of each difference channel, and receiver internal phase shifts with IF phase shifters. It was found that this procedure permitted passive tracking on wideband radiation from the sun, and the same procedure would permit tracking on a wideband noise jammer as well as on an image-frequency jammer.

Use of a fixed-tuned RF preselector restricts the tuning band of the radar system to less than twice the IF. A tunable preselector is often impractical, both because of its loss and the limited tuning rate of mechanically tuned filters. Modern radars tend to use double-conversion receivers with a high frequency for the first IF to permit electronic tuning over a 10% band while eliminating image response.

12.3.5 Two-Frequency Jamming

In the absence of an RF preselector, the radar receiver is vulnerable to a technique known as *two-frequency jamming*, in which two strong signals, separated by the radar IF, are emitted anywhere in the RF bandpass of the radar [1, pp. 253–256]. High jamming levels are required to produce a cross-product in the mixers of the monopulse receivers that will dominate their outputs, suppressing the downconverted target echo. The relative phase of the outputs fails to follow the input phase of the d and s from the radar comparator, and error sensing becomes impossible.

Radar counters to two-frequency jamming are: (1) inclusion of an RF preselector with a bandwidth narrower than the IF, or (2) use of direct amplitude-comparison between the pairs of component beams that are used to form the sum and difference patterns of the antenna. Option (1) is best implemented with double-conversion receivers and a high first IF, to preserve electronic tunability of the radar over a broad band. Option (2) is an alternative if ports are available corresponding to the component beams.

12.3.6 Jamming at the Commutation Frequency

Two-channel monopulse systems such as conopulse (Section 8.17) combine the two difference outputs of the comparator sequentially, to permit processing with only two receiver channels instead of three. This opens a vulnerability to jamming that is amplitude modulated at the commutation frequency of the difference-channel combiner. If the two receiver channels are perfectly matched, no error should result from such AM jamming. But if there is an imbalance between the channels, a fraction of the AM appears at the output and an angle error results. In principle, the commutation frequency does not appear in the transmitted output of the radar, but in most cases there is some leakage or mismatch that causes a small modulation to appear on the transmission, and this can be detected and exploited by the jammer. A similar vulnerability applies to three-channel monopulse when commutation is used to remove bias errors in the detectors (see Section 8.12). The errors that can be produced by AM jamming in this case are small, but they may be sufficient to increase the miss distance of command-guided missiles or gunfire.

References

- [1] A. I. Leonov and K. I. Fomichev, *Monopulse Radar*, Moscow: Soviet Radio, 1970, (in Russian). Translation by W. F. Barton, Norwood, MA: Artech House, 1986.
- [2] D. K. Barton, "Passive Radar Tracking Apparatus," U.S. Patent 3,196,433, July 20, 1965, filed December 4, 1962.
- [3] D. C. Schleher, *Electronic Warfare in the Information Age*, Norwood, MA: Artech House, 1999.
- [4] R. L. Haupt, "Adaptive Nulling in Monopulse Antennas," *IEEE Trans. on Antennas and Propagation*, Vol. AP-36, No. 2, February 1988, pp. 209–215.
- [5] D.-C. Chang, K.-T. Ho, and C.-I. Hung, "Partial Adaptive Nulling on a Monopulse Phased Array Antenna System," *IEEE Trans. on Antennas and Propagation*, Vol. AP-40, February 1992, pp. 121–125.
- [6] R. L. Fante, "Synthesis of Adaptive Monopulse Patterns," *IEEE Trans. on Antennas and Propagation*, Vol. AP-47, No 5, May 1999, pp. 773–774.
- [7] W. P. Plessis, J. W. Odendaal and J. Joubert, "Extended Analysis of Retrodirective Cross-Eye Jamming," *IEEE Trans. on Antennas and Propagation*, Vol. AP-57, September 2009, pp. 2803–2806.
- [8] D. C. Schleher, *Introduction to Electronic Warfare*, Norwood, MA: Artech House, 1986.
- [9] D. K. Barton, *Modern Radar System Analysis*, Norwood, MA: Artech House, 1988.

Chapter 13

Tracking Radar Applications of Monopulse

The AN/FPS-16, a range instrumentation radar designed during the 1950s, has been used several times in previous chapters as an example of a monopulse tracking radar. Details of that radar have been widely presented in the literature, and it serves to illustrate many of the principles discussed in this book. After over fifty years of use, that radar remains in operation at United States and foreign test ranges. Similar monopulse radars have been designed in both the United States and other countries for instrumentation and military applications.

In this chapter we will review several examples of monopulse tracking radars that depart from the technology represented by the AN/FPS-16. Surface-based monopulse radars, including those using phased array techniques, will be covered in the first section, and airborne radars in a second section. The final section will consider a class of monopulse radar whose production numbers have greatly exceeded all the surface-based and airborne systems: the homing seeker, used against both air and surface targets.

13.1 SURFACE-BASED MONOPULSE TRACKING RADARS

13.1.1 AN/FPS-49 and TRADEX Radars

The AN/FPS-49 search/track radar was designed at RCA in the 1950s as an element of the Ballistic Missile Early Warning System (BMEWS). It had been conceived as a vastly scaled-up UHF derivative of the AN/FPS-16, its detection range increased from that radar's 200 km to 4,000 km on 1-m² targets (an increase of 52 dB in scaled parameters of the radar equation). Of that increase, 25 dB was an increase in average power from 1 kW to 300 kW; 17 dB resulted from the antenna

aperture area, scaled from a diameter of 12 ft to 84 ft (3.66m to 25.6m); 7 dB was a reduction in noise figure from 10 dB to 3 dB, and the remaining 3 dB resulted from longer integration time. The TRADEX radar [1, 2], shown in Figure 13.1, was based on the AN/FPS-49 design but included also an L-band channel, multiple polarizations, and pulsed Doppler tracking for measurement of reentry vehicle characteristics at the Kwajalein test range.

TRADEX was the first monopulse radar to use pulsed Doppler tracking, demonstrating that the phase matching required in monopulse receivers could be maintained through the Doppler filtering process. The feed used the five-horn configuration of Figure 4.11, where transmission occurs only through the central horn. Provision is made to shift from linear polarization at 45° or 135° , to right- or left-hand circular polarization. Horns for the difference patterns use horizontal polarization in traverse and vertical polarization in elevation, as was the case with the AN/FPS-49. Thus, only half the power of the echo signal contributed to the difference channel in each coordinate, but the feed horns and comparator network are simplified. Use of circular polarization is necessary for BMEWS to make target

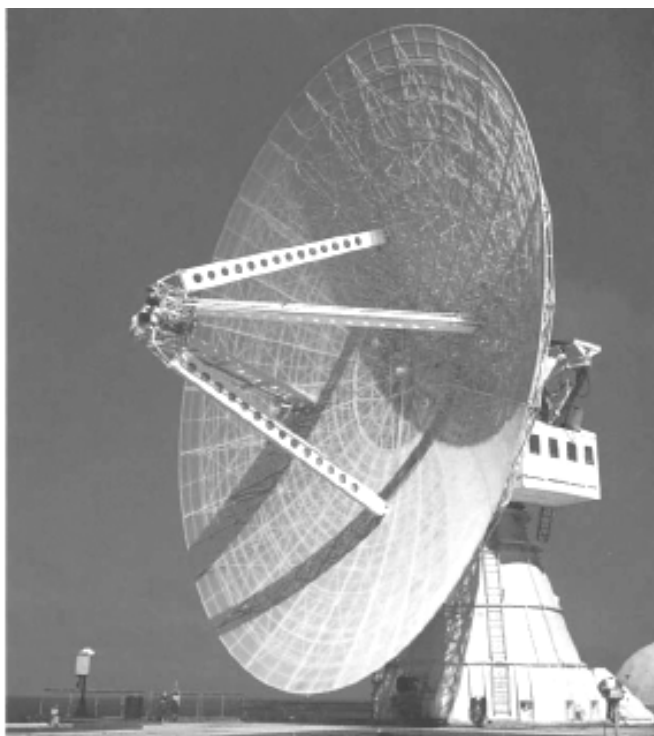


Figure 13.1 TRADEX radar at Kwajalein Atoll. The antenna of the AN/FPS-49 BMEWS radar is similar, but enclosed in a rigid radome for operation in the northern environment.

detection insensitive to the Faraday rotation of the ionosphere. TRADEX, after many modifications and upgrades, remains in use today, while the AN/FPS-49 radars have been replaced by phased array systems.

13.1.2 Patriot AN/MPQ-53 Multifunction Radar

The AN/MPQ-53 radar of the Patriot surface-to-air missile system (Figure 13.2) is a true multifunction radar, in that it performs all the search, multitarget tracking, and missile guidance functions required in the system. The array is a space-fed lens, using the five-layer monopulse feed of Figure 6.9. The feed may be seen raised above the roof of the equipment shelter in Figure 13.2. Its design drew heavily on the multimode technology [3] originated by Hannan at Wheeler Laboratories. The array uses 5,500 nonreciprocal, latching ferrite phase shifters, radiating vertical polarization into space in front of the array through dielectrically loaded circular waveguide elements. Rear radiation focused on the feed is through printed dipoles. Since the phase shifter settings for transmission must be changed for reception, it is possible to place the transmitting horn beside the monopulse receiving horn assembly, as shown in Figure 6.9, avoiding the need for a circulator or other high-power duplexing device. This technique is known as *space duplexing*, and reduces the losses in both the transmitting and receiving paths, as well as allowing more refined monopulse horn designs that avoid the high power levels of the transmitting horns. Solid-state receiver protection (to handle power reflected from the lens) is still needed at the receiver inputs.



Figure 13.2 Patriot AN/MPQ-53 radar. (Figure courtesy of Raytheon.)

Monopulse tracking is performed on up to 100 targets, of which nine may be engaged simultaneously. Since most of the tracking is performed using single-pulse transmissions, the normalization of the monopulse outputs is performed using instantaneous AGC in a feed-forward configuration. The large auxiliary antenna shown in Figure 13.2 communicates with the missile seeker in the so-called target-via-missile (TVM) mode. In this form of semiactive homing, the echoes of the illumination waveform transmitted by the main array are picked up in the seeker antenna, amplified, and transmitted to the radar on this TVM link, where they receive monopulse processing before being used to compute acceleration commands that are returned to the missile. The separate TVM antenna is needed because the missile may be outside the beamwidth of the main array that illuminates the target. Five smaller auxiliary antennas provide inputs for sidelobe cancellation (SLC) loops to protect the main array channels from jamming. Those loops null the interference in all three monopulse channels.

13.1.3 Russian Surface-to-Air Missile (SAM) Guidance Radars

The space-fed array, having appeared initially in the Patriot radar, found favor with Russian designers of monopulse radars used for SAM guidance. The primary examples are the fire control radar of the SA-10 and SA-20 systems, which have been given the NATO names Flap Lid and Tombstone (see Figure 7.2). The lens array of these systems, roughly the same size as in Patriot, operates at X-band, and is composed of 10,000 elements, in which the phase shifters are of the Faraday rotator type. The choice of X-band gives a narrower beam, higher effective radiated power, and improved angular accuracy as compared to C- or S-band used in comparable U.S. systems. A separate search radar is used to designate targets for tracking by the monopulse radar of each system.

The monopulse feed uses the multilayer, multimode principles originated by Hannan, optimizing both the sum and difference illuminations to balance efficiency and difference slope against spillover and taper loss. The polarization duplexer system used in these radars (see Figure 7.3) avoids the loss of the ferrite circulator used in most high-power radars. The array phase shifters constitute the most significant loss in the RF system, as there is no duplexer and only minimal loss from short waveguide lengths and from the radomes covering the polarizing grid and the front face of the lens. The design also avoids the loss normally encountered in solid-state receiver protection devices by using as the low-noise RF preamplifier an electrostatic amplifier that withstands any reflected power from the lens and recovers instantly to amplify received signals with a low noise figure. Total RF losses are in the order of 3 dB lower than in comparable U.S. space-fed arrays.

The same array geometry is used in a series of Russian and Chinese fire control radars for the SA-21 and HQ-9 SAM systems, the latter operating in C-band rather than X-band.

The Russian SA-12 fire control radar, NATO designation Grill Pan, also uses a space-fed lens but with in a more conventional feed approach (Figure 13.3). There are two alternative feeds: one is located on the axis of the lens when it has the tilt shown in the figure, for air-target coverage; a second feed is located to support a tilt to higher elevations, for the system's ballistic-missile defense mode. Both feeds generate circular polarizations, with opposite senses for transmitting and receiving through the Faraday rotator phase shifters.

The figure shows the IFF antenna mounted above the radar array, and three auxiliary antennas that feed SLC systems. These are gimballed for mechanical steering to bring their gains to bear on the sector surrounding the engaged targets.



Figure 13.3 SA-12 Grill Pan fire control radar, with Bill Board surveillance radar in background [4].

As with the auxiliary SLC arrays on the Patriot antenna, the gain of these antennas avoids the need to use large weights in coupling their outputs into the main receiving channels, adding only small extra noise components to those receivers.

13.1.4 Aegis AN/SPY-1 Radar

In naval fire control, the U.S. Aegis AN/SPY-1 and its successor radars are examples of multifunction radar design using monopulse in their tracking modes. Figure 13.4 shows a U.S. Navy cruiser equipped with these radars, of which the aft and portside arrays are visible. A similar pair of octagonal arrays covers the forward and starboard sectors. Each pair of arrays is fed by a transmitter consisting of 32 crossed-field amplifier modules, one module feeding each transmitting sub-array of 128 elements. Transmitter outputs are switched sequentially from one to the other of the antennas in each pair to cover its 180° azimuth (bearing) sector. Additional receiving elements bring the phase-shifter count to 4,480, divided among 140 receiving subarrays of 32 elements each.

The feed design for the AN/SPY-1A system is shown in Figure 13.5. Within each of ten array columns, pairs of 32-element subarrays are combined in magic-Ts. A 0° phase shift (during a transmitter pulse) or 180° phase shift (during the listening period) is introduced in the individual elements of one of the subarrays to



Figure 13.4 U.S. Navy Aegis cruiser, showing the aft/portside arrays of the AN/SPY-1 radar. (Figure courtesy of U.S. Navy.)

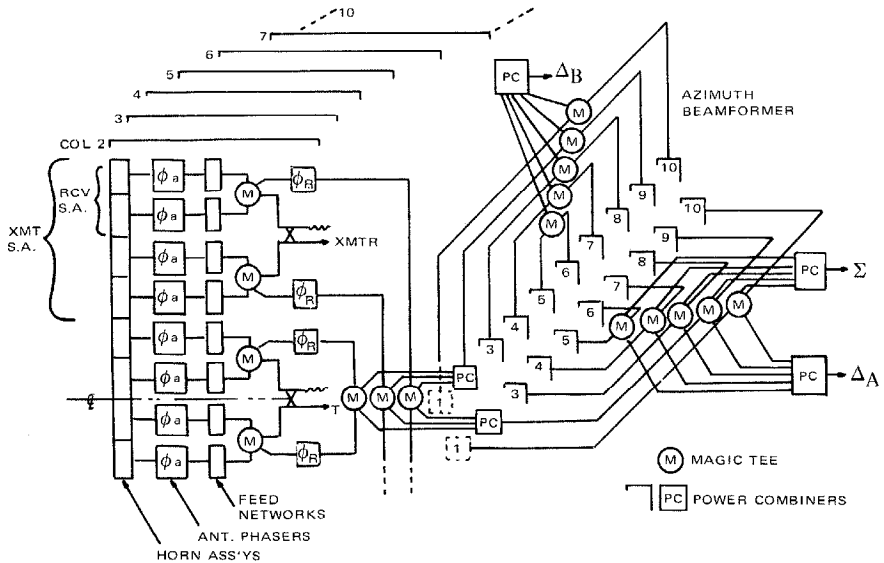


Figure 13.5 Feed network of AN/SPY-1A radar array [5].

connect the pair to either a transmitter or receiver port of the magic-T. Two adjacent pairs are combined (128 elements) and fed from one transmitter module, while separate receiver outputs (64 elements) are retained for combination in the column receiving feed. Each column feed produces a sum and elevation-difference output. The elevation difference outputs of the ten columns are combined in a horizontal network to provide the array elevation difference signal. The elevation sum outputs go to an azimuth network that generates the array azimuth and sum outputs.

In the AN/SPY-1B and subsequent versions of the radar, the receiving subarray structure is refined to avoid the amplitude quantization effects of equal weighting within each 64-element receiving subarray. The refined subarray structure also permits optimization of the monopulse sum and difference illumination functions, using networks similar to the Lopez feed shown in Figure 7.8. The 32-module transmitter design is retained, providing very high total output power from the array as well as graceful degradation of performance in the event of failure of a high-power crossed-field amplifier.

13.2 AIRBORNE MONOPULSE TRACKING RADARS

13.2.1 Multimode Fighter Radars

The multimode fighter radar has evolved over several decades as the dominant sensor for use in fighter/attack aircraft worldwide. Virtually all these radars operate in X-band, and their modes include search, target acquisition, tracking, and ground mapping. A typical example from the era preceding the advent of phased array systems is the AN/APG-63 (Figure 13.6). The photograph shows the complex waveguide network behind the flat-plate antenna, that provides monopulse difference channels as well as the sum channel that is used also for nontracking modes. The monopulse implementation in this radar uses two receiver channels, the difference channel being shared between azimuth and elevation (pitch and yaw) coordinates.

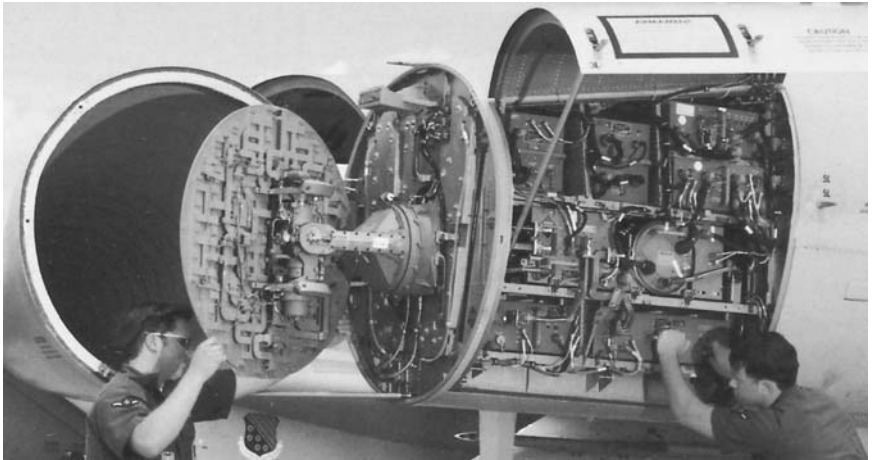


Figure 13.6 AN/APG-63 radar, with radome and equipment bay opened for service. (Figure courtesy of U.S. Air Force.)

13.2.2 Electronically Scanned Fighter Radars

The current standards for multimode airborne radars require electronic scanning, and the active electronically scanned array (AESA) has become the preferred approach. The United States leads in development of these systems, but details of the several current designs remain unpublished. Papers describing the Zhuk-ME, a Russian AESA radar, have appeared, and a model of this radar was shown at the Moscow Air Show in 2005 (Figure 13.7).

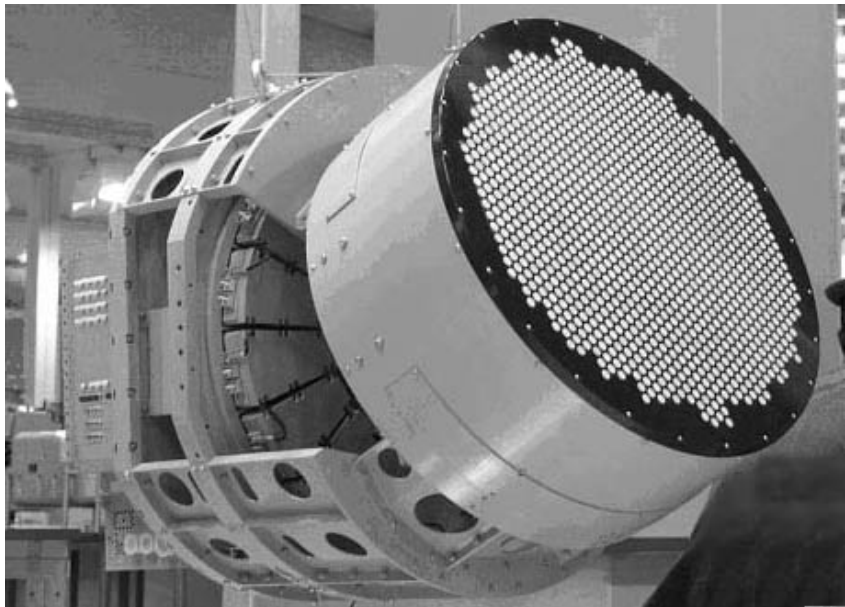


Figure 13.7 Russian Zhuk-ME AESA radar array. (Phazotron photo from 2005 Moscow Air Show.)

The Zhuk-ME is a monopulse array, apparently using the quadrant-split feed design described in Section 7.4.1. The sum and difference patterns presented in [6] are shown in Figure 13.8, following closely the theoretical plots for the quadrant-split illumination function, as shown in Figure 7.5.

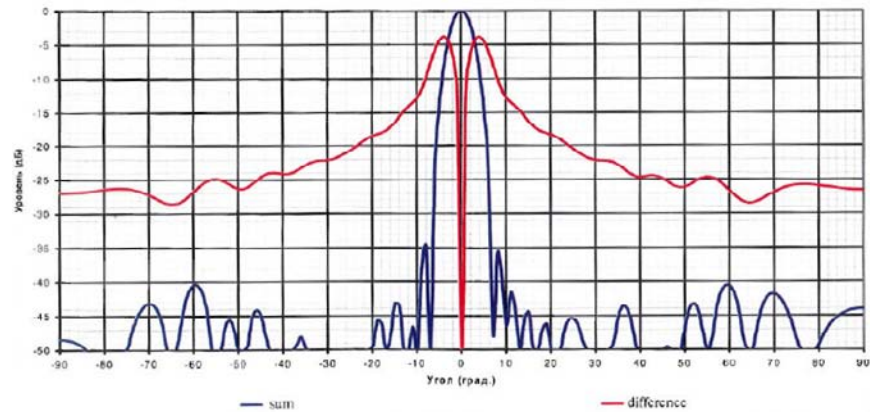


Figure 13.8 Calculated sum and difference patterns of Zhuk array [6].

13.3 MONOPULSE HOMING SEEKERS

The first generations of surface-to-air guided missiles, the U.S. Nike Ajax and Nike Hercules and the Russian SA-2 and SA-3, used command guidance, in which separate tracking radars (Nike) or scanning beams (SA-2, SA-3) obtained data on the target and the interceptor missile, which was then guided by commands computed at the radar site and transmitted to the missile.

The Nike fire control radars used the monopulse technique to achieve the accuracy required for this guidance mode. The SA-2 and SA-3 radars each used a pair of scanning fan beams, narrow in the scanned coordinate, to track both the target and the missile. The SA-10 system initially used a command-guided missile. In each case, the miss distance supported by the radars increased in proportion to the engagement range. This and the inevitable multipath errors in elevation measurement limited the lethal range of the system and ruled out low-altitude engagements.

13.3.1 Semiactive Homing

SAM systems using homing guidance were developed to overcome the errors of command guidance. These initially used the semiactive mode, in which the surface-based radar tracked the target and provided continuous-wave (CW) illumination whose echo was received by the seeker. The U.S. Hawk system and Russian SA-5 and SA-6 used this approach. In Hawk and SA-5 the radar was a CW system whose emission provided both the radar and the seeker with echoes on which to track or home. In the SA-6, the radar tracked on echoes from a pulsed transmission, and the CW illumination, at a different frequency within the same band, was injected into the radar antenna but not used by the radar in tracking.

While the early seeker systems used conical scanning, these were replaced by monopulse seekers as soon as advances in the technology permitted. Both Hawk and the SA-5 used monopulse seekers. The more advanced U.S. Patriot system used a pulse illumination waveform, transmitted in a beam that was slaved to the data from the radar's tracking mode. The seeker in this case forms the monopulse sum and difference signals, and these are transmitted to the radar for processing and development of the guidance commands. The SA-10 also includes a semiactive seeker mode using illumination that is emitted but not tracked by the radar. A monopulse seeker is used. The SA-12 system includes two different illumination antennas and transmitters, separate from the radar.

Air-to-air missiles (AAMs) using semiactive homing followed the same development path as the SAMs, starting with conical scanning and evolving to monopulse. Data on U.S. seekers is sparse, but there have recently been several published papers on Russian seekers. Figure 13.9(a) shows an unusual monopulse antenna design for a semiactive homing missile. This is, perhaps, the only current

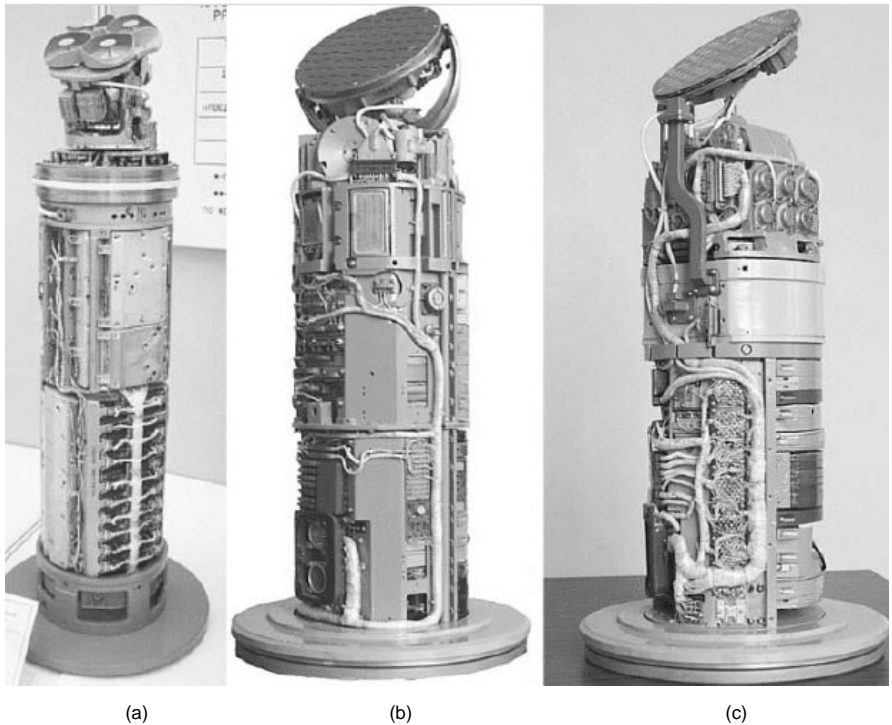


Figure 13.9 Three seekers produced by the Russian company Agat. (a) 9B-1101K semiactive seeker for the Alamo AA-10. (b) 9B-1348E active radar seeker for the AA-10. (c) 9B-1103K active seeker for the AA-12. (Photos courtesy of Agat.)

monopulse system example of the phase-comparison antenna devised by General Electric Company in the 1950s (see Figure 5.5).

13.3.2 Active Homing

The operational limitations of the semiactive homing technique, especially in air-to-air applications, led to intense efforts to develop active radar seekers, many of which use monopulse. The first produced in quantity was the U.S. AMRAAM (designated AIM-120), now in extensive use. It has also migrated to a surface-based defense system, NASAMS (Norwegian Advanced Surface to Air Missile System). The Patriot Advanced Capability (PAC-3) missile includes an active seeker and is designed to achieve direct hits on its targets. As with the semiactive seekers, data is sparse except for sales material originated in Russia. The two active seekers shown in Figure 13.9(b, c) are intended for use on the radar-guided version of the AA-10 (NATO name Alamo) and the AA-12 (NATO name Adder).

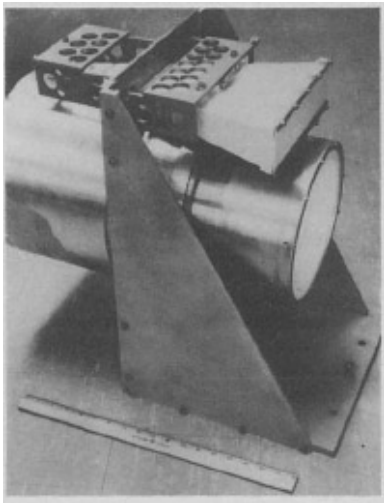


Figure 13.10 Experimental MMW monopulse seeker antenna [7].

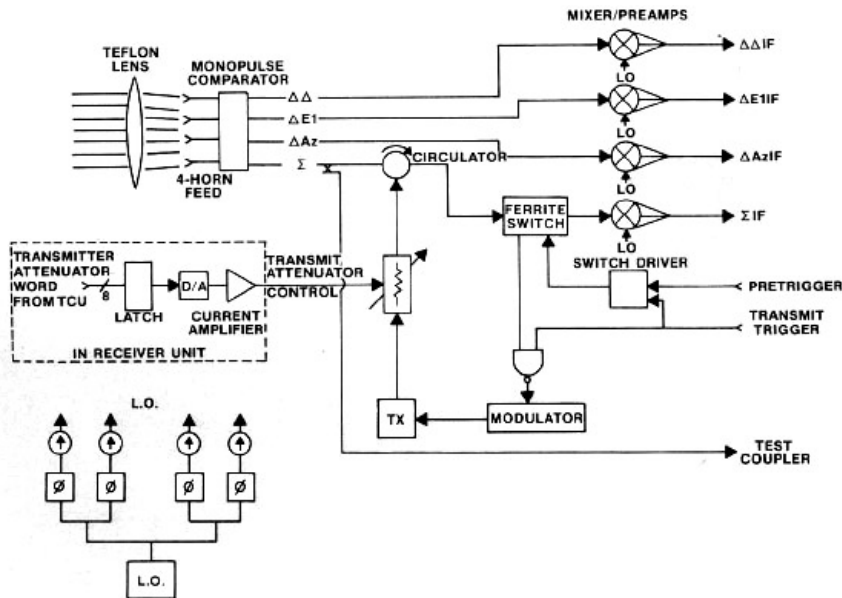


Figure 13.11 Block diagram of experimental MMW monopulse seeker [7].

Monopulse has been applied in development of millimeter-wave (MMW) active seekers for air-to-surface missile guidance. Figure 13.10 shows an experimental MMW antenna design using a 25-cm Teflon dielectric lens [7]. The beamwidth is 1° . A separate fan-beam horn antenna is also mounted on the test fixture. The block diagram of the seeker is shown in Figure 13.11. The transmitter is an impatt diode oscillator with 5W peak power at 100 ns pulsewidth, driven by a ramped pulse that generates a 250-MHz linear FM signal. The fourth monopulse channel, a diagonal-difference channel identified as $\Delta\Delta$ in the diagram, is included to permit reconstruction of the four component beams for experimental purposes.

References

- [1] J. T. Nessmith, "New Performance Records for Range Instrumentation Radar," *Space/Aeronautics*, December 1962, pp. 85–93.
- [2] G. W. Meurer, "The TRADEX Multitarget Tracker," *Lincoln Laboratory J.*, Vol. 5, No. 3, 1992, pp. 317–350.
- [3] P. W. Hannan, "Optimum Feeds for All Three Modes of a Monopulse Antenna: Part I, Theory and Part II, Practice," *IRE Trans. on Antennas and Propagation*, Vol. AP-9, No. 6, September 1961, pp. 444–454 (Part I); pp. 454–461 (Part II).
- [4] D. K. Barton, "Recent Development in Russian Radar Systems," *IEEE International Conf. Radar-95*, Washington, D.C., May 8–11, 1995, pp. 340–346.
- [5] R. M. Scudder and W. H. Sheppard, "AN/SPY-1 Phased-Array Antenna," *Microwave J.*, May 1974, pp. 51–55.
- [6] A. Dolachev, "X-Band Active Phased Array: Scope of Work Report," *Phazotron Information and Analytical Magazine*, Aero India 2007 Special Issue, pp. 17–22.
- [7] J. A. Scheer and P. P. Britt, "Solid-State, 95 GHz Tracking Radar System," *Microw. J.*, October 1982, pp. 59–54.

Chapter 14

Nontracking Radar Applications of Monopulse

The discussions of monopulse throughout this book have concentrated on the accuracy with which tracking radars and homing seekers can measure the angle of arrival of echoes from their targets. The advantages of monopulse, however, can be exploited in other types of radar. Some of these applications will be reviewed briefly in this chapter.

14.1 MONOPULSE 3-D SURVEILLANCE RADARS

A surveillance radar is defined as a radar used to detect, locate, and track targets over a large volume of space. The tracking for this type of radar usually takes the form of *track-while-scan*, defined as [1, p. 1195]:

An automatic target tracking process in which the radar antenna and receiver provide periodic video data from a search scan, together with interpolation measurements, as inputs to computer channels that follow individual targets.

The interpolation (or *beam splitting*) measurements can take the form of signal amplitude readings over a succession of pulses, or monopulse measurements on one or more pulses. The trend in modern surveillance radars has been toward exploitation of monopulse, both to improve the angle accuracy and to perform interpolation with those radars that use only a single pulse in each beam position. This type of radar is characterized as a nontracking application and discussed here because the radar beam does not respond to the presence of targets but instead follows a prescribed scan routine. The associated computer recognizes the target presence by associating detection reports and their coordinates, and forming track files corresponding to the dynamic properties of the desired target types.

14.1.1 Scanning-Beam 3-D Radars: AN/TPS-59 and AN/FPS-117 Examples

The AN/TPS-59 3-D surveillance radar is a scanning-beam system implemented entirely with solid-state electronic circuits. The radar was designed by General Electric Company in the early 1970s to meet a Marine Corps requirement. The trailer-mounted antenna (Figure 14.1) is an array of 54 rows, each with 28 dipole elements, driven by a transmit/receive (T/R) module that contains a power amplifier generating 900W peak power, along with a low-noise amplifier (LNA) for receiving.

In its normal surveillance mode, the radar scans a pencil beam in elevation, covering eight long-range beams that extend from the horizon to 8° elevation, and eleven short-range beams covering from the horizon to 19° elevation. Duplicate coverage of the low beams is necessary because the very long pulses used for long-range detection cause eclipsing of targets out to 150-km range. The antenna

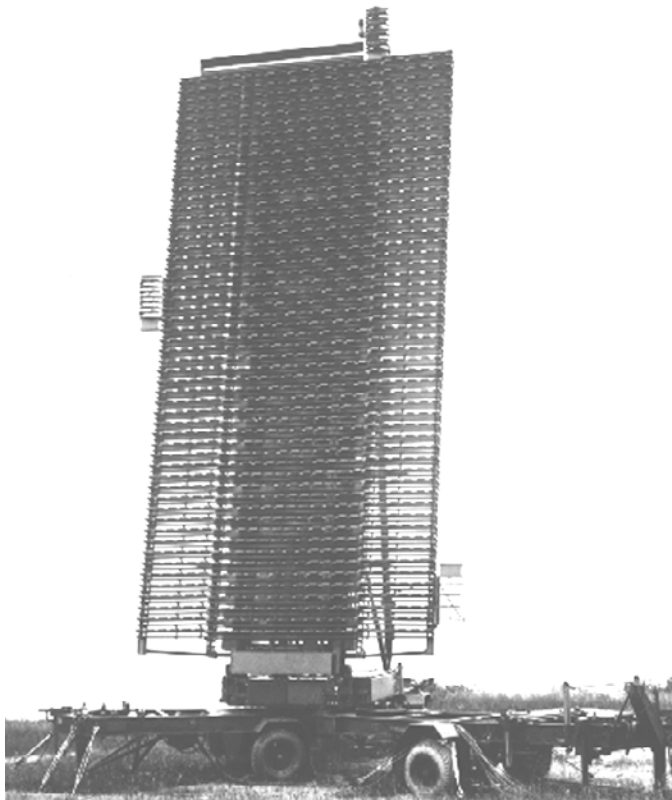


Figure 14.1 AN/TPS-59 long-range 3-D surveillance radar. (Figure courtesy of General Electric Co.)

rotates continuously in azimuth to cover 360° , within which the elevation scans are separated by 2.3° , approximately 72% of the azimuth beamwidth. The long-range beams receive a single pulse, divided into subpulses at different frequencies whose echoes are integrated noncoherently. Most of the short-range beams also receive single pulses, but the three at lowest elevation have three pulses to support MTI. Monopulse is applied in both azimuth and elevation, using the feed network shown in Figure 14.2. Each row feed network couples elements to a sum and an azimuth difference port. The sum port is connected through a circulator to the power amplifier and the LNA of the electronics module. Switches connect the power amplifier or LNA through the row phase shifter to either the transmitting column feed or the sum and elevation difference column feed. The azimuth difference port connects through a separate LNA to the azimuth column combiner.

The elevation column combiner generates conventional sum and difference beams centered that can be scanned to each elevation beam position, and also a pair of displaced sum beams used to minimize multipath errors at low elevation angles. Received signals are downconverted to a 75-MHz IF before passing through rotary joints to the main receivers.

The use of monopulse is necessary in scanning-beam 3-D radars such as the AN/TPS-59 because most of the discrete beam positions in both elevation and azimuth are illuminated with only a single pulse and are spaced almost a beamwidth apart. Interpolation of the angles of the detected targets is necessary to meet

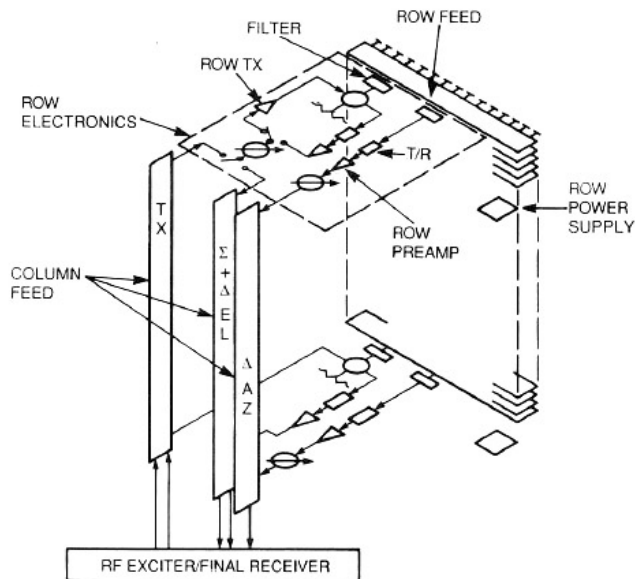


Figure 14.2 AN/TPS-59 antenna feed, showing row and column monopulse networks [2].

the accuracy specification, which calls for azimuth to be measured to 3 mrad and elevation to 1.7 mrad.

The AN/FPS-117 (Seek Igloo) radar designed for use by the U.S. Air Force, uses technology similar to that of the AN/TPS-59, except that the array is broader and uses only 44 rows of elements. These two radars are only examples of the many 3-D radars using the scanning-beam procedure.

14.1.2 Stacked-Beam 3-D Radars: Martello S-723 Example

In contrast to the scanning-beam 3-D radar, a stacked-beam radar illuminates the entire elevation sector through a fan beam on each transmitted pulse. Within this sector, multiple receiving pencil beams are formed in parallel. Advantages of this procedure are that Doppler-based processing can be applied throughout the elevation sector, suppressing airborne as well as surface clutter. A disadvantage is the cost of multiple receivers and availability of only one-way rejection of surface clutter in sidelobes of the upper beams. An example of a modern, solid-state stacked-beam radar is the Martello S-723 (Figure 14.3).

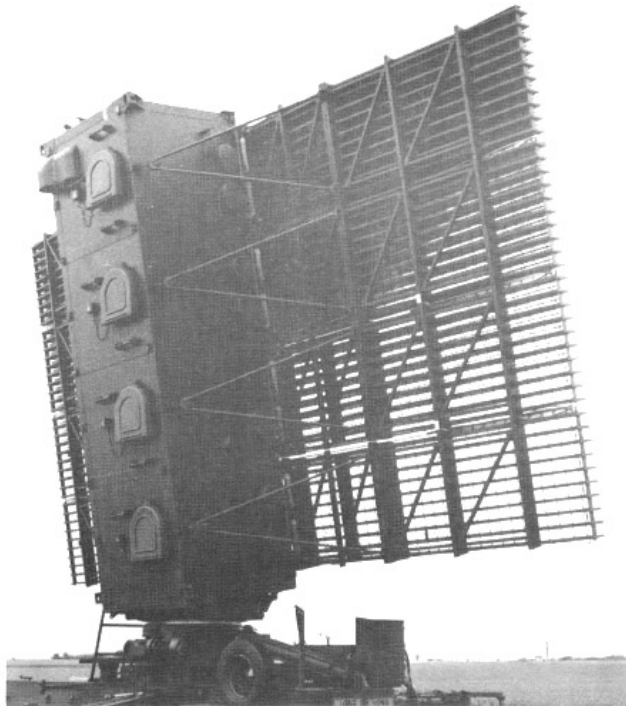


Figure 14.3 Martello S-723 stacked-beam 3-D radar [2].

The Martello S-723 array has 40 rows of 64 dipoles each, with a solid-state T/R module feeding each row. The combined peak power is 132 kW, at a duty cycle of 4%. Use of a duty cycle that is relatively low (for solid-state transmitters) avoids the requirement for transmitting multiple waveforms in each beam, since eclipsing by the transmitted pulse affects only the first 4% of the unambiguous range of the waveform (about 2 km in this case). The 40 row receivers, housed in the central spine of the antenna structure, feed a beamforming matrix that generates eight elevation beams. Monopulse processing in elevation is performed by comparing the amplitude of logarithmic outputs from adjacent beams on each detected pulse, followed by averaging over the multiple pulses during an azimuth beamwidth. Azimuth interpolation within the beamwidth uses the nonmonopulse method common to most 2-D radars that receive pulse trains modulated during scan by the azimuth beamwidth.

14.2 MONOPULSE SECONDARY SURVEILLANCE RADARS

A secondary surveillance radar (SSR) is one in which the return signals are obtained from a beacon (transponder) carried by the target and triggered by the radar's transmitted pulse [3]. The technology evolved from the Identify Friend or Foe (IFF) systems of World War II, and SSRs today are the principal source of data for air traffic control systems worldwide.

A major problem in early SSRs was the presence of unwanted returns triggered by and received in sidelobes of the antenna. The frequencies allocated to SSR are 1,030 MHz for interrogation and 1,090 MHz for response, and the antenna sizes used for SSR typically generate azimuth beamwidths of several degrees at this frequency. The wide beams and sidelobe levels of these antennas would tend to trigger a large number of undesired returns, interfering with proper operation of the air traffic control system. As a result, modern SSR antennas generally include a monopulse-type feed networks in the azimuth coordinate. The difference pattern of this feed is used to transmit a *control pulse* that inhibits response from transponders in the sidelobe region [4]. The principle of operation is similar to the sidelobe blanker used to protect radars from random-pulse interference from emitters in the sidelobes.

The patterns of the SSR monopulse array antenna in its transmitting mode are as shown in Figure 14.4. The *interrogate beam* (sum pattern) has the azimuth beamwidth determined by the wavelength and the width of the SSR antenna. The *control beam* is transmitted through the azimuth difference pattern, formed with a hybrid junction at the center of the antenna. This produces the type of illumination that was shown for a quadrant-split antenna in Figure 7.4 and the patterns shown in Figure 7.5. The high difference sidelobes, extending both sides of the central null, were an undesirable feature of that design for a tracking radar, but are useful in the SSR because they guarantee that the control pulse will exceed interrogation

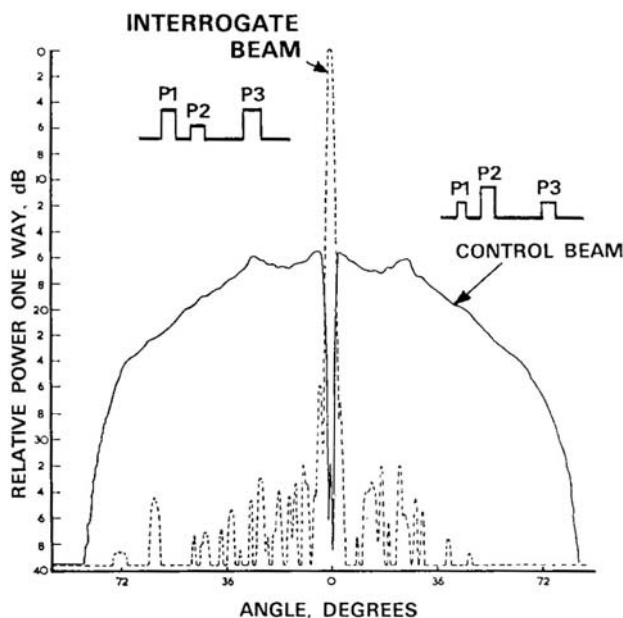


Figure 14.4 SSR antenna interrogate and control beam patterns [3].

pulses everywhere except near the axis. Hence it may be used to discriminate against interrogation other than by the mainlobe of the interrogation beam.

The transmitted pulse group consists of three pulses, of which the first and third (P1 and P3) are transmitted through the narrow interrogation beam. The second pulse (P2) is transmitted through the control beam generated by the difference channel. The transponder compares the amplitudes of the three pulses, and responds only if P1 and P3 exceed P2 by a prescribed ratio. The process is called “interrogator sidelobe suppression” (ISLS or SLS). Different interrogation modes use difference spacing of the P1 and P3 pulses to request different forms of response code for identification and altitude reporting.

The availability of a monopulse difference channel in the SSR antenna permits its use for reducing interference between overlapping response pulse groups (known as *garble*) and for more accurate measurement of their azimuths. The aircraft response to an interrogation consists of a group of some 14 pulses spread over an interval of some 20 μ s, that identify the aircraft and its barometric altimeter reading. In a dense traffic environment there are frequent instances of overlapping responses that would defeat proper decoding by the SSR processor. The ratio of d/s response from aircraft at different azimuth angles provides a means of sorting the response pulses by angle of arrival, and of associating each pulse in the

overlapping groups with its source. The decoded group can then be assigned an azimuth determined from the average of d/s from the multiple pulses.

14.3 OTHER RADAR APPLICATIONS

Apart from tracking and surveillance, there have been several applications of monopulse techniques in other radar areas. Some of these are discussed below to indicate the extent to which monopulse has contributed to the broad field of radar.

14.3.1 Terrain-Avoidance Radar

Military aircraft may be forced to conduct low-altitude penetrations of hostile airspace, flying below the coverage of the surveillance and tracking radars that provide data to the air defense systems. This raises the risk of flying into elevated terrain or obstacles rising above the terrain. The terrain-avoidance radar (usually one of many modes of a nose-mounted airborne radar) offers protection against such collisions. The radar scans a narrow azimuth sector around the aircraft heading, at an elevation angle that permits mapping of the terrain ahead of the aircraft. At each azimuth, the elevation beam illuminates the surface, and monopulse measurements of depression angle to the terrain echoes are performed as a function of range (Figure 14.5).

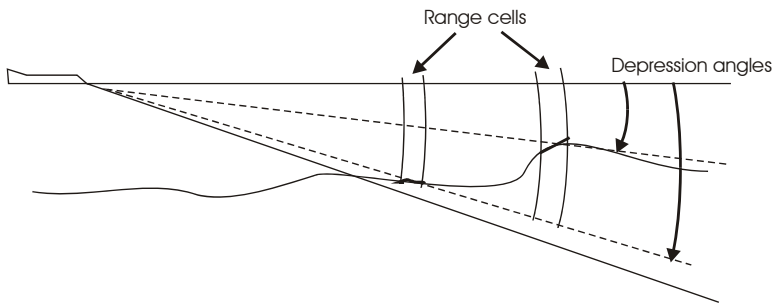


Figure 14.5 Terrain-avoidance beam with monopulse measurement of depression angles.

Data on the terrain profile in the azimuth sector about the aircraft heading are fed to a flight-control computer, which can then determine the risk of collision and adjust the pitch and yaw of the aircraft in time to maintain safe flight. This mode is interlaced with other radar functions, and repeated at a rate adequate to close the flight-control loops.

An application of this technique to helicopter navigation is described in [4]. The antenna in this case was a pair of slotted waveguides mounted one above the

other, feeding two receivers and a phase-sensitive detector. Illumination for the experimental radar was provided by a separate antenna transmitting a CW signal.

14.3.2 Aircraft Low Approach Radar

The use of a monopulse data to improve the resolution of targets on a radar display was discussed by Kirkpatrick in [5]. The same author raised the subject of *monopulse display improvement* (MDI) again [6], proposing use of airborne monopulse radar as a low-approach aid. Experimental data were gathered showing that ground features are useful in navigation toward a runway marked with corner reflectors.

14.3.3 Target Recognition

An experiment performed by the Naval Research Laboratory in the 1970s showed the potential for improved target classification and recognition, as well as reduced glint error, through combined use of high range resolution and monopulse processing [7]. The range resolution of 0.5m was obtained from a 465-MHz linear FM waveform using the stretch processing technique [8], applied to both the sum and difference channels. An example is shown in Figure 14.6, where the aircraft out-

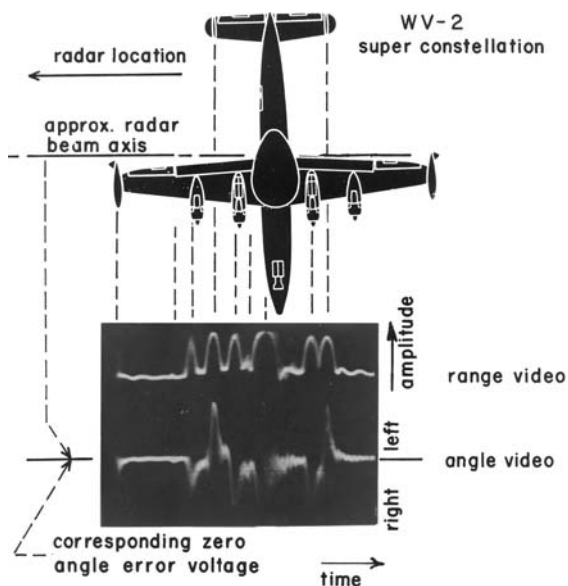


Figure 14.6 High range resolution data on super constellation aircraft in flight. (Photo courtesy of NRL.)

line is compared with the conventional range profile (range video) and the monopulse difference output (angle video).

14.3.4 Displaced Phase Center Antenna Applications

The displaced phase center antenna (DPCA) is used in airborne moving target indication (AMTI) radar to remove the spreading of the clutter spectrum that results from platform motion [9, pp. 3.10–3.20]. The use of monopulse sum and azimuth difference patterns for DPCA and also for compensation of the angular scan effect is shown to provide a large improvement in clutter cancellation. The required antenna designs are more readily implemented than arrays in which individual elements are switched in and out of the array to move the phase center. In addition, changes in platform velocity can be accommodated with a simple change in the weight of the difference channel that is combined with the sum channel for DPCA.

More recently, the more powerful concept of space-time adaptive processing (STAP) has been applied to increase the clutter cancellation in airborne MTI and pulsed Doppler radars. Monopulse sum and difference channels provide the signals necessary for implementation of STAP technology [10], with relatively simple beamforming networks.

References

- [1] IEEE Standard 100, *The Authoritative Dictionary of IEEE Standards Terms*, 7th ed., New York: IEEE Press, 2000.
- [2] Mitre Corporation, *Radar Reference Manual*, Report M87-69, December 1987.
- [3] M. C. Stevens, *Secondary Surveillance Radar*, Norwood, MA: Artech House, 1988.
- [4] K. E. Potter, "Experimental Design Study of an Airborne Interferometer for Terrain Avoidance," *IEE International Conf. Radar-77*, London, October 25–28, 1977, pp. 486–503.
- [5] G. M. Kirkpatrick, "Final Engineering Report on Angular Accuracy Improvement," General Electric Electronics Laboratory, Syracuse, NY, Contract D.A. 36-039-sc-194, 1 August 1952. Reprinted: *Radars*, Vol. 1, *Monopulse Radar*, D. K. Barton, (ed.), Artech House, 1975, pp. 17–103.
- [6] G. M. Kirkpatrick, "Use of Airborne Monopulse Radar as a Low Approach Aid," *IEEE Trans. on Aerospace and Electronic Systems*, Vol. AES-2, No. 3, May 1966, pp. 353–359.
- [7] D. D. Howard, "High Range-Resolution Monopulse Tracking Radar," *IEEE Trans. on Aerospace and Electronic Systems*, Vol. AES-11, No. 5, September 1975, pp. 749–755.
- [8] W. J. Caputi, Jr., "Stretch: A Time-Transformation Technique," *IEEE Trans. on Aerospace and Electronic Systems*, Vol. AES-7, No. 2, March 1971, pp. 269–278. Reprinted: *Radars*, Vol. 3, *Pulse Compression*, D. K. Barton, (ed.), Dedham, MA: Artech House, 1975, pp. 183–192.

- [9] J. K. Day and F. M. Staudaher, "Airborne MTI," Chapter 3 in *Radar Handbook*, 3rd ed., M. I. Skolnik, (ed. in chief), New York: McGraw-Hill, 2008.
- [10] J. Maher, Y. Ahang, and H. Wang, "A Performance Evaluation of $\Sigma\Delta$ -STAP Approach to Airborne Surveillance Radars in the Presence of Both Clutter and Jammers," *IEEE International Conf. Radar-97*, Syracuse, NY, October 14–16, 1997, pp. 305–309.

Chapter 15

Special Topics

This chapter consists of individual sections on supplementary topics which do not fall directly within the scope of the previous chapters.

15.1 DIFFERENCE AND SUM PATTERNS HAVING A RATIO PROPORTIONAL TO ANGLE

The difference-to-sum monopulse ratio d/s is normally a nonlinear function of angle. It is possible, however, to generate sum and difference patterns having a linear characteristic—that is, a d/s ratio exactly proportional to the displacement of the target from the boresight axis in sine space, and therefore very nearly proportional to the off-boresight angle if that angle does not exceed a few degrees. This property of linearity may be useful for certain applications but it requires some sacrifice in other desirable characteristics of the patterns.

15.1.1 General Properties

The description and theory will be developed first for amplitude comparison antennas in which the monopulse axis is on (or close to) the normal to the aperture. This category includes reflectors, lenses, and arrays that are not electronically steerable. Extension to electronically steerable arrays and to phase-comparison monopulse is covered in Section 15.1.7. The present chapter analyzes types of error not covered in other chapters, and presents practical formulas, analytical methods, and other useful information.

Figure 6.6 in Chapter 6 showed three plots of the normalized difference d/s in one angular coordinate versus off-axis angle in that coordinate, for three different values of quint angle of $(\sin x)/x$ component beams. The usual monopulse charac-

teristic (for minimum thermal-noise error) is concave upward, like the lowest curve in the figure. If the squint angle is increased sufficiently, the curve becomes concave downward, like the top curve in the figure. At a certain critical squint angle the curve becomes a straight line, shown by the middle curve in the figure. That squint angle is the one that causes the peak of each $(\sin x)/x$ component pattern to fall at the first null of the other. Strictly speaking, the d/s ratio is proportional to the sine of the angle from the aperture normal rather than to the angle itself, but this distinction is unimportant if the monopulse axis lies in the direction of the normal and the beam is not more than a few degrees wide. Theoretically the proportionality of d/s to the sine of the angle holds true for all angles, including the sidelobes.

Here we will present a simple mathematical derivation of the linear relationship and will calculate the beamwidth, efficiency, sidelobe levels, and monopulse slope of the patterns that have this property. We will then show a linear d/s characteristic can also be obtained from component patterns other than $(\sin x)/x$. The existence of a class of sum-and-difference pattern pairs having a ratio proportional to the sine of the angle was pointed out by Rhodes [1]. He derived equations for the required aperture function (illumination function) of each squinted beam. Here we relate the results to the patterns and illumination functions of the sum and difference, which are usually of more direct interest to a designer or system analyst than the squinted beams.

15.1.2 Applications and Implementation

A linear characteristic may be useful for certain applications even though sum and difference patterns having this property are not generally optimum from the standpoint of low sidelobes and minimum thermal-noise error. Patterns having the linearity property are generated more easily in an array antenna than in a reflector antenna because an array offers greater flexibility in shaping the illumination functions. For example, such patterns could be obtained from a Butler matrix [2].

Strict linearity is an idealized condition that would require perfect equipment, perfectly adjusted. It is doubtful that in practice the equipment tolerance could be kept small enough to maintain the linearity out into the sidelobes, especially near the nulls, which must be coincident in the sum and difference patterns in order for linearity to hold. However, it should not be difficult to obtain linearity throughout the main lobe.

In the analysis and computation of monopulse system performance or errors it is often assumed for convenience that d/s is proportional to angle (or to the sine of the angle). Even when this is not actually the case, the approximation is sometimes acceptable. By using the method to be described, sum and difference patterns that conform to that assumption can be modeled. Of course such models should not be used unless they give a reasonable fit, in the angular region of interest, to the actual patterns that they are supposed to represent.

15.1.3 Derivation of Equations

We assume that the aperture illumination is separable in the two coordinates (as would be the case in a rectangular array, for example). Then the patterns in each coordinate can be analyzed as if they were produced by a line array. A line array of length L , with uniform amplitude and phase illumination, produces the following pattern:

$$f(U) = \frac{\sin(\pi U/2)}{\pi U/2} \quad (15.1)$$

where

- $U = \frac{2L \sin \theta}{\lambda}$; (15.2)
- L = length of antenna;
- θ = angle from beam axis;
- λ = wavelength.

Note that U is a normalized measure of deviation from the axis. It is the ratio of $\sin \theta$ to half of a “standard beamwidth” in sine space, arbitrarily defined as λ/L . If two such beams are formed simultaneously in squinted directions, their sum and difference are given by the following two equations, with a common normalizing factor $\pi/4$ inserted so that the sum pattern is unity when $U = 0$, as will be seen later:

$$s = \frac{\pi}{4} \left[\frac{\sin \left[(\pi/2)(U - U_{sq}) \right]}{(\pi/2)(U - U_{sq})} + \frac{\sin \left[(\pi/2)(U + U_{sq}) \right]}{(\pi/2)(U + U_{sq})} \right] \quad (15.3)$$

$$s = \frac{\pi}{4} \left[\frac{\sin \left[(\pi/2)(U - U_{sq}) \right]}{(\pi/2)(U - U_{sq})} - \frac{\sin \left[(\pi/2)(U + U_{sq}) \right]}{(\pi/2)(U + U_{sq})} \right] \quad (15.4)$$

where

- $U_{sq} = \frac{2L \sin \theta_{sq}}{\lambda}$; (15.5)
- θ_{sq} = squint angle of each beam from crossover.

Choose the following value of U_{sq} :

$$U_{sq} = 1 \quad (15.6)$$

Then (15.3) and (15.4) reduce to

$$s = \frac{\cos(\pi U/2)}{1 - U^2} \quad (15.7)$$

$$d = \frac{U \cos(\pi U/2)}{1 - U^2} \quad (15.8)$$

and their ratio is

$$\frac{d}{s} = U \quad (15.9)$$

which means, according to the definition of U in (15.2), that the normalized difference signal is proportional to $\sin \theta$. If the angles of interest are not greater than a few degrees, the difference between $\sin d$ and d is negligible, and the normalized difference signal is almost exactly proportional to angle off axis.

15.1.4 Characteristics of the Patterns and Illumination Functions

A plot of the monopulse ratio versus $\sin \theta$ is a straight line, as illustrated in Figure 15.1. The line is dotted in the vicinity of the nulls (which occur at the same angles in the sum and difference patterns) because although the mathematical ratio is still given by (15.9), the signal strength is zero or very low. Hence, any attempted measurement of a target in the vicinity of one of those angles would be dominated by noise.

The nulls occur at $U = \pm 3, \pm 5, \pm 7, \dots$. The peaks of the first and second sidelobes of the sum pattern occur at $U = 3.8$ and $U = 5.9$, and have values of -23.0 dB and -30.7 dB, respectively. The peaks of the first and second sidelobes of the difference pattern occur at $U = 3.9$ and $U = 5.9$, and have values of -11.3 dB and -15.3 dB, respectively. A check on these sidelobe levels is obtained by noting that since the peak of the first sidelobe occurs at $U = 3.85$ in both patterns and since $d/s = U$ from (15.9), the first difference sidelobe must be higher than the first sum sidelobe by $20 \log 3.85 = 11.7$ dB, which agrees with the numbers above. The high sidelobes of the difference pattern are caused by the discontinuities where the illumination changes abruptly from a peak value at the ends of the array to zero just beyond the ends.

The sum-pattern beamwidth between one-way half-power points is

$$\theta_{bw} \approx \sin \theta_{bw} = 1.19 \lambda / L \quad (15.10)$$

The half-power points occur at $U = \pm 1.19$.

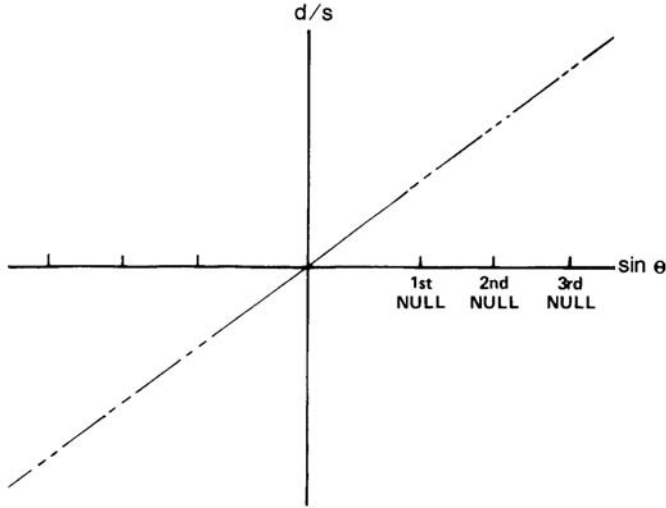


Figure 15.1 Monopulse ratio proportional to sine of angle.

The sum-pattern illumination function is the sum of two terms which generate the two squinted beams. The equation (normalizing coefficient omitted) is

$$i_s(x_n) = \exp(j\pi U_{sq} x_n) + \exp(-j\pi U_{sq} x_n) \quad (15.11)$$

which reduces, after substitution of (15.6), to

$$i_s(x_n) = 2 \cos(\pi x_n) \quad (15.12)$$

In these equations $i_s(x_n)$ is the sum-pattern illumination function expressed as a phasor (complex) voltage and $x_n = x/L$ is normalized distance along the array measured from the center, $-1/2 \leq x_n \leq 1/2$. This illumination has a half-cycle cosine voltage taper which goes to zero at the ends. The difference illumination function is

$$i_d = 2j \sin(\pi x_n) \quad (15.13)$$

which is a half-cycle sine function with peak positive and negative values at the ends. The one-dimensional sum-pattern efficiency is calculated by the following formula:

$$\text{Efficiency} = \frac{\left[\int_{-1/2}^{1/2} i_s(x_n) dx_n \right]^2}{\int_{-1/2}^{1/2} [i_s(x_n)]^2 dx_n} = \frac{\left[\int_{-1/2}^{1/2} \cos(\pi x_n) dx_n \right]^2}{\int_{-1/2}^{1/2} \cos^2(\pi x_n) dx_n} = \frac{8}{\pi^2} \quad (15.14)$$

The monopulse ratio is calculated by using (15.2) and (15.10) to write (15.9) in a form that is normalized to the beamwidth:

$$\frac{d}{s} = U = \frac{2L \sin \theta}{\lambda} = 2.38 \frac{\theta}{\theta_{bw}} \quad (15.15)$$

which means that the monopulse slope is

$$k_m = 2.38 \text{ V/V/beamwidth} \quad (15.16)$$

This is considerably higher than the typical slope of about 1.6 V/V/beamwidth, and it might appear that the higher slope would mean higher sensitivity and therefore a smaller thermal-noise error. However, if the slope is expressed in absolute angular units, such as V/V/degree, the increase over a more typical slope is not so great; when expressed in V/V/beamwidth the increase appears greater than it actually is because the larger squint angle makes the sum beam wider even though each squinted beam maintains constant width. Furthermore, it was shown in Chapter 6 that thermal-noise error is inversely proportional to a performance index equal to the product of difference slope (in absolute units) and sum voltage gain.

The sum gain decreases as the squint angle increases. By entering Figure 6.3 at the two squint angles labeled on the middle and lower curves in Figure 6.6, and comparing the ordinates, it is found that the linear monopulse has 4% larger thermal-noise error than the minimum. Hence there is only a minor penalty in noise error. The main disadvantage of these particular patterns is their high sidelobes.

15.1.5 Computation of Patterns at Indeterminate Points

If these patterns are used in computer modeling of system performance, the computation of the sum pattern from (15.7) generally is straightforward. However, when $U = \pm 1$, both the numerator and the denominator are zero and the quotient is indeterminate. Application of l'Hospital's rule (differentiation of numerator and denominator) yields the value $s = \pi/4$ at those two symmetrical points. In addition to the indeterminacy at the exact points $U = \pm 1$, an erroneous result may be obtained if U is so close to these points that the numerator and denominator are suppressed or excessively rounded off. This problem can be avoided by a first-degree

power series expansion of the numerator and denominator of s in the vicinity of $U = \pm 1$. This gives

$$\cos \frac{\pi U}{2} = \cos \left[\frac{\pi}{2} (1 + \Delta U) \right] = -\sin \left(\frac{\pi}{2} \Delta U \right) \approx -\frac{\pi}{2} \Delta U \quad (15.17)$$

and

$$1 - U^2 = 1 - (1 + \Delta U)^2 = -\Delta U (2 + \Delta U) \quad (15.18)$$

where

$$\Delta U = |U| - 1 \quad (15.19)$$

The ratio of (15.17) to (15.18) is

$$s \approx \frac{\pi/4}{1 + \Delta U/2} \approx \frac{\pi}{4} \left(1 - \frac{\Delta U}{2} \right) \quad (15.20)$$

By use of (15.19) the equation becomes

$$s \approx \frac{\pi}{8} (3 - |U|) \quad (15.21)$$

The computational procedure, then, is to use (15.21) instead of (15.7) when $|U|$ differs from 1 by less than a certain increment. That increment is selected by determining the point at which the particular computer begins to give erroneous results. The approximation is quite close. If (15.20) were carried out to the second power of U , the additional term in the parentheses would be $+(\Delta U/2)^2$. Thus if $|U| - 1 = 0.02$, for example, the error in the use of approximation (15.21) is only 0.01%.

15.1.6 Other Pattern Pairs Having a Constant Monopulse Slope

The particular pair of patterns discussed above is not the only pair having a ratio exactly proportional to the sine of the angle. Rhodes [1] derived an equation for a whole family of aperture illumination functions of squinted beams whose difference and sum have this property. That equation (number 6.4 on page 95 in Rhodes) is reproduced here with some of the symbols changed:

$$|i_{sq}(x_n)| = (\cos \pi x_n)^Z \quad (15.22)$$

where

- $|i_{sq}(x_n)|$ = amplitude of illumination function of each squinted beam;
- x_n = distance from center of aperture, normalized by aperture length;
- $1/2 \leq x_n \leq 1/2$.

The exponent Z can have any nonnegative value, not limited to integers. The required squint angle is independent of Z ; its sine equals $\lambda/2L$.

At this point it is convenient to introduce a measure of monopulse slope, k_U , defined by

$$k_U = \frac{d/s}{U} \quad (15.23)$$

It is recalled from (15.2) that U is proportional to $\sin \theta$. From a relation derived by Rhodes, it is found that

$$k_U = \frac{1}{Z+1} \quad (15.24)$$

Since Z cannot be negative, the largest possible value of K_U is 1. The relation between k_U and the standard measure of monopulse slope k_m (volts per volt per sum-pattern beamwidth), defined in Section 6.4, is

$$\frac{k_m}{k_U} = \frac{2\theta_{bw}}{\lambda/L} \quad (15.25)$$

where θ_{bw} is the half-power sum-pattern beamwidth in radians.

For the pair of patterns treated earlier, $Z = 0$, which means uniform illumination of each squinted beam. If Z is increased, the illumination amplitude taper becomes stronger, causing reduced sidelobes but also reduced efficiency, angular resolution, and monopulse sensitivity. To illustrate this trend, characteristics are compared for $Z = 0$ and $Z = 1$ in Table 15.1. The numbers were calculated with the aid of [3, Table A.2, p. 251].

The family of patterns derived by Rhodes can be extended further by superposition. Consider multiple sum-and-difference pattern pairs, the ratio of each pair having a constant (but different) slope:

$$\begin{aligned} \frac{d_1}{s_1} &= k_{U1}U \\ \frac{d_2}{s_2} &= k_{U2}U \end{aligned} \quad (15.26)$$

Table 15.1 Comparison of Pattern Characteristics

<i>Characteristic</i>	$Z = 0$	$Z = 1$
Illumination function of squinted beams	Uniform	Cosine
Sum illumination function	Cosine	Cosine ²
Difference illumination function	Half-cycle sine	Full-cycle sine
Sum-pattern beamwidth (rad)	$1.19\lambda/L$	$1.44\lambda/L$
Sum-pattern efficiency	0.81	0.66
First sum sidelobe	-23.0 dB	-31.5 dB
Slope k_U	1.0	0.5
Slope k_m	2.38	1.44

By linear superposition of n pairs, form a composite difference pattern

$$d = C_1 \left[a_1 d_1 + a_2 (k_{U1}/k_{U2}) d_2 + \cdots + a_n (k_{U1}/k_{Un}) d_n \right] \quad (15.27)$$

where the coefficients A_1, a_2, \dots, a_n can be chosen arbitrarily, and a composite sum pattern

$$s = C_2 \left[a_1 s_1 + a_2 s_2 + \cdots + a_n s_n \right] \quad (15.28)$$

The coefficients C_1 and C_2 are needed to adjust the total power of d and s to the correct value. Then

$$\frac{d}{s} = \frac{C_1}{C_2} \frac{a_1 k_{U1} s_1 U + a_2 k_{U1} s_2 U + \cdots + a_n k_{U1} s_n U}{a_1 s_1 + a_2 s_2 + \cdots + a_n s_n} = \frac{C_1}{C_2} k_{U1} U \quad (15.29)$$

Thus the composite patterns also produce a constant monopulse slope.

While Rhodes' formulation is useful if one is interested in the illumination function of each squinted beam, a different approach to the problem of generating constant-slope patterns will now be described. This approach is more general, and is expressed in terms of the sum and difference illumination functions, which are usually of more direct interest than the illumination functions of the squinted beams. This method applies to phase-comparison as well as to amplitude comparison monopulse, and is particularly suited to array antennas.

Let $i_s(x_n)$ and $i_d(x_n)$ be the sum and difference aperture illumination functions respectively, as before, and let $s(U)$ and $d(U)$ be the corresponding patterns. Ignoring normalizing coefficients, the patterns are the Fourier transforms of the respective illumination functions. Let the sum illumination be designed to produce the desired sum pattern. By a well-known property of Fourier transforms, the trans-

form of the derivative of $i_s(x_n)$ with respect to x_n is U times the transform for $i_s(x_n)$ itself. Therefore, to obtain a difference pattern proportional to U times the sum pattern, the difference illumination function must be designed to be proportional to the derivative of the sum illumination function. The sum illumination must be zero at the edges of the aperture, otherwise the derivative would have an impulse at each edge.

In applying this method to an array antenna it is immaterial whether the monopulse is classified as amplitude-comparison or phase comparison, as long as the appropriate sum and difference illumination functions can be obtained. The only difference, as explained Chapter 5, is that in amplitude comparison the d and s voltages have 0° (or 180°) relative phase and their illumination functions have 90° relative phase, while in phase comparison the reverse is true. Hence the only modification that may be necessary is to insert the imaginary factor j in the pertinent equations when there is a 90° phase relationship.

15.1.7 Extension to Electronically Steerable Arrays

In electronically steerable arrays the d/s ratio can be made proportional to the displacement of the target direction from the monopulse axis in sine space—that is, proportional to the difference between the sines of the target angle and beam axis, both measured from the normal to the array aperture plane.

The analysis is the same as that of the nonsteerable patterns except that U is replaced everywhere by $U - U_{st}$. The quantity U_{st} is defined by

$$U_{st} = \frac{2L \sin \theta_{st}}{\lambda} \quad (15.30)$$

where θ_{st} is the beam steering angle measured from normal to the array, and U is defined not by (15.2) but by

$$U = \frac{2L \sin(\theta_{st} + \theta)}{\lambda} \quad (15.31)$$

since θ has been defined as the target angle measured from the monopulse axis. Equation (15.5) no longer applies, but U_{sq} remains equal to 1 as in (15.6). In other words the squint is constant in sine space but not in angle space as the beam is steered. As before, the relations apply to each angular coordinate separately.

Equation (15.23) is now modified to

$$\frac{d}{s} = k_U (U - U_{st}) \quad (15.32)$$

so the ratio is proportional to the displacement of the target direction from the monopulse axis in sine space. The ratio can be expressed as a function of angle by using (15.30–15.32):

$$\frac{d}{s} = k_U \frac{2L}{\lambda} \left[\sin(\theta_{st} + \theta) - \sin \theta_{st} \right] \quad (15.33)$$

For small d this reduces to

$$\frac{d}{s} \approx k_U \frac{2L}{\lambda} \theta \cos \theta_{st} \quad (15.34)$$

which means that the monopulse ratio is still approximately proportional to the target angle off axis, but with sensitivity reduced by the cosine of the steering angle.

15.2 THE DIAGONAL DIFFERENCE SIGNAL

It was shown in Section 4.4.3 and in Figures 4.15 and 4.17 that in addition to the sum, the traverse difference, and the elevation difference, a fourth output is available from the monopulse antenna with a four-horn feed. It is the difference between the sums of the two diagonal pairs, and is called the *diagonal difference*. It has also been called the double difference, the second difference, or the quadrupolar signal. This output, which is an unused by-product of the comparator, is usually terminated in a dummy load. The corresponding output from an array antenna of the type illustrated in Figure 7.7 could be obtained if the differences of the column differences were combined instead of being terminated in the dummy loads shown in Figure 7.7(b).

The diagonal difference signal is scarcely mentioned in the technical literature. One paper [4] suggested that it might contain useful information about the angular extent and aspect of a distributed target, but gave no quantitative analysis or specific approach. Here we examine the nature of the diagonal difference in order to determine whether it might be useful for the following purposes:

1. To improve the angle estimates of a single target;
2. To determine the angular location of unresolved targets.

The results of this examination, although based on qualitative reasoning rather than on quantitative analysis, are sufficient to demonstrate that the diagonal difference has little or no general practical value for these purposes, although this conclusion does not negate the possibility of special applications for which the diagonal difference may be found useful. The reasoning follows along the lines of

[5] (where it is called the quadrupolar signal). For the four-horn arrangement shown in Figures 4.15 and 4.17, the four outputs that can be obtained are

$$s = \frac{1}{2}(A + B + C + D) \quad (15.35)$$

$$d_{tr} = \frac{1}{2}[(C + D) - (A + B)] \quad (15.36)$$

$$d_{el} = \frac{1}{2}[(A + C) - (B + D)] \quad (15.37)$$

$$q = \frac{1}{2}[(A + D) - (B + C)] \quad (15.38)$$

In these equations s is the sum voltage, d_{tr} and d_{el} are the traverse and elevation difference voltages, q is the diagonal difference voltage, and A, B, C, D are the voltages from the four horns. The reason for the factor $1/2$ was explained in Chapter 4.

Figure 15.2 is a simulated three-dimensional view of the typical shape of a diagonal difference pattern. One diagonal pair of lobes is positive and the other pair is negative. Along the traverse and elevation axes q is zero by symmetry. At the origin (the boresight direction) there is a saddle point. If the q signal is to be used, it must have its own receiver and must be divided by the sum signal to obtain the ratio q/s , since an angle measurement must be independent of the signal

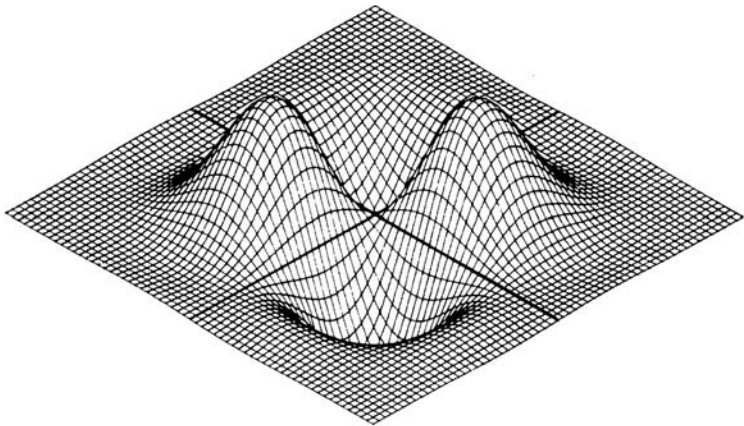


Figure 15.2 Diagonal difference pattern.

strength. Figure 15.3 is another way of visualizing the pattern, this time in the normalized form q/s . The curved lines are approximate shapes of contours of constant q/s . Also shown for comparison are contours of constant d_{tr}/s and d_{el}/s ; these are idealized by being drawn as a rectangular grid, whereas in actuality they may exhibit some “barreling” or “pin-cushioning” because the traverse output is not completely independent of elevation and vice versa.

In the absence of errors, the angular location of a single target is completely determined by measurements of d_{tr}/s and d_{el}/s , so q/s is redundant. However, since there are errors in the measurements, the question is whether an overdetermined solution based on all three would reduce the angle error due to noise. To answer this, we note that at the origin the partial derivatives of q/s with respect to traverse and elevation are zero, since q is a constant (zero) along those axes. It is proved in calculus that if the partial derivative of a continuous function of two coordinates is zero in two orthogonal directions at a given point, it is zero in all directions at that point. This means that q/s has little or no sensitivity to small displacements of the target from the boresight direction, and therefore it is not useful for tracking a target close to boresight. If the target is off axis in traverse but on axis in elevation, q/s has zero sensitivity in traverse. The elevation sensitivity (the slope of q/s versus elevation) is nonzero in this case, but it is lower than the sensitivity of d_{el}/s .

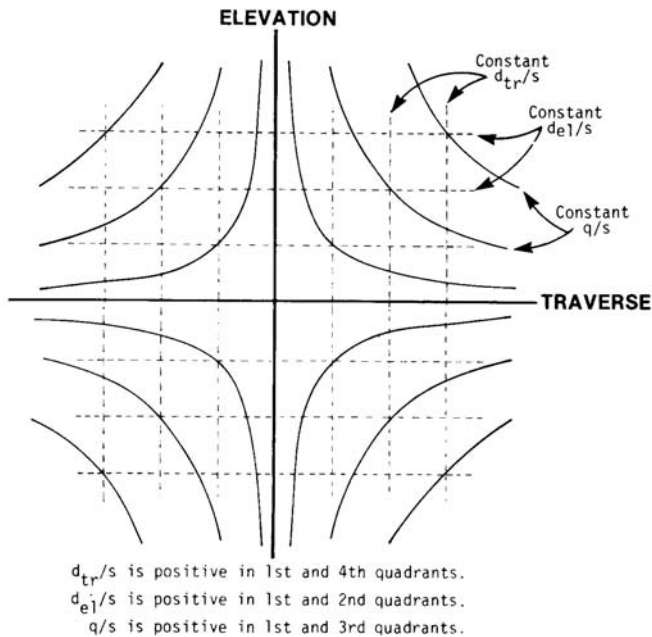


Figure 15.3 Contours of constant d_{tr}/s , d_{el}/s , and q/s .

Therefore combining the two would give negligible improvement and might even degrade the estimate by contributing more noise than signal. A corresponding argument applies if the target is on axis in traverse and off axis in elevation. Improvement in accuracy by overdetermination can be obtained more effectively by measurements of d_{tr}/s and d_{el}/s from multiple pulses rather than just from one.

In the case of two unresolved targets q/s is not redundant. There are six unknowns: two angular components for each target plus the amplitude ratio and relative phase of the pair of targets. As explained in Chapter 9, only the angles are usually desired, but the solutions are not separable. Measurements of the real and imaginary parts of d_{tr}/s , d_{el}/s , and q/s would provide six values related to the six unknowns by a known set of six equations. Thus it might appear that solutions could be obtained for the angular locations of the two targets. Here again, however, the poor sensitivity negates the practical usefulness. As an example, consider two unresolved targets, both at zero elevation but at different traverse angles. The value of q is zero for each target individually and for both together. Therefore the measurement of q/s is of no help in determining the target traverse angles in this example. Other examples are two targets at zero traverse but at difference elevation angles, and one target off axis in traverse only and the other in elevation only. Although these are special examples, they are sufficient to illustrate the generally poor sensitivity of q/s .

Thus, it does not appear that there would be enough benefit (if any) from the use of the diagonal difference signal—at least for the purposes examined here—to justify the complexity and cost of providing the additional receiving channel and monopulse processor that it would require.

15.3 UNITS OF ANGLE AND SINE SPACE

Several types of angular units and sine-space units are employed in the calibration of radar systems and in analysis of the data that they produce. These units are generally the same in monopulse and nonmonopulse systems, except that because of the angular precision available from monopulse, the finer units are more often used. Some units are well known—others are specialized and relatively unfamiliar.

The most universal unit in radar applications, as in other fields, is the *degree*, (1/360 of a circle). However, the *minute* (1/60 of a degree) and the *second* (1/60 of a minute) are uncommon in radar usage. Instead, fractions of a degree are usually expressed in decimal form. This, one-eighth of a degree is written as 0.125° rather than $7'30''$.

The *radian* is defined as the angle subtended at the center of a circle by an arc equal in length to the radius. The radian itself is not used as a practical unit of angular measurement in radar (see milliradian below).

The *milliradian*, which is $1/1,000$ of a radian, is widely used in monopulse radar, especially for small angles of the order of fractions of a degree. The number of milliradians in a circle is $2,000\pi$ or about 6,283. In the International System of Units [6, 7] the standard abbreviation for radian is rad; when combined with the abbreviation for the prefix milli-, it becomes mrad, which is therefore the prescribed abbreviation for milliradian. The abbreviation mr is often seen, but it is nonstandard. The abbreviation mil is also sometimes seen and often heard; besides being nonstandard, it could be confused with the artillery mil, defined in the next paragraph. Nevertheless, mil is a popular oral abbreviation, because mrad and mr are unpronounceable.

The artillery mil is a convenient “rounded” version of the milliradian, used at some U.S. test ranges. By definition, there are exactly 6,400 (rather than approximately 6,283) artillery mils in a circle. Since the difference is less than 2%, the artillery mil and the milliradian may be used interchangeably for approximate values of small angles; in general, however, they should be carefully distinguished.

The *grad* is $1/100$ of a right angle or $1/400$ of a circle. This unit is not used for radar measurements, but may be encountered in some geographic applications in European countries. One grad of latitude is a distance of 100 km (to a close approximation) on the Earth’s surface.

A more recently introduced unit is the *millisine* [8, p. 172]. This is a unit of measurement in sine space (see Sections 2.8, 7.2, and 7.3) rather than angle space, and is particularly suited to planar array antennas. The number of millisines in an angle measured from a specified reference direction is 1,000 times the sine of the angle. For example, 30° corresponds to 500 millisines. The number of millisines in the angular interval between two lines at angles θ_1 and θ_2 from a common reference direction is $1,000(\sin\theta_2 - \sin\theta_1)$, not $1,000\sin(\theta_2 - \theta_1)$. In planar arrays the reference direction is usually understood to be broadside (perpendicular to the array face). The term millisine is nonstandard and cannot be interpreted as “a thousandth of a sine,” as the name would suggest, but it has the merit of convenience in specifying and analyzing performance of an electronically steered array. When beamwidth, angular resolution, and angular precision of an array antenna are expressed in conventional angular units, they are functions of the beam steering angle. When expressed in millisines referenced to broadside, these quantities are nearly independent of beam steering direction and therefore can be specified more compactly. For directions close to the reference direction, the number of millisines is approximately equal to the number of milliradians. The equivalent term millicosine is also sometimes used, the only difference being in the point of view: millicosine refers to the cosines of angles measured from the rectangular coordinate axes of the array (angles α and β), while millisine refers to sines of the complementary angles measured from the principal planes through the broadside direction (angles α' and β').

15.4 COMPARISON WITH RHODES' TERMINOLOGY AND CLASSIFICATION

In the book *Introduction to Monopulse* [1], published in 1959, D. R. Rhodes proposed a classification scheme for the various types of monopulse, and showed that they are related by a unifying set of theoretical principles. Those principles are still valid, and they provide valuable insight into the theoretical foundations of monopulse.

However, because of the advancement and diversification of monopulse functions, applications, and designs since 1959, it was felt necessary in the present volume to modify and expand Rhodes' classification system and to emphasize the individual practical characteristics of the various types of monopulse in addition to pointing out their common theoretical foundations. Some of Rhodes' mathematical terminology has been replaced by engineering terminology more directly identified with the functions and physical components of the monopulse system. A number of topics not covered in Rhodes' small volume, or mentioned there only briefly, have been introduced or expanded. Some of the conciseness of Rhodes' mathematics has been sacrificed in the present volume in favor of fuller step-by-step derivations.

For the benefit of readers of this book who have studied Rhodes' book in the past or who may refer to it in the future, this section gives a brief comparison of the two classification systems and "translations" of some of the terminology.

Rhodes' classification of a monopulse radar rests mainly on two criteria: the type of "angle sensing" and the type of "angle detection." Interposed between these two principal functions there may be an intermediate one called "ratio conversion."

Angle sensing is of two types: amplitude sensing and phase sensing. These depend on the nature of the antenna patterns, and they correspond to the amplitude-comparison and phase-comparison classes defined in Chapter 5 of this book. Rhodes' definitions are worded and illustrated only for reflector or lens antennas, but they can be extended to electronically steered array antennas in the same manner as is done in Chapters 5 and 7 of this book.

Much of Rhodes' theoretical development is expressed in terms of the patterns and illumination functions of the individual component beams¹—that is, the squinted beams with a common phase center or the parallel beams with displaced phase centers—while in the present book the main emphasis is on the sum (or reference) and difference patterns. This is merely a matter of viewpoint, since only a simple transformation (mathematical or physical) is needed to convert component beams to their sum and difference or vice versa. In practice, however, it is usually the sum and difference patterns that are of direct interest to the designer

¹ The term "component beams" is not used in Rhodes. It is used here in the sense defined in Section 2.3.

and user; they have physical reality in the sense of being measurable and producing the voltages that are acted upon by the receivers.

The pair of component beam patterns is characterized by an “angle-sensing ratio,” complex in general, which Rhodes denotes by the symbol $r(u)$, where u is defined as $\pi(d/s)\sin\theta$ and d is the aperture dimension. In the portion of the radar containing the passive components the ratio exists only mathematically. It does not appear physically until a later stage.

If the ratio conversion function is present, it converts the pair of voltages from the component patterns into a different pair having a different ratio, which still exists only mathematically. For example, the output voltages of the pair of component beams may be converted to their sum and difference, or amplitude sensing may be converted to phase sensing or vice versa. The conversions described by Rhodes are accomplished by hybrid junctions or other passive devices. In the terminology of the present book, the device that forms the sum and difference (or the sum and two differences for two coordinate monopulse) is called the comparator (Section 4.4.3), and conversion from amplitude sensing (amplitude-comparison class) to phase sensing (phase-comparison class) or vice versa by means of a 3-dB directional coupler is called “apparent” conversion (Section 5.7) because the classification is regarded here as an inherent property of the antenna patterns, regardless of subsequent conversions. In Rhodes’ terminology, the ratio of the two squinted patterns (in amplitude sensing) or of the two parallel patterns (in phase sensing) is a “multiplicative” ratio, denoted by r_m , and the ratio of the difference to the sum is an “additive” ratio, denoted by r_a . A multiplicative ratio is unity on axis and has reciprocal values at equal positive and negative angles. In amplitude sensing, the multiplicative ratio is the ratio of two amplitudes (with sign), since the phases are equal. In phase sensing, the amplitudes are equal and the ratio is $\exp(j\phi)$, where ϕ is the phase difference between the two component voltages. An additive ratio is zero on axis and has odd symmetry as a function of angle.

The types of circuits that Rhodes calls angle detectors correspond generally to what are called monopulse processors in Chapter 8 of this book. These circuits, which contain active components, act on the pair of voltages whose ratio is r_m or r_a (after ratio conversion, if any) and produce an “angle output,” which is a function of that ratio and can be calibrated with respect to angle.

Rhodes sets up three classes of angle detectors, designated by Roman numerals I, II, and III. Class I is used when the sum and difference voltages are available as inputs. The class I circuit example that Rhodes gives in the first part of his Figure 3.8 and in his Figure 3.9 is the same as the dot-product detector described in Sections 8.8 and 8.9 of this book. Other examples in this book that would also fall in Rhodes’ class I (although their implementation is different from his example) are given in Sections 8.4–8.7.

Rhodes’ class II angle detector operates on input voltages having the same phase but different amplitudes. His example in Figure 3.8 uses logarithmic ampli-

fier-detectors and takes the difference of their outputs as the angle output. This is the same as the processor described in Section 8.12 of this book.

His class III angle detector operates on voltages having the same amplitude but different phases. It consists basically of a phase detector. The processor described in Section 8.13 of this book can be considered a member of that class.

Thus Rhodes' six forms of monopulse are designated as classes IA, IIA, IIIA, and IP, IIP, and IIIP, where the letters A and P denote amplitude and phase sensing. For example, class IIIA would mean that the antenna patterns are of the amplitude-sensing (amplitude-comparison) type, but the pattern outputs have been converted (by a ratio converted such as a 3-dB coupler) to a pair of voltages having equal amplitude but different phases; these voltages are then operated on by a class II angle detector. Examples that are more typical would be IA or IP, since in most cases the beam outputs, whether from an amplitude-comparison or phase-comparison antenna, are converted to their sum and difference, which are then operated on by any of several forms of monopulse processor.

Not all modern monopulse systems fit neatly into Rhodes' classes, particularly with regard to the angle detector (monopulse processor). In fact, some of them are not true monopulse according to his definition because they do not satisfy all of his theoretical postulates (he calls such systems "pseudomonopulse"²). In the present book the definition of monopulse is broadened to include virtually any system that uses simultaneous receiving beams to determine angle of arrival. Furthermore, Rhodes' classes are too broad to distinguish among the various techniques of implementing the same function (since that was not his intention). For these reasons, in Chapter 8 of this book the monopulse processors have been described individually without reference to Rhodes' classification.

References

- [1] D. R. Rhodes, *Introduction to Monopulse*, New York: McGraw-Hill, 1959. Reprint, Dedham, MA: Artech House, 1982. See pp. 92–96 and 102, 105.
- [2] J. L. Butler, "Digital, Matrix, and Intermediate-Frequency Scanning," Vol. III, Chapter 3 of *Microwave Scanning Antennas*, R. C. Hansen, (ed.), New York: Academic Press, 1966.
- [3] D. K. Barton and H. R. Ward, *Handbook of Radar Measurement*, Englewood Cliffs, NJ: Prentice-Hall, 1969. Reprint, Dedham, MA: Artech House, 1984.
- [4] D. B. Anderson and D. R. Wells, "A Note on the Spatial Information Available From Monopulse Radar," *Proc. 5th National Convention on Military Electronics*, IRE-PGMIL, June 1961, pp. 268–278. Reprinted in *Radars*, Vol. 1, *Monopulse Radar*, D. K. Barton, (ed.), Dedham, MA: Artech House, 1974.

² The name "pseudomonopulse" has also been applied to systems in which the signals being compared are not truly simultaneous but are separated by a time interval short enough to minimize the effect of target amplitude fluctuation.

- [5] S. M. Sherman, "Complex Indicated Angles in Monopulse Radar," Ph.D. Dissertation, University of Pennsylvania, 1965 (see pp. 20–24 and 51–53).
- [6] *Metric Editorial Guide*, 3rd ed., Washington, D.C.: American National Metric Council, January 1978.
- [7] *American National Standard Metric Practice*, ANSI/IEEE Std 268-1982, New York: The Institute of Electrical and Electronics Engineers, 1982.
- [8] P. J. Kahrilas, *Electronic Scanning Radar Systems (ESRS) Design Handbook*, Dedham, MA: Artech House, 1976.

List of Symbols

A	Azimuth angle
A	Taylor sidelobe parameter
A, B	Signal voltages into comparator
$A(f)$	Scintillation spectrum
$\dot{A}, \ddot{A}, \ddot{\ddot{A}}$	Azimuth components of velocity, acceleration, and jerk
\mathbf{A}, \mathbf{B}	Vector voltages
a	Amplitude of sine wave
a_1, a_2	Amplitude error of input, output of comparator
a_e, a_o	Even, odd illumination functions
a_m	Modulation voltage
B	Noise bandwidth of scintillation spectrum
B_n	Noise bandwidth of glint spectrum
C	Amplitude constant of two sources
C_1, C_2	Constants in composite difference and sum patterns
c	Noise correlation coefficient
c	Velocity of light
D	Antenna diameter
d	Difference-channel voltage in coordinate of interest
d'	Noise-corrupted difference-channel voltage
d_1, d_2	Erroneous response at input, output of comparator
d_1, d_2	Difference patterns of squinted beam pairs
d_a, d_b	Difference channel voltages of two targets
d_c	Cross-polarized difference channel response
d_{cp}	Cross-polarized difference channel response to jammer
d_{el}	Elevation difference-channel voltage
d_I, d_Q	In-phase, quadrature components of difference signal
d_{tr}	Traverse difference-channel voltage
E	Elevation angle

E_0	Elevation angle of beam axis
E_1, E_2	Fields from two sources
E_a	Elevation angle of normal to aperture
e, e_c	Field strengths of intended, cross-polarized components
e_{cp}	Cross-polarized field from jammer
F_A, F_B	Patterns used to form symmetrical beam ratio
f	Focal length of parabolic antenna reflector
$f(u)$	Voltage pattern of antenna
f_r	Pulse repetition frequency
G_0	Gain of uniformly illuminated antenna
G_j, G_{jr}, G_{jt}	Jammer antenna gain, receiving, transmitting
G_{mlj}, G_{slj}	Jammer antenna mainlobe and sidelobe gains
G_{rep}	Total repeater gain
G_n	Depth of monopulse null
$g(x)$	Illumination function in aperture x -coordinate
g_0	Uniform illumination function
g_d	Difference illumination function
g_{do}	Optimum difference illumination function
h	Aperture height
h_a	Antenna phase-center height
h_t	Target altitude
$I(t), Q(t)$	In-phase, quadrature components of modulated voltage
I, I_d	Sum- and difference-channel interference powers
$i_d(x_n), i_s(x_n)$	Difference- and sum-pattern illumination functions
$i_{sq}(x_n)$	Illumination function of squinted beam
J_b, J_d	Bistatic, direct jammer powers
j	Square root of -1
K	Relative difference slope
K, K'	Scale factors of logarithmic amplifier
$K(\theta)$	Variance of error for steady target
K_0	Optimum relative difference slope
K_v, K_a, K_3	Error coefficients in velocity, acceleration, jerk
K_r	Difference slope ratio
K_θ	Beamwidth constant $= (w/\lambda)\theta_3$
k	Wave number $= 2\pi/\lambda$
k_d	On-axis difference slope

k_m	Normalized monopulse slope
$\frac{k_m'}{k_m}$	Monopulse slope with comparator errors
\bar{k}_m	Average monopulse slope to target angle
k_U	Monopulse slope normalized to angle U
L	Target cross-range span
L	Length of array
L_{pol}	Polarization loss of repeater jammer antenna
$m(t)$	Complex modulation voltage
$N(f)$	Glint spectrum
N_c	Correlated noise power
N_d	Noise power in difference channel
N_{du}	Uncorrelated noise power in difference channel
N_s	Sum-channel noise power
N_{su}	Uncorrelated sum-channel noise power
n	Number of pulses averaged
n_c	Correlated noise component
n_d, n_s	Additive phasor noise voltages
n_{du}, n_{du}	Uncorrelated noise components
n_i	Number of clutter samples with frequency diversity
\bar{n}	Taylor taper parameter
p	Ratio of sum-channel voltages of two targets
$p(S)$	Probability density function of signal power
$p(S, K)$	Signal power pdf, chi-square, $2K$ degrees of freedom
q	Diagonal difference pattern
R	Range
R_1, R_2	Distances to two sources
R_2	Range from jammer to chaff
R_{ab}	Range from target A to target B
R_c	Crossover range in pass course
R_p	Measured power ratio of two targets
r	Power ratio of two targets
r	Specularly reflected multipath component
r_σ	Ratio of effective jammer to target RCS
S	Signal power in sum channel
\bar{S}	Mean signal power of fluctuating target
s	Sum-channel voltage

s'	Noise-corrupted sum-channel voltage
s_0	On-axis sum-channel voltage
s_1, s_2	Sum patterns of squinted beam pairs
s_a, s_b	Sum signals from two targets
s_I, s_Q	In-phase and quadrature components of sum signal
t	Time
t_c	Clutter correlation time
t_o	Averaging time of servo loop
U	Normalized angle from array
U_{sq}	Normalized squint angle
U_{st}	Normalized steering angle
u	Normalized angle
u, v, w	Angles in sine space
u_{ar}	Target traverse angle in sine space
u_{sq}	Squint angle
u_{st}, v_{st}	Steering angles in sine space
v_1, v_2	Squinted-beam voltages
v_1, v_2, v_3, v_4	Voltages at input and output of hybrid junction
v_A, v_B	Voltages from two patterns forming symmetrical ratio
v_{ci}, v_{cq}	In-phase and quadrature components of correlated noise
v_{du}, v_{su}	Normalized uncorrelated noise components
$v_{dvi}, v_{svi}, v_{suq}$	Normalized difference- and sum-channel noise
v_r	Modulated voltage
v_s	Normalized sum-channel noise
v_t	Target velocity
W	Signal bandwidth
$W(\epsilon)$	Probability density function of glint error
w	Aperture width
w	Vector voltage ratio of two targets
x	Horizontal coordinate
x	Real part of complex number
x', y'	I and Q outputs of dot-product detector
x_c	Center coordinate of circle in complex angle
x_n	Normalized distance across array
$Y_a(f)$	Open-loop AGC response
$Y_c(f)$	Closed-loop servo response

$Y_s(f)$	Scintillation error factor
y	Imaginary part of complex number
Z	Exponent of function in squinted-beam illumination
z	Complex number
z_n	Location of zeroes in Taylor pattern
α, α'	Angle from positive x -axis, and its complement
α_{ar}	Target traverse angle from x -coordinate
α'_{sq}	Beam squint angles in sine space
α', α'_{st}	Beam steering angles in sine space
β, β'	Angle from positive y -axis, and its complement
β_n	Servo loop bandwidth
β_{n0}	Design value of servo loop bandwidth
β'_{st}	Beam steering angle in sine space
γ, γ'	Angle from positive z -axis, and its complement
Δ	Difference channel
Δf	Doppler difference of multipath
Δ_f	Agile bandwidth
ΔR	Pathlength difference
Δ_u, Δ_v	Off-axis angle in sine-space coordinates
Δu	Off-axis angle from beam of array
Δv	Off-axis angle from beam of array in elevation
$\Delta\theta$	Angular separation of two targets
Δ_θ	Off-axis error angle
δ	Phase of d relative to s
δ_d, δ_s	Phase angles of d and s relative to arbitrary reference
ϵ	Glint error
ϵ_0	Angle error from cross-eye jammer
$\epsilon_{az}, \epsilon_{tr}$	Azimuth and traverse errors
ϵ_{cp}	Cross-polarization error in monopulse ratio
$\epsilon_{d/s}$	Error in monopulse ratio
ϵ_{lag}	Dynamic lag error
ϵ_x	Cross-range error from cross-eye jammer
ϵ_θ	Error in angular measurement
$\epsilon_{\theta 0}$	Correction adjustment of null during calibration
$\epsilon_{\theta c}$	Bias error in angular measurement from clutter

$\varepsilon_{\theta r}$	Boresight shift from receiver error
η_a	Aperture efficiency
θ	Azimuth angle
θ	Angle from beam axis
θ	Aspect angle of two sources
θ'	Angle measured in beamwidths
θ_a, θ_b	Off-axis angles of two targets
θ_{bw}	Half-power beamwidth
θ_i	Indicated angle
$\bar{\theta}_i$	Mean of indicated angle
θ_{in}	Normalized indicated angle of target pair
θ_{mid}	Angular midpoint between two targets
θ_{sq}	Squint angle of beam
θ_t	Indicated angle
λ	Wavelength
λ_g	Wavelength in waveguide
μ	Angle between vector voltages
μ	Target scatterer distribution parameter
ρ	Radius of circle in complex indicated angle plane
ρ	Correlation coefficient between sum- and difference-channel noise
ρ_0, ρ_s	Fresnel reflection coefficient, specular scattering factor
Σ	Sum channel
σ, σ_c	Intended and cross-polarized target RCS
σ_a, σ_b	Radar cross sections of two targets
σ_b	Bistatic RCS of chaff
$\sigma_{d/s}$	Standard deviation of monopulse ratio
σ_e	Effective RCS of repeater jammer
σ_g	rms cross-range glint
σ_h	rms surface height deviation
σ_{IF}	rms tuning error
σ_s	rms scintillation voltage
σ_{θ}	Standard deviation of angle error
$\sigma_{\theta a}, \sigma_{\theta b}$	On-axis and off-axis error components
$\sigma_{\theta c1}$	Single-pulse clutter error

$\sigma_{\theta ca1}, \sigma_{\theta can}$	On-axis single- and n -pulse clutter errors
$\sigma_{\theta cb1}, \sigma_{\theta cbn}$	Off-axis single- and n -pulse clutter errors
$\sigma_{\theta g}$	rms glint error in angle
$\sigma_{\theta IF}$	rms boresight error from IF tuning
$\sigma_{\theta r}$	rms error from receiver phase and amplitude drift
$\sigma_{\theta s}$	rms scintillation error in angle
τ	Pulsewidth (actual or compressed)
ϕ	Phase of sine wave
ϕ	Relative phase of sum-channel voltages of two targets
ϕ_0	Phase angle of $s + jd$
ϕ_1, ϕ_2	Phase errors at input, output of comparator
ϕ_1, ϕ_2	Phase angles between s and $s + jd$ or s and $s - jd$
ϕ_{ar}	Phase of arriving ray
ϕ_m	Phase of modulation voltage
ϕ_p, ϕ_s	Phase angles of pathlength, reflection coefficient
ϕ_{st}	Steering phase function
ψ_1, ψ_2	Phase angles of directional coupler inputs
ω	Radian frequency of sine wave
$\omega_1, \omega_2, \omega_3$	Break points in servo open-loop response
ω_a	Intersection of 40-dB/octive response slope with axis
$\omega_{az}, \dot{\omega}_{az}$	Azimuth rate and acceleration

About the Authors

Samuel M. Sherman received a Ph.D. in engineering physics from the University of Pennsylvania. As a captain in the U.S. Army, he served as a Radar Design and Development Officer in World War II. After the war he was a research associate at University of Pennsylvania. He then served as a superintendent of the Control Equipment Division at the Naval Air Development Center in Warminster, Pennsylvania.

His major contributions in monopulse radar were at RCA where he was the head of systems engineering and a senior staff scientist. During the early years of his work at RCA, he was a colleague of David K. Barton.

After retirement from RCA, he was the author of the first edition of *Monopulse Principles and Techniques* in 1984. He was a radar consultant and a lecturer in The George Washington University Continuing Engineering Education Program. He published many journal articles and was awarded several patents.

Dr. Sherman worked during the second half of 2010 on this second edition of his book, continuing to provide revised material and review new material through February 2011. He marked his last corrections on February 25, 2011, from the hospital where he passed away on February 28, 2011, at age 96. This book thus represents the last of his many contributions to the art and science of radar.



David K. Barton is a radar system consultant, with a home and office in Hanover, New Hampshire. He attended Harvard College from 1944 to 1949, with a two-year interruption for service in the U.S. Army at White Sands Proving Grounds. He returned to White Sands as a civilian engineer after receiving his A.B. in physics in 1949. In 1953 Mr. Barton transferred to the Signal Corps Laboratories at Fort Monmouth, New Jersey, to initiate development of the AN/FPS-16, the first monopulse instrumentation radar. In 1955 he joined the staff at RCA, where the radar development was carried out, and participated in the test and evaluation of the system. For this work RCA awarded him in 1958 the first David W. Sarnoff Medal for Outstanding Achievement in Engineering. Mr. Barton also scaled up that radar to create in 1960 the AN/FPS-49 radars for the Ballistic Missile Early Warning System, only recently replaced after 40 years of operation in Alaska and Great Britain.



From 1963 to 1984 he was a consulting scientist with Raytheon Company in Wayland and Bedford, Massachusetts, where he originated the radar concepts for the AN/TPS-19 radar-controlled landing system for the U.S. Air Force, and contributed to a number of other radar and guided missile studies and projects. He joined ANRO Engineering in 1984, engaging in radar and missile system studies until his retirement in 2004.

Mr. Barton was elected a Fellow of the IEEE in 1972 and to the National Academy of Engineering in 1997. In 2002 he received the IEEE Dennis J. Picard Medal for Radar Technologies and Applications. He has served on the scientific advisory boards of the U.S. Air Force, the Defense Intelligence Agency, and the Army Research Laboratories. Since 1975 he has been the editor of the Artech House Radar Series, of which this book is approximately the 160th volume.

Index

- Advantages and disadvantages of monopulse, 13–15, 252, 351
- Aegis radar, 342
- Amplitude-comparison monopulse, 5, 7–12, 71–80, 93–103, 105–123, 138–141, 376–378
 - basis for classification, 71–80, 93–103
 - definition, 72
 - equivalence to phase-comparison monopulse, 138–141
- AN/APG-25 radar, 81
- AN/APG-63 radar, 344
- AN/FPQ-6 radar, 107, 118
- AN/FPS-16 radar, 46–48, 54–56, 78–80, 107–108, 113–116, 159–160, 164–168, 173, 230, 259–261, 298, 310, 319, 335
- AN/FPS-49 radar, 337–339
- AN/FPS-117 radar, 354
- AN/MPS-36 radar, 118, 176
- AN/MPQ-53 (Patriot) radar, 121, 339
- AN/SPG-53A radar, 311
- AN/SPY-1A radar, 134–136, 342
- AN/TPQ-27 radar, 176
- AN/TPS-59 radar, 352–354
- Angle of arrival (*see* Direction of arrival)
- Angle tracking (*see* Tracking radar)
- Angular coordinates for monopulse
 - calibration, 128, 147
- Antenna mounts, 13, 32, 45
- Antennas, 46–53, 78–82
 - array (*see* Array antennas)
 - Cassegrain, 51–53, 107, 331
 - lens, 47–49, 129–131, 339, 349–341
 - reflector, 50–53, 91
 - illumination function, 22–24, 74–81, 91–92, 98, 112–113, 125–126, 133, 136–140, 345, 364–370
 - efficiency, 77–82, 112–115, 120–122, 137–138, 365–369
- Aperture, 22, 32
 - sampling, 217, 302, 311
- Applications of monopulse, 3, 6, 15, 337–359
- Array antennas, 25, 66, 125–141
 - active, 126, 345, 352–355
 - adaptive nulling, 323
 - amplitude-comparison or phase-comparison, 98
 - constrained feeds, 132–137
 - coordinates, 33, 128
 - cross-polarized response, 332
 - electronic scanning, 126
 - active, 344
 - electronic steering, 126–129, 370
 - elements, 54, 92, 126
 - frequency steering, 127
 - monopulse in, 125–141
 - optical feeds, 54, 127–129
 - phase center in, 90–92
 - phase steering, 127
 - reflectarray, 129
 - secondary radar, 353
 - space feeds, 128–131
 - special types, 141
 - subarrays, 126–134, 323, 342
 - time-delay steering, 127
 - tracking-radar applications, 339–343
- Artillery mil, 375
- Automatic gain control, 44, 128, 151, 155–158, 163, 171, 174–181, 240–245, 264–268, 318–320, 333
- Axis
 - azimuth, 31, 45
 - boresight, 9–10, 32–36, 255–257, 259–261

- electrical, 9, 259
- elevation, 32
- mechanical, 10, 259
- monopulse, 10, 94, 361, 370
- tracking, 10, 260
- Azimuth, 31–38
- Ballistic Missile Early Warning System, 337
- “Baseline” monopulse radar, 6–13, 24, 41
- Beacon operation, 116
- Beam deviation factor, 116
- Beamwidth, 10, 71, 74
 - constant, 109
 - standard, 290
- Bistatic jamming, 328
- Blockage, 50–53, 65, 105–107, 118
- Boresighting, 11
- Broadside, 34, 90
- Cassegrain antenna, 51–53, 107, 331
- Chaff, 320
- Classification (*see* Monopulse classification)
- Closed-loop tracking
 - bandwidth, 252, 267
 - defined, 27
 - in multipath, 277–280, 305
 - noise errors in, 247
 - of unresolved targets, 218
 - vs. open-loop operation, 247
- Commutation, 170, 336
- Comparators, 63, 57, 63–66
- Complex envelope (*see* Complex signal representation)
- Complex indicated angle, 195–215
 - information derivable from unresolved targets, 188–191, 209–217
 - in multipath, 273, 294–301, 309–311
- Complex ratio, 21, 39–44
- Complex signal representation, 27–31
- Conical scan, 4–5, 14–15, 174–176
- Conopulse, 181–182, 336
- Coordinate transformation, 13
- Correction signal, 2–4, 13, 27, 146
- Corrugated horn, 106, 122
- Cosine factor, 12, 150
- Cosine space (*see* Sine space)
- Countermeasures and
 - countercountermeasures, 317
- Cross-eye jamming, 323–326
- Cross-polarized jamming, 330–332
- Definition of monopulse, 20
- Detection, 12, 73, 121, 165
- dot-product, 158
 - multipath effects, 276
 - of unresolved targets, 203
- Diagonal difference, 26, 40, 63, 209, 349, 371–374
- Difference pattern, 10, 23–25, 65, 71–78, 91, 99, 117–121
- Diffuse scattering factor, 303
- Direction of arrival, 198,
- Directional couplers, 57, 60–63, 68, 97, 100–103, 377
- Displaced phase center, 359
- Displays, 2, 4
- Doppler denial, deception, 318
- Double difference (*see* Diagonal difference)
- Duplexer, 12, 121–123, 131, 165, 340
- Dynamic range of receivers, 69, 118, 145, 150–155, 164, 176, 334
- ECM (*see* Countermeasures)
- Electrical correction signal, 13, 146
- Elevation, 31
- Equivalence of amplitude comparison and phase comparison, 71, 141
- Error correction, 13, 146
- Error signal, 2, 12, 27, 44, 73, 247
- Errors due to
 - boresight axis setting and drift, 256–261
 - clutter, 247–252
 - cross-polarized response, 261–263
 - dynamic lag, 252–255
 - electronic countermeasures, 321–336
 - glint, 27, 190, 213, 227, 263–266, 285, 323, 258
 - inexact monopulse processors, 149, 202, 247
 - multipath, 145, 178, 187, 271–313, 326–328, 346, 353
 - noise (*see* Noise errors in angle measurement)
 - scintillation, 266–268
 - unresolved targets, 161, 187–222, 273, 321, 371–374
- f/D ratio, 107, 261
- Feed horns, 7, 24, 51–57, 108
- Feeds
 - constrained (corporate), 126, 132–136
 - five-horn, 25, 56, 65, 95, 106, 118, 122
 - four-horn, 23, 56, 63–67, 94 108–121, 371
 - Lopez, 122, 135, 343

- multimode, 24, 57, 65, 106, 120–123, 130, 339
- optimization of, 105–113, 118–123, 132–136
- space, 128–132
- twelve-horn feed, 65, 119–123
- Flap Lid radar, 340
- Fresnel reflection coefficient, 274
- Functions of monopulse, 6
- Generic monopulse ECM, 321–329
- Glint (*see* Errors due to glint)
- Graphical symbols, 66
- Grill Pan radar, 341
- History of monopulse, 5
- Hybrid junctions, 9, 23, 26, 57–65
 - directional coupler, 60
 - graphical symbols, 66–68
 - hybrid ring, 59–60
 - magic-T, 58, 66
- I and Q , 12, 30, 41–43, 152–153, 162, 245
- Illumination function, 22–24, 74–81, 91–92, 98, 112–113, 125–126, 133, 136–140, 345, 364–370
- Image-frequency jamming, 318, 334
- Instrumentation radar, 6
- Intelligence applications, 6
- Jamming (*see* Countermeasures)
- Lens antennas, 47–49, 129–131, 339, 349–341
- Linear monopulse ratio, 361
- Magic-T junction, 58, 66
- Milliradian, 375
- Millisine, 375
- Monopulse
 - advantages and disadvantages, 13–15, 252, 351
 - amplitude comparison (*see* Amplitude-comparison monopulse)
 - applications, 3, 6, 15, 337–359
 - axis, 10, 94, 361, 370
 - classification, 71–103, 138–141, 376–378
 - definition, 20
 - functions, 6
 - history, 5
 - nonradar uses, 15, 20
 - optimum, 74–77
 - phase-amplitude, 81, 177–178
 - phase comparison (*see* Phase-comparison monopulse)
 - processors (*see* Monopulse processors)
 - ratio (*see* Complex ratio)
 - single-channel, 179
 - slope (*see* Slope, monopulse)
 - two-channel, 174–177, 336
- Monopulse processors,
 - dot-product detector, 155–162, 201, 216, 242, 245, 377
 - exact, 148–150, 156, 182, 201
 - I and Q , 30, 41–43, 152–153, 162, 245
 - log (v_1/v_2), 166–169
 - noncoherent, 162–165
 - phase and linear amplitude, 150–152
 - phase and log amplitude, 153–155
 - $s + d$ and $s - d$, 165
 - $s + jd$, 170–174
 - summary, 182–184
- Multimode feed, 57, 65, 72, 106, 120–123, 130, 339
- Multimode radar, 343
- Multipath, 271–314, 326–328, 353
 - diffuse, 271, 302–313, 327
 - effect on closed-loop tracking, 277–280
 - errors (*see* Errors due to multipath)
 - “nosediving,” 278, 289, 306–308
 - specular, 221, 271–276, 281, 293, 303–313
 - specular scattering factor, 274
 - stable and unstable nulls, 277–279
- Multipath remedies, 280–302, 307–313
 - aperture sampling, 302, 311
 - beam pattern design, 281
 - complex indicated angle, 294–301, 309–311
 - double-null tracker, 293, 309
 - independent-target methods, 301, 311
 - “low-E” modes, 281, 286, 295–297, 308
 - multiple-beam methods, 301, 311
 - offset-null tracking, 288, 308
 - range or Doppler resolution, 282–285, 307
 - smoothing and averaging, 285, 296–300, 307
 - symmetrical-ratio patterns, 288–293, 301, 308
- Noise errors in angle measurement, 225–247
 - analytical model, 227
 - bias, 225, 231–234, 242, 246
 - probability density function, 233

- closed-loop vs. open-loop, 247
- multiple-pulse averaging, 227, 241
- fluctuating targets, 242–246
- Nonradar uses of monopulse, 15, 20
- Normalization process, 13, 73–75, 128, 144–147, 151–152, 157, 171, 174–182, 213, 226, 240–242, 263–267, 333, 340
- Normalized difference signal, 12, 27, 34, 71, 117, 148, 171, 175, 181, 189, 193, 216, 299, 361–364
- Open-loop operation, 6, 27, 45, 145, 200, 247, 279–281, 285–289, 294
- Paraboloidal-reflector antenna, 7, 50, 107
- Patterns
 - component, 24–26, 72, 90, 94, 102, 107, 140, 162, 182
 - definition of, 24–26
 - reference, 25, 57, 65, 95, 103, 105, 118, 122
 - sum and difference, 10, 24–26, 65, 76–79, 108–110, 128, 137, 330, 355, 361–371
- Pencil beam, 2, 10, 122, 294, 352, 354
- Phase center, 55, 72, 81–95, 102, 141, 274, 201 359, 376
 - of array antenna, 90–92
 - of reflector antenna, 93–96
- Phase-comparison monopulse, 5, 49, 71–74, 80–82, 95–98, 102
 - basis for classification, 71–103
 - definition, 72
 - equivalence to amplitude-comparison monopulse, 71, 141
- Phase front, 82–95, 129, 200
- Phased arrays (*see* Array antennas)
- Pilot pulses, 69, 152, 165, 259
- Polarization
 - circular, 131
 - cross-polarization effects, 261–263
 - duplexing, 130, 340
 - jammer, 326, 330–332
 - reflection coefficient dependence on, 274
 - twisting, 52–53, 331
- Processors (*see* Monopulse processors)
- Product detector, 43–44, 155–161
- Pseudomonopulse, 378
- Pulse repetition frequency (rate), 2, 14, 174–176, 241
- Quadrature component of monopulse ratio, 12, 42, 152, 161, 203, 209, 299
- Quadrupolar signal (*see* Diagonal difference)
- Radar principles, review of, 1
- Radar signature analysis, 221
- Radar targets, 1, 85–89, 193–195
- Range, 2
 - denial and deception, 318–321, 331
 - resolution, 282–284, 307
- Range gate, 3, 146, 157, 174
- Range tracking, 146, 157, 321
- Ranging, 12
- “Rat-race” junction, 59
- Receivers, 12, 46, 68, 72, 146, 151, 165, 178–180, 256–260, 332–336
- Reference pattern, 25, 57, 65, 95, 104 (*see also* Five-horn feed)
- Reflector antennas, 50–53, 91
- Rhodes’ classification, 376–378
- Secant correction, 13, 35
- Second difference (*see* Diagonal difference)
- Secondary radar, 355–357
- Sequential lobing, 3–6, 13–15, 46, 266, 317
- Seekers, 346–349
- Simultaneous lobe comparison, 1, 5, 15, 20–23
- Sine space, 23, 32–36, 90, 126–128, 148, 370–375
- Single-channel monopulse, 179–180
- Slope, monopulse (difference), 71, 74–78, 106, 110–112, 120, 137, 144–178, 230, 257, 290, 294
 - constant, 361–372
 - normalized, 77
 - optimum, 76
 - ratio, 77
 - relative, 75
 - variation with angle, 117
- Space applications, 6
- Space object identification, 6, 221
- Specular scattering factor, 275
- Squint angle, 7–10, 94, 98, 108–118, 168, 361–370
- Strategic applications, 6
- Sum and difference
 - devices for forming, 57–66
 - in array antennas, 73, 127–138
 - notation and terminology, 26
 - patterns, 24, 75–82, 110–115
- Superposition, 191–193, 368
- Tactical applications, 6
- Target recognition, 221, 358

- Terrain-avoidance radar, 357
- Three-dimensional surveillance radars, 351–355
- Tracking radar, 2–6, 27, 46, 200, 252–255, 337–349
- TRADEX radar, 153, 299, 337–339
- Transmission, 12
- Traverse angle, 3, 31–38, 46, 128
- Twelve-horn feed, 65, 106, 119–123
- Two-channel monopulse, 174–177, 336
- Units of angle and sine space, 374
- Unresolved targets, 187–221
 - closed-loop tracking of, 218
 - detection of presence, 203
 - extensions of monopulse techniques, 217
 - mean and variance of indicated angle, 204
 - more than two targets, 219
 - nonindependent targets, 221
 - solving for angles of, 209–215
- Zhuk radar, 345

Recent Titles in the Artech House Radar Series

David K. Barton, Series Editor

Adaptive Antennas and Phased Arrays for Radar and Communications, Alan J. Fenn

Advanced Techniques for Digital Receivers, Phillip E. Pace

Advances in Direction-of-Arrival Estimation, Sathish Chandran, editor

Airborne Pulsed Doppler Radar, Second Edition, Guy V. Morris and Linda Harkness, editors

Bayesian Multiple Target Tracking, Lawrence D. Stone, Carl A. Barlow, and Thomas L. Corwin

Beyond the Kalman Filter: Particle Filters for Tracking Applications, Branko Ristic, Sanjeev Arulampalam, and Neil Gordon

Cognitive Radar: The Knowledge-Aided Fully Adaptive Approach, Joseph R. Guerci

Computer Simulation of Aerial Target Radar Scattering, Recognition, Detection, and Tracking, Yakov D. Shirman, editor

Design and Analysis of Modern Tracking Systems, Samuel Blackman and Robert Popoli

Detecting and Classifying Low Probability of Intercept Radar, Second Edition, Phillip E. Pace

Digital Techniques for Wideband Receivers, Second Edition, James Tsui

Electronic Intelligence: The Analysis of Radar Signals, Second Edition, Richard G. Wiley

Electronic Warfare in the Information Age, D. Curtis Schleher

ELINT: The Interception and Analysis of Radar Signals, Richard G. Wiley

EW 101: A First Course in Electronic Warfare, David Adamy

EW 102: A Second Course in Electronic Warfare, David L. Adamy

EW 103: Tactical Battlefield Communications Electronic Warfare,
David Adamy

Fourier Transforms in Radar and Signal Processing, David
Brandwood

Fundamentals of Electronic Warfare, Sergei A. Vakin, Lev N. Shustov,
and Robert H. Dunwell

Fundamentals of Short-Range FM Radar, Igor V. Komarov and
Sergey M. Smolskiy

*Handbook of Computer Simulation in Radio Engineering,
Communications, and Radar*, Sergey A. Leonov and Alexander I.
Leonov

High-Resolution Radar, Second Edition, Donald R. Wehner

Introduction to Electronic Defense Systems, Second Edition, Filippo
Neri

Introduction to Electronic Warfare, D. Curtis Schleher

Introduction to Electronic Warfare Modeling and Simulation, David
L. Adamy

Introduction to RF Equipment and System Design, Pekka Eskelinen

The Micro-Doppler Effect in Radar, Victor C. Chen

Microwave Radar: Imaging and Advanced Concepts, Roger J.
Sullivan

Millimeter-Wave Radar Targets and Clutter, Gennadiy P. Kulemin

Modern Radar Systems, Second Edition, Hamish Meikle

Modern Radar System Analysis, David K. Barton

*Modern Radar System Analysis Software and User's Manual, Version
3.0*, David K. Barton

Monopulse Principles and Techniques, Second Edition, Samuel M.
Sherman and David K. Barton

MTI and Pulsed Doppler Radar with MATLAB®, Second Edition, D. Curtis Schleher

Multitarget-Multisensor Tracking: Applications and Advances Volume III, Yaakov Bar-Shalom and William Dale Blair, editors

Principles of High-Resolution Radar, August W. Rihaczek

Principles of Radar and Sonar Signal Processing, François Le Chevalier

Radar Cross Section, Second Edition, Eugene F. Knott et al.

Radar Evaluation Handbook, David K. Barton et al.

Radar Meteorology, Henri Sauvageot

Radar Reflectivity of Land and Sea, Third Edition, Maurice W. Long

Radar Resolution and Complex-Image Analysis, August W. Rihaczek and Stephen J. Hershkowitz

Radar Signal Processing and Adaptive Systems, Ramon Nitzberg

Radar System Analysis, Design, and Simulation, Eyung W. Kang

Radar System Analysis and Modeling, David K. Barton

Radar System Performance Modeling, Second Edition, G. Richard Curry

Radar Technology Encyclopedia, David K. Barton and Sergey A. Leonov, editors

Radio Wave Propagation Fundamentals, Artem Saakian

Range-Doppler Radar Imaging and Motion Compensation, Jae Sok Son et al.

Signal Detection and Estimation, Second Edition, Mourad Barkat

Space-Time Adaptive Processing for Radar, J. R. Guerci

Special Design Topics in Digital Wideband Receivers, James Tsui

Theory and Practice of Radar Target Identification, August W. Rihaczek and Stephen J. Hershkowitz

Time-Frequency Transforms for Radar Imaging and Signal Analysis,
Victor C. Chen and Hao Ling

For further information on these and other Artech House titles, including previously considered out-of-print books now available through our In-Print-Forever® (IPF®) program, contact:

Artech House

685 Canton Street

Norwood, MA 02062

Phone: 781-769-9750

Fax: 781-769-6334

e-mail: artech@artechhouse.com

Artech House

16 Sussex Street

London SW1V HRW UK

Phone: +44 (0)20 7596-8750

Fax: +44 (0)20 7630-0166

e-mail: artech-uk@artechhouse.com

Find us on the World Wide Web at: www.artechhouse.com
